UNIVERSITY OF HULL

Surfactant-Nanoparticle Formulations at Calcite-Water and Oil-Water Interfaces for Enhanced Oil Recovery

being a thesis submitted in fulfilment of the

requirements for the degree of

Doctor of

Chemistry

in the University of Hull

by

Hosein Rezvani

May 2023

Acknowledgements

Achievements

PhD publications

- **H. Rezvani**, B.P. Binks and D. Nguyen, Aqueous Surfactant-Nanoparticle Formulations for Enhanced Oil Recovery in Calcite-rich Rocks (in preparation)
- **H. Rezvani,** B.P. Binks and D. Nguyen, Surfactant-nanoparticle mixtures for emulsification of oil and water (in preparation)

Collaboration publications

- A. Khalilnezhad, **H. Rezvani,** A. Talebi, P. Ganji, T. Puntervold and M. Riazi, *Energy Fuels*, 2023, **37**, 11765-11775.
- A.C. Matusse, A. Eleslambouly, B. Rafik, **H. Rezvani,** B.E. Berrehal, B. Richards and G. Wach, *EAGE First Break*, 2023, **41**, 101-112. https://issuu.com/eage/docs/_linked_mr_23199-fb23_june/102.
- A. Khalilnezhad, **H. Rezvani,** A. Abdi and M. Riazi, *in Thermal Methods*. ed. A. Hemmati-Sarapardeh, A. Alamatsaz, M. Don and Z. Li, Gulf Professional Publishing, 2023, ch. 8, pp. 269-314.
- R. Fazlyeva, **H. Rezvani,** A. Askarova, A. Khalilnezhad, A. Cheremisin and M. Riazi, *in Thermal Methods*, ed. A. Hemmati-Sarapardeh, A. Alamatsaz, M. Don and Z. Li, Gulf Professional Publishing, 2023, ch. 5, pp. 155-215.
- **H. Rezvani,** Md A. Islam Khan, A. Khalilnezhad and T. Puntervold, Role of Enhanced Oil Recovery Technologies in Energy Transition, in *Emerging Nanotechnologies and Solutions in Enhanced Oil Recovery,* ed. M. Riazi, A. Hemmati-Sarapardeh, F.B. Cortes, M. Husein and Z. Li, Gulf Professional Publishing, 2024, ch. 18.
- **H. Rezvani,** A. Rezaeyan, S. Tran, Y. Yu and L. Zhang, Recovery Enhancement in Unconventional Shale Resources, *in Unconventional Shale Resources*, Taylor & Francis, 2024, ch. 7 (order of authors not known yet – in preparation).

Awards

- Institute of Engineering and Technology (IET) Postgraduate Research Award 2023 for the impact of research (see IET Website)

Abstract

There is a growing interest in the development of new and innovative enhanced oil recovery (EOR) technologies to reduce the environmental impact of oil production. Surfactant flooding is a well-established EOR method but mainly suffers from high adsorption onto rock or low surface activity resulting in poor EOR. Aqueous surfactant-nanoparticle mixtures have received great attention in different fields like emulsification, foaming, EOR and CO_2 sequestration. The use of nanoparticle-surfactant mixtures can promote a more sustainable and efficient EOR process. However, colloidal particle stability under reservoir conditions is considered a great challenge. In addition, the way synergy works in EOR is not clearly understood.

This thesis aims to formulate a particle-surfactant mixture for an efficient EOR in tight calcite-rich reservoirs with a focus on surfactant adsorption behaviour at fluid-fluid and solid-fluid interfaces in the presence of particles and ions. For this, bare silica particles were sterically stabilized using two silanes, namely epoxy silane (ES) and amino silane (AS), and blended with two commercial surfactants, namely alkyl hydroxysultaine (AHS) or binary zwitterionic-nonionic (ZN) surfactant solution (AHS + nonionic $C_{10-12}E_9$), for both additional steric stabilization and EOR. The effects of particle-surfactant mixtures on reservoir properties including rock wettability, static and dynamic surfactant adsorption onto rock, oil-water interfacial tension and emulsification of oil and water were studied to select effective dispersions for spontaneous oil imbibition in a calcite-rich rock. The blend of ES-coated silica particles and surfactants often showed pH-responsive behaviour at rock-water and oil-water interfaces with particles serving as carriers or surface activity improvers for surfactants resulting in different extents of rock wettability alteration and emulsification. Optimum surfactant concentrations determined from static experiments were found to significantly increase crude oil recovery of Permian brine by $36 \pm 1\%$ original oil in place (OOIP) in secondary spontaneous imbibition which was further enhanced by 14% OOIP on adding only 0.01 wt.% ES-coated silica. The nanoparticle-surfactant formulation was also efficient in producing residual crude oil in tertiary mode (6% OOIP additional oil recovery). The oil recovery results disclosed a high dependence on the emulsification ability of the blends with particle-AHS dispersion producing more stable emulsions and thus more crude oil compared to that of ZN. These findings contribute to the understanding of EOR mechanisms and provide valuable insights for the development of strategies to maximize oil recovery in tight oil reservoirs.

Contents

Chapter 1 Introduction

1.1. Surfactants

1.1.1. Definition

Surface-active substances called surfactants are amphiphiles with hydrophilic head groups and hydrophobic tail groups (Figure 1.1). Depending on the type of head groups or tails, surfactants can be divided into a number of different groups. According to the headgroup charge, they can be anionics, cationics, nonionics, zwitterionics and catanionics while their hydrophobic group could be a hydrocarbon, a small polymer or a fluorocarbon chain.[1]

Figure 1.1. Molecular structure of surfactant.

Tail   Head
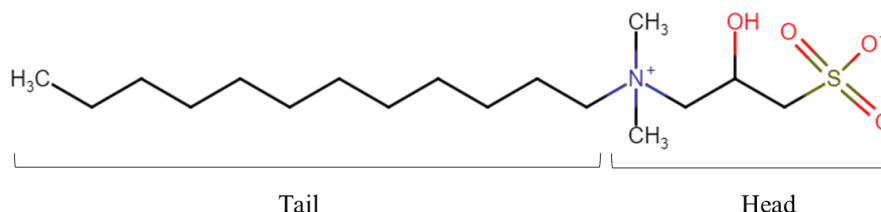
1.1.2. Surfactant aggregation

Surfactant molecules can aggregate in either an aqueous phase or an oil phase if a specific surfactant concentration, or critical micelle concentration (CMC), is attained. The hydrophobic effect, which is the inclination of the hydrocarbon tail group to be away from water molecules, is the primary cause of the aggregation in the aqueous phase. As a result, aqueous surfactant monomers will form normal micelles at the CMC where the head groups make up the shell and the tails are in the core. On the other hand, reverse micelles can be formed in the oil phase in which the hydrophilic head groups form the cores while the hydrophobic tails face the oil phase[1] (Figure 1.2). The free energies of micellization (ΔG°_m) of surfactant (zwitterionic and nonionic) can be calculated using:[2]

$$\Delta G^{\circ}_m = RT \ \ln CMC \qquad (1.1)$$

where R is the gas constant (8.314 J mol^{-1} K^{-1}) and T is the absolute temperature (K).

The hydrophilic–lipophilic balance (HLB) number of a surfactant determines its hydrophilicity or hydrophobicity. HLB numbers below 9 indicate lipophilic surfactants while hydrophilic surfactants have an HLB number above 11.[3]

Figure 1.2. Sketch of monomeric and micellar surfactant in water and oil.
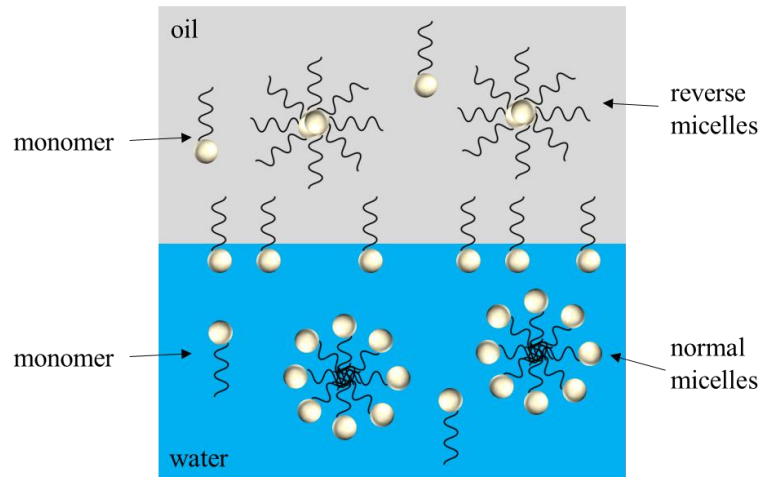
1.1.3. Surfactant adsorption at fluid-fluid interface

Assuming water is in contact with air (or oil), bulk water molecules have similar interactions with neighbouring water molecules in all directions. Water molecules lose half of their connections when they come into contact with air or oil molecules at the air(oil)-water interface. The bulk water-water interactions are mainly hydrogen or dipole-dipole bonding while there are fewer molecules around the water molecules at the interface as the density of the gas is much smaller than that of water resulting in stronger interactions at the interface. Here, surface (interfacial) tension is related to the energy needed to increase the surface area by one unit which causes more water molecules from the bulk (low energy) to move toward the surface. Thus, the bigger the difference between the two phases, the more energy needs to be applied.[8]

Surfactants have high adsorption capabilities at different interfaces. When an aqueous surfactant solution < CMC comes into contact with either air or oil, the hydrophobic effect of the surfactant molecules causes them to diffuse in the aqueous phase to adsorb at the air-water or oil-water interface such that the hydrophobic tail is oriented towards air (oil) and the hydrophilic head is in the aqueous phase (Figure 1.3), increasing interactions between the two phases and lowering surface (interfacial) tension. On increasing surfactant concentration < CMC, a monolayer eventually forms at the CMC where the lowest surface (interfacial) tension is anticipated. Aqueous micelles form in bulk water when the surfactant concentration > CMC rises. Although the quantity of interfacial

molecules does not typically vary, surfactant molecules at the interface are in equilibrium with bulk monomeric or micellar molecules.[4] The surface excess concentration (Γ in mol m^{-2}) and minimum area per molecule (A in nm^2) of nonionic surfactant at the air-water surface can be calculated using the Gibbs adsorption isotherm:

$$\Gamma = -\frac{1}{2.3\ RT}\frac{d\gamma}{d\log a} \qquad (1.2)$$

$$A = \frac{1}{\Gamma_m \times N_A} \qquad (1.3)$$

where γ is the air-water surface tension (N m^{-1}) and a is the activity of the surfactant which can be replaced with surfactant concentration given that CMC happens usually at low surfactant concentrations, Γ_m is the maximum surface excess concentration (mol m^{-2}) and N_A is Avogadro's number (6.022×10^{23}).[5] The constant *2.3* is the conversion factor from the natural logarithm to log10. Zwitterionic surfactants can be considered nonionic for purposes of this equation due to their zero net charged headgroup around neutral pH. The free energy of adsorption ($\Delta G°_{ads}$) of surfactant can be calculated using:[2]

$$\Delta G^{\circ}_{ads} = \Delta G^{\circ}_{m} - \frac{\Pi}{\Gamma_m} \qquad (1.4)$$

where Π is the surface pressure at the CMC which is the difference between the surface tension of DIW and the surface tension at the CMC ($\gamma_0 - \gamma_{CMC}$). Temperature, electrolyte, pressure and pH are only a few of the variables influencing the interfacial behaviour of surfactants.

Figure 1.3. Surface tension between air and water at various surfactant concentrations.
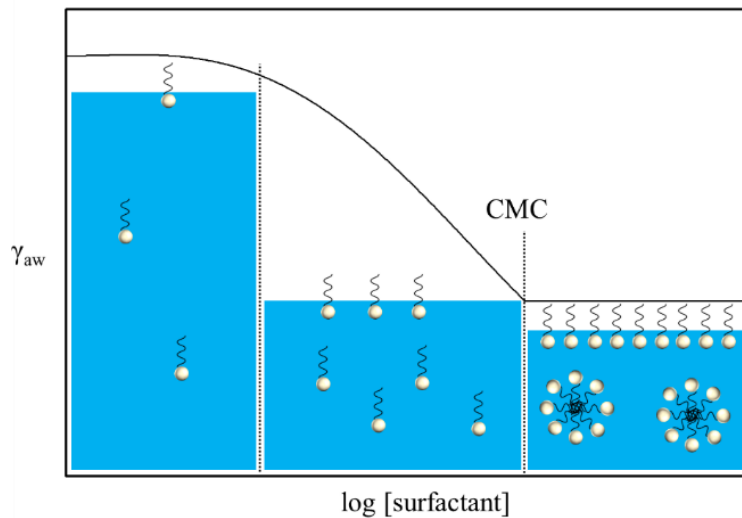
1.1.4. Surfactant adsorption at fluid-solid interface

Surfactants can adsorb at air-solid and liquid-solid surfaces to change the properties of solid surfaces with applications in many fields including detergency, coatings, materials science and EOR. The specific interactions between surfactants and solid surfaces and the adsorption behaviour can differ depending on the type of surfactant (cationic, anionic, or nonionic), the characteristics of the solid surface (charge, roughness and hydrophobicity) and the solution conditions (pH and temperature). Figure 1.4 shows the interactions between different surfactants and solid surfaces. Cationic surfactants are drawn to anionic solid surfaces due to their positively charged head groups. Electrostatic forces dominate the interaction between cationic surfactants and solid surfaces. Anionic surfactants are drawn to cationic solid surfaces due to their negatively charged head groups. Similar to cationic surfactants, electrostatic forces primarily control how anionic surfactants interact with solid surfaces. Adsorption happens when the surfactant's negatively charged head group electrostatically bonds to the positively charged surface. In both types, the surfactant concentration and the charge density on the solid surface are two variables that affect how strong the interactions are. Due to having two charges in their head groups, zwitterionic surfactants can have two types of electrostatic interactions, V-shaped and I-shaped adsorption, depending on the solid charge. Due to the absence of a charged head group, nonionic surfactants exhibit weak electrostatic interactions with charged solid surfaces. Instead, hydrogen bonds and hydrophobic interactions and van der Waals forces control how they interact with solid surfaces. Through physical adsorption, nonionic surfactants can create a monolayer on a solid surface. Surfactant concentration, temperature, and solid surface elements are only a few examples of the variables that affect adsorption.[6, 7]

Figure 1.4. Interactions between different types of surfactants and a charged solid surface.
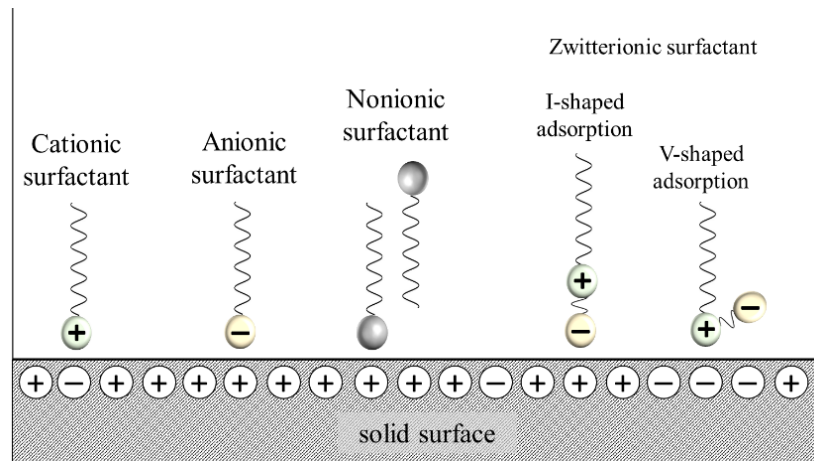
1.2. Colloids

1.2.1. Definition

A colloid is a particular kind of mixture in which one component (minutely dispersed insoluble particles) is suspended within another component. A colloid contains particles that are bigger than atoms or common molecules yet too small to be seen by the naked eye. The usual size range of colloidal particles is between nm and μm. The particles can be made up of various substances such as solid, liquid or gas to form different colloidal systems such as solid particles dispersed in a liquid medium (*e.g.* milk), liquid droplets dispersed in another liquid (*e.g.* emulsion), or gas bubbles dispersed in a liquid (*e.g.* foam). Because of the size, surface characteristics and interactions of the dispersed particles, colloids exhibit particular characteristics and behaviours. Brownian motion (random movement of particles), stability and the ability to scatter light are a few examples of these qualities. Numerous fields, including medicine, food science, materials science, environmental science and petroleum industry, use colloidal systems.[8]

1.2.2. Particle stability

A colloidal system is stable if particles stay suspended in the continuous phase. The total forces operating on the particles determine the particle stability. These forces include van der Waals forces and electrostatic interactions which both contribute to the system's overall free energy. If the interaction energy brought on by the attractive forces existing between the colloidal particles is less than kT (k is Boltzmann constant and T is absolute temperature), the colloid is said to be stable. In this case, the substance will continue to be a suspension because the colloidal particles will either reject or just slightly attract one another. The attractive forces will take control if the interaction energy exceeds kT and the colloidal particles will start to group in the form of aggregation, flocculation, coagulation or precipitation. Reversible aggregation involving lesser attractive forces is referred to as flocculation while precipitation is typically used to describe the phase change from a colloid dispersion to a solid as a result of a perturbation. Coagulation is irreversible and occurs when the forces aggregating the particles together are stronger than any external forces brought on by stirring or mixing.[9, 10]

Colloid destabilisation is the process of aggregating colloidal particles which causes the dispersed phase to separate or settle. Colloidal particles can be made unstable by lowering the electrostatic barrier that prevents colloidal particles from aggregating through salt addition or pH modification. By condensing the counterions in the space between the particles, adding salts to the dispersion can reduce the electric double layers of the

particles to the point where, at specific salt concentrations, electrostatic repulsion completely disappears. Through charge neutralisation, the presence of electrolytes can also lessen the electrostatic attraction between particles. In the absence of particle-particle electrostatic repulsion, van der Waals attraction, which is weak and only operates over short distances, may be the dominant factor in colloidal destabilisation. The closer the particles are to one another, the lower the energy of the interaction (negative), which causes colloid instability. The critical coagulation concentration (CCC) of salt is the point at which the energy barrier between particles is zero or smaller than kT. The electrostatic barrier between particles can therefore be removed by any heat fluctuation, which could cause the system to become unstable. The Shultz-Hardy rule can be used to calculate CCC as follows:[10, 11]

$$CCC = \frac{84 \; \varepsilon^3 \; (kT)^5}{A_H^2 \; e^6 \; Z^6} \tag{1.5}$$

where ε is the water dielectric constant, A_H is the compound Hamaker constant, e is the electron charge, and Z is the ion valency. According to the equation, CCC is inversely related to ion valency to the sixth power. This indicates that the coagulation concentration is reduced by 64 times when $CaSO_4$ (2:2) is used in place of KCl (1:1). Temperature elevation can also destabilize colloids by increasing the Brownian motion and collision of particles.

Colloids can also become unstable when particles are electrostatically grafted with ionic polymers and surfactants. The charged functional groups in the polymers and surfactants can electrostatically adsorb onto the surfaces of the particles, leaving hydrophobic groups outward to bridge with other particles through van der Waals attraction that leads to agglomeration or flocculation.[12]

Colloids can be stabilized using electrostatic stabilization, steric stabilization or a combination of both. The mutual attraction of like electrical charges is the foundation of electrostatic stability. Particle charges are organised in an electrical double layer where the charged particles initially attract counterions (ions with the opposite charge) (Figure 1.5).[13] The zeta potential provides the most convenient means of quantifying the electrostatic attraction between suspended colloidal particles. Derjaguin, Landau, Verwey and Overbeek (DLVO) theory provides a quantitative explanation of the combined impact of van der Waals attraction and electrostatic repulsion on aggregation. Peptization is a standard technique for transforming a precipitate into a colloid by shaking it in the

presence of an electrolyte. pH adjustment also has a great impact on the electrostatic stabilization of colloidal particles.[9]

Steric stabilisation entails the physical and chemical grafting of particles with a layer of a polymer, surfactant or silane to keep them apart in the range of attractive forces. Steric stabilisation provides advantages over electrostatic stabilisation such as being less sensitive to high salinity or particle concentrations and having the option to use both non-aqueous and aqueous phases as solvents.[14, 15]

Figure 1.5. Schematic view of charge distribution around an anionic particle.
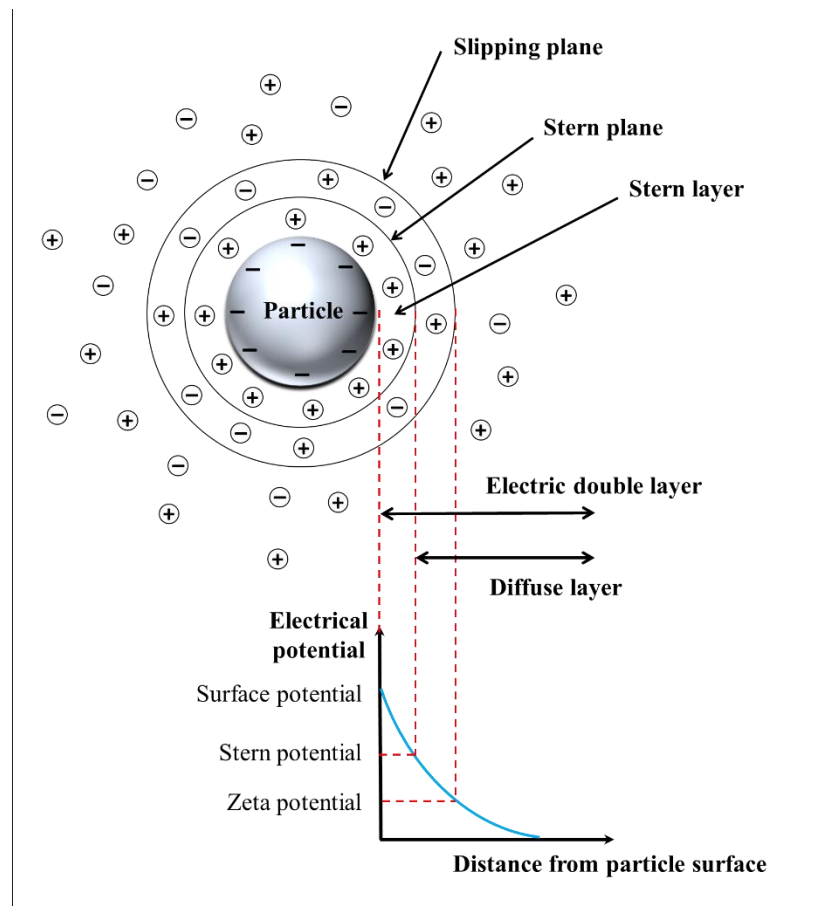
1.3. Solid particles at fluid-fluid interfaces

The adsorption of colloidal solid particles (*e.g.* metal oxides) at fluid-fluid interfaces is of great interest in various fields, including particle-stabilised foams and particle-stabilised emulsions (Pickering emulsions). Particle adsorption at the gas-liquid interface reduces lamella thinning and improves the durability of foam bubbles. Particle adsorption at the oil-water interface creates significant resistance to fusion which delays coalescence in emulsions. Enhanced mechanical characteristics, *e.g.* improved interfacial tension and

dilational or shear surface elasticity, are other benefits of particle adsorption at the liquid-air or liquid-liquid interface.[16]

Similar to surfactants, particle adsorption at the liquid-liquid or liquid-air interface may create a monolayer that aids in the stabilisation of emulsions and foams by providing elastic forces. The monolayer formed as a result of the adsorption of charged particles at an oil-water interface is a two-dimensional assembly with empty spaces between them. This assembly is believed to be a result of van der Waals attraction and repulsive forces (electrostatic, steric and solvation forces). The short-range van der Waals attraction makes particles stay close at the interface while the opposing forces prevent the compact arrangement of like-charged particles.[17] On the other hand, the replacement of part of the fluid interface with a solid particle results in a thermodynamic decrease in free energy that is proportional to the cross-sectional area occupied by the particle. Therefore, although the process of particle adsorption at the interface is kinetically unfavourable, it is thermodynamically ideal. Adsorption may occur naturally or after successfully breaking a significant energy barrier.[18] An interface must favour the adsorption in terms of energy for spontaneous particle adsorption to occur, *i.e.* particles must have lower energy at the interface than in bulk.[19, 20] There are some other factors controlling particle assembly at the fluid-fluid interface including particle surface chemistry, pH, electrolyte, type of oil and thermodynamic conditions (*i.e.* temperature and pressure).[20] Compared to surfactant and polymer molecules which adsorb and desorb at interfaces very quickly, particles, if large enough and with the right wettability, stay irreversibly adsorbed at the fluid-fluid interface. This can considerably increase the stability of emulsion drops and foam bubbles against coalescence and disproportionation by inducing kinetic stability. The wettability of the particles by both fluid phases at the interface is of utmost significance and is determined by the contact angle the particle takes at the interface. Highly hydrophilic ($\theta \sim 0°$) or hydrophobic ($\theta \sim 180°$) particles tend to stay in bulk while partially hydrophobic particles can effectively adsorb at fluid-fluid interfaces (Figure 1.6).

Hydrophilic charged nanoparticles can be activated using different approaches including salt addition, pH adjustment, alcohol addition, the addition of oppositely charged particles, polymers or surfactants and blocking the surface charge of particles by chemical grafting (*e.g.* silanization).[21] It is noteworthy to mention that excessive surface charge reduction by pH adjustment or salt addition may coagulate the particles by shrinking the electric double layer.[16] The stability and thermodynamic characteristics of interfacial monolayers may be impacted by surface modification by ligands (surfactants, silanes, and polymers), which regulate particle-particle and particle-solvent interactions.[19] The significance of

ligands in interactions with the interface or two liquids increases when the particle diameter is equal to the length of the ligand. For a surface-active ligand, the particle shell may be deformed due to the ligand accumulations at the liquid-liquid interface.[19]

Figure 1.6. Particle position at an air-water or oil-water interface according to its contact angle in water.
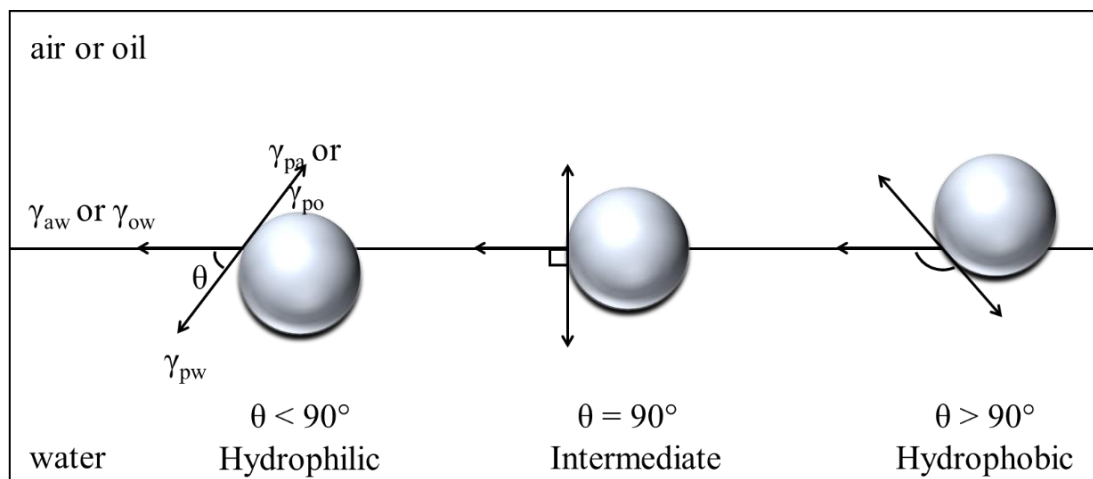
1.4. Solid particles at fluid-solid interface

The adsorption of particles on solid surfaces, in contrast to fluid-fluid interfaces, has not garnered much attention in the scientific literature. While the adsorption behaviour of particles as adsorbates on solid surfaces is rarely addressed, it is frequently studied as an adsorbent. Due to its importance in real-world applications, understanding the adsorption mechanisms of particles on solid surfaces is essential. Particle adsorption on solid surfaces is a significant phenomenon that has applications in many different industries. It can be used in catalysis to promote certain reactions and increase surface reactivity. Additionally, it applies to nanomaterial synthesis, surface coating, sensors and biological applications such as imaging and medication delivery. Particle adsorption on rock surfaces during EOR can alter the characteristics of the rock surface. A variety of surface interaction forces, primarily physical adsorption, chemical adsorption, or a combination of the two, affect particle adsorption on solid surfaces. Chemisorption entails a strong chemical bond between particles and the surface through electron sharing as opposed to physical sorption which involves weaker intermolecular forces like van der Waals interactions (London forces, dipole-dipole attraction, dipole-induced attraction and hydrogen bonding). The surface chemistry of both the particles and the surface, including surface charge, surface functionalization and surface roughness, can have an impact on how particles adsorb to solid surfaces. The properties of particles like composition, size and shape are also important.[7, 22]

1.5. Emulsion

1.5.1. Definition

Emulsions are created when two immiscible liquids such as oil and water are combined with the aid of an emulsifying agent. A surfactant or a combination of surfactants can operate as an emulsifying agent by reducing the interfacial tension between the two fluids and stabilizing the emulsion. There are two types of emulsions: microemulsions and macroemulsions.[23]

Microemulsions are minute colloidal droplets of one liquid dispersed in another liquid as a continuous phase. Usually less than 100 nm in size, microemulsions are clear or translucent and can spontaneously form in the presence of an appropriate surfactant by lowering oil-water interfacial tensions. Microemulsions are thermodynamically stable meaning that the continuous phase (such as water) and the dispersed phase (such as oil droplets) create a stable equilibrium state as a result of the balance of interfacial tensions and the system's free energy. The spontaneous self-assembly of surfactant molecules and the regulation of thermodynamic variables including composition, temperature and pressure influence the composition and structure of microemulsions. The system's free energy is reduced when a thermodynamically stable microemulsion forms allowing for a long time stability without phase separation. [23]

The term "kinetically stable" refers to a property of microemulsions that prevents phase separation or coalescence under dynamic settings or in the presence of external disturbances. Microemulsions keep their small droplet size and homogeneity for a longer period than macroemulsions or conventional emulsions which may spontaneously divide into discrete phases over time. This stability is attained by choosing the proper surfactants, cosurfactants and oil-water compositions that encourage the development of highly structured interfacial structures and inhibit droplet aggregation or coalescence. Kinetic stability guarantees their homogeneity and makes it possible for them to be used as effective delivery methods for a variety of applications.[23]

1.5.2. Microemulsions

The surfactant monomers adsorbed at the oil-water interface are at equilibrium with those in bulk when equal amounts of oil and water are present along with a surfactant at CMC. If the surfactant concentration rises above the critical microemulsion concentration (CµC), where the maximum number of monomers can exist in the water or oil phase, microemulsions begin to form. A constant oil-water interfacial tension that is independent of the surfactant concentration is seen at the CµC. The monomer concentration in the oil

or water phase does not grow past the CμC and stays the same.[24] As a result, according to Winsor, the surplus surfactant forms aggregates in four different ways (Figure 1.7). While Winsor III is a three-phase system, Winsor I and II are two-phase systems. Oil is solubilized in the centre of aqueous micelles in Winsor I to create oil-in-water microemulsions that coexist with extra oil. Winsor II forms water-in-oil microemulsions with extra water by solubilizing water in the hydrophilic cores of reverse micelles in the oil phase. In Winsor III, a third phase forms between the excess oil and water. Winsor IV is a single-phase micellar solution that is thought to be the extension of a middle-phase microemulsion at high surfactant concentrations.[25]

The type of Winsor system is affected by surfactant monolayer curvature which is turn a function of the headgroup and tail group area. The area of the headgroup is typically larger than the tail for a pure ionic surfactant, which tends to create oil-in-water microemulsions with a curved surfactant monolayer around the oil. Surfactants tend to micellize in the oil phase when they are hydrophobic or when there are high electrolyte concentrations.

Figure 1.7. Winsor systems I to IV by Du *et al.*[26]
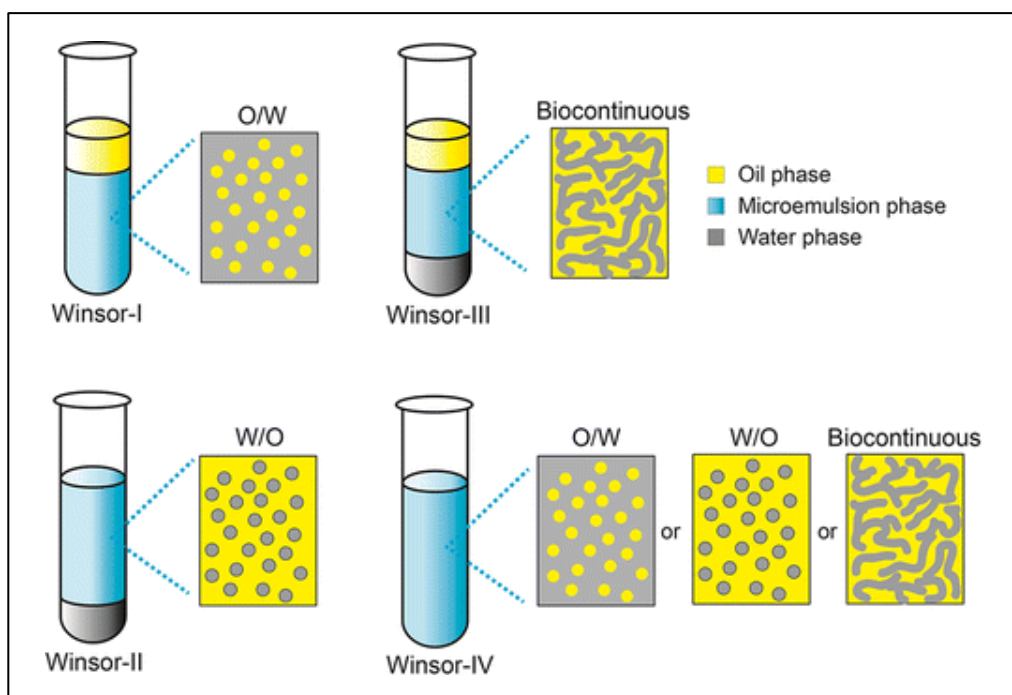
1.5.3. Macroemulsions

Macroemulsions are dispersed liquid-in-liquid systems which are thermodynamically unstable but kinetically stable. As a result of kinetic barriers that prevent phase separation, they can be stable and maintain their emulsified condition for a certain time. Due to their large droplet size (usually a few microns to hundreds of microns), macroemulsions scatter light effectively, giving them a cloudy or opaque appearance. Macroemulsions are not in

a thermodynamic equilibrium condition and will eventually separate into their constituent phases. The high interfacial tension between the immiscible liquids and the large droplet size encourage coalescence and phase separation in them. Unlike microemulsions, macroemulsions do not form spontaneously and require external energy input (vigorous mixing) and the use of emulsifying agents (*e.g.* surfactants) or particles to stabilize the emulsion and prevent phase separation. Oil-in-water, water-in-oil or multiple emulsions (*e.g.* oil-in-water-in-oil) are common types of emulsions depending on the emulsifier, salinity, temperature and volumes of two phases (Figure 1.8).[27]

Particle-stabilized emulsions, or Pickering emulsions, are a type of emulsion where the stability of oil or water droplets is achieved by the presence of solid particles at the interface. These solid particles act as stabilizers, adsorbing onto the droplet surfaces and preventing their coalescence and separation. As described before, particle wettability is important in forming Pickering emulsions. For equal amounts of oil and water, a water-in-oil emulsion is preferable for hydrophobic particles ($\theta > 90°$), and an oil-in-water emulsion is preferred for hydrophilic particles ($\theta < 90°$).[28, 29] There are several mechanisms by which this stabilization happens. The formation of a dense monolayer or multilayer around the emulsion drops and prevention of coalescence can result from particles irreversibly adsorbing at the oil-water interface. The detachment energy is proportional to particle radius, oil-water interfacial tension and particle contact angle and it is maximum when the angle is 90° for a given system. Furthermore, the droplets in the continuous phase can be captured and essentially immobilized if a three-dimensional network of particles is formed in the continuous phase.[16, 28, 29] They can also stabilize the emulsions through electrostatic interactions. For instance, cationic nanoparticles can stabilize anionic oil droplets by creating a double layer around them. This causes the droplets to repel one another and prevents coalescence.[16] Pickering emulsion stability and properties are also influenced by particle size and concentration, the composition of oil and water and the ratio of two phases.[30]

Figure 1.8. Different emulsion types can be formed.

oil-in-water emulsion   water-in-oil emulsion

water   oil

water   oil

water-in-oil-in-water emulsion   oil-in-water-in-oil emulsion
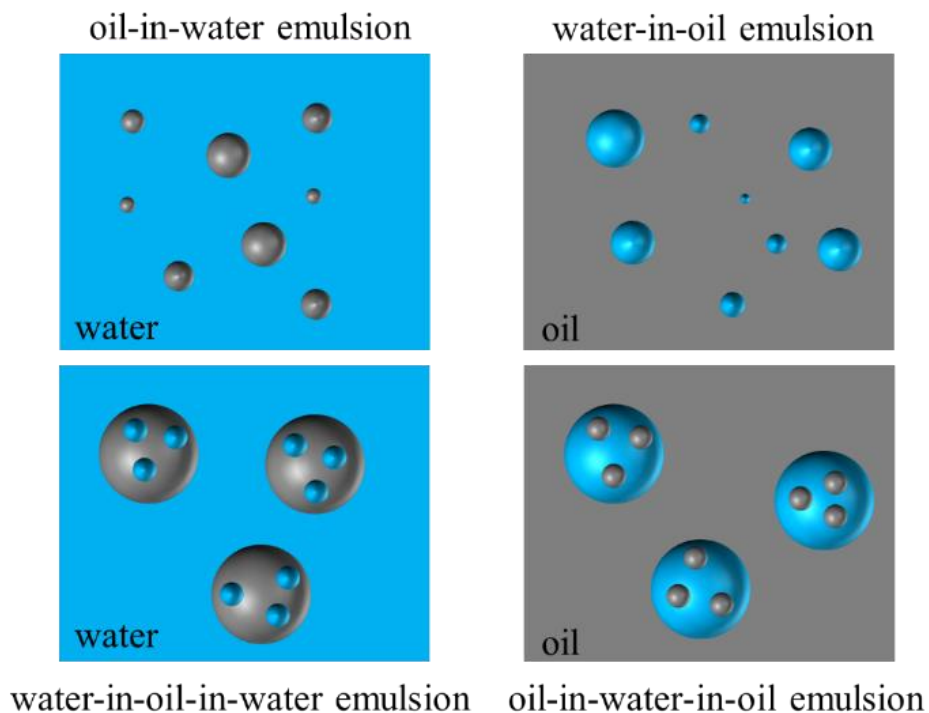
Emulsions can be destabilized through various mechanisms depicted in Figure 1.9. Creaming or sedimentation are the results of large density differences between the two phases. Creaming happens in oil-in-water emulsions in which the less dense oil tends to move to the top while sedimentation happens in water-in-oil emulsions in which the water moves to the bottom due to its higher density. Creaming and sedimentation can be removed by increasing the viscosity or lowering density differences. Flocculation is the aggregation of droplets due to a net attractive force but they do not merge. Coalescence refers to when the droplets irreversibly merge into one big drop due to the breakage of the film between emulsion drops. Ostwald ripening describes the process of larger droplets naturally enlarging and becoming coarser overtime at the expense of smaller ones leading to an alteration of droplet size distribution and the disappearance of smaller droplets.[23]

Figure 1.9. Schematic view of different emulsion destabilization mechanisms.

water-in-oil emulsion

oil-in-water emulsion

Sedimentation

Creaming

Ostwald ripening

Coalescence

Initial emulsion

Flocculation
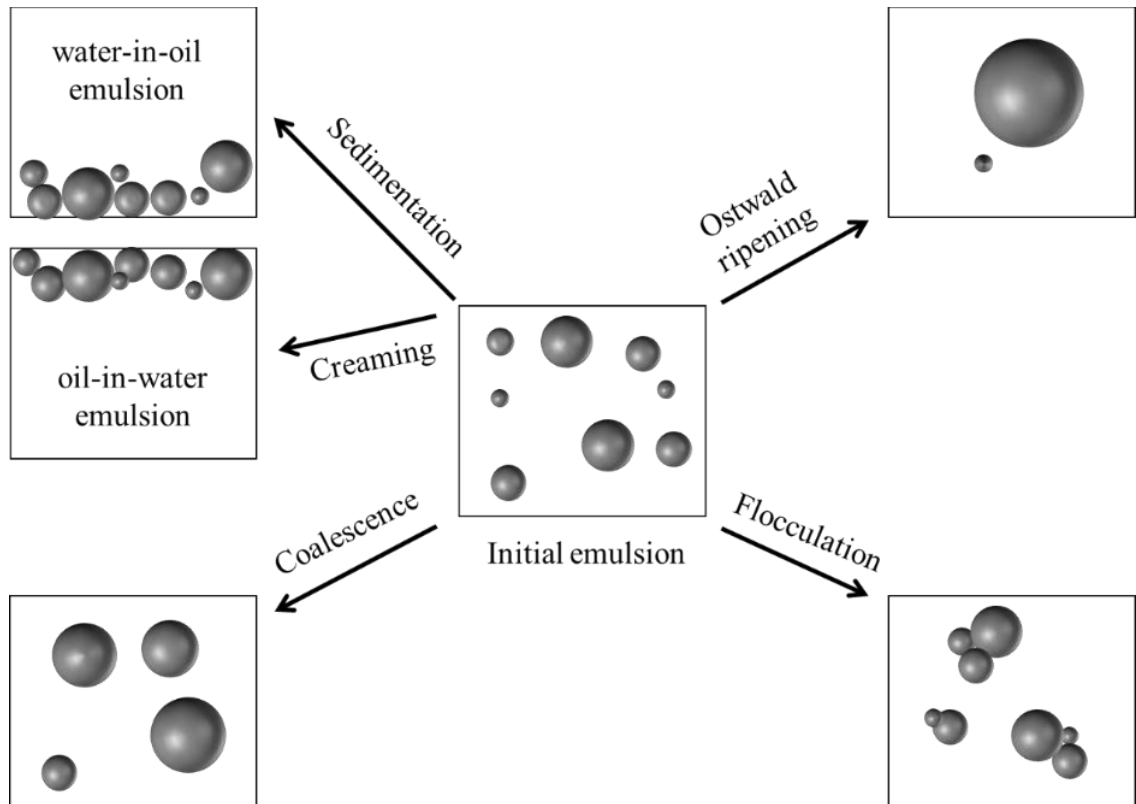
1.6. Future of energy and importance of EOR

The recent 2022 Energy Outlook released by British Petroleum (BP) implies a global shift into renewable energies (*e.g.* wind, electricity and hydrogen) as well as the necessity to cut greenhouse gases (*e.g.* CO_2).[31] Oil and gas reservoirs can play an important role in the energy transition by serving as safe underground storage for greenhouse gases and hydrogen. Storage projects are currently growing in the UK, China, Canada and Norway but mostly lack economic viability. Financial resources may be made available using EOR techniques during the storage process. EOR technologies can also increase oil production from pre-existing reservoirs, reducing the need for additional oil exploration and production. EOR will therefore continue to be important for at least a few decades.[32]

1.7. Oil reservoirs

A huge part of current oil reserves is within tight reservoirs, *e.g.* tight chalks and shales. Shales can serve as both cap rocks and reservoirs. They can be composed of various minerals such as clay, quartz, calcite and occasionally organic materials. The size of pore throats in shales is usually within a nanometre to micrometre which results in an ultralow permeability (mD to nD) which together with their low porosity makes it difficult for the oil to flow through the reservoir leading to a low oil recovery factor of 5% to 15% (lower than that of conventional reservoirs) depending on rock and fluid properties and the maturity of the reservoir. Since oil production rates typically drop by more than 75% in

the first year, more new wells must be drilled which has a significant financial and environmental cost. Therefore, they require specialized techniques, such as hydraulic fracturing and EOR, to extract the oil.[33-35]

Drilling wells into oil reservoirs causes pressure gradients through which oil can be produced naturally. Secondary oil recovery refers to the injection of brine into the reservoir (locally available brine, *i.e.* seawater or produced brine from the reservoir) to increase oil production. Chemicals can be added to the injected brine in secondary mode or later in tertiary mode to increase oil production. Therefore, secondary oil recovery is when all or a large amount of oil is available to the EOR chemical while tertiary oil recovery refers to when residual oil is mostly available. Residual oil is the oil trapped in small pore throats in discontinuous ganglia with high capillary forces which is harder to produce.[33] The capillary pressure (P_c) of a fluid meniscus is given by the Young-Laplace equation:[33]

$$P_c = \frac{2\sigma cos\theta}{r} \tag{1.6}$$

where σ is the oil-water interfacial tension, θ is the three-phase contact angle and r is the radius of curvature. The pressure difference between two immiscible fluids at their interface is known as P_c. It generates the pressure necessary to drive an oil droplet through a pore throat. The capillary pressure present in the pore throats could be so strong that the pressure differences created in the reservoir cannot overcome it. More than 60% of the original oil in place (OOIP) is sometimes still stuck after secondary brine injection. A significant amount of oil, up to 65% OOIP, might be produced using chemical EOR techniques.[36] The equilibrium between viscous forces (pressure gradients caused by the injectant) and capillary forces (oil-water interfacial tension) determines the mobilisation of oil ganglia during flooding, as described by capillary number (N_c):[37]

$$N_c = \frac{v\mu}{\sigma} \tag{1.7}$$

where v is the fluid velocity and μ is the fluid viscosity. Crude oil ganglia start to mobilize when N_c approaches the critical value of $\sim 10^{-5}$. According to reports, oil reservoir pore throats have capillary numbers of $\sim 10^{-6}$. This indicates that capillary forces predominate when it comes to fluid movement in porous media. Values exceeding 10^{-5} show a viscous-dominant fluid flow. The mobility ratio must go down in order to maximise oil recovery. The mobility ratio (M) is defined as the ratio of the mobility of displacing fluid (λ_w) to the mobility of displaced fluid (λ_o) as follows:[33]

$$M = \frac{\lambda_w}{\lambda_o} = \frac{K_{rw}}{K_{ro}} \frac{\mu_o}{\mu_w} \qquad (1.8)$$

where K_{rw} and K_{ro} are the relative permeabilities of water and oil, respectively. A mobility ratio below one is preferred in EOR which can be achieved through a decrease in the relative permeability of water which corresponds to increased oil's relative permeability, increasing water viscosity and reducing oil viscosity. Rock wettability controls oil and water saturations and relative permeabilities which in turn impact the fluid distribution and flow in porous media. Hydrophobic rock wettability and high oil-water interfacial tension induce high negative capillary forces in pore throats offering a low oil recovery by brine injection thus calling for chemical EOR methods. Depending on the type of chemical, EOR can trigger reservoir properties such as rock wettability, oil-water interfacial tension, crude oil viscosity and injected fluid viscosity.[33]

1.7.1. Origin of oil-wetness of reservoir rocks

A solid surface preference for one fluid over another is referred to as wettability. Changes to the surface characteristics of reservoir rocks are referred to as rock wettability alteration. These changes can have an impact on the flow of fluids and the relative permeability of oil and water in the reservoir. The term "oil-wetness" describes a rock surface tendency to be in touch with an oil phase as opposed to a water or gas phase. In reservoir engineering and EOR, it is crucial to comprehend the causes of this rock oil-wetness.

Crude oil is characterized by SARA analysis referring to saturate, aromatic, resin and asphaltene. Saturates are non-polar groups *e.g.* linear, branched or cyclic saturated organics like paraffins.[38] Aromatics are slightly polarizable while resins and asphaltenes are polar. Unlike asphaltenes, resins are soluble in heptane.[39] Resins or polar components of crude oil, normally referred to as natural surfactants, are mainly categorized into acidic and basic groups. The polarity of these compounds usually comes from their heteroatoms *e.g.* nitrogen, oxygen and sulphur in their structure. The presence of oxygen in a structure usually gives it an acidic nature. The most common acidic component is naphthenic acids which usually refer to carboxylic acids, ketones, esters, phenols, alcohols and ethers. Basic polar groups usually have nitrogen in their structure *e.g.* pyridine and quinolone but nitrogen also exists in non-basic groups like carbazole, indole or pyrrole. Commonly found thioalkanes and heterocyclic groups which are derivatives of thiophene usually have sulphur in their structures.[40]

Rock mineralogy, rock surface charge, and pH all affect how hydrophobic the rocks are to a certain extent.[41] Rock hydrophobicity becomes stronger for strongly polar crude oil

where the natural surfactant is abundant. Asphaltenes and polar molecules of crude oil can adsorb or form organic films on the mineral surfaces of reservoir rocks leading to rock oil-wetness. Some rock minerals have inherent hydrophobic properties, encouraging oil-wetness. Certain rock-fluid interactions between the rock surface and the fluids can result in the deposition of hydrophobic substances or the alteration of surface charges leading to oil-wetness. Geological processes, such as diagenesis and rock alteration, can also introduce hydrophobic minerals or modify the surface properties of the rocks contributing to oil-wetness.[42]

The reservoir rock surface is usually charged. These available charged sites resulting from the dissociated surface minerals could act as adsorbents for oppositely charged groups like polar compounds of oil or EOR ionic chemicals, *i.e.* surfactants. The literature has continued to debate the surface charge of oil reservoir rocks since varying surface charges have been recorded.[43, 44] In the case of pure calcite, at high pH (*i.e.* high $[OH^-]$), the calcite surface becomes anionic due to the neutralization of Ca^{2+} and the excess of CO_3^{2-}. However, at neutral or acidic pH, calcite is cationic. In the case of carbonate or shale rocks, due to the presence of other minerals like clay and quartz, a net charge should be considered. The pH and relative dissociation of minerals like Ca^{2+} and CO_3^{2-} as well as other produced complexes, have an impact on the surface charge. In quartz-rich rocks like sandstone reservoirs, the rock surface charge is expected to be negative (pH > 2). In the case of a calcite-rich rock, water on the rock surface promotes the dissociation of polar groups of crude oil, such as stearic acid and calcite, which speeds up the hydrophobization process. The following equilibria can be used to describe how calcite dissociates in water:[45]

$$CaCO_3 \text{ (s)} \rightarrow Ca^{2+} \text{ (aq)} + CO_3^{2-} \text{ (aq)} \tag{1.9}$$
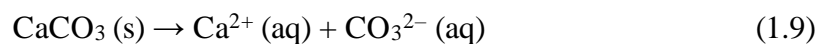
where CO_3^{2-} in water can result in the formation of bicarbonate and carbonic acid as follows:

$$CO_3^{2-} \text{ (aq)} + H_2O \text{ (l)} \rightarrow HCO_3^- \text{ (aq)} + OH^- \text{ (aq)} \tag{1.10}$$

$$HCO_3^- \text{ (aq)} + H_2O \text{ (l)} \rightarrow H_2CO_3 \text{ (aq)} + OH^- \text{ (aq)} \tag{1.11}$$
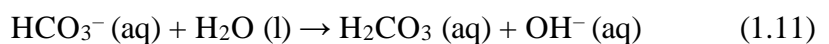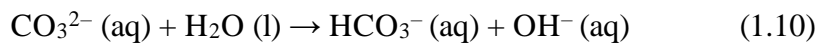
Any of the following equilibria for carbonic acid could occur.:

$$H_2CO_3 \text{ (aq)} \rightarrow H_2O \text{ (l)} + CO_2 \text{ (g)} \tag{1.12}$$

$$H_2CO_3 \text{ (aq)} \rightarrow HCO_3^- \text{ (aq)} + H^+ \tag{1.13}$$
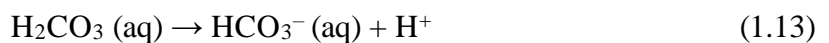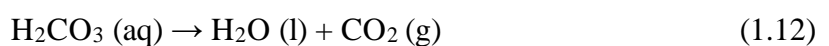
Different equilibria may also be experienced by Ca^{2+} following the dissolution of $CaCO_3$:

(1) The formation of calcium bicarbonate complex through interaction with bicarbonate:

$$Ca^{2+} (aq) + HCO_3^- (aq) \rightarrow CaHCO_3^+ (aq) \tag{1.14}$$

(2) The formation of solid calcium hydroxide complex through interaction with water:

$$Ca^{2+} (aq) + H_2O (l) \rightarrow CaOH^+ (s) + H^+ (aq) \tag{1.15}$$

$$Ca^{2+} (aq) + 2H_2O (l) \rightarrow Ca(OH)_2 (s) + 2H^+ (aq) \tag{1.16}$$
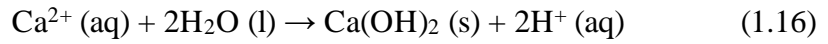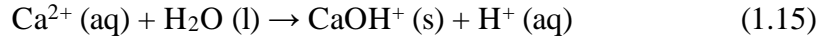
The stearic acid dissociation can be described by:

$$CH_3-(CH_2)_{16}-COOH \rightarrow CH_3-(CH_2)_{16}-COO^- (aq) + H^+ (aq) \tag{1.17}$$
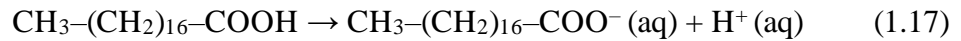
A stearate salt monolayer is chemisorbed on the rock as a result of the reaction between carboxylate and calcium hydroxide ($Ca(OH)_2$) as follows:

$$CH_3-(CH_2)_{16}-COO^- (aq) + -Ca(OH)_2 (s) \rightarrow CH_3-(CH_2)_{16}-COOCa (s) + H_2O \tag{1.18}$$
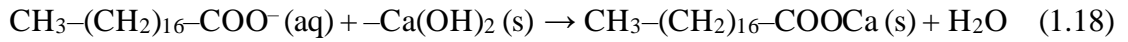
Additionally, stearate can adsorb to the anionic calcium carbonate.:

$$CaOH^+ + -CO_3^- \rightarrow -CO_3CaOH \tag{1.19}$$

$$-CO_3CaOH + CH_3-(CH_2)_{16}-COO^- \rightarrow -CO_3CaOOC-CH_3-(CH_2)_{16} + H_2O \tag{1.20}$$
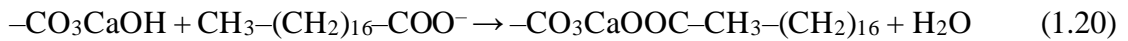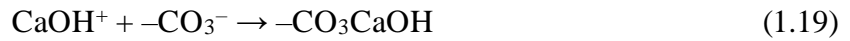
Therefore, Ca^{2+}, HCO_3^- and CO_3^{2-} are the moieties that determine the surface charge of calcite-rich rocks. The development of surface complexes can also be aided by other ions such as H^+ and OH^-. In general, cationic rocks are more susceptible to strong hydrophobization when the pH is low and the crude oil is acidic. Crude oil with high base numbers can render anionic sandstones more oil-wet.[46]

Contact angle measurements are often used to evaluate the wetting properties of a solid surface and the affinity of the surface for various fluids. The contact angle is the angle at which a fluid droplet rests on a solid surface. Considering a water droplet on a solid surface in air, a high contact angle in water towards 180° indicates that the fluid is poorly wetting the surface while a low contact angle towards 0° indicates that the fluid is wetting.[33] The Young equation is a mathematical relationship that describes the link between the contact angle of a fluid droplet on a solid surface and the surface energy of the solid. It is given by:[33]

$$cos\ \theta = \frac{\sigma_{SG} - \sigma_{SL}}{\sigma_{GL}} \tag{1.21}$$

where θ is the contact angle, σ_{SG} is the solid-gas interfacial energy, σ_{SL} is the solid-liquid interfacial energy and σ_{GL} is the gas-liquid interfacial energy (Figure 1.10).

Figure 1.10. Sketch of a liquid drop on a solid surface in air and the corresponding tensions.
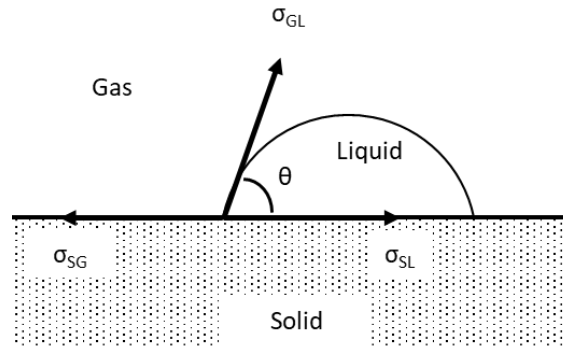
1.7.2. Origin of high oil-water interfacial tension

The high oil-water interfacial tension found in oil reservoirs can be linked to a number of elements that relate to the composition and characteristics of the oil and water phases. The oil-water interfacial tension can increase as a result of the polarity difference between polar water molecules and low polar crude oil. The high oil-water interfacial tension is a result of the chemical composition of crude oil impacting the oil-water interfacial tension. Non-polar saturates usually do not have a large impact on fluid-fluid and fluid-solid interfaces.[38] An additional decrease in the tension between the oil and the water can be brought on by relatively polar aromatics and perhaps aromatic acids. Asphaltenes are made up of various groups such as pyridines, carboxylic acids, pyrroles, phenols and carbonyls as proton acceptors or donators. Most resins are composed of naphthenic aromatic hydrocarbons, which are aromatic rings with alicyclic chains and act as a barrier to prevent precipitation from harming asphaltene. Asphaltene is less interfacially active than resins because of its enormous molecular weight and poor capacity to replace interfacial water and oil molecules. In contrast to less dense resins, asphaltene interfacial layers are solid, elastic and immobile, making them irreversibly adsorbed. Asphaltenes and saturates can raise the tension at the oil-water interface. Another factor contributing to the high interfacial tensions observed in oil reservoirs is the high salinity of the reservoir's formation brine.[47]

1.8. Surfactants for EOR

1.8.1. Oil-water interfacial tension reduction

Surfactants are known to increase the mobility and displacement of oil by decreasing the interfacial tension between oil and water. There are numerous studies on using different types of surfactants for EOR highlighting their ability to reduce the oil-water interfacial

tension to low $(1 - 3$ mN m$^{-1})$ or ultralow levels $(< 0.01$ mN m$^{-1})$.[48-50] Surfactants with smaller CMCs are preferred in EOR signifying improved surface activity and micellization.

Crude oil composition has a large impact on the efficiency of surfactants for oil-water interfacial tension reduction. Zhou *et al.* examined the impact of resin concentration on the oil-water interfacial tension in the presence of two betaine surfactants using a mixture of kerosene and resin. They pointed out that petroleum acids may lower or increase the interfacial tension depending on whether they form a compact monolayer or displace the interfacial betaine surfactant.[51] The simultaneous effects of asphaltene and aqueous surfactants may cause a further reduction in oil-water interfacial tension.

The kind and quantity of ions present in the brine have a significant impact on the effectiveness of surfactants to lower the interfacial tension. Some studies found salt addition helpful in forming a more compact surfactant monolayer at the oil-water interface which further reduces the interfacial tension[52] while others found it detrimental.[53] Low salinity brines (salting-in effect) could act synergistically for oil-water interfacial tension reduction while at high salinities (salting-out effect) the efficiency of the surfactant for interfacial tension reduction decreases.

1.8.2. Solubilization and emulsification

Surfactant flooding for EOR relies heavily on the formation of macro- and microemulsions. The emulsification of oil droplets by surfactants increases the sweep efficiency in micro-heterogeneous zones. By lowering the interfacial tension between oil and water and fostering the contact of oil and water phases, macroemulsions and microemulsions can both enhance oil recovery in surfactant EOR. Due to their greater stability and lower interfacial tensions, microemulsions are preferred in EOR; however, the type of resulting emulsion system in the reservoir will depend on the characteristics of the reservoir.

The Winsor III system is characterised by a very low oil-water interfacial tension that simplifies solubilization, facilitates oil molecule movement through pore channels, and leads to high oil production.[54] This type of emulsion was initially thought to be the main EOR mechanism during micellar flooding while other types of emulsions were underestimated. Significant oil production has been reported at low surfactant concentrations (*e.g.* $0.01 - 0.05$ wt.%) where no middle phase was observed.[55] This signifies that the third phase is not essential for a noticeable EOR.[50, 54] Using various

anionic, nonionic and zwitterionic surfactants and their mixtures, Xiaoxiao *et al.* investigated the effect of emulsification on EOR in cores made with quartz sands and epoxy resin with different permeabilities (5 – 50 mD). They argued that *in situ* emulsification is critical in EOR without causing ultralow interfacial tension, especially in low permeability cores. Efficient emulsification was found helpful in carrying residual oil to reduce oil saturation and blocking pore throats which provide additional pressure differences. The binary mixture of zwitterionic lauramidopropyl betaine and anionic sodium alcohol ether sulphate resulted in more stable oil-in-water emulsions and thus higher oil recovery.[56]

As with oil-water interfacial tension, salts can affect the Winsor systems. For a system consisting of a cationic surfactant along with an alcohol cosurfactant in toluene-water mixtures, the addition of salt was found to cause a progression from a Winsor I to a Winsor III to a Winsor II.[57] The distance between surfactant headgroups in micelles is also reduced upon adding a high concentration of electrolyte which lowers the solubilization of the organic phase.[58]

1.8.3. Rock wettability alteration

Generally, solid wettability alteration happens by either adsorption of new molecules on the surface or the desorption of pre-adsorbed molecules from the surface. When an aqueous surfactant solution is in contact with a solid surface, both tail and headgroups can interact with the surface depending on the properties of the surfactant and surface. The adsorption of surfactant molecules on a solid surface could occur as a result of a variety of attractive forces like hydrogen and covalent bonding, hydrophobic interactions between the pre-adsorbed surfactant molecules and free surfactant molecules, dispersive forces and electrostatic forces.[59-61]

For cationic (*i.e.* rich in calcite) and anionic (*i.e.* rich in aluminosilicates and clays) rocks, a dominance of carboxylates and amine-based groups of crude oil, respectively on the rock surface is expected. For ionic surfactants, ion-pair formation is the common wettability alteration mechanism (Figure 1.11). Cationic surfactants ($R–N^+(CH_3)_3$) interact electrostatically with the anionic carboxylates anchored to the rock surface to produce ion pairs that may be maintained by hydrophobic contacts between the tails, resulting in the complex desorption from the rock surface.[62] The aqueous micelles then solubilize them into their cores making the removal almost irreversible. The complexes can also move into the oil phase through the oil-water interface to form reverse micelles (not preferred). The contraction of the rock-oil-water contact line,[55] the diffusion and

swelling of water on the rock surface[63] and surfactant adsorption onto the rock surface[64] are all effects of the solubilization of the organic component after removal from the rock surface.

For nonionic surfactants, the headgroup can form H-bonds with the rock surface which retains the hydrophobic tails outward for a further hydrophobic-hydrophobic interaction resulting in hydrophilic headgroups outward (Figure 1.11).[65] As a result, a narrow water zone forms on the rock surface, decreasing the oil-water contact angle.[62] To avoid the possibility of a mixed-wet rock during ageing with crude oil, Salehi *et al.* performed spontaneous imbibition tests in hydrophobic polyethylene cores (oil wettability index of 1). This left hydrophobic-hydrophobic interactions between surfactant tails and the polyethylene surface as the only possible interaction for wettability alteration. They observed that hydrophobic-hydrophobic van der Waals interactions are weaker than electrostatic interactions. They claimed that the ethoxy group in sodium laureth sulphate (SLS) diminishes the charge density of the headgroup and allows for a more compact monolayer on the rock resulting in higher adsorption on the rock compared to $C_{12}TAB$.[66]

Standnes and Austad made a significant effort to evaluate the effects of 14 different cationic and anionic surfactants (0.1 – 5 wt.%) in three different brines for EOR in Stevns Klint (SK) cationic chalks utilising two different types of oil (n-heptane and acidic crude oil diluted by n-heptane). They found that brines produced little oil in imbibition tests at 40 °C after 35 days, but 1 wt.% $C_{12}TAB$ in brine produced 65% OOIP due to the rock wettability alteration. Cationics were found to be more efficient in oil recovery than other surfactants. Anionic ethoxylated sulfonate and sodium dodecyl sulphate (SDS) were the most and least efficient in imbibition tests, respectively. Because of the accelerated diffusion of monomers and micelles and decreased solubilization, temperature elevation had a favourable impact on the imbibition of surfactant solutions into rock. Increased solubilization (*e.g.* if [surfactant] >> CMC or if the temperature is low) was found to reduce oil recovery. Unlike non-polar heptane, $C_{12}TAB$ was observed to partition into crude oil (10% mol) at 40 °C *via* the formation of water-insoluble ion pairs. However, their imbibition tests recorded similar imbibition rates implying that rock wettability alteration is independent of surfactant partitioning between phases. Surfactant tail length was found to be effective for oil recovery. The shorter the tail, the larger the CMC and the higher the oil recovery due to a higher monomer concentration. The carbon number of n = 10, 12 resulted in the highest oil recovery. Although having the highest CMC, the oil production by C_8TAB was negligible due to its low hydrophobic interactions with the adsorbed oil groups at the interfaces. The imbibition rate did not depend on surfactant

concentration at surfactant concentrations much above CMC, demonstrating that monomers are primarily responsible for the desorption of crude oil anionic groups from the rock. Below the CMC, oil production was low due to high oil-water interfacial tension and capillary forces in porous media.[62]

Figure 1.11. Different rock wettability alteration mechanisms by cationic, anionic and nonionic surfactants in the absence and presence of inorganic ions.
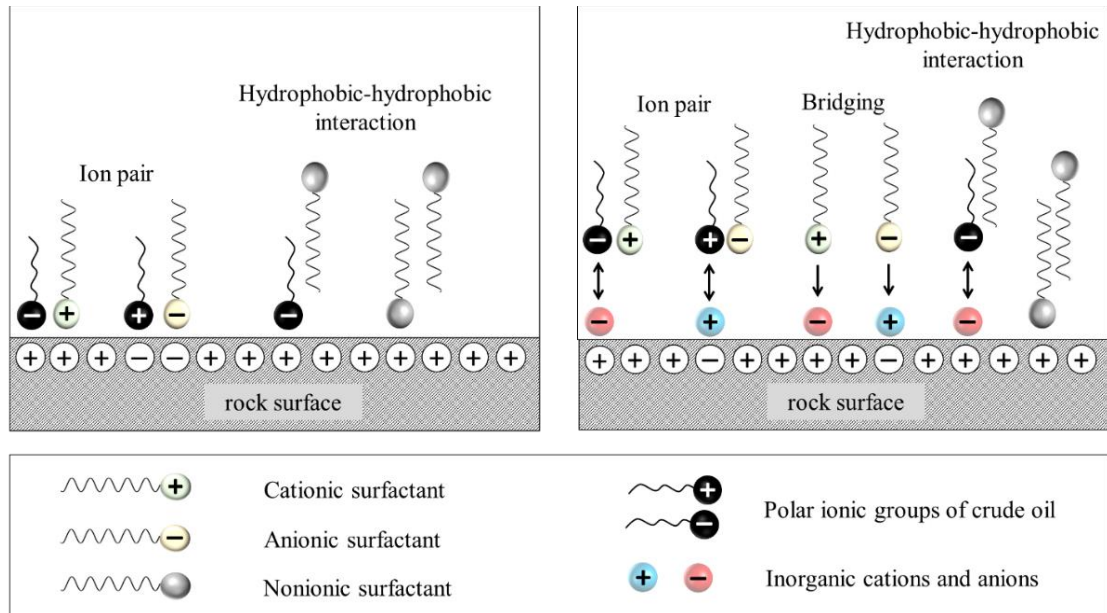
The literature suggests that ionic surfactants with a similar charge to rock are more efficient for EOR. This contrasts with a study by Hou *et al.* who found that cationic CTAB changes quartz wettability more significantly than anionic SLS and nonionic octyl phenol ethoxylate (TX-100). They argued that polar crude oil components (asphaltenes and resins) and quartz surfaces interact in ways other than electrostatic attraction. Other interactions such as polar interactions, ion binding, acid/base interactions and surface precipitation play a part. Ion-pair formation is more prominent for CTAB in crude oil with high acid numbers (large carboxylic groups on rock).[67]

The adsorption of ionic surfactant molecules onto the surface of rocks can be impacted by inorganic ions. Ahmadall *et al.* came to the conclusion that if the rock is mostly cationic or if the brine is rich in Ca^{2+}, cationic surfactant usage owing to the adsorption onto rock would be minimal. They also stated that crude oil with high acid numbers causes high surfactant partitioning through ion-pair formation in a 1:1 ratio which is unfavourable since surfactants moved into the oil phase are inactive in altering rock wettability.[68]

1.8.4. Challenges

The effectiveness of surfactant flooding in EOR is influenced by several variables, including rock mineralogy, crude oil and brine composition, pressure, temperature and salinity. Numerous common surfactants are vulnerable to hydrolysis.[69] Some surfactants degrade at high temperatures, making them pricey and inefficient. Salts and surfactants become more soluble at high temperatures but prolonged exposure might decrease surfactant effectiveness, for example in reducing interfacial tension.[70] Ions such as Ca^{2+} and Mg^{2+} can precipitate surfactants and damage the formation, requiring greater injection pressures but producing little oil.[71]

Surfactant adsorption onto rock can significantly alter the surface characteristics of rock for EOR but surfactant loss near the injector slows surfactant transport and lowers imbibition velocity. This is more critical in tight oil reservoirs like shales where due to their micro- or nanometer pore channels, a larger surface-to-volume ratio and surfactant adsorption could exist.[72] To address this issue, the use of similarly charged ionic surfactants has been proposed but they may not be EOR-wise efficient. In sandstones, alkalis (*e.g.* sodium carbonate) can serve as sacrificial chemicals to increase the negative charge of the rock and hinder the adsorption of anionic surfactants.[73] Polymers can form a monolayer on the rock to prevent high surfactant adsorption[74] but they may cause chromatographic separation due to the different adsorption extents of chemicals onto the rock.[75] Furthermore, polymers or alkalis are expensive and not usually effective at high salinities and temperatures.[76] Increasing salt concentration and pH are other ways of reducing surfactant adsorption on rock[77] but they are limited. Nanoparticles have recently received attention for controlling surfactant adsorption which will be discussed in the next section.

1.9. Nanoparticles for EOR

Solid nanoparticles are nowadays used in different sectors of the oil and gas industries. Due to its strong EOR functionality, availability, simplicity of synthesis and low enrichment cost, silica is the particle that has been the subject of most studies examining various types of nanoparticles for EOR.[20, 78] As well, there has been no change in the specific surface area of silica up to 650 °C.[79] The various roles that nanoparticles could play in EOR are outlined in the sections below.

1.9.1. Oil-water interfacial tension

The effects of bare nanoparticles on the interfacial tension between oil and water have generated some debate in the literature. Although some studies show an interfacial tension

reduction by adding nanoparticles to the aqueous phase,[80, 81] others deny it.[82, 83] The particle size has a great impact. An increase in interfacial tension has also been reported after adding nanoparticles.[84] The aggregation of nanoparticles caused by van der Waals forces predominating over repulsion at high particle loading or high salinity may provide a suitable explanation for this. An optimum particle concentration causing a minimum oil-water interfacial has also been reported by many studies.[85-87] In the case of polar oil, *e.g.* crude oil, interactions between hydrophilic particles and oil molecules at the interface can render particles partially hydrophobic and capable of adsorbing at interfaces. This reduction is not expected for non-polar oils, *e.g.* heptane.

It has been reported that a significant decrease in oil-water interfacial tension by at least two orders of magnitude (< 0.1 mN m^{-1}) is required for enhancing oil and water relative permeabilities and moving a significant percentage of immobilized oil in porous media[20, 88] which is not expected by bare nanoparticles. However, surface functionalization may work to some extent. Wei *et al.* employed nanocellulose treated with –COO$^-$ groups in 1 wt.% NaCl brine at two distinct surface charge densities of 0.72 and 1.51 meq g^{-1}. They noticed that adding modified particles caused the oil-water interfacial tension to decrease from about 30 mN m^{-1} to $1 - 6$ mN m^{-1} which was more pronounced for particles with a greater charge density.[86]

1.9.2. Rock wettability alteration

The use of nanoparticles in EOR techniques to change the wettability of rocks has been investigated. There are studies like[89] that claim nanoparticles rarely change the wettability of rocks for EOR but others show significant changes to rock wettability.[44, 90, 91] Several mechanisms have been highlighted for nanoparticles as rock wettability modifiers. According to Nikolov *et al.*, particles stratify in the film of dispersion generated between an oil droplet and a smooth glass slide submerged in an aqueous silica dispersion (19 nm, 10 vol.%) (Figure 1.12). A monolayer of particles exists in the first layer towards the drop edge, while two and three layers of nanoparticles form in the centre. This particle layering creates structural disjoining pressure, which encourages the dispersion to spread out over the solid surface and releases the oil droplet from the surface. The surface energy and wettability of the solid are altered by the adsorption of nanoparticles at the solid surface.[92] The strength of the disjoining pressure caused by nanoparticles in a crude oil-rock-water system is determined by the sum of attraction (i.e. electrostatic and van der Waals) and repulsion (i.e. electrostatic, structural forces and steric repulsion) between the rock and crude oil. The lowering of attraction forces between crude oil and rock is favoured for

altering rock wettability. The wettability of fluids with low surface tension in the air may be enhanced by the adsorption of metal oxide nanoparticles onto solid surfaces due to their high surface energies. Calcite can chemically react with certain particles, such as silica.[93]

Figure 1.12. Schematic view of silica nanoparticle layering between an oil drop and a glass slide, from Nikolov *et al.*[94]
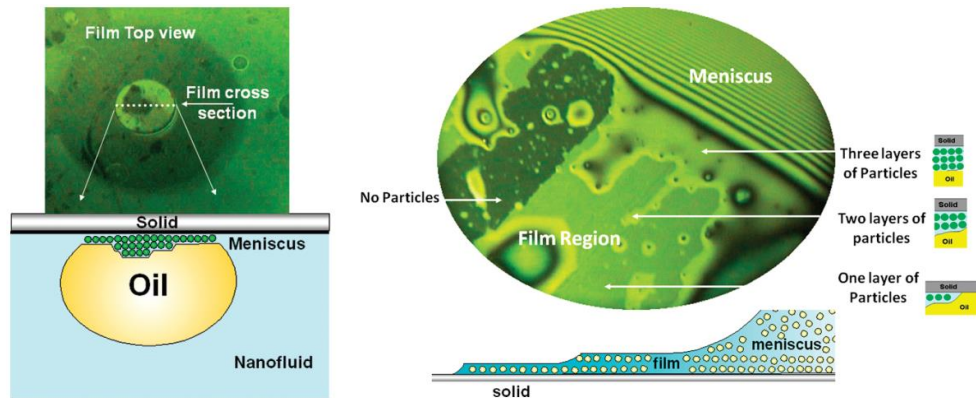
Regarding the effect of electrolytes, previous research showed that NaCl shrinks the electric double layer of both silica particles and the calcite surface, reducing electrostatic particle-calcite repulsion and improving particle adsorption and rock wettability alteration.[95] Na^+ smaller hydration shell allows it to approach the calcite surface more readily than Ca^{2+} and Cl^-, hence reducing or reorganising its hydration shell results in a reduced energy penalty. The energy barrier to particle adsorption on rock is lowered as salt rises. In the interaction energy plot, it also results in the establishment of a secondary minimum that deepens with increasing ionic strength (Figure 1.13).[93] In light of this, it is important to remember that screening particle surface charges might result in formation damage by causing aggregation and sedimentation. As a result, it is important to find the critical salt concentration at which particle adsorption to rock is greatest without sedimentation.

Figure 1.13. Interaction energy vs separation between bare calcite and silica for [NaCl] at 293 K.[93]
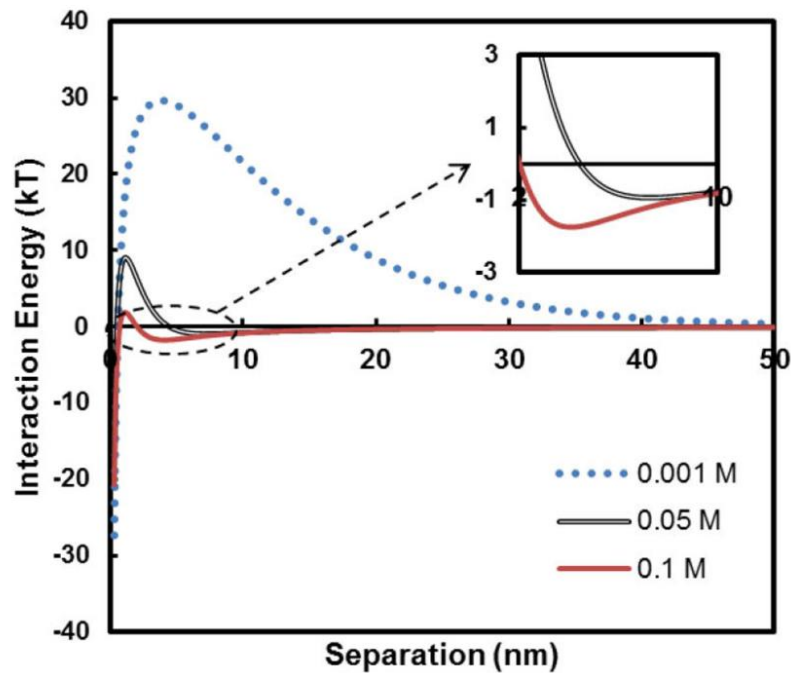
1.9.3. Asphaltene adsorption

Solid asphaltene production from crude oil is known as asphaltene precipitation. Asphaltene has a typically high molecular weight and is capable of self-association and flocculation due to the heteroatoms (N, S and O) in its skeleton which makes it highly polar and likely to deposit in porous media or surface facilities.[96] According to De Boer *et al.*, light crude oil reservoirs are more susceptible to asphaltene deposition if they have high bubble point pressures, high C_1–C_3 and low C_{7+} fractions.[97] Asphaltene deposition can both limit the fluid flow in pore channels and render rock wettability more oil-wet. Nanoparticles are effective in preventing asphaltene deposition. Some nanoparticles are particularly well suited for the adsorption and breakdown of asphaltene due to their high surface-to-volume ratio, adsorptive behaviour and strong catalytic activity. Improved oil recovery and asphaltene stabilisation in the oil phase for up to 8 months were seen after field injections of alumina dispersion into a well with asphaltene deposition around the wellbore.[98]

1.9.4. Oil and water viscosity improvement

Oil viscosity can be reduced and crude oil can be upgraded in situ by catalytic nanoparticles like alumina.[99, 100] Previous research showed that the oil produced by the injection of catalytic Al_2O_3 and NiO nanoparticles is lighter and less viscous.[101] In comparison to TiO_2 and Fe nanoparticles, Shakib *et al.* found that 4 wt.% super-activated carbon reduced viscosity by 91 mPa s when exposed to microwave radiation. This viscosity reduction was caused by the cracking of heavy chemicals in crude oil by nanoparticles as well as a drop in S and N atoms, OH, SH, alkyl, carbonyl, carboxylic

27

acids and aromatic compounds.[102] On the other side, nanoparticles can comparatively raise the viscosity of the injected phase into oil reservoirs when present in adequate concentrations. Both viscosity improvements can reduce the mobility ratio and increase the capillary number which improves oil production.[86]

1.9.5. Nanoparticles in porous media

Particle-particle, particle-fluid and particle-rock interactions as well as thermodynamic or hydrodynamic forces are the possible interactions that nanoparticles may encounter during their lengthy journey in a carrier fluid across a porous medium.[103] These interactions have two main effects on fluid flow: mechanical entrapment and log-jamming. Mechanical entrapment happens when the particle diameter is larger than that of the pore channels.[104] The average pore width in conventional oil reservoir rocks has been reported to be > 2 µm while it is 0.03 – 2 µm in tight sandstone and 5 – 100 nm in shale.[105] Alaskar *et al.* looked at the entrapment of different nanosensors in different types of porous media including Berea sandstones, glass beads and naturally fractured greywacke core. They concluded that spherical nanoparticles with a diameter of less than 200 nm have the best chance of surviving mechanical entrapment while being transported across porous media.[106]

In log-jamming, the particles are still capable of blocking the pore throats although the particle diameter is smaller than the pore channel width. Considering a constant differential pressure during fluid flow in porous media, there is an increase in flow velocity from pores (wider) to channels (narrower) which causes lighter water molecules to move fast into the pore channels while the particles that are left behind build up at the entrance, limiting or obstructing the flow area.[104] While mechanical entrapment can be harmful, log-jamming is seen as a productive EOR mechanism that allows localised particle obstruction of pore throats to direct fluid flow to adjacent intact pores where it can displace oil, leading to EOR.

Particles also have an effect on oil-water interfacial rheology offering a crucial role in multiphase flow in porous media and controls the flow or deformation of oil via pore throats. In oil reservoirs, particle adsorption at the fluid-fluid interface occurs most frequently at confining pressures but when the oil-water interface is compressed or dilated locally, such as by fluid flow through the pore throats, the particle monolayers respond by deforming to release the pressure which causes the particle to either flip in a different direction (which does not happen for spherical particles) or desorb.[107] As a result, the dynamics of multiphase flow in porous media are significantly influenced by particle-

loaded interfaces. In EOR, the interfacial microstructures of nanoparticles and their spontaneous adsorption at the oil-water interface are crucial.

Emulsions and foams stabilized with particles also show improved flow in porous media. Espinoza *et al.* investigated the stability and effectiveness of CO_2 foams (without surfactant) for EOR with silica covered with polyethylene glycol (n = 7). They discovered that particle-stabilized foam can withstand high temperatures and salinities and has a stronger flow resistance ($\times$2–18 higher). Surfactant-stabilized foams could be problematic as the adsorbed surfactant at low concentrations tends to contribute to equilibrium and adsorption at CO_2-water or water-solid interfaces which are absent for particle-stabilized foams due to the high detachment energy of particles.[108]

1.9.6. Challenges

Compared to other available EOR methods, nanoparticles have superior features. For examples, surfactants may not be effective in all reservoir conditions, and they can be costly. Environmental concerns may also arise due to surfactant use. Polymers can improve sweep efficiency by increasing the viscosity of injected water, thus reducing fingering and improving oil recovery but they can be sensitive to reservoir conditions, may require complex mixing and injection systems, and can be expensive. Alkaline chemicals can alter reservoir rock wettability and reduce interfacial tension, enhancing oil recovery but they may not be compatible with all reservoir conditions and can pose environmental and handling challenges. Solvents can be also used for EOR purposes to dissolve oil and improve its mobility, making it easier to recover. However, they can be expensive, pose health and safety risks, and may not be suitable for all reservoirs. Nanoparticles can be engineered to be compatible with various reservoir conditions, including high salinity and high temperature, making them versatile in different geological settings. They are generally considered environmentally friendly as they are mostly mined and enriched from ores compared to some other EOR methods that may involve the use of chemicals with potential ecological concerns.[106] Their small size allows them to penetrate deep into the reservoir rock. This improved mobility can enhance oil displacement.

On the other hand, nanoparticles encounter significant challenges that must be overcome before doing EOR. Application of nanoparticles for EOR requires long-term colloidal stability at high salinity and temperature conditions. They are usually dispersed in seawater and formation brine for EOR with salinities up to 6 wt.%[109] and 30 wt.%,[110] respectively. Oil reservoirs typically have temperatures between 70 °C to 130 °C.[111]

Nanoparticles can potentially form clusters or aggregates at reservoir conditions, leading to scaling issues that can reduce their effectiveness. Thus, steric stabilization through physical or chemical grafting (more effective) or a combination of both is usually required for long-term colloidal stability at reservoir conditions to prevent formation damage.[14] The production and deployment of nanoparticles can be expensive especially if custom-engineered nanoparticles are required to match specific reservoir conditions. High particle adsorption onto rock in porous media is another challenge that could lower the particle concentration and therefore increase costs.[112] It can also reduce rock permeability and cause formation damage.[113] Achieving uniform nanoparticle distribution in the reservoir can be challenging as their small size may lead to loss through filtration or adsorption. Compared to traditional EOR methods, nanoparticles are a relatively new technology in the oil industry, and their field application experience is limited. This can make operators hesitant to adopt them.

All in all, it is noteworthy to mention that the choice of EOR method should be based on the specific reservoir characteristics and economic considerations, and it may involve a combination of methods to maximize oil recovery.

1.10. Nanoparticle-surfactant mixtures for EOR

1.10.1. Motives to mix

Despite having outstanding EOR performance, surfactants face significant obstacles when it comes to their practical application in the field, as was previously outlined. The introduction of particles into surfactant solutions can elicit a spectrum of outcomes, each contingent upon the interplay between particle chemistry and the specific type of surfactant in use. Adsorption and desorption at liquid-liquid, liquid-solid and gas-liquid interfaces are only a few examples of the various phenomena that may be a part of these interactions and have a big impact on the whole EOR process. Particle addition also affects fluid flow through porous reservoir rocks. Here, important elements including capillary pressure, wettability modification and mobility control may be impacted by the interaction between surfactants and particles. Because of this, the success of EOR initiatives rests not only on choosing the right surfactant but also on knowing how the presence of particles and the particulars of the reservoir affect that surfactant behaviour. Therefore, when developing and putting into practise such tactics in the field, considerable consideration and experimentation are essential due to the complex interplay between surfactants and particles in EOR applications.

The subsequent parts of this section will commence by elucidating the intricate dynamics governing the interactions between surfactants and particles at interfaces involving fluid-fluid and rock-fluid phases. Subsequently, an examination of the latest scholarly investigations pertaining to the efficacy and performance of particle-surfactant combinations shall be conducted, thereby providing a comprehensive and up-to-date review of their achievements and outcomes.

1.10.2. Effect on fluid-fluid interface

Small surfactant molecules have a small detachment energy (a few kT) making their adsorption at interfaces reversible and fast, while nanoparticle adsorption (up to 10^3 kT) is irreversible. Particle additions to surfactant solutions can have two effects. The addition of like-charged particles to ionic surfactant solutions can further reduce the air-water and oil-water interfacial tension, while a blend of oppositely charged particles and surfactant can increase the interfacial tension due to surfactant depletion.[78, 114] It is worth mentioning that high particle hydrophilicity is preferred for long-term colloidal stability under harsh reservoir conditions but it reduces particle surface activity. Physical grafting of bare particles with oppositely charged surfactants can render particles hydrophobic and capable of adsorption at the oil-water interface with the possibility of surfactant re-arrangement at the interface.[82] Therefore, an ultralow interfacial tension is not mandatory for the emulsification of oil and water in the presence of nanoparticles and surfactants.[115] In comparison to particles or surfactants alone, prior research has shown that particles covered with surfactants can form more stable foams or emulsions at high temperatures.[116-118] In addition, variations in particle concentrations at the oil-water interface can alter particle density and make the emulsification spontaneous.[115]

1.10.3. Effect on rock-fluid interface

Surfactants with low surface activity are not efficient in EOR, while those with large surface activity are a waste of chemicals and money, leading to the unavailability of surfactants at large distances from the injector. The application of nanoparticles as surfactant carriers in EOR has recently received attention. In this case, the rock surface serves as an adsorbent for both surfactant molecules and nanoparticles. However, Chen *et al.* showed that the adsorption of nanoparticles on rock (sand pack) is lower ($10^{-3} - 10^{-2}$ mg g^{-1}) than that of surfactants ($10^{-1} - 10^0$ mg g^{-1}).[119] Because of their more powerful collisions and hydrogen bonding, Yekeen *et al.* concluded that surfactant molecules adhere to nanoparticles more readily than to rocks[120] resulting in fewer available surfactant molecules for adsorption onto the rock surface. Hydrogen bonds, chemical

bonds, hydrophobic-hydrophobic interaction, and electrostatic attraction are just a few of the forces that the surfactant-particle aggregate can use to interact with the rock surface. Surfactant adsorption on particles depends critically on the stability, size, morphology, and surface area of the particles. Surfactant adsorption on nanoparticles is decreased by particle aggregation. Enhancing the competitive adsorption of surfactants onto nanoparticle surfaces rather than rock surfaces will increase the efficiency and cost-effectiveness of the EOR process.[121, 122]

1.10.4. Literature review

In this section, a comprehensive review of the latest and most pertinent literature concerning particle-surfactant mixtures for EOR has been meticulously conducted. Additionally, within each results chapter later, an exhaustive examination of the relevant literature has been incorporated to facilitate a thorough comparison of the prior findings with the outcomes of this research wherever appropriate.

Previous studies have reported synergy in oil recovery by blending nanoparticles and surfactants. Yekeen *et al.* investigated different nanoparticles including silica, alumina and multiwalled carbon nanotubes in combination with sodium dodecyl benzene sulfonate in glass micromodel for EOR. They observed that the addition of particles to surfactant solutions can lower fingering and channelling of the injected aqueous phase and thus increase oil production. A higher oil production and breakthrough time was found with multiwalled carbon nanotubes which was related to the particle cylindrical shape and the efficient positioning of particle-surfactant aggregate at the liquid-liquid and solid-liquid interfaces to lower the oil-water interfacial tension and contact angle.[123] Xu *et al.* observed improved colloidal stability for Janus silica in 3.5 wt.% brine at 90 °C on adding binary SDS-Tween 60 surfactant. They also reported good oil-water interfacial tension reduction, emulsion stability and rock wettability alternation by the surfactant-particle blends resulting in significant additional oil production in cores.[124] Devakumar *et al.* studied the combination of sodium dodecyl benzene sulfonate and silica nanoparticles in low salinity brine (0.5 wt.% NaCl in DIW) on oil-water interfacial tension and quartz wettability alteration using different oils including n-heptane, n-decane, benzene, toluene, model oils and crude oil. Quartz wettability alteration from oil-wet to water-wet was found more pronounced when using acidic oil. A decrease in surfactant adsorption onto quartz was revealed on raising silica concentration in the dispersion.[125] Wang *et al.* studied the blend of ethyl cellulose nanoparticles and a nonionic surfactant in API brine for foam flooding at high temperatures in fractured carbonate reservoirs. They observed

that the injection of foam stabilized by a particle-surfactant mixture increases oil recovery more than surfactant foam indicating a synergy due to the particle adsorption at the gas-water surface and its ability to divert flow into the rock matrix.[126] Al-shatty et al. studied cationic alumina nanoparticles (hydrophilic and hydrophobic) in a blend with SDS and CTAB for EOR. They observed that the blend of hydrophobic octanoic acid-coated alumina nanoparticles and CTAB increases the oil recovery by 5% compared to CTAB injection alone due to its higher affinity for the oil-water interface.[127] Zhao et al. investigated the blend of sulfonated silicon quantum dots and bitetradecyl sulfobetaine for EOR. They recorded an imbibition recovery of 30% by the blend compared to that of particle dispersion (13%) and surfactant solution (17%) which was linked to the oil-water interfacial tension reduction and rock wettability alteration by the blend.[128] Pereira et al. investigated the blend of Fe_3O_4 nanoparticles and CTAB for EOR. They observed an additional oil recovery of 30% OOIP by the blend in tertiary mode after secondary brine injection which was related to the easier oil displacement by nanoparticles (asphaltene adsorption and rock wettability alteration by disjoining pressure) and surfactant (oil-water interfacial tension decrease).[129] Zhou et al. studied the mixture of silicon quantum dots and 0.1 wt.% alkyl betaine surfactant (n = 12) in 15 wt.% synthetic brine for EOR in Bakken cores (calcite = 52%, quartz = 25%, dolomite = 16%, feldspar + illite = 7%). They revealed that the particle-surfactant mixture can recover an additional 7.5% and 12% OOIP in spontaneous imbibition and core flooding, respectively, compared to surfactant alone. They related this additional oil recovery to the decrease in oil-water interfacial tension and rock oil-wetness. They also claimed that the self-layering of particles in the wedge layer confined between oil drop and rock surface create disjoining pressure leading to oil drop movements.[130] Singh and Mohanty tested a blend of silica nanoparticles coated with 3-glycidyloxypropyl trimethoxysilane (GLYMO) or polyethylene glycol (PEG) and a sulfonate surfactant in API brine for foam flooding in a dual-permeability sand pack. They observed a low oil recovery (33% OOIP) by brine injection due to the channelling of the injected brine in the high permeability region leaving the oil in the low permeability region within while the foam made with surfactant and particles was found to create *in situ* emulsions that blocked the high permeability region and diverted the injected phase towards the low permeability zone to produce more oil.[131] Kumar et al. studied the effect of blending SDBS, silica and carboxymethylcellulose (CMC) on the emulsification of light mineral oil and water. They observed a further oil recovery of 24% OOIP by flooding the Pickering emulsion after conventional water flooding.[132] Cheraghian et al. observed that a blend of fumed silica and SDS can displace more oil ganglia than surfactant alone due to its higher viscosity.[133]

1.10.5. Challenges

For a successful EOR, it is required that the particle and surfactant properties be optimized. The particle-surfactant concentration ratio is an important parameter that should be determined experimentally. As well, in the application of nanoparticles as surfactant carriers, the particles must be stable standalone since any surfactant desorption may cause particle aggregation and sedimentation in porous media. Therefore, steric stabilization of nanoparticles is necessary especially in tight reservoirs to prevent formation damage.[119] The rock mineralogy should be given careful attention in EOR by particles and surfactants. Zhong *et al.* observed that zwitterionic betaine and hydroxysultaine surfactants adsorb on Bakken rock powder more than anionic and nonionic surfactants with and without formation brine (29 wt.%). They related this behaviour to the mixed mineralogy of Bakken rock which had more clay and quartz than calcite. The surfactant adsorption on these anionic minerals was claimed to be dependent on calcium concentration.[134]

1.11. Objectives and outline of this thesis

Surfactant flooding has been a long-standing and proven method for EOR. This technique has demonstrated its ability to effectively reduce oil-water interfacial tension and alter rock wettability, transforming it from oil-wet to water-wet, thereby enhancing oil production.[72] Recently, there has been a growing interest in the use of nanoparticles as a promising tool for EOR. These tiny, versatile particles have garnered attention due to their unique properties and potential benefits in reservoir engineering.

What makes this study particularly intriguing is the emerging trend of combining nanoparticles with surfactants for EOR applications. The synergy between these two components has generated significant curiosity and excitement in the petroleum industry. However, it is worth noting that the precise mechanisms and interactions governing this synergy remain insufficiently understood prompting the need for further research and exploration in this area. This study represents a significant step in bridging this knowledge gap. Its primary objective is to formulate and rigorously test a specialized dispersion of nanoparticles that can withstand the harsh conditions typically encountered in reservoirs. Furthermore, this dispersion will be combined with surfactants to create a unique EOR formulation specifically tailored for calcite-rich rocks which present their own set of challenges and opportunities in the field of petroleum engineering.

The organization of the thesis has been thoughtfully structured to ensure a logical progression of research and presentation of findings. Each chapter builds upon the foundation laid by the previous one, leading to a comprehensive understanding of the

potential of nanoparticles and surfactants in EOR for calcite-rich rock formations. The proposed framework aligns with the following chapters:

In Chapter 2 of this thesis, a comprehensive and detailed exploration of the chemical specifications and the methodologies employed in the research is meticulously presented. This section serves as the foundation upon which the subsequent chapters are built, providing a thorough understanding of the experimental framework and analytical tools employed in the study.

Moving on to Chapter 3, an exhaustive account of the properties of various chemicals is provided. These include a detailed analysis of crude oil, synthesized particles, surfactants and rock materials. The chapter delves into the physical and chemical characteristics of these components, shedding light on their individual properties, which form the basis for subsequent investigations.

Chapter 4 delves into the intricate interplay between aqueous particles, surfactants or their combination and their impact on the fluid-solid interface including air-rock and oil-rock interfaces. This chapter offers a comprehensive examination of how these elements interact and influence the behaviour of fluid-solid interface providing valuable insights into the underlying mechanisms.

In Chapter 5, the focus shifts towards elucidating the behaviour of particles, surfactants, or their blend at the oil-water interface. This section meticulously outlines their role in reducing the oil-water interfacial tension and the emulsification of different oils (including toluene, heptane, heptol and crude oil) and water providing a detailed understanding of their interfacial properties and their potential applications.

The culmination of these investigations leads to Chapter 6 where the effective particle-surfactant dispersions resulting from the previous chapters are utilized in spontaneous imbibition tests conducted on calcite-rich rocks. This chapter showcases the practical applications of the research findings demonstrating their relevance in real-world scenarios.

Lastly, Chapter 7 serves as a synthesis of the key findings of the entire thesis. It offers a comprehensive overview of the research outcomes drawing conclusions based on the cumulative knowledge gathered throughout the preceding chapters. Additionally, this chapter provides a glimpse into potential avenues for future research, highlighting the thesis's contribution to the field and its potential impact on future studies.

Chapter 2 Experimental

The following chapter outlines the chemicals used in the project and their specific characteristics. It also explains the procedures and instruments utilized throughout the study. The methodology mainly includes the synthesis of particles, characterization of all chemicals, chemicals at fluid-rock and fluid-fluid interface and finally oil recovery experiments to prove the efficiency of particle-surfactant dispersions in porous media. This chapter serves as a practical guide, offering insight into how the research was conducted. Its purpose is to provide clarity and accessibility regarding the research process.

2.1   Materials

2.1.1   Water

An Elga reverse osmosis machine initially filtered water. It was then purified using a Milli-Q Ultrafiltration System (Millipore, France). A Jenway 3510 pH meter (Cole-Parmer Scientific Experts, UK) and DMA 35N or 4500 density meters (Anton Paar, Austria) were used to measure the pH and density of different liquids, respectively. Deionized water (DIW) had a surface tension of 72 ± 0.1 mN m^{-1}, pH of 6.5, a density of 0.9973 g cm^{-3} and a viscosity of 0.8872 cP at 25 °C.

2.1.2   Electrolytes

The produced brine from the Permian oilfield (12.56 wt.%, pH = 5.6, density = 1.09 g cm^{-3}) was considered as the electrolyte in this study (Table 2.1). The brine was prepared by dissolving salts in DIW on a magnetic stirrer for a 24 h. Aluminium sulfate solution ($Al_2(SO_4)_3$, 36 wt.%) was received from the sponsor (ChampionX, USA) and used as a pH regulator for dispersions.

Table 2.1. Composition of Permian brine reported by ChampionX (USA) and the salts used in preparation.

Salt	g dm^{-3}	mol dm^{-3}	Supplier	Purity / %
NaCl	117.34	2.007		≥ 99.5
KCl	1.31	0.017	Fisher Scientific	99.5
CaCl$_2$.2H$_2$O	4.03	0.027		99.0
MgCl$_2$.6H$_2$O	1.34	0.006		≥ 99.0
SrCl$_2$	0.81	0.005	Sigma Aldrich	≥ 99.0
NaBr	0.77	0.007		≥ 99.9
DIW	874.40	–		
Total concentration	125.6	–		–
Total ionic strength	–	2.070		

2.1.3 Surfactants

Two commercial surfactant solutions (a zwitterionic solution and a binary zwitterionic-nonionic solution) were received from the sponsor (ChampionX, USA). The zwitterionic surfactant solution was a 50 wt.% alkyl hydroxysultaine (AHS) (also known as dodecyl hydroxypropyl sulfobetaine) and the binary zwitterionic-nonionic (ZN) surfactant solution was a mixture of 32 wt.% AHS and 5 wt.% nonionic C_{10-12} nonaethylene glycol ether ($C_{10-12}E_9$), as shown in Figure 2.1. The pH of both stock surfactant solutions was measured at 8.1 ± 0.1 at 25 °C. The ZN solution contained some proprietary additives for efficient field applications.

Figure 2.1. Structure of (a) alkyl hydroxysultaine (AHS) or 3–dodecyldimethylammonio)–2–hydroxypropane–1–sulfonate, (b) C_{10-12} nonaethylene glycol ether ($C_{10-12}E_9$).

(a)

(b)
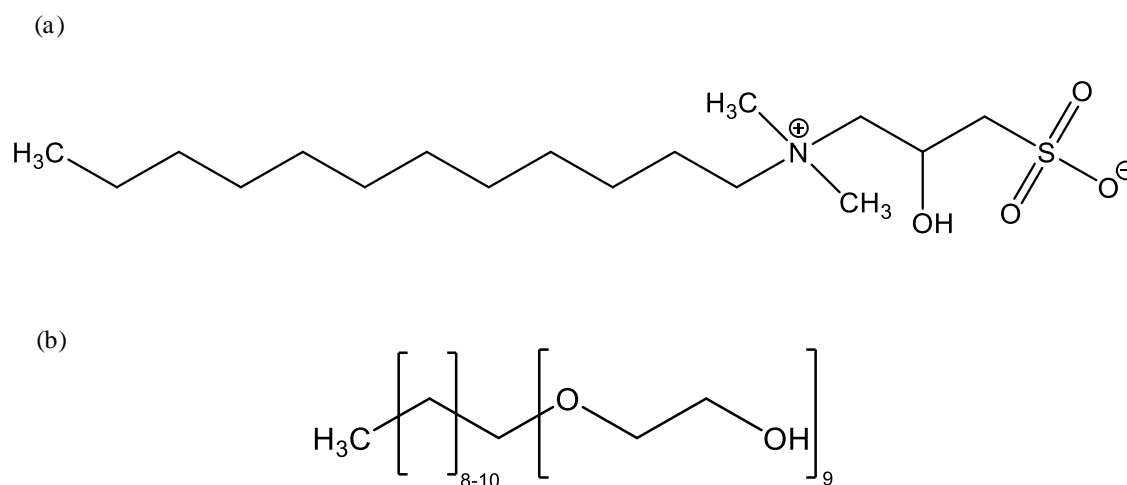
2.1.4   Silanes

Two silanes namely epoxy silane (ES) and amino silane (AS) with a purity of ≥ 98% were used for silanization of bare silica particles to improve their colloidal stability in Permian brine at reservoir temperature (75 °C). The structures of these silanes are shown in Figure 2.2.

Figure 2.2. Structure of (a) AS and (b) ES.
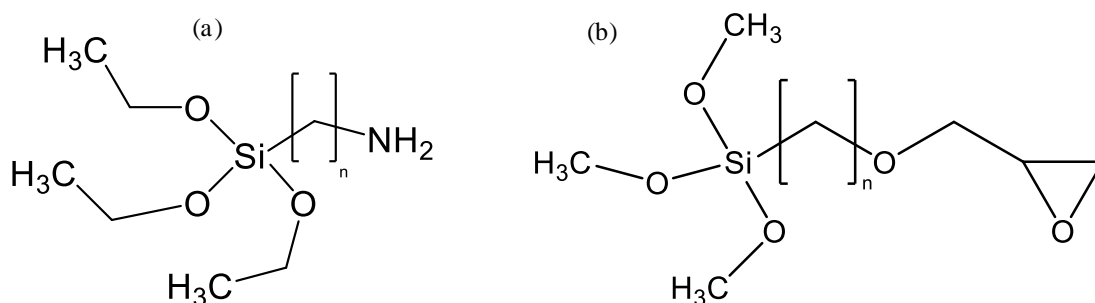
2.1.5   Particles

Stock bare silica dispersion (30 wt.%) with a pH of ~10 was received from ChampionX. The particles were reported to have an average diameter of 9 nm and a surface area of 331 m^2 g^{-1}. ES-coated silica was both synthesized and received from ChampionX (refer to Section 2.2.5 for synthesis). The ES-coated silica dispersion from ChampionX was a 20 wt.% aqueous dispersion with a pH of ~10.

2.1.6   Oils

Four different types of oil including toluene, heptane, heptol and crude oil were used in oil-water interfacial tension measurements and emulsion experiments to examine the effect of oil type. Toluene (ACS reagent ≥ 99.5%, Sigma Aldrich) and heptane (Chromasolv for HPLC ≥ 99%, Honeywell) were purchased and used for preparing heptol (1:1 g g^{-1}) in the lab. These three oils were used as model oil to mimic the main components of crude oil. Dead centrifuged reservoir crude oil from the Permian oilfield (USA) was also received from ChampionX and characterized as will be explained later. Crude oil was mainly used in the contact angle and oil-water interfacial tension measurements and also in oil recovery experiments. For air-rock contact angle measurement, dodecane (≥ 99%) from Research Chemicals Ltd. was used.

2.1.7 Rocks

2.1.7.1 Wolfcamp shale

Shale oil reservoirs represent substantial reservoirs of crude oil within the United States. These reservoirs are characterized by inherently low levels of porosity and permeability, factors which render the natural extraction of oil a formidable challenge. Consequently, there exists a keen interest in the application of innovative EOR technologies aimed at augmenting oil recovery from these reservoirs. Outcrop Wolfcamp shale rock substrates and cores were purchased from Kocurek Industries Inc. (USA) as analogous to the reservoir formation. The substrates were in rectangles of 3 cm by 2 cm with a thickness of 3 mm for contact angle measurements (Figure 2.3). The cores were cylinders of ~ 6.9 cm in length and ~ 3.75 cm in diameter. The outcrop shale is analogous to the formations of the lower Leonardian of Permian (~ 280 million years old).

Figure 2.3. (a) Wolfcamp outcrop shale substrate (b) Wolfcamp outcrop shale core, (c) Stratigraphy of the Midland Basin located in southwestern USA.[135]
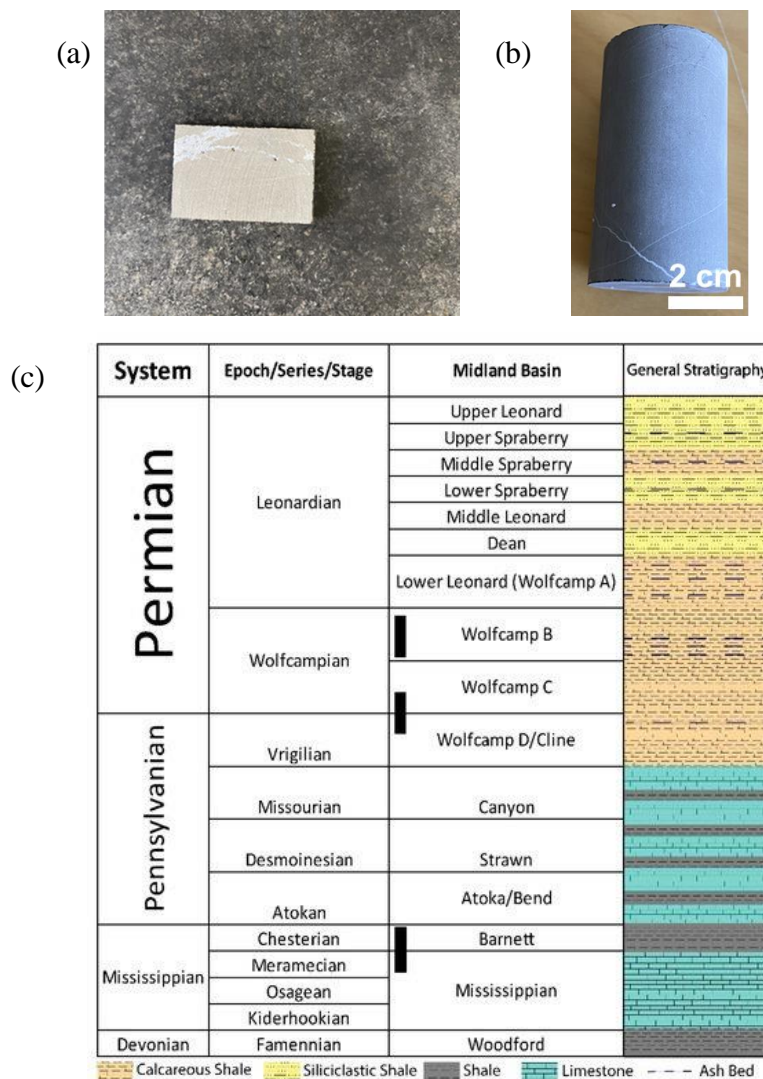
2.1.7.2 Stevns Klint (SK) chalk

SK chalk cores were kindly provided by Smart Water Group (University of Stavanger, Norway). The SK chalk belongs to the Maastrichtian of the upper cretaceous (~ 65 million years old) (Figure 2.4). The samples were taken from Stevns Klint quarry (Denmark). This highly porous (45 – 50%) but low permeable (1 – 5 md) rock is mostly of coccolith (plates or scales of calcium carbonate) matrix, as observed before.[136, 137] However, large bioclasts of uncemented foraminifera (marine organisms) are also observed in the rock texture. The average grain size of the matrix is ~ 1 μm. EDX performed on the rock shows 98% calcite, 1% quartz and trace amounts of other minerals like Mg, S and Al. The pore size distribution of SK chalk by mercury injection capillary pressure shows a range of pore sizes (80 nm up to a few micrometres) with a mean pore diameter of ~ 500 nm. The SK chalk properties are similar to Ekofisk and Valhall oil reservoirs.[138]

Figure 2.4. Stratigraphy of the North Sea Chalk reservoirs and the outcrop at Stevns in Denmark. The grey vertical bar shows the age and location of the outcrop sample taken. Fm: formation and Ma: mega annum (1 million years).
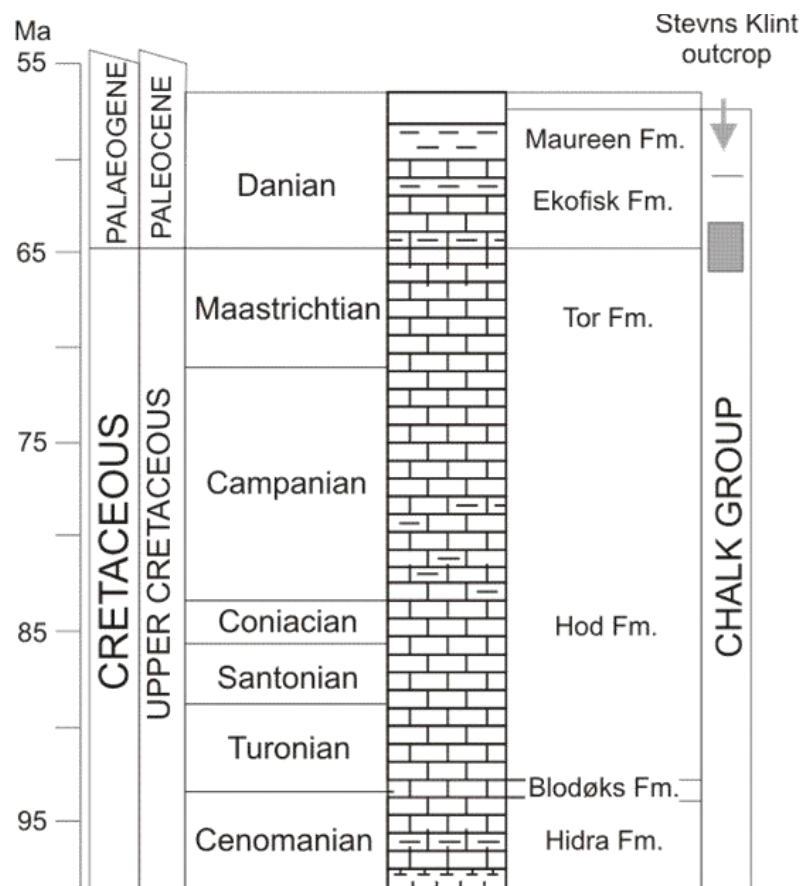
2.1.8   Other chemicals

Sodium hydroxide (99%, Fisher Scientific), glacial acetic acid (> 99%, Fisher Scientific) and hydrochloric acid (37%, Fisher Scientific) were used for pH adjustment either in the synthesis of particles or resulting particle dispersions. Amicon® ultra-15 centrifugal filters were purchased from Merck Company and used for particle filtration in the synthesis of silane-coated silica. The filter tubes had a molecular weight cut-off of 30,000 Da. Sterile 33-mm diameter Startlab syringe filters with polyethersulfone or hydrophilic polyvinylidene fluoride membranes were used for filtration of dispersions during the synthesis of particles (pore sizes of 0.22 µm or 0.45 µm). High pressure high temperature 35 cm^3 glass tubes (CG-1880-02, Chemglass Life Sciences) were purchased and used for particle stability inspections at high temperatures. The chemicals used for the determination of surfactant concentration using Epton titration are listed in Table 2.2.

Table 2.2. Chemicals used in this study.

Chemical	Purity / %	Supplier	Molecular weight / g mol^{-1}
Disulphine blue (Patent Blue VF)	Pure indicator grade	ACROS	566.7
Dimidium bromide	95	Sigma Aldrich	380.3
Aqueous Hyamine 1622 solution (0.004 M)	For titration, standardized with reference SDS	Merck	448.1
Absolute ethanol	≥ 99.8	Honeywell	46.00
Chloroform	99.2	VWR Chemicals	119.38
Sulphuric acid	>95 Analytical reagent grade	Fisher scientific	98.07
Phenolphthalein indicator	ACS Reag. Ph. Eur.	Merck	318.30
SDS	Specially pure, ≥ 99	BDH	288.38

2.2   Methods

2.2.1   Characterization of crude oil

The dead crude oil sample from ChampionX was centrifuged and characterized by density, pH and acid/base number measurements. The modified American Society for Testing and Materials (ASTM) methods (ASTM D664 for acid number and ASTM D2896 for base number) by Fan and Buckley were used for the determination of acid and base number [139] using potentiometric titration by a T50 automatic titrator (Mettler Toledo, UK) (Figure 2.5). The instrument includes two electrodes (for acid and base number measurements),

a dosing unit, a display and titration stands. Table 2.3 shows the solutions required for measurements. The electrode and propeller of the instrument were first cleaned with DIW and ethanol. The electrodes were calibrated using three pH buffers of 4, 7, and 10 (AnalaR® Normapur grade, VWR) and appropriate standard solutions depending on the type of electrode. In both acid and base number titrations, the measurement was first performed for a blank solution (50 cm^3 appropriate titration solvent + 1 cm^3 appropriate spiking solution) denoted blank measurement. Then, 0.5 cm^3 of crude oil sample was added to a new blank solution and the acid or base number was measured by titration. In all steps, the weight of added components was measured. The instrument automatically measures the acid or base number for the crude oil sample.

Figure 2.5. T50 Mettler Toledo titrator used for the measurement of acid/base number of crude oil.

Table 2.3. Solutions used for acid and base number measurements of crude oil.

Solution	Acid number	Base number
Electrode electrolyte	3 M KCl in DIW	Saturated sodium perchlorate in 2-propanol
Standard solution	0.2 g potassium hydrogen phthalate diluted to 500 cm^3 with DIW	0.2 g potassium hydrogen phthalate diluted to 250 cm^3 with acetic acid
Titration solvent	500 cm^3 Toluene 494 cm^3 2-propanol 6 cm^3 DIW	Methyl isobutyl ketone
Titrant	2.8 g KOH (>85%) diluted to 1000 cm^3 with 2-propanol	5 cm^3 perchloric acid (70%) 15 cm^3 acetic anhydrite diluted to 1000 cm^3 with acetic acid
Spiking solution	0.5 g stearic acid diluted to 100 cm^3 with acid titration solvent	0.5 g quinoline diluted to 100 cm^3 with decane

2.2.2 Characterization of surfactants

2.2.2.1 Thermal and salinity resistance

Surfactants can degrade at high temperatures or precipitate by ions. Appropriate concentrations of AHS and ZN surfactants were prepared in Permian brine and added to high pressure high temperature glass tubes and monitored at 100 °C for a month for spotting precipitation. To investigate the thermal stability of surfactants, thermogravimetric analysis (TGA) was performed on AHS and ZN surfactants. For this, AHS and ZN samples were dried at 100 °C and analyzed using a Perkin-Elmer TGA 4000 instrument.

2.2.2.2 Air-water surface tension

The critical micelle concentration, CMC, of AHS and ZN surfactants was determined using air-water surface tension measurements using K11 force tensiometer (Kruss, Germany) and the du Nouy ring method. Dynamic surface tension was measured until a standard deviation of < 0.1 mN m^{-1} for the last five measurements was reached. The average was then reported as the equilibrium surface tension. The measurements were performed at 25 °C for different concentrations of ZN and AHS surfactants (0 – 1 wt.%) in DIW and Permian brine. The effect of particle loading (0 – 0.1 wt.%) on the surface tension of blends of AS- or ES-coated silica and surfactant was also investigated.

2.2.2.3 Charge of micelles

The charge behaviour of AHS and ZN surfactants with pH was investigated using zeta potential measurements. First, zeta potentials of different concentrations (0.1, 1.0 and 2.0 wt.%) of AHS and ZN surfactants in DIW were measured at 25 °C. An appropriate surfactant concentration was then selected to inspect the charge alteration of the surfactant headgroup with pH. A range of pH from 2 to 11 was inspected using 1 M HCl and 1 N NaOH.

2.2.3 Properties of bare silica

The stability of bare silica particles alone or in blend with AHS and ZN surfactants in DIW and Permian brine at 25 °C and 75 °C were inspected with time using the picturing technique.

2.2.4 Synthesis of amino silane (AS)-coated silica particles

Procedures from previous studies were followed for amine functionalization of bare silica.[140-142] To oligomerize the silane, 1.5 g AS was added to a vessel containing 15 g

acetic acid (5 wt.%) and was stirred on a magnetic stirrer for 20 min at room temperature of ~20 °C (pH ~ 4.4). NaOH (1 N) was then added to the mixture to bring the pH up to ~8. Afterwards, 1 g bare silica dispersion (30 wt.%) was added dropwise to the mixture under stirring within 2 min, which turned the mixture turbid (resulting pH 8.5). The mixture was then slowly heated to 65 ± 1 °C using a water bath on a magnetic stirrer and allowed to stir for 20 h. The final blueish dispersion was cooled to room temperature. Using Amicon ultra-15 centrifugal filters, the dispersion was centrifuged at 5,500 rpm and washed with DIW four times. Finally, 5 cm^3 DIW was added to the subnatant and sonicated for 30 min using a water bath sonicator (FB15051, Fisher Scientific, USA). Figures 2.6 and 2.7 show the setup and sketch of reactions involved in the synthesis of AS-coated silica, respectively. The synthesis allows the silane molecules to attach to the silica surface, forming covalent bonds through hydrolysis and subsequent condensation reactions.

Figure 2.6. (a) The setup used for the synthesis of AS-coated silica, (b) initial turbid dispersion and (c) final blueish dispersion.

Figure 2.7. (a) Bare silica nanoparticles and AS and (b) AS-coated silica particles.

(a)

silica +

(b)
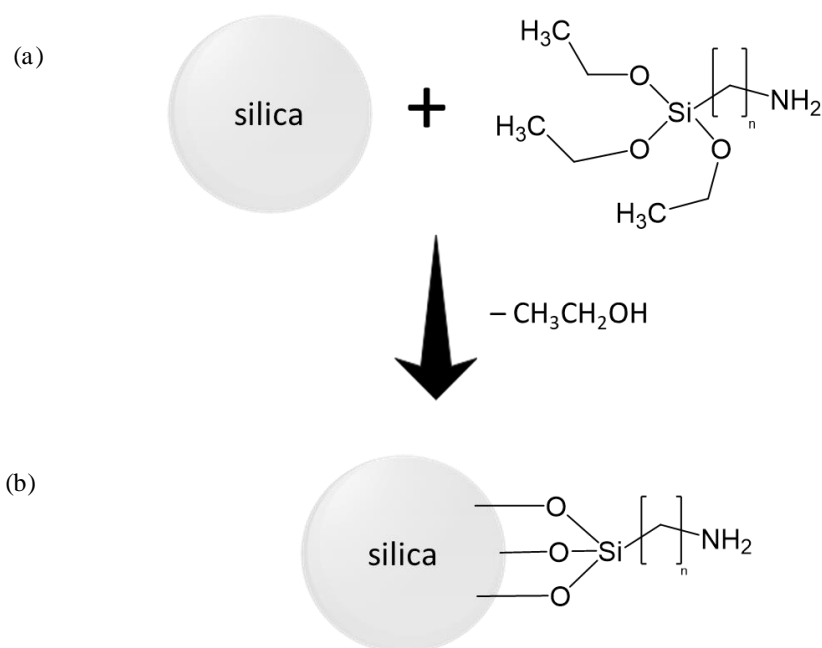
silica

2.2.5   Synthesis of epoxy silane (ES)-coated silica particles

2.2.5.1   Protocol of ChampionX

First, the protocol proposed by ChampionX was followed to surface-modify bare silica particles through a series of hydrolysis-condensation reactions. Figure 2.8 shows the photo and scheme of the setup used for the synthesis. As shown, the setup includes an overhead stirrer, a glass rod with a Teflon blade, a dropping funnel, a three-neck round bottom flask, a heating mantle, a spiral condenser, N_2 gas and a bubbler filled with silicone oil. Briefly, 100 g DIW was loaded to 50 g bare silica (30 wt.%) in a multi-neck round bottom flask and allowed to stir at 300 rpm to prepare 150 g of 10 wt.% bare silica dispersion. The dispersion was heated gradually using the heating mantle to reach $60 \pm 1\ °C$. The weight ratios of ES/silica dispersion and ES/HCl (0.01 M) were selected at 0.35 and $0.30\ \mathrm{g\ g^{-1}}$, respectively. Thus, 53 g ES was added to 182.4 g 0.01 M HCl in a separate beaker and allowed to stir to acid catalyze ES at room temperature of $20 \pm 1\ °C$. Different hydrolysis times (5 – 120 min) were tried to see the effect of time on the final product. The hydrolyzed ES was then added dropwise to the heated bare silica dispersion using a dropping funnel at different stirring speeds (100–600 rpm) within 3 to 12 min, which turned the dispersion turbid. Once the addition was finished, the pH was adjusted to ~10 using a solution of 10 wt.% NaOH. The reaction was held at $60 \pm 1\ °C$ for 24 h and the dispersion was then cooled to room temperature.

Figure 2.8. The setup used for the synthesis of ES-coated silica particles.

45

	1.	Overhead stirrer
	2.	Glass rod with a Teflon blade
	3.	Dropping funnel
	4.	Three-neck round bottom flask
	5.	Heating mantle
	6.	Spiral condenser
	7.	Bubbler
	8.	Support stand
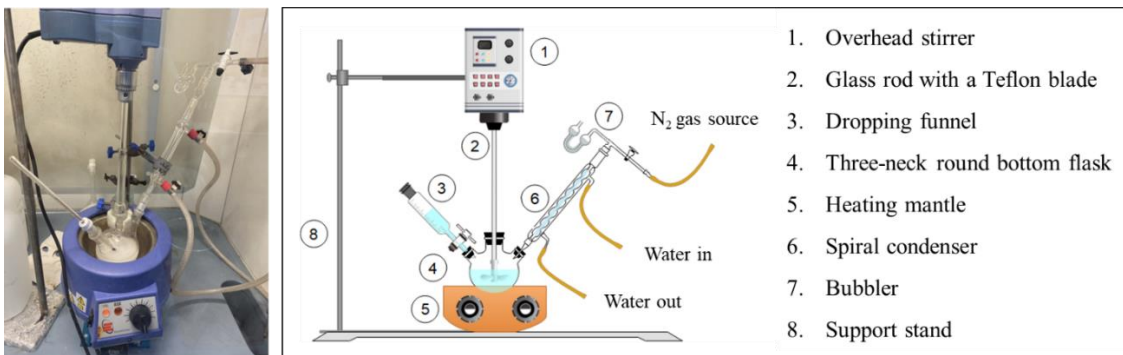
2.2.5.2 Protocol of previous literature

The synthesis was based on the literature.[12] Various ES/ bare silica dispersion ratios of 0.11, 0.25, 0.51 and 1.00 (cm^3 g^{-1}) were used during the synthesis to investigate the effect of coating extent of ES on the particle stability in brine. Also, different initial bare silica concentrations of 30, 17, 8, 4 and 2 wt.% were used at a constant ES/silica dispersion ratio of 0.51 cm^3 g^{-1}. Briefly, the stock bate silica dispersion (30 wt.%) was first diluted. ES and 0.01 M HCl (pH 2) were mixed with a silane/acid volume ratio of 1:6 and stirred for 5 min at room temperature to acid-catalyze the silane. The addition of hydrolyzed ES to the bare silica dispersion was performed in three ways to investigate the effect of the addition rate of ES to the silica dispersion on the ES coating extent and ultimate particle stability in the brine:

(i) One-step method: The whole aqueous ES was added dropwise to the silica dispersion stirring at room temperature. The pH of the mixture was then increased to 10 by 2 N NaOH solution. The mixture was allowed to stir at 60 °C for 24 h using a water bath.

(ii) Two-step method: Half of the aqueous ES was added dropwise to the silica dispersion in a vial under stirring and the mixture was stirred for 2 h at the room temperature of 25 ± 2 °C. Then, the second half of the aqueous ES was added dropwise to the mixture. The pH of the mixture was kept at ~10. The mixture was gradually heated to 60 °C and allowed to stir for 22 h in a water bath.

(iii) Four-step method: The aqueous ES was divided into four portions and added dropwise to the dispersion stirring at the room temperature of 25 ± 2 °C every 40 min. After each addition, the mixture was stirred for another 40 min at room temperature. The pH of the mixture was kept at ~10. The whole mixture was then stirred at 60 °C for 22 h using a water bath.

In all cases above, it was observed that the addition of aqueous ES to the bare silica dispersion turns the dispersion turbid at a pH of ~10. In each case, after 24 h reaction, the

mixture was washed four times (4 min) with DIW using 30,000 g mol^{-1} centrifuge filters at 5,500 rpm to remove the excess silane. DIW was added to the subnatant followed by bath sonicating for 30 min and passing through a 0.22 µm syringe filter to separate large aggregates (if any). A small amount was dried overnight at 80 °C to determine the ES-coated silica concentration.

2.2.5.3 Modified synthesis route

The same setup and steps in Section 2.2.5.2 with different ratios were followed in this synthesis route. In this case, the amount of ES needed was calculated based on the weight of particles in the dispersion. Therefore, ES/silica particle weight ratios of 0.25, 0.51, 0.75 and 1.00 (g g^{-1}) and a ES/HCl (0.01 M) weight ratio of 1:6 were used. Magnetic stirring and a water bath were used during the synthesis. The desired amount of ES and 0.01 M HCl (pH 2) were mixed for 5 – 10 min at 20 ± 2 °C. The addition of aqueous ES to the bare silica dispersion was performed in two steps. Half of the hydrolyzed ES was added dropwise to the bare silica dispersion stirring at room temperature within 5 min, which turned it turbid after a few minutes. The mixture was allowed to stir for 2 h at room temperature. The second half of aqueous ES was then added dropwise in 5 min. The pH of the mixture was kept at ~10. The dispersion was then heated slowly to 60 °C using a water bath within 1 h (to prevent aggregation) and was allowed to stir for 20 h at 60 °C. After 20 h, the dispersion was cooled to room temperature. The final steps in Section 2.2.5.2 including filtration, centrifugation and sonication were removed in this synthesis route. Figure 2.9 shows a sketch of reactions involved in the synthesis of ES-coated silica. The synthesis of particles occurs through a series of hydrolysis-condensation processes.

Figure 2.9. (a) Initial ES, (b) hydrolysed ES by HCl at pH 2 and (c) grafting of ES on a silica particle surface.
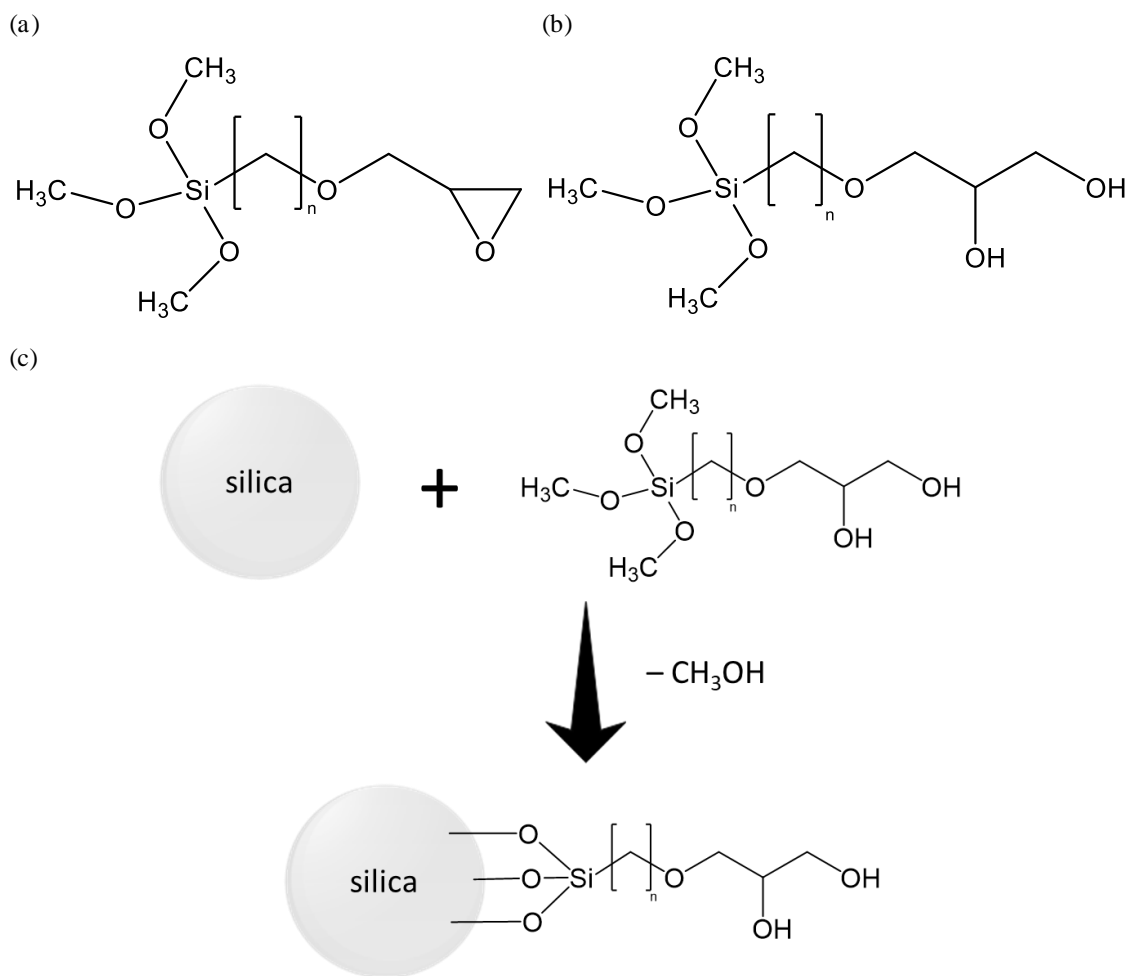
2.2.6 Characterization of particles

2.2.6.1 Visual stability inspection

The visual stability of bare silica and silane-coated silica (ES or AS) with/without AHS or ZN surfactants in DIW or Permian brine was inspected at room temperature and 75°C using photos. A TC120 oil bath (Grant, UK) was used to set the temperature at $75 \pm 2\ °C$.

2.2.6.2 Particle diameter and zeta potential

The initial particle diameter and zeta potential of different concentrations of bare silica, synthesized AS-coated silica and ES-coated silica with or without AHS or ZN surfactants in DIW or Permian brine were measured at 25 °C using a Zetasizer Nano-ZS instrument (Malvern, UK). For visually stable dispersions with no visual aggregation or sedimentation, long-term particle diameter and zeta potential measurements after standing at a temperature for a while were performed to quantitatively analyse turbidity. It is noted that UV-vis was performed on the silane-coated silica but a characteristic wavelength was not found to be used for turbidity analysis. Drying was also tried but it failed due to the low particle and high salt concentrations (will see later).

It is noted that the ionic strength of Permian brine (~2.1 M) exceeds the limit of the instrument (0.15 M), thus zeta potential measurements were not possible for dispersions of particles in Permian brine.

The refractive index (RI) of different solutions and dispersions was measured at 25 °C using a Hilger Abbé refractometer (Hilger & Watts Ltd., UK) equipped with a water bath. The viscosity of Permian brine was calculated at 1.0626 cP using the Zetasizer Nano-ZS software calculator by considering the brine composition. The RI and viscosity calculator of the software showed good accuracy. The RI of Permian brine by the refractometer and software was measured at 1.355 and 1.350 at 25 °C, respectively. The RI of bare silica was obtained from the literature.[143] For the ES-coated silica and AS-coated silica dispersions, it was assumed that the surface of particles is completely covered by silanes. Therefore, the RI of ES (1.429) and AS (1.420) provided by Sigma-Aldrich were used.

For dispersions containing blends of nanoparticles and surfactant in DIW, at low surfactant concentrations (< 1 wt.%), the viscosity of dispersions was assumed to be equal to that of background *i.e.* DIW (0.8872 cP) or Permian brine (1.0626 cP). It has been reported that the dielectric constant of DIW remains unchanged for [NaCl] < 0.1 M.[144] Regarding the surfactant concentrations used in this study (< 1 wt.% ~ 0.02 – 0.03 M), the dielectric constant of DIW (78.5) is unchanged for the zeta potential measurements. Low aluminium sulphate concentrations (0.005 wt.%) used in dispersions are not expected to change the RI and viscosity of the dispersant. Table 2.4 shows the parameters used for particle diameter and zeta potential measurements.

2.2.6.3   X-ray diffraction (XRD)

The XRD of bare silica, AS-coated silica and ES-coated silica (sent by Championx) was performed using an Empyrean X-ray Diffractometer (Malvern PANalytical, UK) operating in Bragg-Brentano geometry using copper $K\alpha_1$ radiation (λ = 1.540546 Å) and a PIXEL detector. A scanning range of 5° to 65° with a step size of 0.02° was selected.

Table 2.4. Parameters used for particle diameter and zeta potential measurements at 25 °C using the Zetasizer.

Dispersion	Dispersant	Dispersant viscosity (cP)	RI	
			Material	Dispersant

bare silica	DIW	0.8872	1.4585	1.333
	Permian brine	1.0626		1.355
bare silica + surfactant	DIW only	0.8872	1.4585	1.333 – 1.336 [a]
AS-coated silica	DIW	0.8872	1.4200 [e]	1.333
	Permian brine	1.0626		1.355
AS-coated silica + surfactant	DIW	0.8872	1.4200	1.333 – 1.336 [a]
	Permian brine	1.0626		1.355 – 1.357 [a]
ES-coated silica	DIW	0.8872	1.4290 [e]	1.333
	Permian brine	1.0626		1.355
ES-coated silica + surfactant	DIW	0.8872	1.4290	1.333 – 1.336 [a]
	Permian brine	1.0626		1.355 – 1.357 [a]

[a] For surfactant concentrations of 0.001 – 2.000 wt.%.

2.2.6.4 Degree of silanization

TGA was performed on the ES-coated silica (sent by ChampionX) and AS-coated silica (synthesized in the lab.) using a Perkin-Elmer TGA 4000 instrument to determine the surface silane coverage. An aliquot of dispersions was first added to a 30,000 g mol^{-1} centrifuge tube and washed four times with DIW at 5,500 rpm for 15 min to remove the unreacted silane. DIW was then added to the subnatant and the dispersion was sonicated for 15 min in a water bath. The sample was dried in an oven of 80 °C for 24 h and then heated under air to 110 °C in the instrument (20 °C min^{-1}) at which it was held for 20 min to remove the remaining water. The temperature was then increased to ~760 °C with the same heating rate to determine the organic content. The organic coverage of particles was calculated by:[145, 146]

$$\phi_i = \frac{f_{org}}{(1 - f_{org}) \times SSA \times MW} \times 10^6 \tag{2.1}$$

where ϕ_i is the organic coverage in µmol m^{-2} of the particle surface, f_{org} is the weight loss fraction due to the loss of particle surface organic molecules obtained from TGA, SSA is the specific surface area of bare silica (331 m^2 g^{-1}) and MW is the molecular weight of the silane in g mol^{-1} that can be removed by TGA. Considering the structure of silane, methyl/ethyl groups are removed by hydrolysis during the synthesis of silane-coated silica. Silicon and oxygen atoms of silane have a strong bond to the surface of silica through siloxane linkages thus they cannot be removed at this temperature window (Figure 2.10).

Considering 4.6 available SiOH groups per nm^2 of bare silica surface as the typical density of reactive silanol sites on colloidal silica[1] and Avogadro's number ($6.022 \times 10^{+23}$), a full monolayer of silane on a silica surface is 7.6 µmol ligand m^{-2}. Therefore, the silane coverage can be calculated by ϕi divided by 7.6 for both particle types.

Figure 2.10. (a) AS-coated silica and (b) ES-coated silica structures. The removable parts of silanes during TGA are bordered in red.
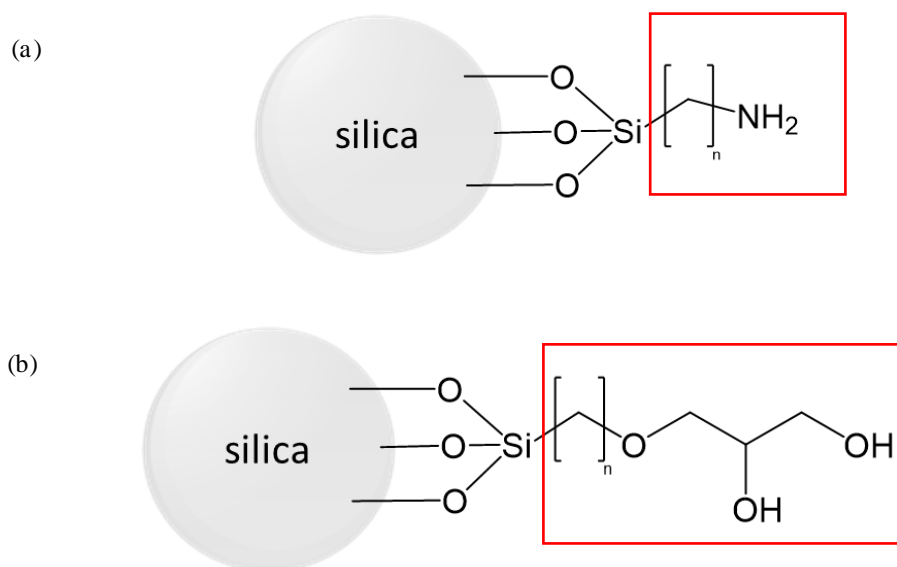
2.2.6.5 Surface activity

The surface activity and to some extent surface wettability of synthesized particles were investigated by air-water surface tension measurements for different particle concentrations in DIW and Permian brine at 25 °C using K11 force tensiometer (Kruss, Germany) and the du Nouy ring method. Any surface activity of particles can result in particle adsorption at air-water surface to reduce the air-water surface tension. Therefore, by measuring surface tension, the particle surface activity can be assessed which is seen as large surface pressures (different between neat air-water surface tension and final surface tension with particles at surface). Dynamic surface tension was measured until a standard deviation of < 0.1 mN m^{-1} for the last five measurements was reached. The average was then reported as the equilibrium surface tension.

2.2.7 Characterization of rock

2.2.7.1 Milling and powder size

Wolfcamp shale rock chunks received from Kocurek (USA) were first crushed to < 3 mm pieces using a Denbigh No. 3 fly press (UK) and then powdered using a Siebtechnik T750 milling instrument (Germany). Sieves with different pore sizes were used to classify

51

powdered shale into different size groups of < 63 µm, 63 – 212 µm, 212 – 425 µm, 425 – 1000 µm and 1 – 3 mm. The first three size groups were selected for subsequent experiments. 0.1 wt.% of shale powder was dispersed in DIW in a water bath for particle diameter measurement using a Mastersizer 2000 instrument (Malvern, UK). Different repeats were performed and the results were averaged and reported with standard deviation.

2.2.7.2 XRD

The XRD of Wolfcamp shale was performed on powder using an Empyrean X-ray Diffractometer (Malvern PANalytical, UK), as described before. Rietveld refinement was used to determine the mineralogy of rock.

2.2.7.3 Surface charge and zero-point charge

The zeta potential of shale powder (< 63 µm) in DIW was measured at different pHs. The pH of dispersions was adjusted using 1 M HCl and 1 N NaOH. For the determination of the zero-point charge (ZPC) of shale, the powder addition/pH drift method was used.[147] To a series of 20 cm^3 glass vials, 10 cm^3 of 0.01 M NaCl or Permian brine was added. The pH of solutions was adjusted to 2 – 11 using 1 N NaOH and 1 M HCl (pH$_1$). 1 g shale powder (< 63 µm) was added to the vials and equilibrated for 48 h using an orbital shaker (Stuart, UK) at 200 rpm at room temperature (Figure 2.11). The final pH (denoted as pH$_2$) was measured. Using a plot of $\Delta pH = pH_2 - pH_1$ *vs* pH$_1$, the ZPC was determined where $\Delta pH = 0$.

Figure 2.11. Equilibrating rock powders with electrolytes on a shaker.

2.2.7.4 Surface area

The Brunauer-Emmett-Teller (BET) surface area of $63-212$ µm and $212-425$ µm shale powder was measured using a Micromeritics TriStar Porosimeter. The samples were first degassed for three hours by a nitrogen capillary tube in a heated well at 80 °C to remove the moisture. The measurement is based on the physical adsorption of N_2 onto the adsorbate surface at a constant bath temperature (77.5 K) and the amount of surface-bound nitrogen to determine N_2 monolayer coverage. The interaction between N_2 molecules and the adsorbate relies on relatively weak intermolecular forces. The nitrogen pressure was then gradually increased to reach an adsorption-desorption equilibrium. N_2 multilayers can occur due to the nitrogen interacting with pre-adsorbed nitrogen molecules at low analysis temperatures. The linear section (monolayer coverage) of the BET plot was used to compute the specific surface area with the assumption that the molecular cross-sectional area of nitrogen molecules (packing parameter) is 0.162 nm^2. The parameters of the process are expressed by:[148]

$$C \propto \exp\frac{E_1 - E_L}{RT} \tag{2.2}$$

where C is the multilayer adsorption parameter to account for interactions between adlayers of N_2, E_1 and E_L are the heat of adsorption for the first and second subsequent N_2 layers (kJ mol^{-1}), R is the universal gas constant (8.314 J mol^{-1} K^{-1}) and T is the analysis temperature (K). C is a function of the enthalpy of the adsorption and is positive since adsorption here is an exothermic process. The BET isotherm can be written as:[148]

$$\frac{1}{V[(\frac{P_0}{P}) - 1]} = \frac{1}{V_m C} + \frac{C - 1}{V_m C}(\frac{P}{P_0}) \tag{2.3}$$

where V is the amount of N_2 gas adsorbed at a given relative pressure (P/P_0), P is the absolute pressure in the tube and P_0 is the saturation vapour pressure of the adsorbate. V_m is the monolayer capacity which is the volume of gas at standard temperature and pressure (STP). A plot of $\frac{1}{V[(\frac{P_0}{P}) - 1]}$ vs $(\frac{P}{P_0})$ gives a linear line by which V_m and C can be estimated:

$$V_m = \frac{1}{slope + intercept} \tag{2.4}$$

$$C = \frac{1}{V_m \times intercept} \tag{2.5}$$

The BET specific surface area (SSA) is then given by:[148]

$$SSA = \frac{V_m \; \sigma \; N_A}{m \; v} \tag{2.6}$$

where V_m is the monolayer volume (m^3), σ is the N_2 packing value (0.162 nm^2 or 1.62×10^{19} m^2), N_A is Avogadro's number (6.023×10^{23}), m is the adsorbate mass (g) and v is the gas molar volume. The pore volume of the rock sample can be determined by Gurvich rule:[149]

$$V_p = \frac{V_{ads.}^{sat.}}{\rho_L} \tag{2.7}$$

where V_p is the total pore volume ($cm^3 \; g^{-1}$), $V_{ads.}^{sat.}$ is the adsorption volume at saturation (usually before condensation at $P/P_o = 0.9$) and ρ_L is the density of liquid nitrogen (0.808 g cm^{-3}).

2.2.8   Rock wettability analysis

Assessing rock wettability alteration involves a range of techniques and measurements to understand how the interaction of fluids and surfaces affects the wetting properties of rocks. There are different methods to evaluate rock wettability such as contact angle measurement, Amott-Harvey index and API wettability test. The last two provide only qualitative information rather than quantitative measurements. Amott-Harvey index does not offer information about the interactions at the solid-liquid interface and the API wettability test is limited to assessing spontaneous imbibition, which may not capture dynamic wettability changes during displacement processes. Contact angle measurement, on the other hand, involves measuring the angle formed at the interface between a liquid droplet and a solid surface (rock). It benefits from a direct and quantitative measure of wettability and high sensitivity to surface interactions. It is also useful for characterizing

individual mineral grains or specific surfaces. Therefore, contact angle measurement has been used in this study for rock wettability analysis.

2.2.8.1 Polishing

The Wolfcamp shale substrates received from the supplier had some artificial surface lines induced during trimming which might affect the droplet shape and contact angle (Figure 2.12a). Therefore, they were first polished using a polishing machine to remove the large lines (Figure 2.12b) and then polished using silicon carbide suspensions (Figure 2.12c). Two grit sizes of 400 and 600 were prepared in DIW. The rock substrates were rubbed against two flat glass plates covered with a thin layer of suspension to make the rock surface polished. They were then washed with DIW in separate vials in a bath sonicator several times until the supernatant became clear. They were finally dried at 90 °C for a day.

Figure 2.12. (a) Bare Wolfcamp shale substrates as received from the supplier, (b) after polishing with a polishing machine and (c) after polishing with silicon carbide.
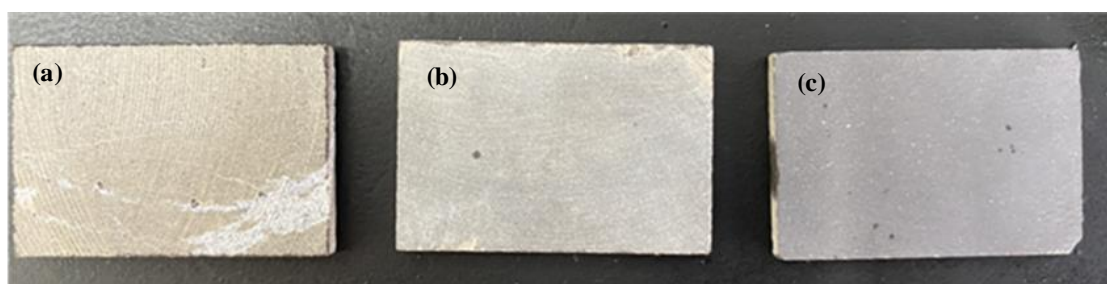
2.2.8.2 Ageing

Dried polished rock substrates were placed vertically in crude oil in separate glass vials for uniform hydrophobization. The process was performed at a room temperature of 20 ± 2 °C for a month (Figure 2.13).

Figure 2.13. (a) Wolfcamp shale substrates standing vertically in crude oil in separate glass vials during ageing and (b) aged substrates.
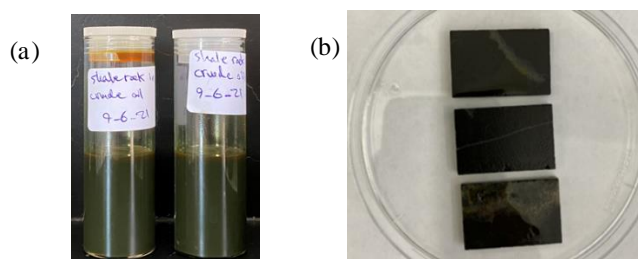
2.2.8.3 Contact angle measurements

The inverted sessile drop method (Figure 2.14) using a DSA 10 instrument (Kruss, Germany) was used to measure the three-phase contact angle of oil droplets on the oil-wet rock substrates immersed in water. The setup includes a glass cuvette, substrate holders, a U-shaped needle, a camera and a PC. The contact angle of crude oil droplets on oil-wet shale substrates immersed in DIW was first measured to ensure sufficient oil-wetness and minimum uncertainties in subsequent results. The substrates with sufficient hydrophobicity (contact angles through the water phase $> 150°$) were chosen for the main experiment. Before contact angle measurements, the oil-wet substrate was gently dried with air to remove excess oil. Contact angle measurements of DIW, n-dodecane and crude oil drops on both bare rock and oil-wet shale substrates in the air ($\theta_{a,w}$ and $\theta_{a,o}$) were also measured at room temperature of 18 ± 2 °C.
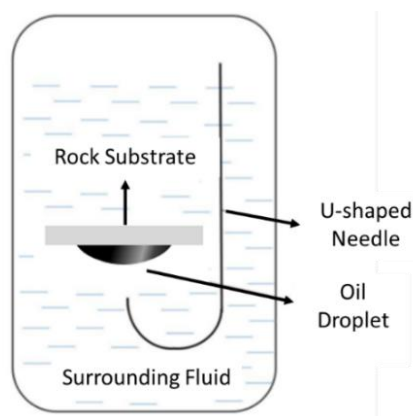
Figure 2.14. Inverted sessile drop method for contact angle measurements.

Different concentrations of ES-coated silica ($0 - 0.1$ wt.%), AS-coated silica ($0 - 0.1$ wt.%), AHS or ZN surfactant ($0 - 0.1$ wt.%) or a blend of particles and surfactant in DIW or Permian brine served as wettability modifiers. For the treatment process, the oil-wet substrates were placed vertically in a treating fluid in a glass vial with a cap for up to 48 h at room temperature (Figure 2.15). Treatment times of 0.5, 1.5, 3, 24 and 48 h were selected to investigate the effect of the contact time of the oil-wet substrate with the treating fluid on the extent of the wettability alteration. At each treatment time, the substrate was removed and placed horizontally on a holder in a glass cuvette filled with DIW or Permian brine (depending on the background). Multiple 5 µL oil droplets were injected underneath the oil-wet substrate using a long U-shape needle mounted on a Gastight 50 microliter syringe (Hamilton, USA). The oil droplet profiles on the rock were photographed over time and equilibrium contact angles were measured using ImageJ software. Contact angle measurements were repeated 3 times and for each repeat at least 8 oil droplets were placed on different areas on both sides to account for the rock

heterogeneity and reproducibility. The average values are reported with error bars. Contact angle measurements started on unpolished rock substrates which had artificial lines on their surface making drop shape variable and then continued on polished rock to investigate the effect of surface roughness on the drop shape and thus contact angle.

Figure 2.15. A typical picture of oil-wet rock substrates placed vertically in treating fluids in glass vials with a cap at room temperature.

2.2.8.4 Scanning electron microscopy (SEM) and energy dispersive X-ray (EDX) spectroscopy

Dispersions of particles and surfactant with the lowest oil-water contact angle were selected for SEM and EDX. 1 g of rock powder (212 – 425 μm) was added to 19 g of each candidate solution/dispersion and the mixture was stirred magnetically for 24 h at 25 ± 0.5 °C in a water bath. The rock powder was then separated and dried in an oven at 90 °C for 24 h. A Zeiss EVO-60 SEM equipped with a LaB6 emitter at its second emission peak was used for SEM imaging. With a 20 kV accelerating voltage and a 40 uA beam current, secondary electron pictures in the high vacuum mode (chamber pressure $< 5 – 10$ mbar) were acquired with a working distance of ~ 8 mm. An Oxford X-max 80 detector connected to Inca 1.2 software was used to gather spectra with a count rate of 1000 to 2000 counts per second for 30 seconds. For comparison, the analysis was also conducted on bare rock powder (no treatment) and powder treated with DIW and Permian brine.

2.2.9 Adsorption of surfactant onto rock powder

The extent of AHS or ZN surfactant adsorption onto rock powder was analyzed with/without a fixed concentration of ES-coated silica in DIW and Permian brine. 1 g rock powder and 19 cm^3 of solutions/dispersions were added to a glass vial and stirred magnetically in a water bath at 25 ± 0.5 °C for 24 h (Figure 2.16). The mixture was centrifuged for 10 min at 7,500 rpm and the supernatant was collected using a syringe and passed through a 0.45μm membrane filter to separate rock particles. Three different methods were tried for the determination of surfactant concentration: conductivity measurement, Epton titration and surface tension measurement.

Figure 2.16. Appearance of mixtures of rock powder and different dispersions/solutions.

2.2.9.1 Conductivity measurement

The conductivity of different concentrations of AHS and ZN in DIW and Permian brine were first measured by a 4510 Jenway conductivity meter (UK) at 25 ± 0.5 °C using a water bath to create calibration curves. The instrument was first calibrated by 0.01 M KCl solution standard with a conductivity of 1413 µS cm^{-1} at 25 °C. The conductivity of the supernatants was then measured and converted into surfactant concentration using calibration curves.

2.2.9.2 Epton titration

ASTM D 3049-89 (2003) Protocol was followed for the determination of surfactant concentration.[150] First, a few drops of a pre-made phenolphthalein solution (1 wt.% phenolphthalein in 95 wt.% ethanol) were added to the sample and neutralized to faint pink with 1 N NaOH (Figure 2.17). 1 cm^3 of supernatant was added into a 100 cm^3 mixing cylinder with a stopper. 2 cm^3 of the acid indicator solution (0.07 mM disulphine blue, 0.21 mM dimidium bromide and 0.1 M sulphuric acid in DIW) or basic indicator solution (0.07 mM disulphine blue, 0.21 mM dimidium bromide and 0.2 M sodium hydroxide in DIW) (Figure 2.18) were added to the mixing cylinder followed by 15 cm^3 of chloroform. Depending on the charge of surfactant, 0.004 M aqueous Hyamine 1622 solution or 0.0034 M and 0.001 M SDS solution serving as titrant was added to the mixing cylinder using pipettes. The mixture was hand shaken for 15 sec after each titrant addition and monitored until the emulsions phase separated. The changes in colours with the addition of titrant were monitored to find the endpoint at which the emulsions are expected to break easily and shortly. The added volume of titrant ($V_{tit.}$) in cm^3 was used to estimate the active concentration of the sample (C_s) in M:

$$C_s = \frac{V_{tit.} \times C_{tit.}}{V_s} \tag{2.8}$$

where $C_{tit.}$ is the concentration of titrant (M) and V_s is the volume of the sample (cm^3) used in the titration. The experiment was first performed for known concentrations of SDS and Hyamine as control.

Figure 2.17. 0.1 wt.% AHS surfactant in DIW with few drops of phenolphthalein solution (1 wt.% in 95 wt.% ethanol) neutralized to faint pink by 1 N NaOH (pH$_1$ = 7.80 and pH$_2$ = 9.63 at 19.5 °C).

Figure 2.18. (a) Acid indicator solution containing 0.07 mM disulphine blue, 0.21 mM dimidium bromide and 0.1 M sulphuric acid at pH = 1.2 at 20°C. (b) Basic indicator solution containing 0.07 mM disulphine blue, 0.21 mM dimidium bromide and 0.2 M sodium hydroxide at pH = 13 at 20 °C.
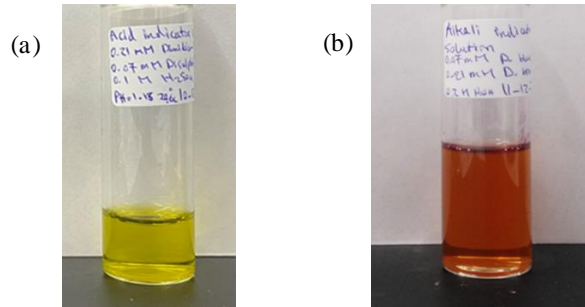
2.2.9.3 Surface tension measurement

Pre-CMC surface tension curves were used to determine the aqueous surfactant concentration in the supernatant. The dilution of supernatant was done where required using the appropriate diluent. The process was repeated three times and the average with standard deviation was presented.

2.2.9.4 Modelling

The amount of surfactant adsorbed onto rock (Q_e) is given by[151]

$$Q_e = \frac{(C_o - C_e)\,\text{V}}{\text{m}} \tag{2.9}$$

where C_o and C_e are the initial and equilibrium surfactant concentrations, respectively (mg cm^{-3}), V is the volume of solution (19 cm^{-3} here) and m is the weight of shale powder (1 g here). The surfactant adsorbed per m^2 of rock powder is given by[151]

$$amount\ adsorbed\ (\frac{mg}{g}) = \frac{Q_e}{\text{A}} \tag{2.10}$$

where A is the surface area of shale powder (m^2 g^{-1}) obtained by BET analysis. The experimental data were fitted to different adsorption isotherms including Sips, Langmuir, Freundlich, Redlich-Peterson and Temkin models (Table 2.5).

Table 2.5. Different adsorption isotherms used in this study.[152]

Model	Equation	Comments
Sips	$$Q_e = \frac{Q_m(K_S C_e)^n}{1 + (K_S C_e)^n}$$	Q_m: saturation adsorption (mg g^{-1}) K_S: Sips constant (L mg^{-1})^n n: exponent
Langmuir	$$Q_e = \frac{Q_m K_L C_e}{1 + K_L C_e}$$	Q_m: saturation adsorption (mg g^{-1}) K_L: Langmuir constant (L mg^{-1})
Freundlich	$$Q_e = K_F (C_e)^{\frac{1}{n}}$$	K_F: Freundlich constant (L mg^{-1}) n is a constant and 1/n is surface heterogeneity
Redlich-Peterson	$$Q_e = \frac{K_{RP} C_e}{1 + \alpha_{RP} C_e{}^n}$$	K_{RP}: Redlich-Peterson constant (L mg^{-1}) n: exponent α_{RP}: Redlich-Peterson constant (L mg^{-1})^n
Temkin	$$Q_e = \frac{RT}{b} \ln (K_T C_e)^n$$	K_T: adsorption capacity (L mg^{-1}) b: sorption heat (J mol^{-1})

2.2.10 Oil-water interfacial tension

Interfacial tension measurements between different oils including toluene, heptane, heptol (1:1 g g^{-1}) and crude oil and different aqueous phases including different concentrations of AHS or ZN with/without different ES-coated silica concentrations (0.01 – 0.1 wt.%) in DIW and Permian brine were measured using a Site 04 spinning drop tensiometer (Kruss, Germany) at 25 °C and 60 °C (Figure 2.19). The tensiometer supports tensions of 0.0001 – 100 mN m^{-1} with a rotation speed of up to 10,000 rpm. It consists of a stationary steel chamber with an inside rotating glass capillary. The chamber comes with side optical windows which facilitate visual observations into the capillary by a camera. The camera has two magnification lenses (2.5X and 5.0X) and is capable of axial movement (x, y and z directions). Tilting of the stage and hence the chamber-capillary assembly is possible where required to bring the droplet in the middle of the capillary. The eyepiece of the camera has an inside measuring Vernier scale which can be set on the upper and lower edges of the rotating elongated droplet to measure the diameter. An E100 Lauda bath was used to set the temperature using circulating oil inside the chamber around the rotating capillary.

Figure 2.19. Site 04 spinning drop tensiometer.

Control

unit

60
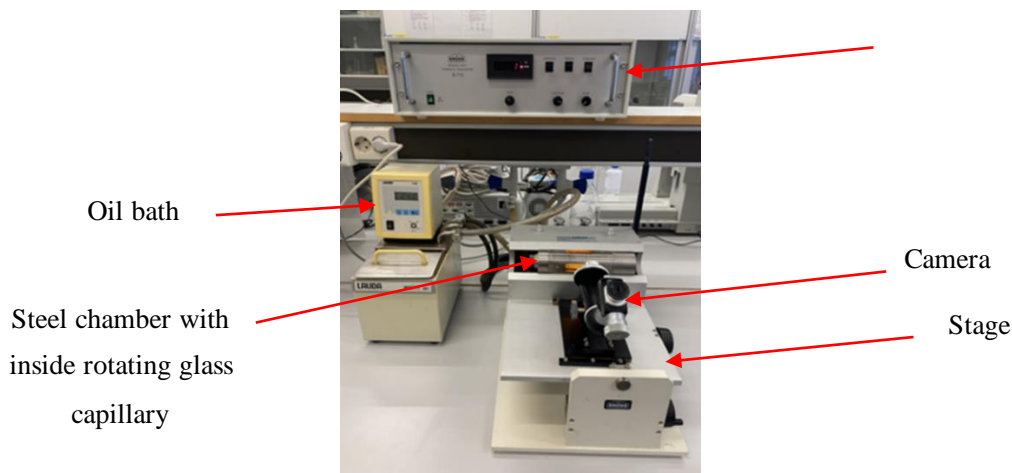
Before measurements, the glass capillary was first washed with DIW and acetone. The aqueous phase was first injected into the capillary using a syringe followed by injection of an oil drop (5 – 10 µm) using a Gastight 50 microliter syringe (Hamilton, USA) in the middle of the capillary. After setting the temperature, the rotation speed was gradually increased. For low tensions, a rotation speed of 3000 – 4000 rpm and for high tensions, higher rotation speeds of up to 9,000 rpm were required. The initial measurements showed that the diameter changes for these systems occur mostly in the first 30 min however up to 60 min was allowed to ensure an equilibrium. The oil-water interfacial tension (σ) in mN m^{-1} is given by:

$$\sigma = e(v.d)^3.n^2.\Delta\rho \tag{2.11}$$

where e is the unity factor (3.427×10^{-7} mN cm^3 min^2 m^{-1} g^{-1} mm^{-3}), v is the enlargement factor (mm sdv^{-1}), d is the drop diameter (sdv), n is the rotation speed (rpm) and $\Delta\rho$ is the difference in density between the aqueous and oil phase ($\rho_w - \rho_o$) (g cm^{-3}). In this method, the rotation speed should be enough such that the oil drop length is at least four times higher than the drop diameter for the equation to be applicable. In the above equation, the enlargement factor depends on the refractive index (RI) of the oil and aqueous phase inside the capillary glass as well as that of circulating oil and temperature. This factor was determined by a calibration wire of known diameter (1 mm). After cleaning and filling the capillary with the appropriate aqueous phase, the temperature was set and the wire diameter placed inside the capillary was measured by the two lenses. The enlargement factor (v) was then calculated in mm sdv^{-1} for both lenses by:

$$v = \frac{wire\ diameter}{measured\ diameter} \tag{2.12}$$

For calibration, the interfacial tensions of DIW and toluene, heptane and heptol (1:1 g g^{-1}) were measured.

2.2.11 Emulsification of oil and water

The stability and preferred type of emulsion formed by mixing different oils including toluene, heptane, heptol (1:1 g g^{-1}) and crude oil and different concentrations of AHS or ZN (0 – 0.1 wt.%) with/without AS- or ES-coated silica (0 – 0.1 wt.%) in DIW or Permian brine were investigated. Accordingly, 5 g of either phase was gently added to a glass vessel and homogenized using a T25 digital ultra Turrax homogenizer (IKA, China) for 2 min at 13,000 rpm at room temperature.

For the determination of the preferred type of emulsion, an emulsion drop test was performed. For an oil-in-water emulsion, the emulsion droplets sediment in oil and disperse in water. For a water-in-oil emulsion, the droplet disperses in oil and floats in water. Immediately after homogenization, optical microscopic images of the emulsion were taken using an Olympus BX51 microscope fitted with a GXCAM U3-18 digital camera. Calibration of microscope lenses was performed first using a calibration ruler.

The emulsion droplet diameter was determined using a Mastersizer 2000 instrument. 1 cm^3 of the formed emulsion was added to 99 cm^3 DIW in the dispersion unit of the instrument and the droplet volume mean D[4,3] was determined. Between each measurement, the dispersion unit was washed with DIW and ethanol. Table 2.6 presents the parameters used in drop size measurements.

The stability of emulsions was monitored with time at room temperature from photos, and the fraction of oil (f_o) and water (f_w) resolved were calculated based on the following equations:

$$f_o = \frac{oil\ phase\ height}{initial\ oil\ phase\ height\ before\ homogenization} \quad (2.13)$$

$$f_w = \frac{aqueous\ phase\ height}{initial\ aqueous\ phase\ height\ before\ homogenization} \quad (2.14)$$

Therefore, $0 \leq f \leq 1$ with $f = 0$ and $f = 1$ showing no resolving of the phase and total phase resolved, respectively. The effect of pH reduction on emulsification was investigated by adding HCl or $Al_2(SO_4)_3$.

Table 2.6. Refractive indices and densities used for the measurement of emulsion droplet diameter.

Chemical	RI at 25 °C	Density / g cm^{-3}
DIW	1.3330	0.997
Toluene	1.4950	0.865

n–Heptane	1.3855	0.684
Heptol (1:1 g g^{-1})	1.4265	0.759

2.2.12 Oil recovery tests

2.2.12.1 Candidate injectants

The static results from rock wettability analysis, oil-water interfacial tension measurements and surfactant adsorption on rock were considered for determining candidate dispersions to test in spontaneous imbibition.
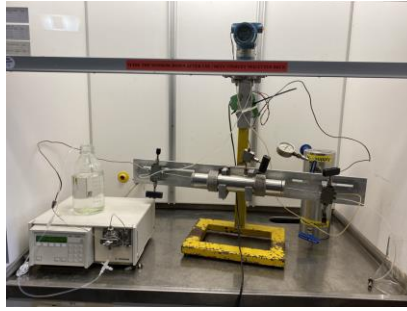
2.2.12.2 Shale cores

Shale oil reservoirs are unconventional tight reservoirs with a micro- to nanometre pore throat size. That is why fracking is usually used for oil production in these reservoirs. Therefore, the injectivity of calcite-rich shale cores was tested for imbibition tests. They were first weighed (as reference) and dried in an oven of 90 °C until reaching a stable weight (2 – 3 days). The dried weight was measured and showed no change in weight compared to the initial weight, meaning no initial fluid inside. They were then used in the following scenarios for inspecting injectivity and saturation possibility:

2.2.12.2.1 Injection of DIW or heptane at room temperature

Figure 2.20 shows the core flooding setup used. The setup includes a 307 High-Performance Liquid Chromatography (HPLC) pump (Gilson, USA) with a DIW feeding bottle, a Hasler core holder, a Rosemount digital differential pressure (DP) transmitter (Emerson, UK), a confining pressure around the core by N_2-pressurized DIW, a collection Erlenmeyer flask and appropriate tubing/valves. The shale core was first mounted in a rubber sleeve and placed inside the core holder. DIW or heptane injection was performed with a confining pressure of 20 bar, a pressure limit of 10 bar and an injection rate of 0.1 cm^3 min^{-1} at room temperature. The injection and differential pressures were monitored throughout the experiment. After the core was taken out, the excess liquid on its surface was removed with a tissue before being weighed and compared to its dry weight.

Figure 2.20. Core flooding setup used for injectivity test of shale cores.

2.2.12.2.2 Vacuum saturation with heptane at room temperature

Figure 2.21 shows the setup used for vacuum saturation of shale cores with heptane. The setup includes a desiccator with a lid equipped with two valves: one connected to a vacuum pump and the other to an overhead container of heptane using tubing. The core was placed in a plastic container containing two small balls at the bottom to allow for oil saturation from underneath. The lid O-ring of the desiccator was covered with a thin layer of Dow Corning high vacuum grease for better sealing. The core was first vacuumed for 40 min. Heptane was then introduced and allowed 24 h to saturate the core. After the core was removed, the excess liquid on the surface of the core was wiped off with a tissue before it was weighed and compared to its dry weight.

Figure 2.21. Setup used for vacuum saturation of shale cores with heptane.


2.2.12.2.3 High pressure saturation with heptane at room temperature

The core was placed in a steel cell and filled with heptane. Using the setup in Figure 2.20, heptane was injected into the cell using a transfer cylinder to pressurize the core to 50 bar at room temperature. Five days were allowed for heptane to saturate the core at high pressure. Before being weighed and compared to its dry weight, the excess liquid from the core surface was wiped off using a tissue.

2.2.12.2.4 High pressure high temperature (HPHT) saturation with crude oil

Six shale cores were placed in two large steel cells with marble balls at the bottom and between the cores to allow oil contact with cores in all directions. The cells were filled with crude oil and pressurized using a transfer cylinder of crude oil to 70 bar. They were then aged for two weeks in an oven of 120 °C (Figure 2.22). Once the cores were taken out, the excess oil on the surface of the cores was wiped off with a tissue before being weighed and compared to their dry weight.

Figure 2.22. Setup used for HPHT saturation of Wolfcamp shale cores with crude oil.
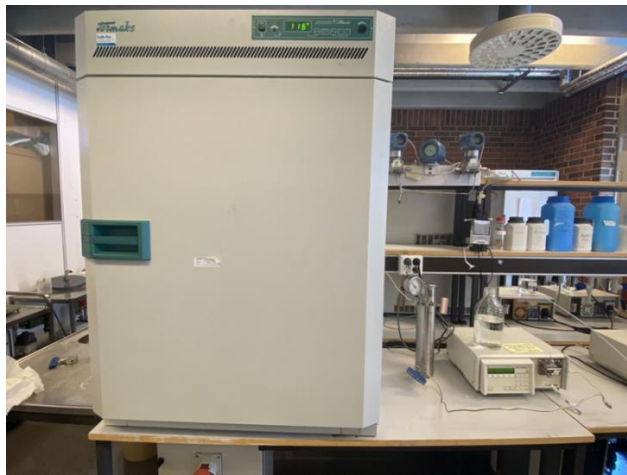
2.2.12.3 Chalk cores

An outcrop SK chalk block was chosen for drilling several cores using a driller (Figure 2.23a). The cores were drilled from the block in the same direction to prevent permeability heterogeneity. They were then shaped using a lathe (Figure 2.23b) and cut using a trimmer (Figure 2.23c) into a suitable diameter (~3.8 cm) and length (~7 cm) for flooding setup. Figure 2.23d shows the photos of a typical core after these steps. The exact dimensions of the cores were then measured using a digital caliper. The cores were moved with extreme care because SK chalks are delicate and brittle.

Figure 2.23. (a) Driller, (b) lathe, (c) trimmer and (d) final core for the experiment.

(a) (b)
(c) (d)
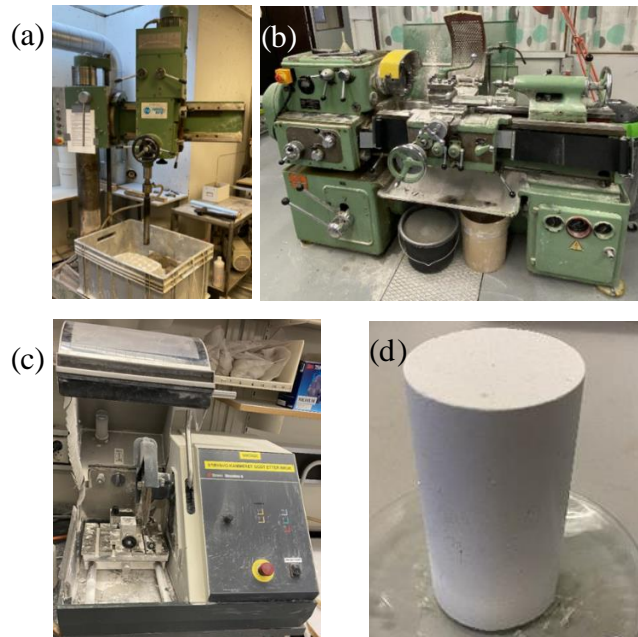
2.2.12.4 Core cleaning

SK chalks are rich in sulphate which repels and prevents the adsorption of anionic groups of crude oil (*i.e.* carboxylic groups) onto the cationic rock during oil saturation and ageing, resulting in a more water-wet rock. More importantly, as the sulphate content of rock varies, different initial wettability may be achieved after the ageing of cores which creates uncertainties in results.[153] Thus, cleaning of rock with DIW was performed first to remove sulphate salts. The same core flooding setup as in Figure 2.20 was used for cleaning. The core was mounted in the rubber sleeve of the core holder using a small vacuum pump to facilitate a simple, failure-free movement of the delicate core. 5 pore volumes (PV) of DIW (~200 cm^3) were injected into cores with an injection rate of 0.1 cm^3 min^{-1} at room temperature. The confining pressure and the pump pressure limit were kept at 20 ± 2 bar and 10 bar, respectively. The removal of sulphate from cores was checked by adding BaCl$_2$ to the outlet samples (Figure 2.24). The addition of BaCl$_2$ to a sulphate-rich sample creates a turbid solution due to the formation of BaSO$_4$ precipitates while no turbidity is expected in a sulphate-free sample. Previous studies using the ion chromatography technique show that at least 5 PV is required to ensure the complete removal of sulphate.[137]

Figure 2.24. Barium chloride added to (a) a sulphate-rich sample taken from the core after 27 cm^3 (~0.7 PV) injection of DIW, (b) a nearly sulphate-free sample taken after 160 cm^3 (~ 4 PV) DIW injection.

(b)

(a)
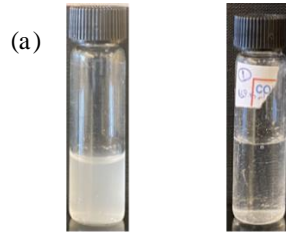
2.2.12.5 Absolute permeability measurement

Permeability is an important parameter of rock and is the ability of a rock to pass fluids through. Following cleaning, the permeability of the cores was measured using the same setup to continue DIW injection at 0.05, 0.10 and 0.15 cm³ min⁻¹ until a stable pressure difference was achieved. The permeability was then calculated using the single-phase flow Darcy equation as follows:[33]

$$Q = \frac{K \, A \, \Delta P}{\mu \, L} \qquad (2.15)$$

where Q is the flow rate (cm³ sec⁻¹), K is permeability (D), A is the injection area (cm²), $\Delta P = P_1 - P_2$ is the pressure difference (atm), μ is the liquid viscosity (cP) and L is the core length (cm) (Figure 2.25). The permeability from different flow rates was averaged and reported with standard deviation. The cores were then dried at 90 °C until they reached a steady weight.

Figure 2.25. Core parameters in the Darcy equation for permeability measurements.
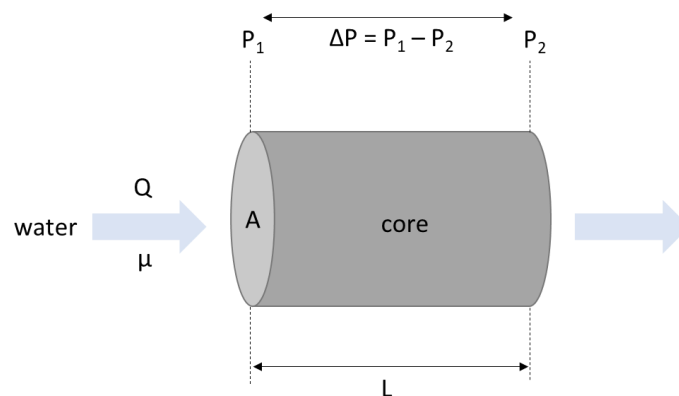
2.2.12.6 Brine saturation

Permian brine (12.56 wt.%) was 10-time diluted with DIW and used for brine saturation using the setup shown in Figure 2.21. Five dried cores were cooled to room temperature and weighed. The cores were first vacuumed for 15 min to a pressure of 0.3 mbar followed by the dropwise addition of diluted brine (with a density of 1.008 g cm⁻³ at 25 °C) from the overhead container. Cores were taken out of the desiccator after being fully saturated

67

with diluted brine for 30 min. The excess brine on the core surface was removed by a tissue before being weighed. The pore volume (V_p) of the cores in cm^3 was estimated as the weight of brine over the brine density (ρ in g cm^{-3}) as follows:

$$V_p = \frac{W_{sat.} - W_d}{\rho} \tag{2.16}$$

where W_d and $W_{sat.}$ are the dried and saturated core weights, respectively (g). The porosity of a rock is defined as the pore volume over the bulk volume (V_b) of the core as follows:

$$\emptyset = \frac{V_p}{V_b} \times 100 \tag{2.17}$$

$$V_b = \pi r^2 L = \frac{\pi D^2 L}{4} \tag{2.18}$$

where r and D are the core radius and diameter, respectively (cm). The saturation of a phase in rock is defined as the volume of the phase over the pore volume of the rock. Water or brine saturation (S_w) can be given by:

$$S_w = \frac{V_w}{V_p} \times 100 \tag{2.19}$$

The brine-saturated cores were placed on a porous plate in a desiccator with silica gel at the bottom to reach a brine saturation of 10% in 4 – 5 days by monitoring the weights daily (Figure 2.26). They were then placed in plastic containers with screws at room temperature for three days for homogeneous distribution of brine in rock.

Figure 2.26. (a) Brine-saturated core on a porous plate in a desiccator with bottom silica gel, (b) cores with $S_w = 10\%$ in plastic containers for three days to reach stable phase distribution.
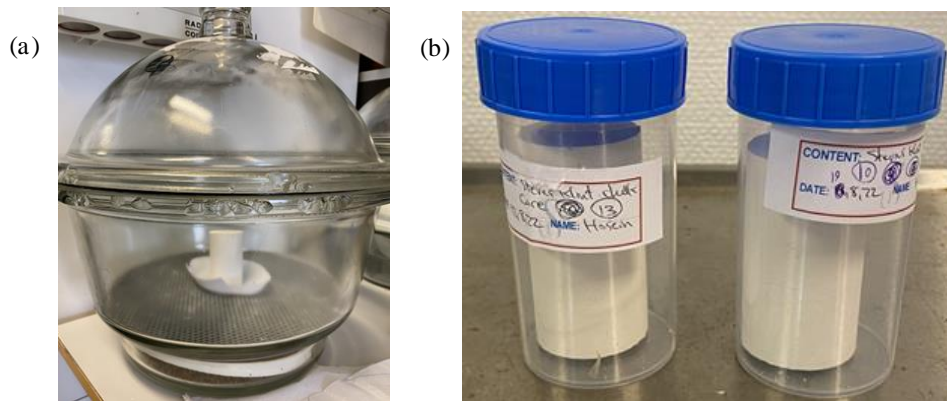
2.2.12.7 Crude oil saturation

The previous core flooding setup was upgraded to that shown in Figure 2.27 to allow for crude oil injection (5 PV ~ 200 cm^3) into the cores ($S_w = 10\%$) from both sides at 50 °C.

The oil saturation process included two left- and right-side oil injections which were proceeded and followed by high pressure saturation. The injection cylinder, core holder, tubing and valves were first cleaned with heptane and DIW and dried with N_2. A core was placed in a rubber sleeve in the core holder using a vacuum. After applying confining pressure and opening all valves inside the oven, a big vacuum pump was connected to the outside outlet valve and the vacuum of the dead-end closed system was performed for 1 h until stabilizing at a pressure of 0.3 mbar. The outside outlet valve was then closed and the vacuum pump was turned off. The oven was turned on to reach 50 °C before starting the pump to inject ~ 40 cm^3 of fresh crude oil (> 1 PV to account for dead volume in tubing) at 0.5 cm^3 min^{-1} with a pressure limit of 6 bar and confining pressure of 20 bar through the inlet valve. As the outlet valve was closed, the pump reached its pressure limit and stopped after around 1 PV injection. This step was to saturate and pressurize the core with crude oil to dominate the available capillary pressures (4 − 5 bar) of small pore throats and evenly saturate the core. The outlet valve was then opened to release the pressure.

The pump was then set to inject 2 PV (~80 cm^3) fresh crude oil into the right side of the core at 0.2 cm^3 min^{-1} at 50 °C with a pressure limit of 6 bar and confining pressure of 20 bar by opening the right inlet and left outlet valves and closing the other two inside the oven. Using the same settings but opposite valves, 2 PV (~80 cm^3) crude oil was also injected into the left side of the core at 50 °C.

The oven was then turned off for the setup to cool to room temperature in a few hours. The first pressurization step was repeated at room temperature to account for the rock expansions at high temperatures. All valves inside the oven were opened and the outside outlet valve was closed. The pump was set to inject a few cm^3 of crude oil at 0.5 cm^3 min^{-1} with the same settings into the core to pressurize it at room temperature. When reaching its pressure limit at 6 bar, the pump was stopped, and the pressure was released by opening the outside outlet valve. In all steps above, the produced oil was collected separately for each core for re-use in the ageing process.

Figure 2.27. (a) Core flooding setup used for saturation of cores with crude oil, (b) Hasler core holder inside the oven, (c) scheme of setup. P, V and E refer to pipelines, valves and equipment used in the setup, respectively. TI and PI are temperature and pressure indicators, respectively. The red dashed box is the oven.

(a)

(b)

(c)
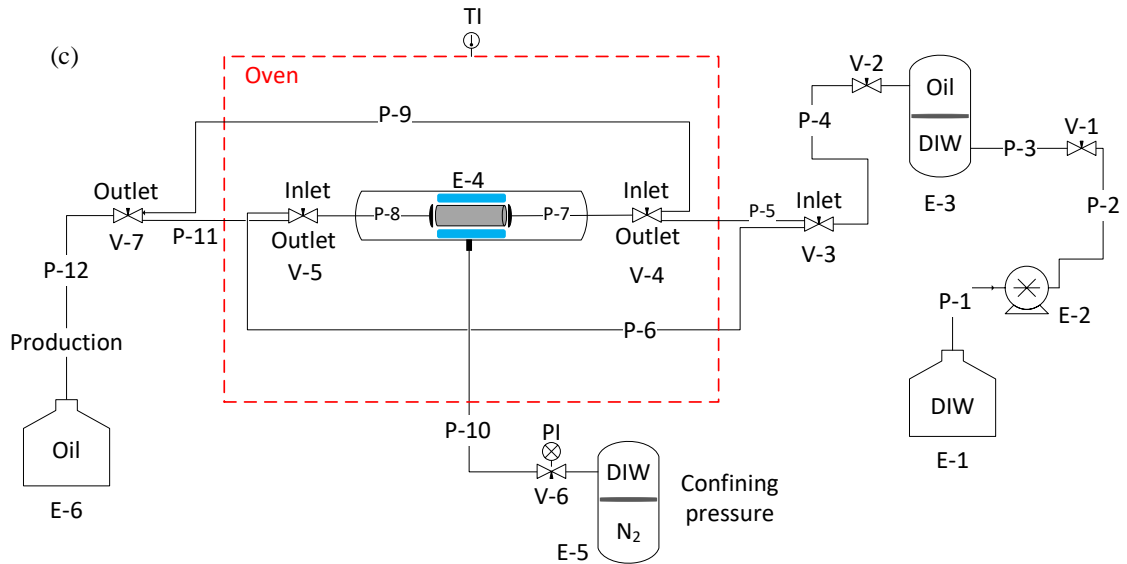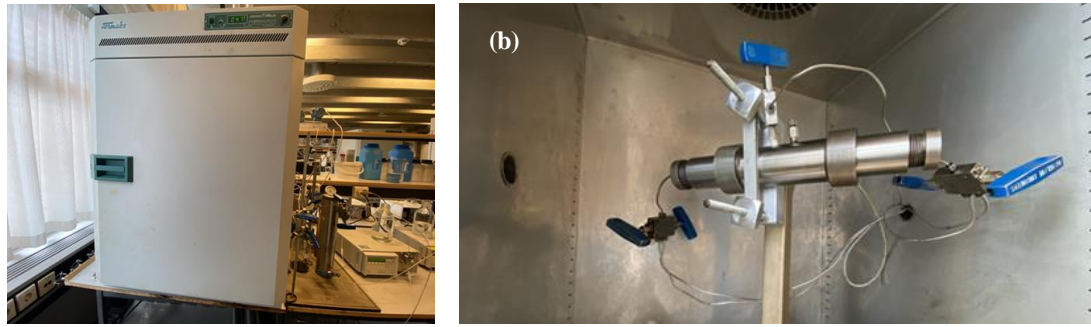
2.2.12.8 Core ageing

Before measuring the weight of the cores as a reference, excess oil on their surface was thoroughly cleaned with a tissue. The oil-saturated cores were then placed in HPHT ageing cells with two small marble balls at the bottom and were filled with oil collected from the oil saturation step. The cells were then closed and placed in an oven of 75 °C for two weeks for ageing to reduce water-wetness (Figure 2.28).

Figure 2.28. (a) Crude oil-saturated core with $S_w = 10\%$, (b) cores in ageing cells in an oven of 75 °C.

(a)

(b)
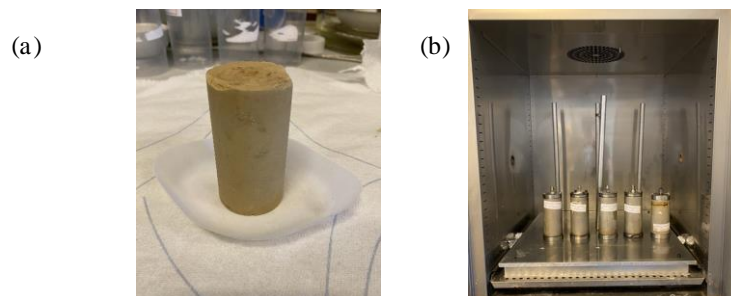
2.2.12.9 Spontaneous imbibition tests

The aged cores were removed from the oven after two weeks and allowed to cool to room temperature. They were weighed after being wiped with a tissue to remove any extra oil

70

from the surface. The weight of the original oil in place (OOIP) was calculated by comparing core weights before and after oil saturation and converted to volume using crude oil density (0.81 g cm^{-3} at 25 °C).

Figure 2.29 shows the setup used for the spontaneous imbibition test. The setup includes an HPHT steel imbibition cell, a large transfer cylinder with a pressure gauge, a burette and valves/tubing as required. The cores were placed in imbibition cells with two small marble balls at the bottom to allow imbibition from all directions. The cells were filled with imbibition fluids and the transfer cylinder containing 1 L of the imbibition fluid pressurized to 10 bar using N$_2$ fed the imbibition cell during the oil production reading.

After setting up different parts, 24 h at room temperature was allowed to ensure that the system is leak-free. On the next day, the oven was turned on at 75 °C and air removal was performed after a few hours through the outside valve. The oil production was recorded daily by a burette. The recovery factor (*RF*) and imbibition rate were calculated by:

$$RF \ (\%) = \frac{cumulative \ oil \ production}{OOIP} \times 100 \qquad (2.20)$$

$$Imbibition \ rate \ (\frac{mL}{d}) = \frac{oil \ production}{time} \qquad (2.21)$$

The imbibition tests were performed in both secondary and tertiary modes.

Figure 2.29. Photos and scheme of the setup used for spontaneous imbibition test. P, V and E refer to pipelines, valves and equipment used in the setup, respectively. TI and PI are temperature and pressure indicators, respectively. The red dashed box is the oven.
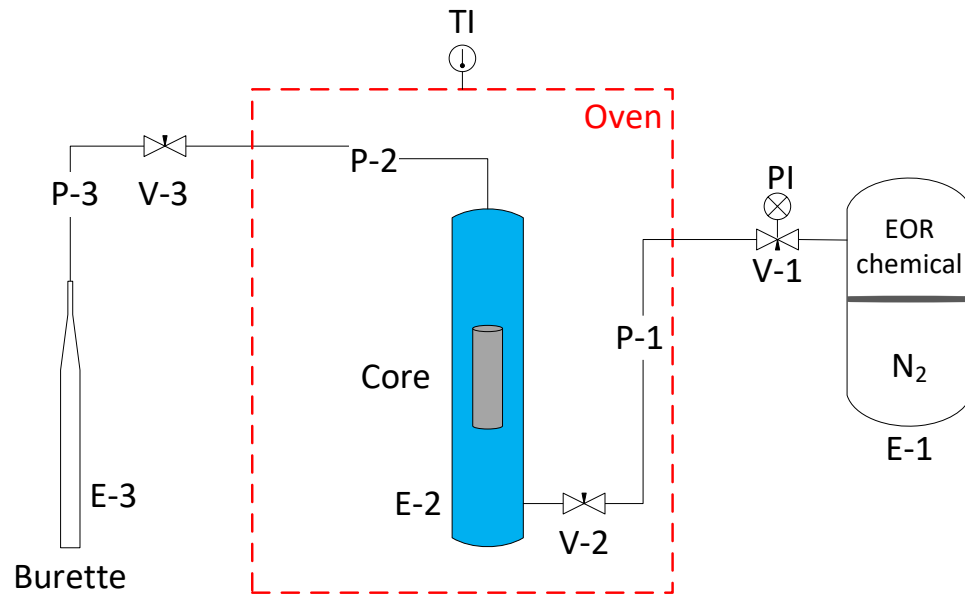
2.2.12.10 Dynamic adsorption of chemicals onto rock during flooding

2.2.12.10.1 Surfactant

Candidate dispersions/solutions for imbibition tests were considered for this investigation. The extent of adsorption of AHS or ZN onto cores with/without ES-coated silica was inspected in flowing mode. The previous core flooding setup was equipped with an N_2 back pressure regulator (BPR) and autosampler (Figure 2.30). The core cannot produce until the injection pressure is equal to the back pressure (10 bar) which aids in pressurisation and pressure stability during flooding.

After cleaning the setup, the tubing and valves were flushed with Permian brine. The clean cores (no oil) were weighed and placed in a sleeve in the core holder using a vacuum. The two transfer cylinders 1 and 2 were filled with Permian brine and appropriate dispersion/solution. The air was removed from cylinders and tubing by allowing the pump to inject a few cm^3 before turning on the oven at 75 °C. With all valves inside the oven and bypass valves open, Permian brine was first injected to the core at 0.5 cm^3 min^{-1} at 75 °C with a back pressure of 10 bar, a confining pressure of 18 ± 1 bar and a pressure

limit of 20 bar. After around 1.35 PV injection, the first droplet of brine was observed in the outlet when the injection pressure reached ~10 bar. The flow rate was then reduced to 0.1 cm^3 min^{-1} and allowed to inject a few cm^3 before closing the bypass valves. Permian brine injection was performed for 7 PV (~280 cm^3) to equilibrate the rock surface with ions. The injection of AHS or ZN in Permian brine with or without ES-coated silica was then performed with the same settings for 5 PV (~200 cm^3). Injection pressures, differential pressures and temperature were recorded with time (or injected PV) in the above stages. The autosampler connected to the outlet of the setup was set to sample from production every 80 min (8 cm^3 samples). The surface tension of samples was then measured at 25 °C using the du Nouy ring tensiometer to investigate the amount of surface-active agent in the samples. The core was removed from the core holder after cooling to room temperature and weighed after drying the excess surface fluid.

2.2.12.10.2   ES-coated silica

In addition to inspecting the static stability of ES-coated silica in glass vials, the particle stability was inspected in porous media during flooding. An empty clean core was flooded by first Permian brine (7 PV) and then a dispersion of 0.01 wt.% ES-coated silica in Permian brine (3 PV) at 75 °C with the same procedures as described before. Pressure differences were monitored for detecting any blockage of the pore throats which is shown as pressure build-up.

Figure 2.30. (a) Photos and (b) scheme of core flooding setup. P, V and E refer to pipelines, valves and equipment used in the setup, respectively. TI and PI are temperature and pressure indicators, respectively. DP is a differential pressure transmitter and BPR is a back pressure regulator. The red dashed box is the oven.

(a)
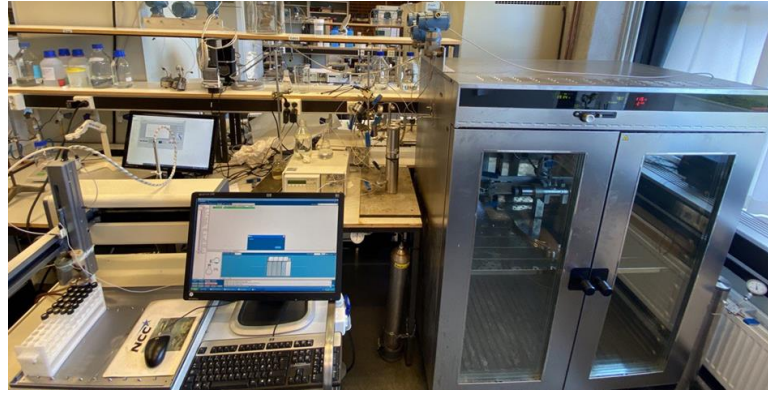
(b)
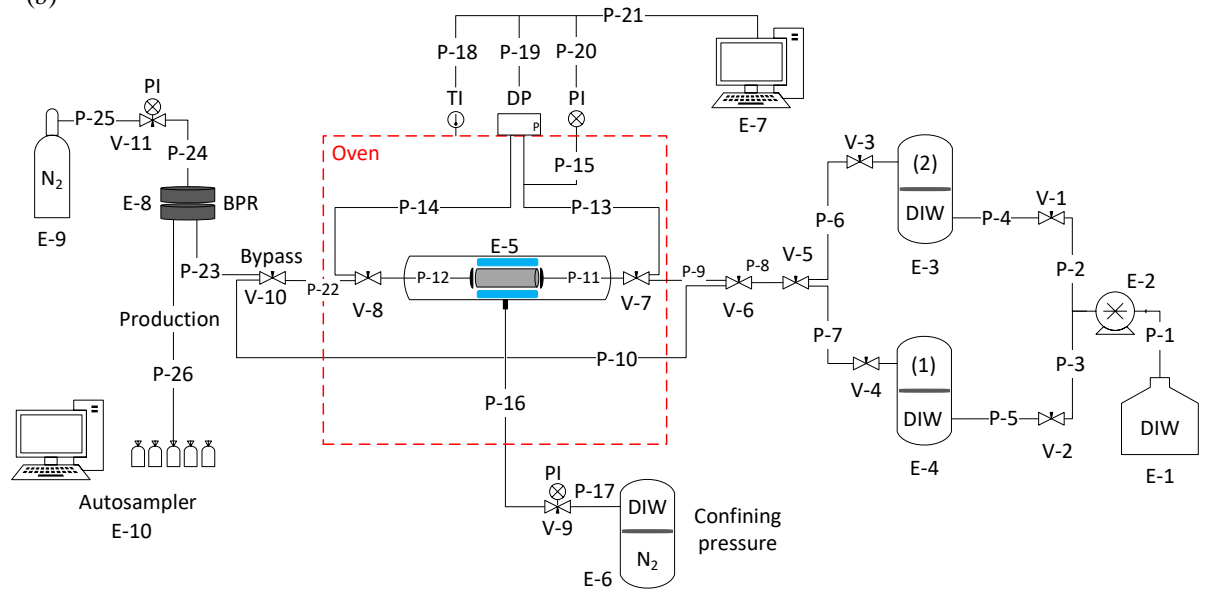
Chapter 3 Properties of crude oil, surfactant, particles and rock

This chapter reports on the properties of the main chemicals involved in the EOR process including crude oil, surfactants, particles and rock. This initial characterization helps with understanding the behaviour of the materials in different systems of oil-water, oil-rock and water-rock in subsequent experiments.

3.1 Properties of crude oil

Understanding the behaviour and properties of crude oil is essential for optimizing chemical EOR methods. Table 3.1 presents the specifications of the Permian crude oil sample sent by ChampionX. According to the SARA (saturates, aromatics, resins and asphaltenes) analysis of the crude oil based on the extraction method, the crude oil is mostly paraffinic, with a low content of asphaltene (1 %) and polar chemicals (1.4 %). The total acid and base numbers are significant because they indicate the degree of oil-wetness of the reservoir rock.[154] They are both low here indicating that the oil is not highly polar which agrees with the SARA analysis. Furthermore, it is observed that the polar acidic groups in crude oil are relatively lower than the basic groups.

Table 3.1. Specifications of crude oil.

Property	Value	Units
Polar (resin)	1.4	
Aromatic	9.4	
Paraffin	32	%
Asphaltene	< 1	
Total acid number	0.25	
Total base number	0.45	mg KOH g^{-1}
pH at 25 °C	7.5 ± 0.2	–
Density at 25 °C	0.8133	g cm^{-3}

The density of crude oil shows a light crude oil with a density close to that of water. This implies that a normal chemical EOR strategy seems to be enough for this reservoir without the need for thickeners like polymers. However, due to the small pore throats usually found in tight oil reservoirs and subsequently high capillary pressures, the trapped oil would be high necessitating EOR with surfactants.[155]

3.2 Properties of surfactants

Zwitterionic surfactants are known for their wide isoelectric range, perfect water solubility, stability in a wide range of pH values, stability in high salinity brine and their ability to solubilize both polar and non-polar compounds. However, they should be carefully characterised before being used in an EOR strategy.[156]

3.2.1 Thermal and salinity tolerance

Figure 3.1 shows the appearance of surfactant solutions. The surfactants did not show any precipitation in Permian brine after a month at 100 °C.

For the thermal tolerance, TGA was performed on surfactants. TGA is usually accompanied by a differential thermogravimetry (DTG) curve which is produced as the first derivative of the weight with relative to temperature or time. DTG facilitates change visualisation and identifies inflection points for detailed interpretations. Figures 3.2 and 3.3 show the TGA-DTG of surfactants initially and after 30 d standing at 100 °C. The results show a small weight loss up to 150 °C (due to the water removal) followed by a more significant weight loss (at > 270 °C) due to the oxidation of hydrocarbon groups of the tails for both surfactants. When the organic molecules react with oxygen from airflow at high temperatures, oxides such CO_2, H_2O, and CO are produced which is referred to as combustion or combustion-like oxidation. The same small weight loss and subsequent larger weight loss are also observed when TGA was performed on the samples standing at 100 °C for a month. Overall, excellent thermal stability up to 150 °C (less than typical reservoir temperature) is shown with both surfactants. Therefore, both are tolerant of reservoir temperatures for EOR operations.

Figure 3.1. Appearance of 0.1 wt.% AHS or ZN surfactant in DIW and Permian brine after standing at 100 °C for a month.
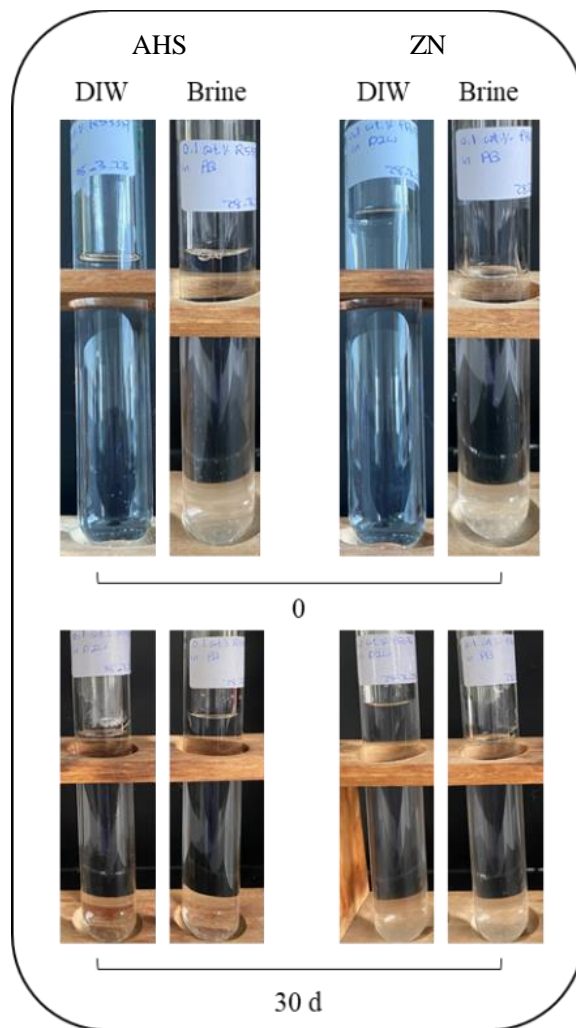
Figure 3.2. Initial and long-term TGA and DTG of AHS surfactant. The long-term TGA was performed on 0.1 wt.% surfactant in DIW after standing at 100 °C for 30 days.

Figure 3.3. Initial and long-term TGA and DTG of ZN surfactant. The long-term TGA was performed on 0.1 wt.% surfactant in DIW after standing at 100 °C for 30 days.

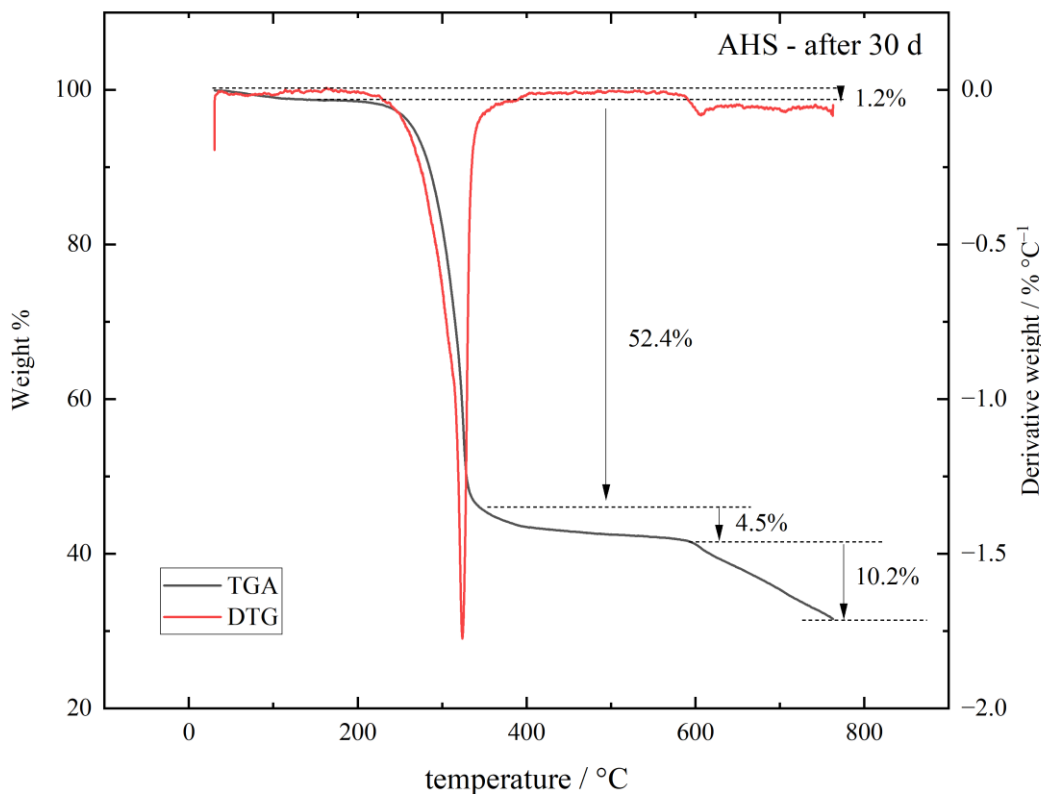### 3.2.2 Micelle charge

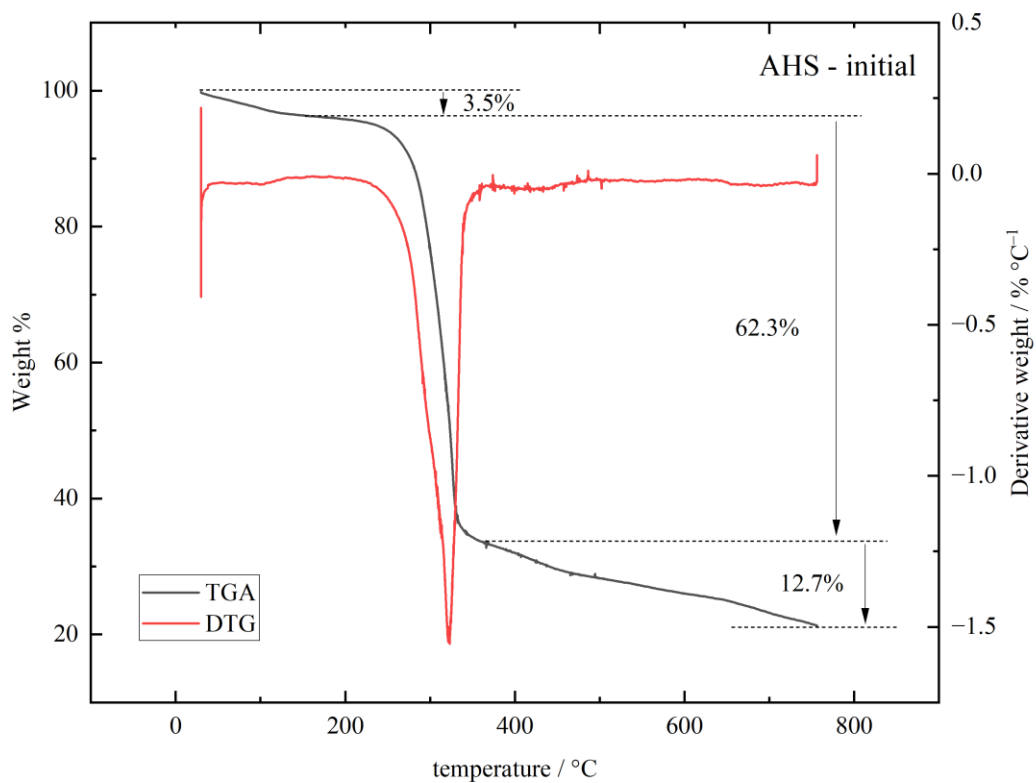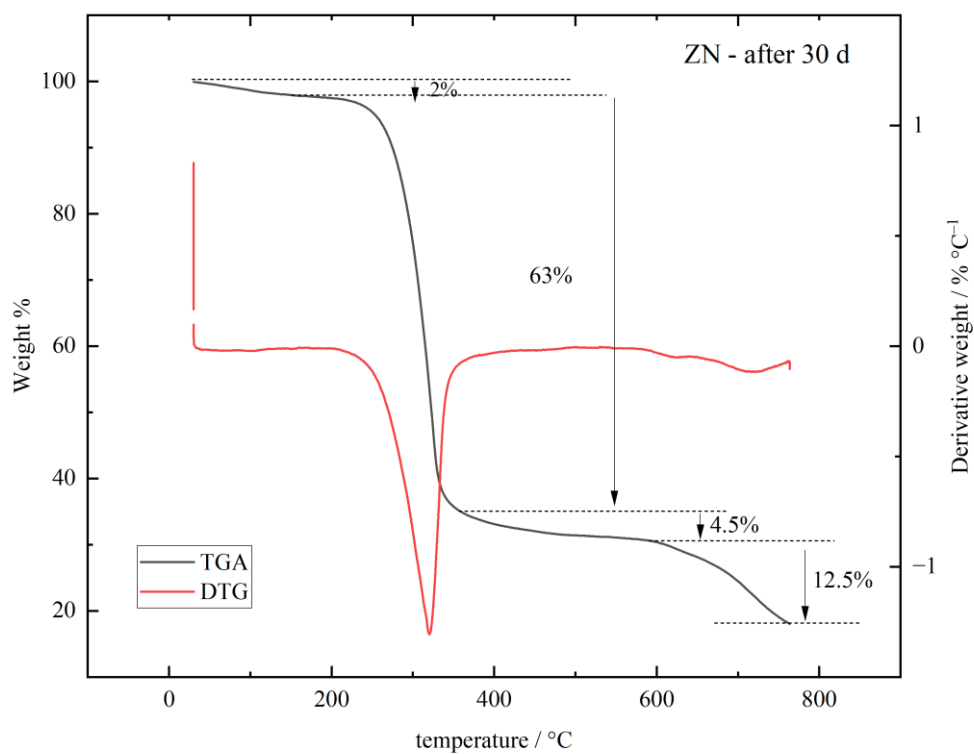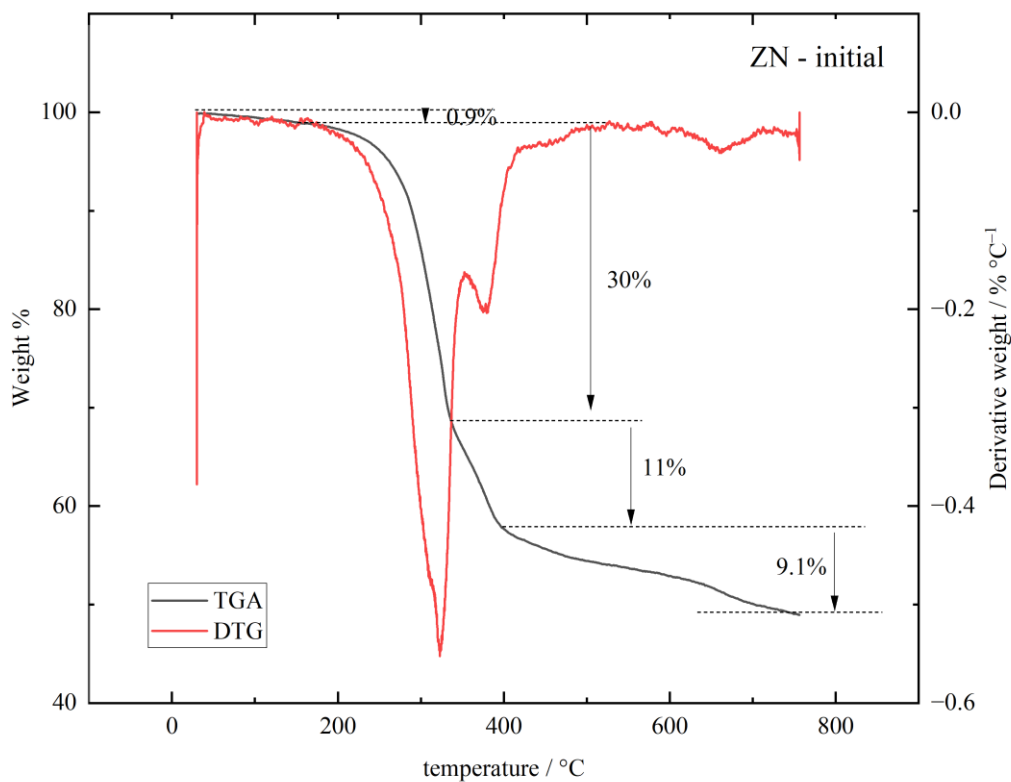The headgroup charge and the overall stability and solubility of zwitterionic surfactants are influenced by pH. The headgroup charge may influence the surfactant ability to interact with rock, oil and water and to alter the interfacial tension between these

phases.[157] The alkyl hydroxysultaine surfactant used in this study as AHS is a type of zwitterionic surfactant that contains an alkyl chain and a quaternary ammonium group which is attached to a sulfonate group by isopropyl alcohol as a spacer. ZN however is a binary mixture of AHS and a minor amount of nonionic $C_{10-12}E_9$ surfactant. In this study, the zeta potential of surfactant micelles was measured to determine the charging behaviour of AHS and ZN surfactants with pH. A preliminary investigation was performed with zeta potential measurements of different concentrations of surfactant in DIW for selecting a suitable concentration (see Appendix A.1). Figure 3.4 shows the zeta potentials of AHS and ZN in DIW at concentrations well above CMC at different pH values. The AHS surfactant shows a net zero charge at a pH of 5.5 – 8.0 at 25 °C while this region is narrower for the ZN surfactant (pH = 7.5 – 8.4). In these regions, the headgroup of the surfactants is neutral with the positive charge of the ammonium being balanced by the negative charge of the sulfonate group. Below this range, both surfactants showed a more positive charge because of the protonation of the sulfonate group which leaves the cationic quaternary ammonium determining the headgroup charge. At high pH, due to the deprotonation of the sulfonate group, the negative charge of the surfactant headgroup becomes dominant which renders the surfactant weakly anionic. Similar observations have been made before on the charging behaviour of zwitterionic surfactants with pH.[116, 158, 159] In addition, ZN has relatively lower zeta potential values due to the presence of nonionic surfactant monomers in alkyl hydroxysultaine micelles. It is noted that zeta potential measurements of surfactants in Permian brine were not possible due to the instrument limitations with high ionic strength solutions.

Figure 3.4. Zeta potential measurements of AHS and ZN surfactants in DIW at different pH values at 25 ± 0.1 °C. The concentration of surfactant is 0.1 wt.%.
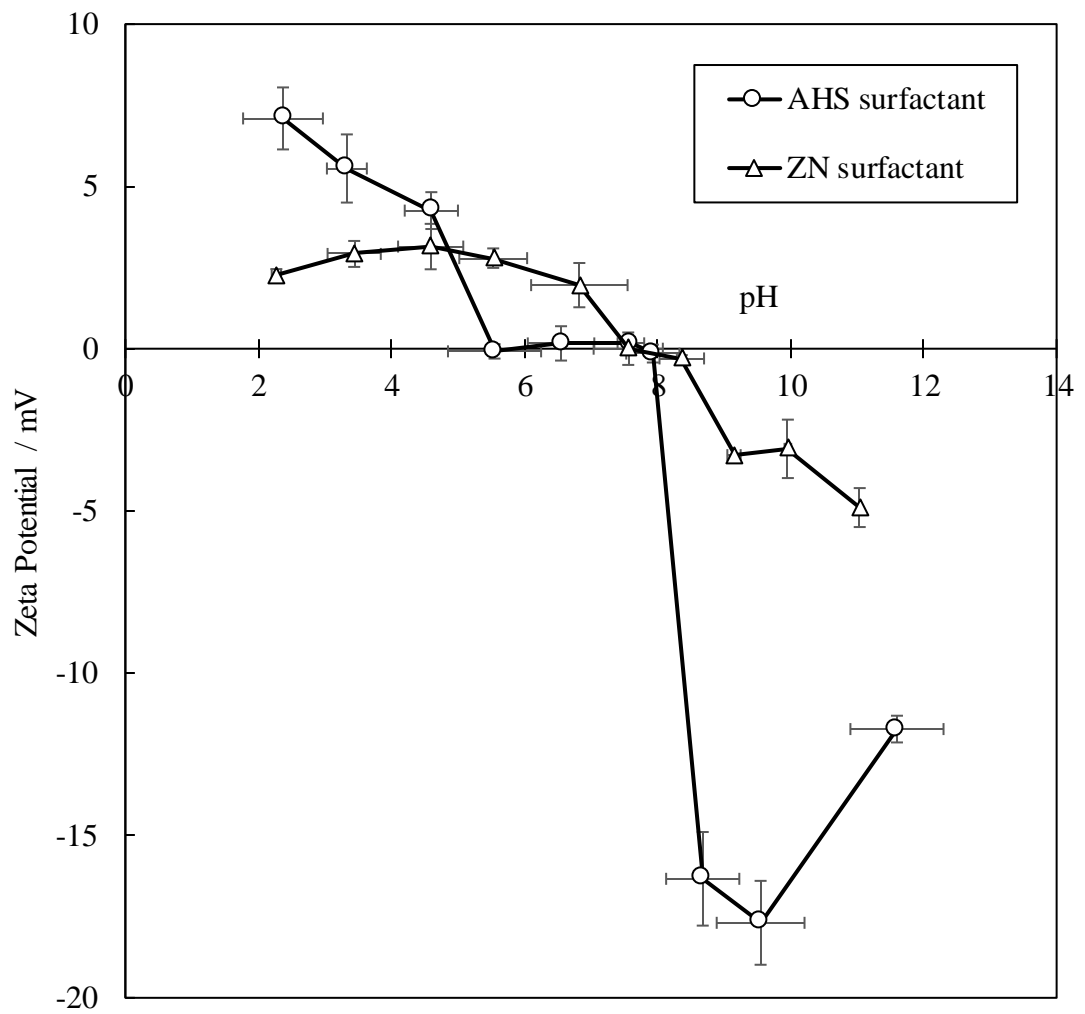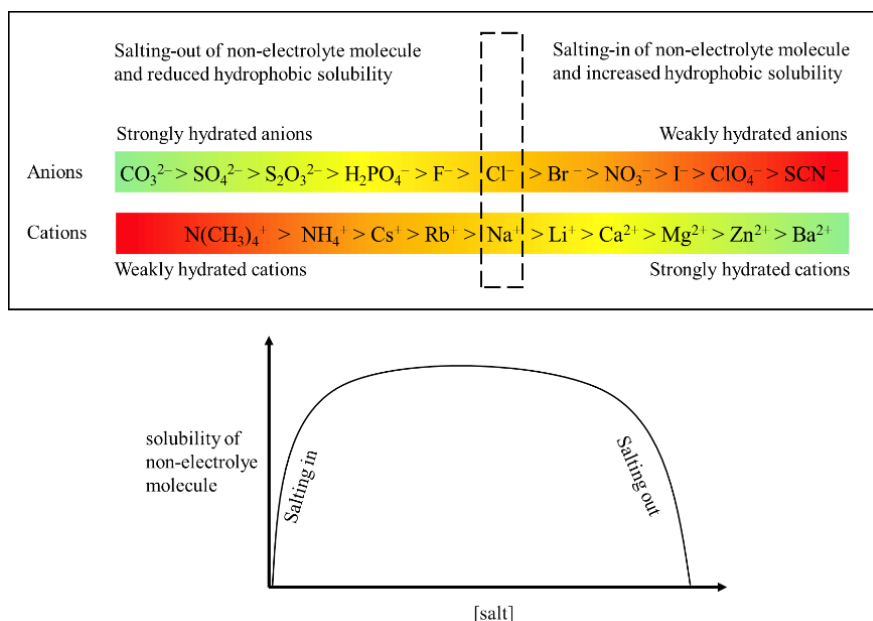
3.2.3 Air-water surface tension

3.2.3.1 Effect of electrolyte

Ions can have a significant effect on the air-water surface tension due to their interactions with interfacial water molecules which disrupt hydrogen bonding. The Hofmeister series (Figure 3.5) is widely used to investigate the effect of ions on surface tension by dividing them into water structure makers (well-hydrated ions with a high ionic charge (Z) to radius (R) ratio) and water structure breakers (poorly-hydrated ions with a low Z/R ratio).[160] Therefore, anions like CO_3^{2-} are least likely to lower the surface tension because of their strong hydration whereas I^- and Br^- can significantly adsorb to the air-water surface to reduce the surface tension.[161] In addition, cations are more effective in surface tension reduction than anions.[5, 160] In this study, the surface tension of DIW was measured as 72 ± 0.1 mN m^{-1} at 25 °C (consistent with the literature[162, 163]) which was increased to 74.3 ± 0.2 mN m^{-1} on adding Permian salts. Langmuir argued that this increase is due to the depletion of ions close to the air-water surface[164] which was later explained by the electrostatic repulsion between ions and their images at the air-water surface[165] and repulsion from the Gibbs dividing surface due to the ionic hydration.[166] All these theories are mainly true for a single salt solution at low concentrations of < 1 M. Nevertheless, the strong electrolyte (2.1 M) used here is a mixture of different ions that is expected to create a complex arrangement of ions at the air-water surface that depends on several factors, such as the relative concentration of ions, pH and temperature making simplified Hofmeister model efficient.

Figure 3.5. The Hofmeister series and ion hydration effect on the solubility of non-electrolyte molecules.

The air-water surface tensions of different concentrations of AHS and ZN surfactants in DIW and Permian brine at 25 °C are presented in Figure 3.6. For zwitterionic AHS, no

change in surface tension is observed on adding brine mainly due to the charge neutrality of the headgroup as observed by previous authors.[167, 168] The addition of Permian salts impacts the air-water surface tensions of ZN solutions. At very low ZN concentration, the surface tension of the surfactant in brine is higher than that of DIW while close to the CMC it is reversed. It is thought that it is the nonionic $C_{10-12}E_9$ in ZN that lowers the surface tension around the CMC when adding salts due to the salting-out effect.[169] It is hypothesised that at low ZN concentrations, ions dominate the few adsorbed surfactant monomers at the air-water surface resulting in higher surface tension while a lower surface tension is achieved ~ CMC where more surfactant monomers adsorb.

The presence of salts can affect the CMC of surfactants and thus their tendency to form micelles. The CMC of AHS in DIW and Permian brine at 25 °C was 0.01 wt.% and 0.005 wt.%, respectively while that of ZN was 0.02 wt.% and 0.003 wt.%, respectively. The specific effect of the salts on micellization can depend on the type and concentration of the salts, as well as the chemical structure and charge of the surfactant. Considering cationic and anionic surfactants, the addition of inorganic counterions shrinks the electric double layer around the headgroup which subsequently lowers the electrostatic repulsion between headgroups and provides easier micellization at lower monomer concentrations.[170] This electrostatic effect is expected to be absent for nonionic and zwitterionic surfactants with no charge and zero net charges in the isoelectric region, respectively. It is indeed the salting-in and salting-out of the hydrophobic group which mostly contributes to the CMC alteration of these surfactants.[171, 172] The solubility of zwitterionic and nonionic surfactants decreases with increasing electrolyte concentration. The salting-out effect terminates the initial hydration structure of the hydrophobic group of these surfactants, promoting the surfactant hydrophobic ability for easier micellization. The larger the electrolyte concentration, the lower the CMC. Ions with high hydration ability can salt out the hydrophobic group of these surfactants and lower the CMC while less hydrated ions can salt in the hydrophobic groups to raise the CMC.[5] The total impact of salts on surfactant is thought to be the combination of their effects on both the hydrophilic group and hydrophobic group in monomeric (both groups are affected) and micellar forms (only the headgroup is affected). Thus, the hydrophobic group in monomer form is important for solubility. For zwitterionic and nonionic surfactants, the following linear relationship between CMC and salinity has been proposed:[173]

$$log\ CMC = -K \times [salt] + C \qquad (3.1)$$

where *K* and *C* are both constants. This equation holds for [salt] < 1 M. For zwitterionic surfactants with a strong dependence of the headgroup charge on pH, the electrostatic

effect may appear at high or low pH where the surfactant turns ionic. Previous studies also show that even at zero net charge pH, zwitterionic surfactants are weakly anionic for two main reasons. First, the negative charge of the headgroup is located on the end of the molecule and the positive group is in the middle part which makes the charge density more concentrated in the negative part. Second, it is mostly the anionic group that interacts with inorganic cations in micellar form. Thus, electrostatic contribution, in addition to the strong effect of salting out, plays a role in lowering the CMC of zwitterionic and nonionic surfactants even at neutral charge pH. Cations with a low valence-to-radius ratio (Z/R) and a low hydrating radius are more efficient at placing between the headgroups in micelles and weakening the electrostatic repulsion for more favourable micellization.[174]

Figure 3.6. Equilibrium air-water surface tension as a function of (a) AHS and (b) ZN concentration in DIW and Permian brine at 25 ± 0.2 °C. The horizontal dashed and dotted lines show the surface tension of pure DIW and Permian brine, respectively. The vertical red dashed lines show the CMC. The standard deviations are less 0.1 mN m^{-1}.
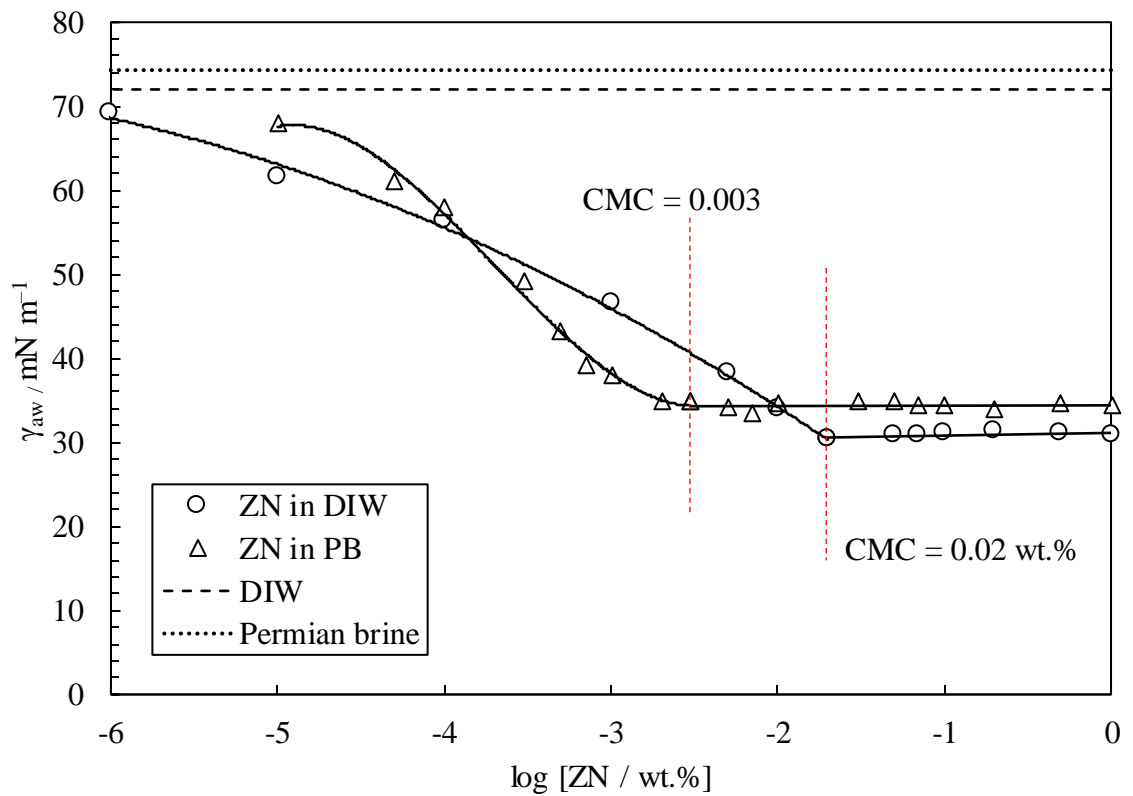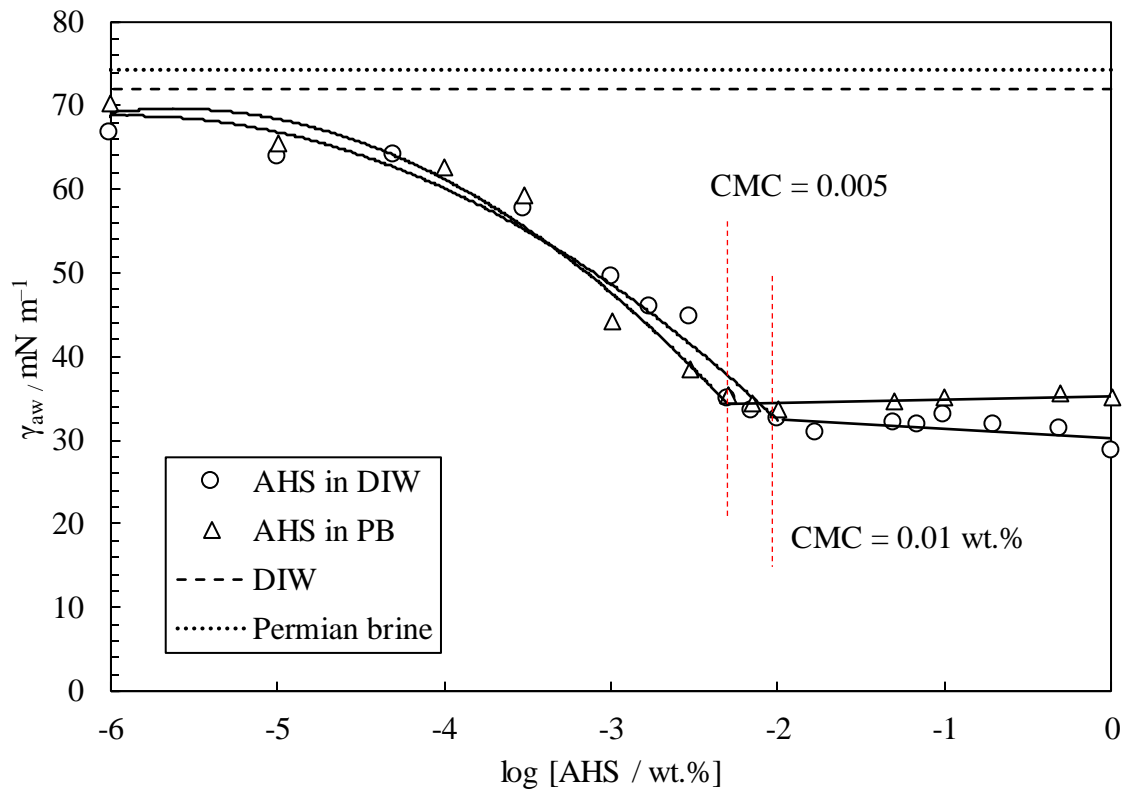
Figure 3.7 shows the surfactant adsorption at the air-water surface below the CMC for AHS and ZN in DIW and Permian brine, respectively. Surface excess concentration increases with surfactant concentration in DIW and Permian brine for both surfactants as more and more surfactant molecules adsorb at the air-water surface until a maximum (Γ_m)

at around the CMC is reached. Salts can considerably impact equilibrium surfactant behaviour by affecting the CMC, equilibrium surface tension and aggregation number. The presence of salts reduces the electrostatic repulsion between surfactant headgroups at the air-water surface providing a more compact monolayer at the air-water surface. Therefore, higher surfactant adsorption at the air-water surface is expected in the presence of salts. Here, Permian salts increase the surfactant adsorption close to the CMC which is more significant for ZN, as discussed earlier.[175]

The thermodynamic parameters of the micellization and adsorption of surfactants are presented in Table 3.2. The surface concentration and the area per molecule of both surfactants increase and decrease on the addition of salts, respectively proving higher adsorption and a more compact monolayer in the presence of salt. Overall, the surface concentration of AHS in DIW and Permian brine is higher than that of ZN while its area per molecule is lower. The free energies of micellization and adsorption are all negative indicating that micellization and adsorption are spontaneous for both surfactants. The free energy of micellization increases in magnitude upon adding salt for both surfactants meaning that Permian salts have eased micellization (*i.e.* the process is more spontaneous). AHS in DIW has a higher magnitude of free energy of micellization than ZN in DIW reflecting that AHS forms micelles more readily than ZN. This behaviour is reversed for surfactants in Permian brine. The free energy of adsorption of ZN is higher than that of AHS both in DIW and Permian brine implying that ZN is more surface-active.

Figure 3.7. AHS and ZN surfactant adsorption at the air-water surface as a function of surfactant concentration in DIW and Permian brine at 25 ± 0.2 °C. The vertical red dashed lines show the CMC.
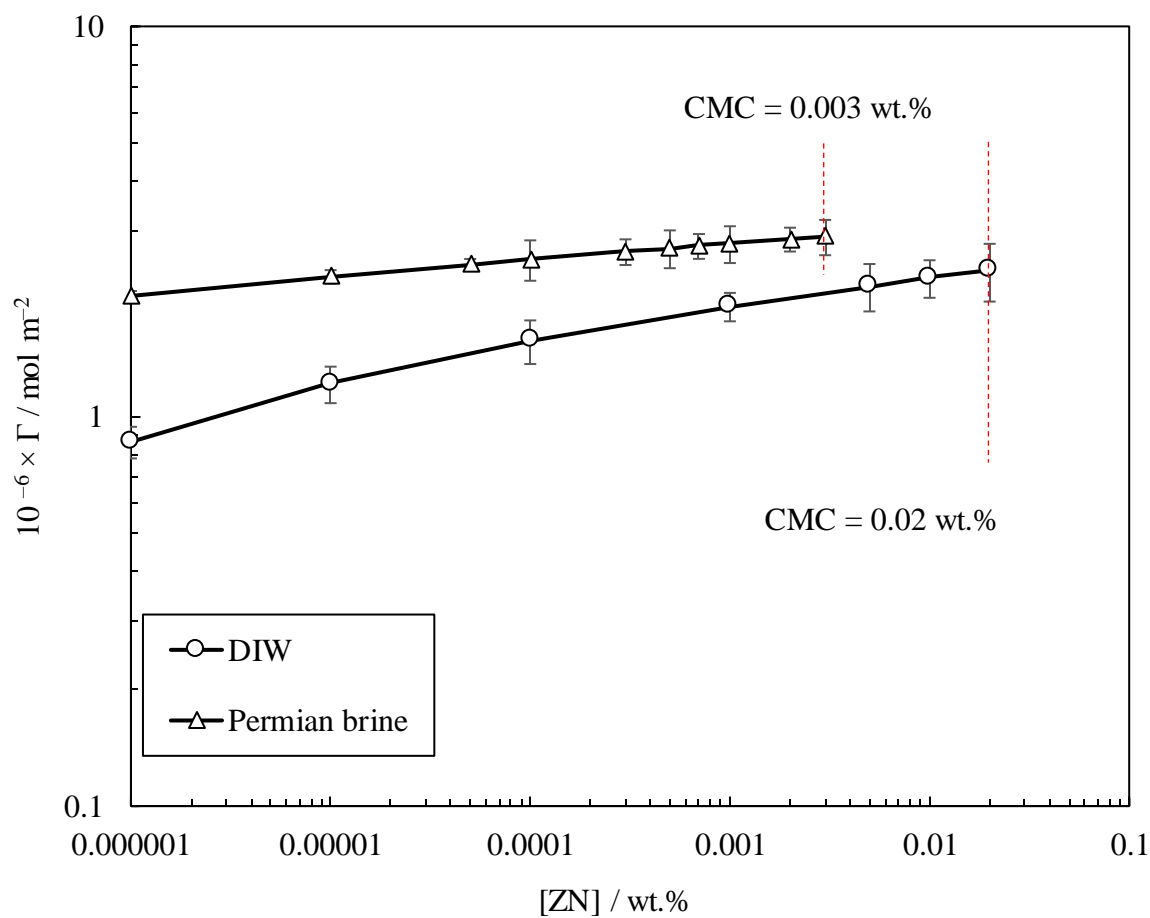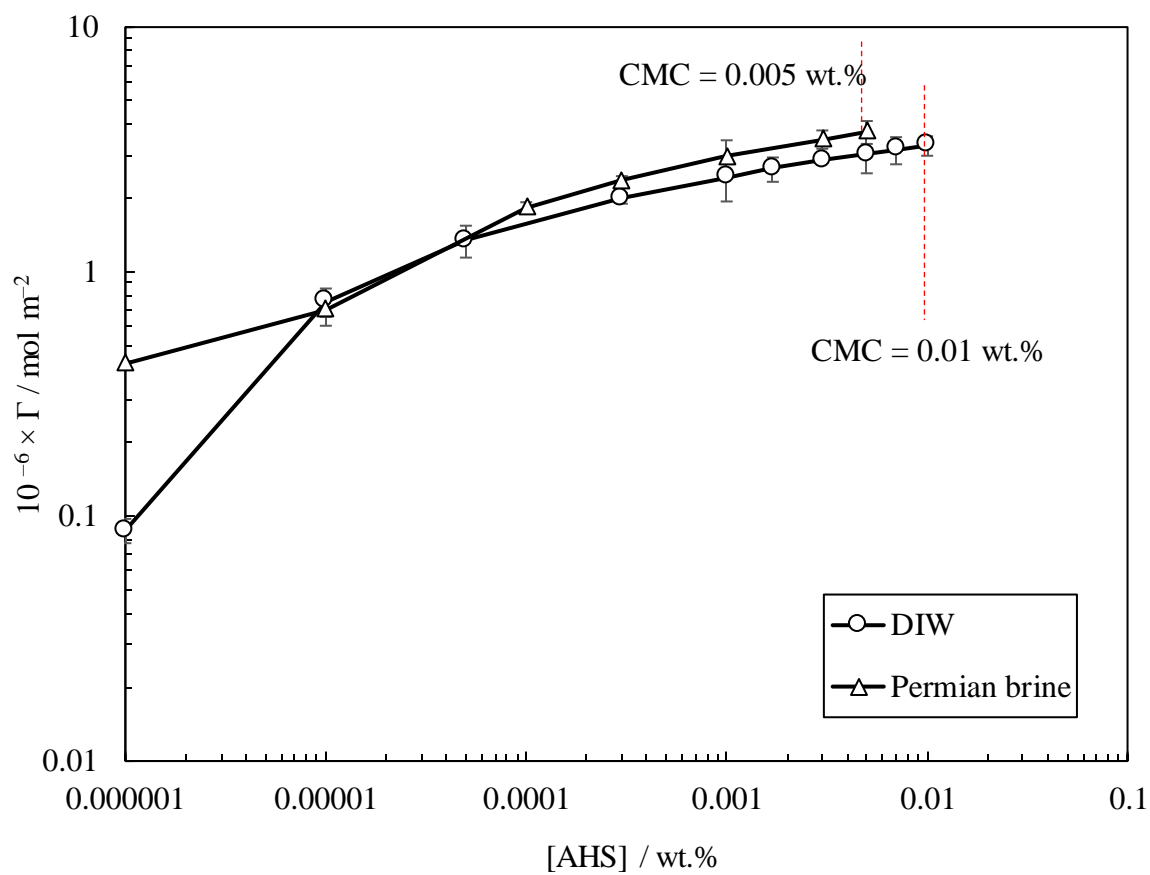
Table 3.2. Effect of adding ES-coated bare silica on thermodynamic parameters of micellization and adsorption of AHS and ZN in DIW and air-water surface, respectively at 25 °C.

Surfactant	[particle] / wt.%	CMC / wt.%	$10^{-6} \times \Gamma_m$ / mol m^{-2}	A / nm^2 per molecule	Π / mN m^{-1}	$-\Delta G^{\circ}_m$ / kJ mol^{-1}	$-\Delta G^{\circ}_{ads}$ / kJ mol^{-1}
AHS in DIW	0	0.01	3.3	0.5	39	20.2	32.3
	0.01	0.02	3.8	0.4	37	18.5	28.1
	0.05	0.025	3.9	0.4	37	17.9	27.4
	0.1	0.03	4.6	0.3	39	17.5	26
AHS in Permian brine	0	0.005	3.7	0.4	37	21.9	31.8
	0.01	0.007	2.8	0.6	35	21.1	33.8
	0.05	0.008	2.5	0.7	37	20.8	35.5
	0.1	0.008	2.3	0.7	37	20.8	36.9
ZN in DIW	0	0.02	2.4	0.7	42	18.5	36.1
	0.01	0.025	2.7	0.6	40	18	33.2
	0.05	0.03	2.7	0.6	41	17.5	32.8
	0.1	0.03	2.7	0.6	43	17.5	33.4
ZN in Permian brine	0	0.003	2.8	0.6	37	23.2	36.1
	0.01	0.006	2.3	0.7	37	21.5	37.5
	0.05	0.008	1.5	1.1	38	20.8	46
	0.1	0.008	2.3	0.7	37	20.8	36.8

3.2.3.2   Effect of surfactant type

Figure 3.6 also compares the effect of surfactant type on air-water surface tensions with and without Permian salts at 25 °C. The surface tensions at the CMC are the same for both surfactants in DIW but they increase on the addition of Permian salts. Although the CMC of ZN in DIW is higher than that of AHS, the CMCs are nearly the same in the presence of Permian salts. ZN caused a lower air-water surface tension < CMC than AHS both in DIW and Permian brine due to the presence of nonionic C_{10-12} nonaethylene glycol ether in ZN. Mulqueen and Blankschtein compared the air-water surface tensions of a 1:1 mixture of a zwitterionic n-dodecyl-N, N′-dimethylamino betaine (C_{12}betaine) and a nonionic n-dodecyl-β-D-maltoside (C_{12}maltoside). They discovered that nonionic surfactants have lower surface tensions than zwitterionic surfactants. There is no synergism (*i.e.* increased surface activity) with the binary mixture since the surface tensions of the mixture lie between those of the individual surfactants.[176] Hines *et al.* reported that raising the C_{12}betaine surfactant concentration when blended with nonionic C_{12}maltoside increases the air-water surface tension of the mixture.[177] Since the concentration of nonionic surfactant in ZN is minor (5 wt.%), a significantly lower surface

tension by ZN is not expected. AHS forms a monolayer of zwitterionic alkyl hydroxysultaine at the air-water surface whereas the monolayer formed by ZN is expected to be a mixture of alkyl hydroxysultaine and nonionic $C_{10-12}E_9$ (Figure 3.8). This monolayer becomes more complex with the addition of inorganic counterions. Figure 3.7 shows the effect of the surfactant type on the surface excess concentration of surfactants. ZN has a higher surface excess concentration in both DIW and Permian brine at low surfactant concentration whereas it is reversed close to the CMC but the difference is negligible.

Figure 3.8. Schematic representation of surfactant monolayer at the air-water surface for AHS (top) and ZN (bottom) surfactants in DIW and Permian brine at isoelectric region.
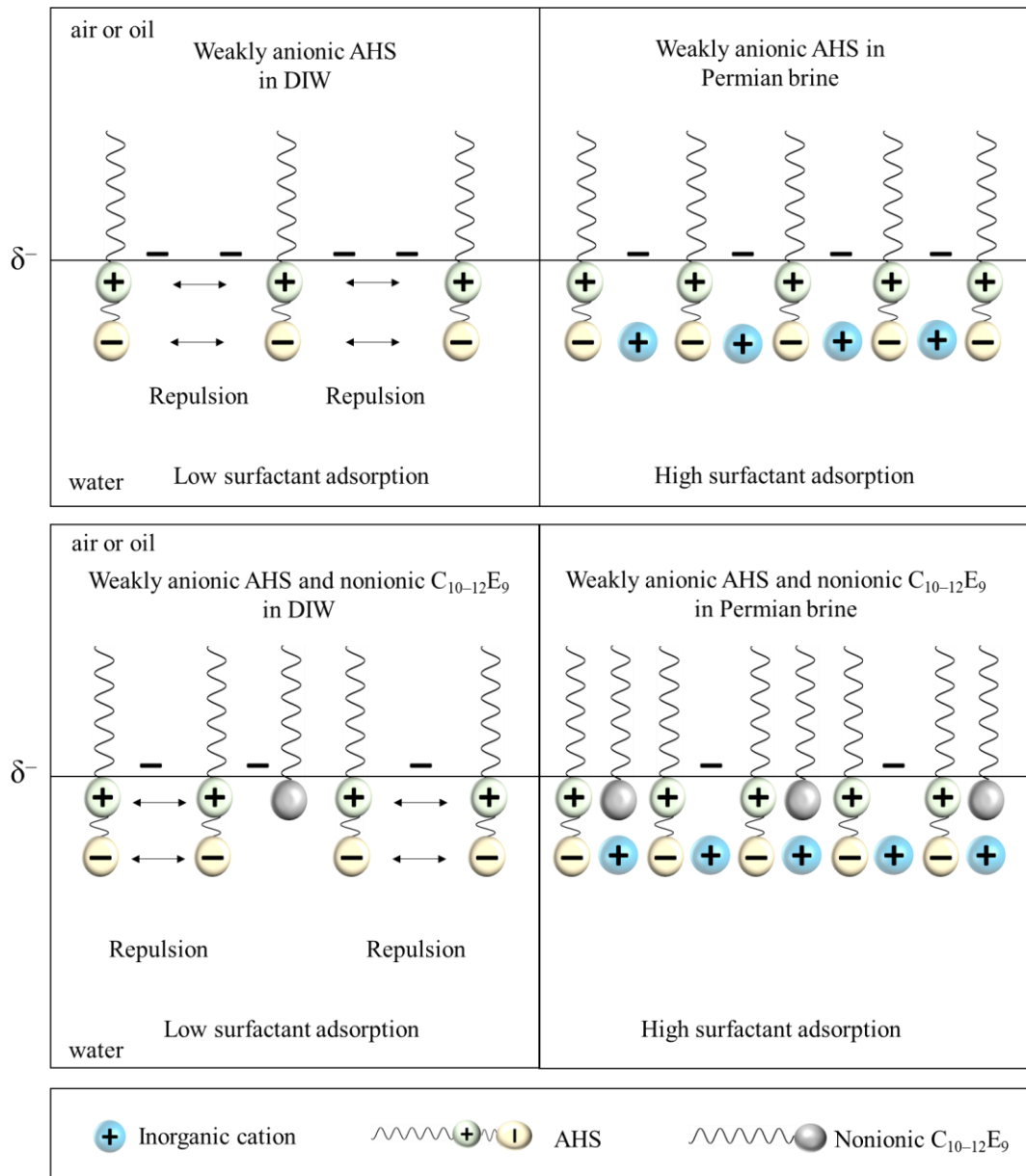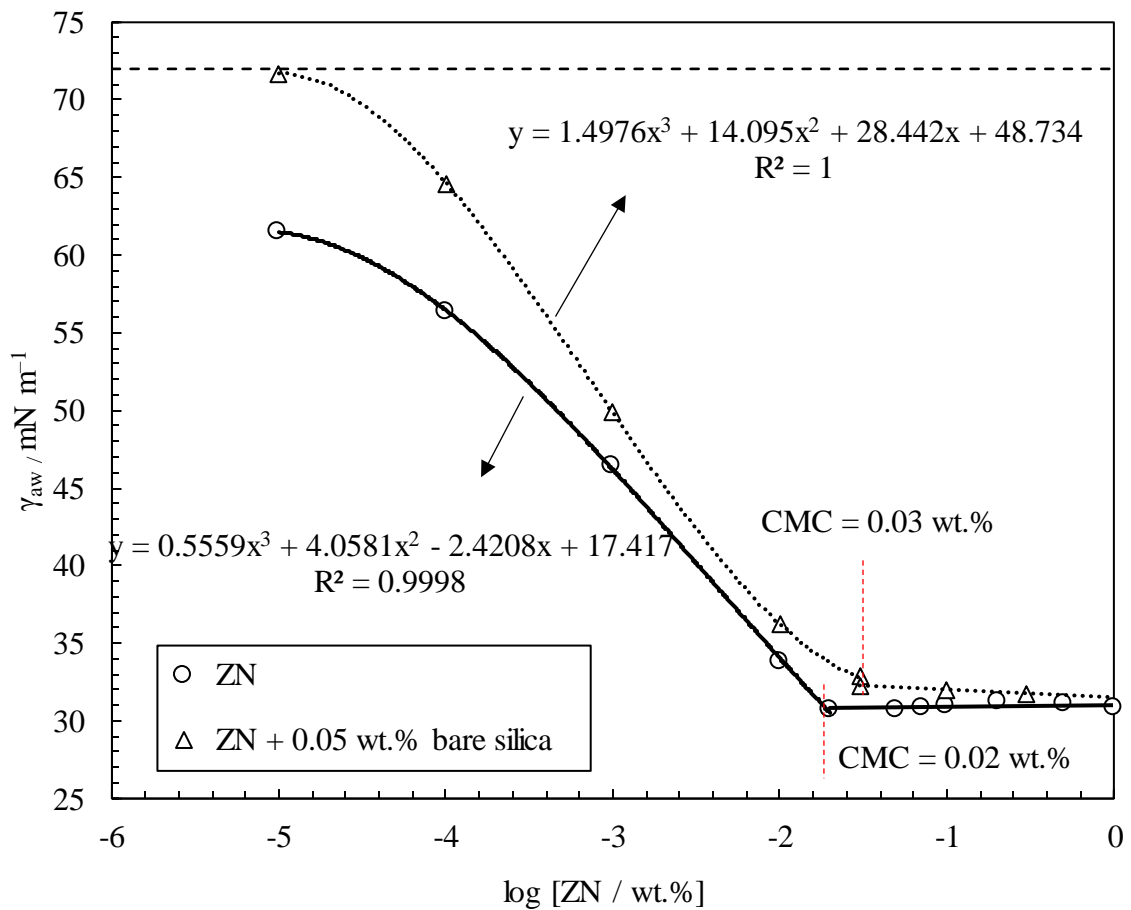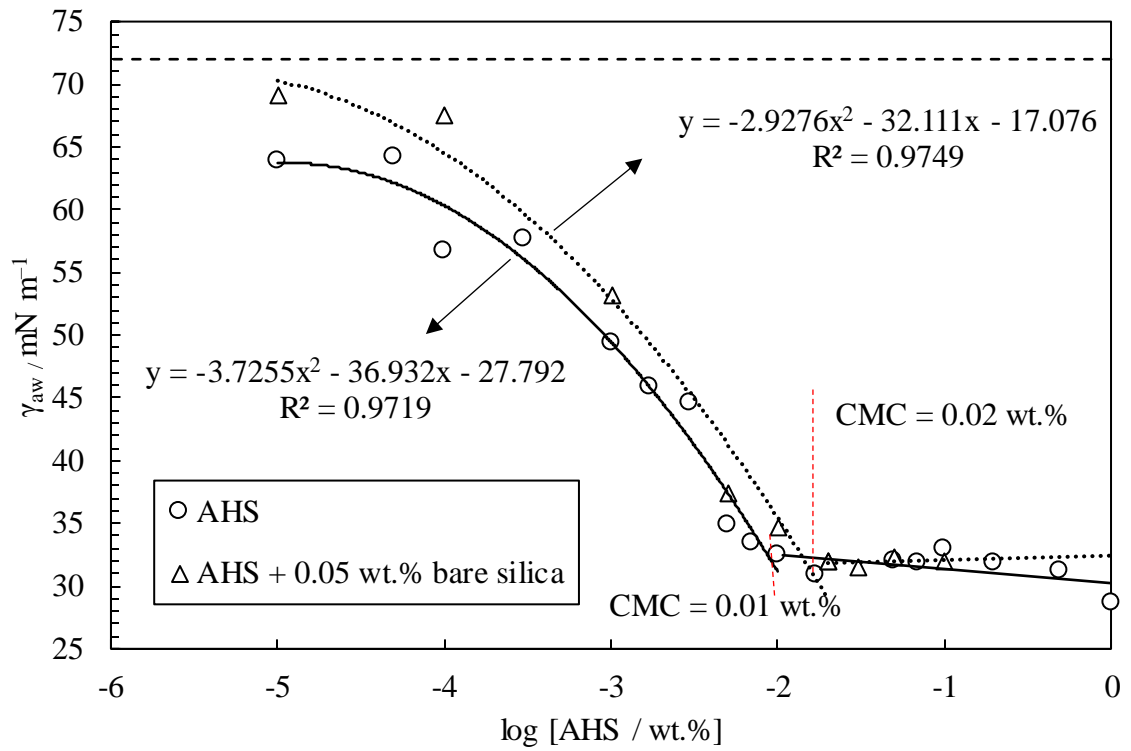
3.2.3.3.1 Bare silica

In any adsorption process between an adsorbent and an adsorbate, there are four main types of interactions: hydrophobic bonds, π electron polarization, van der Waals London dispersion forces and electrostatic interactions. These interactions are not present in all systems and are highly dependent on the type of adsorbent and adsorbate used.[178] Of these interactions, electrostatic interactions are considered strong. Bare hydrophilic silica is not expected to reduce the air-water surface tension due to the lack of surface activity and the electrostatic repulsion between particles (pH > 3) and the air-water surface.[179] For blends of ionic surfactants and charged bare particles in DIW, electrostatic repulsion or attraction between surfactant and particles can develop depending on charges.[180] Figure 3.9 shows the effect of adding 0.05 wt.% bare silica on the surface tensions of AHS and ZN in DIW. The addition of bare silica to both surfactant solutions increased the air-water surface tension (more so for ZN), implying an electrostatic attraction between anionic silica and cationic quaternary ammonium of the surfactant leaving less free surfactant molecules to adsorb at the air-water surface. The interactions between bare silica and zwitterionic surfactant are thought to be weak at the isoelectric region (pH = 5.5 – 8.0 at 25 °C) in comparison to cationic surfactants. For the nonionic surfactant available in ZN, hydrogen bonding between the surfactant headgroup and particle surface is also possible. The addition of particles to surfactant solutions also increases the CMC of the surfactant. The surface tension measurements of blends of bare silica and surfactants in Permian brine were not possible due to the lack of dispersion stability in the brine.

Lee *et al.* studied the effect of hydrophobization of silica on the particle monolayer at the air-water surface. They claimed that physical grafting of silica with cationic surfactants hydrophobized the particles with amphiphilic features at the air-water surface capable of reducing surface tension. The lower the chain length, the stronger the packing of particles.[181] Therefore, it is thought that along with free surfactant molecules, the grafted particles also adsorb at the air-water surface and have a role in reducing the surface tension. This grafting is essential in EOR processes where the goal of blending particles and surfactant is to prevent the surfactant from high adsorption onto the rock. The surfactant molecules adsorbed on the particle surface can desorb and adsorb at the air-water surface.

Figure 3.9. Equilibrium air-water surface tension as a function of surfactant concentration in DIW with or without 0.05 wt.% bare silica at 25 ± 0.2 °C. The horizontal dashed line shows the surface tension of DIW. The vertical red dashed lines show the CMC. The standard deviations are less than 0.1 mN m^{-1}.

$$y = -2.9276x^2 - 32.111x - 17.076$$
$$R^2 = 0.9749$$

$$y = -3.7255x^2 - 36.932x - 27.792$$
$$R^2 = 0.9719$$

CMC = 0.02 wt.%

CMC = 0.01 wt.%

○ AHS

△ AHS + 0.05 wt.% bare silica

$$y = 1.4976x^3 + 14.095x^2 + 28.442x + 48.734$$
$$R^2 = 1$$

$$y = 0.5559x^3 + 4.0581x^2 - 2.4208x + 17.417$$
$$R^2 = 0.9998$$

CMC = 0.03 wt.%

CMC = 0.02 wt.%

○ ZN

△ ZN + 0.05 wt.% bare silica

3.2.3.3.2 ES-coated silica

As for bare silica, adding 0.01 wt.% ES-coated silica increased the surface tension and CMC of AHS in DIW, however a decrease in surface tension is observed at higher particle

concentrations (Figure 3.10). The CMC remains unchanged for [particle] > 0.01 wt.%. The electrostatic attraction between the positive headgroup of zwitterionic surfactant and ES-coated silica is believed to be weaker than bare silica and cationic surfactant due to the silane coating (lower reactive silanol groups) and lower charge density in zwitterionic surfactant headgroup. Hydrogen bonding is still possible between the particles and the surfactant.[182, 183] There is a systematic decrease in surface tension upon raising particle concentration from 0 to 0.1 wt.% for AHS in Permian brine which is more noticeable at low surfactant concentrations. The interactions between particles and surfactant and the surfactant monolayer at the air-water surface are complicated on adding ions. Through total organic carbon measurements, Hu *et al.* concluded that cations like Mg^{2+} and Ca^{2+} can neutralize anionic silica and limit the alkyl hydroxysultaine adsorption on particles.[184] The presence of sodium ions has also been found to be effective in lowering the adsorption of zwitterionic betaine surfactant onto silica surfaces. The higher the sodium concentration in the electrolyte, the weaker the interactions between surfactant and silica.[185] It is difficult to investigate the interactions between particles and surfactants with ions or monolayer formation at the surface when a mixture of different salts is used. Similar observations are available in the literature for the blend of silica coated with polyethylene glycol (6 – 9 EO units) and C_{12-15} linear alcohol ethoxylate (9 EO units) surfactant in API brine (8 wt.% sodium chloride and 2 wt.% calcium chloride) in which the surface tension in the presence of particles and ions at low surfactant concentrations is lower than that of surfactant alone in brine while similar surface tensions are achieved close to the CMC (as observed here).[186] The potential reason is the increased pH upon raising particle concentration in the blend which renders the surfactant anionic which electrostatically repelled towards the surface by anionic particles resulting in lower surface tension. The surface activation of particles by surfactant and their contribution to the air-water surface in forming a mixed monolayer with surfactant and ions may also account for this decrease. The CMC of AHS in Permian brine does not change significantly on adding particles. The thermodynamic parameters of micellization and adsorption of AHS and ZN with or without Permian salts and ES-coated silica particles are presented in Table 3.2.

Figure 3.10. Effect of ES-coated silica loading on equilibrium air-water surface tension as a function of AHS surfactant concentration in DIW and Permian brine at 25 ± 0.2 °C. The curves are polynomial fits to experimental data with a correlation coefficient of $R^2 > 0.94$.
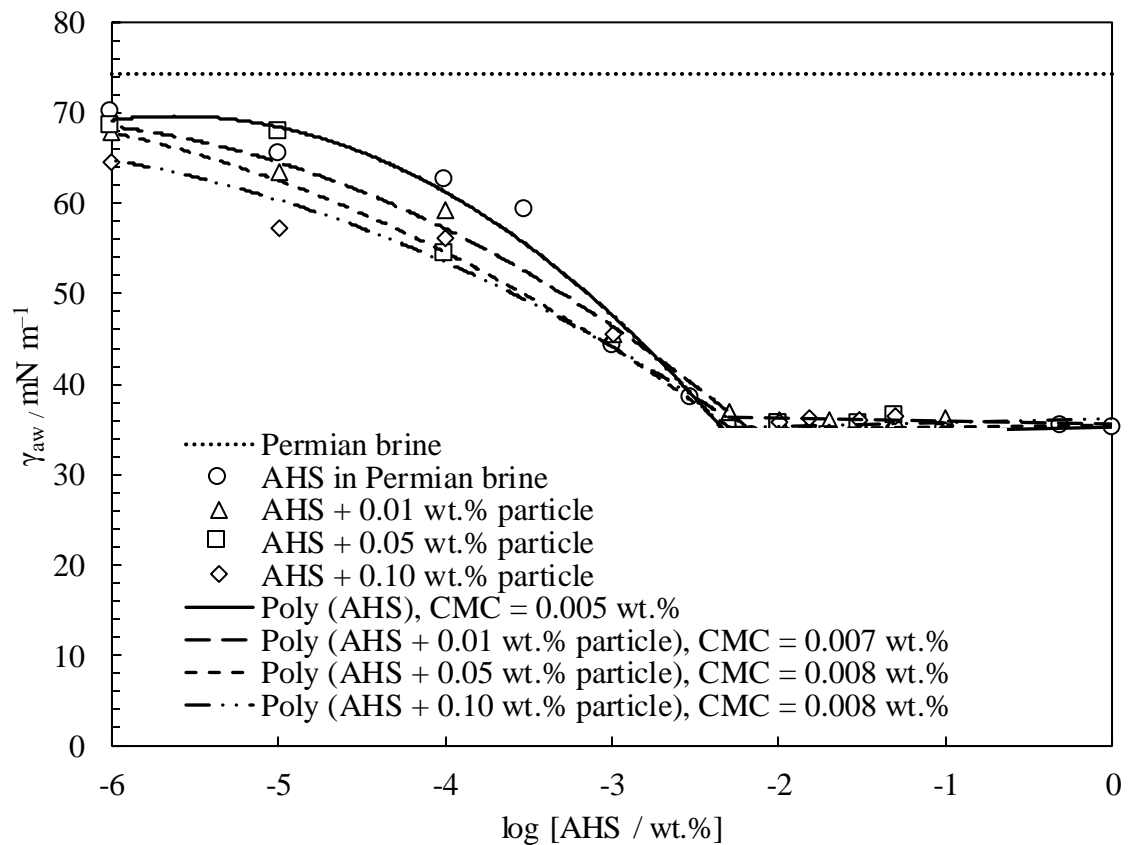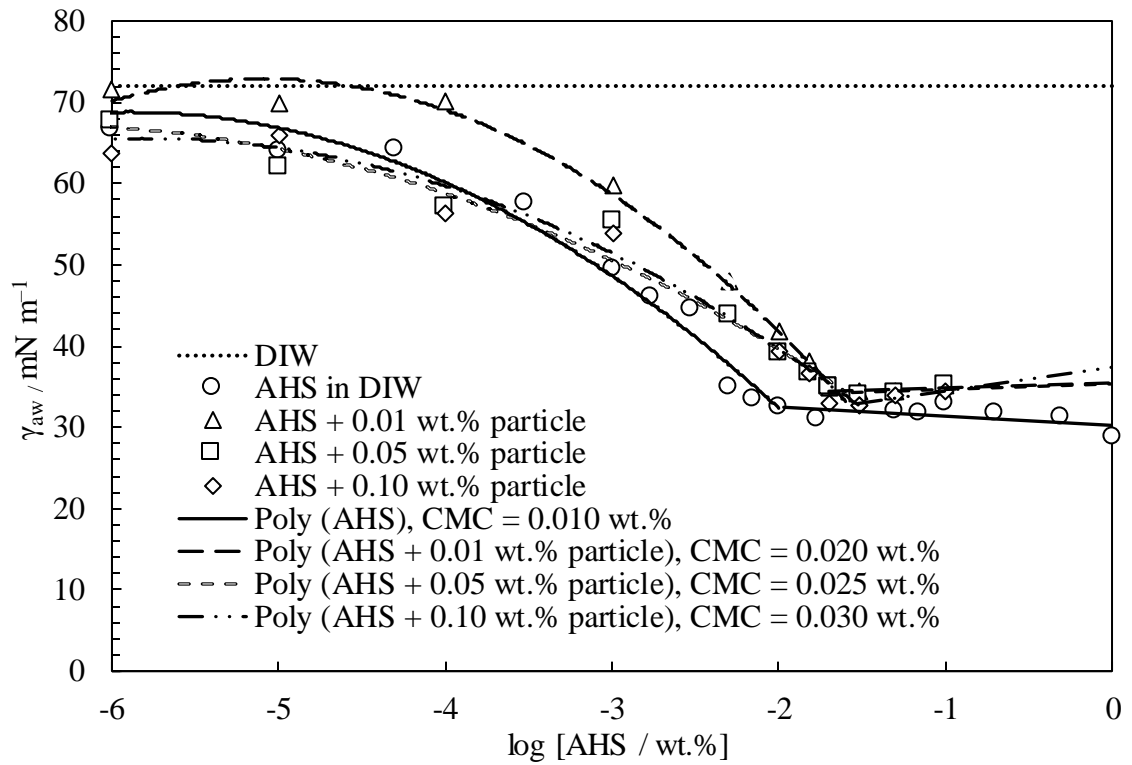
Figure 3.11 shows the air-water surface tensions of ZN in DIW with and without different concentrations (0 – 0.1 wt.%) of ES-coated silica. Like AHS, adding particles up to 0.05 wt.% increases the surface tension of ZN in DIW. For 0.1 wt.% particle loading, the

surface tension of the blend in DIW is lower than that of surfactant alone at low surfactant concentrations, but they are the same at concentrations close to the CMC. The CMC of ZN in DIW increases with the addition of ES-coated silica particles to surfactant solutions. The same interactions between particles and AHS explained earlier exist here between ZN and particles; however, the nonionic surfactant in ZN can contribute to the micellization and monolayer formation at the air-water surface. ES-coated silica particles do not show a clear effect on the air-water surface tensions of ZN in Permian brine. The surface tensions in the presence of particles are lower than those of surfactant alone at low surfactant concentrations while the behaviour is reversed when approaching the CMC. Raising the particle loading from 0.01 to 0.1 wt.% also does not affect the surface tensions of the blend considerably. There is a slight rise in the CMC of ZN in Permian brine on the addition of 0.01 wt.% particles, but no significant change was found at higher particle concentrations.

Figure 3.11. Effect of ES-coated silica loading on equilibrium air-water surface tension as a function of ZN surfactant concentration in DIW and Permian brine at 25 ± 0.2 °C. The curves are polynomial fits to experimental data with a correlation coefficient of $R^2 > 0.96$.
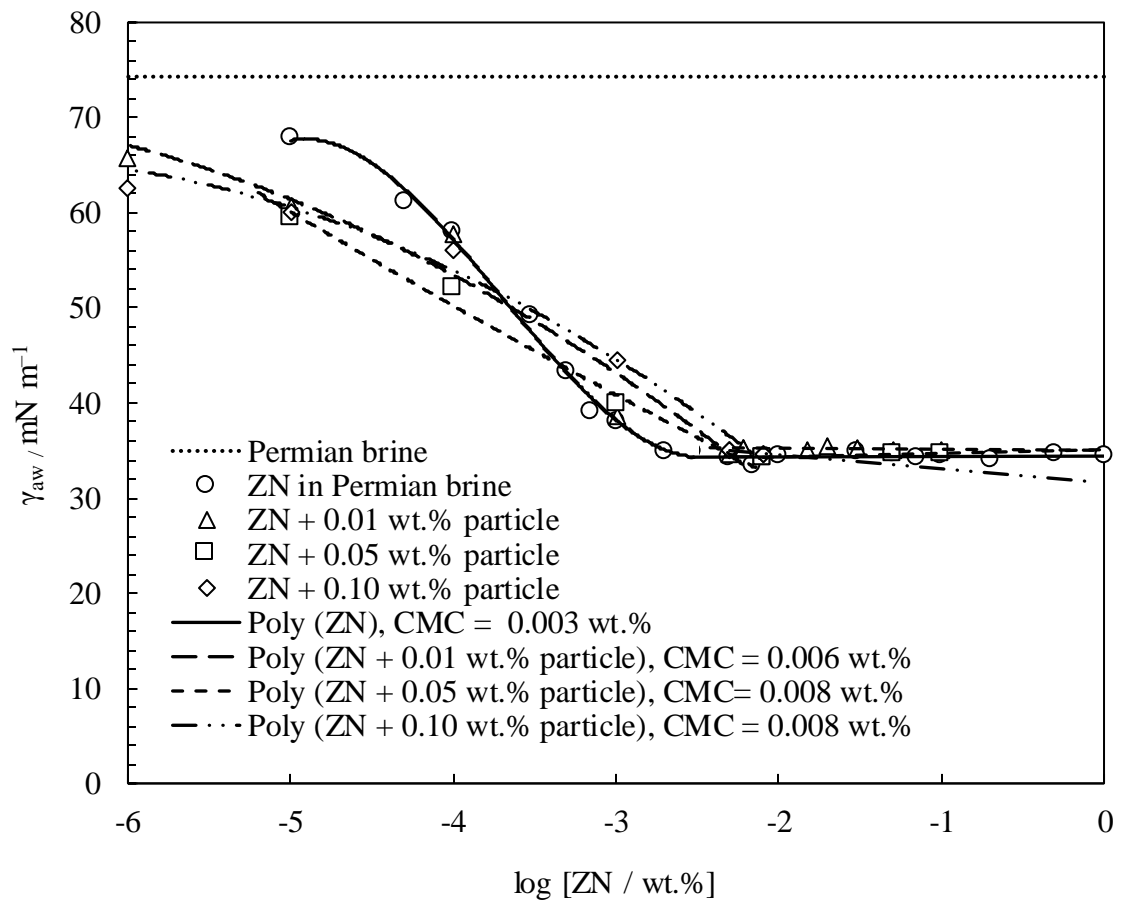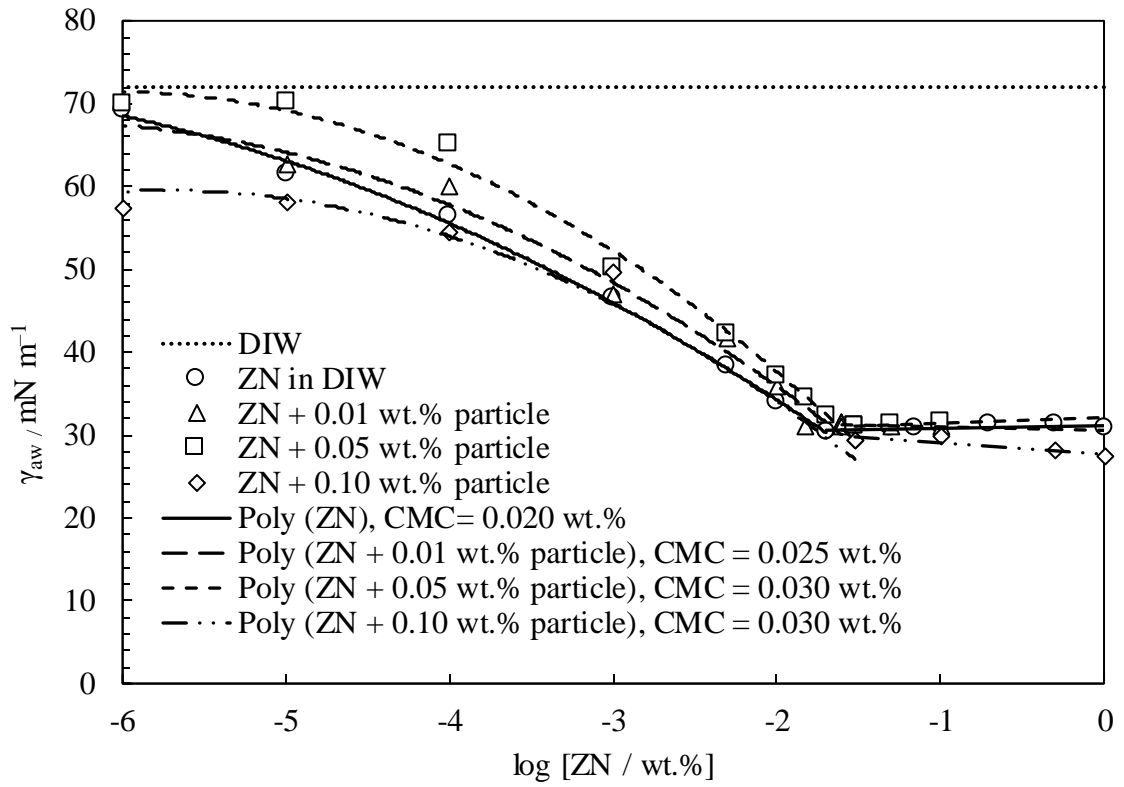
3.3 Properties of bare silica particles

Several important features should be investigated when using nanoparticles for EOR: particle size, surface chemistry, surface area, particle stability and compatibility with other EOR chemicals like surfactants.[187] These properties determine the success or failure of the operation. Before investigating the properties of silane-coated particles, the stability of bare silica particles alone or in a blend with surfactant in DIW and Permian brine was studied at low and elevated temperatures as a control. This investigation can also provide information on the particle-surfactant interactions in high salinity and high temperature environments.

3.3.1 Particles alone

Bare silica particles were long-term stable in DIW at all concentrations at low temperatures (Figure 3.12) due to the particle-particle electrostatic repulsion because of the deprotonation of surface silanol groups at high pH (~10). However, sediments were observed in dispersions > 2 wt.% (not typically used in EOR) after a while upon increasing the temperature to 75 °C due to the increased Brownian motion and particle collisions.[29] The particle stability was reduced significantly upon adding Permian brine, especially at high temperatures. The dispersion with 5 wt.% silica in brine gelled after 3 h due to the formation of an aggregated network of particles at high particle loading and high electrolyte concertation.[188] Generally, introducing salts into dispersions shrinks the electric double layer of particles. Considering Permian brine concentration (12.6 wt.% or 2.1 M), the particle-particle electrostatic repulsion is completely removed on adding ions (*i.e.* no electrostatic barrier) leaving van der Waals attraction acting on particles. Herein, the energy of interaction would be negative which aggregates the particles when they approach and collide with each other. Based on the Schultz-Hardy rule, multivalent ions are more detrimental to colloidal stability (critical coagulation concentration, or CCC α $\frac{1}{z^6}$ where Z is the ion valence).[189, 190] The variations in initial particle diameter and zeta potential with bare silica concentration in DIW are shown in Figure 3.13. The particle diameter in DIW was 16 ± 1 nm. Note that particle diameter at high concentrations is not the true size because of particle-particle interactions. The zeta potential of particles in DIW was measured as -42 ± 1.3 mV. The initial particle diameter of 0.05 wt.% bare silica in Permian brine was measured as 51 ± 1 nm. No particle diameter and zeta potential measurements were possible for other dispersions in Permian brine.

Figure 3.12. Appearance of dispersions containing different concentrations (0.05 – 5 wt.%) of bare silica in DIW (top) and Permian brine (bottom) at 25 °C and 75 °C at different times. The pH values were measured at 25 °C.

Figure 3.13. Variation of the initial particle diameter and zeta potential of bare silica with particle concentration in DIW at 25 °C.

98
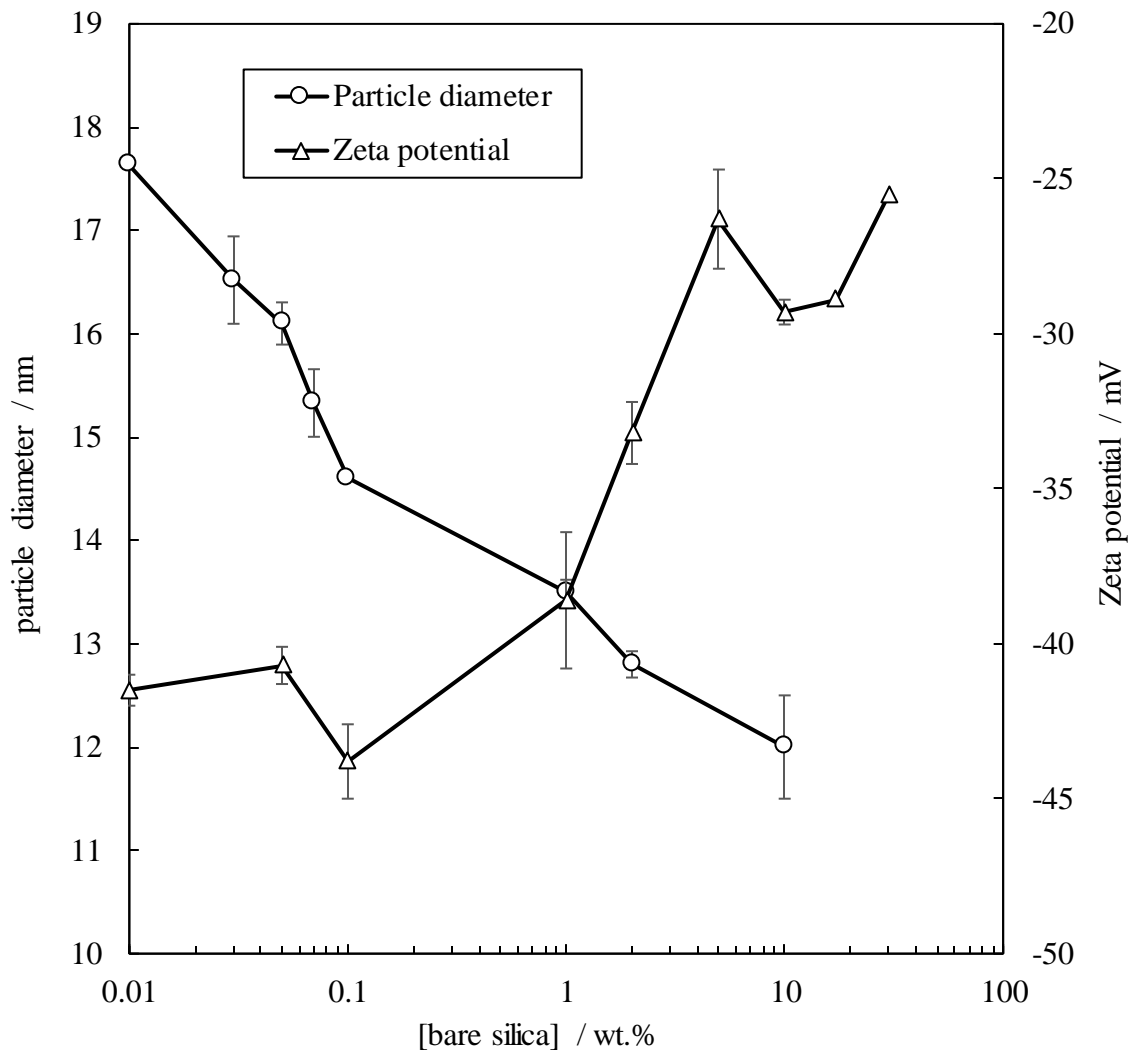
Aluminium sulphate is mainly used as a coagulating agent to promote particle collision by neutralizing particle charges in the purification of drinking water. In neutral or slightly

alkaline water, $Al_2(SO_4)_3$ dissolves to form a gelatinous precipitate of aluminium hydroxide ($Al(OH)_3$) and weak sulfuric acid:[191]

$$Al_2(SO_4)_3 + 6\,H_2O \rightarrow 2\,Al(OH)_3 + 3\,H_2SO_4 \qquad (3.2)$$

The sulfuric acid can reduce the pH which agrees with the pH measurements of the dispersions here (4.1 ± 0.1 at 20 °C). The effect of adding aluminium sulphate on the zeta potential of different concentrations of bare silica in DIW was investigated. The zeta potential of bare silica increased from -42 ± 1.3 mV to around zero with the addition of 10% aluminium sulphate. All dispersions were sedimented due to the termination of electrostatic repulsion caused by the charge neutralization of the particle surface by the electrolyte.

3.3.2 Blends of particles and AHS surfactant

Figure 3.14 shows the appearance of a fixed 0.1 wt.% bare silica in a blend with different AHS concentrations in DIW and Permian brine at different temperatures. The dispersions were stable for 80 days at both temperatures at low surfactant concentrations (< 0.2 wt.%) in DIW. For higher AHS concentrations, sedimentation occurred immediately after preparation and increased in less than a day. For the blend in Permian brine, all dispersions were initially turbid and sedimentation occurred in half an hour at both temperatures. As discussed earlier, at high pH (*i.e.* low [AHS] in the blend), the anionic sulfonate group of the zwitterionic surfactant is dominant. Therefore, there is a weak electrostatic attraction between anionic silica and the cationic headgroup of surfactant. At high surfactant concentrations (pH ~ isoelectric pH at 5.5 – 8.0), stronger electrostatic interactions between the surfactant and particle surface exist which leaves the hydrophobic chains of the surfactant oriented outward. The van der Waals attraction between surfactant tails on the particle surface can dominate the particle-particle electrostatic repulsion when particles are at a certain distance leading to particle aggregation and sedimentation. As proof of this, the initial particle diameter and zeta potential of the blend were measured in DIW at 25 °C (Figure 3.15). The plot shows that an increase in AHS concentration up to 0.1 wt.% where the surfactant is anionic does not change the initial particle diameter and zeta potential significantly. However, raising the AHS concentrations > 0.1 wt.% increases the particle diameter sharply up to ~ 3400 nm at 2 wt.% AHS because of the interactions between particles and surfactant (at pH ~ 8 where the surfactant turns zwitterionic). The zeta potential also increases with an increase in surfactant concentration toward zero, reflecting more interactions between particles and the surfactant headgroup and thus fewer charged sites on particles. These results agree with stability photos in which sedimentation was observed in dispersions with surfactant

concentrations > 0.2 wt.%. No particle diameter and zeta potential measurements were possible for the blend in Permian brine due to the fast sedimentation after preparation. Observations made during the preparation of these dispersions showed the addition of a small amount of NaCl (1 wt.%) to the aggregated blend of 0.1 wt.% bare silica and 0.5 wt.% AHS in DIW can reduce the turbidity and aggregation; however, the turbidity increased on the addition of Permian salts into a stable dispersion of 0.1 wt.% bare silica and 0.1 wt.% AHS in DIW (Figure 3.16). The reduction of the electrostatic attraction between the anionic particle and the positive headgroup of the zwitterionic surfactant by NaCl may be responsible for the first observation. In the presence of Permian salts however, a complete charge neutralization of particle surfaces by different ions (primarily multivalent cations) occurs which causes the particle-particle electrostatic repulsion to vanish (no electrostatic energy barrier) and the van der Waals attraction to dominate.[192]

Figure 3.14. Appearance of dispersions containing a fixed 0.1 wt.% bare silica in a blend with different concentrations of AHS in DIW (top) and Permian brine (bottom) at different times. The pH values were measured at 25 °C.
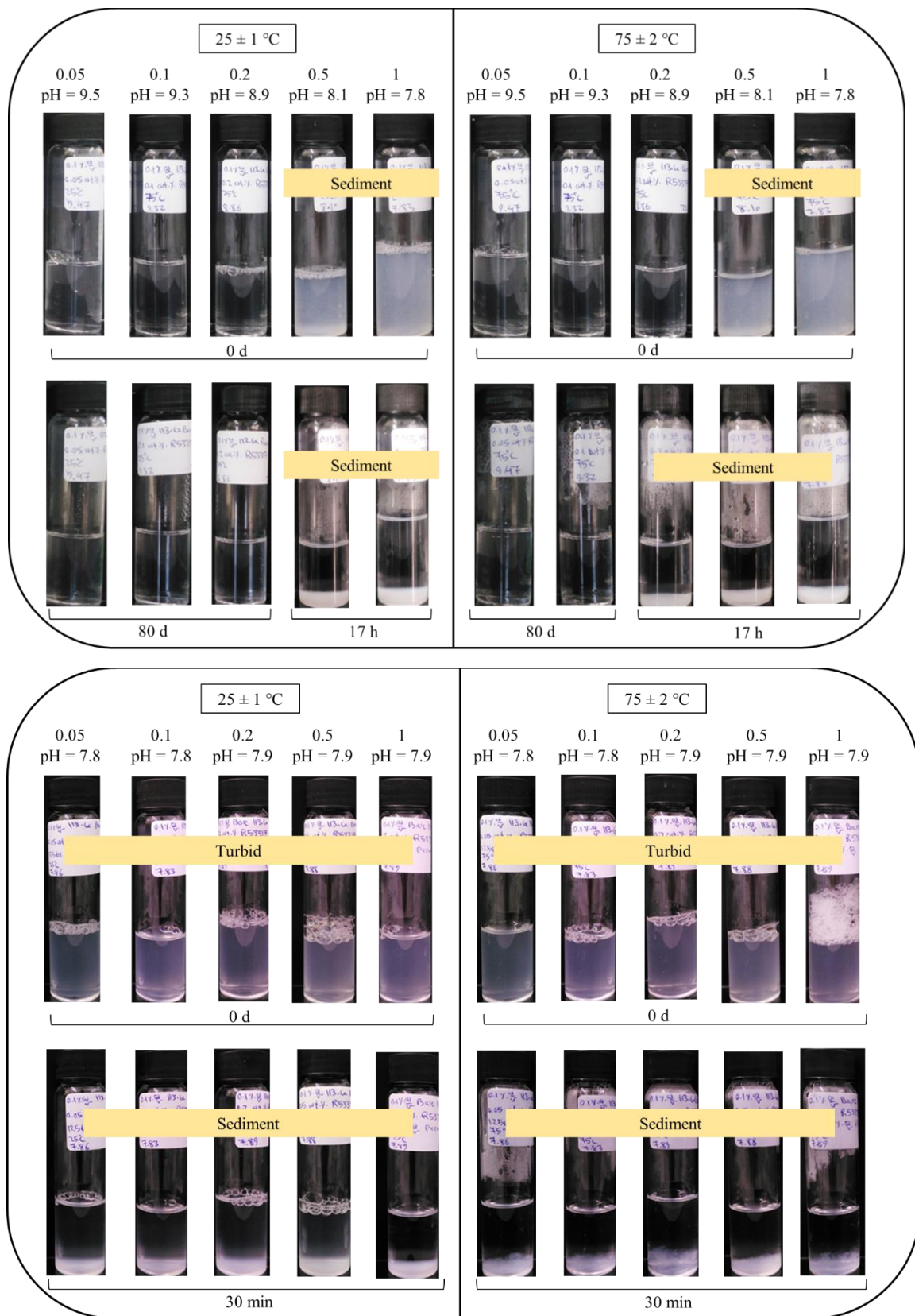
Figure 3.15. Initial particle diameter and zeta potential of a fixed 0.1 wt.% bare silica in a blend with different AHS concentrations in DIW at 25 °C. The zeta potential of 0.1 wt.% bare silica in DIW is -43 ± 1 mV at 25 °C. The pH of the blends decreases from 9.8 to 7.9 on increasing surfactant concentration.
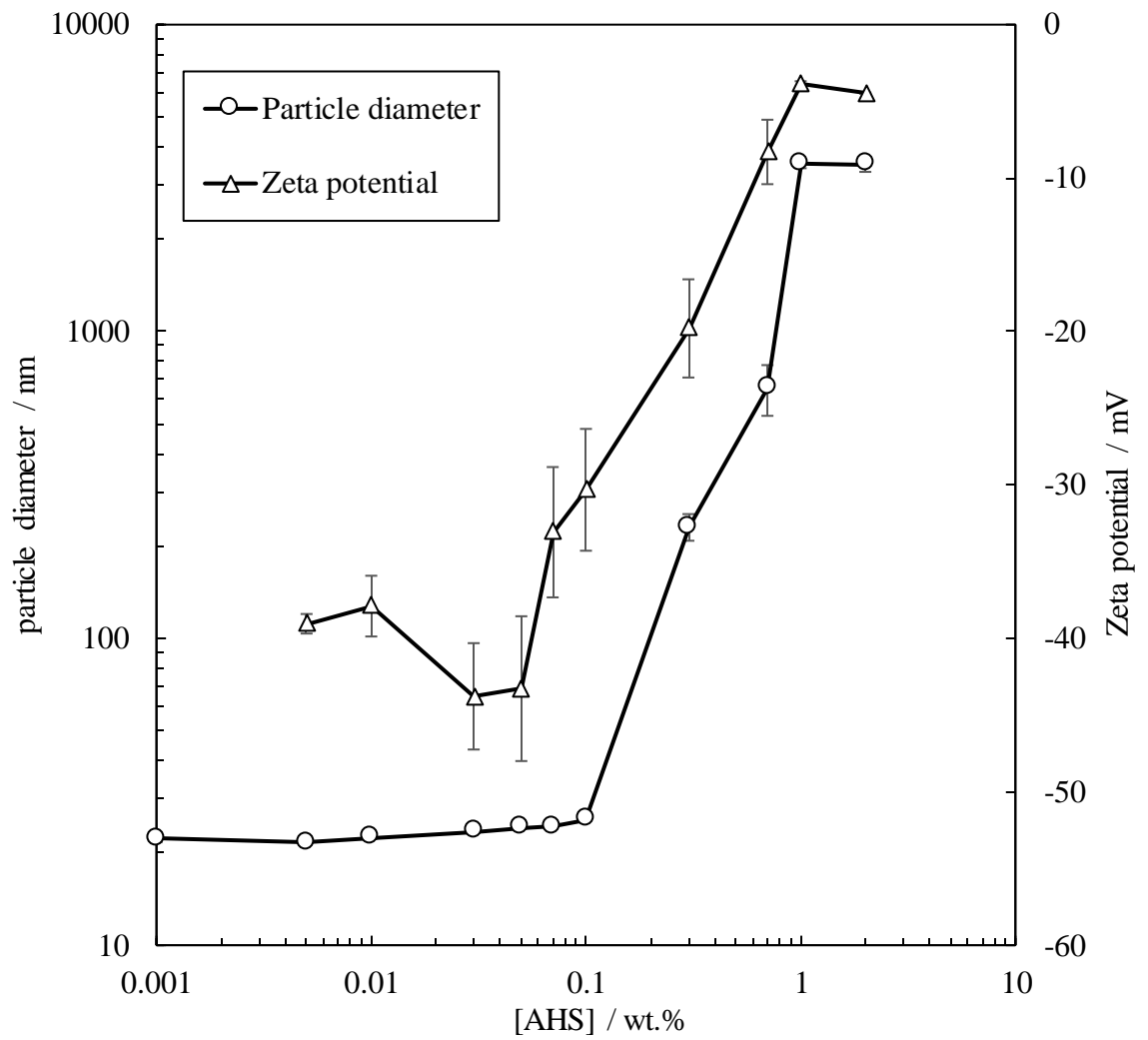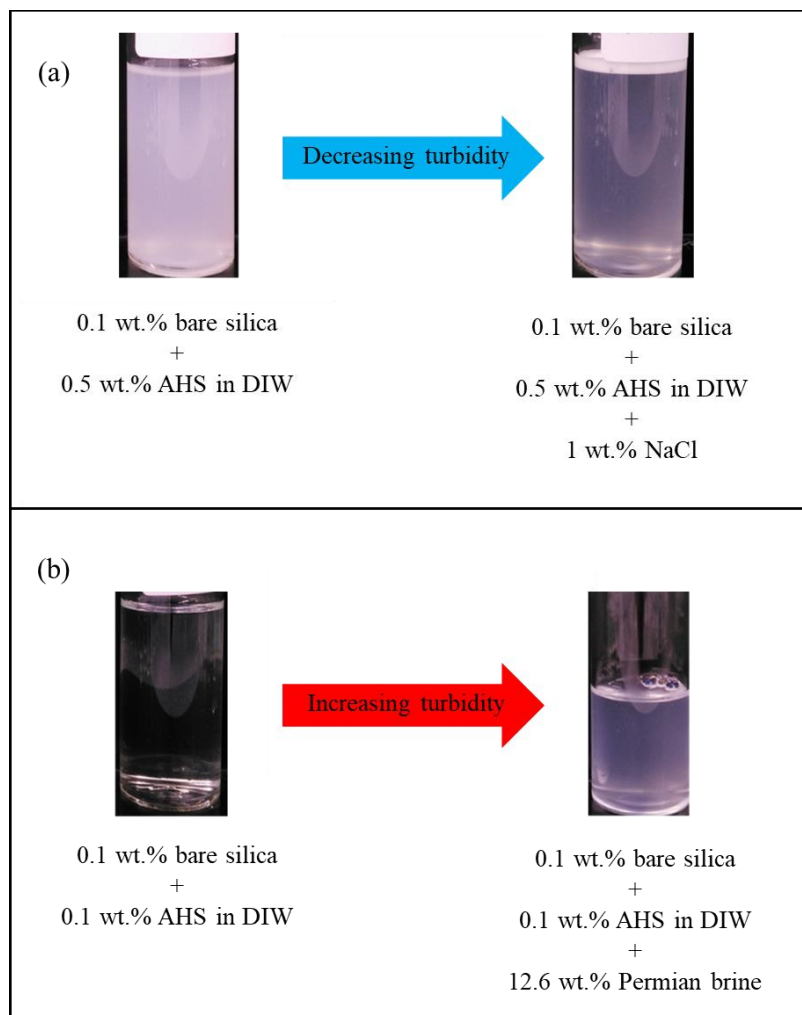
Figure 3.16. Effect of adding (a) 1 wt.% NaCl or (b) Permian brine (12.56 wt.%) on the turbidity of dispersions of 0.1 wt.% bare silica in a blend with 0.1 wt.% or 0.5 wt.% AHS at 20 °C.

(a)

0.1 wt.% bare silica
+
0.5 wt.% AHS in DIW

Decreasing turbidity

0.1 wt.% bare silica
+
0.5 wt.% AHS in DIW
+
1 wt.% NaCl

(b)

0.1 wt.% bare silica
+
0.1 wt.% AHS in DIW

Increasing turbidity

0.1 wt.% bare silica
+
0.1 wt.% AHS in DIW
+
12.6 wt.% Permian brine

3.3.3 Blends of particles and ZN surfactant

Figure 3.17 shows the appearance of 0.1 wt.% bare silica in a blend with different ZN concentrations in DIW and Permian brine at two temperatures. Like AHS, the dispersions

of bare silica and ZN in DIW were stable at both temperatures for a long time (85 days) at low surfactant concentration (< 0.1 wt.%) while rapid sedimentation was observed at higher surfactant concentrations at both temperatures. For blends in Permian brine, fast sedimentation was observed in all dispersions at both temperatures immediately after preparation. The same interactions discussed earlier between silica and AHS exist here. There is also a possibility that the nonionic $C_{10-12}E_9$ present in ZN contributes to adsorption on the particle surface through hydrogen bonding between the surfactant headgroup and the particle surface.

Figure 3.18 presents the initial particle diameter and zeta potential of a fixed 0.1 wt.% bare silica in a blend with different ZN concentrations in DIW at 25 °C. Like AHS, raising the ZN concentrations in the blend increased the particle diameter and zeta potential to around 3700 nm and – 6 mV, respectively. No successful measurements were achieved for surfactant concentrations above 0.5 wt.% in the blend due to the particle instability. As the blend in Permian brine was so unstable, particle diameter and zeta potential measurements were not possible.

Figure 3.17. Appearance of dispersions containing a fixed 0.1 wt.% bare silica in a blend with different ZN concentrations (given in wt.%) in DIW (top) and Permian brine (bottom) at different times. The pH values were measured at 25 °C.
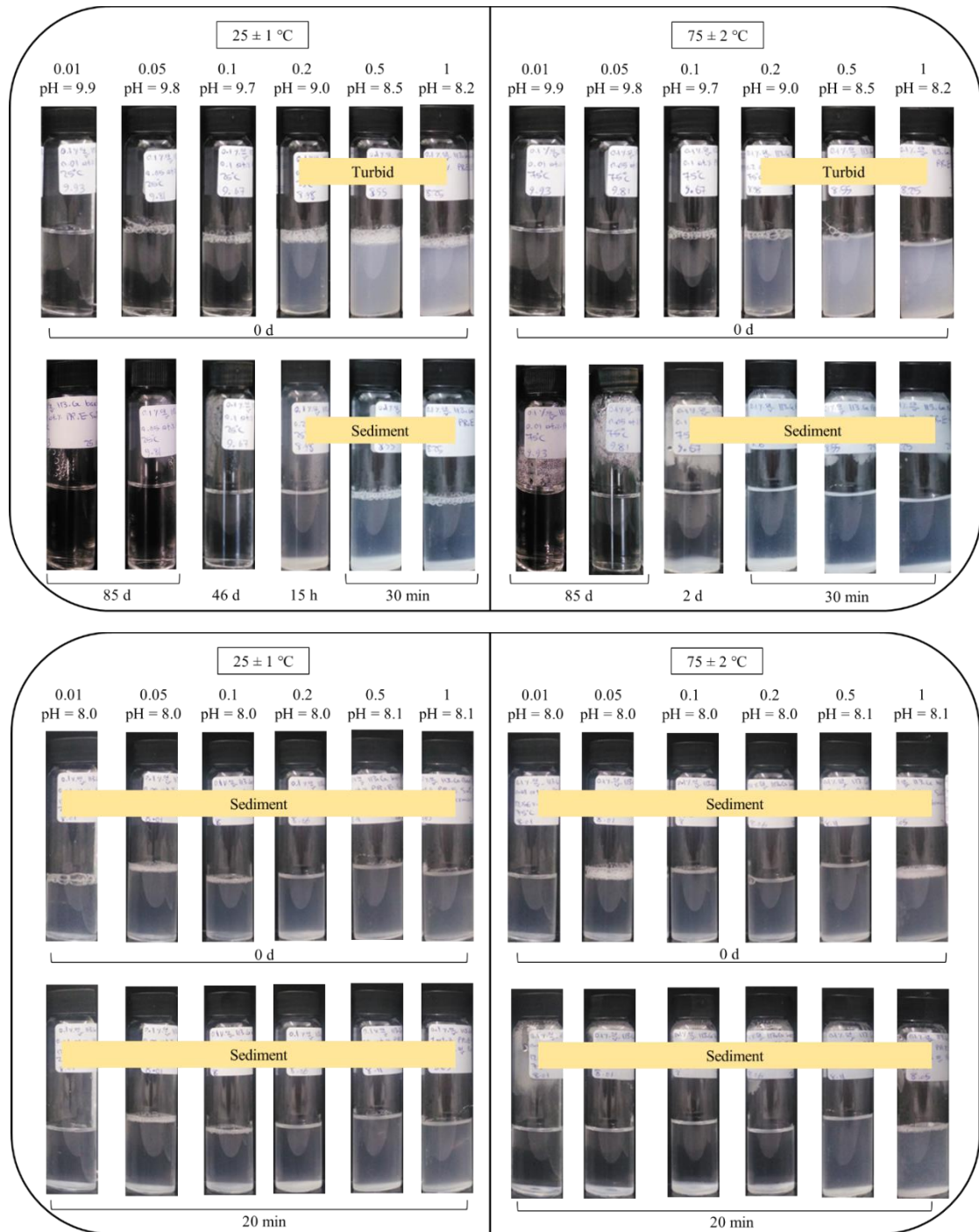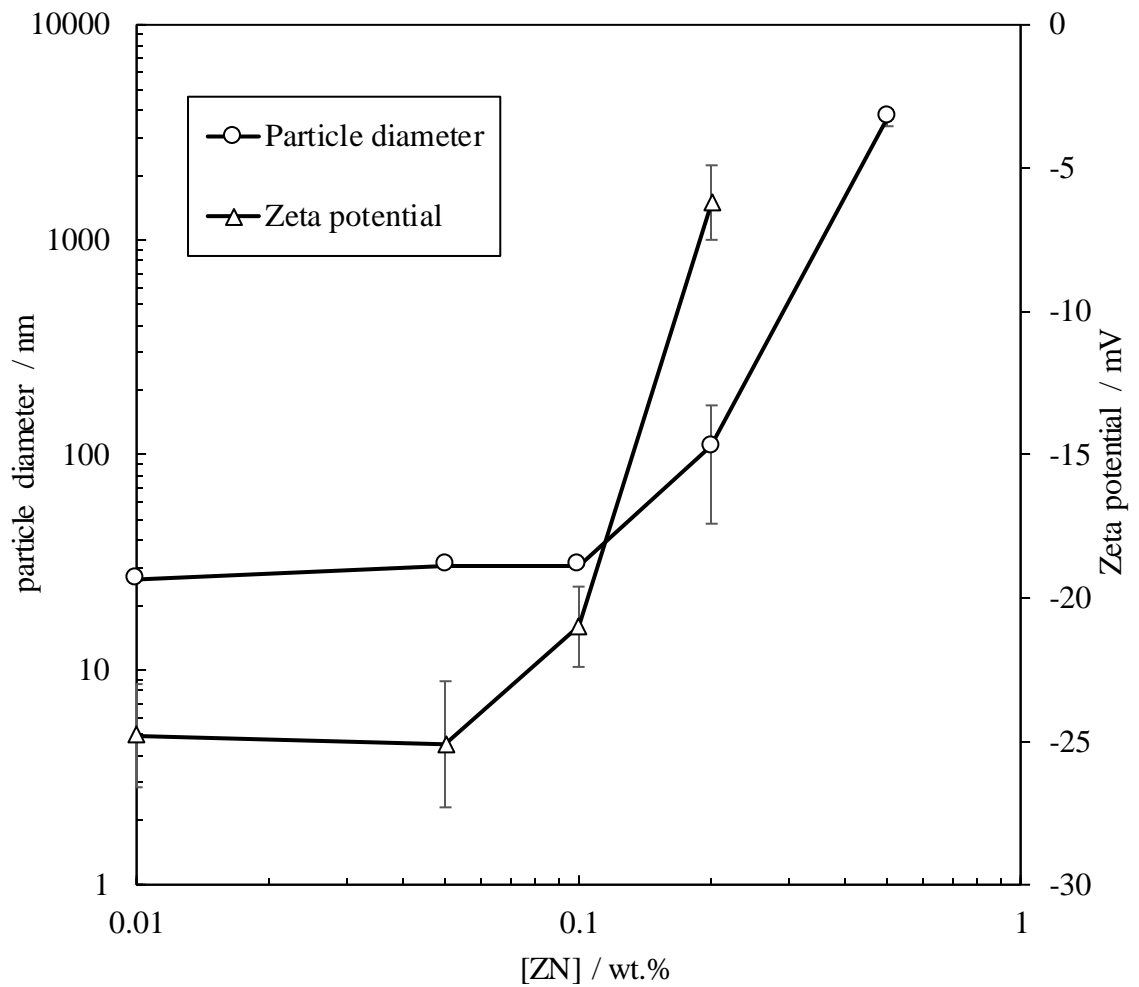
Figure 3.18. Initial particle diameter and zeta potential of a fixed 0.1 wt.% bare silica in a blend with different ZN concentrations in DIW at 25 °C. The zeta potential of 0.1 wt.% bare silica in DIW is -43 ± 1 mV at 25 °C. The pH of the blends decreases from 9.9 to 8.2 with increasing surfactant concentration.

106

3.4 Properties of AS-coated silica particles

One of the key challenges in using nanoparticles for EOR is ensuring their stability under the high temperature and salinity conditions found in oil reservoirs over a long period. To improve particle stability, researchers have explored several approaches including steric stabilization (*i.e.* physical and chemical grafting), electrostatic stabilization (*i.e.* pH

adjustment) or the blend. In this part, the properties of sterically and electrostatically stabilized AS-coated silica particles alone or in a blend with surfactant were determined to understand their behaviours in the EOR process.

The silanization of particles is performed through a series of hydrolysis and condensation process during which the silanes chemically adsorb onto the surface of particles through siloxane linkage (Si–O–Si). Condensation of silanes by oligomerization and polymerization is possible particularly if the silane is not sufficiently hydrolysed in the first step. The chemical grafting of silanes onto silica can be also monodentate, bidentate or tridentate depending on number of silane reactive group interacting with particle surface silanol group.

3.4.1 XRD

XRD is a technique that can be used to identify the crystal structure and composition of nanoparticles. It operates by illuminating a sample with an X-ray beam and measuring the diffraction patterns.[193] Amorphous silica (XRD $2\theta = 17 \pm 4°$) is usually made at low calcination temperatures (110 ± 40 °C) while crystalline silica (XRD $2\theta = 26 \pm 1°$) needs temperatures up to 1000 °C.[194] It is documented that particle surface activity decreases with increasing silica crystallinity due to the formation of regular lattices and powerful silica-oxygen bonds. The peak indexing at $2\theta = 22°$ in Figure 3.19 is the characteristic peak of amorphous silica. The XRD analysis by Xpert Highscore shows that silica is tridymite (a high-temperature polymorph of silica, $Si_{80}O_{160}$). The crystal system of silica was found to be anorthic (or triclinic). Additional peaks as a result of coating silica particles with AS are observed at $2\theta = 43°$ and $50°$ which are indicative of chemical reactions that happened between the core silica and the shell alkoxy silane in the synthesis process.[195] No further peaks in the pattern indicate the absence of impurities in the sample.

3.4.2 Extent of salinization

TGA works by measuring the mass loss as a function of temperature to determine the amount and stability of coating material (organic and inorganic) present on nanoparticles under different temperature conditions. It is a useful technique for studying the properties of coated nanoparticles and can be used to optimize the coating process or assess the performance of the coated nanoparticles in a particular application.[196] Figure 3.19 shows the TGA results of AS-coated silica. There are three main weight loss regions occurring in the sample. The first small weight loss happens up to 150 °C and is related to the removal of water from the sample. The second one occurs from 150 °C to 380 °C and is probably related to the degradation of silane physically adsorbed onto silica particles. The

last weight loss (from 380 °C to 760 °C) is associated with the oxidation of silane molecules chemically adsorbed on particle surface. Oxides like CO_2, H_2O and CO are created when the organic molecules of the silane react with oxygen from airflow at high temperatures. Combustion or combustion-like oxidation are common names for this process. The proximity and strength of the chemical connections between the silanes and the particle surface determine the oxidation temperature of silane. The lower the oxidation temperature, the weaker the chemical bond. Slightly positive values (due to the heat release) in the DTG profile are here visible at high temperatures showing a high oxidation temperature. In addition, it is inferred that the silane is predominantly chemisorbed on particles as seen by the chemical and physical silane uptake on silica (0.21 mg as opposed to 0.12 mg).

Overall, considering a 9.1% weight loss from 150 °C to 760 °C for the loss of organic ligand, the organic coverage (ϕ_i) on silica is calculated at 5.15 µmol silane m^{-2} of the silica. Given that 7.64 µmol silane per m^2 of silica surface gives a full silane monolayer, the AS coverage on silica in this sample is calculated at 68 % of a full monolayer.

Figure 3.19. XRD (top) and TGA/DTG (bottom) of AS-coated silica.
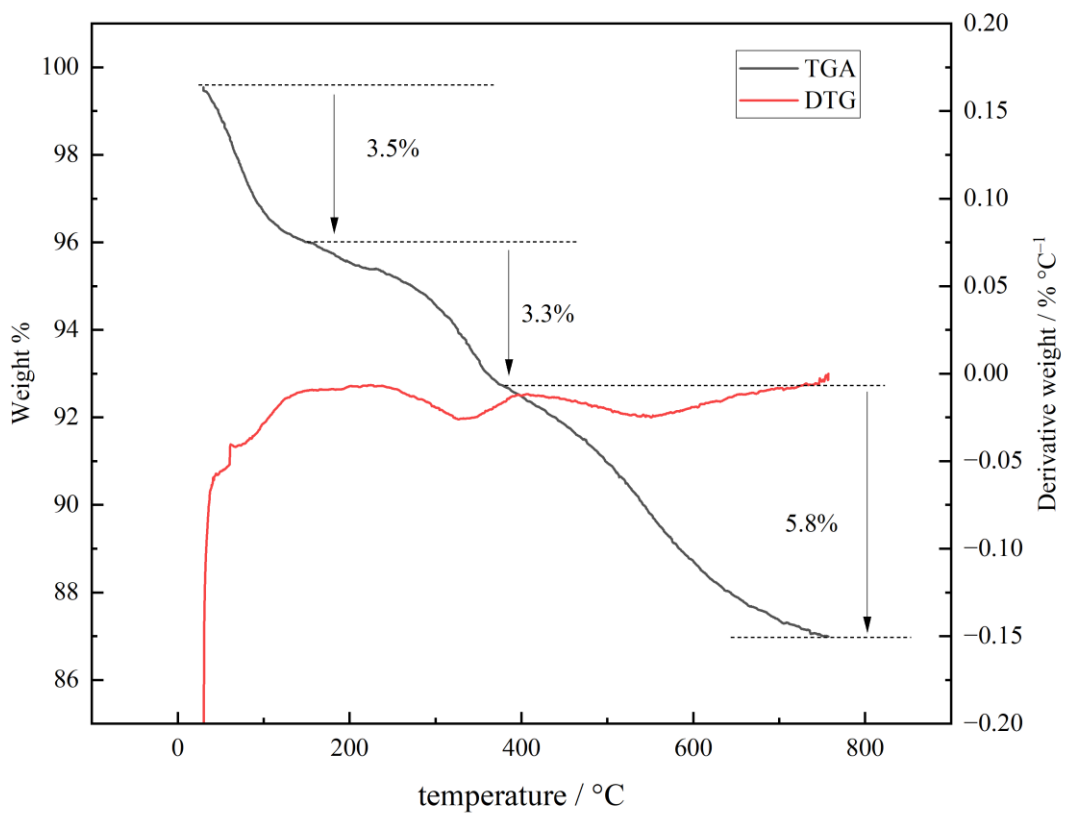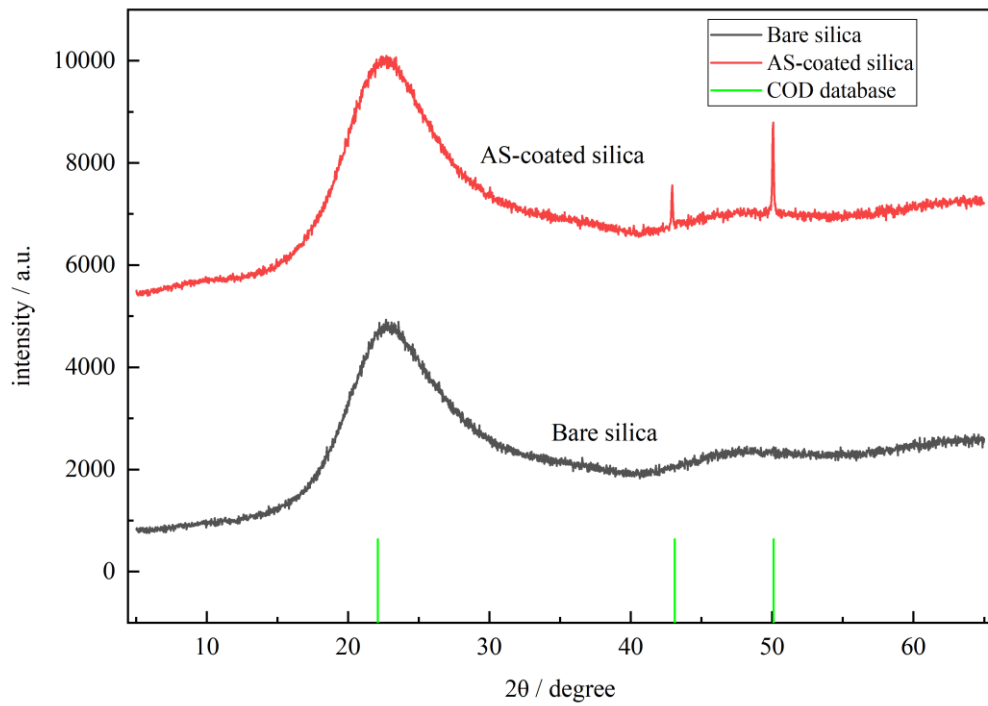
3.4.3 Particle stability

Figure 3.20 shows the stability of 0.1 wt.% AS-coated silica in the presence and absence of 0.1 wt.% ZN in DIW and Permian brine at the original and reduced pH (by HCl) at

two temperatures. In particle dispersions at the original pH, the particles were sedimented both in DIW and Permian brine in a few days at low temperatures. The sedimentation was faster (3 h) at 75 °C. As shown, the particles became long-term stable (~ 7 months) in DIW and Permian brine by reducing the pH of dispersions at both temperatures. AS becomes protonated and cationic below pk_a of the amino group (NH_2) at ~ 9.[197] Regarding the isoelectric point of bare silica $(2-4)$ [198] and high silane coverage on particles (~ 68 %), AS-coated silica is expected to have an isoelectric point close to that of AS *i.e.* $8 - 9$, as measured before.[140] At original pH (8.1 – 8.6), the silane is uncharged but the particles are overall weakly anionic due to the uncoated sites on silica leading to aggregation and sedimentation due to the negligible particle-particle electrostatic repulsion which is intensified at higher temperatures. Ions can screen the charges and increase the agglomeration rate. At low pH, amino groups are protonated to NH_3^+ and the particles become net cationic creating electrostatic repulsion between particles. Therefore, the particles are sterically and electrostatically stabilized in Permian brine at high temperatures for the long term. The low pH used here is just to ensure a reasonable gap with the original pH. The same improved particle stability is expected around reservoir pH (6.5).

Figure 3.21 shows the initial particle diameter and zeta potential of dispersions. Protonation of the particle surface was found to reduce the initial particle diameter in DIW by ~ 10 nm. The zeta potential of particles in DIW at the original pH was ~ 0, as expected. A positive zeta potential (~ + 30 mV) was observed at low pH. Therefore, anionic bare silica has been reversed in charge with amine functionalization (-42 to $+30$ mV). The initial diameter of 0.1 wt.% AS-coated silica particles in Permian brine at an original pH of 8.2 and a reduced pH of 4 was measured at 50 ± 1 nm and 30 nm ± 2, respectively at 25 °C. The higher initial diameter of the original pH dispersion agrees with its short-term stability in visual inspections. The addition of ZN increased the stability of particles in DIW at the original pH significantly: from 5 to 180 days at 25 °C and from 3 hours to 16 days for dispersions at 75 °C. Although the particle stability in Permian brine also increased on adding ZN at 25 °C (1 day to 160 days), the particle stability improvement at high temperature was not enough for EOR purposes (3 hours to 3 days). All dispersions became long-time stable upon pH reduction. Table 3.3 compares the initial particle diameter and stability of 0.1 wt.% AS-coated silica with and without 0.1 wt.% ZN in DIW and Permian brine at original pH and reduced pH at two temperatures.

Figure 3.20. Appearance of dispersions containing 0.1 wt.% AS-coated silica in the absence (top) and presence (bottom) of 0.1 wt.% ZN in DIW and Permian brine at the original pH and reduced pH by HCl at two temperatures at different times.
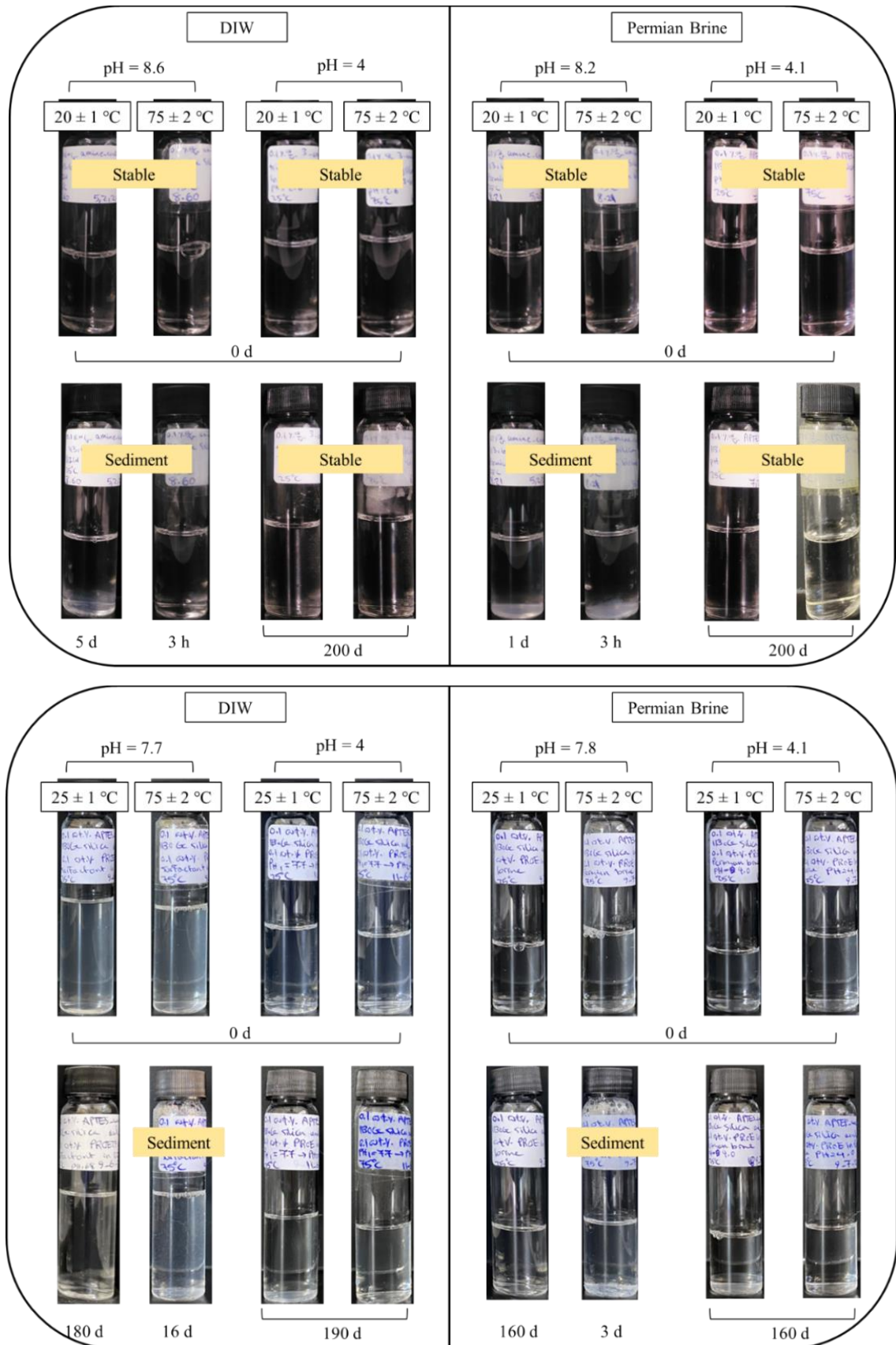
Figure 3.21. Initial particle diameter and zeta potential of different concentrations of AS-coated silica in DIW at 25 °C. The original pH was 8.1 – 8.6 which was reduced to 4.3 – 5.2 by HCl.
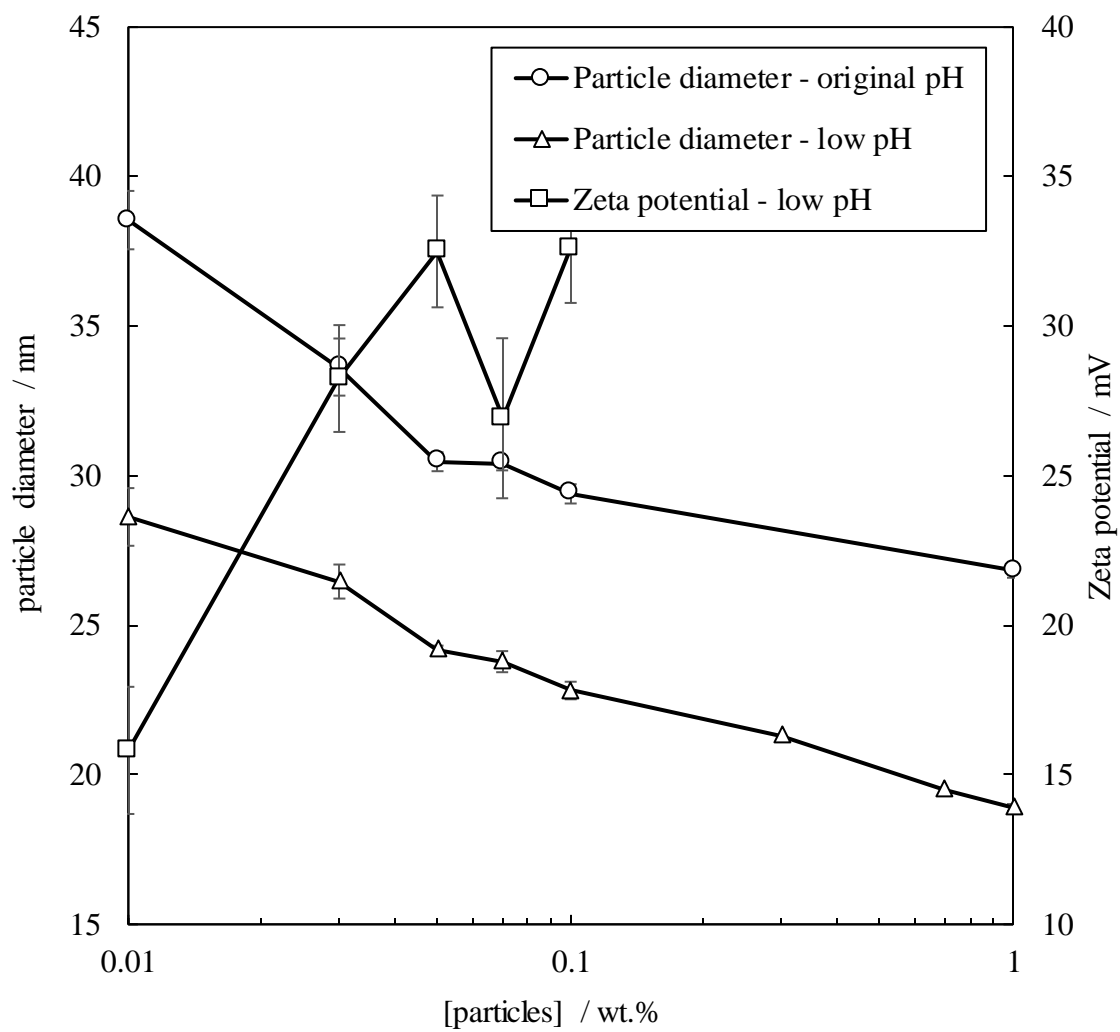
113

Table 3.3. Initial particle diameter of dispersions of 0.1 wt.% AS-coated silica with or without 0.1 wt.% ZN surfactant in DIW and Permian brine at 25 °C at original pH and reduced pH (4) by HCl.

| [ZN] / wt.%	pH at 25 °C	Solvent	Diameter / nm	Stability to sedimentation / days	
				25 °C	75 °C
–	Original	DIW	30 ± 2	5	< 1
	Reduced		23 ± 1	200	200
0.1	Original		30 ± 3	180	16
	Reduced		24 ± 1	190	190
–	Original	Permian brine	50 ± 1	1	< 1
	Reduced		30 ± 2	200	200
0.1	Original		164 ± 37	160	3
	Reduced		47 ± 1	160	160

3.5 ES-coated silica particles

3.5.1 Synthesis routes

3.5.1.1 Synthesis route from ChampionX

115

Following the ChampionX synthesis route, the final dispersions were turbid after a 24-hour reaction time at 60 °C, although they should have been blueish. The turbidity reflects a large extent of particle aggregation which must be avoided. The synthesis route was repeated several times and the following controls were performed during the synthesis, but no success was achieved (Figure 3.22):

(i)   During the hydrolysis of ES by HCl, the pH of the mixture was monitored to remain in the range of 2.0 – 2.2. A higher pH could reduce the solubility of the silane in water and lower the hydrolysis efficiency. 1 M HCl was added to bring the pH down to the range where required. The mixture of ES and HCl was initially hazy but turned clear after stirring for 3 min. The hydrolysis time was extended to 120 min to ensure complete silane hydrolysis. In addition to magnetic stirring, overhead stirring with speeds up to 500 rpm was also performed to create higher shear and a good vortex during the hydrolysis to prevent silane aggregation.

(ii)   The reaction between bare silica and ES was performed both in the presence and absence of N_2 gas (the condenser and bubbler were removed).

(iii) To ensure a good vortex during the addition of hydrolyzed ES to the bare silica dispersion, higher speeds up to 600 rpm were tried to prevent aggregation of particles and silane. The silane addition time was also extended to 30 min.

Figure 3.22. Synthesis of ES-coated silica based on the route from the sponsor: (a) clear bare silica dispersion at 60 °C, (b) a relatively turbid dispersion immediately after the addition of all aqueous ES at 60 °C, (c) increased turbidity after stirring for 20 min at 60 °C, (d) after 24 h reaction at 60 °C.
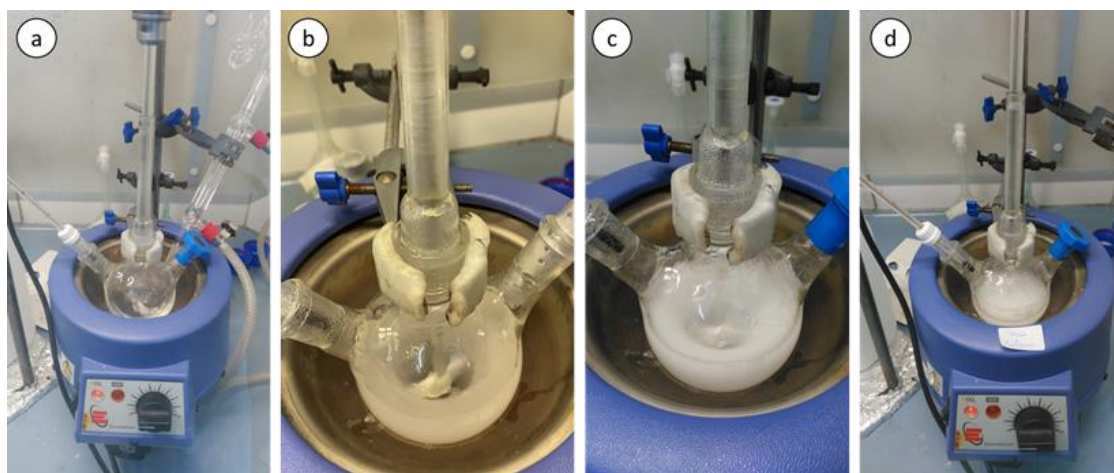

3.5.1.2 Synthesis route from literature

All ES/silica <u>dispersion</u> ratios of 0.11, 0.25, 0.50 and 1 cm^3 g^{-1} resulted in final turbid dispersions after 24 h. However, the turbidity was removed for [silica] $\leq$ 4 wt.% at a constant ES/silica dispersion ratio of 0.50 cm^3 g^{-1} but some large aggregates were found

at the bottom of vials indicating that the silane volume is still high (Figure 3.23). As the final dispersions were filtered, some particle stability inspections were performed for the particles synthesized by this method at different ratios (see Appendix A.2).

Figure 3.23. Effect of initial bare silica concentration on the final turbidity of ES-coated silica dispersions in the synthesis using a constant ES/silica dispersion of 0.50 cm^3 g^{-1}.
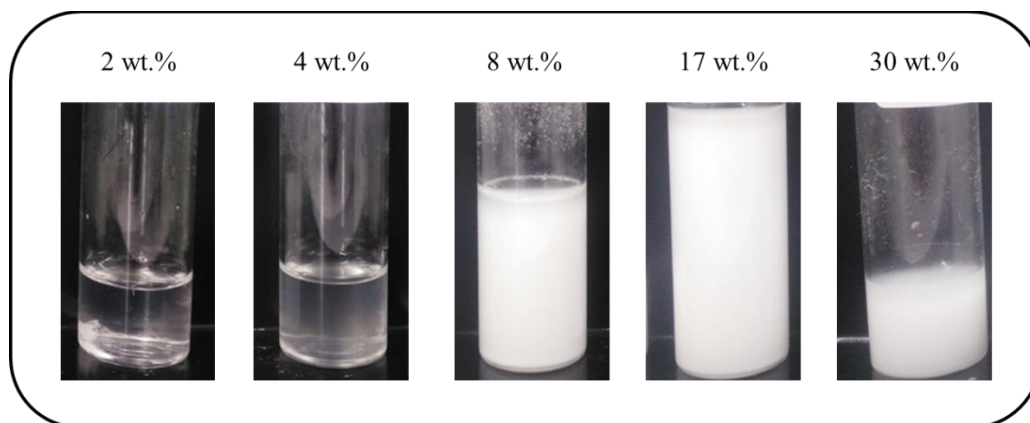
3.5.1.3 Modified synthesis route

It was revealed that previous methods used high ES volumes in the synthesis which caused particle aggregation. Using a typical density of reactive silanol sites on colloidal silica (4.6 SiOH groups per nm^2 of bare silica) [1] and Avogadro's number ($6.023 \times 10^{+23}$), 7.64 µmol ES per m^2 of silica is required for full silane coverage on bare silica which equals 0.6 g ES per g of bare silica using its specific surface area (331 m^2 g^{-1}) and silane molecular weight (236.3 g mol^{-1}). Since the density of ES is 1 g cm^{-3}, weight and volume can be used interchangeably here. It is noted that this amount is for pure ES and a monodentate reaction during silanization (*i.e.* one-to-one interactions between silane monomers and the surface silanol group on silica). Oligomerization of silanes or bidentate reactions is possible during the chemisorption of silane on silica. [199]

A range of ES/silica particle ratios (0.25 – 1.00 g g^{-1}) was tried during the synthesis to inspect the effect of silane volume (weight) on the final dispersion turbidity in the synthesis. Figure 3.24 shows a summary of the observations made during the synthesis of ES-coated silica by this method for different ES/particle ratios. The final dispersions after a 24 hour reaction time were monitored for a few days for possible particle aggregation and sedimentation. As seen, for small ratios up to 0.50 g g^{-1} (slightly below the value required for a full monolayer) the final dispersions were blueish with no turbidity after synthesis. The dispersion synthesized with 0.75 g ES per g silica (above the value required for a full monolayer) was blueish but had small aggregates with a diameter of up to ~ 1

mm at the bottom. The dispersion with the highest ES/silica ratio (1 g g^{-1}) was turbid with large aggregates and by-products with a diameter of ~ 1 – 3 mm at the bottom of vials. Any higher ratio above 1 g g^{-1} is expected to have higher turbidity and aggregation, as previously observed. The dispersions synthesized with 0.25 and 0.50 g g^{-1} did not show any aggregation or sedimentation after a few days of standing at room temperature; however, partial and complete sedimentation was observed with dispersions made with 0.75 g g^{-1} and 1 g g^{-1}, respectively. Therefore, particle stability inspections in DIW and Permian brine were only performed for the dispersions with ES/particle ratios of 0.25 and 0.50 g g^{-1} (see Appendix A.3).

The effect of the silane mass used during the synthesis of ES-coated silica on the initial particle diameter in DIW and Permian brine at 25 °C showed that the initial particle diameter in DIW and Permian brine is constant for ES/silica particle ratios up to 0.5 g g^{-1} while increasing sharply for the ratios above 0.75 g g^{-1} which is above the silane weight required for a full monolayer (0.6 g g^{-1}) (Figure 3.25).

Figure 3.24. Summary and appearance of dispersions during the synthesis of ES-coated silica by the modified synthesis route for different ES/silica particle ratios of 0.25, 0.50, 0.75 and 1 g g^{-1}.
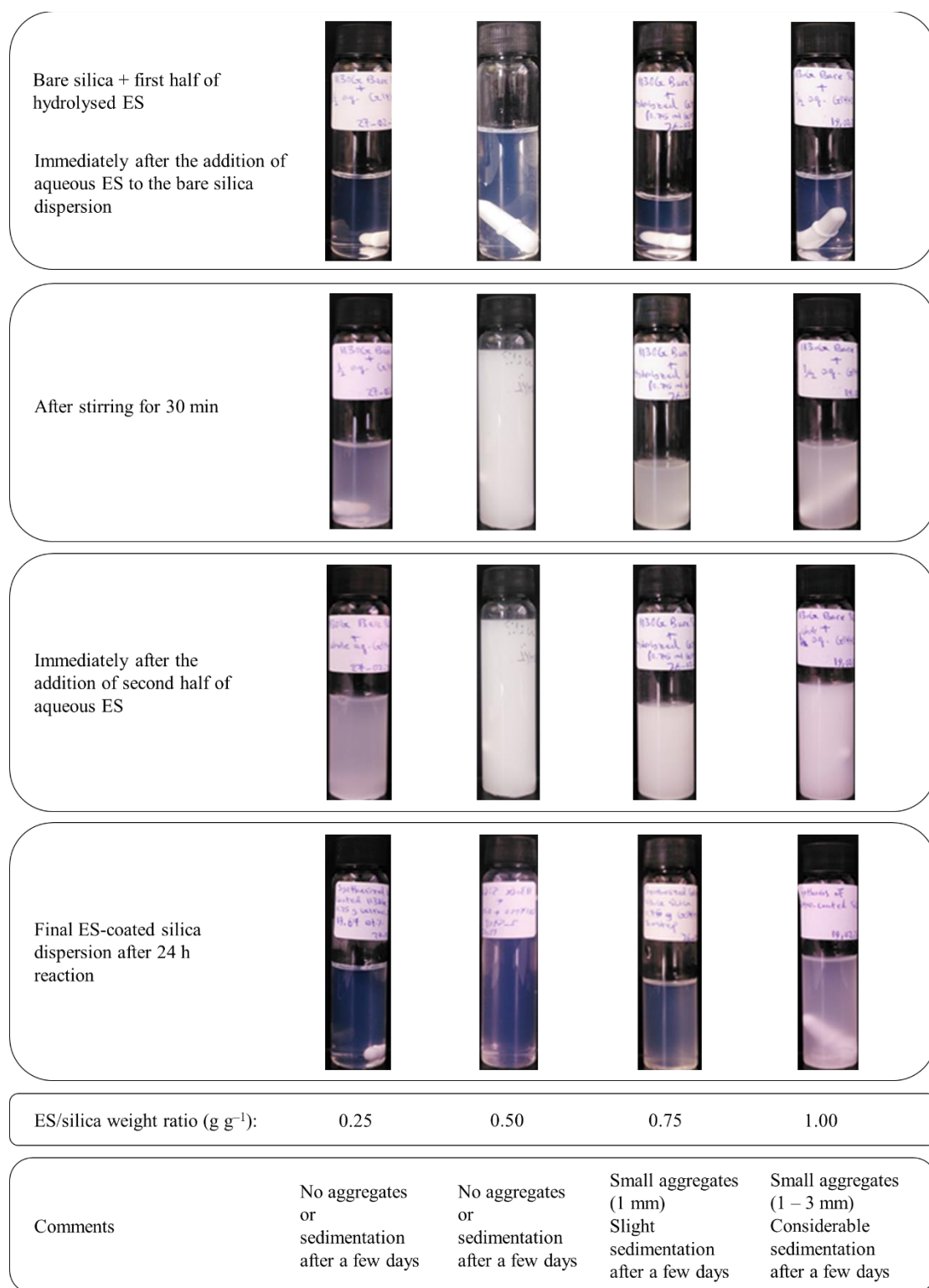
	0.25	0.50	0.75	1.00
Bare silica + first half of hydrolysed ES				
Immediately after the addition of aqueous ES to the bare silica dispersion				
After stirring for 30 min				
Immediately after the addition of second half of aqueous ES				
Final ES-coated silica dispersion after 24 h reaction				
ES/silica weight ratio (g g⁻¹):	0.25	0.50	0.75	1.00
Comments	No aggregates or sedimentation after a few days	No aggregates or sedimentation after a few days	Small aggregates (1 mm) Slight sedimentation after a few days	Small aggregates (1 – 3 mm) Considerable sedimentation after a few days

Figure 3.25. Effect of ES mass used during the synthesis of ES-coated silica on the initial particle diameter in DIW and Permian brine at 25 °C. The particles were synthesized with different silane/silica particle ratios by the modified synthesis route. The particle concentration was 0.1 wt.% in all dispersions.
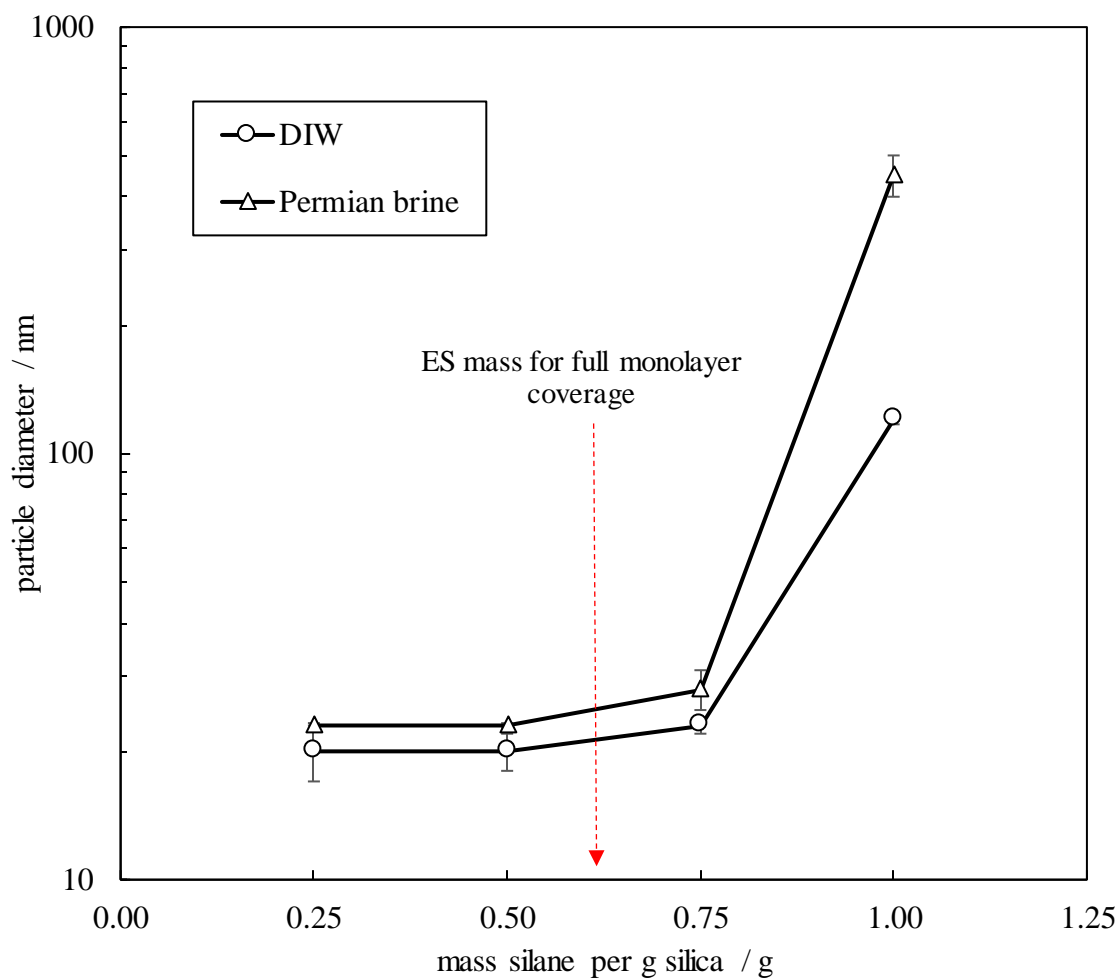
3.5.2 Properties

After optimization of the synthesis of ES-coated silica using different methods and silane/particle weight ratios, the synthesized particles from the sponsor were used in the

subsequent experiments to ensure reproducible results. As for AS-coated silica, the properties of ES-coated silica were first investigated to understand the later effects of particles alone or in a blend with surfactants on the oil-water, oil-rock and water-rock systems for EOR.

3.5.2.1 XRD

Figure 3.26 compares the diffraction patterns of bare silica and ES-coated silica. As explained earlier, the peak at $2\theta = 22°$ is the characteristic peak of amorphous silica. The intensity of this peak is almost the same for both AS- and ES-coated silica. The XRD analysis by Xpert Highscore shows that silica is tridymite (a high-temperature polymorph of silica, $Si_{80}O_{160}$). The crystal system of silica was found to be anorthic (or triclinic). Like AS, ES-coated silica has additional peaks at $2\theta = 43°$ and $50°$ as compared to bare silica which are related to the grafting of silica with silane by covalent bonds in the synthesis process. The intensity of these peaks is significantly higher for ES-coated silica but this cannot provide information on the coating extent of silane on particles as the intensity is a function of different setting parameters like micro-strains (*i.e.* the extent of distortion in the crystalline lattice), size, doping and vacancy.[195] No further peaks in the pattern prove the absence of impurities in the sample.

3.5.2.2 Extent of silanization

Figure 3.26 shows the TGA results of ES-coated silica. As described before, the small initial weight loss up to 150 °C is related to the removal of water from the sample. The second weight loss occurs from 150 °C to 370 °C and is associated with the degradation of silane physically adsorbed onto silica particles. The last weight loss (from 370 °C to 760 °C) is associated with the oxidation of silane molecules chemically adsorbed on particle surface. When the organic molecules of the silane react with oxygen from airflow at high temperatures, oxides like CO_2, H_2O and CO are formed. High oxidation temperatures are observed implying strong chemical bonds between silane and particles. The silane is predominantly chemisorbed on particles due to the higher chemical uptake of silane on silica.

Considering a 15.4% weight loss from 150 °C to 760 °C for the loss of organic ligand, the organic coverage (ϕ_i) on silica is calculated at 4.1 μmol silane m^{-2} of the silica. Given that 7.64 μmol silane per m^2 of silica surface gives a full silane monolayer, the ES coverage on silica in this sample is calculated at 55% of a full monolayer. Note that the

weight percentage is unchanged up to 200 °C indicating that the silane can tolerate the typical reservoir temperatures (70 – 130 °C) [111] without degradation.

Figure 3.26. XRD (top) and TGA/DTG (bottom) of ES-coated silica.
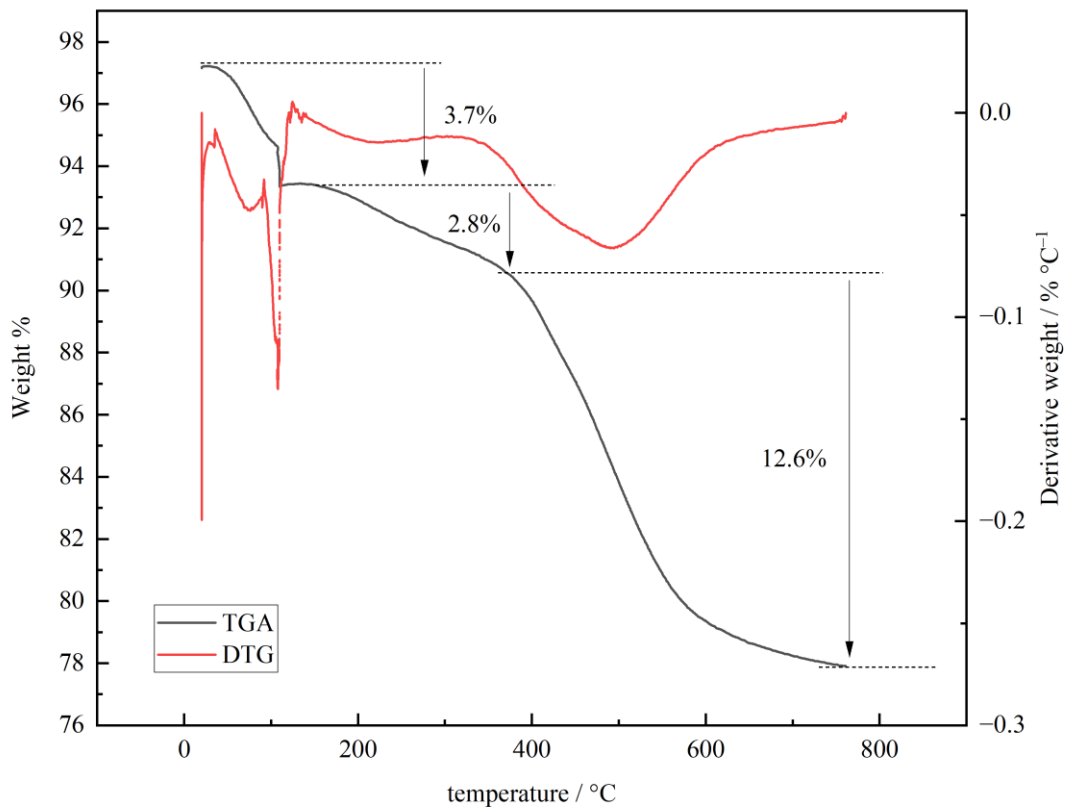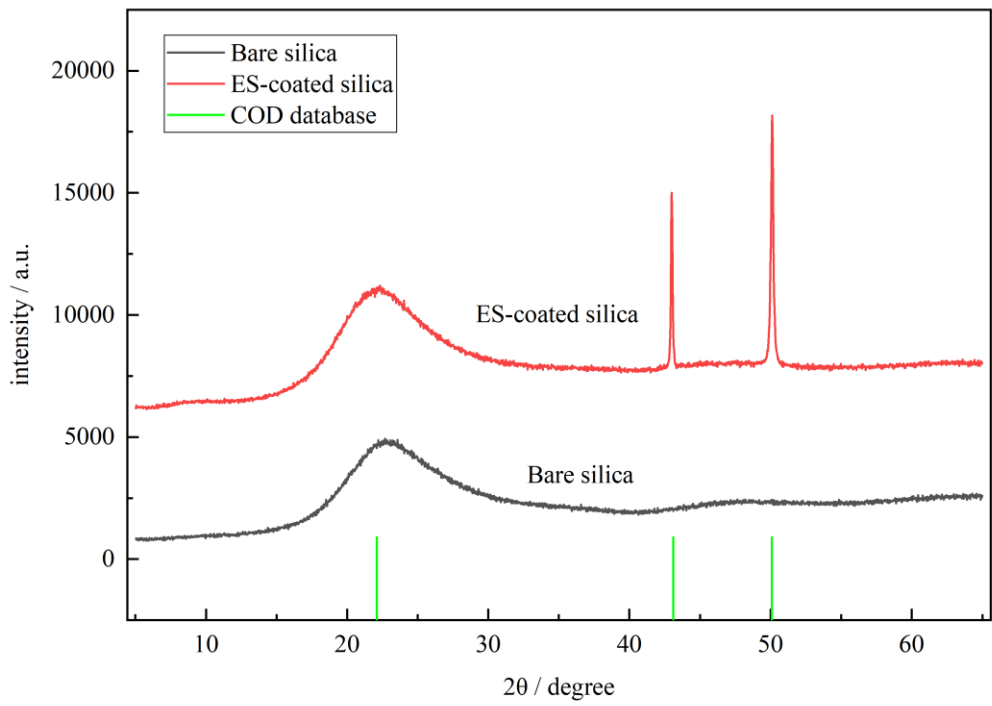
3.5.2.3 Particle stability

The stability of ES-coated silica with or without different concentrations of AHS and ZN surfactants in DIW and Permian brine was investigated at low and elevated temperatures visually and by particle diameter/zeta potential measurements. Since low particle concentrations (< 0.1 wt.%) are usually economically and technically viable for EOR purposes, 0.1 wt.% particles were chosen for stability inspections here. The objective of this part is to inspect and stabilize (if required) the sterically stabilized ES-coated silica for long-term colloidal stability at high salinity and high temperatures for EOR.

3.5.2.3.1 Particles in DIW and Permian brine

Figure 3.27 shows the stability of 0.1 wt.% ES-coated silica in DIW and Permian brine at original pH and reduced pH. The dispersions in DIW at the original pH were stable for 60 days at both temperatures and are expected to be stable for longer times. The dispersion in Permian brine was stable at the low temperature for two months while sedimentation was observed in the one at 75 °C after a week (not enough for EOR purposes). The long-term particle stability in DIW is mainly due to the electrostatic (charge-induced particle-particle repulsion) and steric (hindrance of ES) stabilization. Note that a full monolayer of silane on silica was not achieved during the synthesis of ES-coated silica. Thus, the uncoated sites on the surface of particles are at the highest charge density at high pH (9 – 10) due to the largest deprotonation of surface silanol groups. These negatively charged sites electrostatically attract the cations of the brine, especially Ca^{2+} and Mg^{2+}, which results in the charge neutralization of particles and the disappearance of particle-particle electrostatic repulsion. If steric hindrance by silane is not enough, particle aggregation and sedimentation happen due to the dominance of van der Waals attraction which is intensified at high temperatures due to high Brownian motion and particle collisions. Ions such as Mg^{2+} and SO_4^{2-}, on the other hand, have low activity at low temperatures.[52, 200] At high temperatures however the H-bonds around the ions are broken and the activity of the ions increases which finally increases their contribution to the aggregation and sedimentation of particles. That is why sedimentation occurred in a dispersion of particles in Permian brine at 75 °C while the low temperature dispersion was stable for two months.

The stability of the same dispersions was also investigated at an acidic pH (by HCl) (Figure 3.27). As indicated, the dispersions containing particles in Permian brine were stable at both temperatures for around 7 months by pH reduction. The extent of cation attraction and screening of particle surface charges by cations decreases significantly with pH reduction and as a result, the dispersions were made stable for a long time. Note that if silane hindrance was not available, the pH reduction was expected to destabilize the

particles in Permian brine at high temperatures due to the reduced electrostatic repulsion between particles.

All dispersions of 0.1 wt.% ES-coated silica in DIW and Permian brine at the original pH (8.8 – 10.0) and reduced pH by HCl (~ 4) had an initial particle diameter of 23 ± 3 nm at 25 °C. Although pH reduction did not affect the initial particle diameter, it considerably extends the particle stability in brine at high temperatures as observed earlier. The zeta potential of particles in DIW was measured at $- 27 \pm 1$ mV which was reduced to $- 13.9 \pm 1$ mV on reducing pH. This decrease in zeta potential is associated with the protonation of silanol groups at low pH. Figure 3.28 presents a comparison of the initial particle diameter and zeta potential of bare silica and ES-coated silica in DIW at 25 °C. The higher particle diameter and zeta potential of ES-coated silica are due to the silane coverage on the surface of silica and the termination of silanol groups by silane, respectively.[12]

Figure 3.27. Appearance of dispersions containing 0.1 wt.% ES-coated silica in DIW and Permian brine at the original and reduced pH (by HCl) at two temperatures at different times.
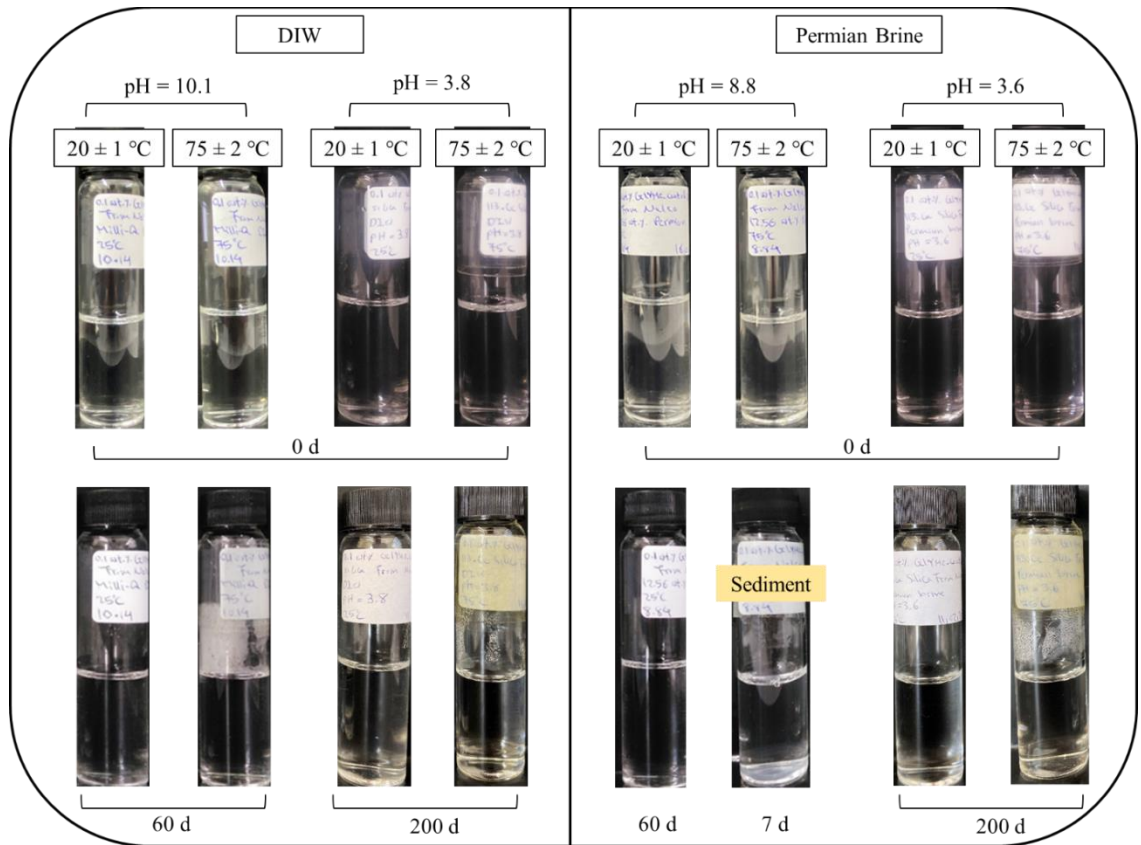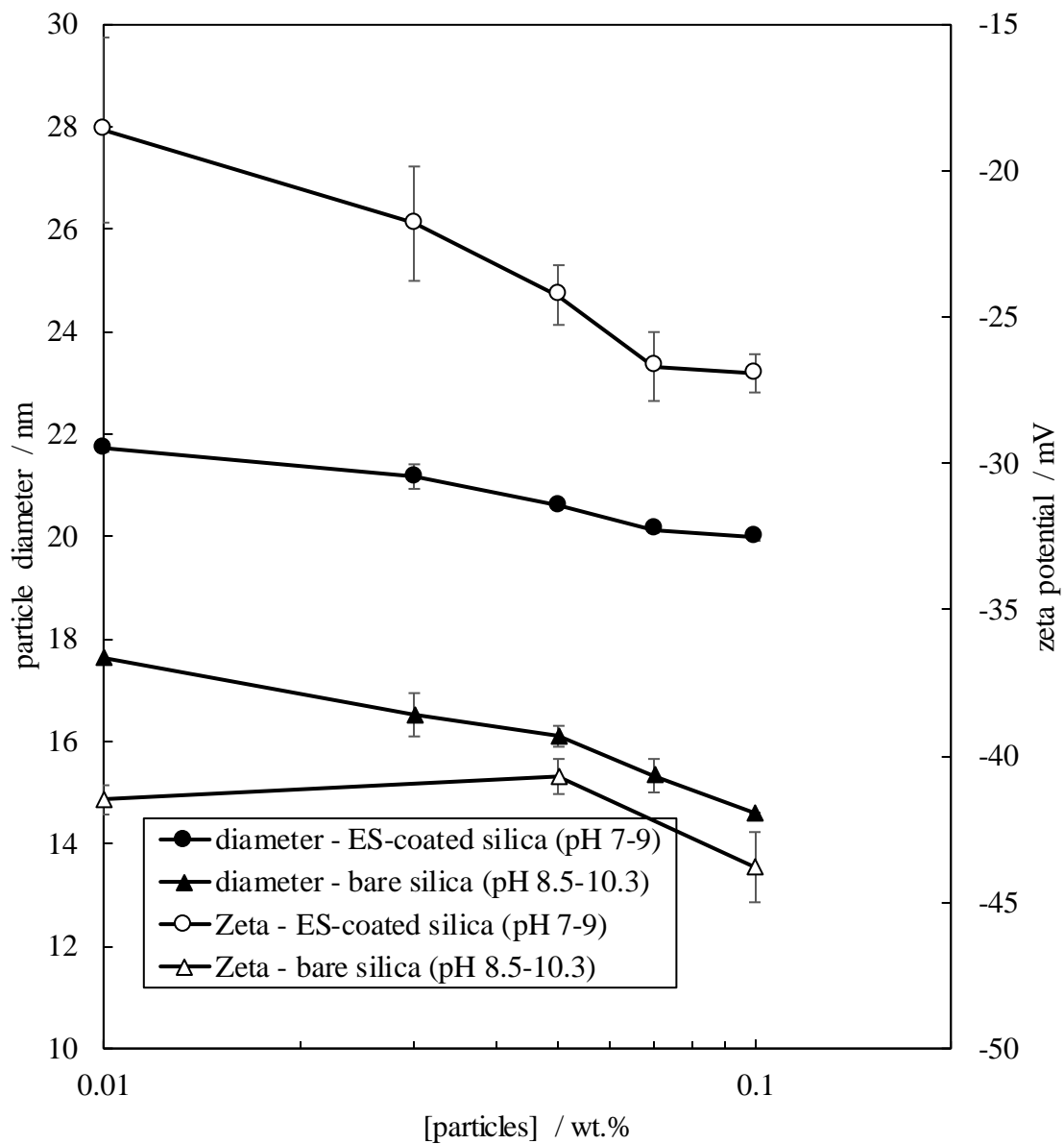
Figure 3.28. Effect of ES coverage on the initial particle diameter and zeta potential of bare silica at 25 °C.

The effect of pH reduction on the re-dispersibility of particles in a sedimented dispersion of ES-coated silica in Permian brine was also investigated. Figure 3.29 shows the stability of 0.1 wt.% ES-coated silica in Permian brine (original pH = 8.8 at 23 °C) with time. When sedimentation happened in the dispersion at 75 °C, the pH of both dispersions was reduced to 3.5 at 20 °C using HCl. The dispersions were then stirred for 30 min before being monitored for stability once more. Interestingly, the particles became re-dispersed with pH adjustment and were stable for a long time (180 days). This observation implies that pH reduction is effective in controlling the particle surface charges and reducing the electrostatic attraction between brine cations and anionic particles even after initial sedimentation. This is critical for EOR processes where long-term particle stability in a high salinity brine and high temperature is required.

The same effect was observed when using aluminium sulphate in dispersions. Figure 3.30 shows the stability of blends of ES-coated silica and aluminium sulphate ($Al_2(SO_4)_3$) in DIW and Permian brine. The concentration of $Al_2(SO_4)_3$ in these dispersions was kept at 10% of the particle concentration. As shown, all dispersions were stable for more than 6 months on the addition of aluminium sulphate. As explained before, the dilute sulfuric acid produced on the addition of $Al_2(SO_4)_3$ can reduce the pH of dispersions (4.4 ± 0.1 at 20 °C) and the particle-cation electrostatic attraction which improves the particle stability. The zeta potential of particles in DIW was found to increase to around zero on adding aluminium sulphate to all dispersions at 25 °C but the particles survived aggregation thanks to the steric stability induced by ES. In the absence of silane hindrance, bare particles aggregate and sediment upon adding electrolyte due to the surface charge neutralization as observed before. The initial particle diameter of all dispersions in DIW and Permian brine at original and reduced pH was 25 ± 3 nm. Like HCl, aluminium sulphate did not affect the initial particle diameter but long-term stabilized the particles in brine at high temperatures.

Figure 3.29. Appearance of dispersions containing 0.1 wt.% ES-coated silica in Permian brine at two temperatures at different times (initial pH = 8.8 at 20 °C). When sedimentation occurred, the pH of both dispersions was reduced to 3.5 using HCl.
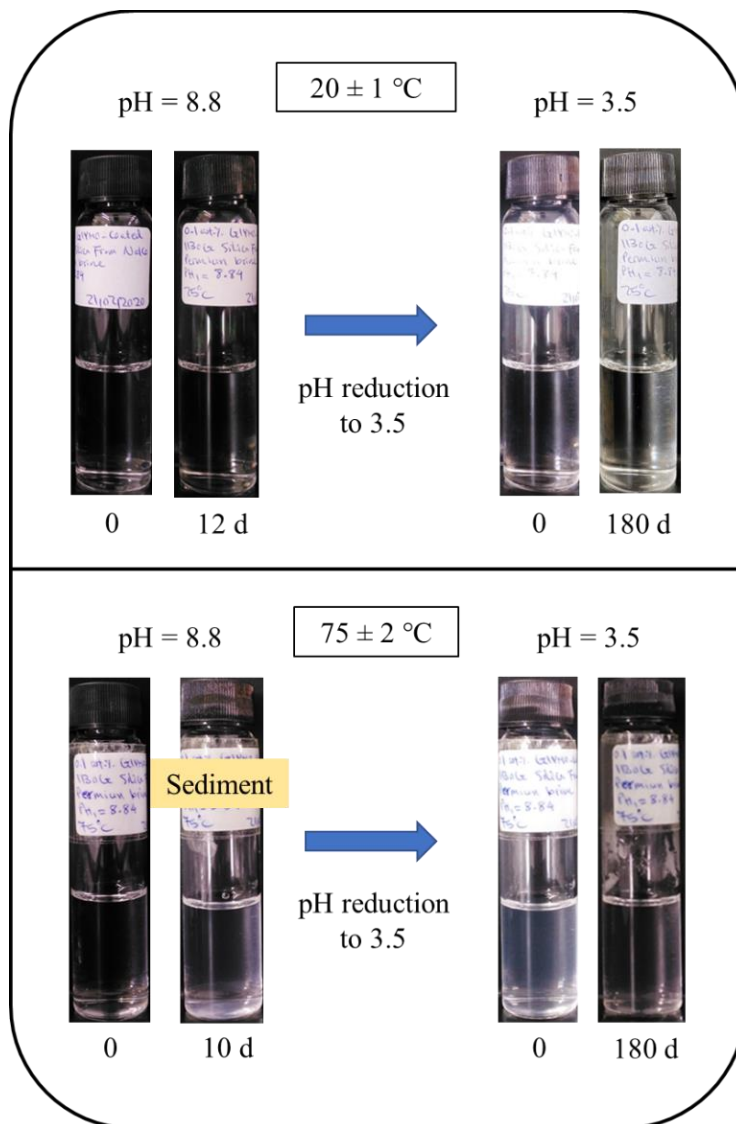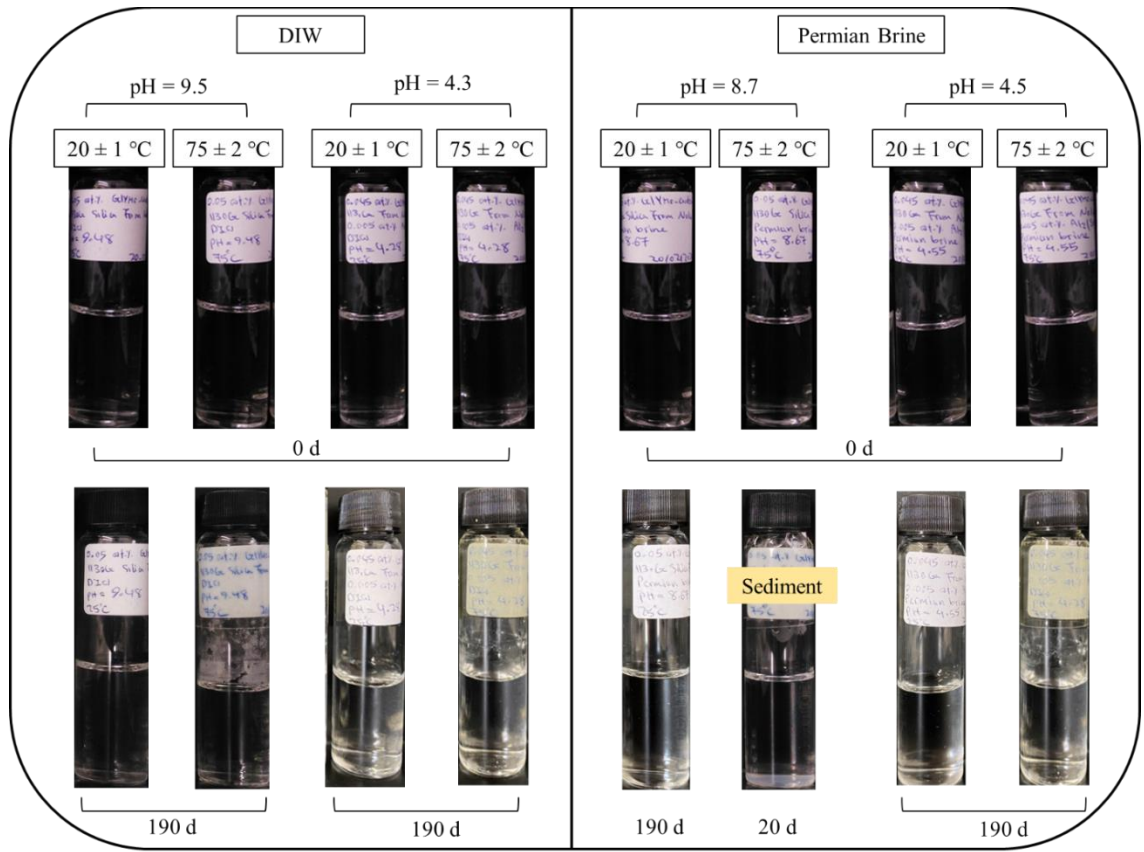
Figure 3.30. Appearance of dispersions containing 0.05 wt.% ES-coated silica with and without 0.005 wt.% aluminium sulphate in DIW and Permian brine at two temperatures.

3.5.2.3.2 Blends of particles and AHS surfactant

The stability of nanoparticles in a blend with surfactants is important in EOR processes. Figure 3.31 shows the stability of 0.1 wt.% ES-coated silica in a blend with different AHS concentrations (0.001 – 1 wt.%) in DIW and Permian brine at original pH. As seen, all dispersions in DIW were stable at both temperatures for a long time. The dispersions in Permian brine at the low temperature were also stable for more than 6 months while sedimentation was observed in the ones at 75 °C after nearly 2 – 4 weeks.

At relatively high electrolyte concentrations, surfactant can stabilise nanoparticles in dispersions in two different ways. The headgroups of the surfactant molecules adsorb onto the nanoparticle surface when an oppositely charged surfactant is added to a colloidal dispersion, leaving the hydrocarbon chains toward the water phase. This creates a barrier between the particles, preventing them from coming into close contact and aggregating. When two nanoparticles get close to one another, the chains overlap, stabilising the dispersion sterically by creating extra osmotic pressure and elastic forces. However, if this energy barrier is dominated by *e.g.* ions, particle aggregation occurs. The increased charge of the particle surface can also produce a stable dispersion electrostatically preventing the particles from colliding and aggregating when the tails of surfactants adsorb on the particle surface or when the surfactant monolayer on the nanoparticle surface changes to a bilayer at high surfactant concentrations. The first mechanism is thought to be stronger than the second one at high electrolyte concentrations. When the surfactant adsorbs onto the surface of nanoparticles, it can reduce the surface energy of the nanoparticles, making them less likely to aggregate.[122]

Figure 3.32 shows the effect of AHS concentration on the initial particle diameter and zeta potential of ES-coated silica particles in the blend at 25 °C. As shown, the initial particle diameter decreases with an increase in surfactant concentration in the blends due to the increased electrostatic adsorption of surfactant molecules on the particle surfaces which agrees with the increased zeta potential of particles towards zero on increasing AHS concentrations in the blend.

Figure 3.31. Appearance of dispersions containing 0.1 wt.% ES-coated silica in a blend with different concentrations of AHS surfactant in DIW (top) and Permian brine (bottom) at original pH at two temperatures.
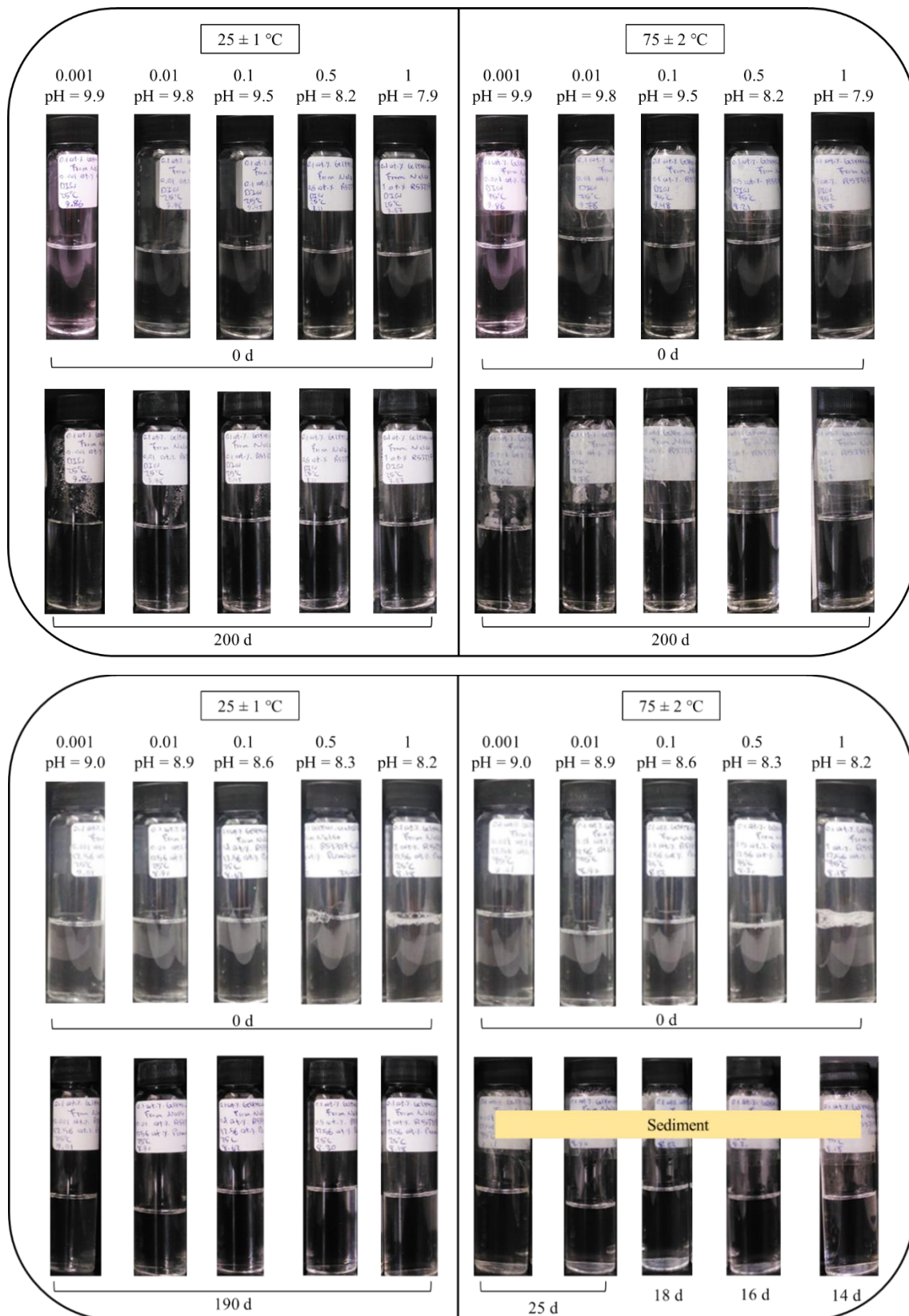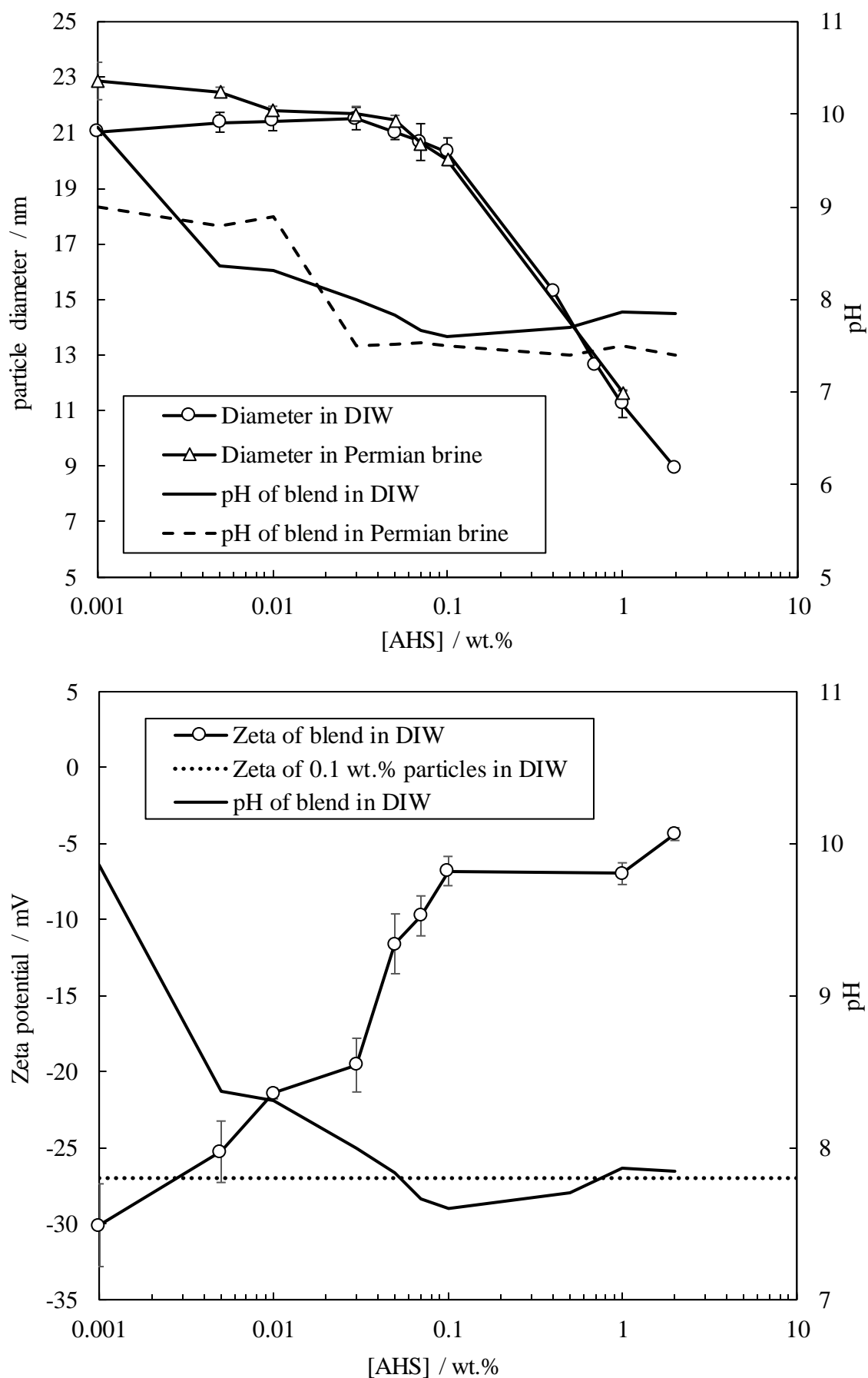
Figure 3.32. Initial particle diameter (top) and zeta potential (bottom) of 0.1 wt.% ES-coated silica in a blend with different concentrations of AHS surfactant at 25 °C.

3.5.2.3.3 Blends of particles and ZN surfactant

Figure 3.33 shows the appearance of dispersions containing 0.1 wt.% ES-coated silica in a blend with different concentrations of ZN surfactant (0.001 – 1 wt.%) in DIW and Permian brine at the original pH. The dispersions of particles in DIW were all stable at both temperatures up to 200 days except for high surfactant concentrations of 0.5 and 1 wt.% at 75 °C which showed sedimentation after one day. All dispersions in Permian brine kept at the low temperature were stable for up to 200 days while sedimentation was observed in the ones at 75 °C. For [ZN] $\leq$ 0.1 wt.%, sedimentation was slower (after 3 – 4 weeks) whereas the dispersions with 0.5 and 1 wt.% ZN became turbid at 75 °C after a day. An increase in the initial particle diameter was observed for both dispersions when the surfactant concentration was > 0.1 wt.% (Figure 3.34). With an increase in ZN concentration from 0.001 wt.% to 0.07 wt.% in the blend in DIW, the zeta potential changed from – 27 mV to – 3 mV and remained unchanged at higher surfactant concentrations up to 1 wt.%.

Figure 3.33. Appearance of dispersions containing 0.1 wt.% ES-coated silica in a blend with different concentrations of ZN surfactant in DIW (top) and Permian brine (bottom) at original pH at two temperatures.

Figure 3.34. Initial particle diameter and zeta potential of 0.1 wt.% ES-coated silica in a blend with different concentrations of ZN surfactant in DIW and Permian brine at 25 °C.

135
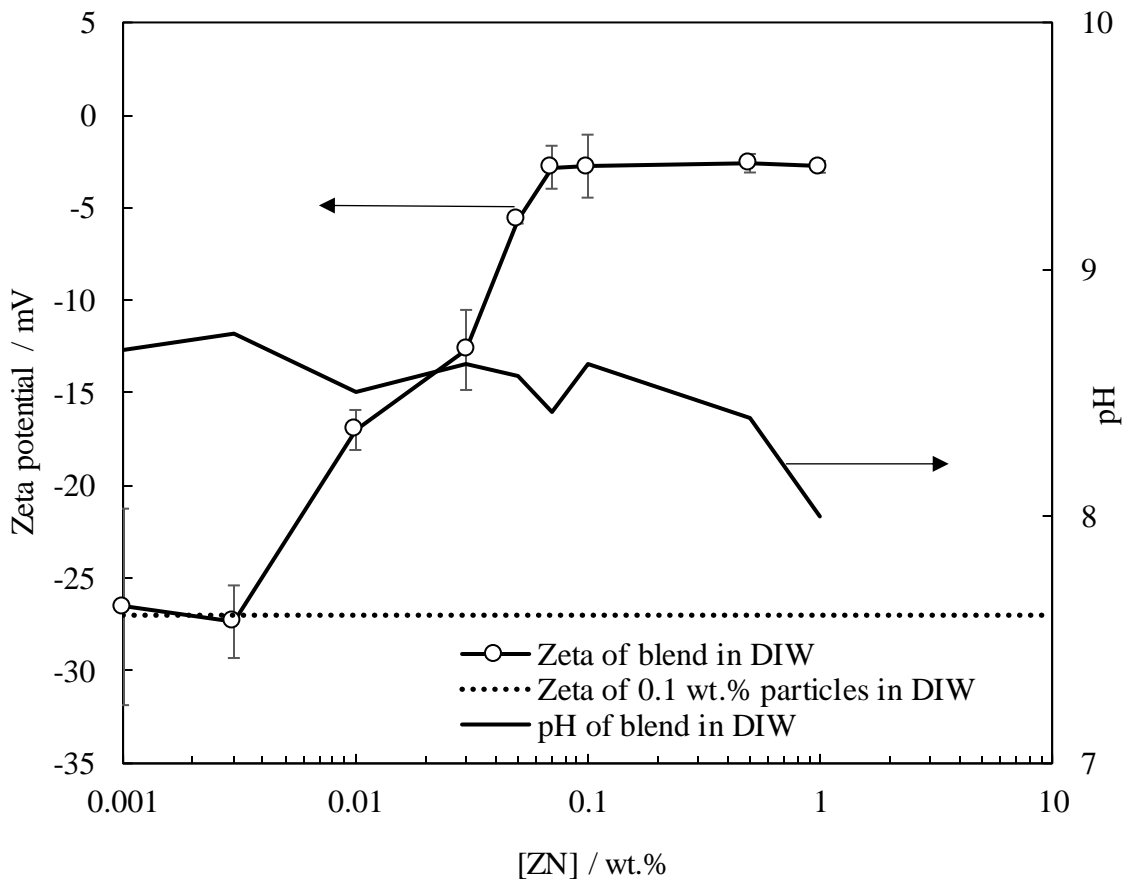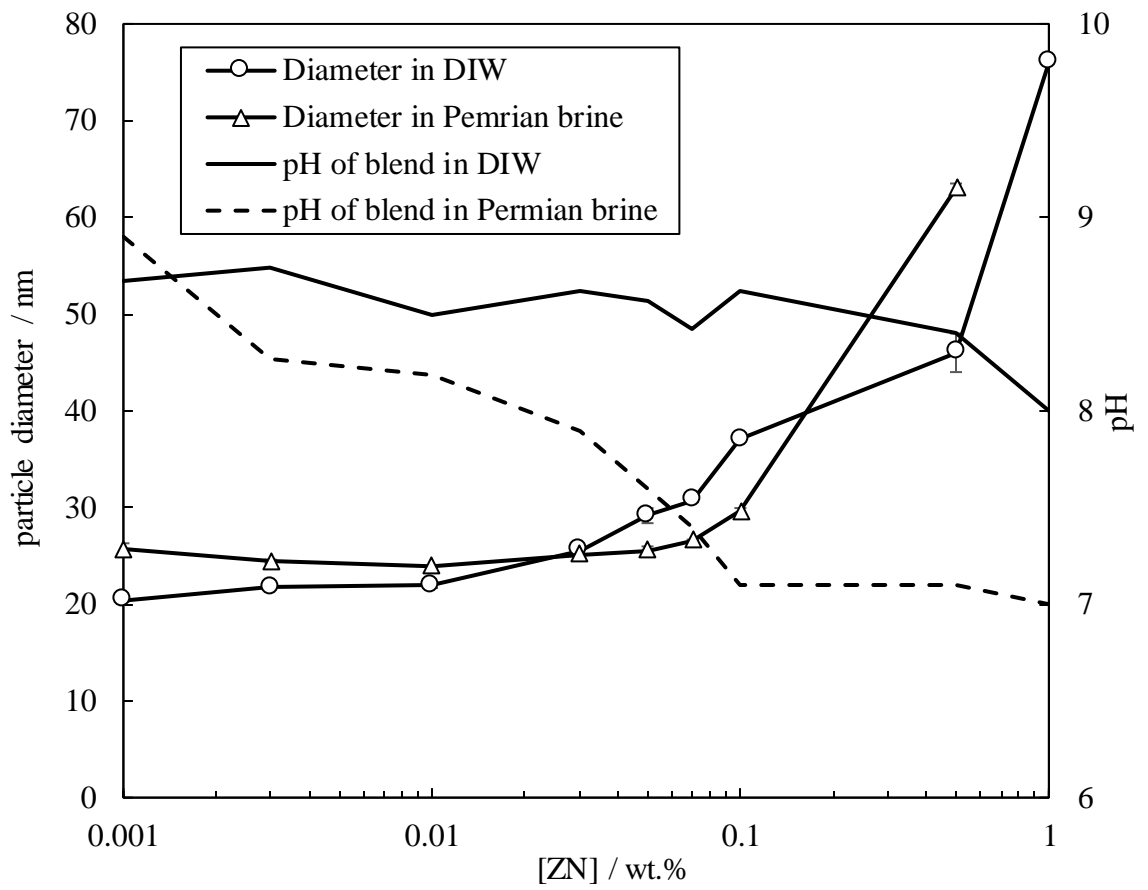
3.5.2.4 Particle surface activity

Large changes in air-water surface tensions on adding particles can be interpreted as particle surface activity. Figure 3.35 shows the air-water surface tension of different concentrations of ES-coated silica in DIW and Permian brine at the original and reduced pH at 25 °C. As seen, surface tensions decrease from the reference lines (surface tensions of DIW and Permian brine) upon adding particles but this reduction is not large. As described earlier, ES-coated silica particles have hydroxyl groups on both uncoated and coated sites (due to the opening of the ES epoxy ring by hydrolysis during synthesis). However, the hydrocarbon group in the silane tip can indue partial hydrophobicity given that the ether bond is flexible enough to bend at the air-water surface. This is usually possible when the silane coverage is small enough to provide sufficient spaces between silane molecules grafted on silica to bend freely. In the case of high silane coverage on silica however, the particles become large and grafted silanes cannot freely bend thus they have to expose the hydroxyl groups to the surface which makes them purely hydrophilic and non-surface active.[12] Regarding the silane coverage on silica (55%) and the surface tension measurements here, ES-coated silica particles are not thought to be highly surface active.

The similar charges of particles and air-water surface electrostatically prevent high particle adsorption but pH reduction can reduce the charges of both, enabling more particle adsorption at the air-water surface, consistent with more surface tension decrease on pH reduction. The adsorption energy of spherical particles at an air-water surface can be calculated using:[201]

$$\Delta E = \frac{(\gamma_o - \gamma)\ \pi r^2}{\eta} \tag{3.3}$$

Where γ_o and γ are the surface tensions of DIW or Permian brine and dispersions (mN m^{-1}), r is the particle radius (nm) and η is the packing parameter (0.91 for closely packed monolayer). This equation is valid assuming that the particle contact angle is 90°. Figure 3.36 shows the variation of adsorption energy with particle concentration at 25 °C. At the original pH, the adsorption energy was almost independent of particle concentration when particles were in DIW but became more negative with raising the particle concentrations in Permian brine. At low pH, a decrease and increase in adsorption energy are observed with increasing particle concentrations in DIW and Permian brine, respectively.

Figure 3.35. Air-water surface tension of different concentrations of ES-coated silica in DIW (upper) and Permian brine (lower) at original and reduced pH at 25 °C. The dashed lines are the surface tensions of DIW and Permian brine.
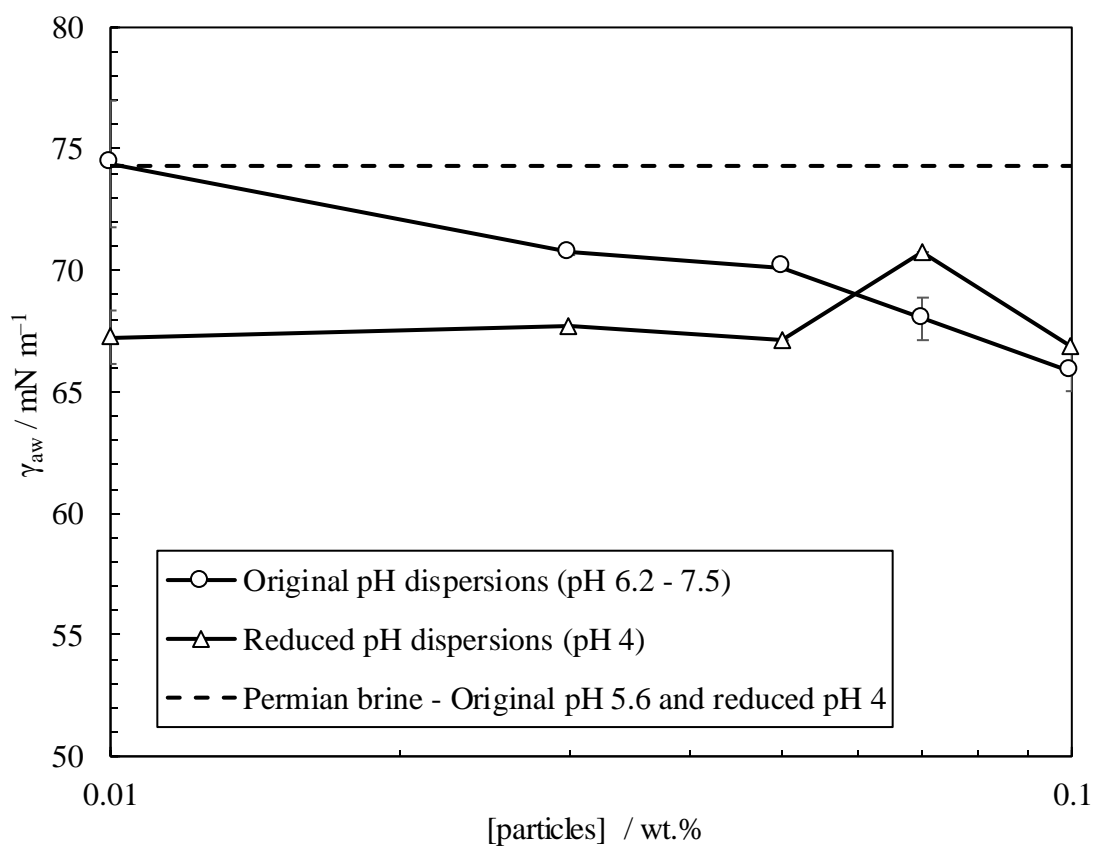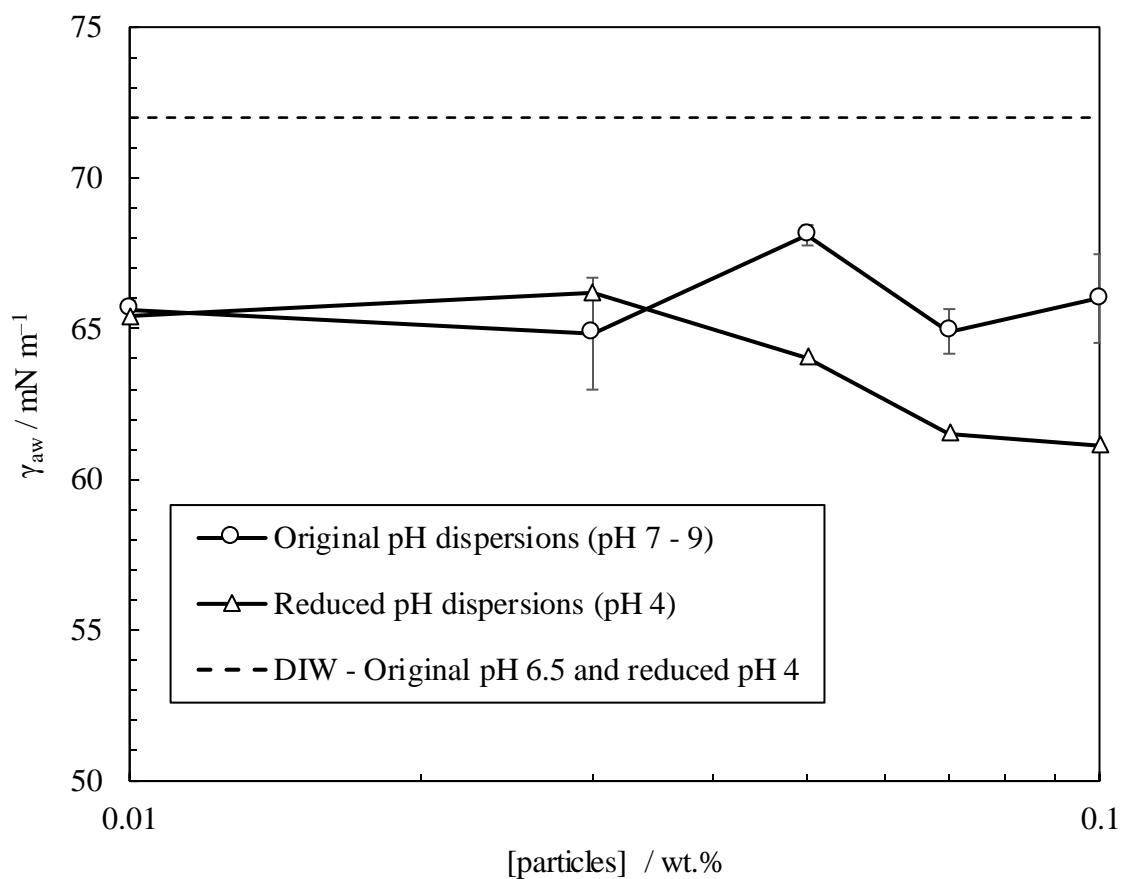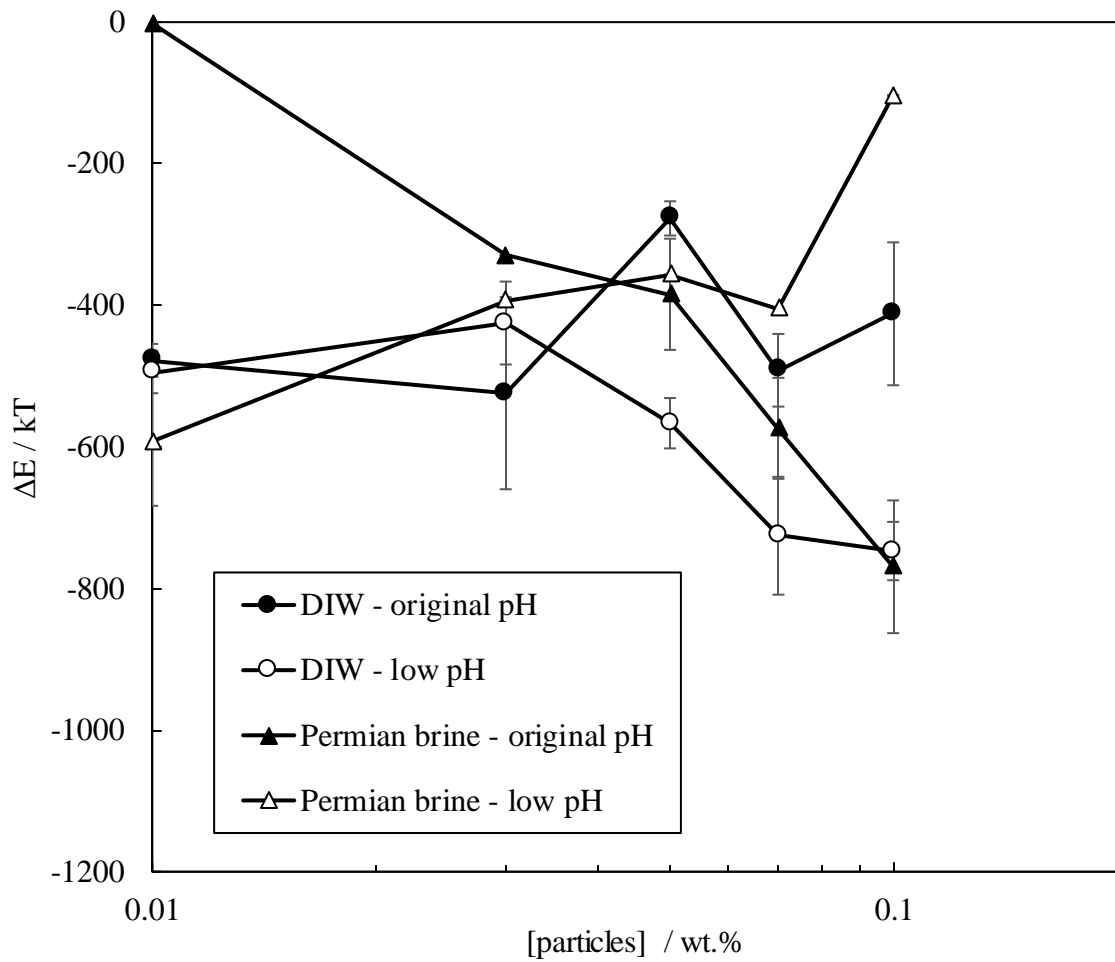
Figure 3.36. Adsorption energy (ΔE) of ES-coated silica particles in DIW and Permian brine at air-water surface at 25 °C under different pH environments.

3.6 Properties of rock

The surface chemistry, roughness, surface area, pore size and pH are important features of the rock in chemical EOR. For example, certain minerals may interact with surfactants in specific ways or the pH of the reservoir may alter the surfactant ability to adsorb onto

139

the surface. Thus, the properties of the rock will determine the nature and strength of its interactions with EOR chemicals like surfactants and particles, and these interactions can significantly impact the effectiveness of the EOR technique in the reservoir.[158]

3.6.1 Powder size and XRD

As explained in the methodology, the Wolfcamp shale sample was powdered and sieved into different size groups. Figure 3.37 shows the size distribution and XRD of shale powder. The XRD peaks match a rock consisting mostly of calcite. The crystal system of calcite was found to be hexagonal. The peak indexing at $2\theta = 22°$ is indicative of quartz (filled square). The calcite peaks have been shown in filled circles in the figure. The Rietveld refinement shows 97.20 ± 0.06 % calcite and 2.80 ± 0.06 % quartz in the sample.

Figure 3.37. (Top) Particle size distribution of shale powder of different sieve groups (the values on top of each distribution show the volumetric weighted average D[4, 3]). (Bottom) XRD of shale (10 µm).
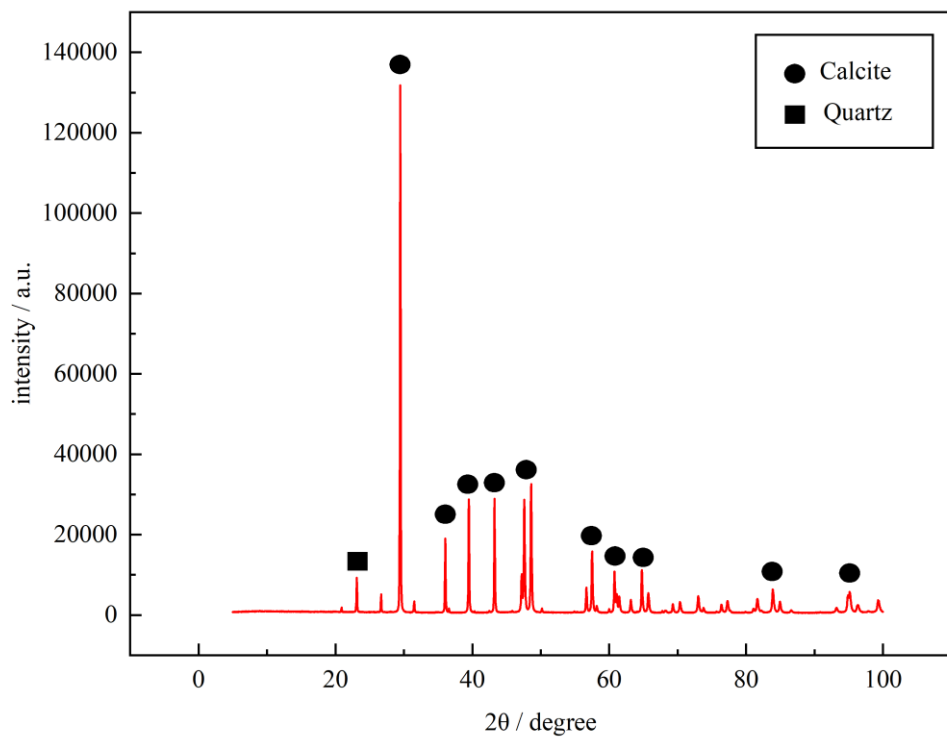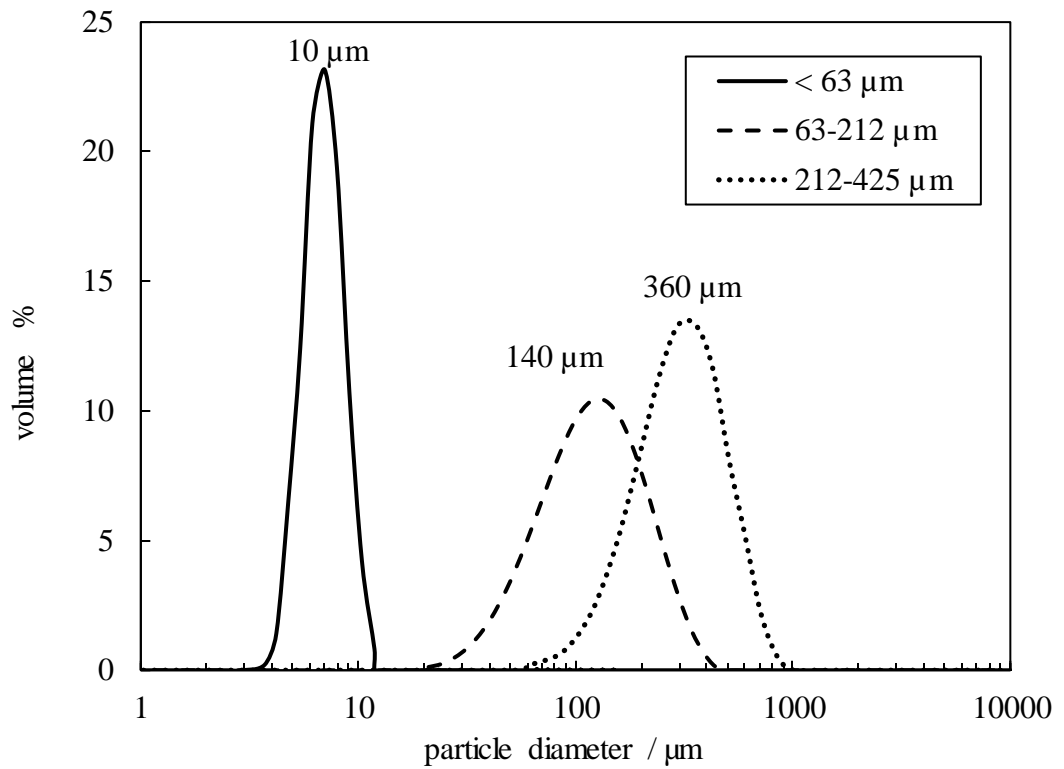
3.6.2 Charge of shale

The ZPC is the pH at which the rock surface has a zero net charge. The rock surface will have a positive and negative charge at pH values below and above the ZPC, respectively. The ZPC of a rock is determined by the chemical composition of the minerals present in

the rock, as well as the type and concentration of ions present in the surrounding fluids (*i.e.* water or oil). Common minerals that can contribute to the ZPC of rock include quartz, clay, carbonates and oxides. The ZPC of rock is an important factor to consider in chemical EOR techniques since the rock charge affects the adsorption of the chemicals which can impact the efficiency of the EOR process.[158]

Figure 3.38 shows the variations in pH with the initial pH of shale powder (10 µm) in two electrolytes for ZPC determinations. According to the figure, the ZPC of shale powder in 0.01 M NaCl is ~ 9.3 which is near that of calcite at ~ 9.[202] Previous studies show that NaCl is ineffective in calcite-water systems for changing ZPC[45] necessitating the determination of ZPC in Permian brine. The ZPC of shale powder is reduced to ~ 8 on adding Permian brine. The zeta potentials of different concentrations (0.01 – 0.1 wt.%) of 10 µm shale powder in DIW (original pH = 9.6 ± 0.2 > pH_{ZPC}) at 25 °C were – 18 ± 1 mV independent of shale concentration. In addition to the effect of pH, the shale also has 3% quartz (SiO_2) which is anionic at this pH. Figure 3.39 shows the effect of pH on the zeta potential of shale in DIW. As seen, the zeta potential is negative at all pH values for both suspensions. Saxena *et al.* looked into how pH affected the charge of bentonite, carbonate and sandstone in DIW. For all three rock samples, they noticed a nearly zero zeta potential at high (12) and low (2) pH and a negative charge at other pH values. The samples were at their most anionic at neutral pH (7 ± 1). While bentonite's negative charge was related to the hydroxyl groups of the basal planes of its layered structure, that of sandstone was attributed to the silanol groups (SiOH) formed by water molecules and consequent deprotonation of them at the rock surface. They claimed that the anionic carbonate charge was influenced by the presence of other minerals like quartz or the dissociation of calcium ions in water.[121] Here, the negative charge of shale at low pH is related to the dissolution of calcite which leaves the anionic quartz creating a negative zeta potential.

Figure 3.38. Determination of ZPC of shale powder (10 µm) in 0.01 M NaCl and Permian brine using the pH drift method. pH_1 and pH_2 represent the initial and equilibrium (after 48 h) pH of suspensions, respectively.
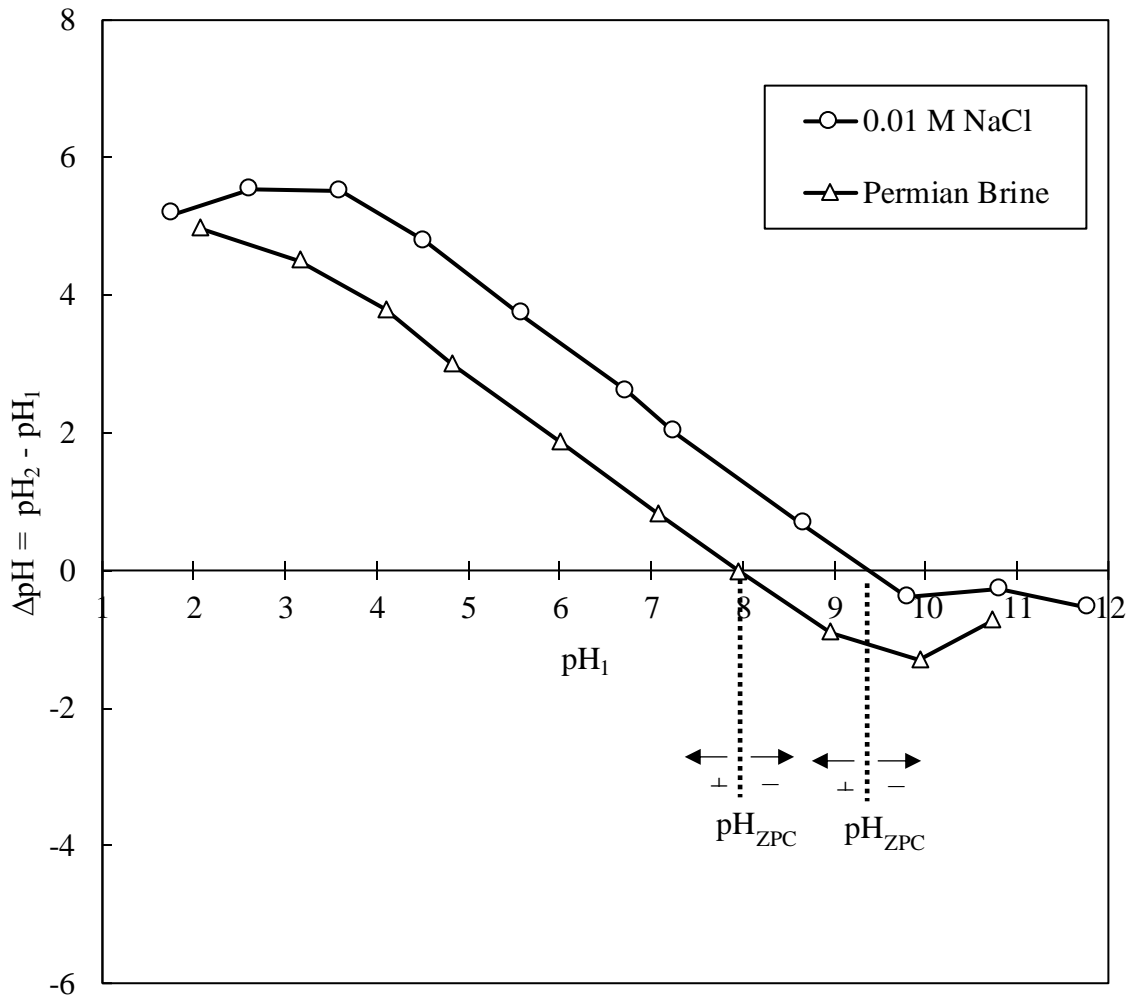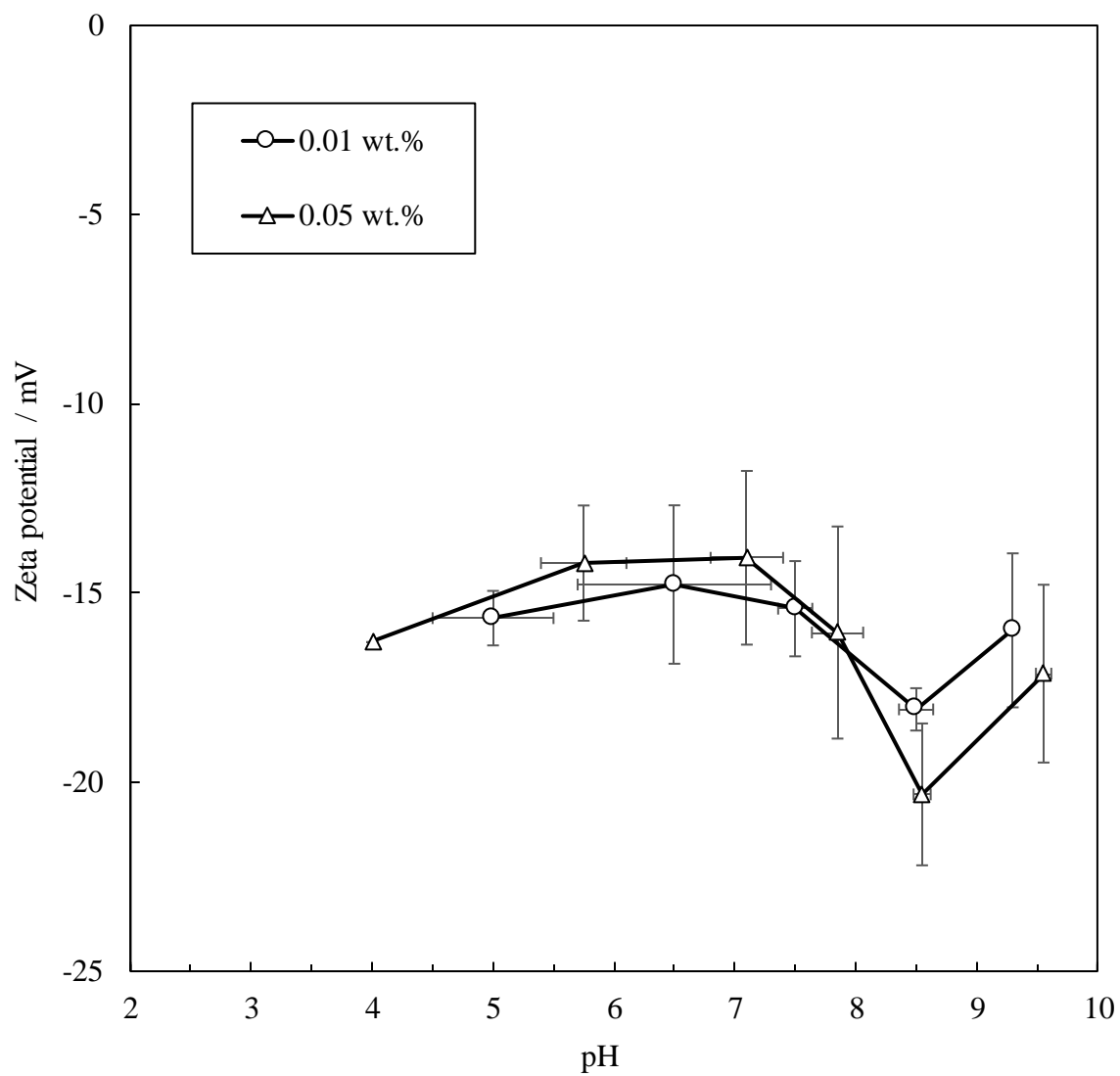
+

Figure 3.39. Variation of zeta potential with pH for different concentrations of 10 µm shale powder in DIW at 25 °C. 1 N NaOH and 1 M HCl were used for pH adjustment.
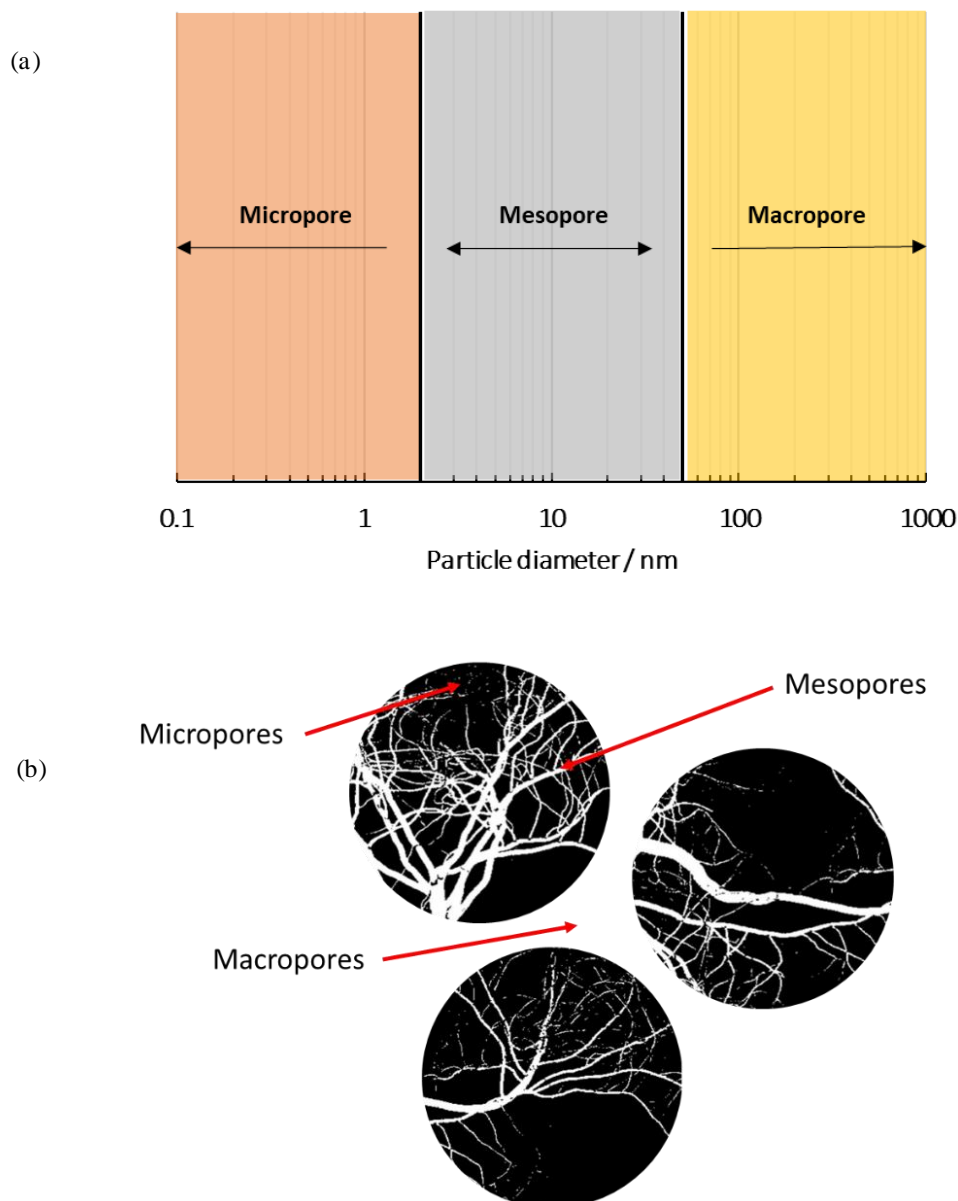
3.6.3 Surface area and pore size

Pores are the openings in solid surfaces into which liquids, gases and particles can enter. Reservoir rocks must be porous to store hydrocarbon. Sedimentary background, diagenesis (*i.e.* post-deposition physical and chemical changes in sediments), compaction by overburden, cementation (*i.e.* precipitation of mineral matter in the pore spaces) and dissolution are key factors determining the average pore size, pore size distribution and pore structure in oil reservoirs.[203] The International Union of Pure and Applied Chemistry (IUPAC) classifies pores into micropores, mesopores and macropores.[204] Micropores and mesopores are arranged within rock grains but macropores, also known as interparticle pores, are mostly created between particles (Figure 3.40).

Figure 3.40. (a) Size range and (b) visual representation of different pore types defined by IUPAC.

Brunauer–Emmett–Teller (BET) analysis is a useful tool to investigate the surface area, pore structure and pore size distribution of porous materials like rock. BET theory is an extension of the Langmuir adsorption isotherm and considers multilayer gas adsorption in which gas molecules can adsorb onto the surface in infinite layers but with no inter-layer interactions. Applying to each of these layers, the BET model assumes that gas molecules behave ideally to form a monolayer with a homogenous surface and no adsorbate-adsorbate interactions. The surface sites have equal adsorption energies for adsorbate, and the upper layer is in equilibrium with the vapour phase. BET analysis usually comes with adsorption/desorption isotherms which are used for the analysis of the surface area, pore size and pore structure.[148]

Shale powder with an average particle diameter of 140 µm and 360 µm was selected for cryogenic nitrogen BET analysis at 77 K (Figure 3.41). As the rock was degassed initially, dosing nitrogen into the analysis tube makes atoms first adsorb onto the surface of the smallest pores *i.e.* micropores. As the relative pressure (P/P$_o$) increases, nitrogen will adsorb on the external surfaces and also on the surface of bigger pores *i.e.* mesopores and macropores until a monolayer forms (typically at P/P$_o$ = 0.3 – 0.5) which is used for BET surface area calculations.[148] Both adsorption isotherms have a positive curvature at low relative pressures due to the adsorption being done more on energetically favourable sites. Both plots show a type II adsorption isotherm and a macroporous sample (> 50 nm), according to the Brunauer-Deming-Deming-Teller (BDDT) classification.[205] As relative pressure increases, adsorption volumes increase linearly in both, allowing us to calculate the BET surface area. At high relative pressures, the isotherms continue to increase until saturation is achieved. The final adsorption rise in both plots is due to the nitrogen-nitrogen multilayers on a non-porous sample or to the incomplete filling of a macroporous sample. The isotherm behaviour and type here are in agreement with the study by Liu *et al.* on shales.[206] When the adsorption process was finished, *i.e.* when the highest adsorption pressure was reached and the adsorption volume was determined, the relative pressure was gradually reduced and the volume of nitrogen desorbed from the rock was determined for both powder sizes (Figure 3.41). The desorption isotherms in both figures show type H3 hysteresis.[207] The presence of hysteresis usually implies the presence of porosity in the sample but a sharp rise in adsorption at high relative pressures shows the dominance of meso- and macropores in the rock which are not filled as saturation is reached. The hysteresis is basically because of the different processes occurring during adsorption and desorption. Pore filling by condensation happens during adsorption while pore emptying performed by evaporation happens during desorption. Condensation starts

from the pore walls and continues towards the centre of the pores until they are filled. On the other hand, emptying starts from the top of the pores downwards until they are all empty. Figure 3.42 shows the transformed plot of isotherms for both shale powder sizes. The slope and intercept of the linear regression lines fitted to experimental data points of the adsorption isotherm were used to calculate the BET surface area. Adsorption isotherms give information about pore sizes while desorption isotherms can show how open or restricted pore throats are. Table 3.4 presents the BET parameters and pore volumes of the samples. The large BET values imply that the rock has a high potential for adsorbing chemicals in EOR. The small pore volumes show that the shale rock is tight with low porosity.

Barrett-Joyner-Halenda (BJH) analysis can help to determine the average pore size and pore size distribution in the rock. Figure 3.43 shows the BJH pore size distribution of two shale powders which is the mathematical slope of the cumulative pore volume (V) in the log scale *versus* the pore diameter (D). As can be seen, there are no significant peaks below 100 nm while the plots increase at pore widths > 120 nm, confirming that the rock is mostly macroporous (> 50 nm pore width). Typically, if macropores are larger than 200 – 300 nm, they are too big to be filled with nitrogen as saturation approaches which leads to the final rise in the plots. Therefore, the BET method has a limitation for pore sizes above 200 – 300 nm.

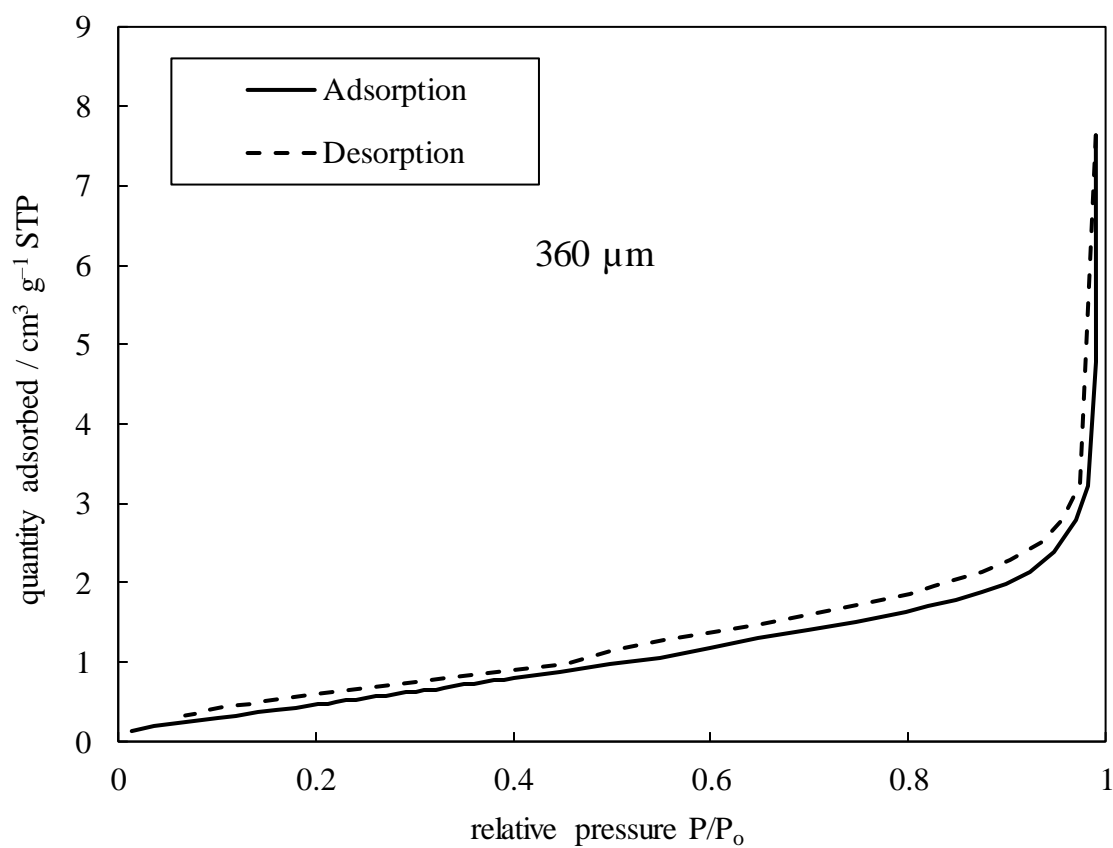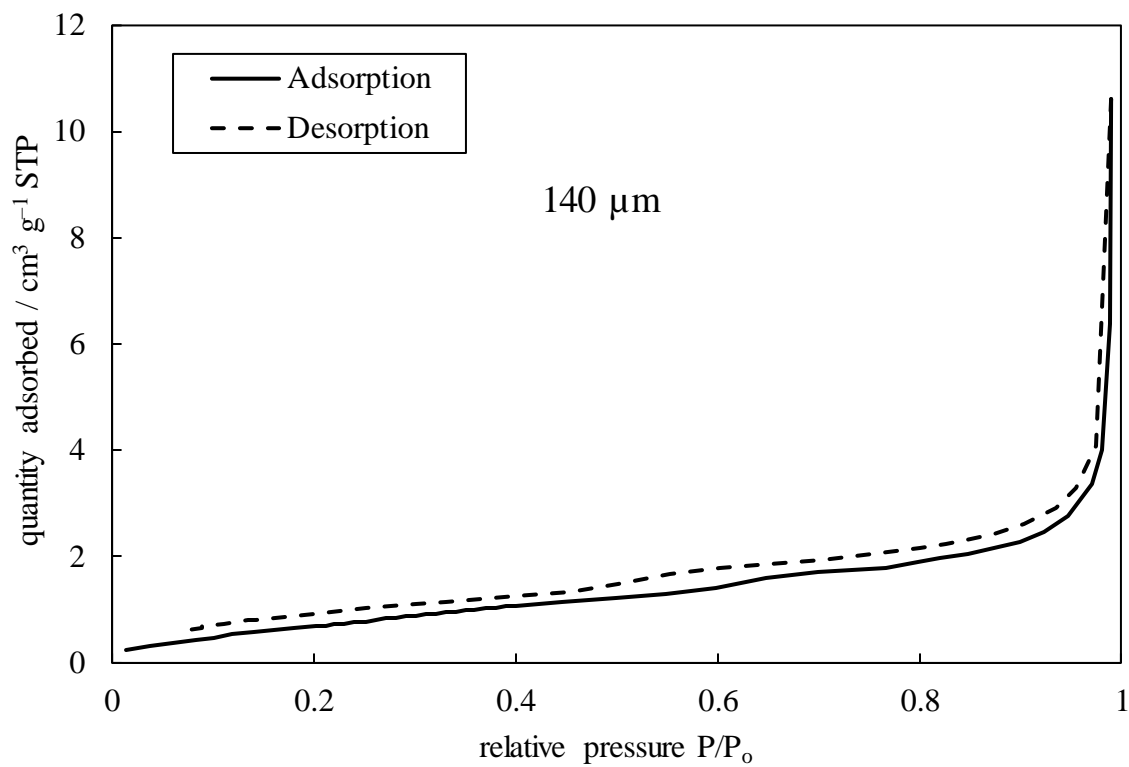**Figure 3.41.** Adsorption and desorption isotherms of N_2 at 77 K on two shale sizes of 140 µm and 360 µm.

Figure 3.42. BET transform plots of adsorption isotherms for two shale powder sizes of $140\,\mu$m and 360 μm. Here, V is the quantity adsorbed at each relative pressure (P/P$_\text{o}$).

148
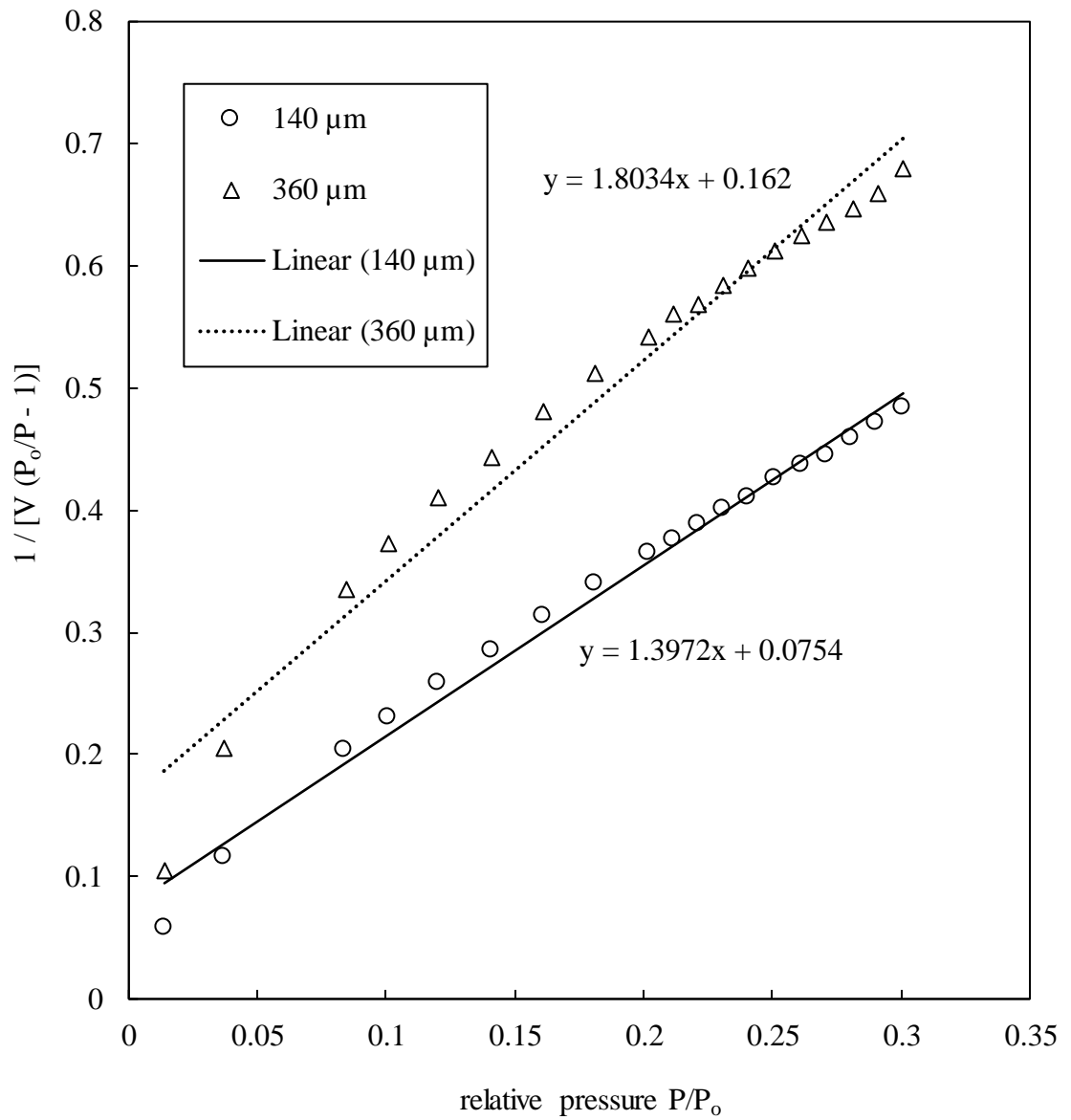
y = 1.8034x + 0.162

y = 1.3972x + 0.0754

Table 3.4. BET parameters calculated for the two shale powder sizes of 140 µm and 360 µm.

Diameter / μm	Slope / g cm⁻³ STP	Y-intercept / g cm⁻³ STP	BET constant C	V_m / cm³ STP g⁻¹	Correlation coefficient	BJH pore volume / cm³ g⁻¹	BET surface area / m² g⁻¹
140	1.397 ± 0.036	0.075 ± 0.007	19.52	0.68	0.99	0.016	2.95 ± 0.07
360	1.803 ± 0.080	0.162 ± 0.017	12.13	0.51	0.98	0.011	2.21 ± 0.09

Figure 3.43. BJH pore size distributions from adsorption isotherms of N_2 onto two shale powder sizes.
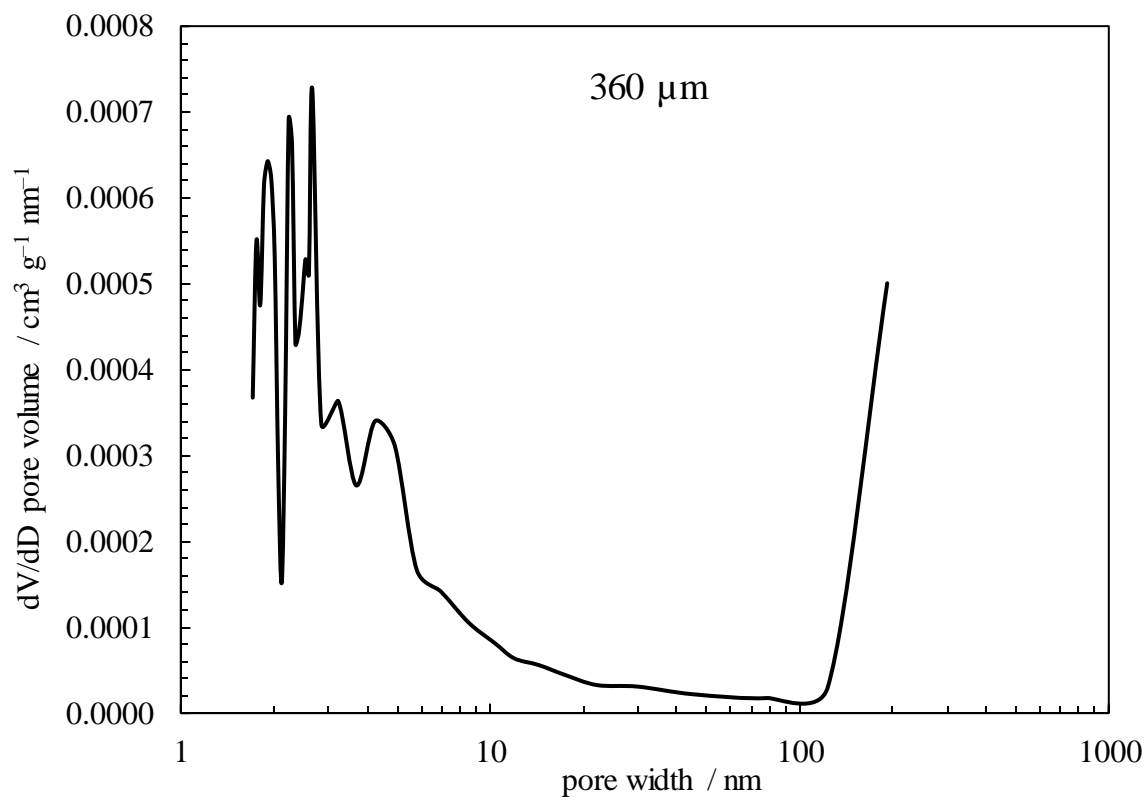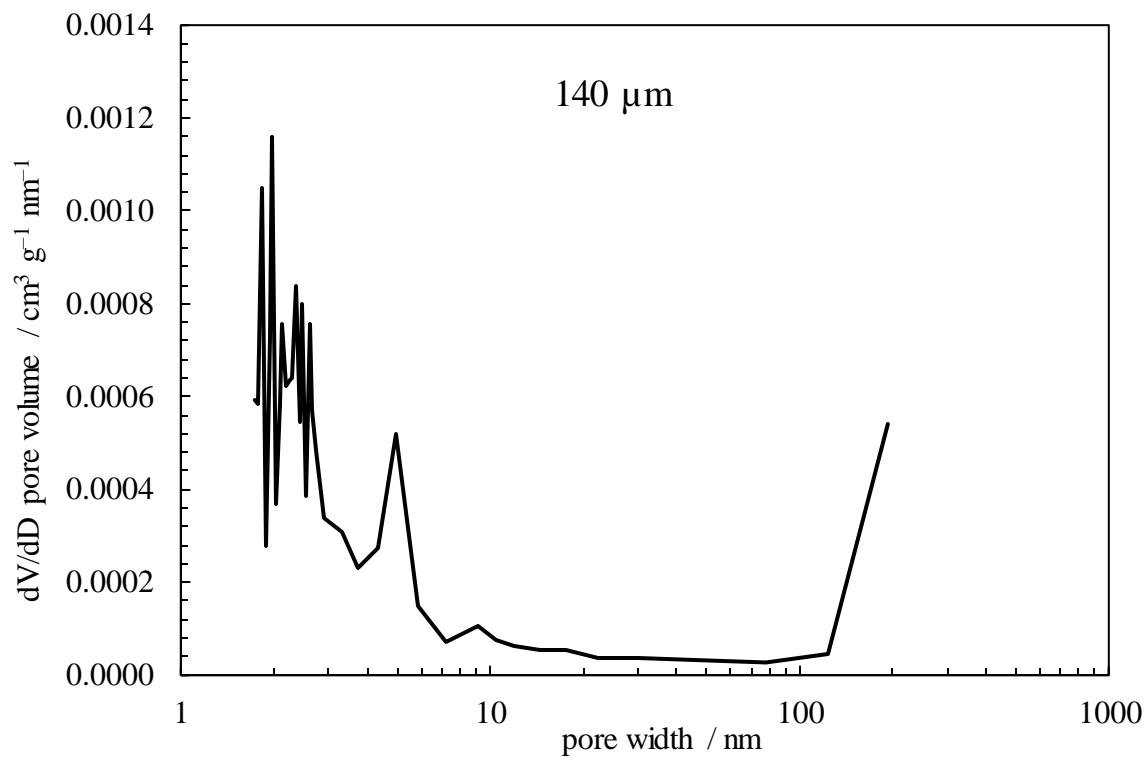
3.7 Summary of finding

In this chapter, the properties of chemicals including particles, surfactants and rocks were determined using different techniques. The findings could be summarized as follows:

- Although stable in DIW, bare silica (d = 16 nm, ζ = – 42 mV) experienced quick sedimentation in Permian brine at 75 °C. When blended with AHS surfactant, raising surfactant concentration to 2 wt.% in DIW (pH ~ pH_{ZPC}) increased the particle diameter sharply up to ~ 3400 nm and the zeta potential towards zero because of the interactions between particles and surfactant leading to sedimentation. When the blend was in Permian brine, sedimentation occurred quickly at both temperatures. Similar observations were made with ZN surfactant.

- Anionic bare silica was successfully reversed in charge with amine functionalization (30 mV at low pH) which was confirmed by XRD and TGA (68% coverage). At the original pH (ζ ~ 0), the particles were sedimented both in DIW and Permian brine in a few days even at low temperatures but they became long-term stable (~ 7 months) at both temperatures by the protonation of particles at low pH. Unlike 25 °C, the particle stability improvement in Permian brine on adding ZN surfactant at 75 °C was not enough for EOR purposes (3 h to 3 d) but they became long-term stable (~ 6 months) on reducing pH.

- The literature synthesis method was modified and optimized using various ESE/silica particle ratios (0.25 – 1.00 g g^{-1}). The initial particle diameter in both DIW and Permian brine was constant (22 nm) for ES/silica particle ratios up to 0.5 g g^{-1} while it increased sharply to 120 – 450 nm for ratios above 0.75 g g^{-1} (> 0.6 g g^{-1}, monolayer ratio) which must be avoided to prevent particle aggregation and silane waste. TGA results showed a thermal tolerance from 110 °C to 200 °C and a silane coverage of 55% indicating hydrophilic particles (by hydroxyl groups) with partial hydrophobicity (by silane hydrocarbon groups). Particle adsorption energy at the air-water surface was almost independent of [particle] in DIW at the original pH (– 400 kT) but it became more negative (– 800 kT) on raising [particle] in Permian brine. At low pH, the adsorption energy became more and less negative on increasing [particle] in DIW and Permian brine, respectively.

- A higher particle diameter (23 nm) and zeta potential (– 27 mV) were measured with ES-coated silica compared to bare silica. Unlike low temperatures, ES-coated silica particles were sedimented in Permian brine at the original pH at 75 °C after a week. Unlike the initial diameter, the zeta potential of particles in DIW increased to – 14 mV and ~ 0 on adding HCl and aluminium sulphate, respectively but the particles

survived aggregation thanks to the steric hindrance by silane. This electrostatic stabilization by pH could also re-disperse and long-term stabilize sedimented particles in Permian brine (for 180 days at 75 °C) implying the effect of particle surface charge on the ion-particle and particle-particle electrostatic interactions and stability of sterically stabilized particles even after sedimentation which is critical in EOR processes.

- The addition of AHS or ZN surfactant to ES-coated silica in DIW was found to add electrostatic stabilization to sterically stabilized particles. However, the particle stability improvement was not sufficient in Permian brine at 75 °C (only up to 3 weeks) due to the high temperature and ions limiting electrostatic grafting of particles with surfactant.

- ZN surfactant had a narrower net zero charge pH (7.5 – 8.4) and smaller zeta potentials (± 5 mV) in DIW at 25 °C compared to AHS surfactant (pH$_{ZPC}$ = 5.5 – 8.0 and ζ = 7 to – 18 mV) due to the presence of its nonionic $C_{10\text{-}12}E_9$ monomers. For the same reason, ZN surfactant had a lower air-water surface tension (< CMC) both in DIW and Permian brine. The CMC of both surfactants and the free energy of micellization decreased and increased, respectively on adding Permian brine due to the salting-out and electrostatic effects. The free energy of adsorption of ZN surfactant was more negative than that of AHS surfactant both in DIW and Permian brine implying that ZN surfactant is more surface-active.

- The addition of bare silica to both surfactant solutions increased the air-water surface tension and CMC (more so for ZN surfactant). The free energies of micellization and adsorption became less negative upon adding bare silica implying less favourable micellization and surfactant adsorption at the air-water surface. The addition of low concentrations of ES-coated silica increased the surface tension and CMC of AHS and ZN surfactants in DIW. The CMC of surfactants in Permian brine increased slightly upon adding 0.01 wt.% particles but no significant change was observed at higher [particle]. For AHS in Permian brine, there was a systematic decrease in surface tension upon raising [particle] implying increased surface activity of the surfactant while no clear effect was found in that of ZN surfactant.

- The ZPC of calcite-rich shale in 0.01 M NaCl was measured as ~ 9.3 which was reduced to ~ 8 when it was in Permian brine. The adsorption and desorption of N$_2$ on and from shale showed a type II adsorption isotherm and H3 hysteresis (presence of pores inside the rock). BJH pore size distribution showed a macroporous rock (> 50 nm pore width) with low pore volumes (0.011 – 0.016 cm^3 g^{-1}) confirming a tight

shale. The shale showed a large BET surface area $(2.21 - 2.95 \text{ m}^2 \text{ g}^{-1})$ for adsorbing chemicals in EOR.

Chapter 4 EOR chemicals in air-rock and liquid-rock systems

In chemical EOR, the terms "water-rock" and "oil-rock" interactions refer to the interactions of rock with water and oil, respectively in a reservoir which can have a significant effect on the efficiency of EOR processes and the overall recovery of oil from the reservoir. These interactions can be influenced by a variety of factors including the rock wettability, the rock surface energy and the physiochemical properties of water and oil. In general, water is more likely to wet and adhere to a rock surface if the rock is more hydrophilic (water-loving) and if the surface energy of the rock is high while oil is more likely to wet a more oleophilic (oil-loving) rock that has a low surface energy. In a typical chemical EOR, an important goal is often to alter the wettability of the rock from (strongly) oil-wet to intermediate or water-wet in order to increase the recovery of oil from the reservoir. This is often carried out by adding surface-active chemicals like surfactant, polymer or nanoparticles to the injected aqueous phase to modify the wetting properties of the rock and alter its affinity for water or oil.

This chapter reports the effectiveness of EOR chemicals used in this study including AHS and ZN surfactants, ES-coated silica particles and Permian brine ions on the rock wettability alteration. The impact of adding particles on the adsorption of AHS and ZN surfactants onto rock was also studied. The results were further discussed by EDX-assisted SEM.

4.1 Contact angle measurement

4.1.1 Air-water and air-oil contact angle

Figure 4.1 shows the contact angles of water and n-dodecane drops on bare and oil-conditioned shale (hydrophobized with crude oil) in air with time. As time increases, the water droplets shrink due to imbibition into the pores of the rock. The water droplet forms an initial contact angle of 102 ° on bare shale and 117 ° on oil-conditioned shale showing an intermediate wettability against water.[208] The n-dodecane droplets spread initially on both bare and oil-conditioned shale implying that the ageing process and duration were sufficient for the hydrophobization of the substrates.

Figure 4.1. (a) Dynamic contact angles of water droplets and (b) initial contact angles of n-dodecane droplets on bare shale and oil-conditioned shale in air at 20 ± 2 °C.
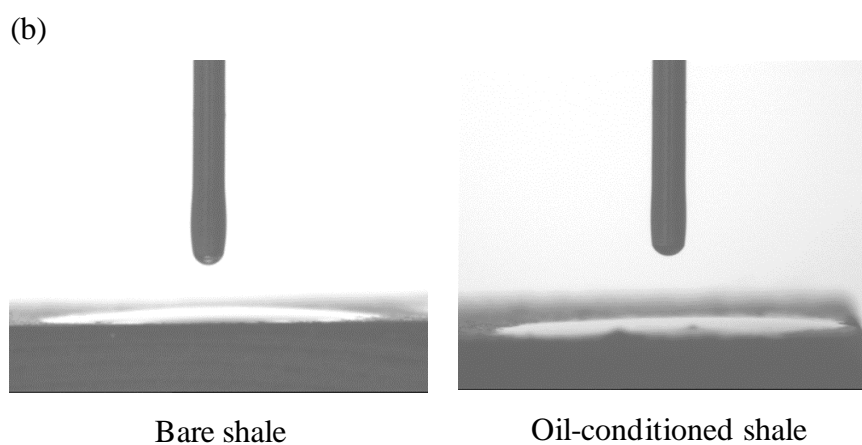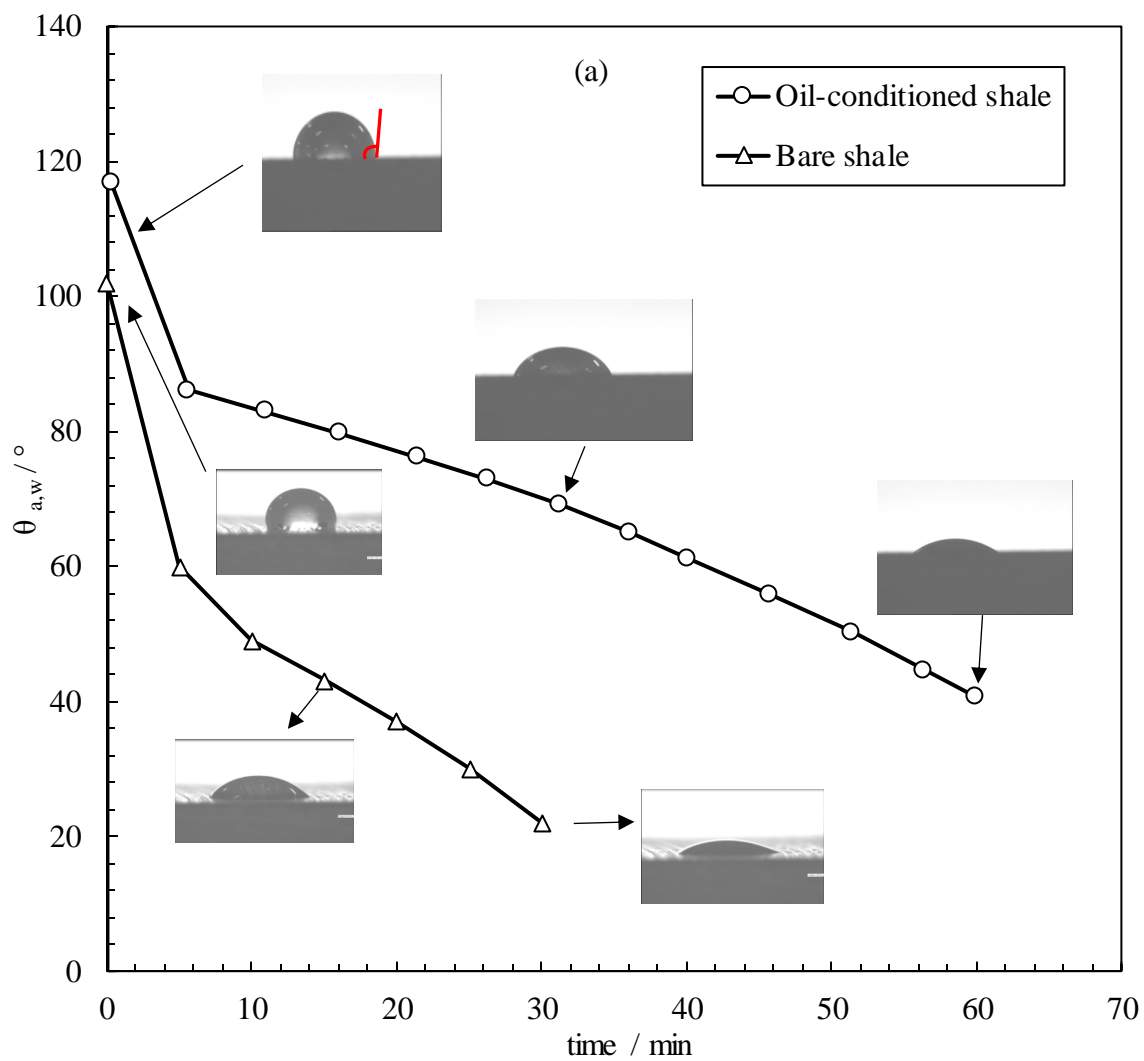
4.1.2 Oil-water contact angle

4.1.2.1 Hydrophobicity of shale substrates

In order to investigate the degree of hydrophobicity of rock substrates obtained by ageing with crude oil, the contact angles of fresh crude oil drops on the oil-conditioned substrates immersed in DIW and Permian brine were measured through water after allowing the drop to reach equilibrium for around 10 minutes. At this time, almost no further change in contact angle with time was observed. In both cases, the oil drops were observed to spread on the shale substrates initially (Figure 4.2). Longer immersion in DIW and Permian brine up to 48 h did not reduce the hydrophobicity noticeably implying that both are ineffective in altering rock wettability necessitating the use of EOR chemicals like surfactants and particles. The oil-water contact angle after 24 h immersion in DIW or Permian brine was measured as 171 ± 8 ° showing a strong hydrophobization of shale with crude oil during the ageing process. This contact angle was considered as a reference for subsequent investigations. The shale used in this study was calcite dominant (97.2% calcite + 2.8% quartz) with a ZPC in 0.01 M NaCl at pH ~ 9.3. At around neutral pH, calcite is expected to be cationic. However, the presence of quartz can also provide some anionic sites on the surface of the rock. The total acid number (0.25 mg KOH g^{-1}) and total base number (0.45 mg KOH g^{-1}) of crude oil show a higher presence of cationic polar groups in the crude oil facilitating the adsorption of cationic components of the oil onto anionic sites of the rock.

Figure 4.2. Equilibrium crude oil droplets on oil-conditioned shale substrates treated with DIW and Permian brine for up to 48 h. The measurements were performed under DIW and Permian brine, respectively.
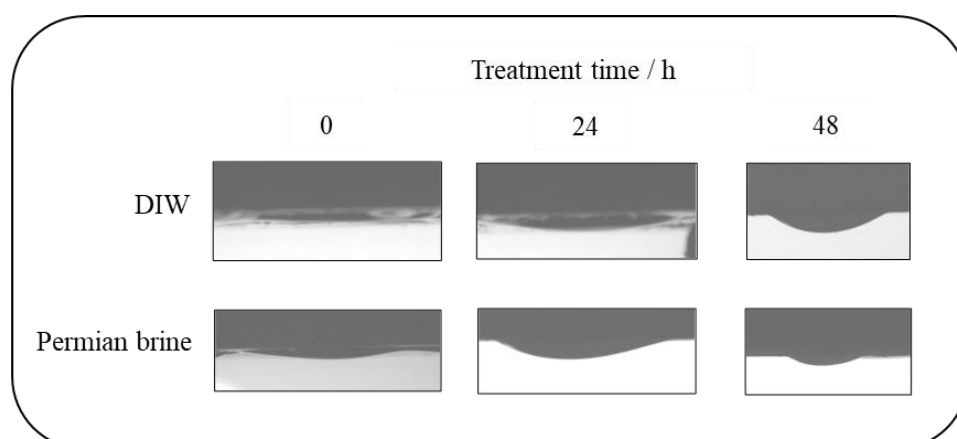
4.1.2.2 Effect of treatment time

The term "treatment time" refers to the duration of contact between the wettability modifier and the oil-wet rock. Measuring the contact angle with treatment time can show not only the dynamic contact angle behaviour but also the time when a minimum contact angle can be seen. The latter shows the maximum power of the chemical for rock wettability alteration with no significant later change. Surfactant and particle adsorption at the liquid-liquid and liquid-rock interfaces is time-dependent. As the treatment time increases, the contact angle may decrease, increase or reach a plateau. This can occur due to various chemical or physical processes such as the adsorption, removal or alteration of oil-wetting agents or the formation of a thin film of water on the rock surface.

In this study, the variation of the contact angle of crude oil droplets on oil-conditioned unpolished shale in DIW was investigated at different treatment times. For this, the oil-conditioned shale substrates were placed in the modifier (solutions or dispersions) for up to 48 h. At certain times (0.5, 1.5, 3, 24 and 48 h), the substrates were removed from the treating fluid and the contact angle of fresh oil drops on the substrates was measured under DIW or Permian brine (depending on the background of the solution or dispersion). The treatment time beyond which the contact angle change was negligible was chosen for subsequent measurements. Also, 10 min were allowed in all measurements for the oil droplets to reach equilibrium on the solid surfaces.

As shown in Figures 4.3 and 4.4, the contact angle decreased noticeably only after 0.5 h of treatment although larger reductions can be seen at longer treatment times. For ZN in DIW, at least 24 h is required to observe the maximum contact angle reduction and no further significant decrease is observed up to 48 h. When ZN is in Permian brine, the contact angle reduction to minimum is faster and occurs after 1.5 h beyond which no further significant change is observed. The decrease in the electrostatic repulsion between surfactant headgroups and charged sites on the shale surface upon the addition of ions may account for this faster wettability alteration. For particles in DIW and Permian brine, 24 h appears to be suitable for a noticeable contact angle reduction and no considerable reduction is observed up to 48 h. Therefore, a treatment time of 24 h was chosen for subsequent experiments.

Figure 4.3. Effect of treatment time on the contact angle of crude oil droplets on oil-conditioned unpolished shale treated with different ZN concentrations in DIW (top) and Permian brine (bottom) for up to 48 h. The black dashed line shows the contact angle of oil droplets on shale treated with DIW or Permian brine.
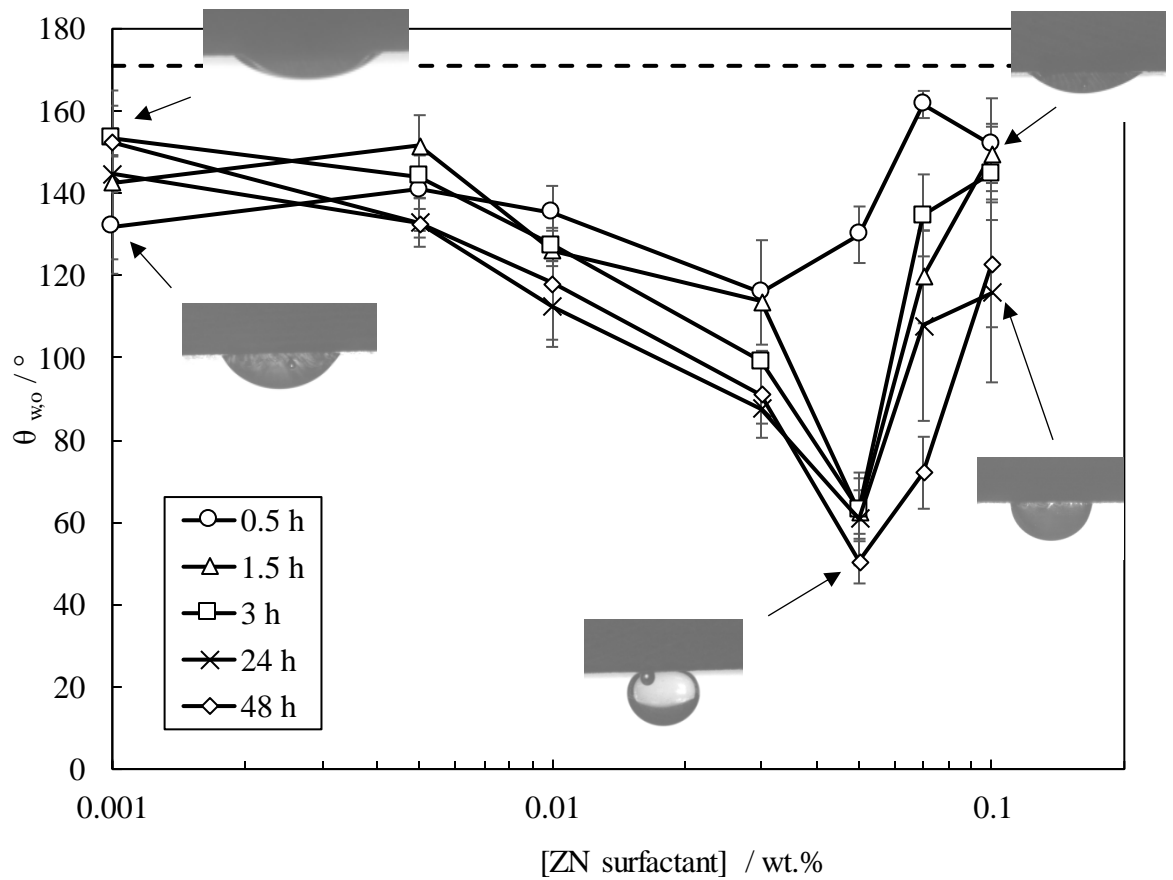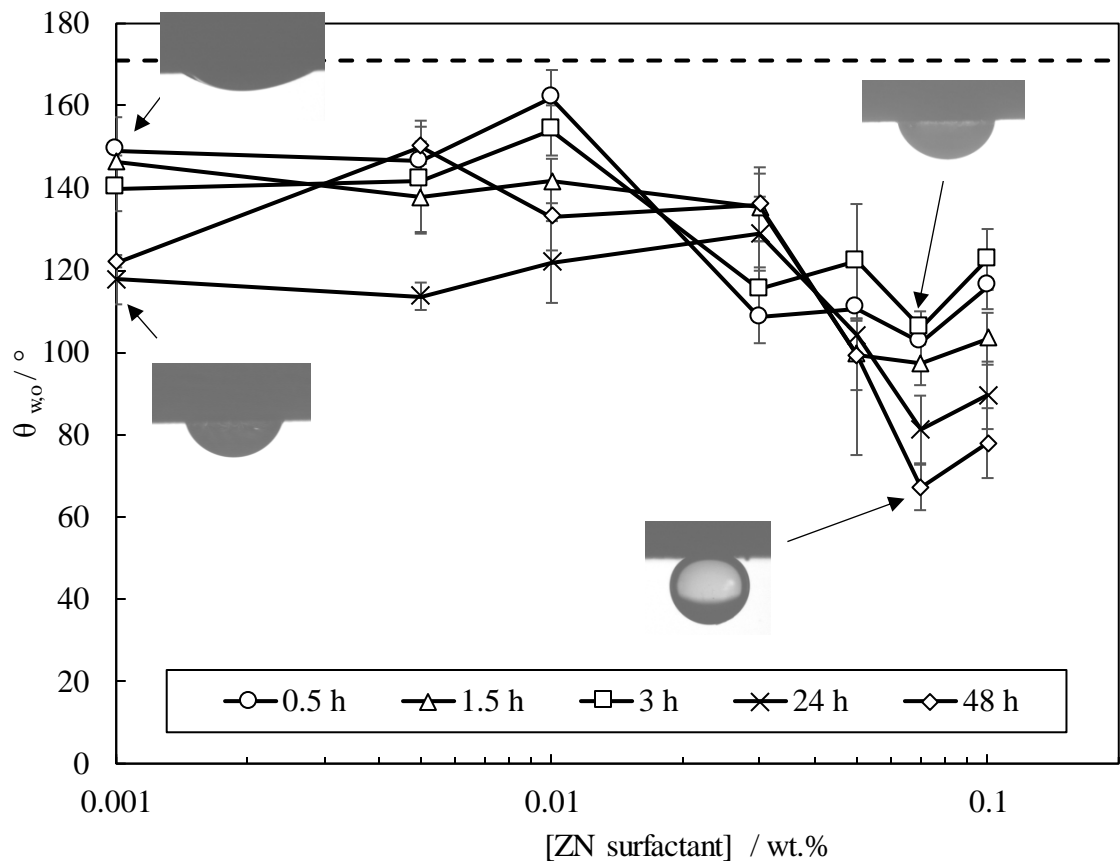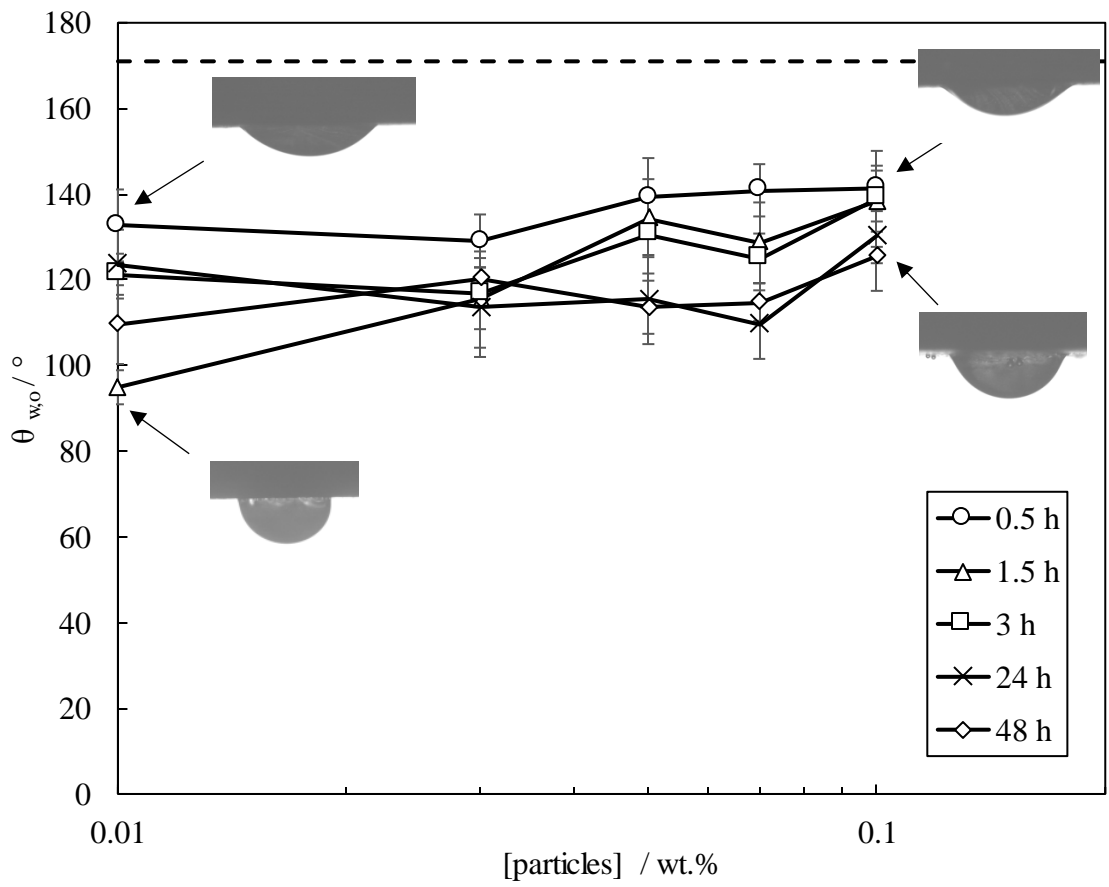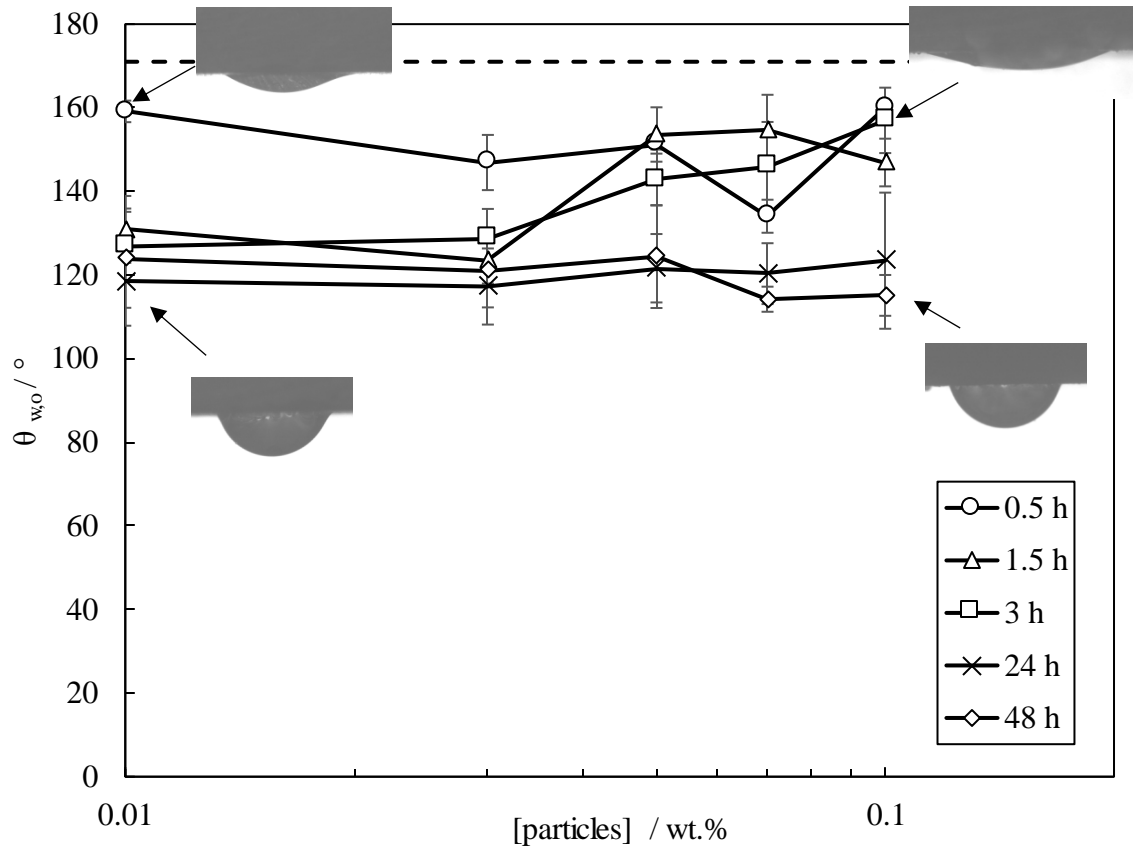
Figure 4.4. Effect of treatment time on the contact angle of crude oil droplets on oil-conditioned unpolished shale treated with different ES-coated silica concentrations in DIW (top) and Permian brine (bottom) for up to 48 h. The black dashed line shows the contact angle of oil droplets on shale treated with DIW or Permian brine.

159

4.1.2.3 Effect of polishing rock

160

The bare shale substrates received from the supplier had artificial surface lines induced during trimming. To remove this surface roughness, the substrates were polished as explained in the methodology. To investigate how polishing the substrates affects the oil-water contact angles, measurements were performed on both unpolished and polished shale. Figures 4.5 and 4.6 show the oil-water contact angles for different ZN solutions and ES-coated silica dispersions on polished and unpolished shale. The oil-water contact angles are higher on polished shale substrates in all plots. Due to the lower surface roughness, a polished rock surface is typically more hydrophobic than an unpolished surface which can lead to a higher contact angle. This is because the liquid droplet will have a harder time adhering to a smooth surface than to a rough surface. In other words, it is easier to detach the oil droplet from a rough surface due to its partial adherence to the surface. The change in surface roughness and wettability can also affect the way that oil and other fluids interact with the rock which can have implications for EOR processes such as surfactant flooding. Therefore, substrates with machine-induced roughness must be avoided in wettability studies to reduce uncertainties and misinterpretations. In all subsequent contact angle measurements, polished shale substrates were aged in crude oil and used.

Figure 4.5. Effect of polishing shale substrates on contact angles of crude oil droplets on oil-conditioned shale treated for 24 h with different ZN surfactant concentrations in DIW (top) and Permian brine (bottom) at the original pH. The black dashed line shows the contact angle of oil droplets on oil-conditioned shale treated with DIW or Permian brine.
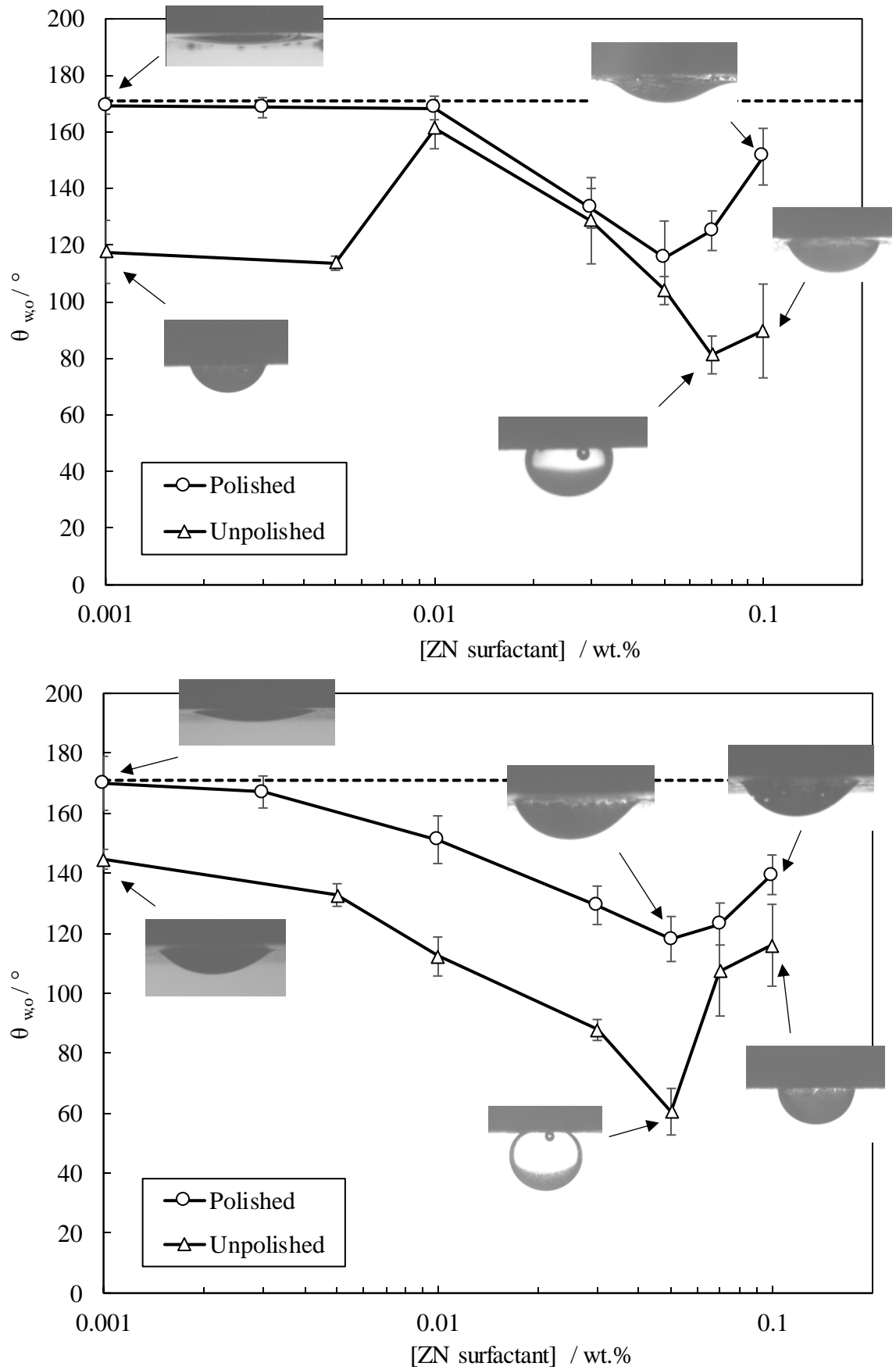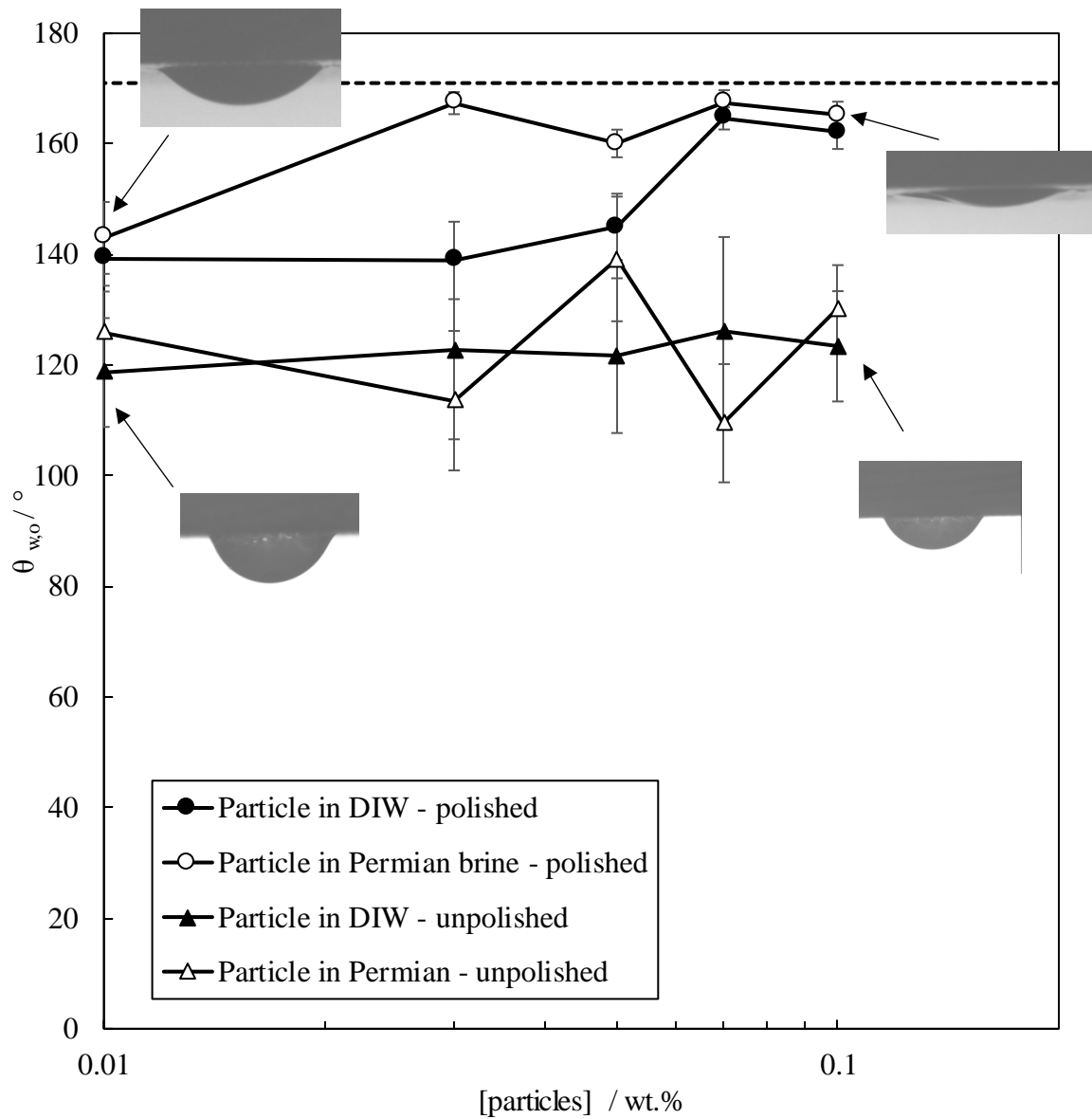
Figure 4.6. Effect of polishing shale substrates on contact angles of crude oil droplets on oil-conditioned shale treated for 24 h with different ES-coated silica concentrations in DIW and Permian brine at the original pH. The black dashed line shows the contact angle of oil droplets on oil-conditioned shale treated with DIW or Permian brine.

162

4.1.2.4 Effect of surfactant type and concentration

Surfactant flooding is not well known in tight oil reservoirs due to their complexity *i.e.*
low porosity and permeability. However, some studies have revealed that adding

surfactants reduces rock hydrophobicity and increases both water imbibition and oil production making them promising.[209-212] In this part, the effect of surfactant type and concentration on rock wettability alteration is studied. An initial investigation was also performed on oil-water contact angles measured on substrates immersed in equilibrated surfactant solutions or the background *i.e.* DIW (see Appendix B.1). It was revealed that the oil-water contact angles are almost the same with both. Therefore, for more convenience and control during measurements, the substrates were immersed in DIW or Permian brine in subsequent contact angle measurements.

Figure 4.7 shows the contact angle measurements with AHS and ZN in DIW and Permian brine. The measurements show that the rock wettability alteration is more noticeable for AHS (zwitterionic alkyl hydroxysultaine) compared to ZN (mixture of AHS and nonionic $C_{10-12}E_9$) when surfactants are in DIW. On increasing surfactant concentrations in DIW, the contact angle decreases to a minimum after which it increases again. Previous researchers reported the same observation with commercial zwitterionic surfactants (unknown formula) on Wolfcamp and Eagle Ford shales[34] and with zwitterionic octadecyl sulfonyl betaine and nonionic alkylphenol ethoxylates on Chinese shales with no explanation.[213] The surfactant concentration causing this minimum is considered the optimum surfactant concentration which is economically important in field applications. According to the results, the minimum contact angle by AHS is 64° and that of ZN is 115° both at 0.05 wt.%.

The zwitterionic AHS surfactant can adsorb onto various charged sites because of its positive and negative charges. The electrostatic attraction between the charged sites on the rock surface and the oppositely charged headgroup of the surfactant balances the electrostatic repulsion produced by the like-charged surfactant headgroup which has a similar polarity to the charge on the rock surface. These two opposing forces can make surfactant molecules adsorb in different ways on the rock surface, as schematically shown in Figure 4.8. The anionic sites on the rock surface can attract the cationic ammonium group of the zwitterionic surfactant and repel the anionic sulfonate group resulting in V-shaped adsorption.[214] On the other hand, the rock cationic sites attract the anionic sulfonate group of the surfactant and tend to be away from the cationic ammonium group resulting in normal I-shaped adsorption.[215] The zwitterionic surfactant may adopt L positioning if the rock surface is cationic which occupies a larger surface area and leads to lower adsorption density. In this study, since the rock was mostly calcite and net cationic, I-shaped adsorption is expected to be dominant, however, the anionic sites of the rock (*e.g.* quartz minerals, CO_3^{2-} and HCO_3^{-}) can serve V-shaped adsorption for the

surfactant. Comparing these two orientations, I-shaped adsorption causes a lower adsorption area per molecule and thus a higher adsorption density on the rock.

Zwitterionic surfactants can electrostatically attract oppositely charged groups of the crude oil adsorbed on the rock surface to form ion pairs (Figure 4.8) which are then stabilized by hydrophobic interactions of the surfactant tails and desorbed from the rock surface.[62] The aqueous micelles then solubilize these hydrophobic complexes into their cores which makes the removal process almost irreversible. Strong H-bonds between surfactant headgroup and the rock surface are possible for the nonionic $C_{10-12}E_9$ present in ZN given that it is hydrophilic enough (high ethylene oxide number), allowing the hydrophobic tail of the surfactant to be oriented outward for additional hydrophobic-hydrophobic interaction with free surfactant molecules. By creating a narrow water zone between oil-wet rock and oil drops, this creates a bilayer with hydrophilic headgroups outward on the rock surface and decreases the contact angle[65] (Figure 4.8). It has been documented that weak van der Waals forces between the surfactant tails only temporarily adsorb surfactant to solid surfaces but strong electrostatic forces can result in persistent adsorption and the loss of the surfactant from the aqueous phase. Therefore, compared to ion pair formations by electrostatic attraction, a lower rock wettability alteration is expected by nonionic surfactants.[62]

Figure 4.7. Equilibrium contact angles of crude oil droplets on oil-conditioned polished shale treated for 24 h with different concentrations of ZN or AHS surfactant in DIW (top) and Permian brine (bottom). The black dashed line shows the contact angle of oil droplets on oil-conditioned shale treated with DIW or Permian brine.
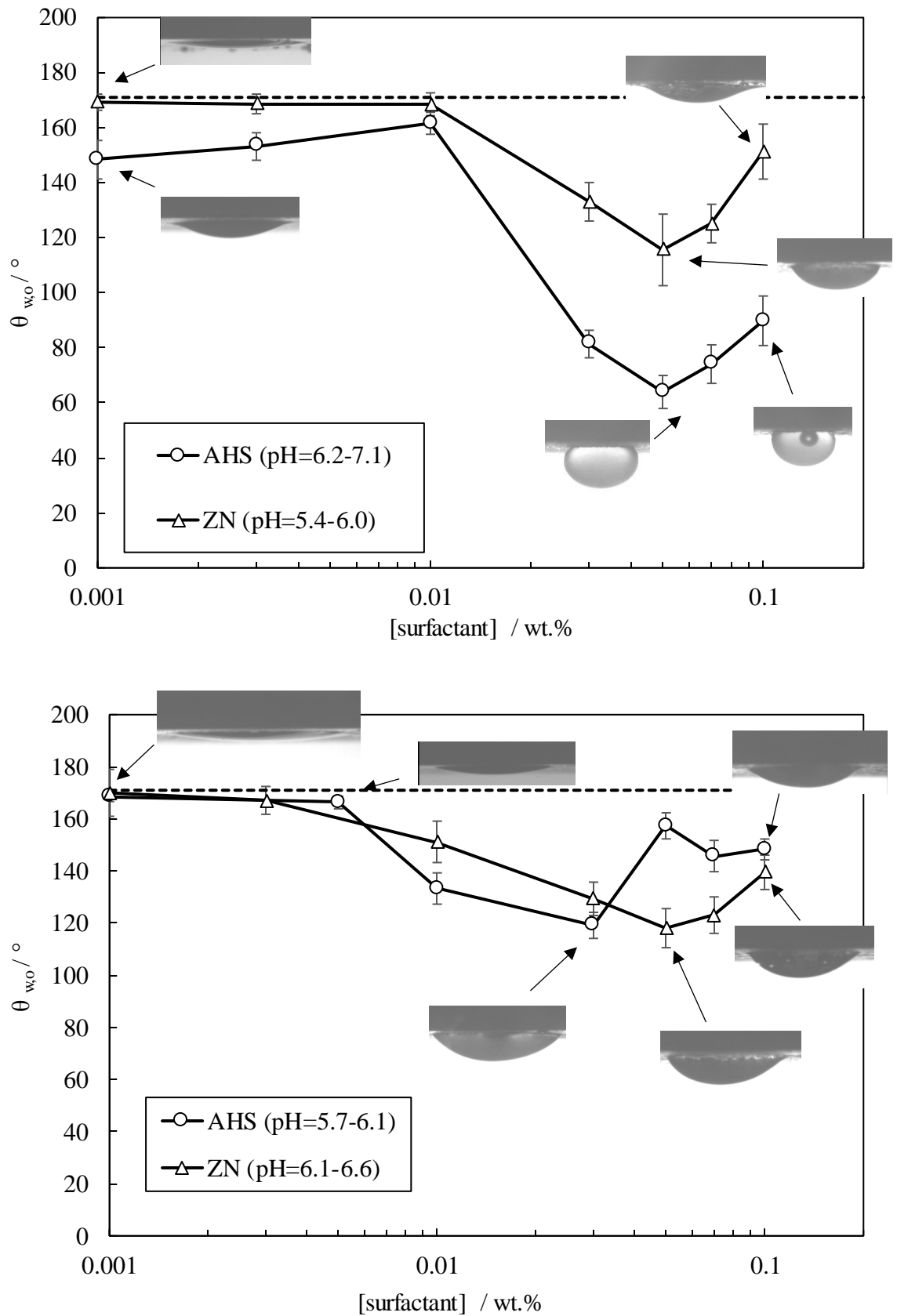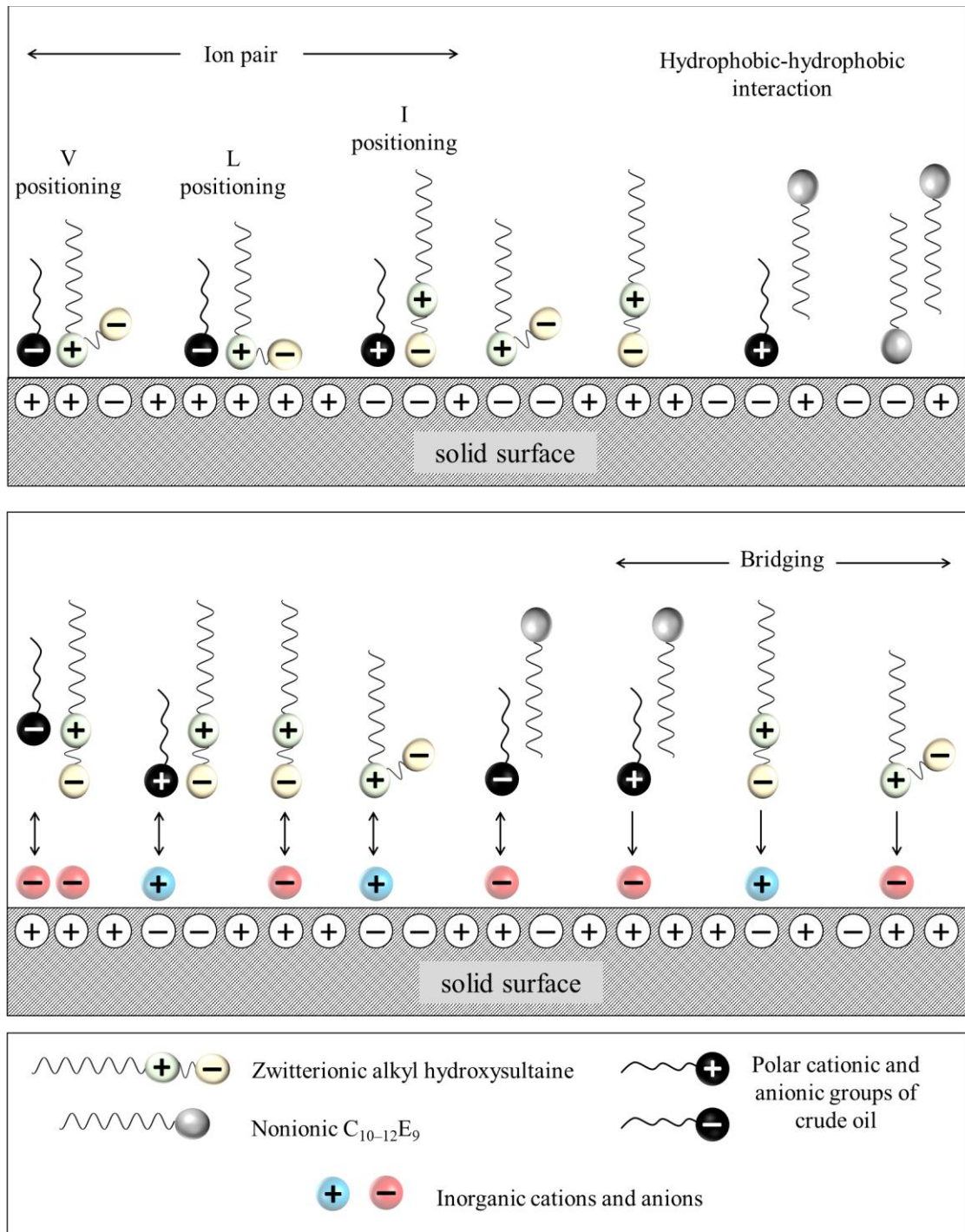
Figure 4.8. Schematic representation of the wettability alteration of calcite-rich rocks by zwitterionic and nonionic surfactant molecules in the absence (top) and presence (bottom) of inorganic salts.

4.1.2.5 Effect of electrolyte

Electrolytes can affect the adsorption behaviour and surface activity of surfactants at different interfaces. Figure 4.7 shows the contact angle measurements for AHS and ZN in Permian brine. It is observed that the addition of Permian salts increases the minimum

contact angle that can be achieved by AHS from 64° to 119° but it has a negligible effect on that of ZN. ZN has the same minimum contact angle at the same surfactant concentration with or without Permian salts (117 ± 2 °). The AHS concentration for the minimum contact angle is lower than that of ZN (0.03 wt.% *versus* 0.05 wt.%).

In reviewing the literature, ions have different effects on the performance of surfactants in rock wettability alteration. Ions are capable of reducing the electrostatic repulsion between surfactant headgroups adsorbed on the surface which makes them arrange more compactly on the solid surface.[216] In this case, increasing salt concentrations increase surfactant adsorption onto the rock with tails outward which increases hydrophobicity.[217] The adsorption of ionic surfactant onto like-charged solid surfaces is also possible in the presence of inorganic counterions which results in higher surfactant adsorption.[218] The ions could lower the electrostatic attraction between surfactant headgroups and a solid surface and thus reduce the surfactant adsorption onto the surface.[217, 219, 220] This may account for the higher oil-water contact angles by AHS in the presence of Permian brine here, consistent with the reduced AHS adsorption on the rock on adding brine (see Section 4.2.2). For the nonionic surfactant in ZN, hydrogen bonding could exist between the headgroup of the surfactant and the solid surface. However, in addition to the weak wettability modification ability of nonionic surfactants, high concentrations of electrolyte can increase the chemisorption of counterions on reactive sites of solid surfaces which makes nonionic surfactants ineffective for wettability alteration.[221] These mechanisms are schematically shown in Figure 4.8. The type and composition of the electrolyte are also important. For example, it has been reported that at a fixed total concentration, the addition of divalent cations such as Ca^{2+} and Mg^{2+} can lower the adsorption of surfactant onto rock while monovalent cations such as Na^+ and K^+ can enhance the adsorption[217, 220] (see also Section 4.3). Since a mixture of salts has been used here, it is not possible to identify the effect of each ion.

### 4.1.2.6 Effect of particles alone

The effect of nanoparticles on rock wettability alteration in EOR is an active area of research. Nanoparticles, if sufficiently surface-active, can alter the rock wettability by modifying the surface properties of the rock making it more hydrophobic or hydrophilic. This can change the way that oil and water interact with the rock, making it easier to

extract oil from it. Studies have found that certain types of nanoparticles, mostly metal oxides such as silica, titanium dioxide and iron oxide, can be effective in altering rock wettability. Here, the size, concentration and surface functionalization of the nanoparticles are important and can affect their effectiveness. However, more research is needed to fully understand the mechanisms behind and the optimal conditions for nanoparticles to be used in EOR.[222]

Bare silica in DIW (*i.e.* 0.01 – 0.1 wt.%) was first tested as a wettability modifier as a control. Due to particle instability, measurements were not possible with dispersions in Permian brine. Figure 4.9 shows the oil-water contact angle for different bare silica concentrations. As seen, even a low concentration of bare silica (*i.e.* 0.01 wt.%) can reduce the contact angle noticeably by ~ 60°. The contact angle decreased further to ~ 40° on increasing the particle concentration to 0.05 wt.%, implying a hydrophilic surface. However, higher particle loading leads to a rise in contact angle.

Particle layering between the oil drop and the solid surface is responsible for the development of a disjoining pressure and the spreading of the dispersion on the solid surface. There is an adsorption competition between silica particles and crude oil components on the rock surface. Once the disjoining pressure exceeds the adhesion force between the oil drop and the rock surface, the oil drop starts to detach leaving the surface more water-wet. Particle adsorption also changes the surface energy and wettability of the solid surface. Therefore, the disjoining pressure could also be improved by the hydration of adsorbed particles.[92] Since bare silica particles are hydrophilic, they are hydrated by water molecules. Thus, when they adsorb onto the rock surface, they increase the number of water molecules on the oil-wet rock rendering the rock more water-wet.[223] There is also a chance that adsorbed bare silica on the rock will interact covalently or electrostatically with crude oil components which makes the particles hydrophobic.[93] This explains why the hydrophobized particles boost rock hydrophobicity once again at high particle loading, as several earlier investigations have also discovered.[113, 224]

Figure 4.9. Equilibrium contact angles of oil droplets on oil-conditioned polished shale treated with different concentrations of bare silica in DIW. The black dashed line shows the contact angle of oil droplets on oil-conditioned shale treated with DIW.
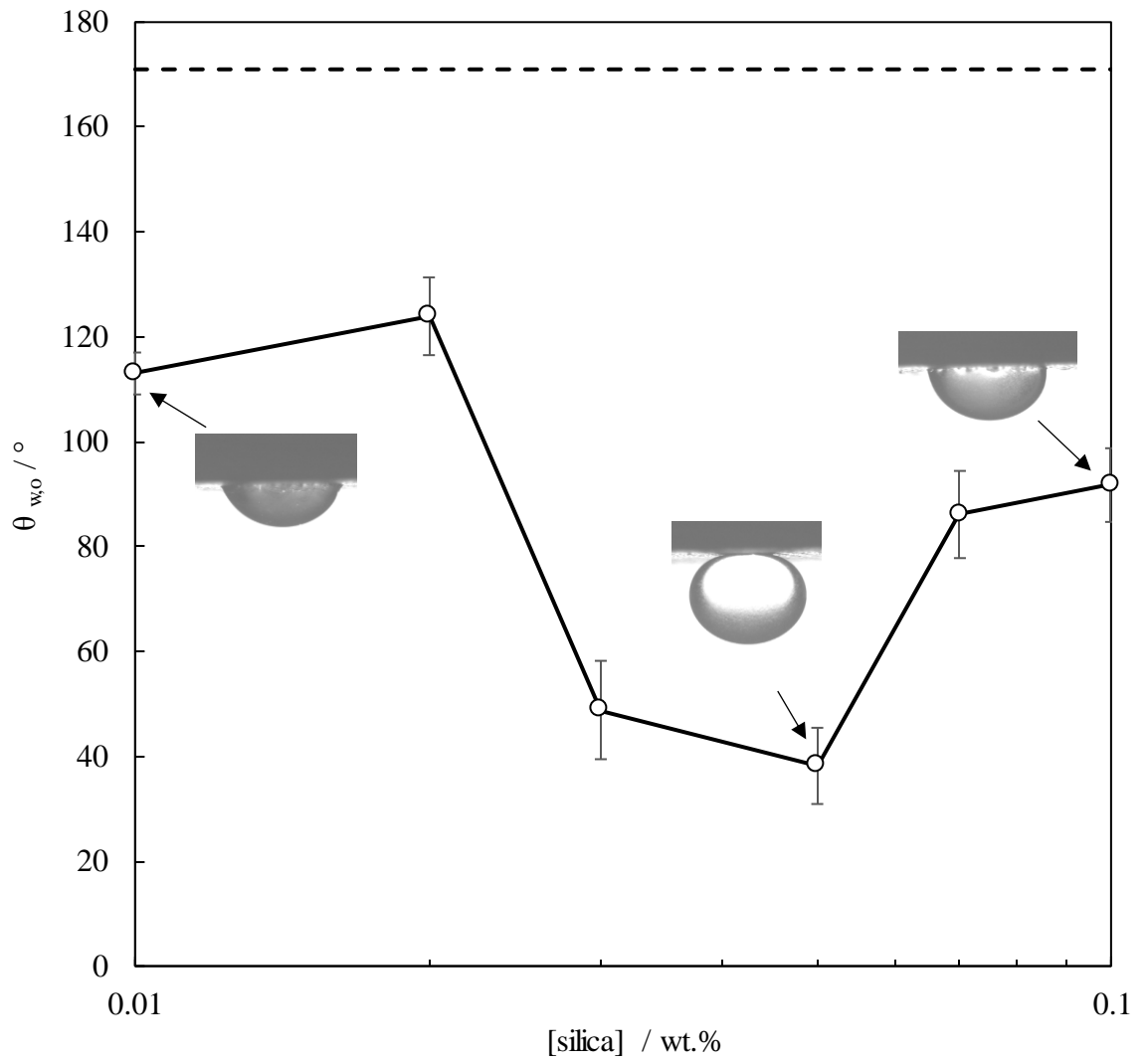
The oil-water contact angles with AS-coated silica are presented in Appendix B.2. Figure 4.10 shows the oil-water contact angles for different concentrations of ES-coated silica in DIW and Permian brine. As shown, the particles cannot change the rock wettability

significantly. The greatest contact angle reduction ($30 \pm 2°$) occurs at 0.01 wt.% particles, resulting in a final contact angle of $141 \pm 2°$ for particles in both DIW and Permian brine, which is insignificant for EOR. The literature on the effect of ES-coated silica on rock wettability alteration is scarce. In a major attempt, Jang *et al.* studied the effect of ES-coated silica in API brine on the wettability alteration of kerosene-conditioned dolomite (93% $CaMg(CO_3)_2$) and limestone (99% $CaCO_3$) substrates. Their particles had a lower silane coverage than the particles used in this study which in turn led to a rise in the surface activity of the particles as discussed before (see surface tensions of dispersions in Chapter 3). They found that a high particle concentration (1 wt.%) in API brine can alter the wettability of both substrates from oil-wet to water-wet or an intermediate wet condition.[146] Using a lower grafting density (13.8%), Hadia *et al.* investigated the effect of ES-coated silica in seawater (2.9 wt.%) and NaCl brine (3.5 wt.%) on the wettability alteration of Berea sandstone (91% quartz), Bentheimer sandstone (99% quartz) and Austin chalk (100% calcite) hydrophobized by a light paraffinic crude oil sample. They observed a contact angle reduction of $25 \pm 4°$ on Berea and Bentheimer sandstones and a decrease of 40° on calcareous Austin chalk by 1 wt.% particles which were attributed to the hydrophilic nature of particles adsorbed on the rocks. Because of the dissimilar charges of particles and calcite, the particles were claimed to be more effective in altering the wettability of calcite-rich rocks.[225] As reviewed, previous studies have used a high particle concentration for rock wettability alteration. This is both uneconomical and highly risky in field applications due to the formation damage from possible particle aggregation at high concentrations especially in tight reservoirs.

It was revealed in Chapter 3 that the synthesized particles have low surface activity at the air-water surface. Based on the oil-water contact angle measurements here, a lack of surface activity of particles on the rock surface is also evident, unlike the particles used in the literature discussed above. The potential reason for this could be the higher grafting density on ES-coated silica synthesized in this study which increases the hydrophilicity of the particles through hydroxyl groups on ES. This high silane coverage however provides significantly longer dispersion stability in high salinity Permian brine (12.56 wt.%), which was lacking in previous studies. This in turn reduces the risk of permeability reduction due to particle aggregation in the pore throats of the rock. Another reason could be the pH of the dispersions here at which the particles have a different charge density. At high particle concentrations, the pH of dispersions increases which results in a higher number of negative charges on particle surfaces. As a result, the adsorbed anionic particles on the rock surface attract the oppositely charged components of crude oil more

strongly which promotes the hydrophobicity of both the particles and the rock surface.[93, 113, 224] This is the reason why a greater oil-water contact angle is seen as the concentration of ES-coated silica increases.

The oil-water contact angles with particles show the necessity to add surfactant for noticeable rock wettability alteration and EOR. The low ability of ES-coated silica to reduce the oil-water contact angle is consistent with the findings of Alzobaidi *et al.* who investigated the effect of various nanoparticles grafted with cationic (N-trimethoxysilylpropyl-N,N,N-trimethylammonium chloride), nonionic (N-3-triethoxysilylpropyl gluconamide) and anionic (3-trihydroxysilyl propyl methylphosphonate and 3-(trihydroxysilyl)1-propanesulfonic acid) ligands on the wettability alteration of calcite substrates aged with model oil (0.01 M stearic acid in decane). They reported that the particles grafted with the cationic ligand are more effective in changing the calcite wettability for three main reasons: the steric repulsion between particles close to the three-phase contact line, the poor adsorption of cationic particles on cationic calcite and finally the high desorption of carboxylates from the calcite by cationic particles which causes the lower oil-water interface close to the rock to have smaller negative charges and thus lower attraction towards calcite.[226] The first mechanism holds for the ES-coated silica used in this study. As ES is nonionic, the electrostatic attraction between the grafted ligand and the rock surface is absent but hydrogen bonding could still exist. Instead, the negative charge of ungrafted sites on silica can have a share in the electrostatic adsorption of particles on the rock surface which reduces the positive charge of the rock surface and leads to a reduction in the attraction between crude oil components and the rock surface and thus a wettability alteration. However, compared to bare silica, this electrostatic adsorption is not expected to be strong for ES-coated silica due to the blocking of 55% of charge sites on silica by the silane. That is why the oil-water contact angles by bare silica are significantly lower than those of ES-coated silica. As the particles are anionic, they cannot interact with the carboxylates of the crude oil, however electrostatic interactions with cationic components of the crude oil, like nitrogen-based groups, are possible.[227,]

It is worth emphasizing that the current investigation has utilized a relatively limited rock surface area (small substrate) to evaluate the influence of nanoparticles on rock wettability. In field scale applications, the interconnected nature of rock pore throats becomes particularly relevant. Aqueous nanoparticles, owing to their small size, possess the capability to penetrate tiny small pores and traverse pore throats, thereby accessing new rock surfaces with the potential to alter rock wettability. As the process of wettability

modification propagates through this intricate network of interconnected pores, its ramifications extend to a considerably larger volume of the rock. This phenomenon has the propensity to enhance the mobility of oil within the reservoir and augment the displacement of hydrocarbons. Consequently, it may culminate in a more efficient and comprehensive process of enhanced oil recovery on a large scale.

Figure 4.10. Equilibrium contact angles of crude oil droplets on oil-conditioned polished shale treated for 24 h with different concentrations of ES-coated silica in DIW and Permian brine. The black dashed line shows the contact angle of oil droplets on oil-conditioned shale treated with DIW or Permian brine.
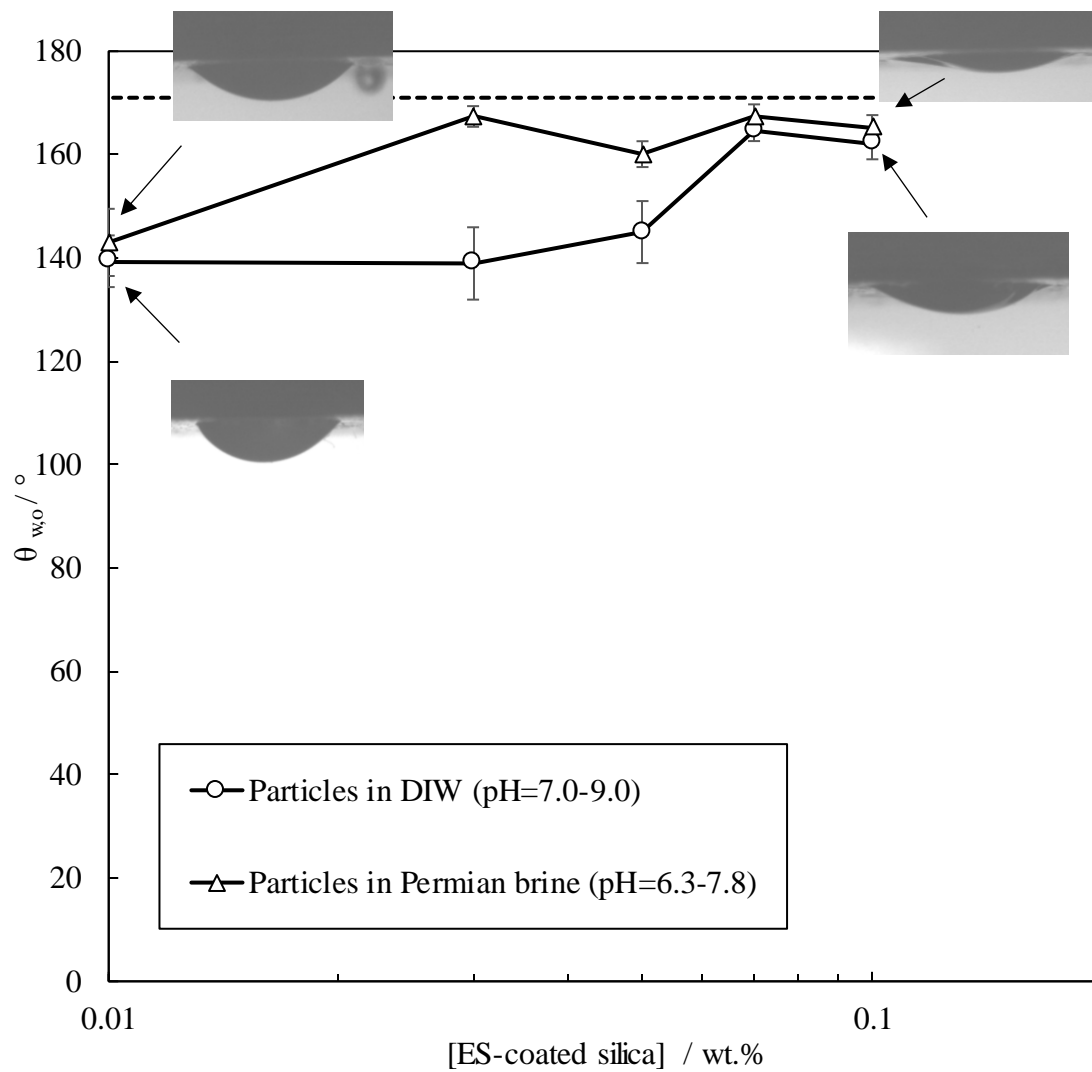
4.1.2.7   Effect of blends of particles and surfactant

Nanoparticles can have different effects on the surface activity of surfactants. Some studies have shown that adding nanoparticles like metal oxides can enhance the

adsorption and surface activity of surfactant leading to improved wettability alteration of rocks[228, 229] while others show the role of particles in reducing the adsorption of surfactant onto rocks to save surfactant.[119] Both effects depend on the size, shape and surface properties of the nanoparticles as well as the properties of the rock and surfactant used.

Figure 4.11 shows the oil-water contact angle and pH measurements of blends of AHS and ES-coated silica in DIW. As can be seen, the oil-water contact angle increases upon increasing AHS concentration below the CMC (*i.e.* 0.01 wt.%) in the blend. The contact angle then sharply decreases to 48° – 74° upon raising surfactant concentrations to 0.03 – 0.05 wt.% in all blends above which either remains constant or increases. This behaviour is observed in all blends with all particle loadings. The surfactant concentration at which a minimum contact angle occurs is considered the optimum surfactant concentration in the blend. The same optimum surfactant concentration and increasing contact angle beyond a minimum have also been observed with the blends of hexadecyl trimethylammonium bromide and sodium dodecyl sulfate and silica and alumina nanoparticles on different shale samples by previous researchers.[230] Zhong *et al.* stated that at low surfactant concentrations, the synergy of the blend of particles and surfactant is mainly due to the free spaces between adsorbed surfactant molecules on the solid surface that can be used by particles, but fewer particles can adsorb at high surfactant concentrations due to the high number of adsorbed surfactant molecules leading to the inefficiency of the blend and hydrophobicity again.[229] The minimum contact angle here is 48° which is observed with the blend containing 0.01 wt.% particles and 0.03 wt.% AHS in DIW. This minimum contact angle is lower than that of particles alone or surfactant alone in DIW indicating a synergy in rock wettability alteration by blending the chemicals. Tang *et al.* studied silica coated with quaternary amine silane and nonionic ES in a blend with different cationic, anionic and nonionic surfactants in a formation brine for wettability alteration of calcite substrates aged with light and heavy crude oil. They observed an additional decrease in oil-water contact angle with the blend of cationic particles and cationic tetradecyl trimethylammonium bromide surfactant compared to the individual chemicals which was related to the desorption of crude oil components from the calcite surface by the surfactant through ion-pair formation and the steric repulsion between the particle-loaded oil-water interface and calcite. The blend of ES-coated silica and cationic surfactant was less effective in altering calcite wettability.[228] The zwitterionic AHS can form ion pairs with both anionic and cationic components of crude oil on the rock surface or oil-water interface. It is thought that a mixed monolayer of particles and surfactant is formed on the rock that has created this synergy. Because of

the high adsorption of surfactant on the rock at high surfactant concentrations, particles adsorb less readily, causing the oil-water contact angle plot to rise.

The change in pH with particle or surfactant affects the charge of the zwitterionic AHS and particles. As mentioned before, the isoelectric region of AHS in DIW is at pH 5.5 – 8.0. The surfactant becomes cationic and anionic at pH values below and above this isoelectric range, respectively which in turn affects its interactions with the rock surface, crude oil components and particles. In the isoelectric region, there is a transition in charge type from positive (pH 5.5) to negative (pH 8.0) by deprotonation of the sulfonate group. Figure 4.11 shows that high concentrations of particles and surfactant increase the pH towards the upper limit of the isoelectric region where the number of negative headgroups of the surfactant is relatively higher than the positive group. This may create repulsion between anionic particles and weakly anionic surfactant molecules, making surfactant molecules adsorb more on the rock surface, consistent with increased AHS adsorption onto the rock at high particle and surfactant concentrations (see Section 4.2).

Figure 4.11. (Top) Equilibrium contact angles of crude oil droplets on oil-conditioned polished shale treated for 24 h with different AHS concentrations in DIW with or without different ES-coated silica concentrations. The black dashed line shows the contact angle of oil droplets on oil-conditioned shale treated with DIW. (Bottom) The pH of different blends at 20 ± 1 °C.
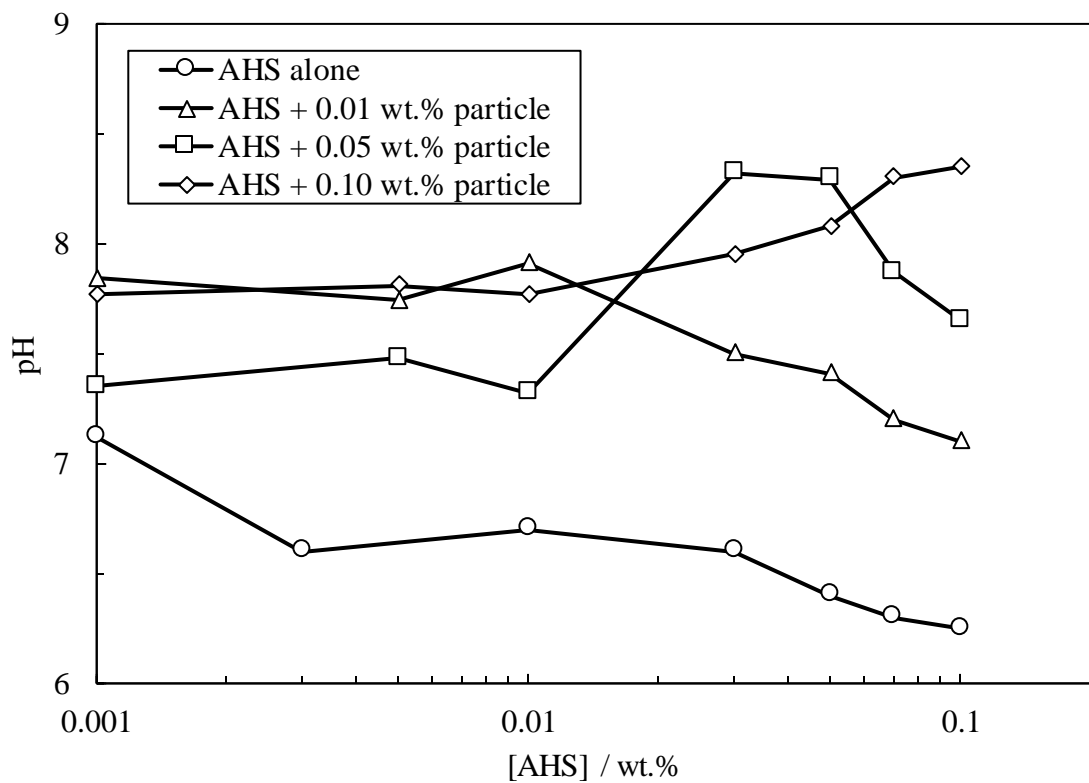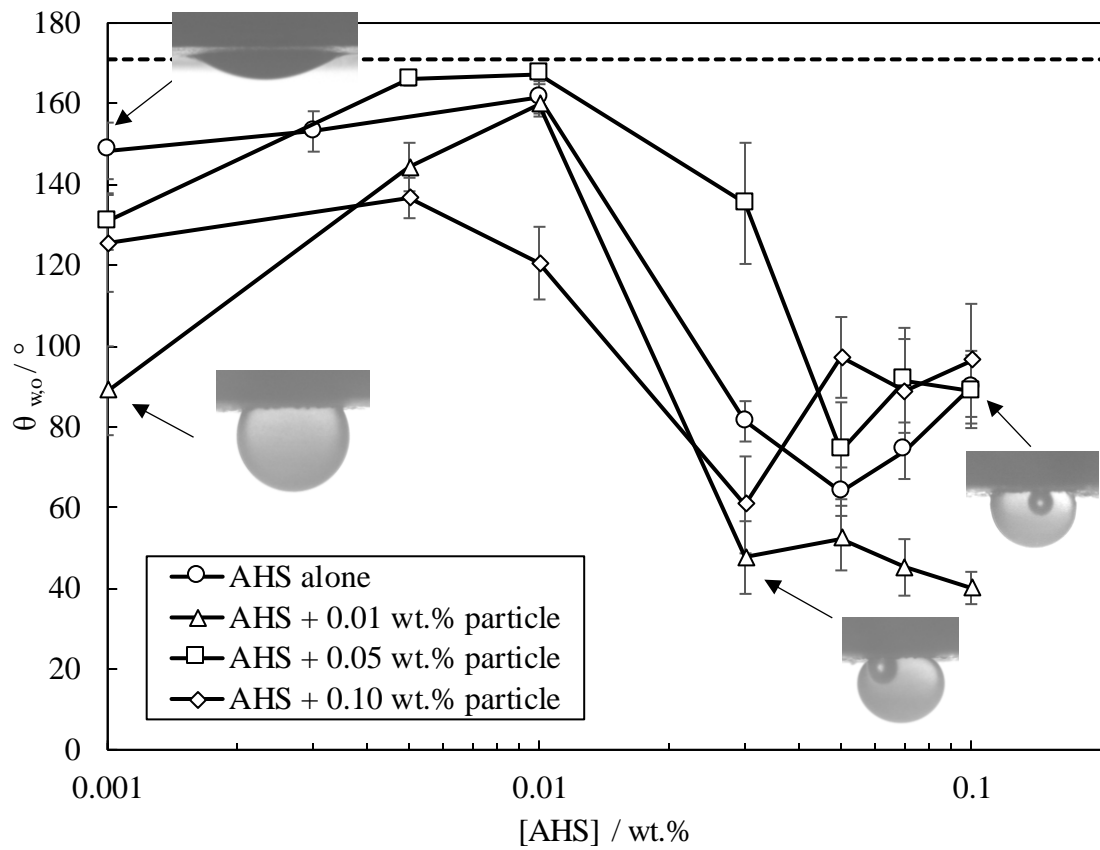
Figure 4.12 shows the oil-water contact angle and pH measurements for blends of AHS and ES-coated silica in Permian brine. As for the blends in DIW, a minimum contact angle at intermediate surfactant concentrations above the CMC and an increasing contact

angle at high surfactant concentrations are observed. The minimum contact angle here is 85° – 90° which is observed at 0.03 wt.% and 0.05 wt.% AHS in a blend with 0.01 wt.% and 0.05 wt.% particles, respectively. In comparison with the contact angles by surfactant alone in Permian brine, a reduction of 30° and 72° is observed at 0.03 wt.% and 0.05 wt.% AHS on the addition of 0.01 wt.% and 0.05 w.% particles, respectively. These further contact angle reductions agree with the increased AHS adsorption onto rock due to the addition of particles to Permian brine (see Section 4.2.3.1). Due to economic considerations, the blend with the lower particle (*i.e.* 0.01 wt.%) and surfactant concentrations (*i.e.* 0.03 wt.%) is chosen as the optimum formulation for rock wettability alteration. It is also noted that the contact angle rise at high surfactant concentrations is more pronounced for the blends in Permian brine than in DIW.

Comparing Figures 4.11 and 4.12, one can observe that the addition of Permian brine to blends of AHS and ES-coated silica has increased the oil-water contact angle, as was also observed with surfactant alone before. The same behaviour has also been reported by previous researchers. Okunade *et al.* reported that for a blend of carbon nanotubes and SDS, increasing NaCl concentrations increases the oil-water contact angle and hydrophobicity of bare shale.[230] As the salinity of Permian brine is high (12.6 wt.% or 2.1 M), such behaviour is not unusual. The brine provides higher adsorption of surfactant onto rock and adsorbed particles with tails pointing outward which promotes hydrophobicity of both particles and the rock surface (see Section 4.2.31).

There is an increase in the pH of AHS in Permian brine on the addition of particles which is negligible for 0.01 wt.% particles but becomes noticeable at higher particle loadings. A rise in pH causes the surfactant to become weakly anionic, as explained earlier, which develops electrostatic repulsion between anionic particles and surfactant that promotes the adsorption of the surfactant on the rock (as observed in Section 4.2.3.1) and induces more wettability alteration compared to AHS alone in Permian brine.

Figure 4.12. (Top) Equilibrium contact angles of crude oil droplets on oil-conditioned polished shale treated for 24 h with different [AHS] in Permian brine with or without different ES-coated silica concentrations. The black dashed line shows the contact angle of oil droplets on oil-conditioned shale treated with Permian brine. (Bottom) The pH values of blends at 20 ± 1 °C.
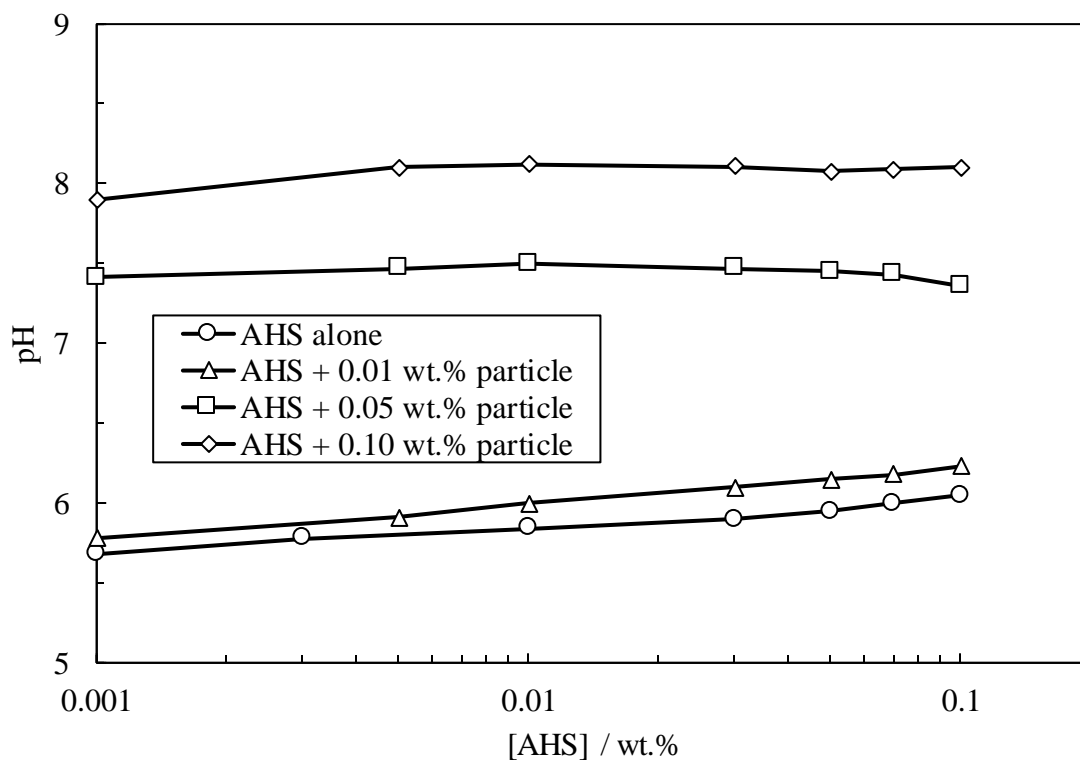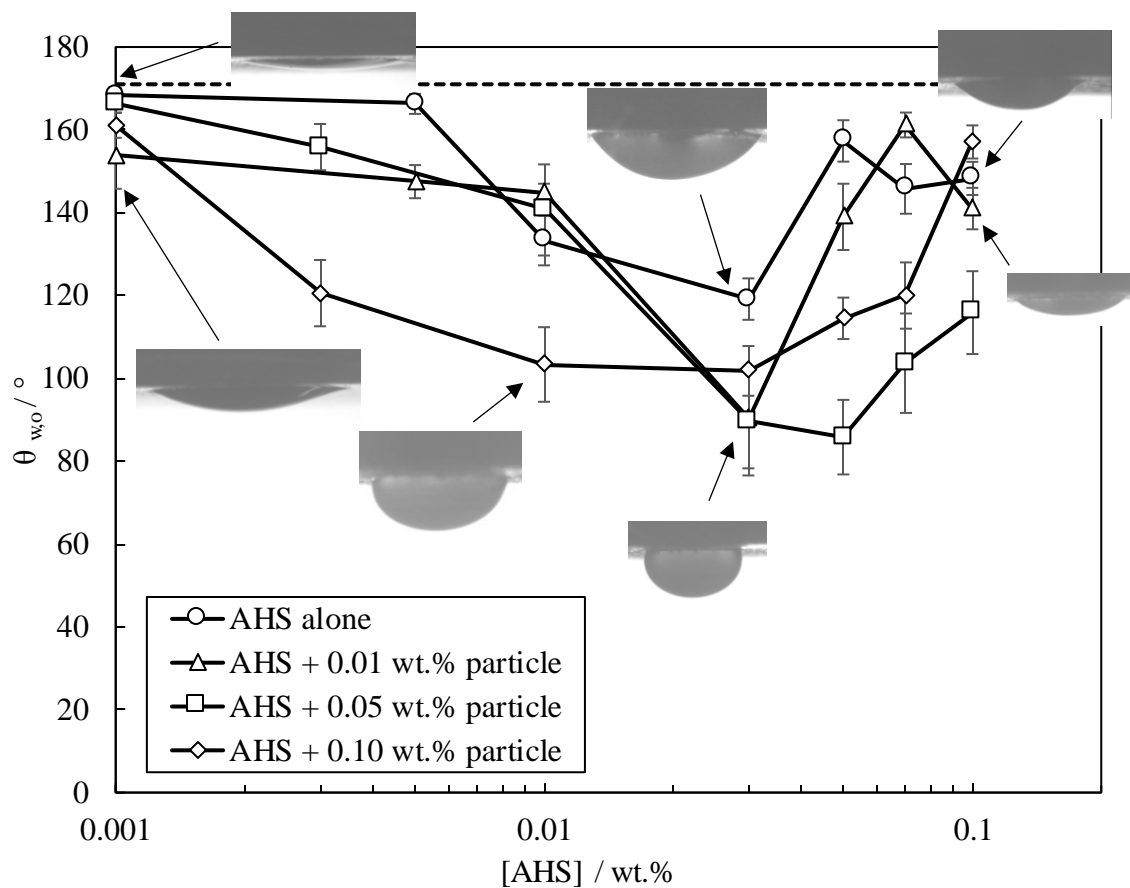
Figure 4.13 shows the oil-water contact angle and pH measurements for blends of ZN and ES-coated silica in DIW. The plot shows a minimum contact angle of 64° for the blend containing 0.01 wt.% particles and 0.07 wt.% ZN in DIW. Compared to the contact angle

by 0.07 wt.% ZN in DIW, a further 61° reduction in contact angle is observed upon the addition of 0.01 wt.% particles. The same interactions explained between AHS and particles or the rock surface apply to ZN. The hydrophobic tail of the $C_{10-12}E_9$ is still pointed outward for further hydrophobic-hydrophobic interaction with free surfactant molecules, while its headgroup can establish H-bonds with the rock surface and particles. On the particle and rock surfaces, this creates a bilayer with hydrophilic heads pointing outward.[62, 65] As explained before, the wettability alteration caused by nonionics is weak and reversible.

In the absence of particles, the pH of ZN in DIW is below the isoelectric range (pH = 7.5 – 8.4) which makes ZN mostly cationic. With the addition of particles, the pH increases which turns the surfactant zwitterionic and facilitates the interactions with anionic particles and cationic rock surfaces through V-shaped and I-shaped adsorption, respectively. At high particle loadings (0.1 wt.%), the surfactant mostly adsorbs onto the particle surface which makes the blend less effective for rock wettability alteration due to the surfactant depletion. This is consistent with the reduced ZN adsorption on the rock with the addition of particles in DIW (Section 4.2.3.2).

Figure 4.13. (Top) Equilibrium contact angles of crude oil droplets on oil-conditioned polished shale treated for 24 h with different ZN concentrations in DIW with or without different ES-coated silica concentrations. The black dashed line shows the contact angle of oil droplets on oil-conditioned shale treated with DIW. (Bottom) pH values of blends at 20 ± 1 °C.
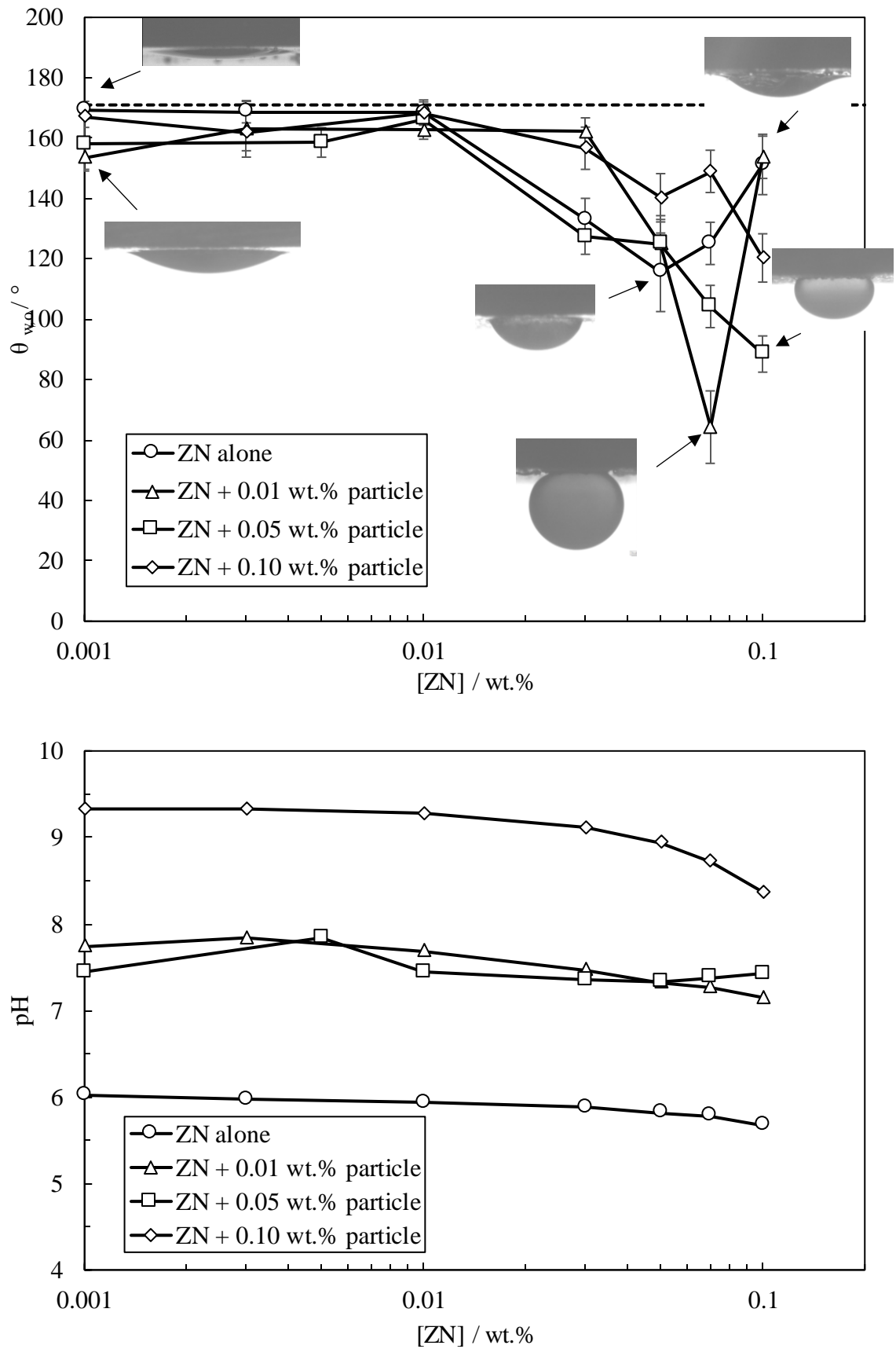
Figure 4.14 shows the oil-water contact angle and pH measurements for blends of ZN surfactant and ES-coated silica in Permian brine. There is a minimum contact angle at 0.05 wt.% ZN in all blends with different particle concentrations. The lowest contact

angle (56°) is observed with 0.01 wt.% particles and 0.05 wt.% ZN in Permian brine which resulted in an additional reduction of 62° compared to that of surfactant alone at the same concentration. Furthermore, the addition of Permian brine to the blends of ZN and particles has reduced the optimum surfactant concentration from 0.07 wt.% to 0.05 wt.%. The pH of ZN solutions decreases with the addition of 0.01 wt.% particles but increases at higher particle concentrations. It is thought that the adsorption of surfactant molecules on the surface of particles makes them partially hydrophobic and surface-active. This agrees with the reduced ZN adsorption onto the rock with the addition of particles in Permian brine (see Section 4.2.3.2). However, high surfactant concentrations can increase the hydrophobicity of particles which is consistent with zeta potential measurements earlier where an increase in the zeta potential of particles towards zero was observed upon increasing surfactant concentration. High adsorption of surfactant onto the rock with tails pointing outward at high concentrations can also induce hydrophobicity, as discussed earlier.

Figure 4.14. (Top) Equilibrium contact angles of crude oil droplets on oil-conditioned polished shale treated for 24 h with different ZN concentrations in Permian brine with or without different ES-coated silica concentrations. The black dashed line shows the contact angle of oil droplets on oil-conditioned shale treated with Permian brine. (Bottom) pH values of blends at 20 ± 1 °C.
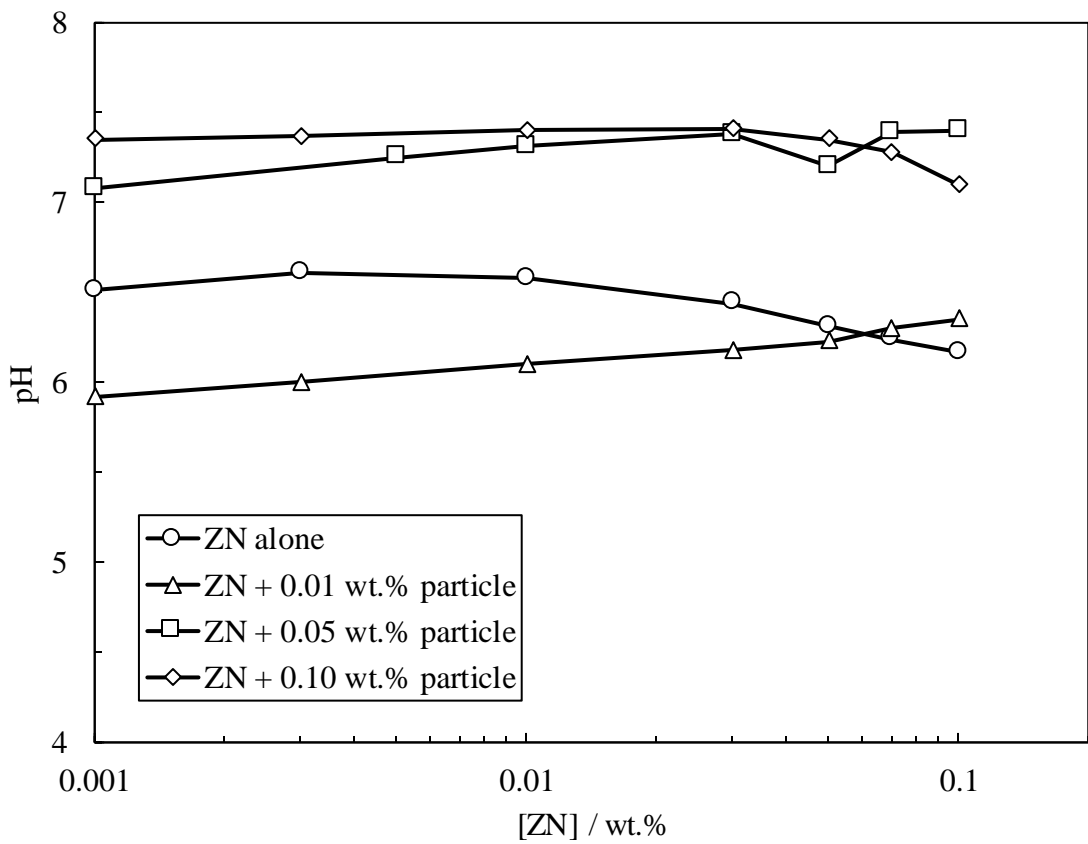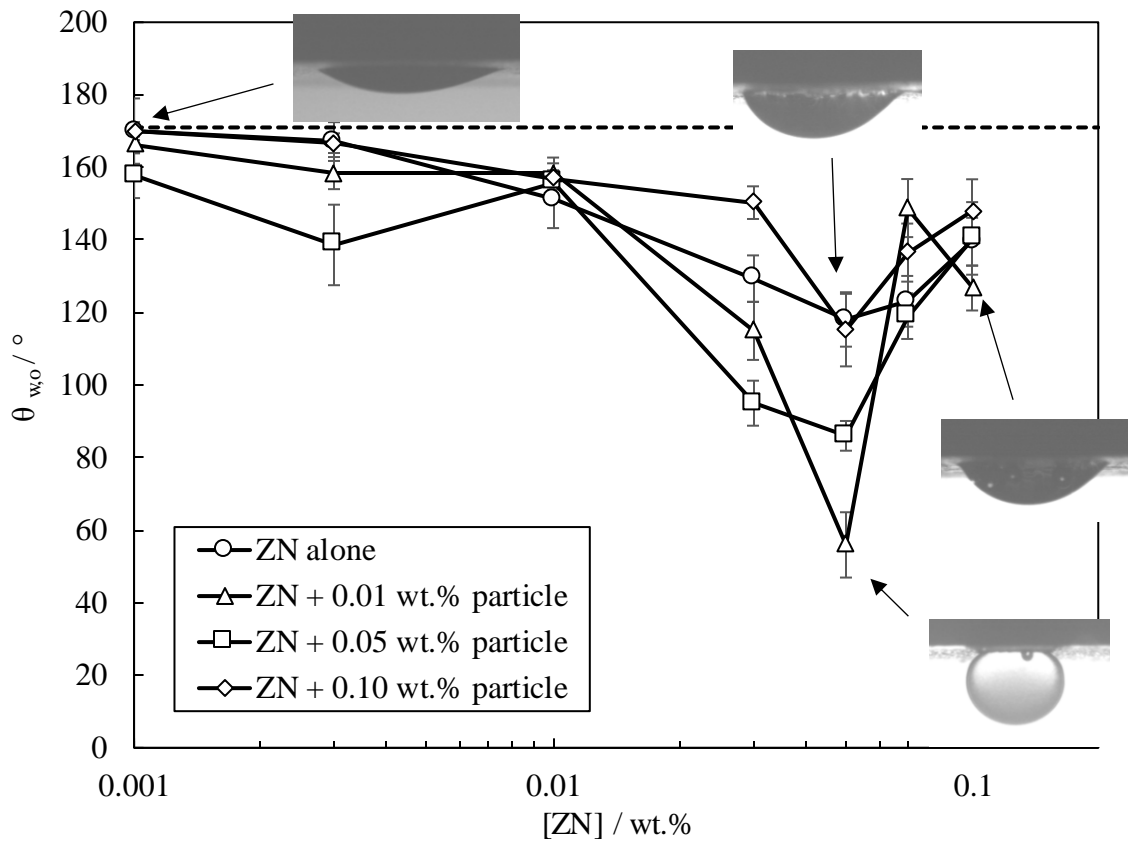
4.1.2.8   Effect of pH on contact angle

The effect of pH on the ability of blends containing 0.1 wt.% ES-coated silica and

different concentrations of ZN in Permian brine to alter the wettability of oil-conditioned

rock was investigated (Figure 4.15). The pH reduction was performed with 1 M HCl. As shown, a decrease in pH reduces the wettability alteration ability of the dispersion such that the same minimum contact angle happens at a higher surfactant concentration which is not economical in field applications. The charge of surfactant, particles and rock is affected by pH, as are their interactions. At pH 4, the positive charge on the zwitterionic surfactant would be more prominent and the particles would become less anionic due to the protonation of silanol groups. As carboxyl groups have a pK_a of 4, they are expected to be neutral or weakly anionic at this pH. Therefore, a weak attraction between the cationic surfactant and anionic silica nanoparticles or crude oil carboxylates exists at low pH. The adsorption of cationic surfactant on cationic rock is also negligible. At high pH (> 8.5), the positive charge on the surfactant would be less prominent and the particles and carboxylates of crude oil are more anionic. Thus, weak electrostatic attraction between the anionic surfactant and anionic particles or crude oil carboxylates is expected. In this case, the particles may electrostatically repel the anionic surfactant to adsorb excessively on the rock resulting in hydrophobicity again, as observed before. The optimum formulation achieves the greatest contact angle reduction at intermediate pH (~ 7) where the surfactant has both positive and negative charges in the headgroup and the particles are moderately charged. This could be due to the partial hydrophobization of particles by surfactant and electrostatic attraction between crude oil components and particles or surfactant which have a significant effect on rock wettability alteration.

It is noted that calcite dissolution can happen at low pH which is itself a cause of wettability alteration by creating a new surface free. Sjöberg and Rickard proposed three pH regimes to discuss the rate of calcite dissolution in aqueous solutions. The dissolving rate is linearly proportional to $[H^+]$ at pH < 4 and independent of $[H^+]$ at higher pH levels (> 5.5). Between these two, a transitional regime exists where the $[H^+]$ dependency changes.[231] Here, although expected to be helpful, calcite dissolution has not improved the rock wettability alteration at low pH probably due to the newly created surface serving as a new adsorbent for the adsorption of the crude oil components or excess aqueous surfactant.

Figure 4.15. Effect of pH on equilibrium contact angles of crude oil droplets on oil-conditioned polished shale treated for 24 h with dispersions of 0.1 wt.% ES-coated silica in a blend with different ZN concentrations in Permian brine at the original pH and reduced pH. The black dashed line shows the contact angle of oil droplets on oil-conditioned shale treated with Permian brine.
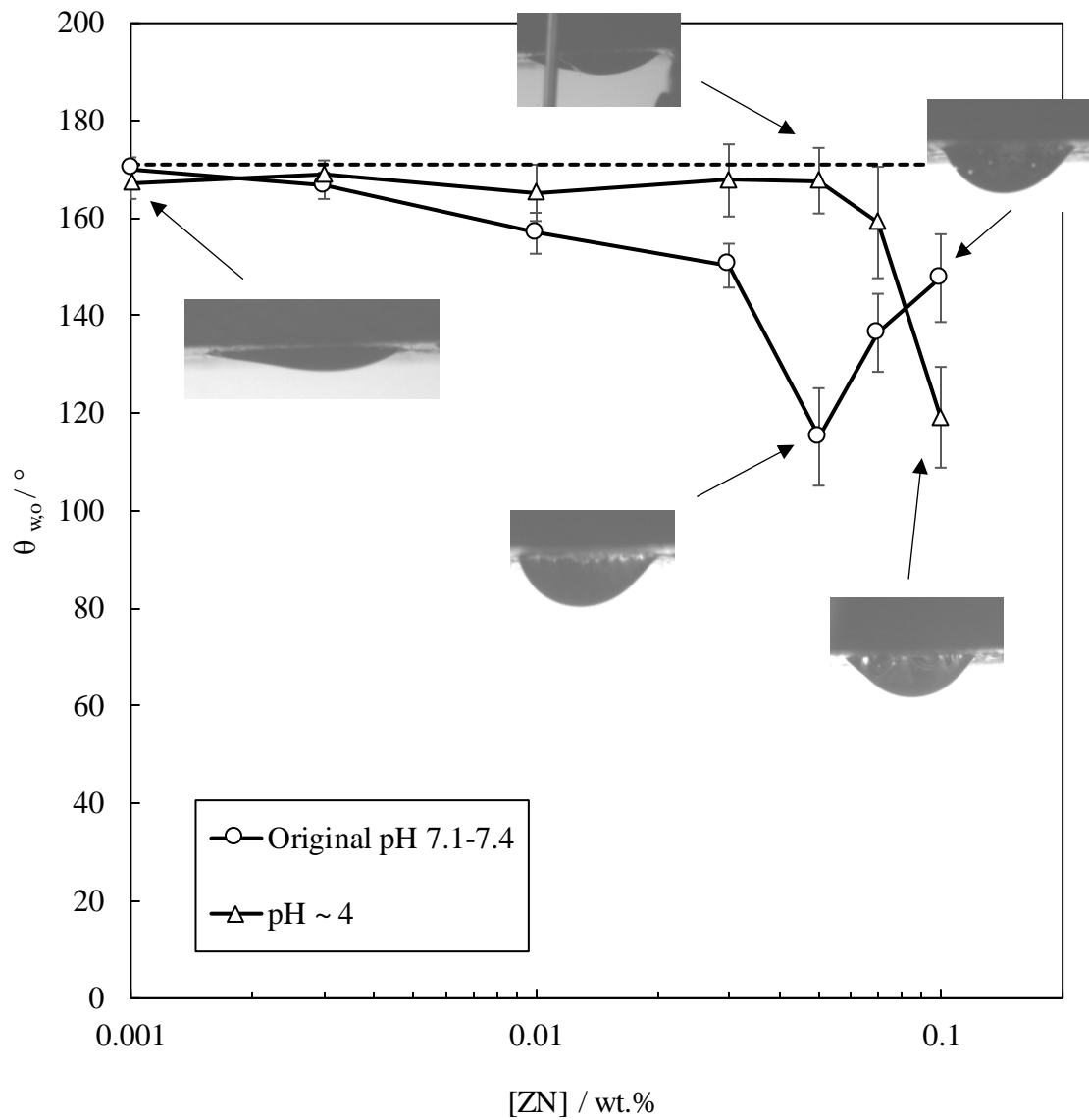
4.2 Adsorption of surfactant onto rock

Several variables including the surface charge of the reservoir rock, kind of surfactant, temperature, pH and salinity of the aqueous phase influence surfactant adsorption onto

oil reservoir rocks.[121] When choosing a surfactant to use in EOR, careful consideration must be given to the loss of surfactant owing to high adsorption onto rock since it can result in a large reduction in its positive performance and a waste of money. The modification of reservoir rock wettability is a benefit of surfactant adsorption, though.[232] Zwitterionic surfactants have a high potential for use in EOR due to their ability to strongly adsorb onto a range of reservoir rocks such as carbonates and sandstones. Additionally, they are less affected by divalent cations such as calcium and magnesium which are known to inhibit the adsorption of other types of surfactants (cationic and anionic) on reservoir rocks. Being dependent on pH, their headgroup charge can change which makes the surfactant behave differently in rock wettability alteration.[233] Recently, the addition of nanoparticles to surfactant solutions has gained popularity for reducing surfactant adsorption onto the rock in EOR.

In this part, the equilibrium adsorption of AHS and ZN onto calcite-rich shale at 25 °C was investigated. The effect of electrolytes and the concentration of ES-coated silica particles on the adsorption of surfactants were studied. The experimental data were modelled with different non-linear adsorption isotherms including Sips, Langmuir, Freundlich, Redlich-Peterson and Temkin models using the Solver add-in in Excel. The correlation coefficients of the models were used for comparing the isotherms (see Appendix B.3). The results showed that the experimental data are best fitted with Redlich-Peterson and Sips isotherms (highest R^2). The Redlich-Peterson model was used here in discussions.

4.2.1 Effect of surfactant type and concentration

Figure 4.16 compares the equilibrium surfactant adsorption onto the rock with the initial and equilibrium surfactant concentrations in DIW and Permian brine. The amount of AHS surfactant adsorbed onto rock increases almost linearly upon increasing the initial surfactant concentration in DIW, while it reaches a plateau when the surfactant is in Permian brine. When ZN is in DIW, a maximum is observed in the adsorption profile which approximately corresponds to the concentration where a minimum oil-water contact angle was previously observed. The adsorption of ZN onto rock increases linearly in the presence of Permian salts. The Redlich-Peterson adsorption parameters are listed in Table 4.1. The maximum adsorption for ZN is also observed in this plot. A similar maximum and then decreasing adsorption has also been observed in previous studies for CTAB and ionic liquids adsorbed onto Berea sandstone.[151]

Because of its anionic sulfonate and cationic quaternary ammonium groups, the zwitterionic AHS can have both a hard (I-shaped) and a soft (V-shaped) adsorption onto the rock surface, respectively. The latter is weaker since the sulfonate headgroup is required to bend for the positive group to interact with the solid surface and is repelled by the like-charged solid surface. As a function of concentration, this duality acts as the driving force behind the cooperative adsorption and coalescence of surfactant aggregates.[234] However, these electrostatic interactions between the headgroup of the surfactant and the rock surface have been found to occur effectively at low surfactant concentrations while it is mainly the interactions between the hydrophobic tails of the surfactant and the rock that take effect at high surfactant concentrations.[7, 235, 236] The nonionic surfactant in ZN can also have hydrogen bonding with the rock surface which turns into a weak bilayer at high surfactant concentrations. The amounts of surfactant adsorbed on this shale are consistent with those of anionic C_{15-18} internal olefin sulfonate, nonionic nonylphenol ethoxylate and cationic cetyl trimethylammonium bromide adsorbed onto calcite-rich (Eagle Ford, Wolfcamp and Marcellus formations) and quartz-rich (Mancos formation) shales.[237]

Figure 4.16. Equilibrium AHS and ZN adsorption onto shale *versus* the initial (top) and equilibrium (bottom) surfactant concentrations in DIW and Permian brine at 25 °C. In the lower plot, the points show the experimental data and the curves show the Redlich-Peterson adsorption isotherm.
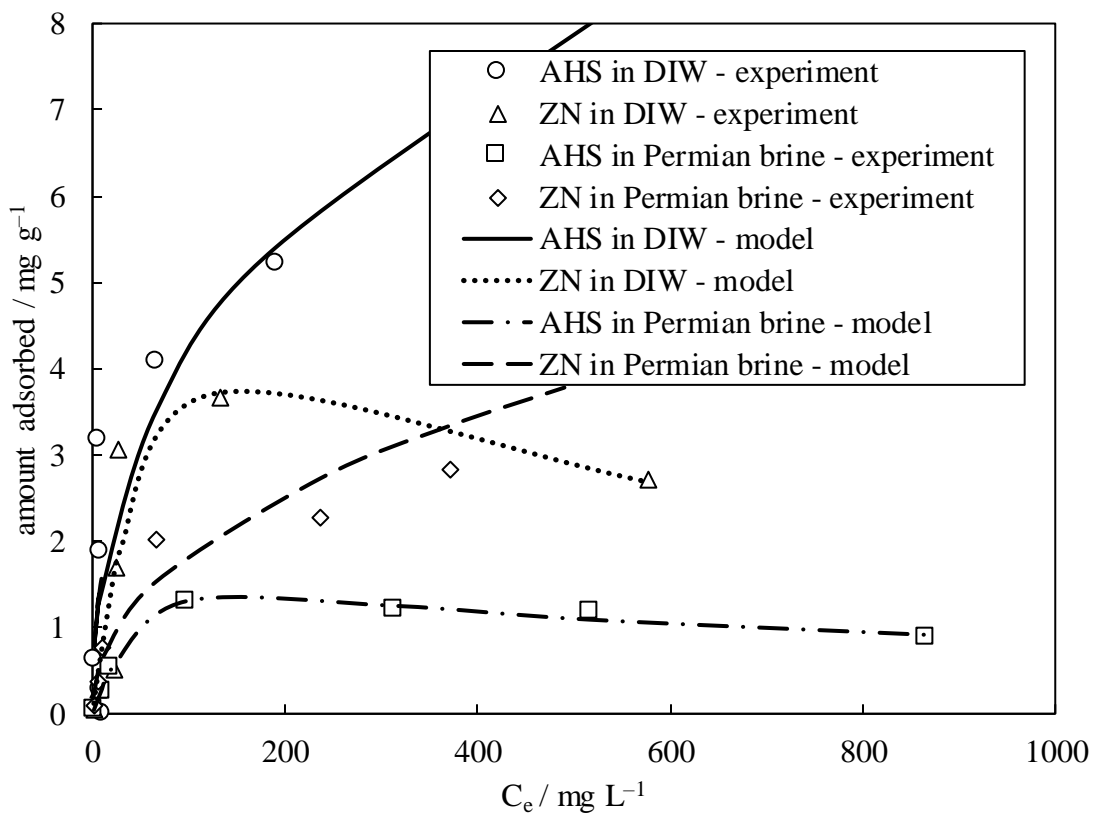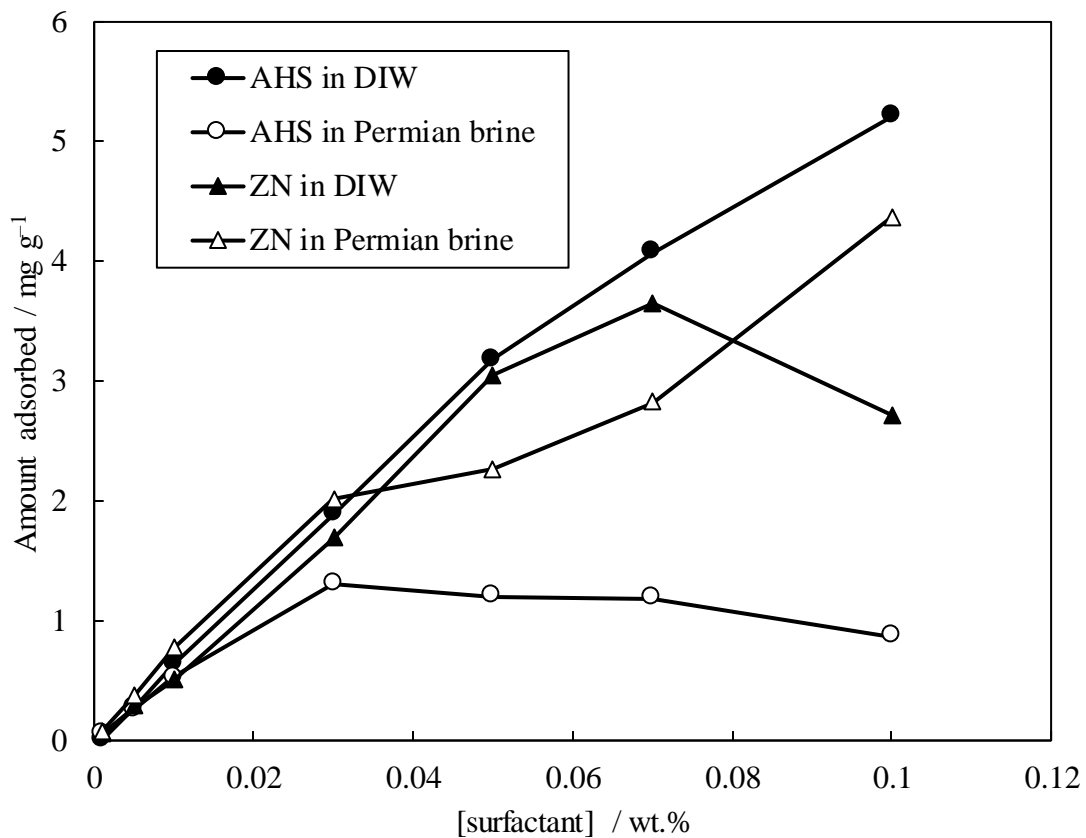
Table 4.1. Parameters of the Redlich-Peterson adsorption model fitted to the experimental data related to the amount of AHS and ZN adsorbed onto shale with or without different concentrations of ES-coated silica in DIW and Permian brine at 25 °C.

Surfactant	[particle] / wt.%	Solvent	Redlich-Peterson model parameters		
			K_{RP}	α_{RP}	n
AHS	0	DIW	12.33	19.32	0.59
	0.01		0.019	3×10^{-7}	0.55
	0.05		0.017	7×10^{-9}	0.07
	0.10		0.03	2×10^{-5}	0.13
	0	Permian brine	0.03	0.001	0.41
	0.01		0.06	0.002	0.48
	0.05		0.009	2×10^{-5}	0.89
	0.10		0.03	2×10^{-5}	0.13
ZN	0	DIW	0.08	0.001	0.46
	0.01		0.07	0.002	0.34
	0.05		0.008	1×10^{-5}	0.83
	0.10		0.05	0.001	0.41
	0	Permian brine	1.22	5.05	0.55
	0.01		0.07	0.02	0.10
	0.05		0.20	0.008	0.45
	0.10		0.09	0.002	0.51

K_{RP} (L mg^{-1}) and α_{RP} (L mg^{-1})^n are Redlich-Peterson constants. n is an exponent.

4.2.2 Effect of electrolyte

Figure 4.16 also shows the effect of adding Permian salts on the adsorption of AHS and ZN onto the rock at 25 °C. With the addition of Permian brine, the amount of AHS adsorbed onto the rock decreases. This observation is compatible with the oil-water

contact angles with AHS solutions where it was found that Permian salts reduce the wettability modification ability of AHS. For ZN, the amount adsorbed onto shale is lower in the presence of ions at intermediate initial surfactant concentrations (*i.e.* 0.03 – 0.07 wt.%) but it exceeds that of ZN in DIW when the surfactant concentration is above this range.

The literature shows that inorganic salts have three main effects on the adsorption of surfactant on solid surfaces depending on ion concentration and valence. Ions can increase surfactant adsorption onto the rock by reducing surfactant-surfactant electrostatic repulsion on the rock surface[216] but high salt concentrations increase hydrophobicity due to excess surfactant adsorption.[217] Ions can reduce surfactant adsorption by reducing surfactant-rock electrostatic attraction.[219] The last effect is dependent on the salt type. Nevskaia *et al.* reported that increasing NaCl concentrations increases the chemisorption of ions on reactive sites of quartz surfaces which reduces the adsorption of nonionic TX-100 surfactant onto the solid but the addition of $CaCl_2$ increases the surfactant adsorption due to the sufficient screening of the quartz surface charge. For anionic surfactants, the addition of cations can reduce the quartz surface charge and increase adsorption.[221]

As reviewed, most studies in the literature used a single salt brine but the brine used here is a mixture of different salts at a high concentration which makes it difficult to talk about the role of each ion. For zwitterionic surfactants with both charges in the headgroup, the interactions are complex in the presence of ions, as previously described. However, it is thought that the addition of Permian salts to zwitterionic AHS solutions could screen the electrostatic attraction between the anionic sulfonate group of the surfactant and cationic sites on the shale which leads to reduced adsorption of surfactant onto the rock and thus a smaller wettability alteration. An increase in the minimum oil-water contact angle from 64° to 119° with the addition of Permian brine to the AHS solutions was observed before which confirms this hypothesis. For ZN, the change in adsorption onto the rock with the addition of Permian brine is not significant (Figure 4.16) which agrees with the same contact angles measured with and without the salts. It is also thought that the intense adsorption of ZN onto the rock at high surfactant concentrations in the presence of ions is possible which makes the rock surface partially hydrophobic again.[217] This is in agreement with the increasing oil-water contact angle at high surfactant concentrations beyond the minimum observed before. Comparing the adsorption amounts of the two surfactants onto shale, the zwitterionic AHS has higher adsorption when the surfactants are in DIW, particularly at high surfactant concentrations, while ZN adsorption exceeds in the presence of Permian ions. The potential reason could be the increased adsorption

of the nonionic surfactant in ZN onto the rock with the addition of salts, particularly divalent counterions.[221]

4.2.3   Effect of adding particles

4.2.3.1   AHS

Figures 4.17 and 4.18 show the effect of adding ES-coated silica particles on the adsorption of AHS onto the rock with initial and equilibrium surfactant concentrations in DIW and Permian brine, respectively. The plots show a decrease in AHS surfactant adsorption onto rock upon addition of 0.01 wt.% particles in DIW while no significant change is observed in the adsorption plot at higher particle concentrations. This agrees with oil-water contact angle measurements where it was observed that particle concentrations above 0.01 wt.% in DIW do not change the contact angle considerably. It is also observed that the effect of particles on decreasing surfactant adsorption is more pronounced when the initial surfactant concentration is large.

When the blend of AHS and particles was in Permian brine, the addition of particles increased AHS adsorption onto rock which is more significant at intermediate initial surfactant concentrations. This increase in adsorption is small when using 0.01 wt.% particles but becomes significant at higher particle concentrations. It is noted that when optimum surfactant adsorption onto rock is reached, the highest rock wettability alteration is expected. Additional surfactant adsorption onto the rock with tails outward increases the rock hydrophobicity. Here, 0.01 wt.% particles have helped the surfactant adsorb onto rock more to induce the highest wettability alteration but higher particle loadings have increased the surfactant adsorption onto rock significantly which promotes hydrophobicity. There is also a maximum in the adsorption profile at 0.03 – 0.05 wt.% surfactant for all blends in Permian brine above which the adsorption decreases again. The surfactant concentration causing this maximum is the same as the one at which a minimum oil-water contact angle was observed.

Figure 4.17. Amount of AHS adsorbed onto shale at 25 °C *versus* initial (top) and equilibrium (bottom) surfactant concentration in DIW for different concentrations of ES-coated silica. In the lower plot, the points show the experimental data and the curves show the Redlich-Peterson adsorption isotherm.
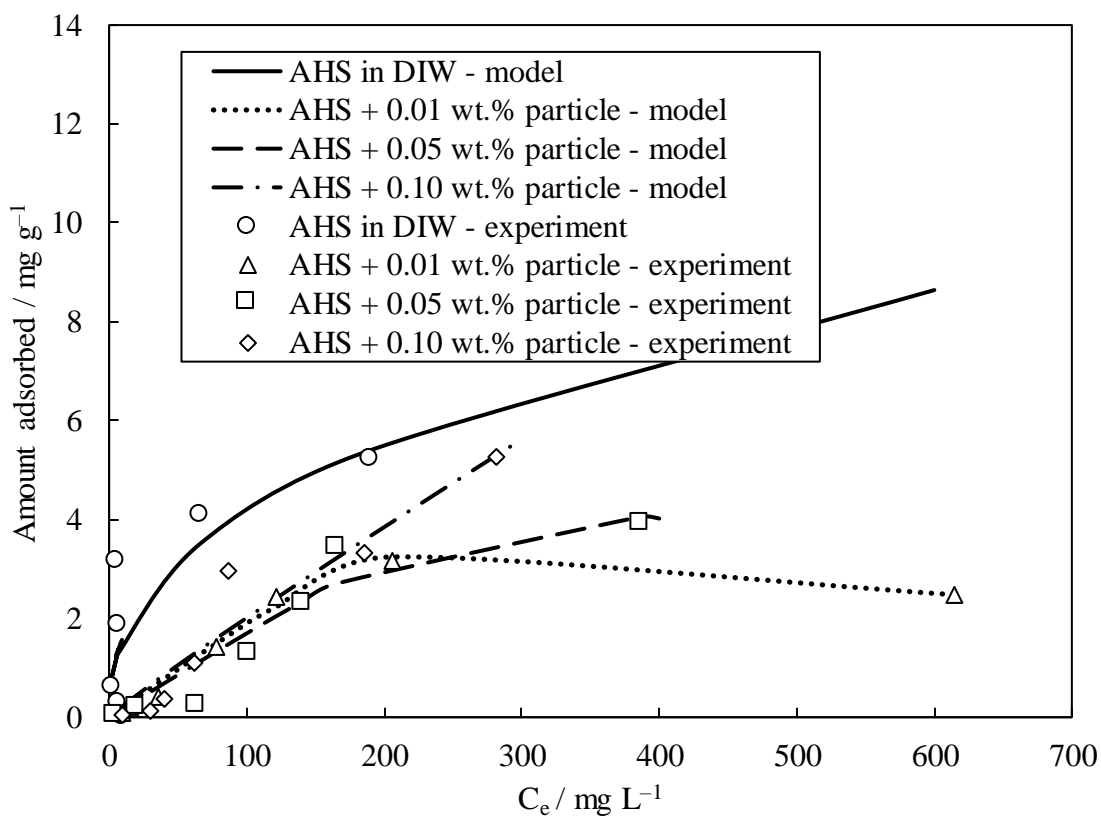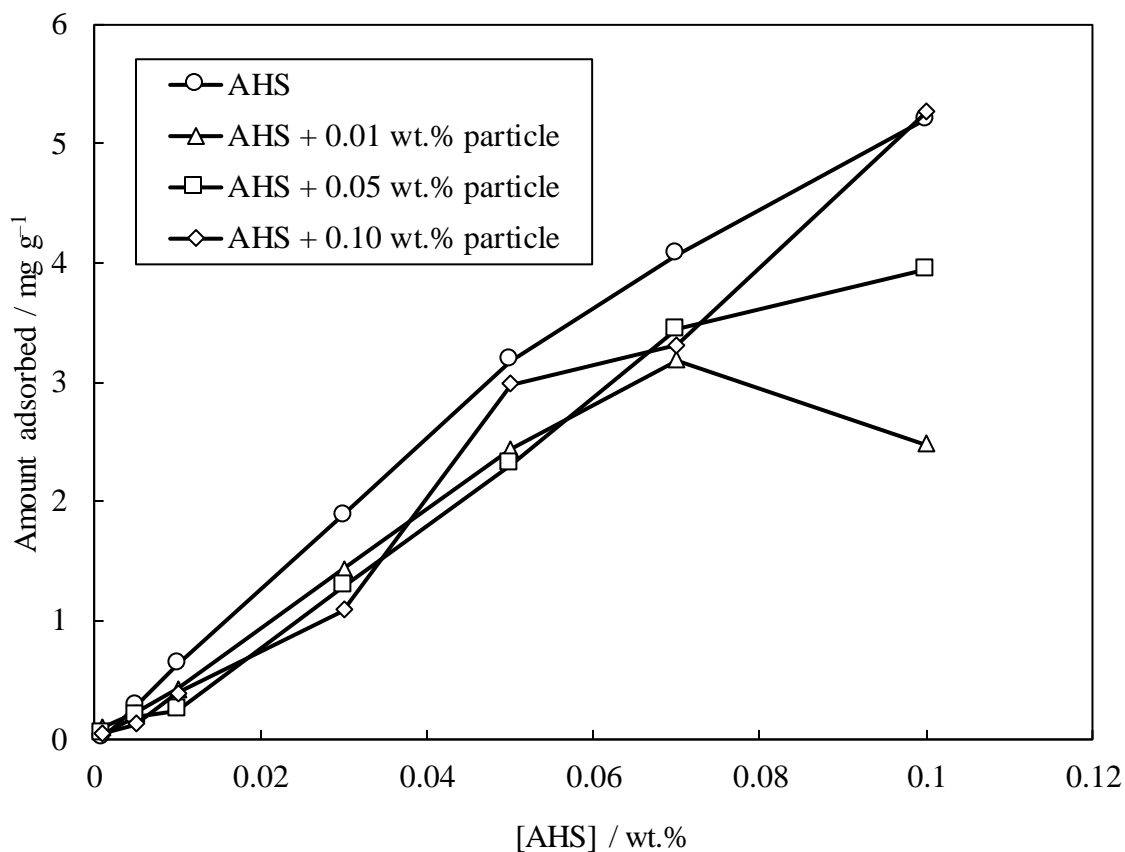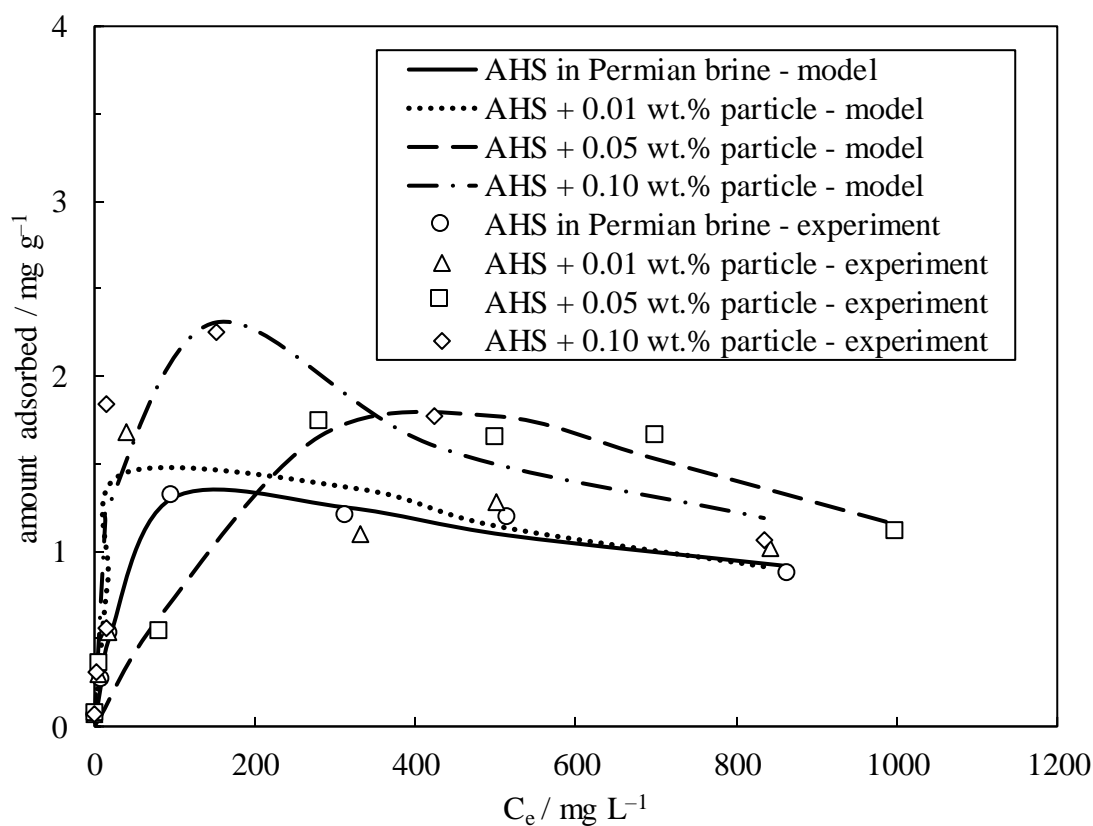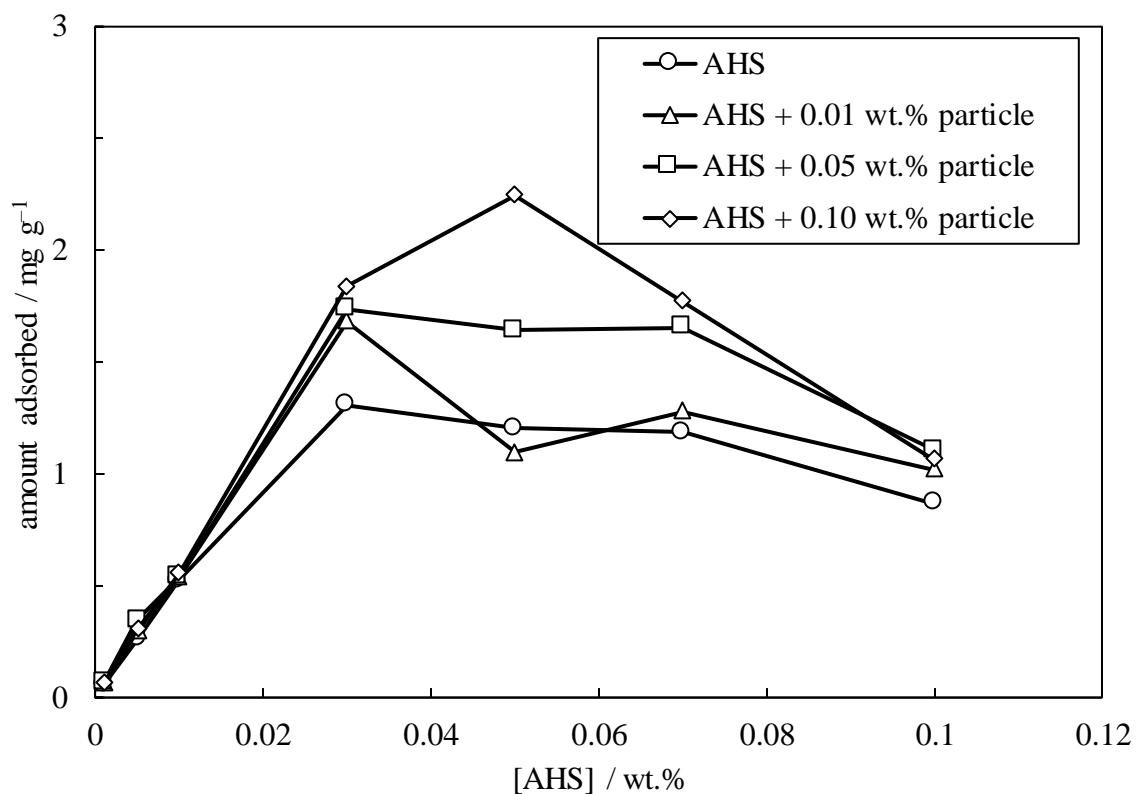
Figure 4.18. Amount of AHS adsorbed onto shale at 25 °C *versus* initial (top) and equilibrium (bottom) surfactant concentration in Permian brine for different concentrations of ES-coated silica. In the lower plot, the points show the experimental data and the curves show the Redlich-Peterson adsorption isotherm.

4.2.3.2 ZN

Figures 4.19 and 4.20 show the effect of adding particles on the adsorption of ZN onto the rock in DIW and Permian brine, respectively. As shown, the addition of particles reduces the ZN adsorption onto rock both in DIW and Permian brine. The same effect was reported by Zhong *et al.* who observed a significant reduction in the adsorption of zwitterionic cocamidopropyl hydroxysultaine surfactant onto Berea sandstone (70% quartz) in API brine by using ES-coated silica particles which was linked to the electrostatic interactions between the positive headgroup of the surfactant and anionic particles that can reduce the attraction between anionic particles and the cations of the brine by chelate effects; therefore, the surfactant-grafted particles may have a higher surface charge in comparison with that of particles in the brine which results in synergy.[229] For the blends in DIW, the reduced ZN adsorption onto the rock by particles becomes small at large initial surfactant concentrations. When the blends are in Permian brine, the effect of particles on decreasing ZN adsorption onto rock is mainly significant at large initial surfactant concentrations. The same maximum in the adsorption profiles is also observed here which is more noticeable for the blends in Permian brine. The surfactant concentrations in the blends causing these maximum adsorptions (0.05 – 0.07 wt.%) are the same as the ones causing minimum oil-water contact angles. The decreasing adsorption above the maximum also corresponds to the increasing oil-water contact angle at high surfactant concentrations. Table 4.1 presents the parameters of the Redlich-Peterson adsorption model fitted to the experimental data.

The reduction in surfactant adsorption onto the rock by particles is more critical in tight oil reservoirs like shales which have a larger surface area. Optimizing the dispersion formulation is required to achieve sufficient adsorption onto the rock for wettability alteration while avoiding surfactant loss. It has been reported that surfactant adsorption at particle surfaces is higher than that at gas-water surfaces but lower than that at oil-water interfaces. Therefore, it is most likely that $\Delta G < 0$ when using nanoparticles as surfactant carriers. In other words, the surfactant molecules tend to spontaneously leave the particle surface to adsorb at oil-water and oil-solid interfaces.[119] In this situation, the lack of sufficient steric stability leaves the particles aggregated. It is also noted that unlike at the liquid-liquid interface, when nanoparticles adsorb at the rock surface they are bound to the solid surface with no lateral mobility[19] which makes the adsorption process irreversible. The mixed particle-surfactant monolayer formed on the rock surface is likely constant due to the high attachment energy.

Figure 4.19. Amount of ZN onto shale at 25 °C *versus* initial (top) and equilibrium (bottom) surfactant concentrations in DIW for different concentrations of ES-coated silica. In the lower plot, the points show the experimental data and the curves show the Redlich-Peterson adsorption isotherm.
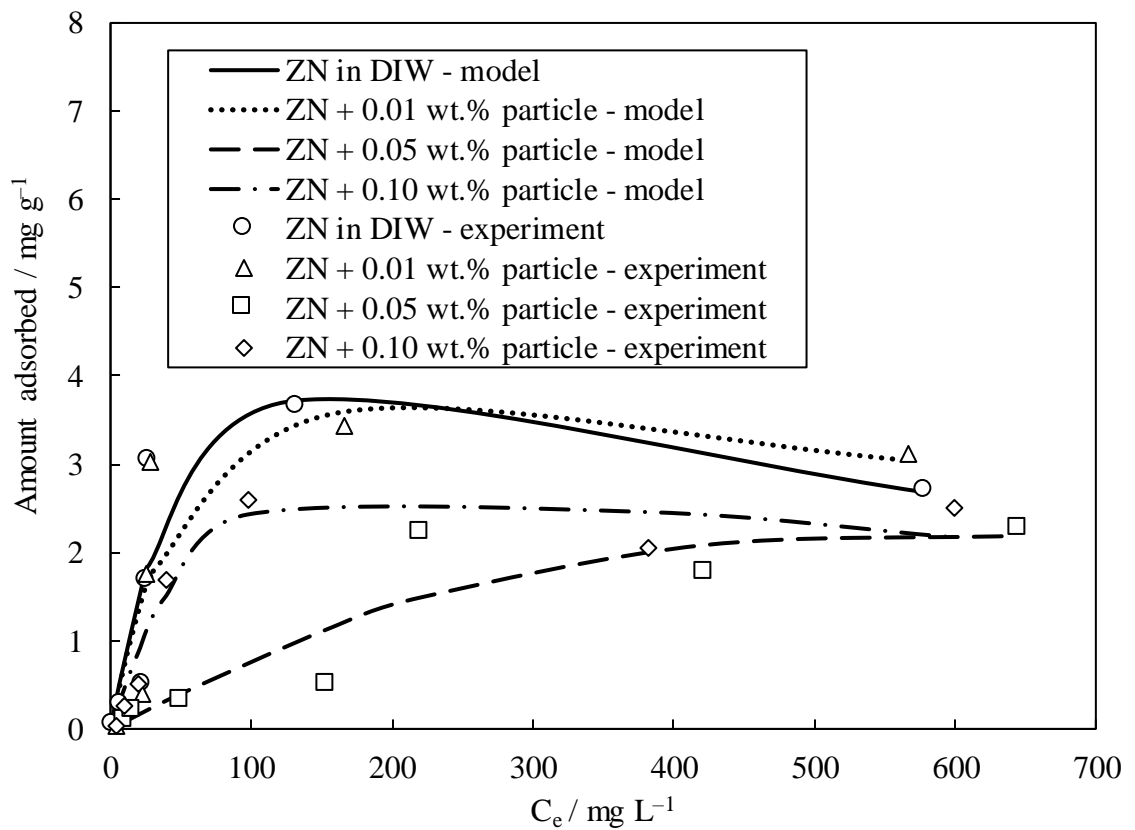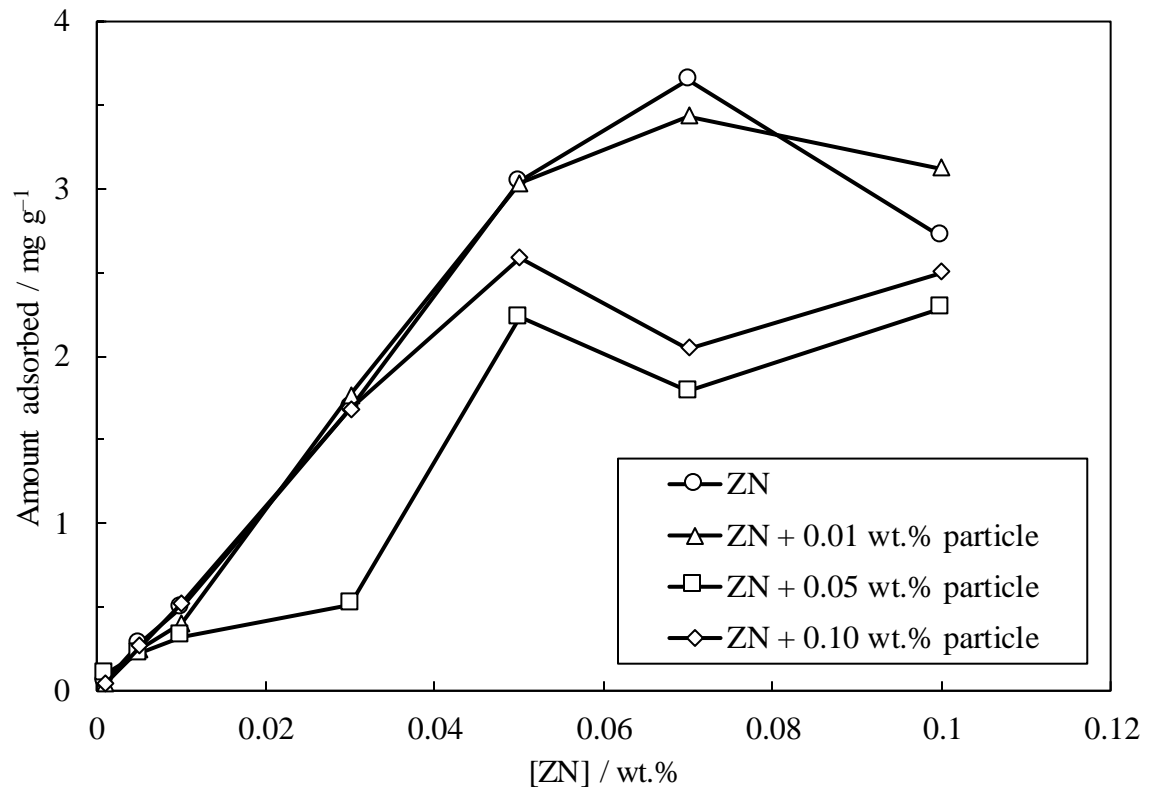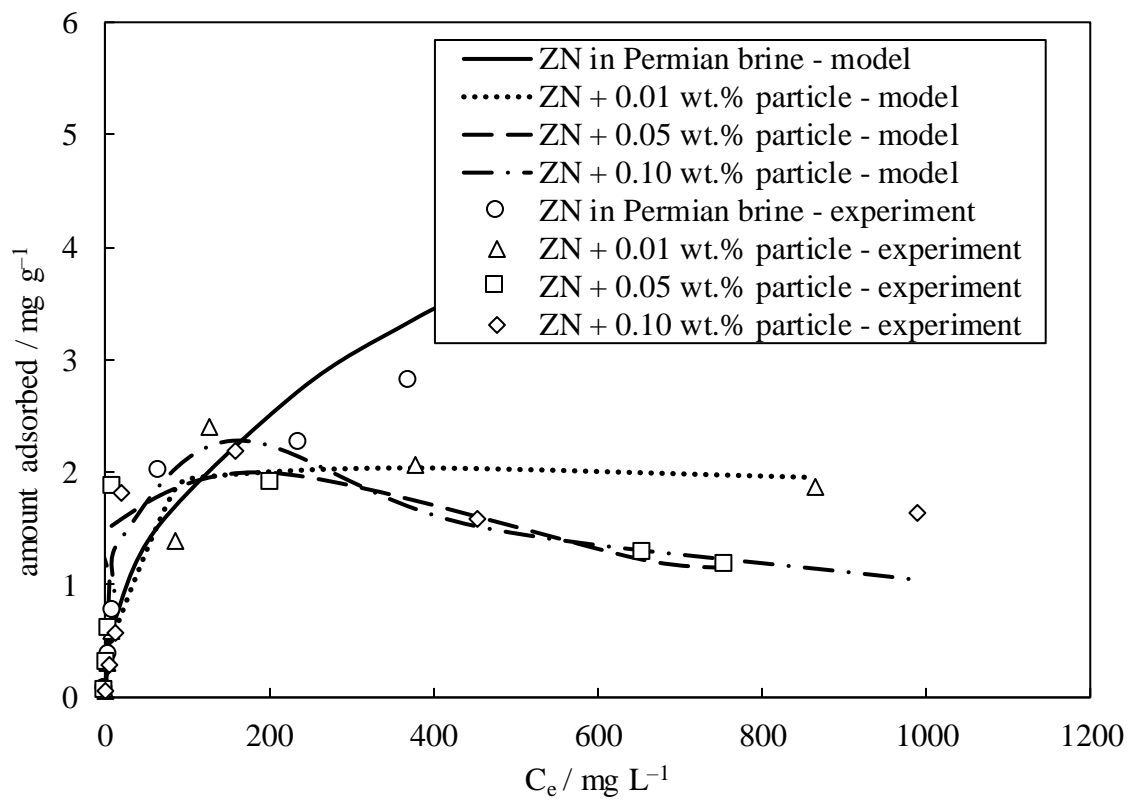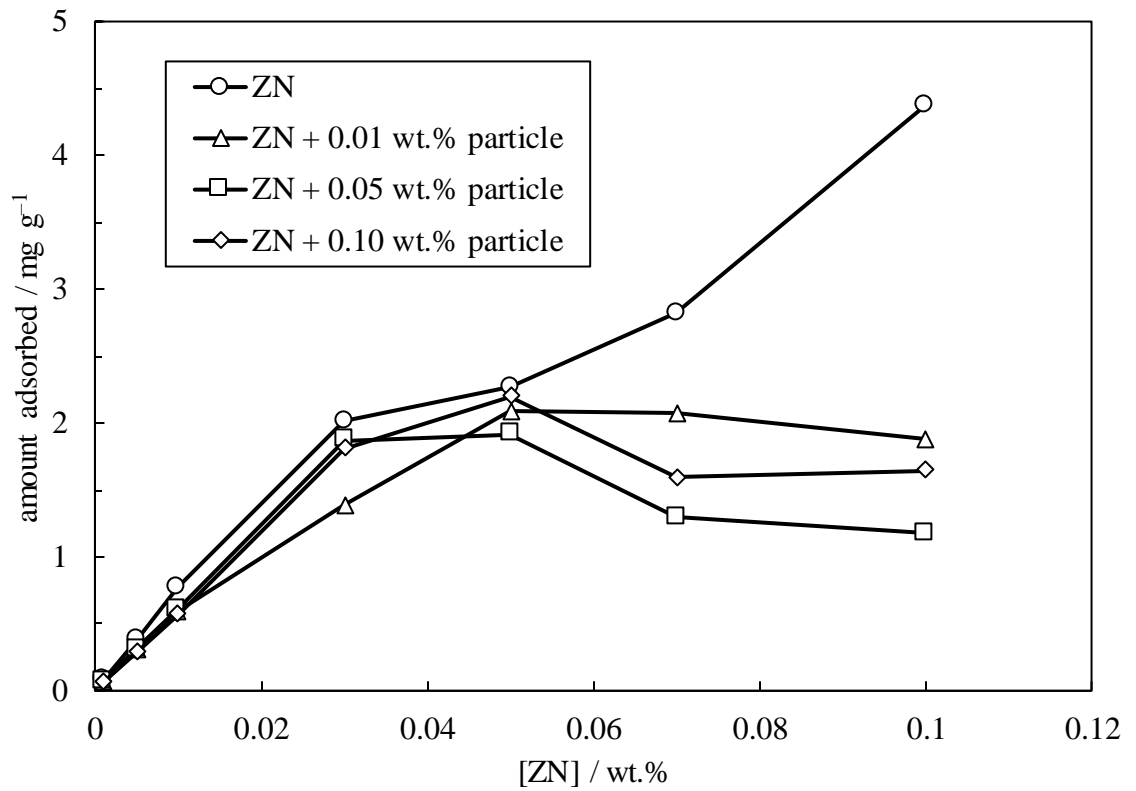
Figure 4.20. Amount of ZN adsorbed onto shale at 25 °C *versus* initial (top) and equilibrium (bottom) surfactant concentration in Permian brine for different concentrations of ES-coated silica. In the lower plot, the points show the experimental data and the curves show the Redlich-Peterson adsorption isotherm.

4.3 SEM and EDX

EDX-assisted SEM is a useful technique for identifying the wettability alteration of a rock caused by a chemical in EOR. SEM can be used to inspect the surface morphology of the rock and spot morphological alterations that might happen as a result of a change in wettability. On the other hand, EDX can be used to determine the chemical composition of the sample and identify any changes that could have altered the surface wettability. The combination of SEM and EDX provides a comprehensive understanding of the wettability alteration. In this study, the surface morphology and composition of the shale treated with the optimum dispersion of 0.01 wt.% ES-coated silica and 0.03 wt.% AHS surfactant in Permian brine were inspected by SEM-EDX. The dispersion selected here was the most effective dispersions in the wettability alteration based on contact angle measurements (see Section 4.1.2.7). For comparison, the SEM-EDX of the bare rock and rock treated with DIW, Permian brine, the blend in DIW and the individual chemicals in DIW and Permian brine were also performed.

Figures 4.21 and 4.22 compare the SEM images taken from the bare shale and the shale treated with different solutions and dispersions at 25 °C. As shown, the addition of ions, particles and surfactants changes the surface morphology of the minerals.

Figure 4.23 shows the EDX of 10-micron bare rock powder treated for 24 h with different chemicals (ES-coated silica particles and AHS) in DIW at 25 °C. The plot shows the atomic percentage of the main elements of the system related to calcite (calcium, oxygen and carbon), quartz (silicon and oxygen), nanoparticles (silicon, oxygen and carbon) and surfactant (carbon and oxygen). The atomic percentages of other elements were negligible. As previously observed, the bare rock (without treatment) is mostly comprised of calcium, carbon and oxygen showing a high calcite content. Treatment of rock with DIW does not change the composition significantly. However, by treating the rock with 0.01 wt.% ES-coated silica in DIW, the percentage of surface silicon atoms increases by 10 times (from 0.5% to 5%) indicating the adsorption of particles on the rock surface which is accompanied by a higher and lower number of oxygen and calcium atoms, respectively compared to bare rock. With the treatment of rock with AHS solution, a relative rise in oxygen percentage compared to that of bare rock is observed, probably due to the adsorption of the sulfonate group on the rock, which is accompanied by a drop in calcium percentage due to the reduction of adsorption sites. The percentage of silicon atoms here is the same as in the bare rock, as expected. By treating the rock with the blend of particles and surfactant, the percentage of surface oxygen is as high as the particle dispersion or

surfactant solution and no rise in the number of silicon atoms as a result of the adsorption of particles on the solid is observed compared to that of bare rock probably due to the interference caused by the surfactant-particle interactions. The number of calcium atoms decreases when treating the rock with the blend compared to bare rock.

Figure 4.24 shows the EDX of the bare rock treated for 24 h with the different chemicals in Permian brine. As shown, with the treatment of rock with Permian brine, the percentages of carbon and oxygen atoms increased and decreased, respectively. The percentage of ions present in Permian brine like chlorine, sodium and potassium also increased as expected. It is difficult to discuss the changes in other elements due to the interference of the brine ions but by comparing Figures 4.23 and 4.24, one can observe that the addition of Permian salts reduced the oxygen percentage but left the calcium and carbon numbers almost unchanged. The percentage of chlorine, sodium and potassium ions decreased when the rock was treated with particles in brine, probably due to the adsorption of ions onto the particle surface. When treating the rock with the surfactant solution, the percentage of carbon and oxygen increased and decreased, respectively compared to that of bare rock as a result of the adsorption of surfactant onto the rock while a further decrease in the percentage of the three brine ions (chlorine, sodium and potassium) was observed possibly due to the ions serving as counterions for surfactant headgroups.

The EDX-SEM of the rock treated with the blend of ZN and particles was not performed since the same results were expected and no comparison could be made with that of AHS.
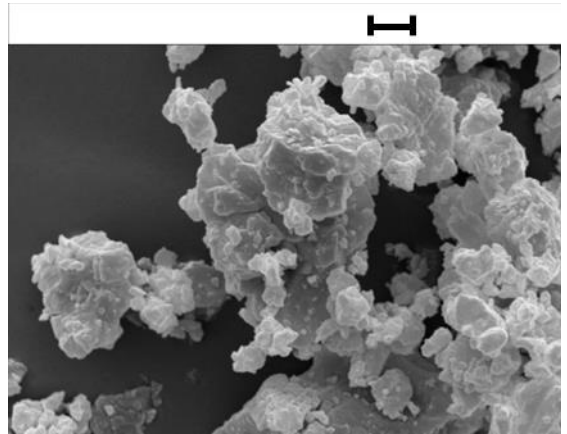
Figure 4.21. SEM images of 10-micron bare shale powder treated for 24 h at 25 °C with various solutions and dispersions in DIW. The scale bars show 2 µm.
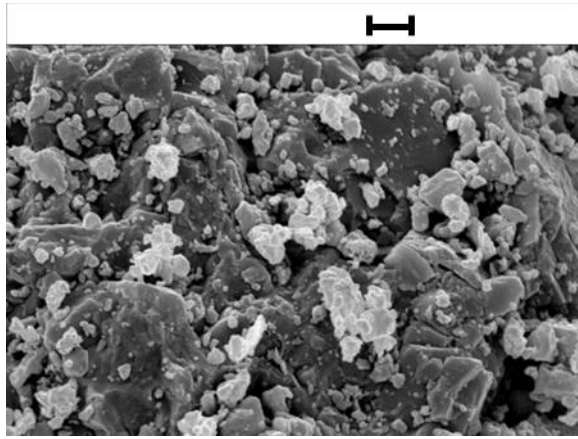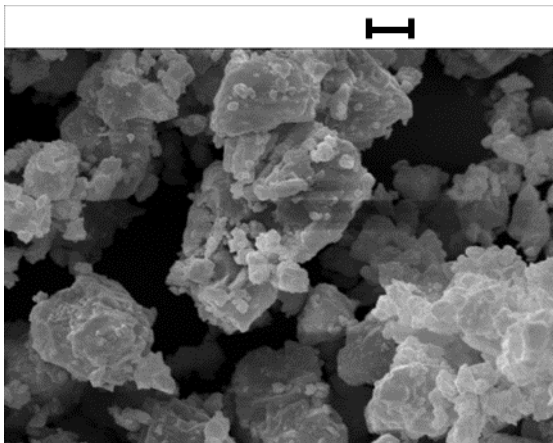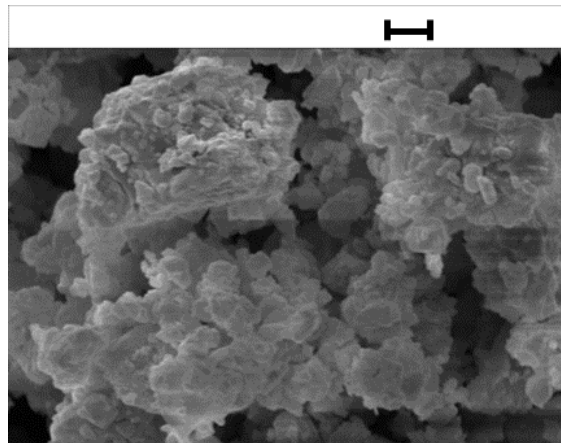
Bare shale

DIW
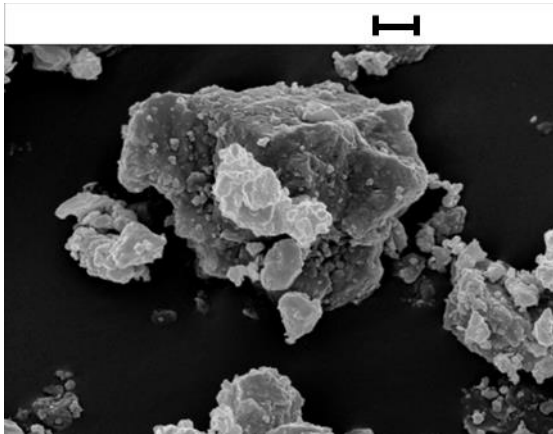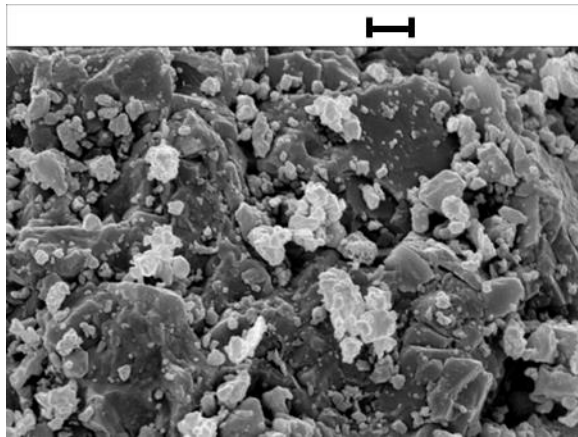

0.01 wt.% ES-coated silica in DIW
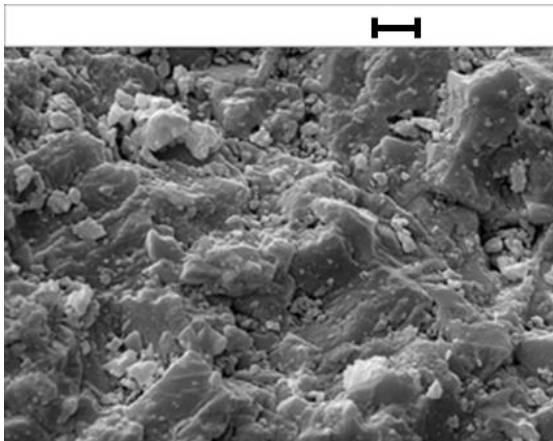

0.03 wt.% AHS in DIW

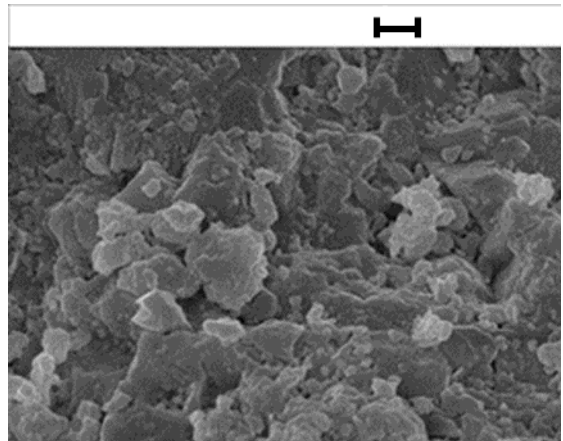0.01 wt.% ES-coated silica and 0.03 wt.% AHS in DIW

Figure 4.22. SEM images of 10-micron bare shale powder treated for 24 h at 25 °C with various solutions and dispersions in Permian brine. The scale bars show 2 µm.
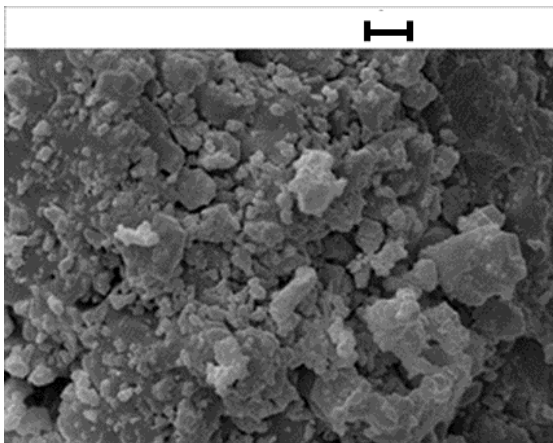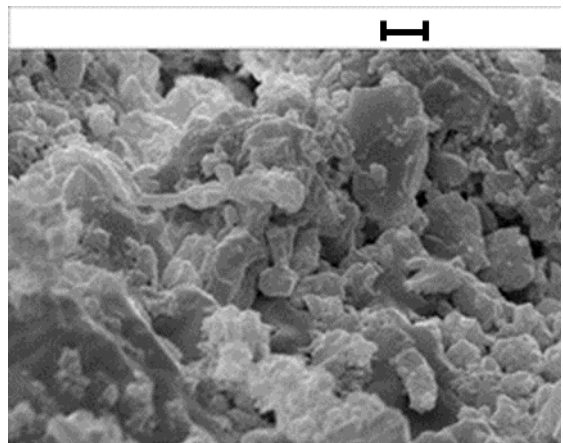
Bare shale

Permian brine

0.01 wt.% ES-coated silica in Permian brine

0.03 wt.% AHS in Permian brine

0.01 wt.% ES-coated silica and 0.03 wt.% AHS in Permian brine

Figure 4.23. EDX taken from 10-micron shale powder after treatment with DIW, 0.01 wt.% ES-coated silica in DIW, 0.03 wt.% AHS in DIW and the blend of 0.01 wt.% ES-coated silica particles and 0.03 wt.% AHS in DIW for 24 h at 25 °C.
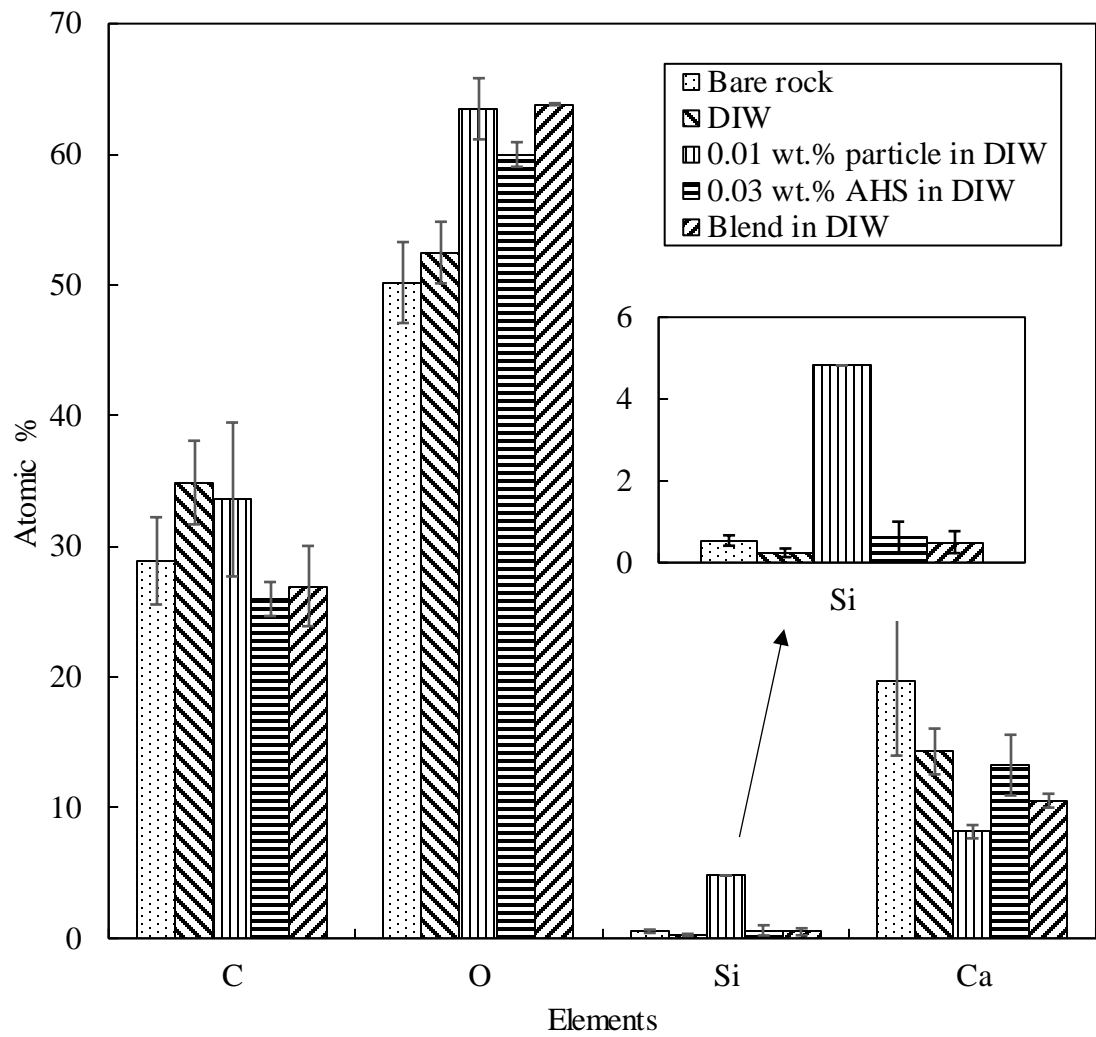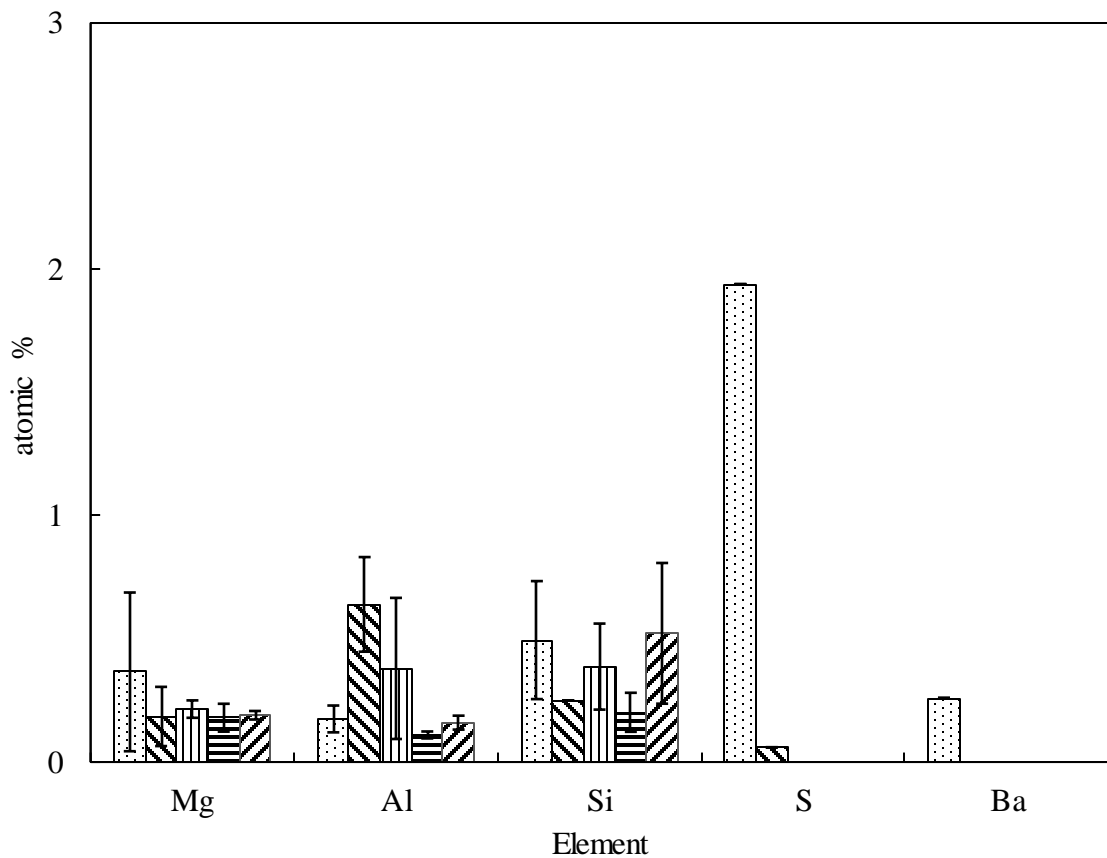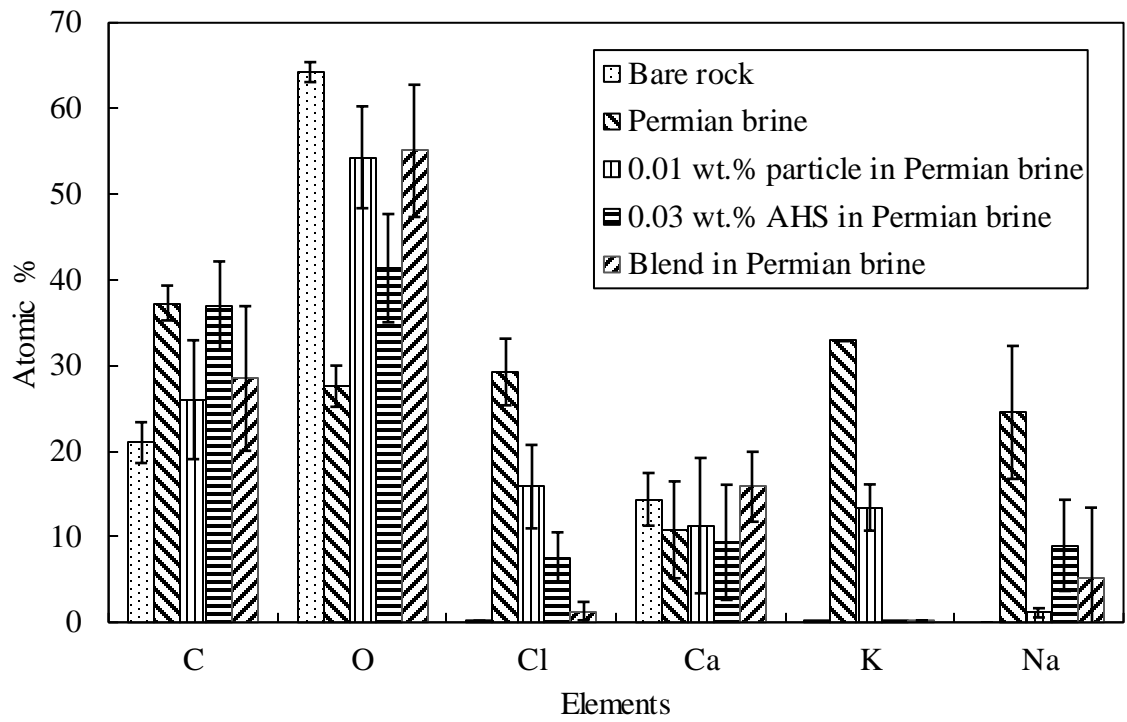
200

Figure 4.24. EDX taken from 10-micron shale powder after treatment with Permian brine, 0.01 wt.% ES-coated silica in Permian brine, 0.03 wt.% AHS in Permian brine and the blend of 0.01 wt.% ES-coated silica particles and 0.03 wt.% AHS in Permian brine for 24 h at 25 °C.

4.4 Summary of findings

The adsorption of surfactants (with and without particles) at the rock-fluid interface were described in this chapter. The findings could be summarized as follows:

- A decreasing crude oil-water contact angle from ~ 171° to 64° by AHS and 115° by ZN surfactant was observed at 0.05 wt.% in DIW due to the ion-pair formation by zwitterionic surfactant and hydrogen bonding by $C_{10-12}E_9$ in surfactant (weaker). An increasing contact angle was seen at higher [surfactant] probably due to the I- and V-shaped adsorption of excess surfactant molecules on the rock surface.

- When Permian brine was added, both surfactants resulted in the same contact angle (~ 118°) but with a lower [AHS]. Permian brine addition increased the minimum contact angle by AHS due to the reduced surfactant-rock electrostatic attraction by ions, consistent with the reduced adsorption of AHS on rock powder when adding brine.

- A decreasing contact angle to ~ 40° was observed on increasing [bare silica] to 0.05 wt.% in DIW beyond which hydrophobicity increased again.

- A pH-dependent behaviour was observed with AS-coated silica. At low particle loading (low pH), rock wettability alteration was negligible due to the similar charges of particles and rock, while at high [particle] (isoelectric point), larger rock wettability alteration (by ~ 25°) was observed due to the interactions of weakly anionic particles with cationic rock and crude oil groups.

- ES-coated silica was not also efficient in rock wettability alteration (maximum 30° decrease at 0.01 wt.%). As ES is nonionic, charge reversal with pH is absent for these particles but they can have hydrogen bonding and electrostatic interactions (by anionic uncoated sites) with charged rock and crude oil polar groups. Particle adsorption can reduce the rock positive charge leading to reduced attraction between crude oil components and the rock surface. This mechanism is not strong for ES-coated silica compared to bare silica explaining its lower wettability alteration power.

- A minimum contact angle (48°) was observed with blending 0.03 wt.% AHS and 0.01 wt.% ES-coated silica in DIW indicating a further contact angle decrease of 91° and 16° compared to minimums by particles and surfactant alone, respectively.

- The particle-surfactant mixture showed a pH-responsive behaviour in which particles can act as surfactant carriers (isoelectric pH) or surface activity improvers (high pH). The former provides interactions between the zwitterionic surfactant and anionic particles (V-shaped adsorption) or cationic rock (I-shaped adsorption). The latter led to a simultaneous increase in oil-water contact angle and AHS adsorption onto rock powder at high [particle] and [AHS]. A minimum contact angle (90°) was observed with the same blend in Permian brine indicating a further reduction of 30° and 53°

compared to minimums by AHS and particles alone, consistent with the increased AHS adsorption onto the rock on adding particles in Permian brine.

- The blends of 0.07 wt.% ZN surfactant and 0.01 wt.% ES-coated silica in DIW resulted in a minimum contact angle of 64° indicating a further 51° and 75° reduction in contact angle compared to minimums by ZN and particles, respectively. The same pH-dependent behaviour was observed with ZN surfactant and particles. The blend of 0.01 wt.% particles and 0.05 wt.% ZN surfactant in Permian brine minimized the contact angle to 56° indicating an additional reduction of 62° and 87° compared to minimums by surfactant and particles alone, respectively. Unlike AHS, ZN surfactant adsorption could hydrophobize particles, consistent with reduced ZN surfactant adsorption from Permian brine onto rock powder when adding particles.

- The optimum pH of the blend for achieving a minimum contact angle was revealed to be ~ 7 where the surfactant is zwitterionic and the particles are moderately anionic leading to the largest electrostatic interactions between surfactant and particles or crude oil components which have a significant effect on particle and rock wettability.

- Although expected to be helpful, calcite dissolution increased rock hydrophobicity at low pH probably due to the free rock surface serving as an adsorbent for crude oil components or excess aqueous surfactant.

- Both AHS and ZN surfactants exhibited high adsorption onto the rock in both static (rock powder) and dynamic (cores) modes (more so for powder) due to the aerobic lab. conditions.

- Higher static AHS adsorption onto rock was observed when the surfactants were in DIW while the adsorption of ZN surfactant was higher in Permian brine. The latter was also observed in dynamic mode.

- Permian brine reduced static AHS adsorption onto rock consistent with an increased oil-water contact angle after adding brine.

- When ZN surfactant was in DIW, a maximum was observed in its static adsorption profile which approximately corresponded to the concentration where a minimum oil-water contact angle was observed. Permian brine had a small effect on static ZN surfactant adsorption onto rock consistent with unchanged oil-water contact angles with and without salts.

- A decrease in static AHS adsorption onto rock was observed upon the addition of 0.01 wt.% particles in DIW while no significant change was observed at higher [particle], consistent with insignificant oil-water contact angle changes observed at [particle] > 0.01 wt.%. When the blend of AHS and particles was in Permian brine, the addition

of particles increased both static and dynamic (smaller change) AHS adsorption onto the rock.

- The addition of particles reduced both static and dynamic adsorption of ZN surfactant onto rock both in DIW and Permian brine. Unlike those of AHS, the interactions between the headgroup of the nonionic surfactant in ZN surfactant and the particle surface are independent of the salinity leading to more ZN surfactant savings.

- The surface morphology of rock was shown to change in SEM images when treated with blends of particles and AHS. The EDX results disclosed the adsorption of anionic ES-coated silica (10-time increase in silicon atoms) and AHS (rise in oxygen atoms and decrease in calcium atoms) onto the cationic rock. A decrease in calcium atoms was also seen with the blend of particles and AHS in DIW. Particles and AHS were revealed to serve as an adsorbent for brine ions leading to reduced counterion adsorption onto the rock.

Chapter 5 EOR chemicals in oil-water systems

By lowering the interfacial tension between crude oil and water and promoting emulsification, surfactant flooding can improve oil recovery. The extent of interfacial tension reduction and subsequent mixing of the oil and water phases are determined by the ability of surfactant molecules to adsorb at the oil-water interface. The flow resistance is reduced as a result and oil may be displaced more successfully.

This chapter reports the adsorption behaviour of AHS and ZN at the oil-water interface through interfacial tension measurements and emulsion tests using different oils including toluene, heptane, heptol $(1:1 \text{ g g}^{-1})$ and crude oil. The effects of adding Permian brine and ES-coated silica particles to surfactant solutions on the oil-water interfacial tension and the emulsification of oil and water have also been studied.

5.1   Oil-water interfacial tension

As a reference, the interfacial tensions between different oils and DIW or Permian brine were measured at $25 \pm 0.5 \,°C$ (Table 5.1). According to the results, the interfacial tension between pure oils and DIW decreases as follows: heptane > heptol > toluene, which is in agreement with the literature values reported before.[238, 239] Such low oil-water interfacial tension is anticipated given the light nature of the crude oil.

The chemical characteristics of the oil phase such as its polarity and the presence of surface-active agents affect the interfacial tension between oil and water. Toluene is an aromatic hydrocarbon with a partial polarity. Due to its symmetrical molecular structure and the delocalization of its electrons, the benzene ring itself is non-polar. Nevertheless, the methyl group is polar because of the difference in electronegativity between the carbon and hydrogen atoms (hydrogen atoms are slightly positive but carbon atoms are slightly more electronegative). Therefore, toluene is partially soluble in polar solvents like water and mostly soluble in non-polar solvents.[240] Compared to non-polar oils like heptane, polar oils often have lower interfacial tensions with water. This is due to the reduced intermolecular interactions at the oil-water interface and the larger interfacial oil molecules. On the other hand, because of their weak polarity, non-polar oils like heptane and more or less heptol (due to the presence of heptane in it) frequently exhibit higher

interfacial tensions with water caused by stronger intermolecular interactions between the oil and water phases.[240, 241] The complex mixture of hydrocarbons that make up crude oil has varied degrees of polarity and surface-active agents, and the way this affects the oil-water interfacial tension can be quite different. Moreover, crude oil may contain additional elements including asphaltenes and sulphur compounds that may have an impact on its surface-active agents and oil-water interfacial tension.[242]

Table 5.1 also shows that the oil-water interfacial tensions increase with the addition of Permian brine for all oils. Some studies show that high concentrations of ions reduce the electrical double layer of the oil-water interface and increase the interfacial tension.[243] Other studies link the rise to the disruption of the equilibrium attraction between interfacial molecules due to the salting-out effect. Salts dissociate and hydrate in water. Since water molecules interact with oil molecules at the oil-water interface, they provide lower hydrogen bonding, encouraging ions to move to the bulk which increases the bulk salt concentration, makes the surface excess concentration of salts negative and raises the interfacial tension as follows:[52, 244]

$$dγ = -RT \sum Γ_i \, dln α_i \tag{5.1}$$

where R is the universal gas constant, T is the temperature, $Γ$ is the surface excess concentration and $α$ is the chemical activity of solutes.

Table 5.1. Measured interfacial tensions between various oils and DIW or Permian brine (12.6 wt.%) at 25 ± 0.5 °C.

Aqueous phase	Oil phase	Interfacial tension / mN m^{-1}
DIW	Toluene	39.1
	Heptane	52.1
	Heptol (1:1 g g^{-1})	45.8
	Crude oil	10.4
Permian brine	Toluene	41.4
	Heptane	54.0
	Heptol (1:1 g g^{-1})	47.5
	Crude oil	12.6

5.1.1 Effect of surfactant type and concentration

Figure 5.1 shows the impact of the kind and concentration of surfactant (> CMC) in DIW or Permian brine on the interfacial tension between various oils and water at 25 °C. Upon adding the surfactants, they diffuse in the aqueous phase to adsorb at the oil-water interface with non-polar tails drawn to the organic phase and the polar headgroups

interacting with the aqueous phase. As a result, a monolayer of surfactant molecules forms at the interface[245] resulting in a considerable reduction in oil-water interfacial tension even at CMC compared to reference values (Table 5.1). In the absence of surface-active agents in the oil phase (for pure oils), the surfactant tails mostly interact with interfacial oil molecules (if any) while polar groups can adsorb at the oil-water interface to form a mixed monolayer with the aqueous surfactant to lower the tension when using crude oil.[246] When the surfactants are in DIW, increasing surfactant concentration above the CMC further reduces the interfacial tension to a minimum at 0.03 wt.% beyond which it reaches a plateau or slightly increases. Similar minimum and increasing interfacial tensions on raising surfactant concentrations have been observed before and are linked to the solubilization of the oil phase by adsorbed surfactant which reduces its concentration at the oil-water interface and results in a slight increase in interfacial tension.[70, 246, 247]

The predominant surfactant in ZN is zwitterionic AHS with a trace quantity of nonionic polyoxyethylene alkyl ethers ($C_{10-12}E_9$). They are frequently employed in combination with other kinds of surfactants like zwitterionics to accomplish certain qualities like improved micellization, solubilization, emulsification and wetting.[248] The addition of a nonionic surfactant to a zwitterionic surfactant solution can have a variety of effects on lowering the interfacial tension between oil and water. Adding a nonionic surfactant to a zwitterionic surfactant may have no impact on the interfacial tension between oil and water, depending on the specific qualities of the surfactants and the concentration used.[248] The interfacial tension reduction may be smaller than anticipated as a result of the two surfactants competing for adsorption at the oil-water interface when the nonionic surfactant is added. This may happen if the nonionic surfactant concentration is too high or if the nonionic surfactant has a longer hydrophobic tail than the zwitterionic surfactant which favours adsorption at the interface.[248] This effect does not hold here as the concentration of nonionic surfactant is low in ZN. The binary nonionic-zwitterionic mixture may lead to synergy in reducing the oil-water interfacial tension. Yan *et al.* observed that combining double-chain, single-head nonionic Guerbet alcohol ethoxylates with zwitterionic didodecylmethyl hydroxylpropyl sulfobetaine can further reduce the crude oil-brine interfacial tension due to the co-adsorption of surfactants. In this case, the solubilization of zwitterionic surfactant can be improved by adding nonionic surfactant and the surfactant molecules can be packed more effectively at the oil-water interface.[249] Here, using the binary nonionic-zwitterionic mixture (ZN) in DIW further reduces the interfacial tension between heptane and water compared to AHS, while the reduction is negligible for those of toluene, heptol and crude oil. The lowest and largest interfacial

tensions are achieved with slightly polar toluene (with high interfacial oil molecules) and non-polar heptane (with weak interfacial oil molecules), respectively with those of heptol and crude oil lying between them. The interfacial tension between crude oil and both surfactant solutions is greater than toluene probably as a result of the electrostatic repulsion between the headgroups of adsorbed aqueous and crude oil surfactants which prevents an effective mixed monolayer at the oil-water interface.[246]

The interfacial surfactant concentration and size affect the oil-water interfacial tension. For instance, betaine surfactants have been found to be unable to achieve ultra-low interfacial tension due to the flat position of their hydrophilic headgroup at the oil-water interface, which inhibits a compact monolayer. However, the interfacial tension can decrease more if crude oil is high in fatty acids due to the mixed monolayer that can be formed at the interface.[250] When the surfactants are in Permian brine, the interfacial tension between water and toluene, heptane and heptol does not change on raising the surfactant concentration > CMC while it gradually increases for crude oil which is due to the reduced interfacial surfactant with the solubilization of the organic phase on increasing surfactant concentration.[246] Using the binary nonionic-zwitterionic mixture (ZN) in Permian brine can further reduce the interfacial tension compared to AHS which is more pronounced for heptane and crude oil. The reduction in the crude oil-water interfacial tension on the addition of nonionic surfactant is more pronounced when the surfactant is in Permian brine which is linked to the presence of salts that screen the electrostatic repulsion between aqueous and crude oil surfactant headgroups and allows for a mixed monolayer consisting of aqueous zwitterionic and nonionic surfactants as well as the crude oil polar groups at the oil-water interface.[246] Because of this, when the surfactants are present in Permian brine, crude oil exhibits the lowest interfacial tension.

Figure 5.1. Effect of surfactant type and concentration in DIW (upper) or Permian brine (lower) on the interfacial tension between different oils and water at 25 ± 0.5 °C.
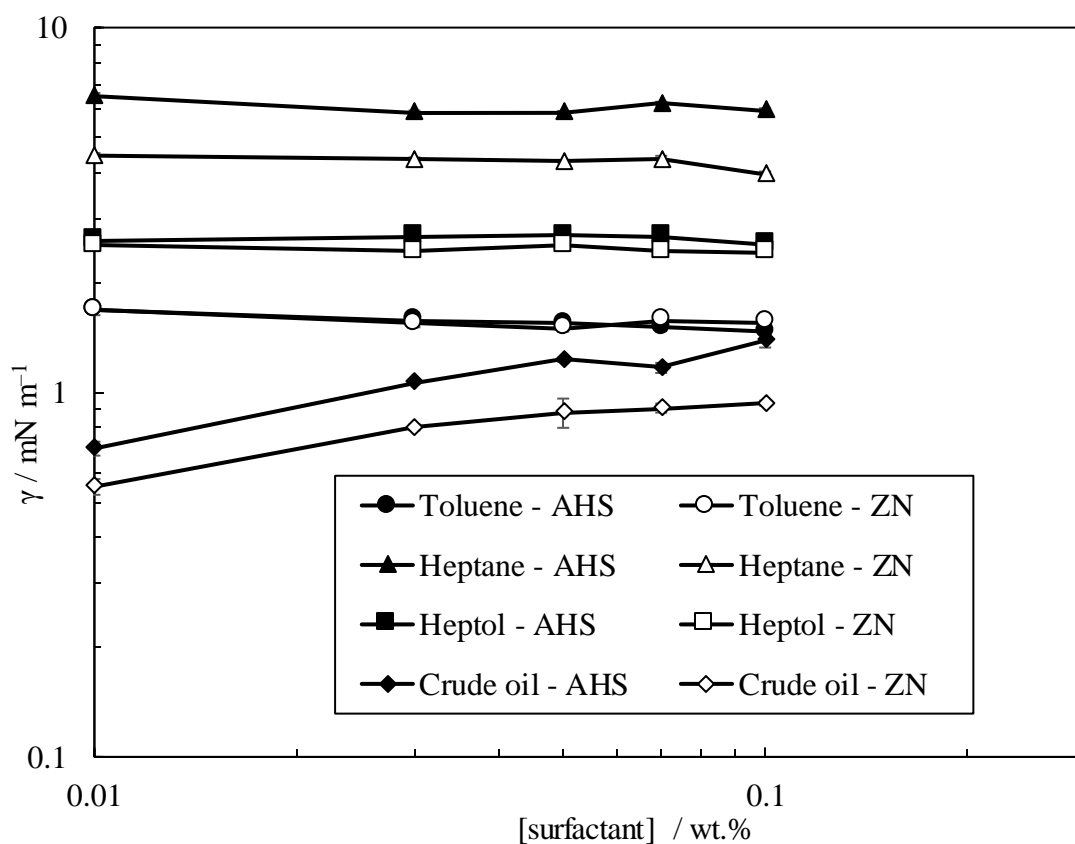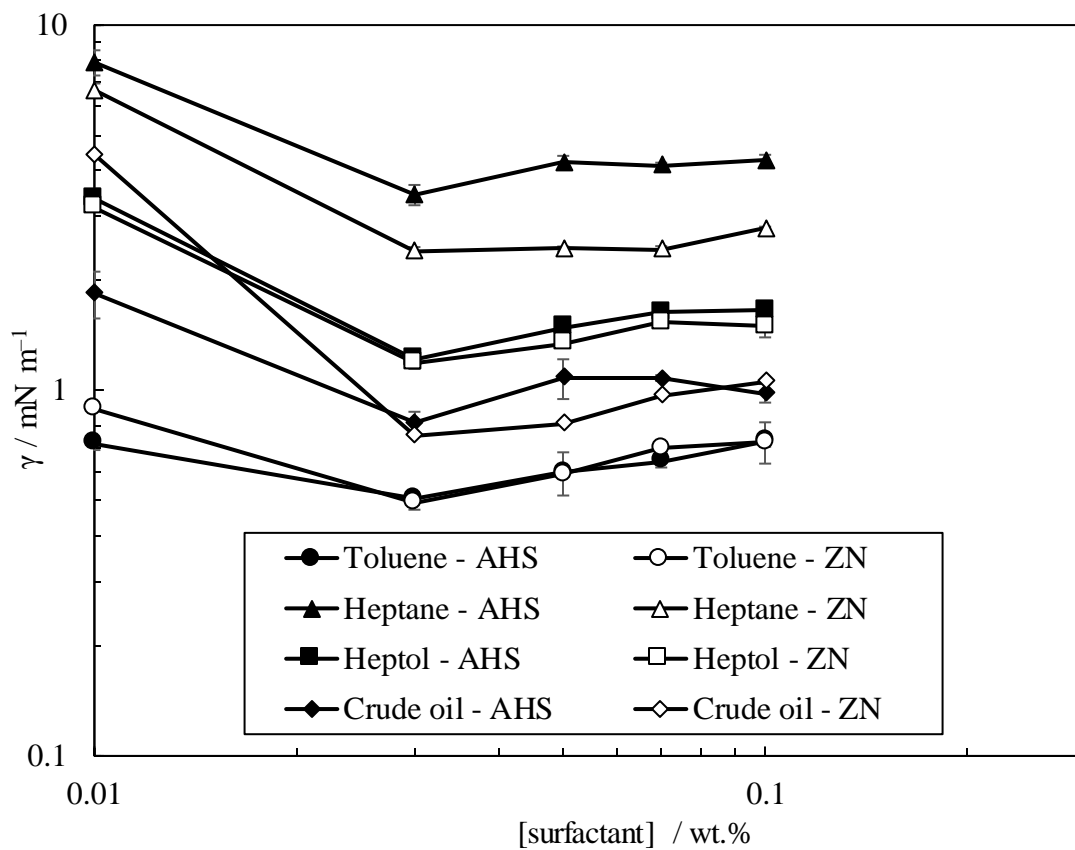
5.1.2 Effect of electrolyte

The solubility, stability and adsorption behaviour of zwitterionic surfactants can change in the presence of ions which can have an impact on how well they work in EOR. Permian brine is a mixture of various ions that may influence the surface activity of surfactants and in turn their effects on the interfacial tension between water and the organic phase. Depending on the concentration of salt, the presence of salt can have both salting-in and salting-out impacts on the micellization and adsorption behaviour of zwitterionic surfactants. At low salt concentrations (salting-in effect), the salt ions can shield the repulsive electrostatic interactions between the charged surfactant headgroups and lower the CMC. This may lead to a more effective micellization process and a reduction in the surface tension of the solution. The salting-out effect (at high [salt]) can reduce the solubility of the surfactant and increase the degree of counterion binding. As a result, the micellization process may be less effective and the surface tension of the solution may rise. The type of ions is also important. The presence of kosmotropic salts such as sodium sulphate can lead to a more pronounced salting-out effect while the presence of chaotropic salts such as sodium thiocyanate can lead to a more salting-in effect.[174] Ren claimed that the specific mechanism of the salt effect on micellization of the zwitterionic amino sulfonate surfactant is related to the competition between electrostatic interactions and counterion binding as well as the ion-specific effects of the salts on the water structure and solvation of the surfactant headgroups.[174]

An increase in oil-water interfacial tension is observed when adding Permian brine to both surfactant solutions (Figure 5.1). When salts are added to water, they dissociate and interact with water molecules through dipole-ion bonding. The surfactant headgroups will have dipole-dipole and hydrogen bonding with water molecules but their tails will have covalent bonding with the oil at the interface. The addition of low salt concentrations lowers the electrostatic repulsion between the surfactant molecules adsorbed at the oil-water interface which allows for a more compact surfactant monolayer and a further reduction in the interfacial tension. In this regard, divalent cations like Ca^{2+} are more efficient in reducing interfacial tension than monovalent ones like Na^+ since they are dissociated more.[251] However, the ions compete with the surfactant molecules for the available hydration sites at the oil-water interface as the salinity of the brine rises. At high salinity, the ions largely adsorb at the oil-water interface which leads to an increase in the interfacial tension due to interfacial surfactant depletion. Herein, cation-alkane interactions are potent non-covalent interactions at the oil-water interface.[252] The surfactant molecules may also aggregate in solution and form micelles as a result of the

high salt content which will decrease their availability for adsorption at the oil-water interface. As a result, zwitterionic surfactants become less effective at reducing the interfacial tension between oil and water in high salinity brine.[48] Similar increases in oil-water interfacial tension with the addition of high salinity brine have also been observed for other surfactants.[253] It is worth noting that the rise in the oil-water interfacial tension on the addition of Permian brine to surfactant solutions is more significant when using toluene here which is associated with its reduced polarity with increasing salinity which in turn lowers the interfacial oil molecules for interactions with adsorbed surfactants.[240, 241]

5.1.3 Effect of adding particles

5.1.3.1 AHS

Figures 5.2 to 5.5 show the effect of adding different concentrations of ES-coated silica particles to AHS solutions on the interfacial tension between different oils and water at 25 °C. When using the blend in DIW, interfacial tension reaches a minimum at 0.03 wt.% AHS and then increases with a further increase in the AHS concentration to 0.1 wt.% at all particle concentrations for all oils. When the blend is in Permian brine, increasing interfacial tension is observed when raising the surfactant concentration from 0.01 wt.% to 0.1 wt.% in all particle concentrations which is more pronounced when using heptane and crude oil. In this case, the minimum interfacial tension occurs at the lowest surfactant concentration (CMC = 0.01 wt.%). According to Zhong *et al.*, the synergy of the mixture of particles and surfactants at low surfactant concentrations is primarily caused by the free spaces between adsorbed surfactant molecules at the interface that can be used by particles but at high surfactant concentrations due to the high number of adsorbed surfactant molecules fewer particles can adsorb which results in the inefficiency of the mixture.[229] Here, the pH of the blend is high at low surfactant concentrations resulting in electrostatic repulsion of anionic surfactant by anionic particles towards the interface and more oil-water interfacial tension reduction. However, the pH decreases to the isoelectric region on increasing surfactant concentrations in the blend leading to interactions between particles and surfactant and less interfacial surfactant.

The plots also show that the addition of particles to AHS solutions slightly reduces the oil-water interfacial tension in some cases but there is no clear effect of increasing particle concentration in the blend. The same unclear behaviour was observed in air-water surface tension measurements before. It is thought that a mixed monolayer of particles, zwitterionic surfactant and ions accompanied by natural surfactants (in the case of crude

oil) is responsible for the interfacial tensions observed here. As observed in Chapter 3, the electrostatic grafting of the zwitterionic surfactant onto hydrophilic anionic ES-coated silica makes particles partially hydrophobic, implying a higher capability for adsorbing at the oil-water interface, as observed by previous researchers.[28, 254] For instance, Saien and Bahrami found that silica nanoparticles with oleic acid coating that have been further modified with SDS surfactant (< CMC) can lower the maximum excess concentration (Γ_{max}) at the hexane-water interface. Due to their greater surface area at the hexane-water interface, this reduction is more noticeable when using larger nanoparticles. A higher particle adsorption at the oil-water interface is caused by an increase in bulk particle-particle steric stabilisation caused by an increase in aqueous particle concentration. Additionally, they discovered that the addition of nanoparticles to the SDS solutions resulted in a greater negative standard Gibbs free energy, indicating improved spontaneity of particle adsorption at the interface.[78] Contrary to when they adsorb at the liquid-solid interface where they are bound to the solid surface, when nanoparticles adsorb at the oil-water interface, they are imprisoned at the interface perpendicular to the interface plane. However, this does not indicate that they are unable to migrate laterally. Nanoparticles can move and regain equilibrium by releasing internal or external strains thanks to this lateral mobility at the liquid-liquid interface.[19] The natural surfactants in crude oil move towards the oil-water interface when crude oil and water are in contact. The adsorbed nanoparticles at the oil-water interface can interact with natural surfactants to lower the oil-water interfacial tension or repel them to the bulk oil which could raise the interfacial tension.[255]

As explained earlier, high salt concentrations can disorganize the surfactant layer at the oil-water interface which leads to the inefficiency of the surfactant molecules in reducing the oil-water interfacial tension. However, nanoparticles can lessen this impact by serving as a large surface area adsorbent for salt ions which prevents the ions from depleting the interfacial surfactant. The hydrophobized particles themselves may potentially have an impact on the interfacial tension as well.[245]

Figure 5.2. Effect of adding ES-coated silica particles to AHS in DIW (upper) and Permian brine (lower) on the interfacial tension between toluene and water at 25 ± 0.5 °C.
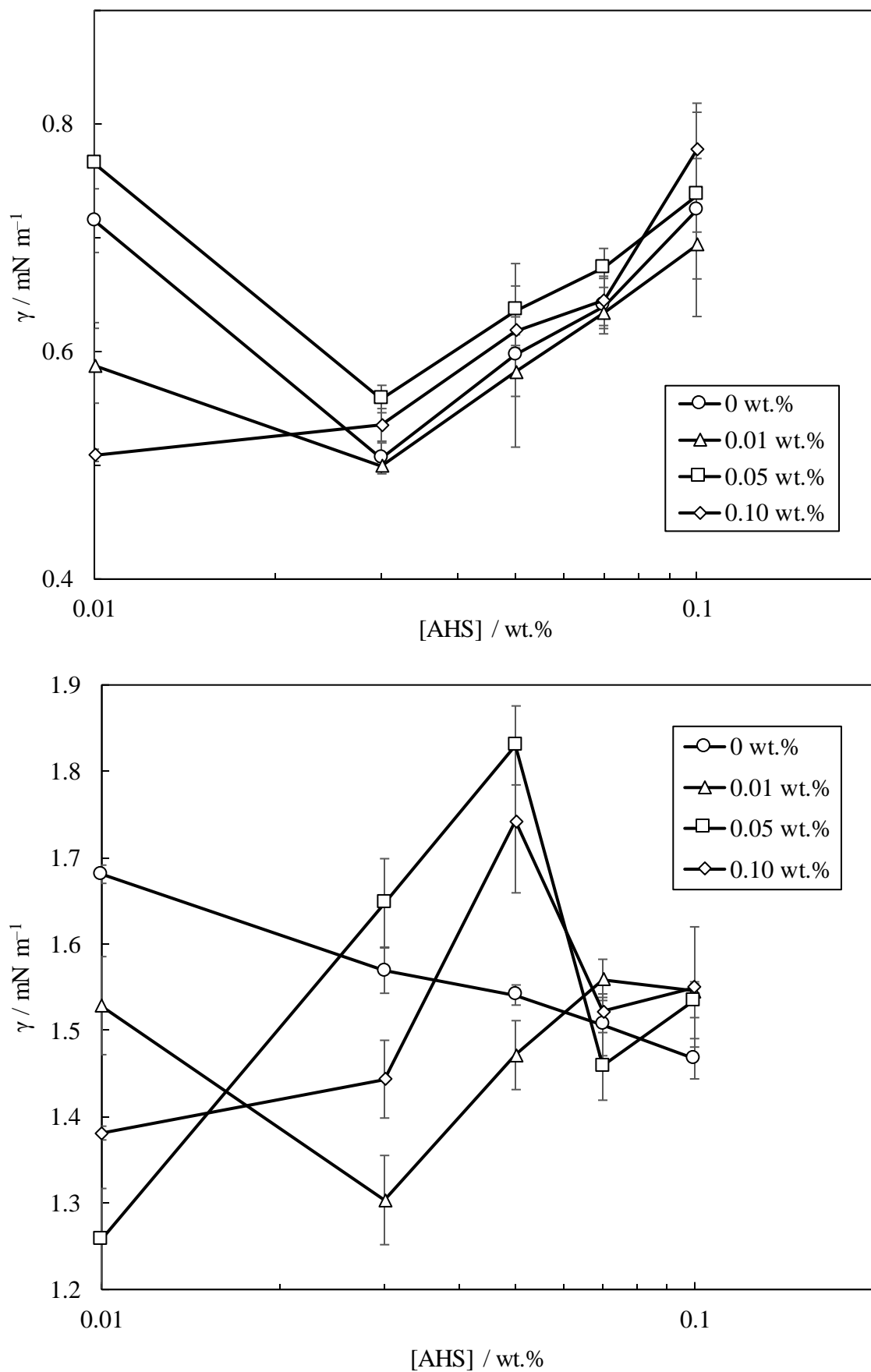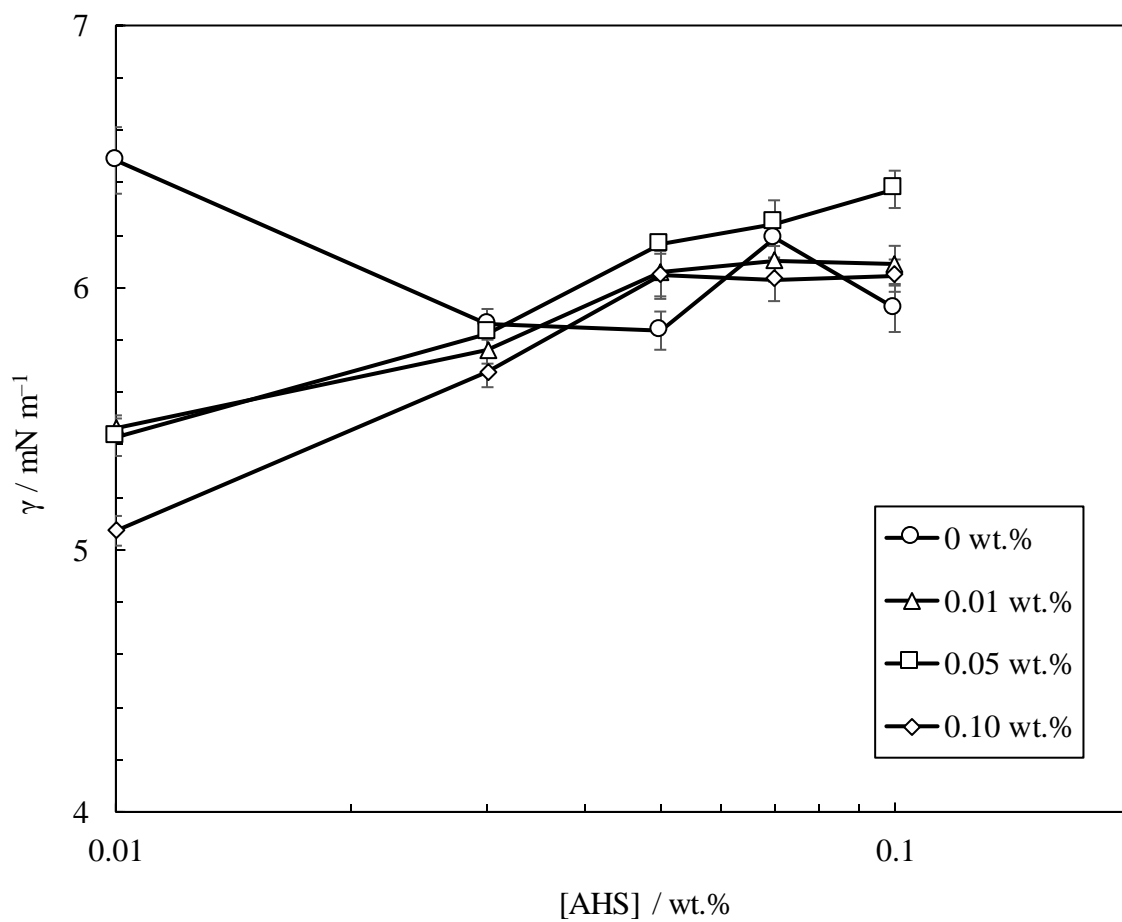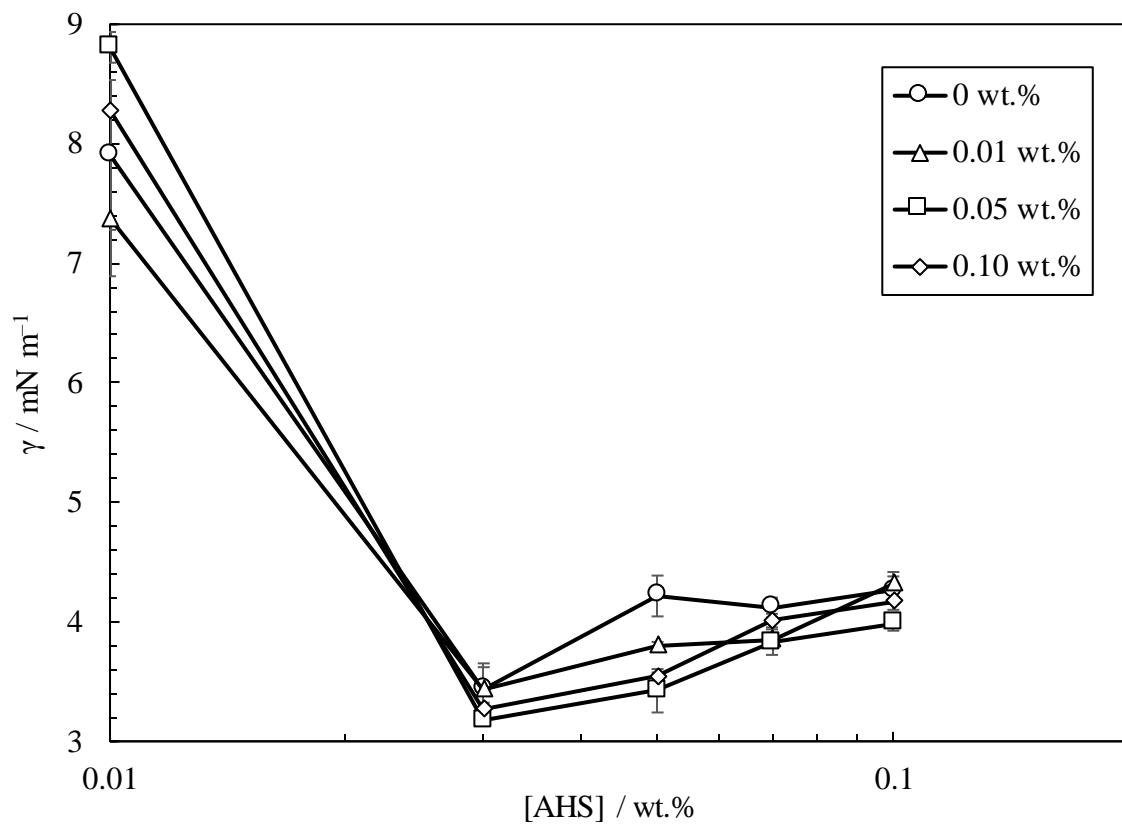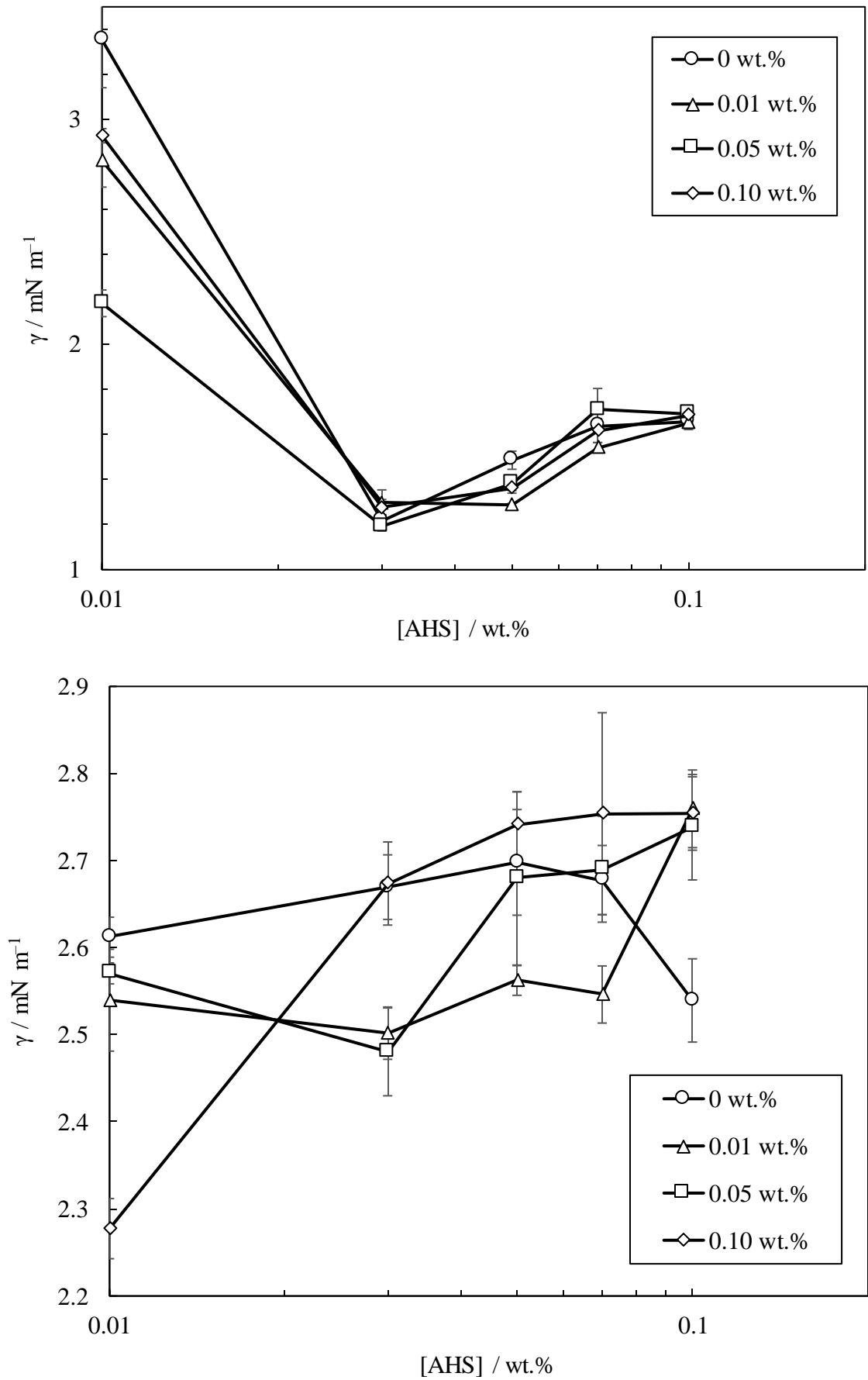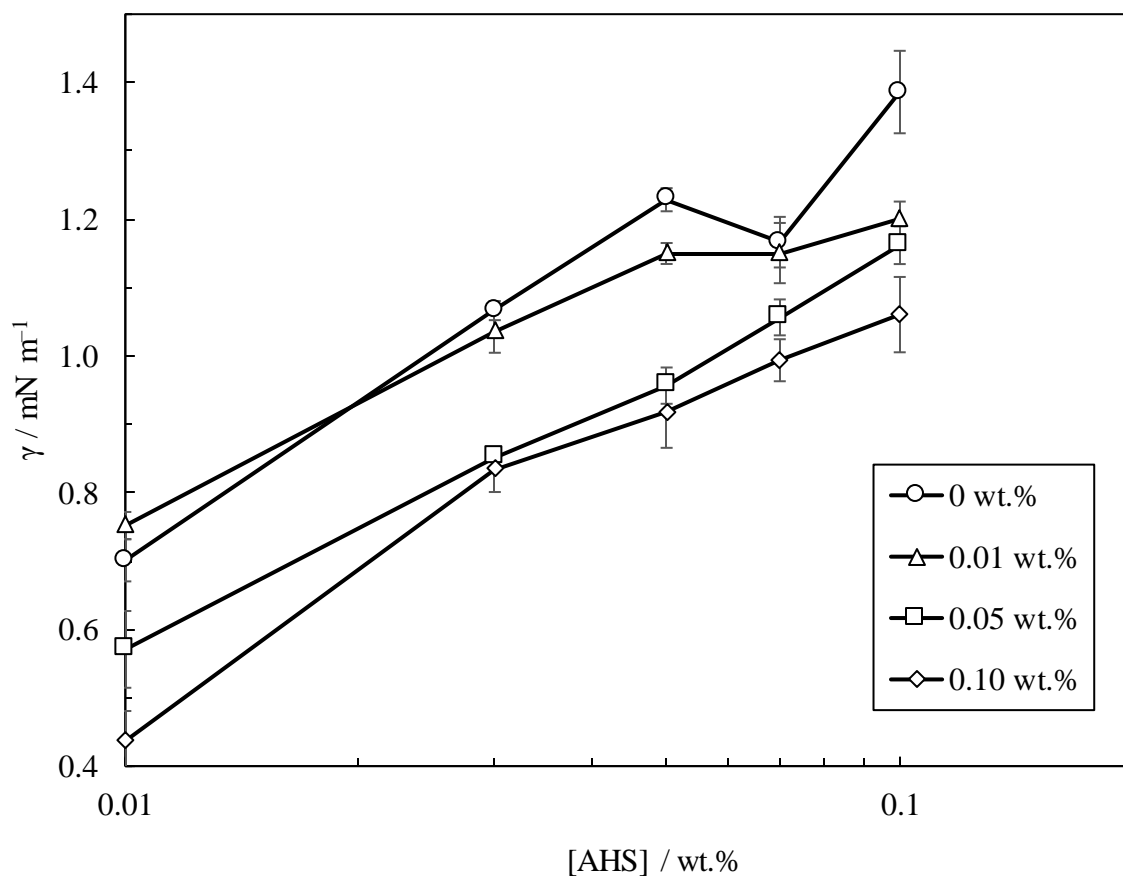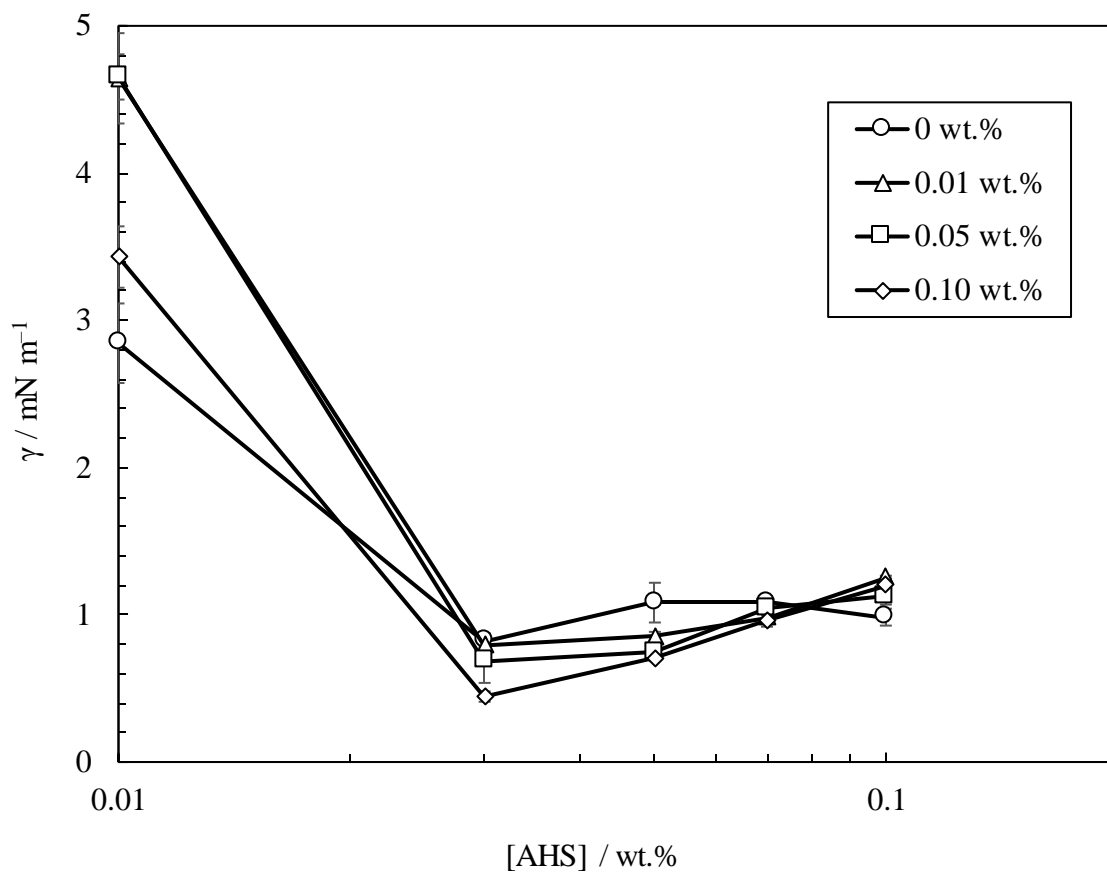
Figure 5.3. Effect of adding ES-coated silica particles to AHS in DIW (upper) and Permian brine (lower) on the interfacial tension between heptane and water at 25 ± 0.5 °C.

Figure 5.4. Effect of adding ES-coated silica particles to AHS in DIW (upper) and Permian brine (lower) on the interfacial tension between heptol (1:1 g g^{-1}) and water at 25 ± 0.5 °C.

215

Figure 5.5. Effect of adding ES-coated silica particles to AHS in DIW (upper) and Permian brine (lower) on the interfacial tension between crude oil and water at 25 ± 0.5 °C.

216

5.1.3.2 ZN

217

Figures 5.6 to 5.9 show the effect of adding ES-coated silica particles to ZN solutions on the interfacial tension between different oils and water at 25 °C. All blends of ZN and particles in DIW exhibit the same minimum interfacial tension at 0.03 wt.% surfactant and increasing interfacial tension at higher surfactant concentrations for all oils, as was the case with AHS. A minimum is observed in the plot of interfacial tension related to toluene and 0.05 wt.% ZN in Permian brine at all particle loadings while almost a plateau is observed in those of heptane and heptol. Like AHS, the interfacial tension between crude oil and Permian brine increases with an increase in ZN concentrations in the blend at all particle loadings. Increasing particle concentration in the blend in DIW has systematically reduced the crude oil-water interfacial tension while no clear effect of particle concentration is observed in the plots of other oils. Mostly, 0.05 wt.% particles are more efficient in giving the minimum interfacial tension between pure oils and water for the blends in both DIW and Permian brine while it is 0.1 wt.% for crude oil and the blend in DIW. For the blend in Permian brine, the minimum is mostly observed with the blend of 0.01 wt.% particles. The same mechanisms explained before for AHS are thought to apply to ZN. The nonionic surfactant in ZN can also form hydrogen bonds with particles but the interactions are weaker than the electrostatic attractions between charged surfactants and particles. The nonionic surfactant can also contribute to the mixed monolayer at the oil-water interface.[249]

Figure 5.6. Effect of adding ES-coated silica particles to ZN in DIW (upper) and Permian brine (lower) on the interfacial tension between toluene and water at 25 ± 0.5 °C.
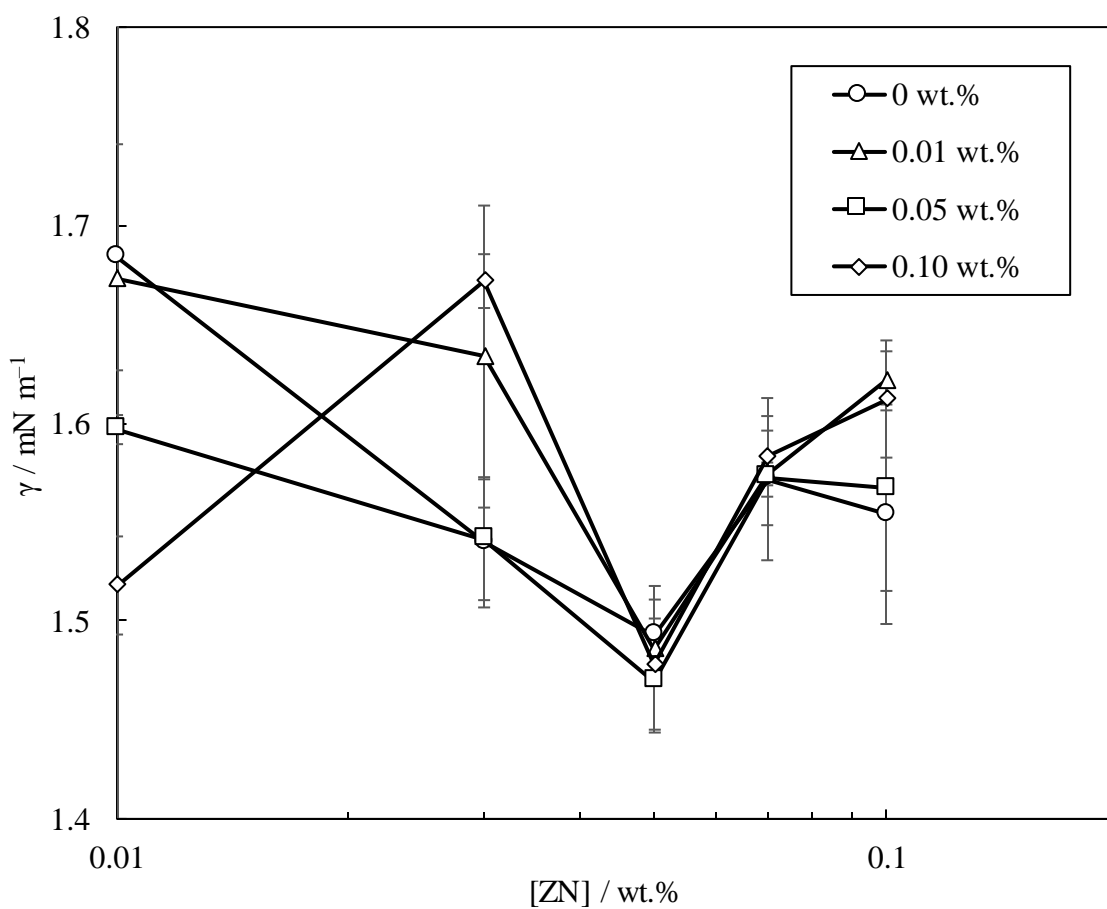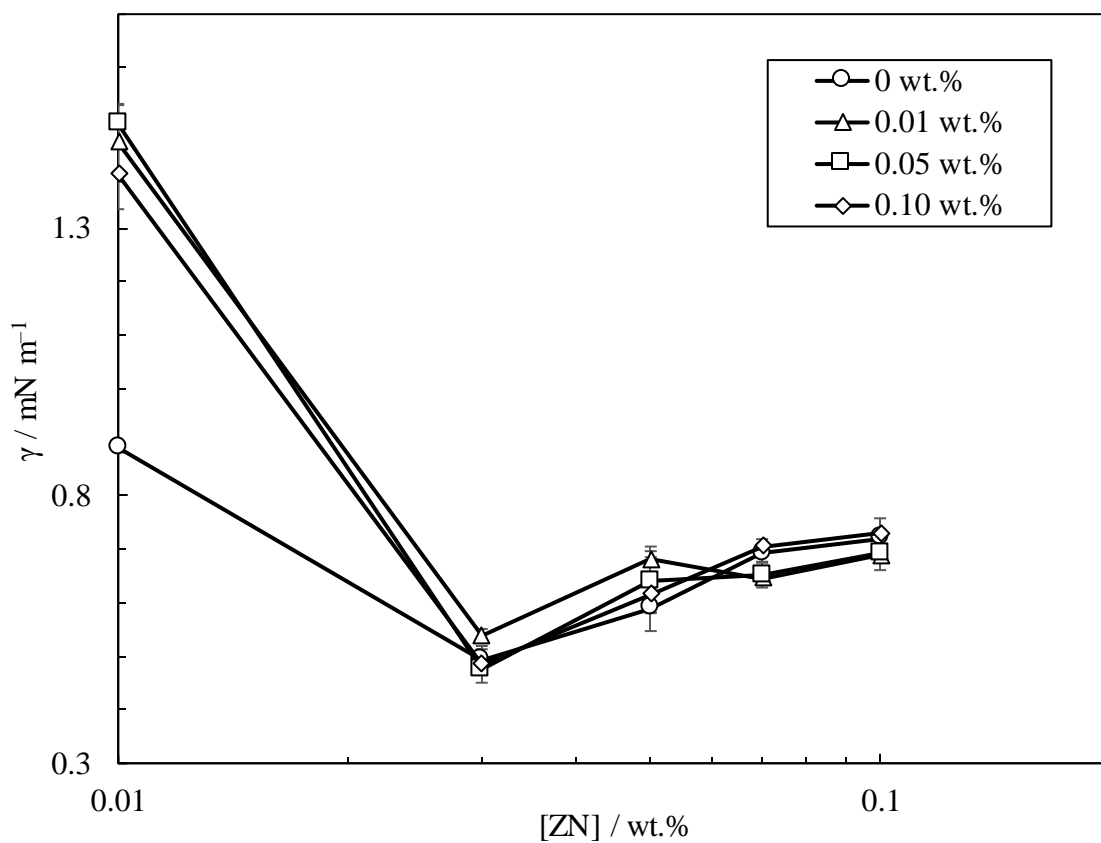
Figure 5.7. Effect of adding ES-coated silica particles to ZN in DIW (upper) and Permian brine (lower) on the interfacial tension between heptane and water at 25 ± 0.5 °C.
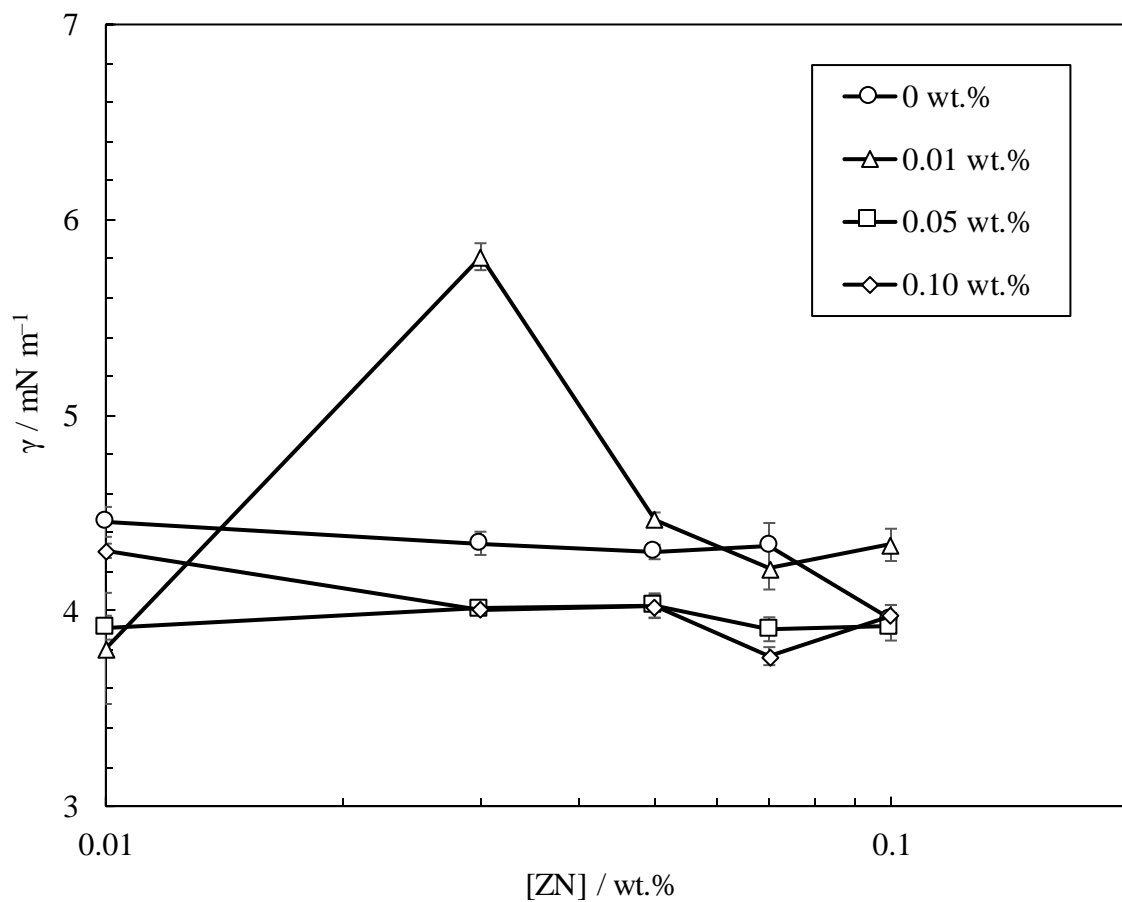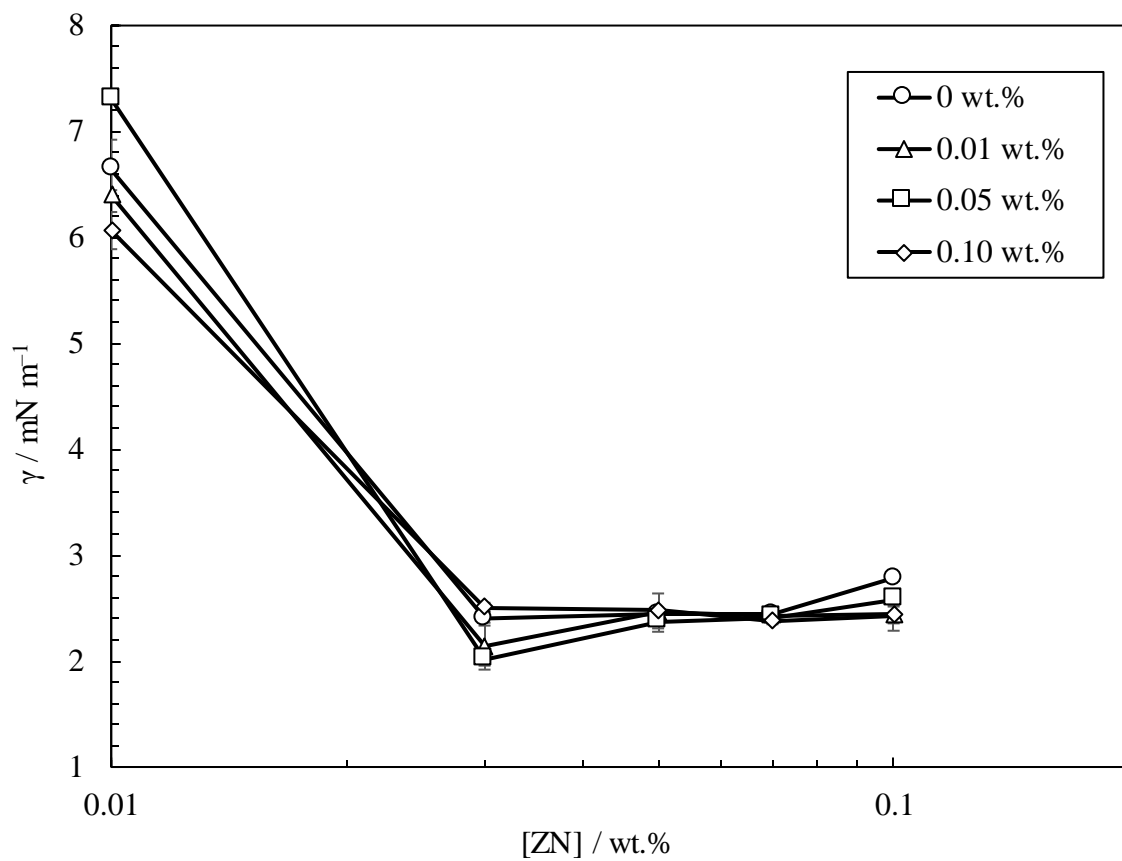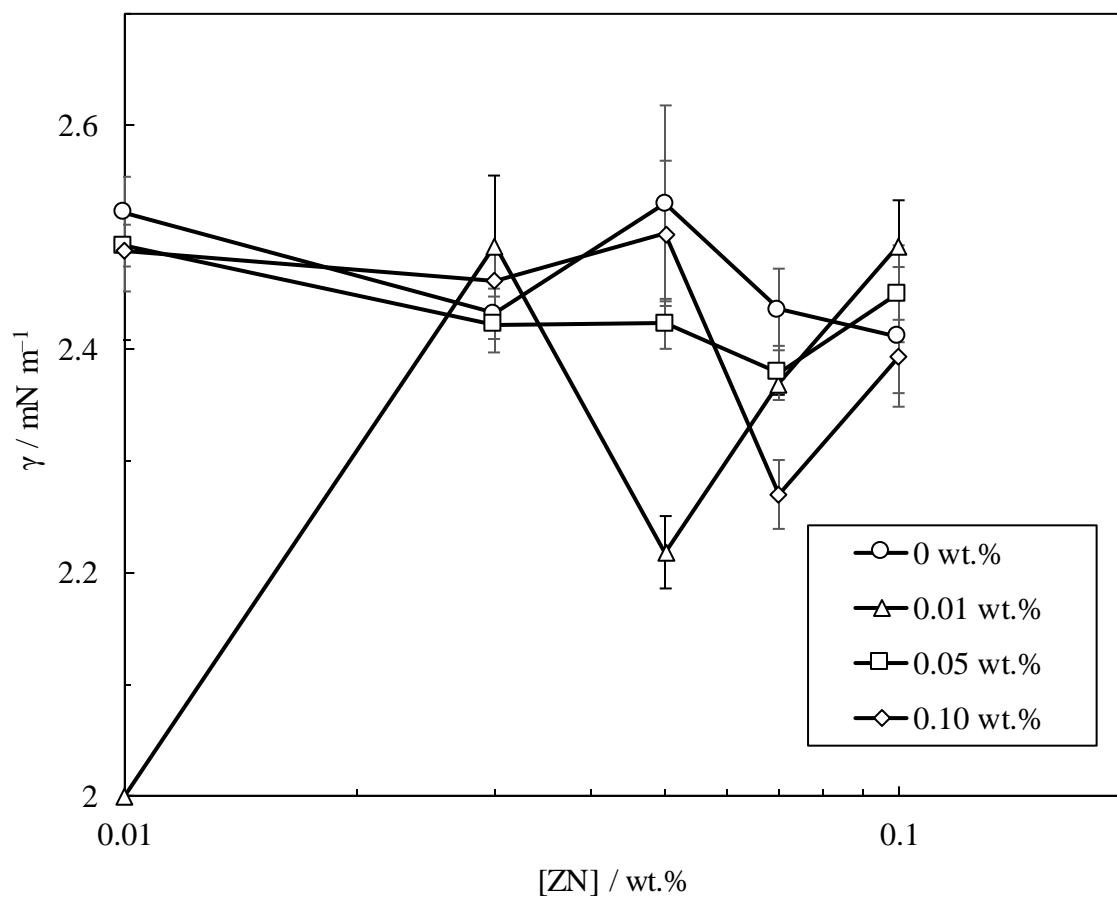
Figure 5.8. Effect of adding ES-coated silica particles to ZN in DIW (upper) and Permian brine (lower) on the interfacial tension between heptol (1:1 g g^{-1}) and water at 25 ± 0.5 °C.
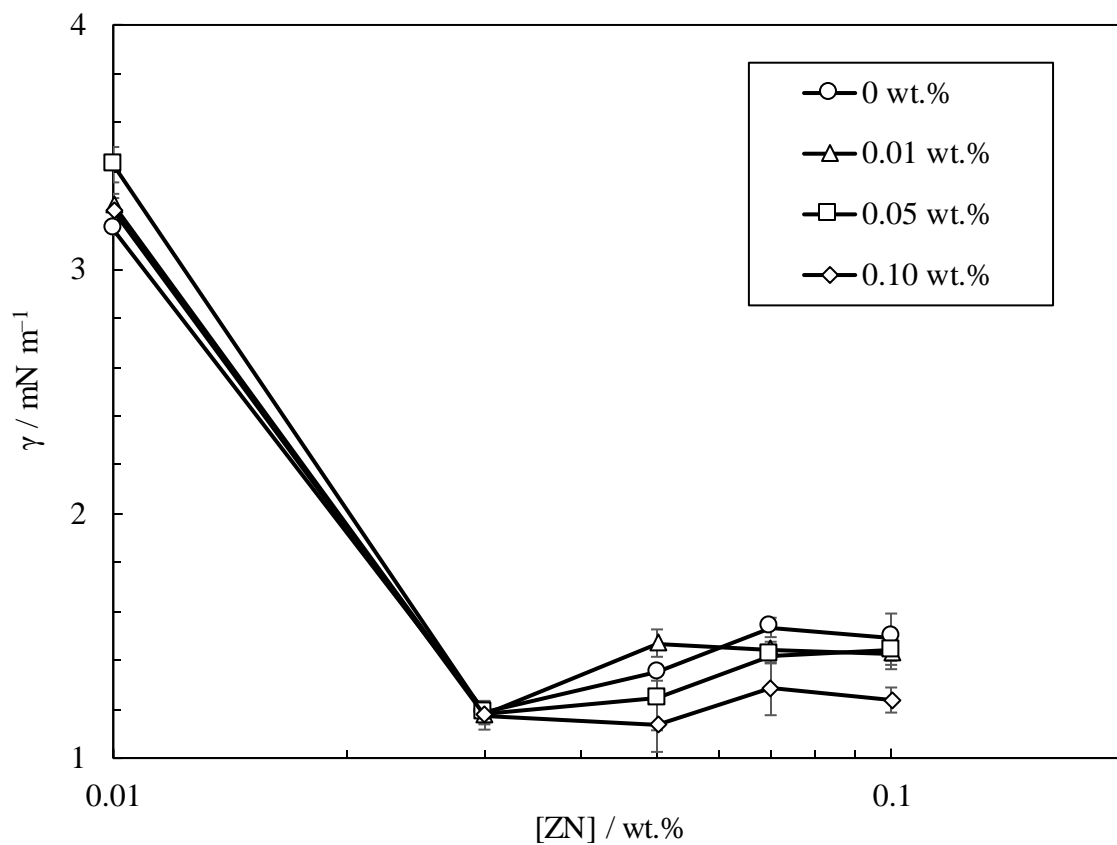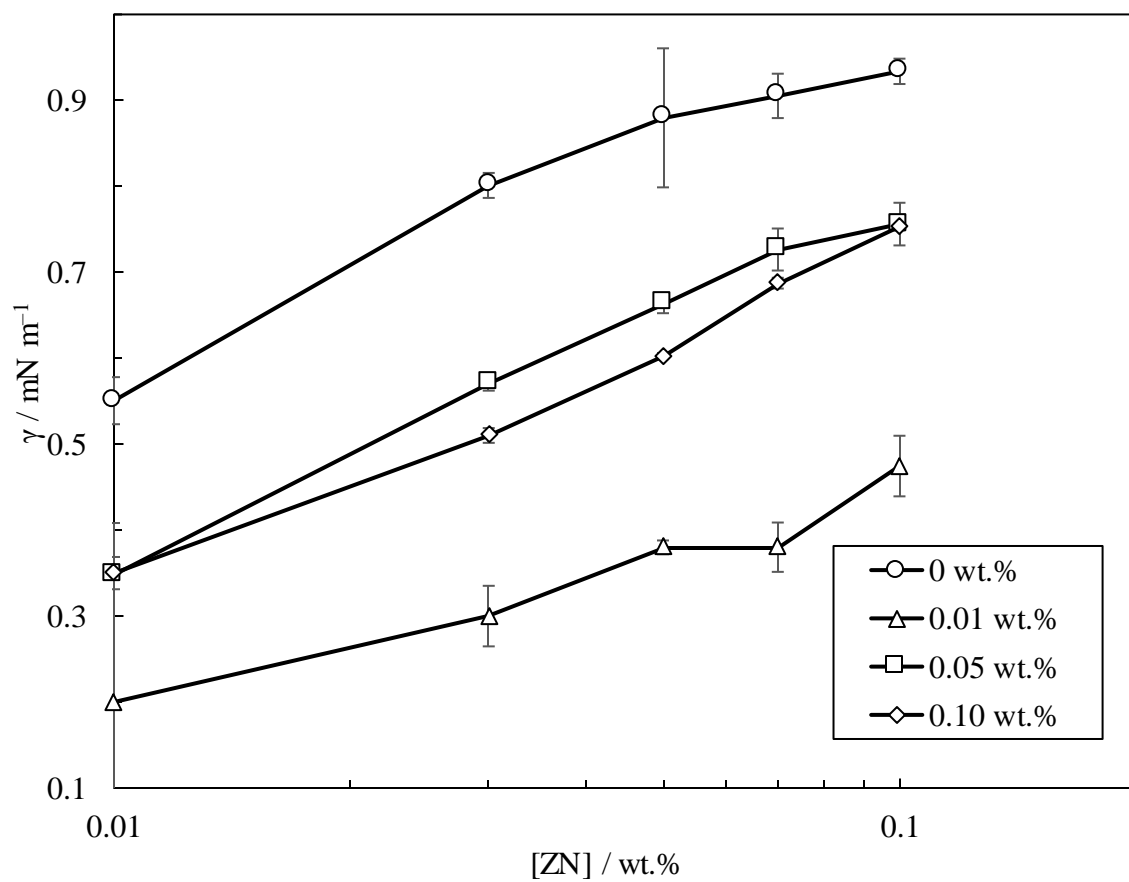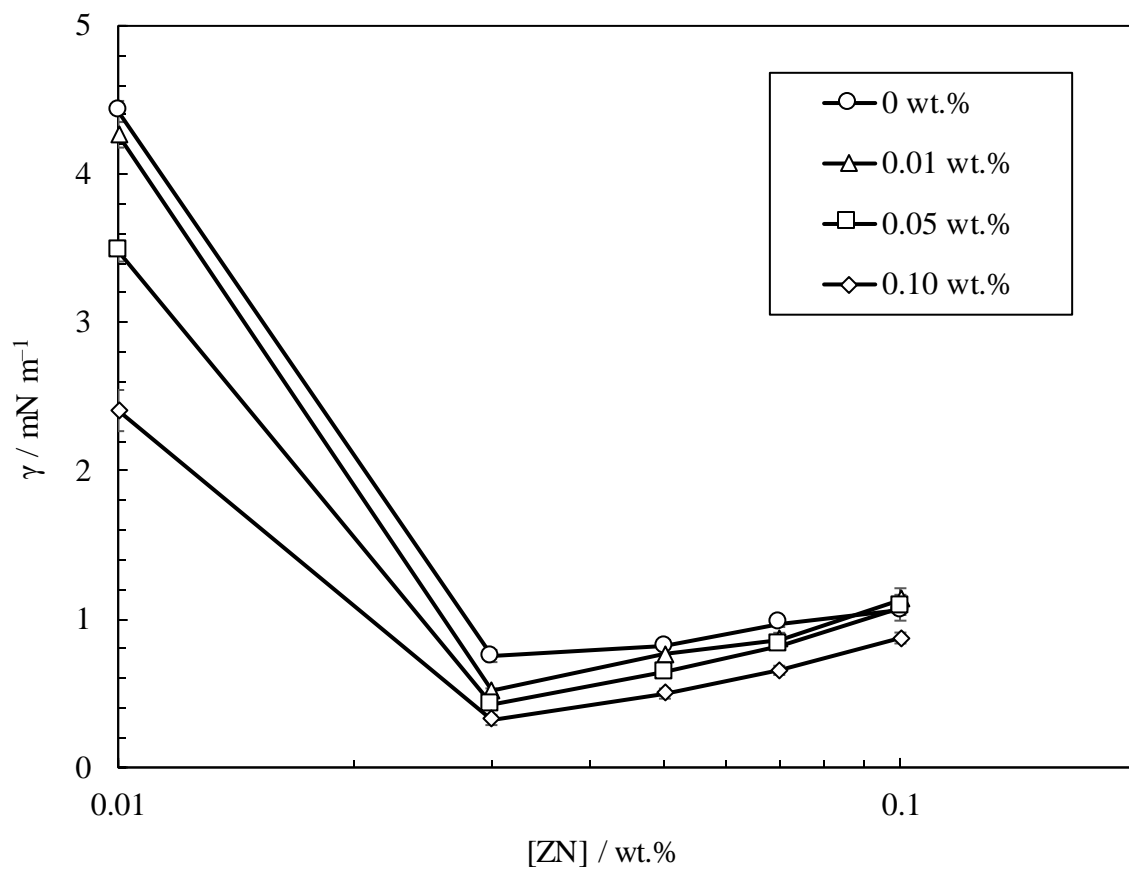
Figure 5.9. Effect of adding ES-coated silica particles to ZN in DIW (upper) and Permian brine (lower) on the interfacial tension between crude oil and water at 25 ± 0.5 °C.

5.1.4 Effect of oil type

Polar toluene and crude oil have the lowest interfacial tension regardless of the surfactant type in DIW due to their high contribution to the monolayer at the oil-water interface. Non-polar heptane has the largest interfacial tensions at all surfactant concentrations (0.01 – 0.1 wt.%) and particle concentrations (0 – 0.1 wt.%) while those of heptol (1:1 g g^{-1}) range between these minimum and maximum values. For the same reasons, when using the surfactants in Permian brine, crude oil followed by toluene has the lowest interfacial tension at all surfactant and particle concentrations but those of heptane continue to have the highest interfacial tension.

5.1.5 Effect of temperature

As EOR chemicals are usually used in brine in the applications, the effect of temperature on the interfacial tension between crude oil and water for different blends of AHS or ZN and particles in Permian brine has been investigated (Figures 5.10 and 5.11). Figure 5.10 shows that increasing the temperature from 25 °C to 60 °C lowers the interfacial tension at low AHS concentrations both in the presence and absence of particles but the interfacial tension at 60 °C exceeds that of low temperature at high AHS concentrations. A significantly higher interfacial tension is achieved upon increasing the temperature at all ZN concentrations with and without particles in Permian brine (Figure 5.11). A larger slope is observed in the plots of interfacial tension *versus* surfactant concentration upon increasing the temperature which is more pronounced for ZN.

Generally, the oil-water interfacial tension decreases with an increase in temperature.[256] However, the relationship depends on the oil composition, salinity and presence of surface-active agents.[52] When temperature or salinity increases, zwitterionic surfactants are not usually affected and no turbidity is seen.[257] However, their surface activity changes when both change. Some researchers state that zwitterionic surfactants typically perform better as temperature rise because of their increased solubility and diffusion coefficient which can result in both lower interfacial tensions and shorter times to achieve a minimum interfacial tension.[258, 259] Some authors have reported increased oil-water interfacial tension on increasing temperature when using crude oil and brine. The hydration of the surfactant headgroups can be destroyed by high concentrations of Ca^{2+} or Na^+ acting as counterions. This causes the surfactant to shift from the oil-water interface to the oil phase, progressively increasing the interfacial tension. This effect is more pronounced at high temperatures.[260] Temperature elevation also weakens the solvation of surfactant molecules at the oil-water interface which consequently increases

the interfacial tension.[261] An inverse relationship between decane-water interfacial tension and temperature has also been observed for nonionic surfactants due to the reduced solubility of ethylene oxides of the surfactant in water at high temperatures.[49, 262, 263] Therefore, the larger slope observed in the plot of interfacial tension with ZN concentration may be related to the additional rise in interfacial tension caused by the nonionic surfactant present in ZN.

In addition to the effects of temperature on surfactants, the type of particles and their interactions with the surfactant or oil-water interface are important when a mixture of particles and surfactant is used. The particles may have a smaller effective surface area and be less effective at reducing interfacial tension if aggregated due to temperature rise. This latter effect is absent here as the particles were found to be long-term stable in Permian brine at higher temperatures (75 °C). Increasing temperature has been shown to enhance particle adsorption and desorption, which in turn rejects the adsorbed natural surfactants of crude oil to the bulk oil and increases the oil-water interfacial tension.[255]

Figure 5.10. Effect of temperature on the interfacial tension between crude oil and water for different concentrations of AHS alone (upper) or AHS in a blend with 0.01 wt.% ES-coated silica (lower) in Permian brine.
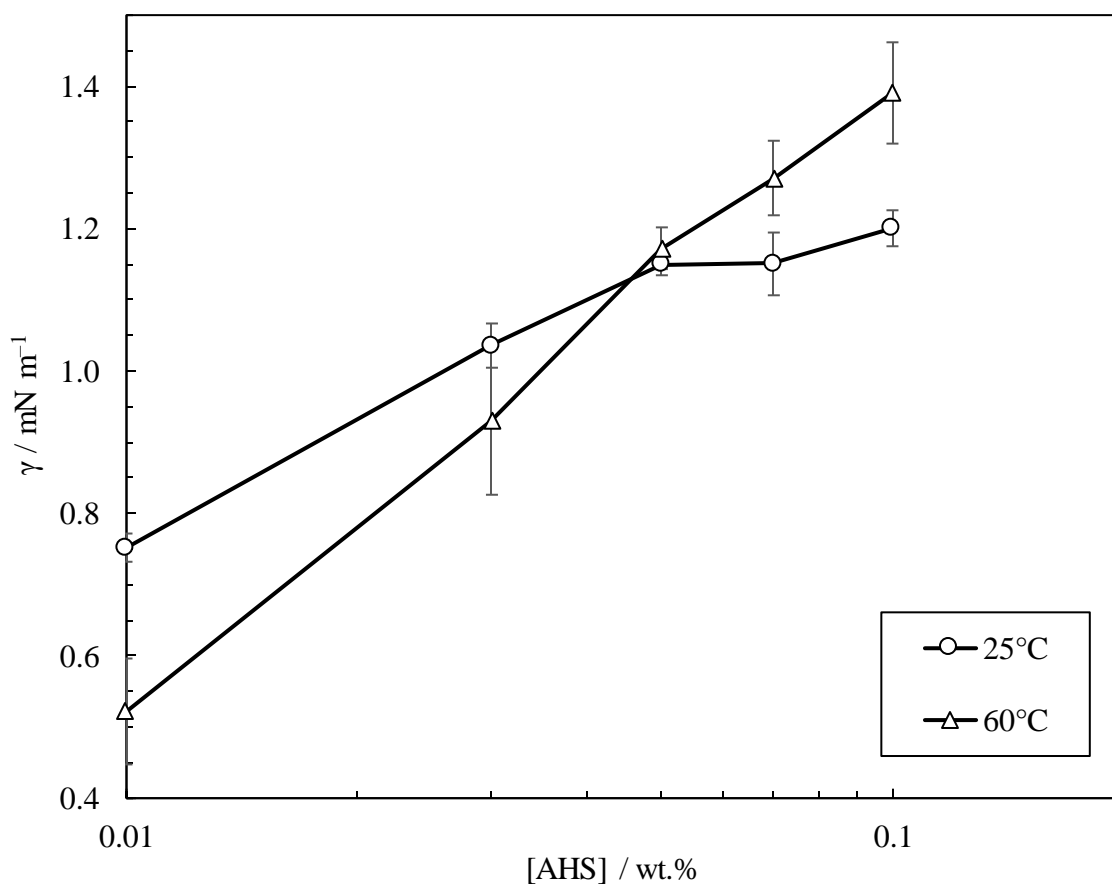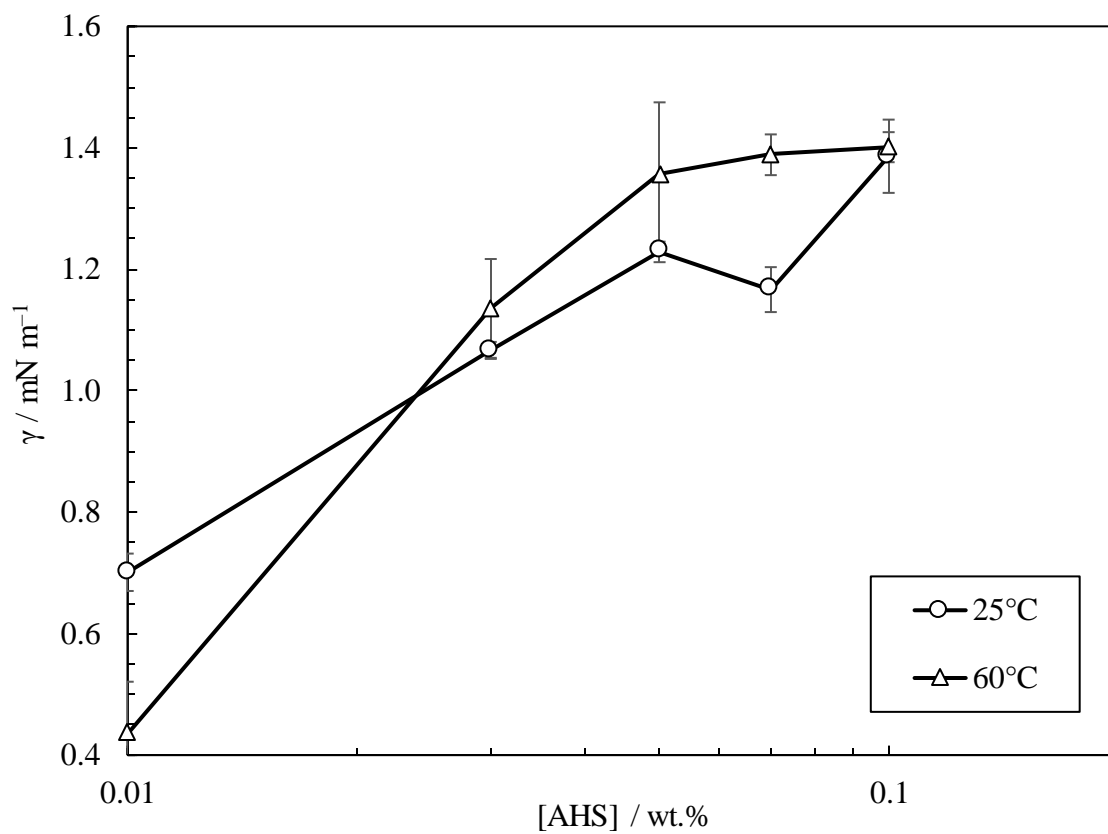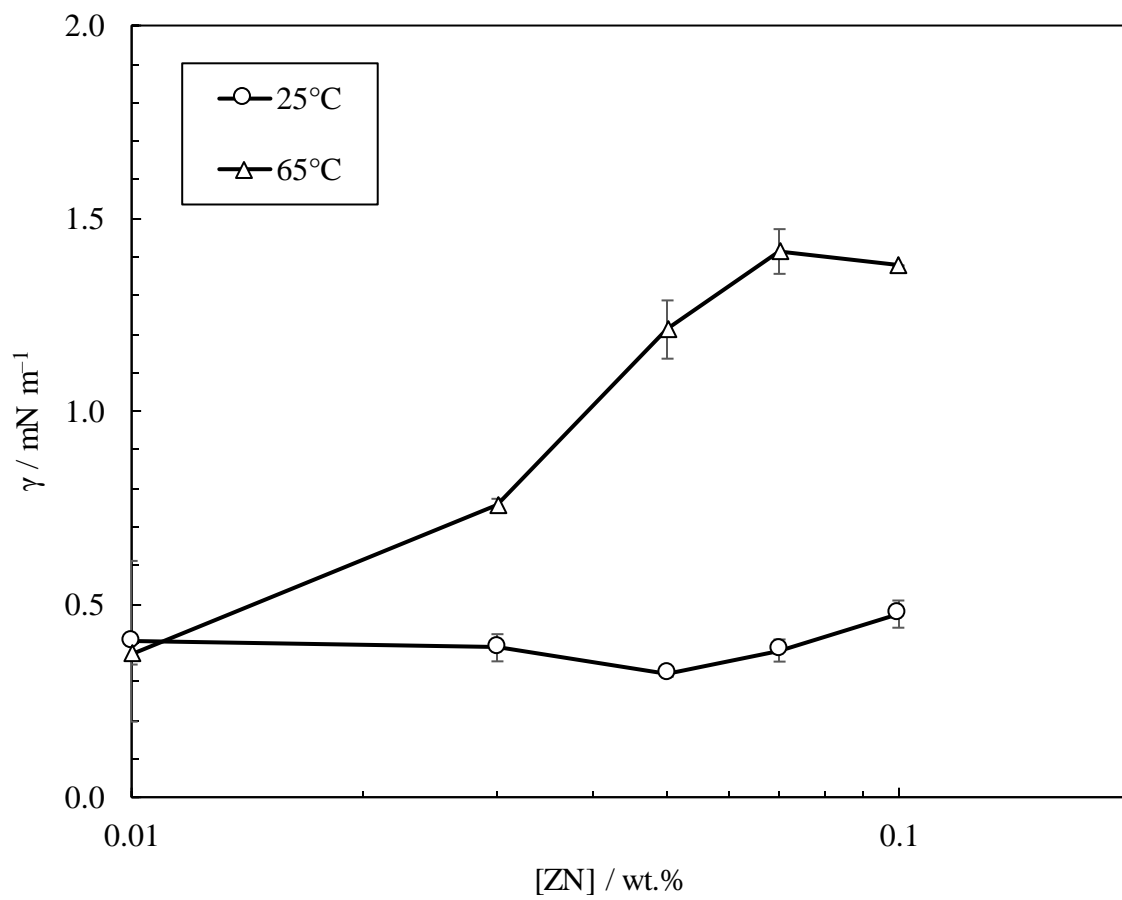
Figure 5.11. Effect of temperature on the interfacial tension between crude oil and water for different concentrations of ZN surfactant alone (upper) or ZN in a blend with 0.01 wt.% ES-coated silica (lower) in Permian brine.
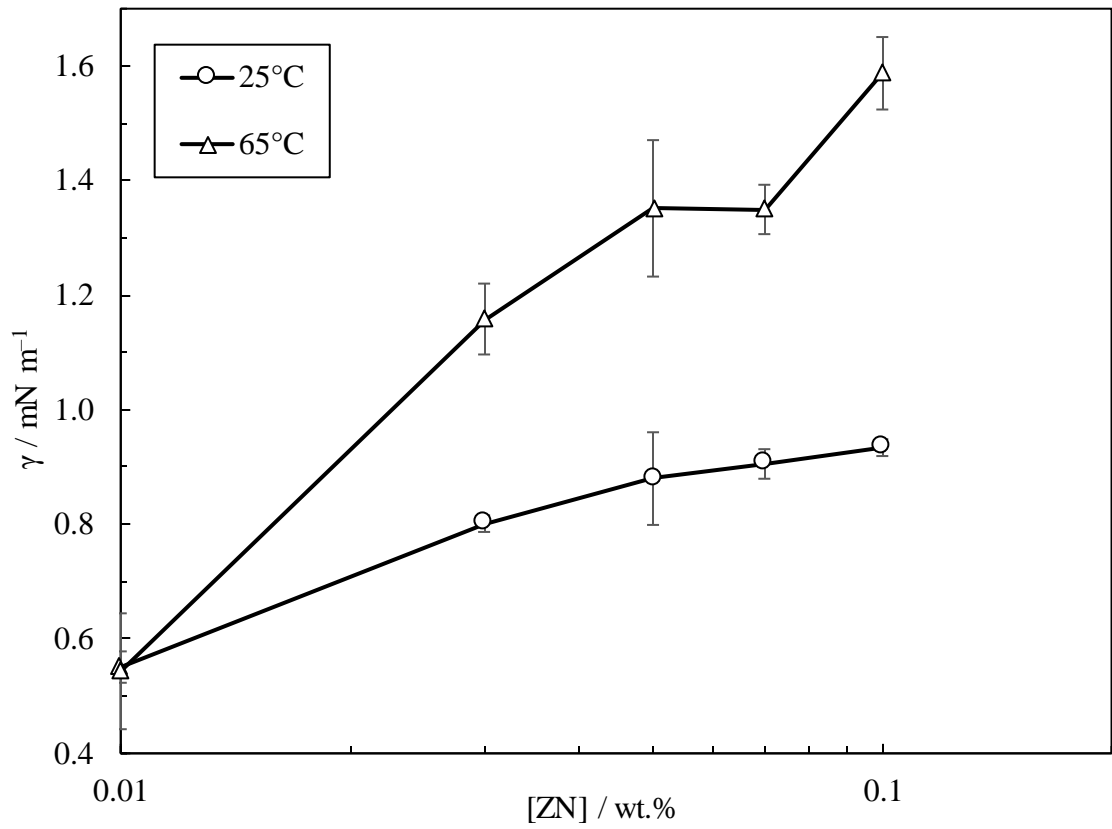
225

5.2 Emulsions of crude oil and water

There are a number of challenges in emulsion research with crude oil as opposed to pure oils like toluene and heptane. The behaviour of emulsions made with crude oil can vary depending on the oil composition (polar group content like petroleum acids), processing methods and the presence of impurities (water and fines like rock particles). Therefore, it can be challenging to replicate the results when using crude oil for emulsification without prior knowledge about the adsorption behaviour of chemicals. Although some of the emulsion experiments in this work were initially carried out with crude oil, pure oils were primarily employed to lessen the uncertainty in the outcomes for the above reasons.

5.2.1 DIW and Permian brine

Figure 5.12 shows the appearance and the fractions of oil and water resolved from the oil-in-water emulsions from crude oil and DIW or Permian brine with time. The emulsion of crude oil and DIW faced significant coalescence and creaming in an hour while that of Permian brine was more stable to coalescence and creaming in a month.

The emulsification of crude oil and water can be significantly impacted by the presence of inorganic ions like sodium, potassium, calcium and magnesium in Permian brine. Previous studies show that an increase in salinity can improve the emulsification of oil in brine due to the enhancement of interfacial oil-water viscoelasticity. However, there exists an optimum salinity above which no additional improvement in emulsification is observed. In oilfields, the potential reason is the adsorption of fines (clay or calcium carbonate particles from rock during crude oil flow in porous rock) together with charged oil groups at the oil-water interface which forms Pickering emulsions.[264, 265] The Hofmeister series, as presented in Chapter 3, is believed to hold here regarding the effects of cations on the emulsification of crude oil and water: $Mg^{2+} > Ca^{2+} > Na^+ > K^+$. Sulfate and hydrogen phosphate are the most effective anions in emulsification [265] which are absent in the Permian brine used in this study. The formation of oil-in-brine emulsions is also a function of the crude oil composition. For instance, stearic acid can quickly produce emulsions even when the crude oil is in contact with DIW but heptanoic acid role is noticeable when certain ions exist in the brine.[266] As Permian brine is high in NaCl, it is thought that it is mostly sodium ions providing a more compact monolayer of crude oil polar at the oil-water interface to stabilise the emulsions here. The microscope photos of these emulsions are presented in Figure 5.13.

Figure 5.12. Appearance and fractions of oil (f_o) and water (f_w) resolved from oil-in-water emulsions formed from 5 g crude oil and 5 g DIW or Permian brine.
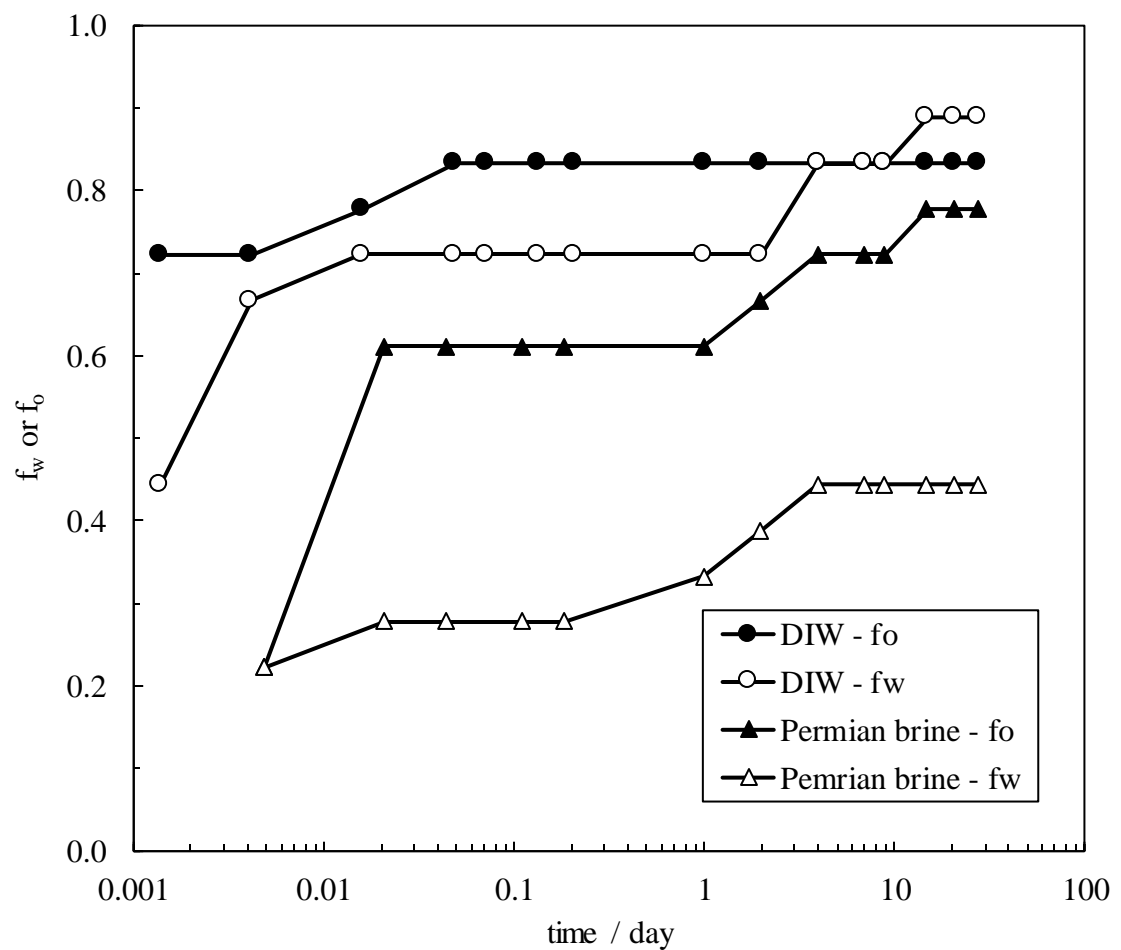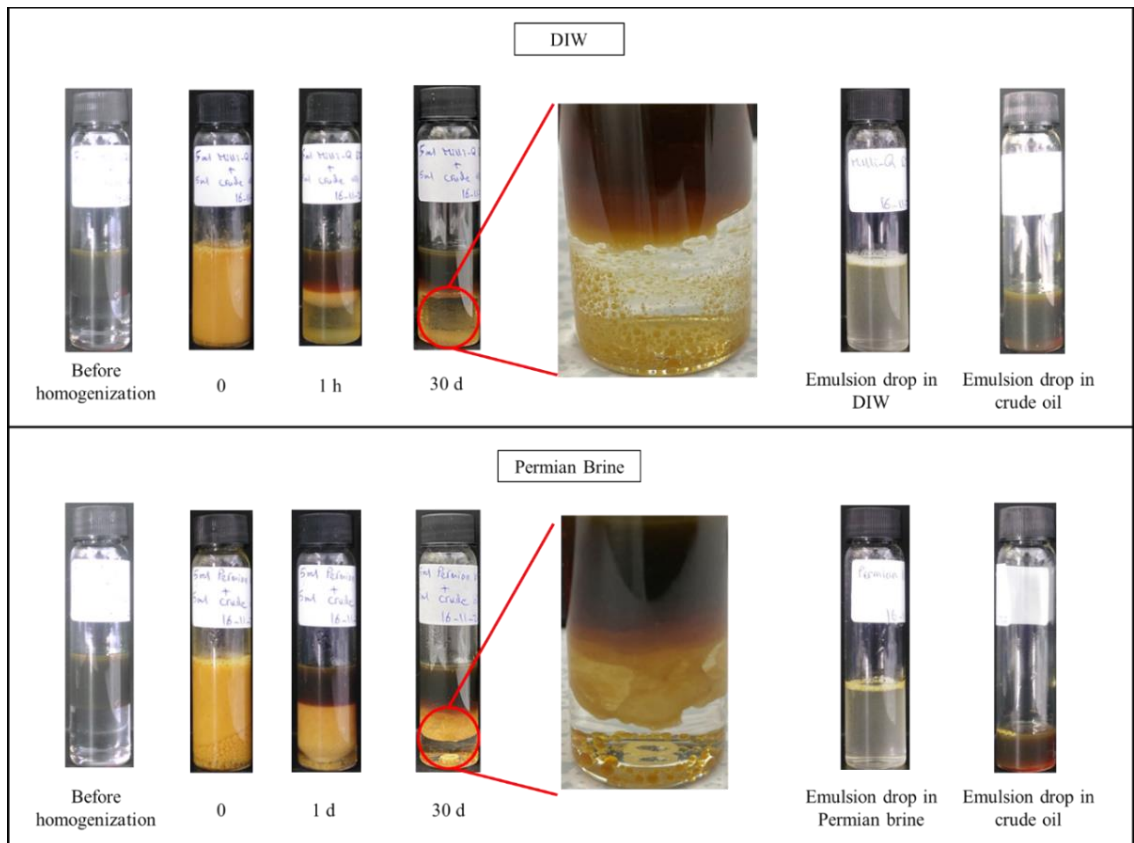
Figure 5.13. Initial microscope images and drop diameters of oil-in-water emulsions made from 5 g crude oil and 5 g of different solutions and dispersions.
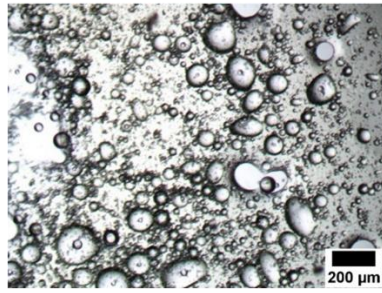
DIW
84 ± 11 μm
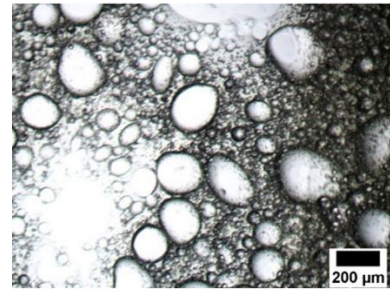
Permian brine
87 ± 13 μm
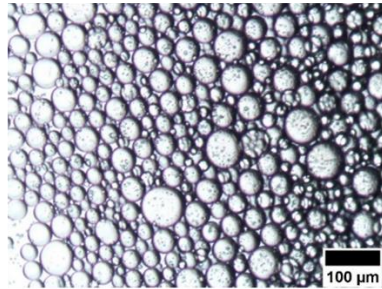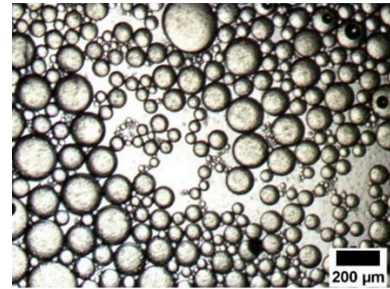
0.1 wt.% ZN in DIW
27 ± 5 μm

0.1 wt.% ZN in Permian brine
85 ± 14 μm
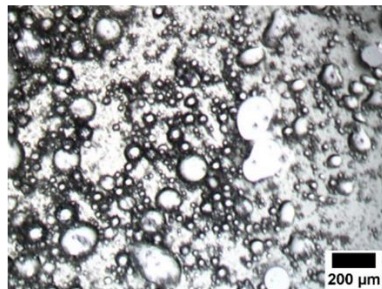
0.05 wt.% silica in DIW
97 ± 15 μm
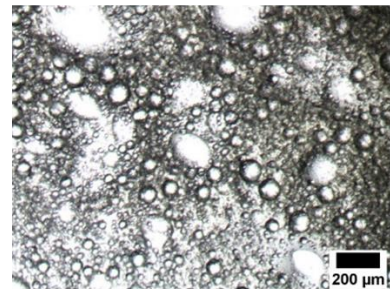
0.05 wt.% silica in Permian brine
51 ± 10 μm
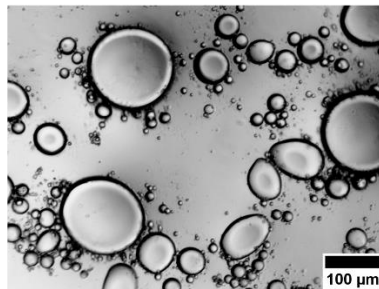
0.01 wt.% ES-coated silica in DIW
110 ± 15 μm

5.2.2 ZN

Both emulsions made with crude oil and 0.1 wt.% ZN in DIW and Permian brine showed coalescence and creaming after an hour which increased after 3 weeks (Figure 5.14).

229

Coalescence and creaming were higher with the addition of Permian brine to ZN solutions. Compared to the emulsions of crude oil and DIW or Permian brine alone, the addition of ZN created more spherical drops. The drop diameter of the emulsion made with ZN in DIW was smaller than that of no surfactant emulsions however those of Permian brine and ZN in Permian brine were the same. The microscope images of these emulsions are shown in Figure 5.13. Initially, the rapid diffusion of aqueous surfactant molecules (zwitterionic and nonionic surfactants of ZN) and crude oil surfactants (polar groups like petroleum acids) to the neat oil-water interface creates a mixed interfacial surfactant monolayer which is followed by a time-dependent movement of adsorbed crude oil surfactants to the aqueous phase to produce mixed micelles with ZN surfactant. This is evidenced by the brownish colour of the resolved water. The latter may also pose a rise in oil-water interfacial tension.[246] When ZN is in Permian brine, the electrostatic interactions between aqueous and crude oil surfactants are reduced, resulting in a lower number of interfacial surfactant molecules and quicker phase separation. This is accompanied by the demulsification power of ZN which was discussed in detail later.

5.2.3   Bare and ES-coated silica particles

When hydrophilic bare silica is used in DIW, the electrostatic attraction between anionic particles and the cationic polar group of the crude oil makes the particles partially hydrophobic to create a Pickering emulsion. This hydrophobization is lower for ES-coated silica due to the silane coverage resulting in lower emulsion stability. The emulsion stability to coalescence and creaming also decreased significantly on adding 0.01 wt.% ES-coated silica to DIW. Sediment was observed on adding Permian brine to bare silica dispersion however the particles became slightly dispersed (weakly aggregated) after stirring the dispersion vigorously for 30 min (Figure 5.15) which is ideal for emulsification purposes, as observed in the previous studies.[28, 29] Oil-in-water emulsions initially more stable to coalescence and creaming were observed when bare silica was in Permian brine. However, both emulsions (bare silica in DIW and Permian brine) had the same degree of coalescence in the long term (Figure 5.16). The initial microscope photos of these emulsions are shown in Figure 5.13. Table 5.2 summarizes the results on emulsions made from crude oil.

Figure 5.14. Appearance and fractions of oil (f_o) and water (f_w) resolved from oil-in-water emulsions formed from 5 g crude oil and 5 g of 0.1 wt.% ZN in DIW or Permian brine.
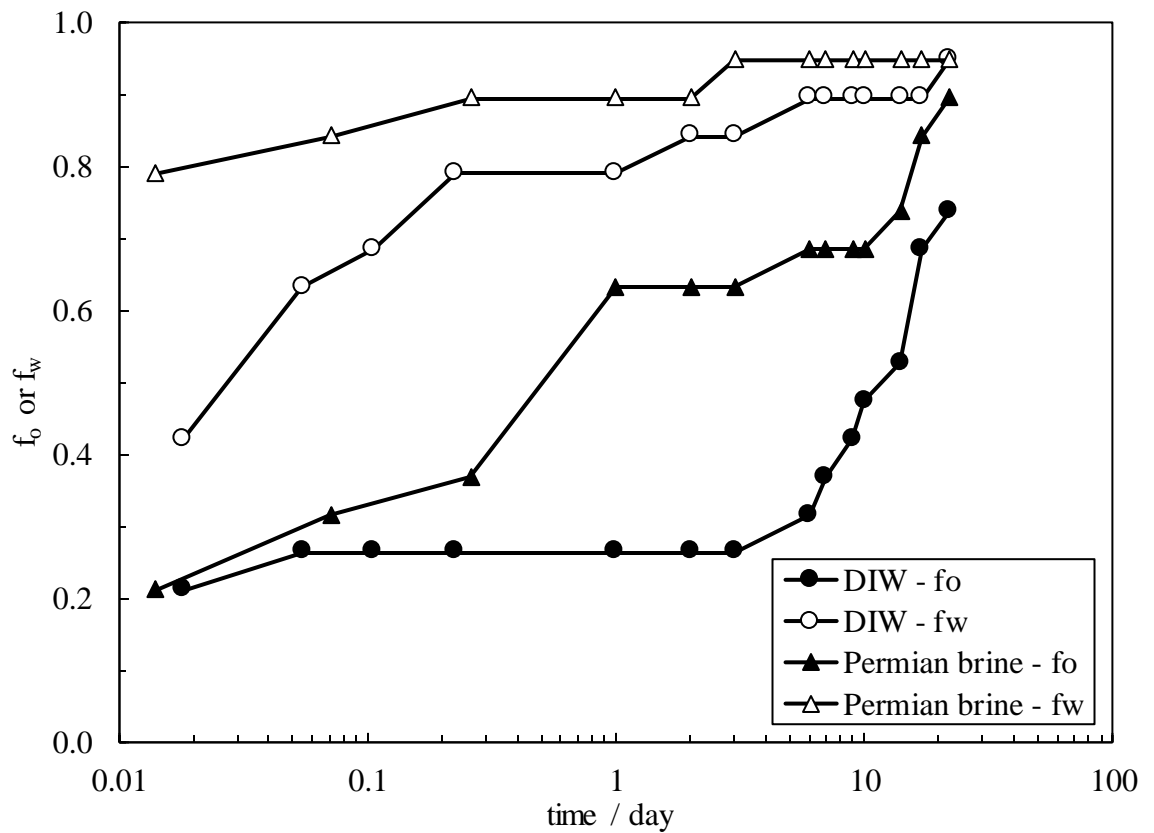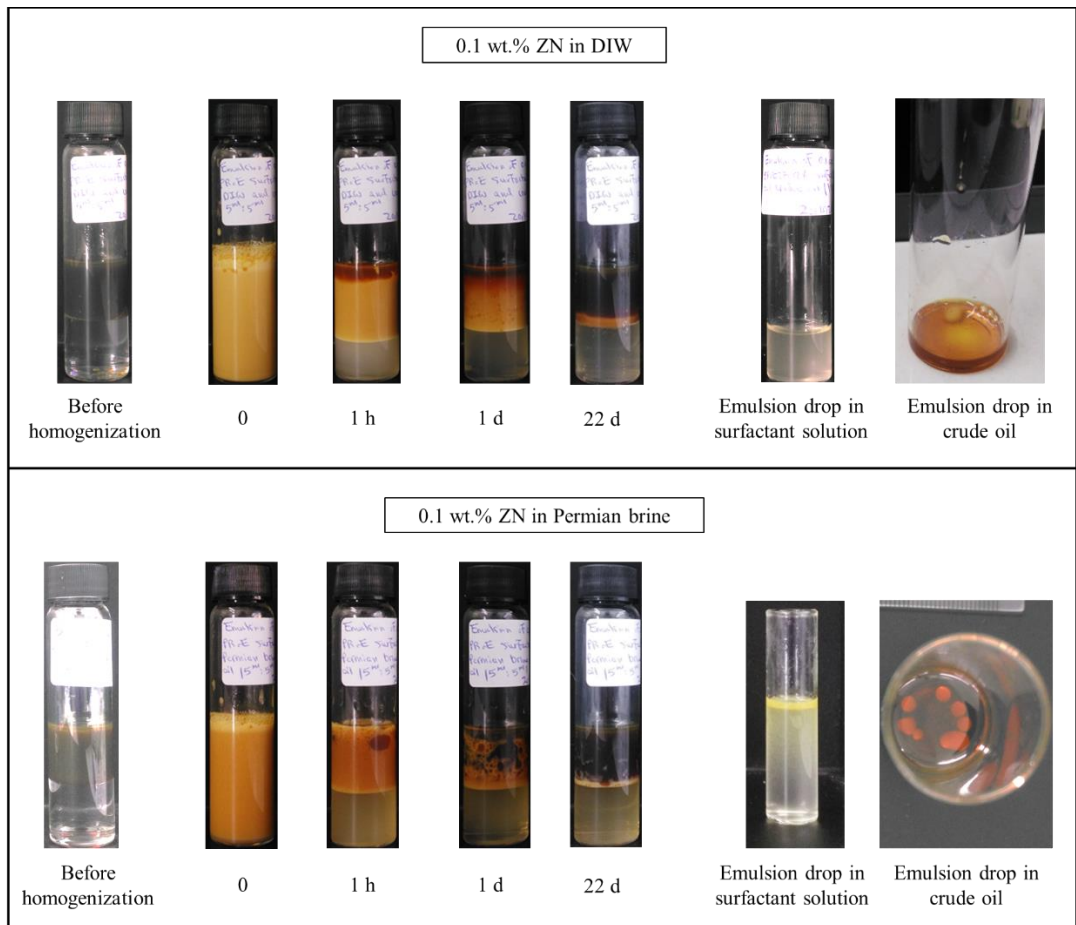
Figure 5.15. Appearance of oil-in-water emulsions from 5 g crude oil and 5 g of dispersions of bare silica or ES-coated silica.
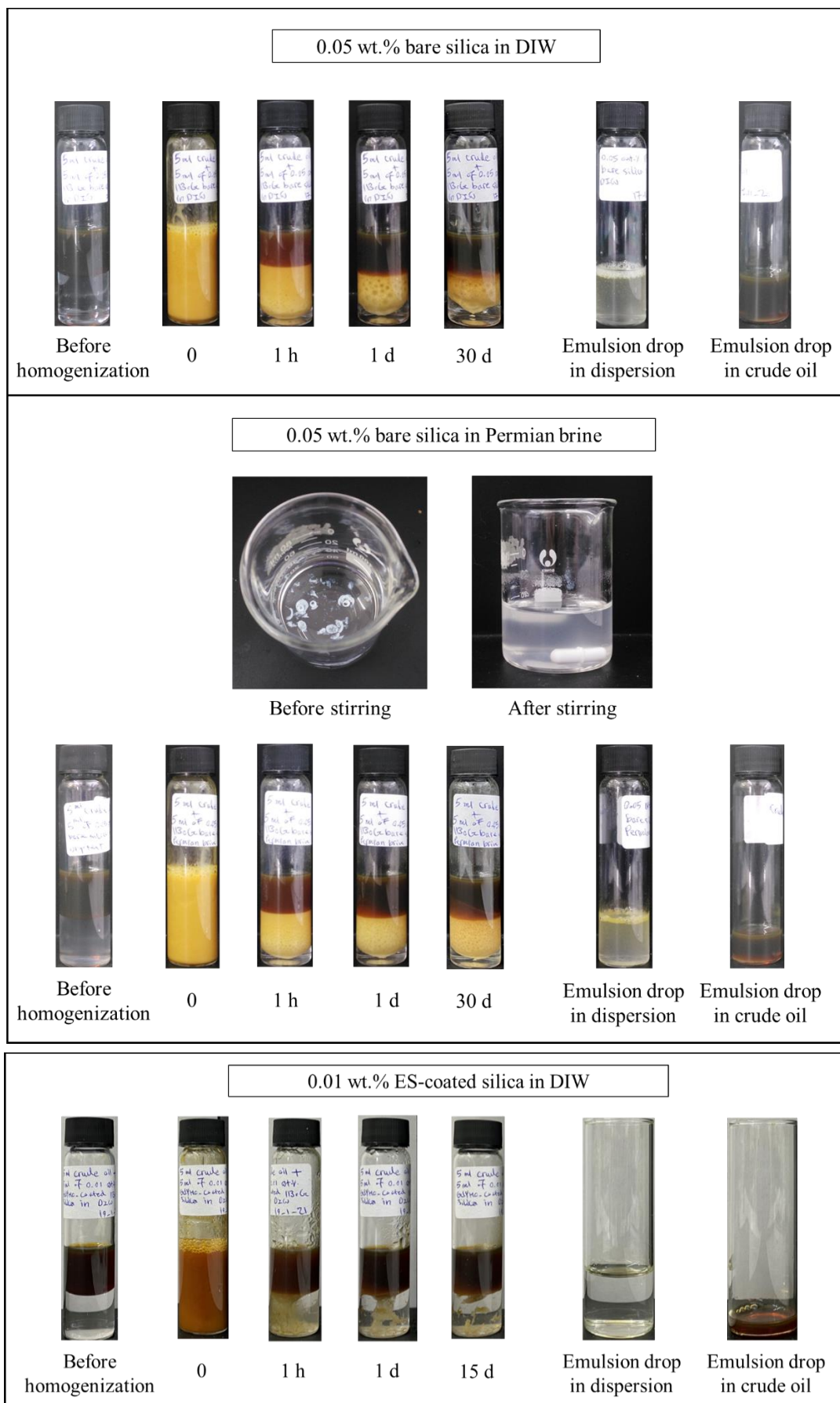
Figure 5.16. Fractions of oil (f_o) and water (f_w) resolved from oil-in-water emulsions formed from 5 g crude oil and 5 g of (a) 0.05 wt.% bare silica in DIW or Permian brine, (b) 0.01 wt.% ES-coated silica in DIW.
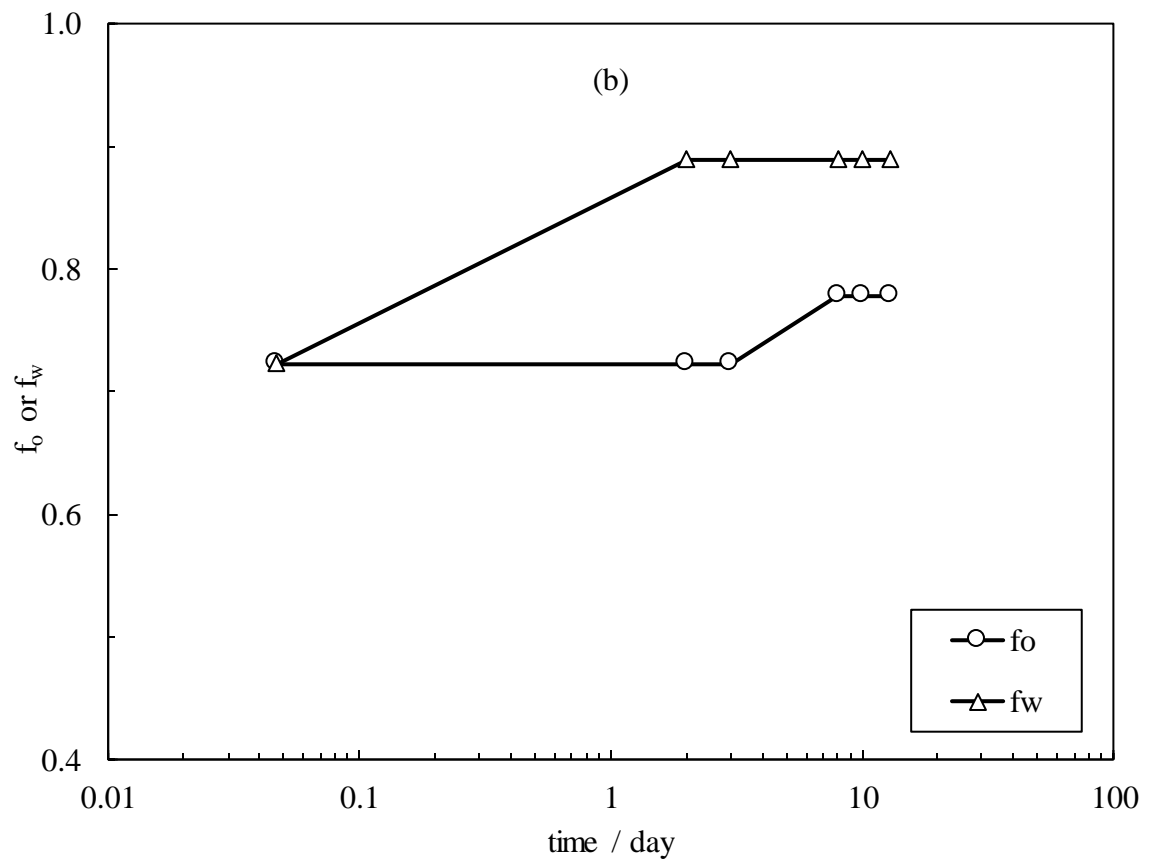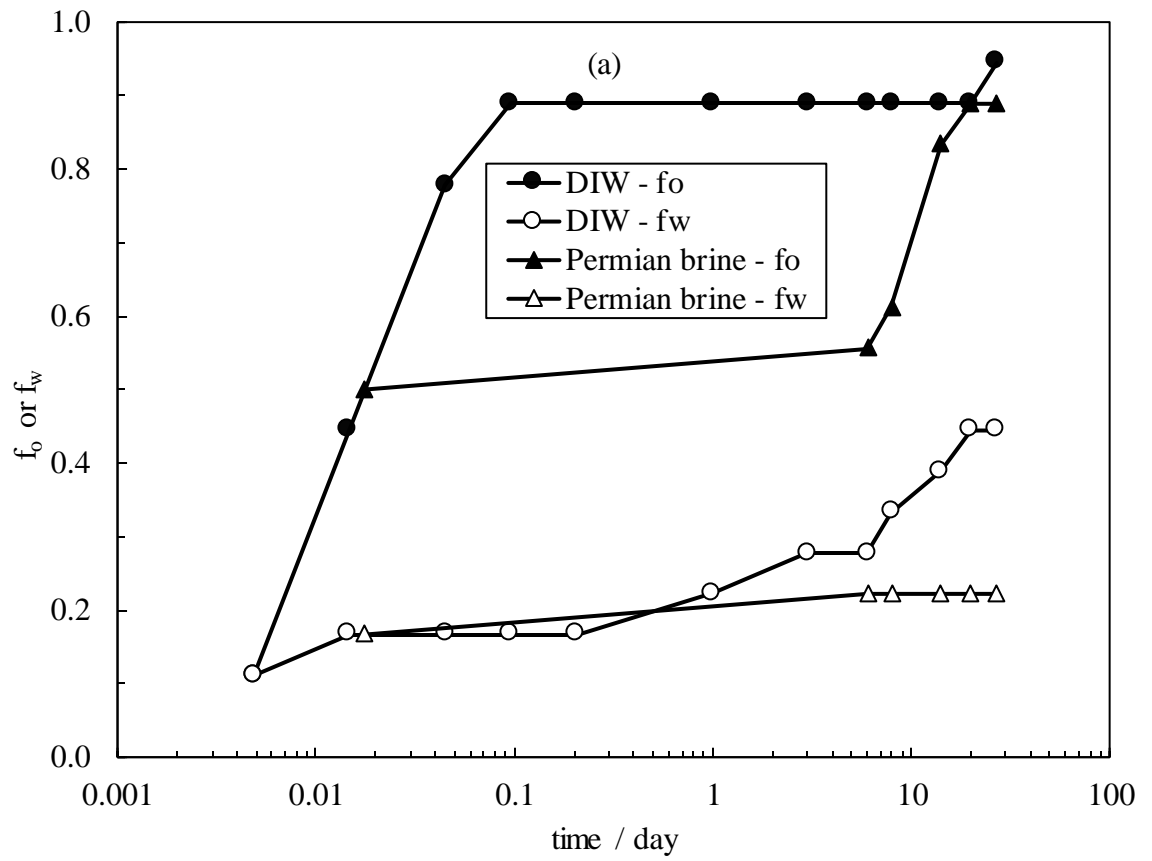
Table 5.2. Summary of results on oil-in-water emulsions from crude oil and different ZN solutions or bare silica and ES-coated silica in DIW and Permian brine (12.6 wt.%) after 3 – 4 weeks.

Aqueous phase	f_o	f_w	Comment
DIW	0.8	0.9	
			Mostly sodium ions interact with crude oil polar groups to stabilize the emulsions initially.
Permian brine	0.8	0.4	Both had the same initial drop diameter.
0.1 wt.% ZN in DIW	0.7	0.9	Permian brine made coalescence and creaming faster.
			Brine ions lowers the electrostatic interactions between aqueous and crude oil surfactants at the oil-water interface resulting in a lower number of interfacial surfactants. This is accompanied by
0.1 wt.% ZN in Permian brine	0.9	0.9	the demulsification power of ZN.
			The addition of ZN to DIW reduced the initial drop diameter but had no effect on that of Permian brine.
0.05 wt.% bare silica in DIW	0.9	0.4	
0.05 wt.% bare silica in Permian brine	0.9	0.2	Particle hydrophobization extent by crude oil: bare silica > silane-coated silica
			Slightly aggregated bare silica particles in Permian brine can stabilize the emulsions more initially.
0.01 wt.% ES-coated silica in DIW	0.8	0.9	

5.3 Emulsions of pure oils and water

5.3.1 Effect of surfactant type and concentration

5.3.1.1 Toluene

234

Figure 5.17 shows the effect of the surfactant type and concentration on the emulsification of toluene and water. The figure shows considerable coalescence and creaming in all emulsions by two surfactants in DIW within a day with an exception at 0.05 wt.% ZN which had no coalescence but significant creaming over the first day. This emulsion had a fraction of oil and water resolved as 0.5 and 0.9, respectively after a month but the phases separated after 3 months. It is observed that the addition of Permian brine to both surfactant solutions makes more emulsions of toluene and water however the emulsions with ZN in Permian brine were only short-term stable. Figure 5.18 shows the effect of surfactant type on the fractions of oil and water resolved from these emulsions after 100 days. All emulsions made with surfactants in DIW were phase separated after 3 months. AHS in Permian brine (> 0.03 wt.%) produced emulsions more stable to coalescence (f_o < 0.2) after around 3 months compared to those of ZN (f_o > 0.8). An initial decrease in creaming was observed in emulsions with surfactants in Permian brine but it increased after 100 days. The type of surfactant had no significant impact on how well the emulsions creamed. Due to the significant difference in density between the aqueous and oil phases, density-driven creaming is common in these emulsions.

When the zwitterionic surfactant is in DIW, the surfactant molecules adsorb at the oil-water interface but the adsorption is limited due to the electrostatic repulsion between the adsorbed surfactant headgroups. The negative headgroup of AHS surfactant and the anionic oil-water interface experience another electrostatic repulsion as a result of the relatively high charge density of the toluene-water interface which prevents the alkane tail of the surfactant from being completely solvated in the oil phase.[240] Being slightly polar, toluene molecules have random adsorption at the oil-water interface. Consequently, there are weak random interactions between the tails of the surfactant molecules and the toluene molecules that have been adsorbed, which leads to unstable emulsions.

The addition of salts can lower the electrical double layer of the interface and headgroup-headgroup repulsion, resulting in less interfacial charge and more surfactant adsorption with elongation of their linear tails in the oil phase [267] which increases emulsification. Previous research has also shown that zwitterionic and nonionic surfactants become less soluble as electrolyte concentration rise. In the salting-out region, the salts break down the initial hydration structure of the hydrophobic groups of the surfactants, enhancing their hydrophobicity and facilitating simpler micellization to prevent exposure of their hydrophobic tails in the aqueous phase. In addition, when salinity rises, more and more water molecules are taken up by salt ions, leaving less of it available to interact with the surfactant headgroups in the aqueous phase.[268] Heavily hydrated ions like Na^+ can salt

out the hydrophobic groups of the surfactant more.[5] Da *et al.* made a similar observation regarding the effect of high salt concentrations on surfactant adsorption at a gas-water interface. They stated that the addition of 22 wt.% brine of various salts can encourage the zwitterionic cetyl betaine surfactant molecules to adsorb more at the CO_2-water interface due to the decrease in surfactant headgroup hydration and the decrease in the electrostatic repulsion of the adsorbed surfactant headgroups.[269] Adding salts can also help generate more micelles which can help increase the structural disjoining pressure and in turn the stability of foams or emulsions.[270] All these reasons may explain the higher emulsification of water and toluene when Permian brine is added to AHS solutions.

The nonionic C_{10-12} nonaethylene glycol ether in ZN can improve the power of zwitterionic R83397 can further lower the interfacial tension, stabilize the emulsion and prevent droplet coalescence. In comparison to AHS, lower air-water and oil-water interfacial tensions were found in the presence of ZN. Other advantages of nonionic surfactants include enhanced solubilization and improved compatibility with various oils.[169] The ZN solution was created by ChampionX as a commercial product using a proprietary demulsifier to destabilize oilfield emulsions. Because of this, less stable emulsions are seen in this investigation when ZN is present, despite more emulsification being predicted due to the presence of the nonionic surfactant.

The initial drop diameters decrease for both surfactants as surfactant concentrations rise (Figure 5.19). No drop diameter measurements were possible for emulsions made with AHS in DIW due to the quick phase separation. It is observed that the addition of Permian brine increases the drop diameter of the emulsions made with ZN although they are more stable to coalescence. Comparing the drop diameters of the emulsions made with surfactants in Permian brine, AHS produces larger drops but remains stable for longer times. After 100 days, the emulsions with AHS in Permian brine had a rise in their drop diameters by 20 ± 10 µm while that of ZN in Permian brine was 10 ± 10 µm. Figure 5.20 shows the initial microscope images of the oil-in-water emulsions formed by toluene and surfactant solutions. As shown, increasing AHS concentrations from 0.03 wt.% to 0.1 wt.% in Permian brine has no effect on the shape of drops but it makes the drop size distribution wider such that drops of different sizes with flocs are observed at 0.1 wt.% while they are equally sized at 0.03 wt.%. The emulsions made with 0.005 wt.% and 0.01 wt.% ZN in Permian brine were unstable but had small droplets in the resolved aqueous phase that disappeared after a day. A wide size distribution is also observed in the emulsions formed by ZN in Permian brine, reflecting unstable emulsions with droplets of different diameters. The presence of drop flocs at high surfactant concentrations is due to the high salinity of

the brine. Similarly, it has been observed that foams made with surfactants in high salinity brine have an increase in interfacial dilatational elasticity and bubble flocs which help the foam stabilize.[271]

Figure 5.17. Effect of surfactant type and concentration on oil-in-water emulsions of 5 g toluene and 5 g solutions of AHS or ZN (given in wt.%) in DIW and Permian brine at different times.

Figure 5.18. Effect of surfactant type and concentration on the fractions of oil (upper) and water (lower) resolved from oil-in-water emulsions of 5 g toluene and 5 g solutions of AHS or ZN in DIW and Permian brine after 100 days.

238

Figure 5.19. Initial and long-term emulsion drop diameter with surfactant concentration for oil-in-water emulsions from 5 g toluene and 5 g solutions of AHS or ZN in DIW and Permian brine.
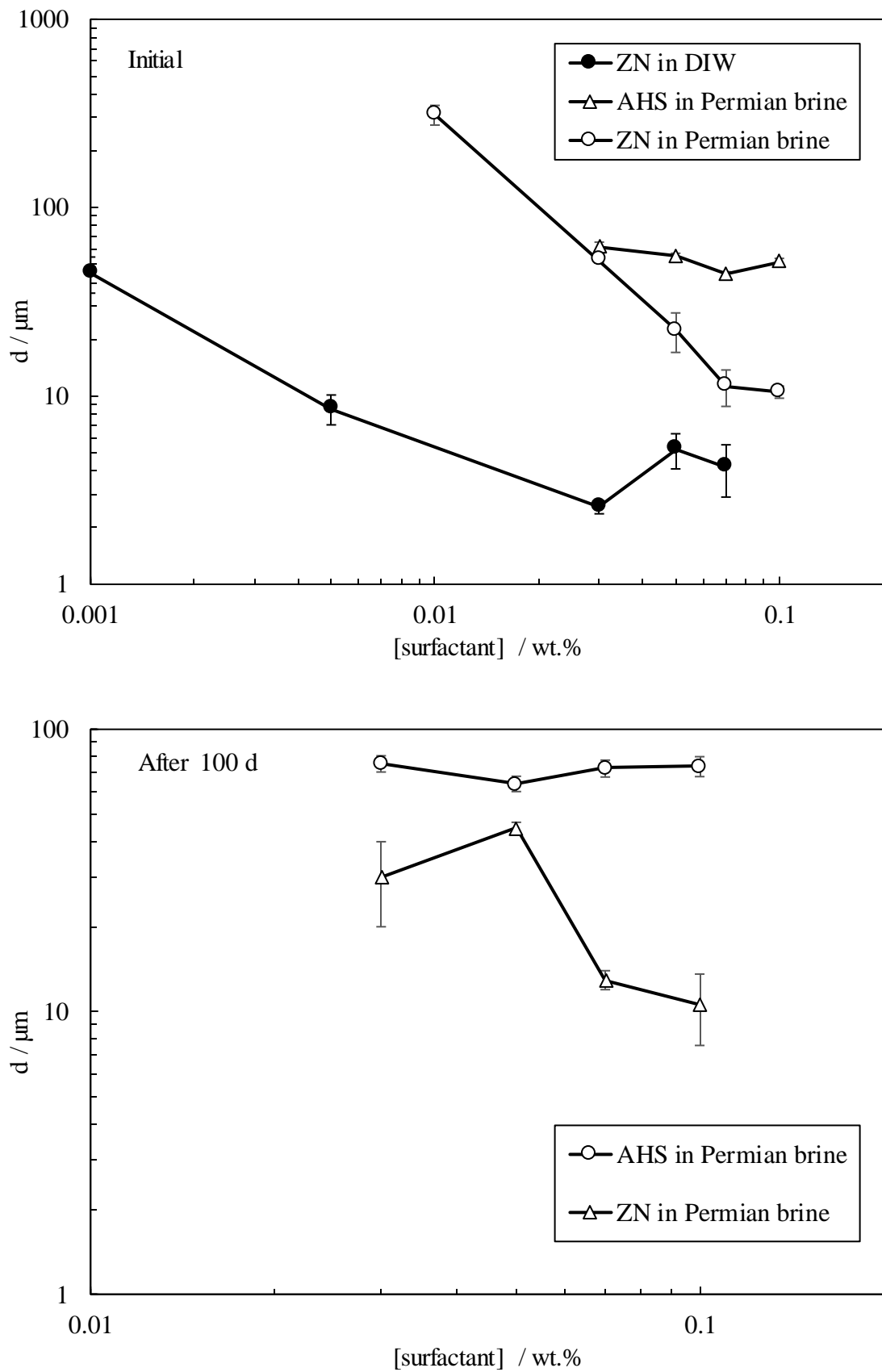
Figure 5.20. Optical microscope images taken immediately after preparation of oil-in-water emulsions of 5 g toluene and 5 g solutions of AHS and ZN. Concentrations are given in wt.%.

240

AHS in Permian brine

0.03 0.05 0.07 0.1

ZN in DIW

0.001 0.005 0.01 0.03

0.05 0.07 0.1

ZN in Permian brine

0.01 0.03 0.05

0.07 0.1

5.3.1.2 Heptane

Figure 5.21 shows the effect of surfactant type on the emulsification of heptane and water. All the emulsions formed by ZN in DIW and Permian brine were phase separated within a day. The emulsions made with AHS in DIW (> 0.05 wt.%) were more stable to coalescence than those in Permian brine which were phase separated within a week (Figure 5.22). The emulsions of 0.07 and 0.1 wt.% AHS in DIW showed slight coalescence after two months (f_o = 0.25). Both surfactants were ineffective in reducing creaming. Figure 5.23 shows the initial drop diameter measurements of the emulsions made with heptane and different concentrations of AHS in DIW and Permian brine. The addition of Permian brine can reduce the drop diameter in the emulsions formed by AHS. No measurements were possible for the emulsions made with ZN solutions due to the quick phase separation. Figures 5.24 and 5.25 show the initial microscopy of these emulsions. The addition of Permian brine to R55397 solutions has produced a more monomodal drop distribution.

When the zwitterionic AHS is in DIW, the surfactant molecules tend to adsorb at the oil-water interface with tails toward the oil phase and headgroups facing water. The negative headgroup of the surfactant (sulfonate group) tends to be farther away from the anionic oil-water interface while the positive headgroup (quaternary ammonium) would be placed in the thick double layer (high charge density) of the interface. Here, the anionic headgroups of the adsorbed surfactants serve as a physical barrier to prevent the oil droplets from meeting one another. Previous research demonstrates that because heptane molecules are non-polar, they prefer to stay in the bulk of the oil phase and rarely adsorb at the heptane-water interface.[240] In this case, surfactants extend their tails towards the bulk of the oil phase far enough to interact with the heptane molecules to enhance the emulsification.[272] The interfacial double layer contracts when salts are added, and it is believed that the accumulation of counterions at the oil-water interface prevents surfactants from adsorption, hence raising the interfacial tension between oil and water, as observed earlier. In addition, because there are weak interfacial heptane molecules accessible, there would be fewer interactions between the oil phase and surfactant tails at the interface, leading to poor emulsification. Binary nonionic-zwitterionic solution (ZN) is thought to be capable of improving the emulsification but the emulsions are quickly broken due to the demulsification ability of ZN.

Figure 5.21. Effect of surfactant type and concentration on oil-in-water emulsions of 5 g heptane and 5 g solutions of AHS or ZN (given in wt.%) in DIW and Permian brine.
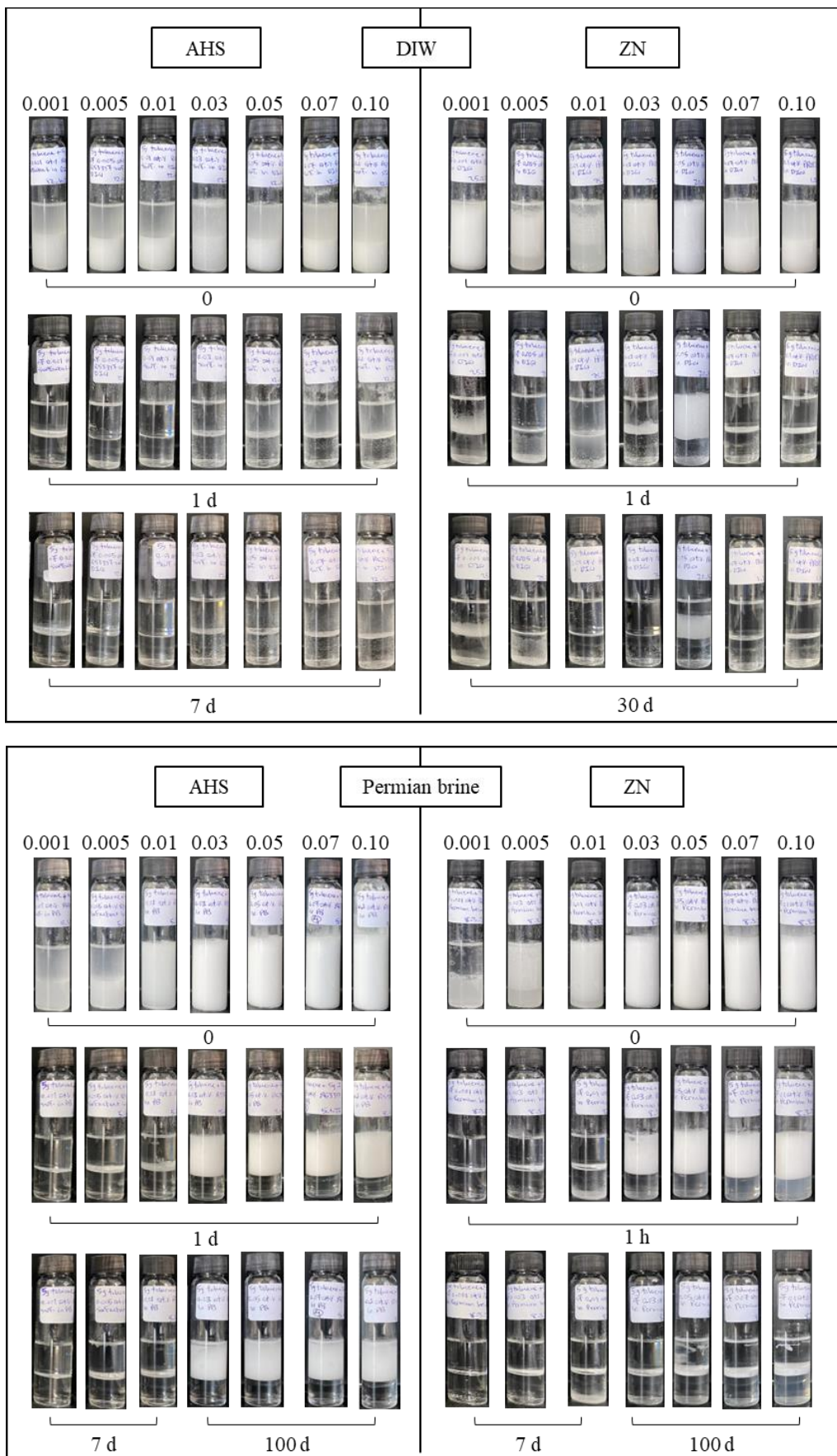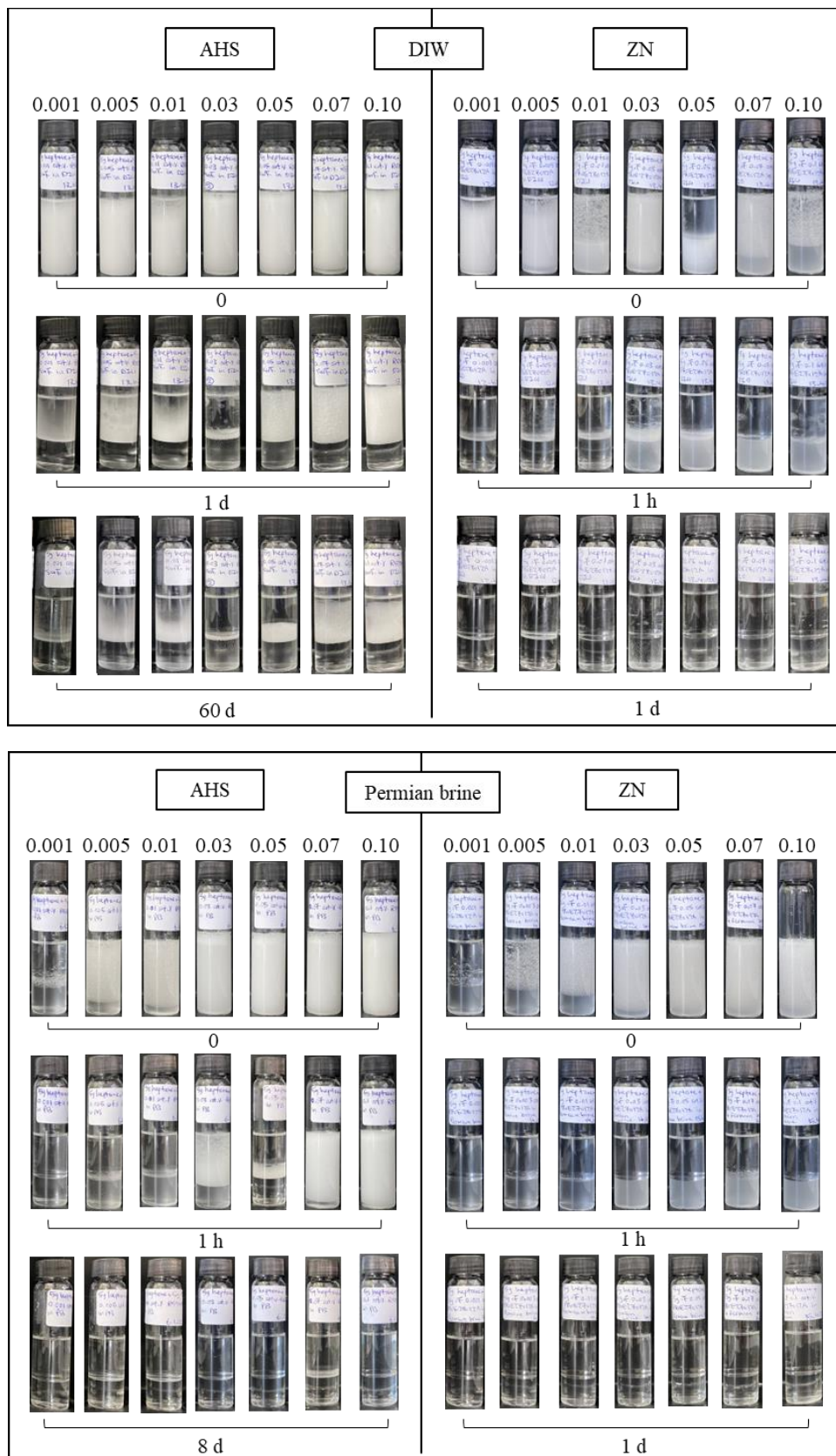
Figure 5.22. Effect of surfactant type and concentration on the fractions of oil (upper) and water (lower) resolved from oil-in-water emulsions from 5 g heptane and 5 g solutions of AHS and ZN in DIW after two months.

243

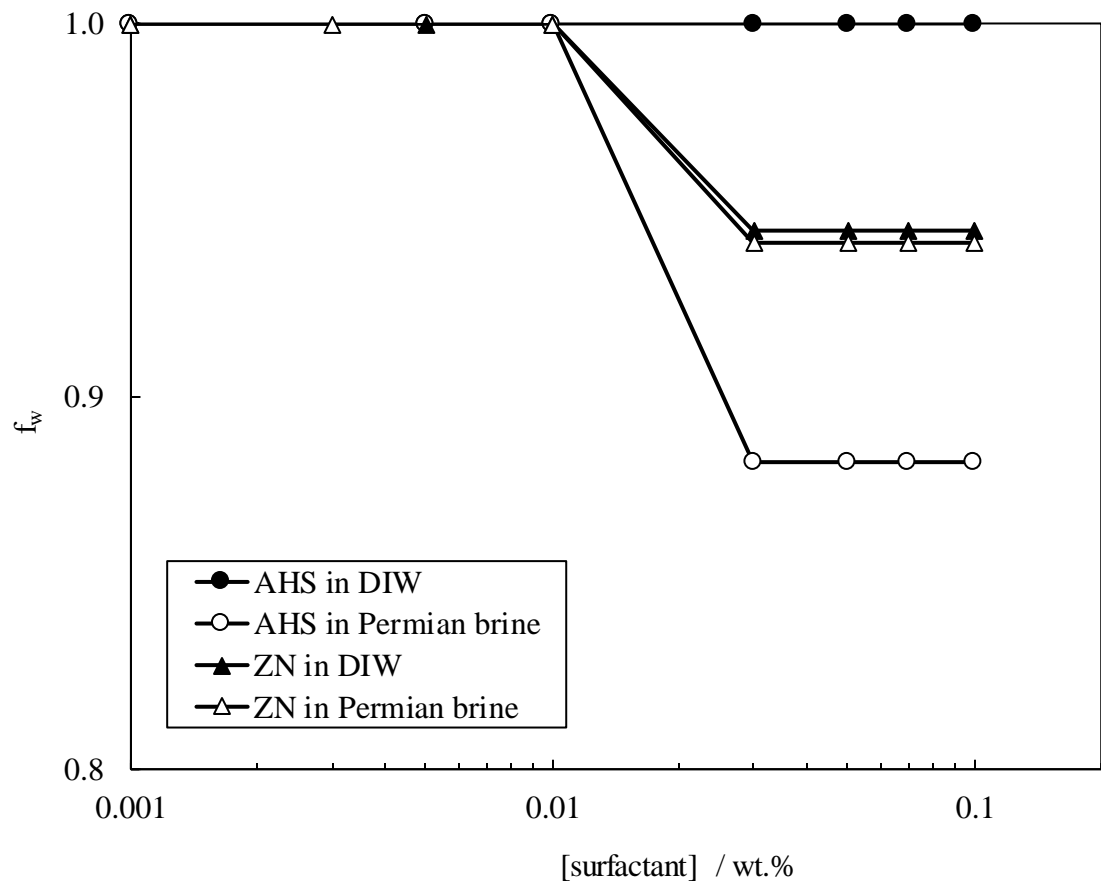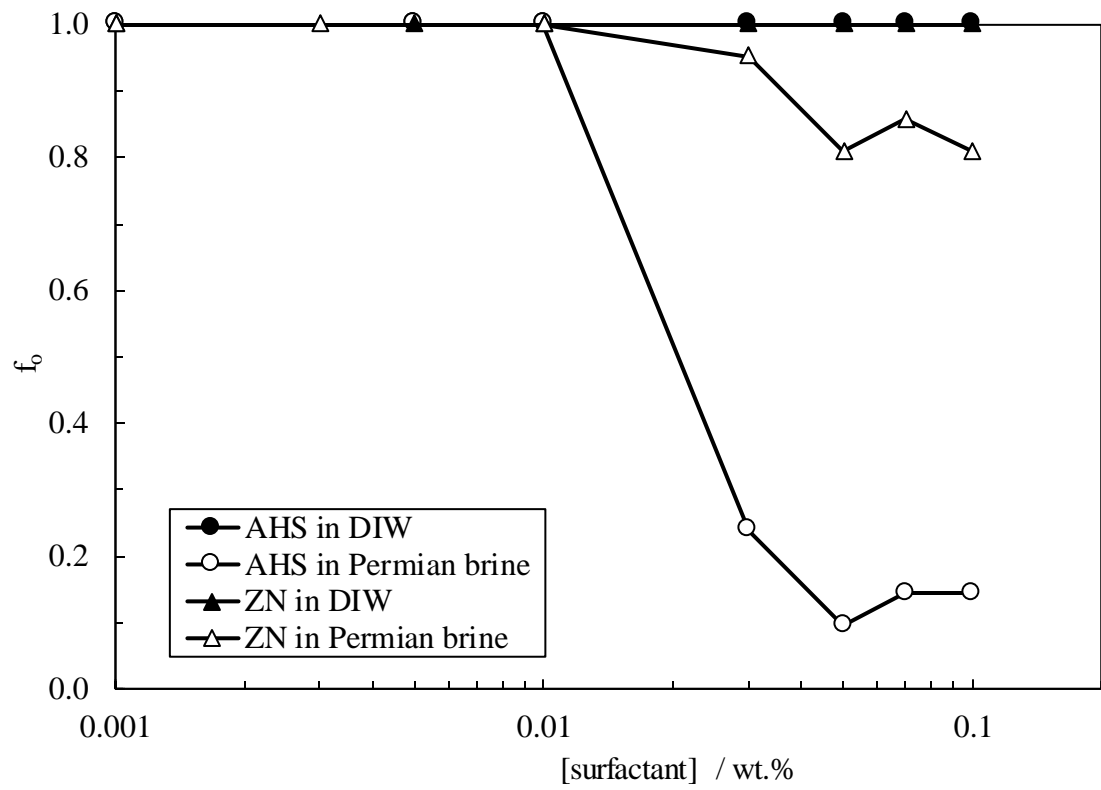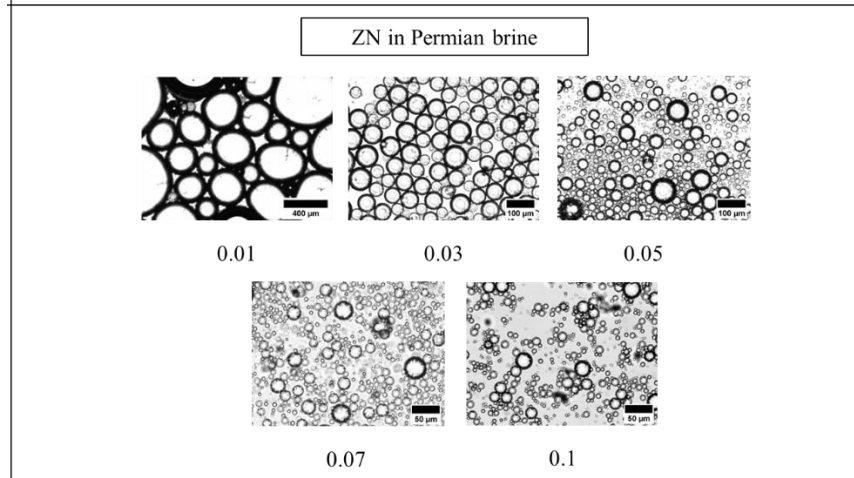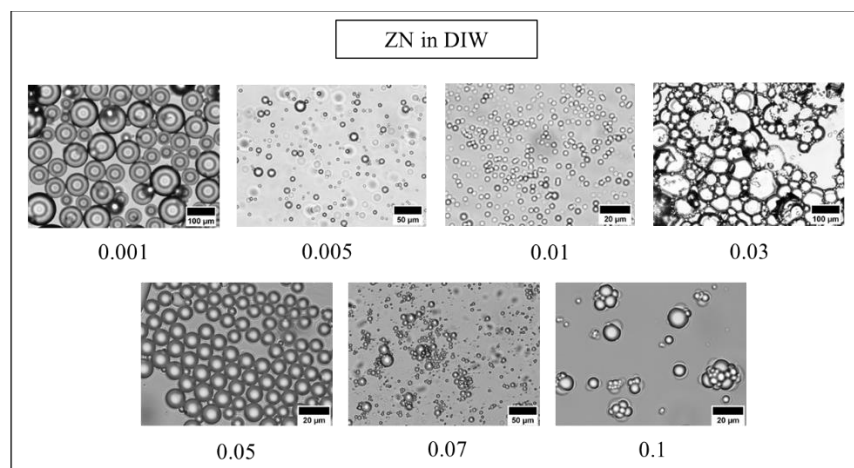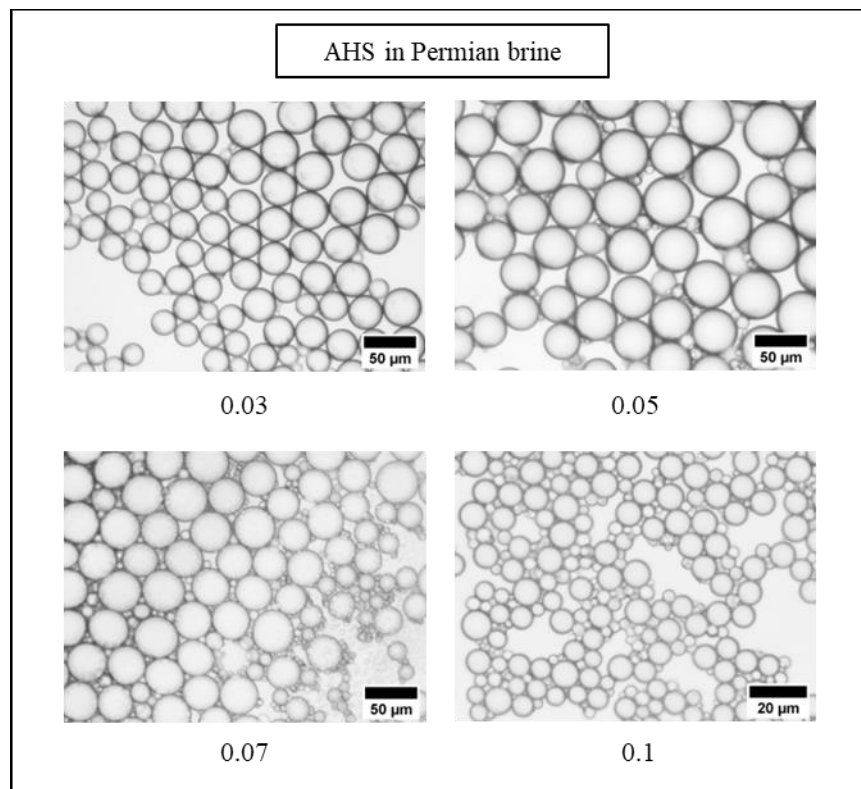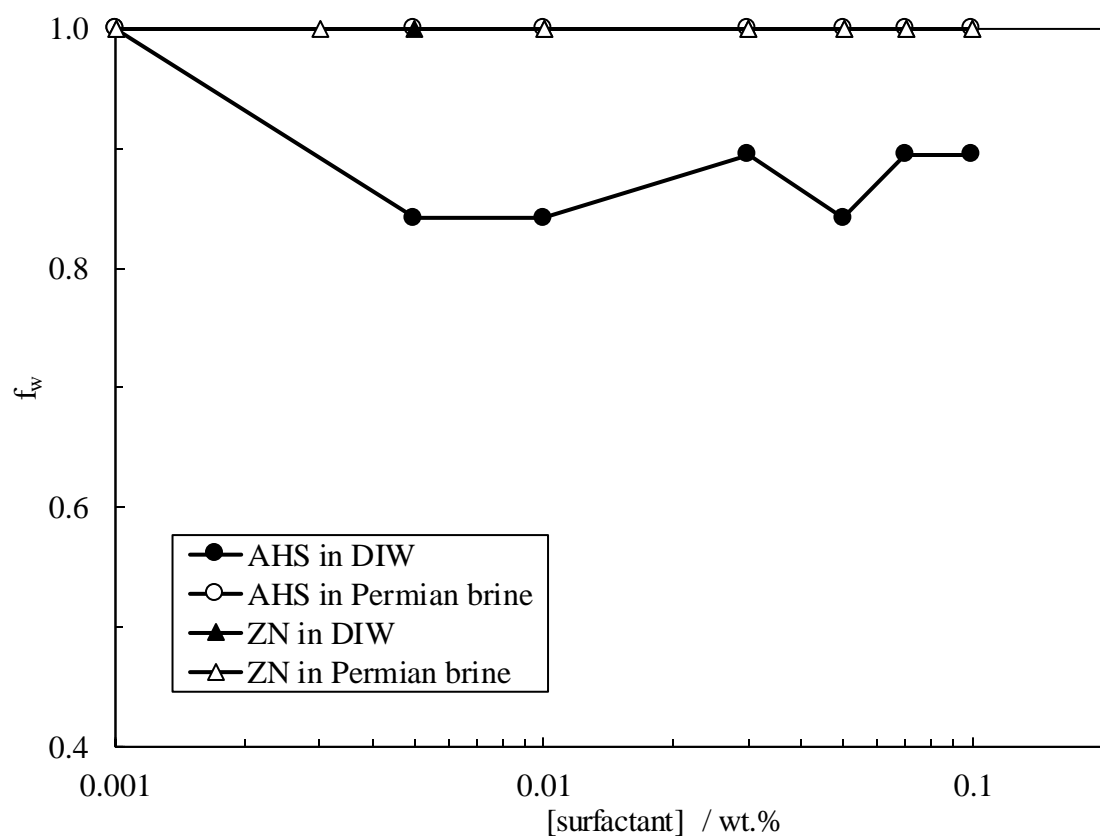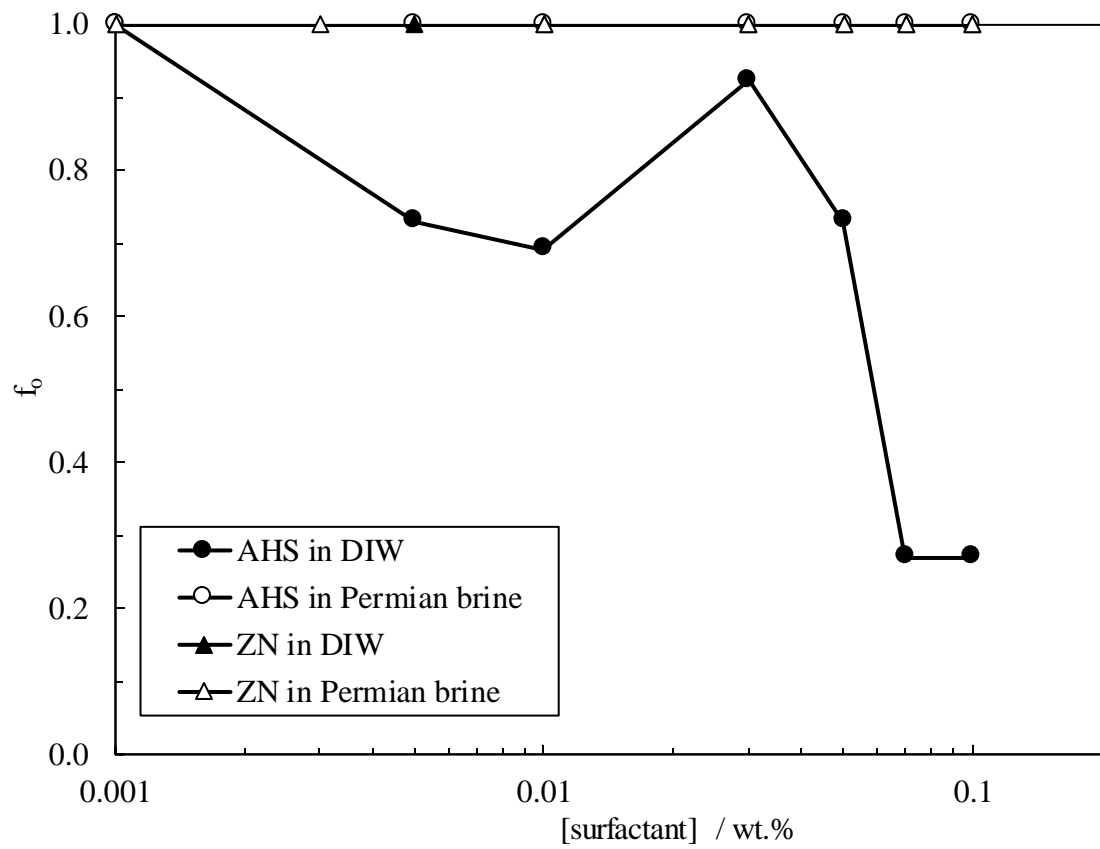**Figure 5.23.** Initial emulsion drop diameter vs surfactant concentration for oil-in-water emulsions from 5 g heptane and 5 g solutions of AHS in DIW and Permian brine.

Figure 5.24. Optical microscope images taken immediately after preparation of oil-in-water emulsions from 5 g heptane and 5 g solutions of AHS (given in wt.%) in DIW and Permian brine.

Figure 5.25. Optical microscope images taken immediately after preparation of oil-in-water emulsions from 5 g heptane and 5 g solutions of ZN (given in wt.%) in DIW or Permian brine.

246

DIW

0.001   0.005   0.01
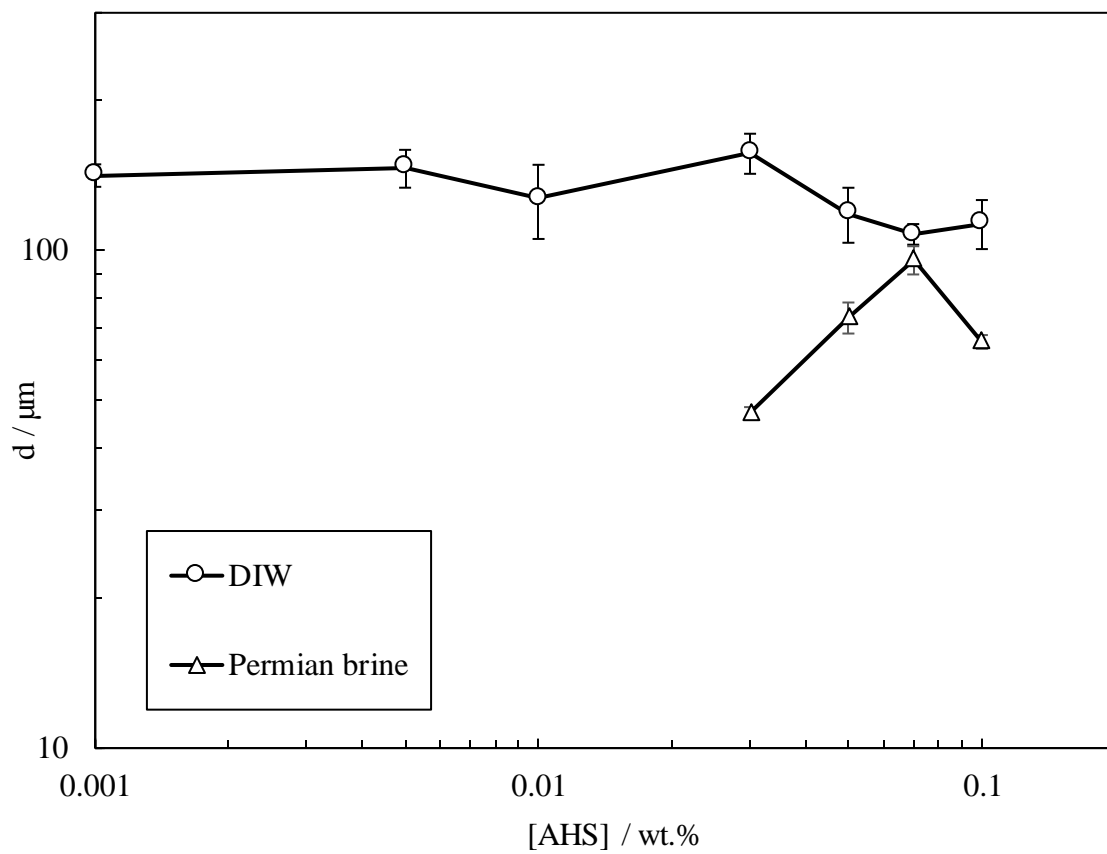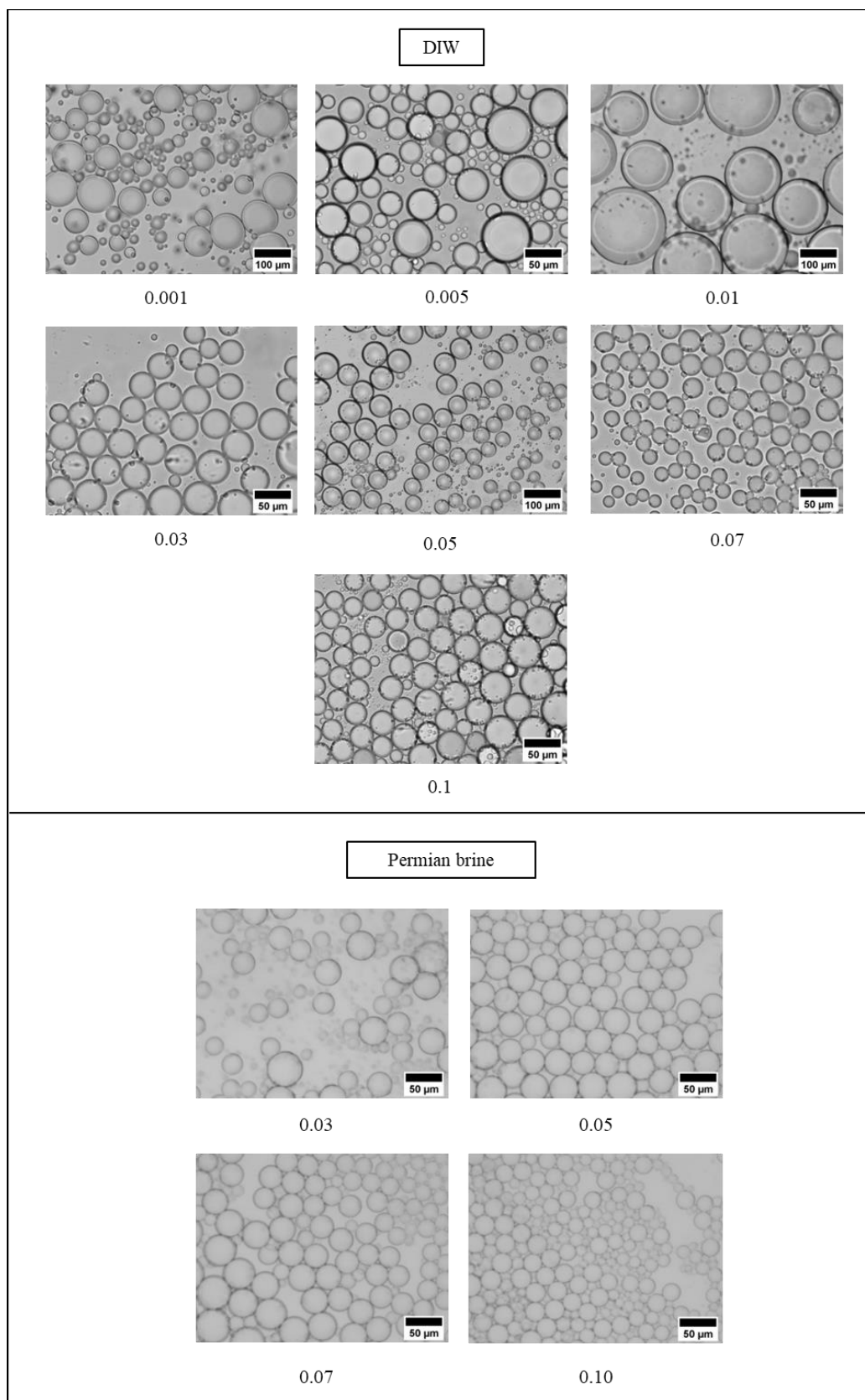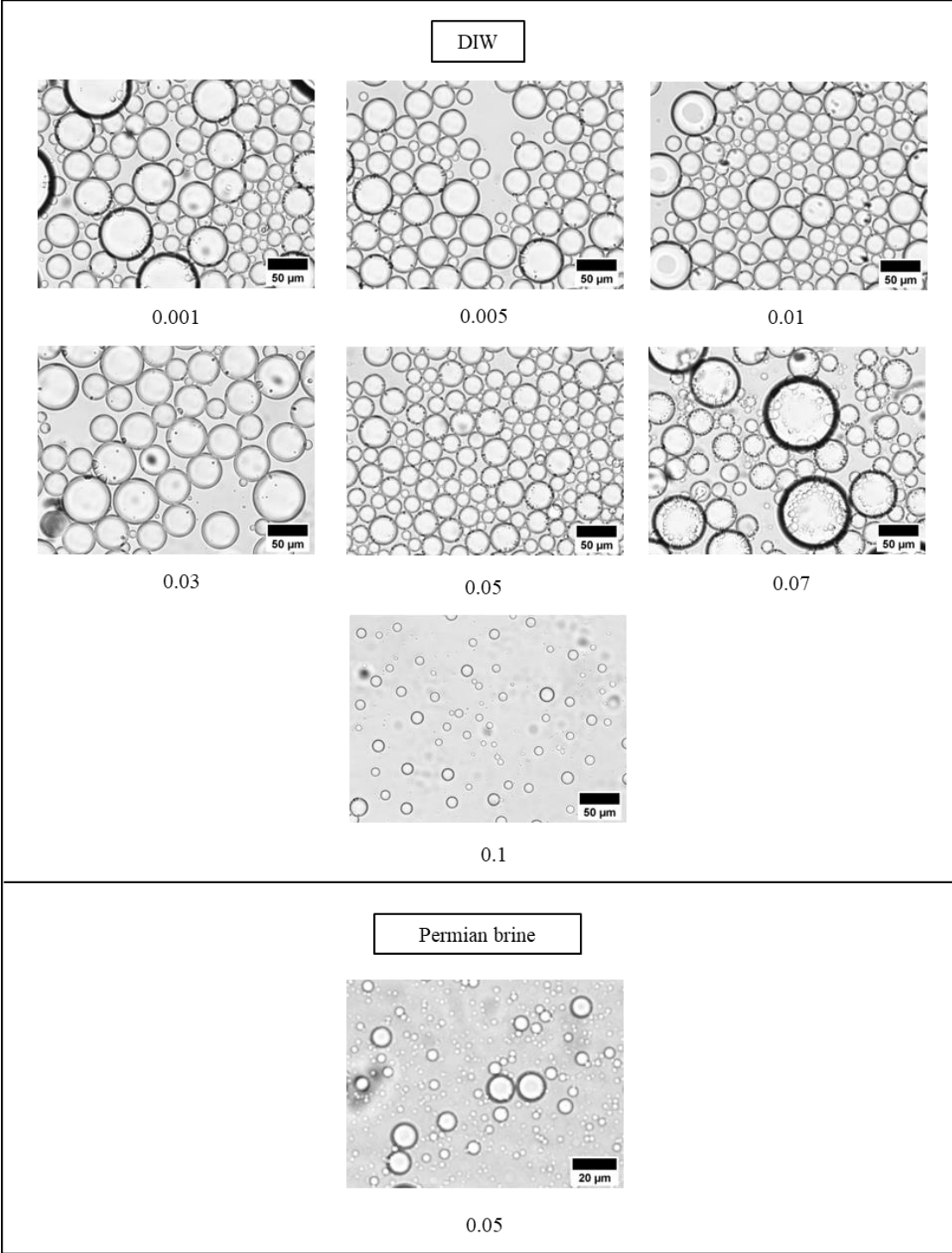
0.03   0.05   0.07

0.1

Permian brine

0.05

5.3.1.3   Heptol

Figure 5.26 shows the emulsification of heptol and water with different solutions of AHS and ZN. All emulsions made with ZN in both DIW and Permian brine experienced phase separation within a day. Emulsions made with AHS in DIW and Permian brine ($>$ 0.03 wt.%) were initially stable to coalescence but creamed significantly. The emulsion made with 0.1 wt.% AHS in DIW remained stable for a long time with negligible coalescence. The fractions of oil and water resolved from this emulsion after 100 days were around 0.2 and 0.8, respectively (Figure 5.27). The emulsions made with 0.05 wt.% and 0.07 wt.% AHS in Permian brine also showed good stability to coalescence up to 100 days (f_o = 0.2 – 0.3). Like toluene, the addition of Permian brine to AHS solutions increased the emulsification of heptol and water at 0.05 – 0.07 wt.% but did not have any effect on that of ZN.

Previous studies show that increasing the polarity of the oil phase reduces the van der Waals energy while increasing the electrostatic and interaction energies. In other words, van der Waals interaction dominates at a weakly polar oil-water interface whereas electrostatic interaction dominates at a polar oil-water interface.[240] As the polarity of the oil increases *e.g.* when replacing heptane with toluene, the work of adhesion ($W_a = \gamma_{oil-air} + \gamma_{air-water} - \gamma_{oil-water}$) between water and oil increases as a result of decreasing oil-water interfacial tension and increasing air-oil surface tension. Thus, the adsorption capability of the oil molecules at the oil-water interface decreases as follows: toluene $>$ heptol $>$ heptane.[241, 272] Therefore, the emulsification behaviour of heptol is anticipated to be a combination of separate oils *i.e.* toluene and heptane. Note that the heptane/toluene ratio of 1:1 g g^{-1} means a slightly higher heptane volume in the mixture (56 vol.% heptane + 44 vol.% toluene), offering a higher effect of heptane. Therefore, the slightly polar toluene of the heptol gives it local oil adsorption at the oil-water interface with a high interfacial charge density while the non-polar heptane molecules are mainly in the bulk of the oil phase and have a lower interfacial charge. Thus, the interfacial behaviour of heptol (1:1 g g^{-1}) is controlled by both.[241] Except for the highest surfactant concentration, the emulsions made with heptol and AHS in DIW are often unstable, similar to those made with toluene, which is due to the high electrostatic repulsion between the anionic headgroup of the surfactant and the local anionic toluene-water interface. The emulsion of heptol and 0.1 wt.% AHS in DIW has a higher stability to coalescence than that of heptane alone. High concentrations cause more elongation of surfactant tails in the bulk of the oil phase to interact with heptane molecules which is accompanied by the role of toluene as described. When Permian brine is added, more stable emulsions are produced at an intermediate AHS concentrations like that of toluene

due to the reduced electrostatic repulsion between the surfactant headgroup and the interface by ions. For ZN, the phase separation occurs extremely quickly for the surfactant both in DIW and Permian brine which is more similar to the behaviour of heptane.

Figure 5.28 shows the initial drop diameters of these emulsions. There is a decrease in the emulsion drop diameter on increasing AHS concentrations both in DIW and Permian brine. No considerable change is seen in the drop diameters upon adding Permian brine to AHS solutions. Figure 5.29 shows the initial microscope images of these emulsions. Spherical, monosized emulsion droplets are observed in the emulsions of low AHS concentrations (0.03 wt.%) in DIW while they turn multimodally distributed with drop flocculation at high surfactant concentrations (> 0.07 wt.%). Spherical droplets are observed in all emulsions of AHS in Permian brine with drop flocs at high surfactant concentrations. The photos of emulsions made with ZN solutions are presented in Figure 5.30. The emulsions of ZN in Permian brine were unstable so the photos are related to the drops dispersed in the resolved aqueous phase.

Table 5.3 summarizes the results on emulsions from different oils and AHS and ZN in DIW and Permian brine.

Figure 5.26. Effect of surfactant type and concentration on oil-in-water emulsions of 5 g heptol (1:1 g g^{-1}) and 5 g solutions of AHS or ZN (given in wt.%) in DIW and Permian brine.
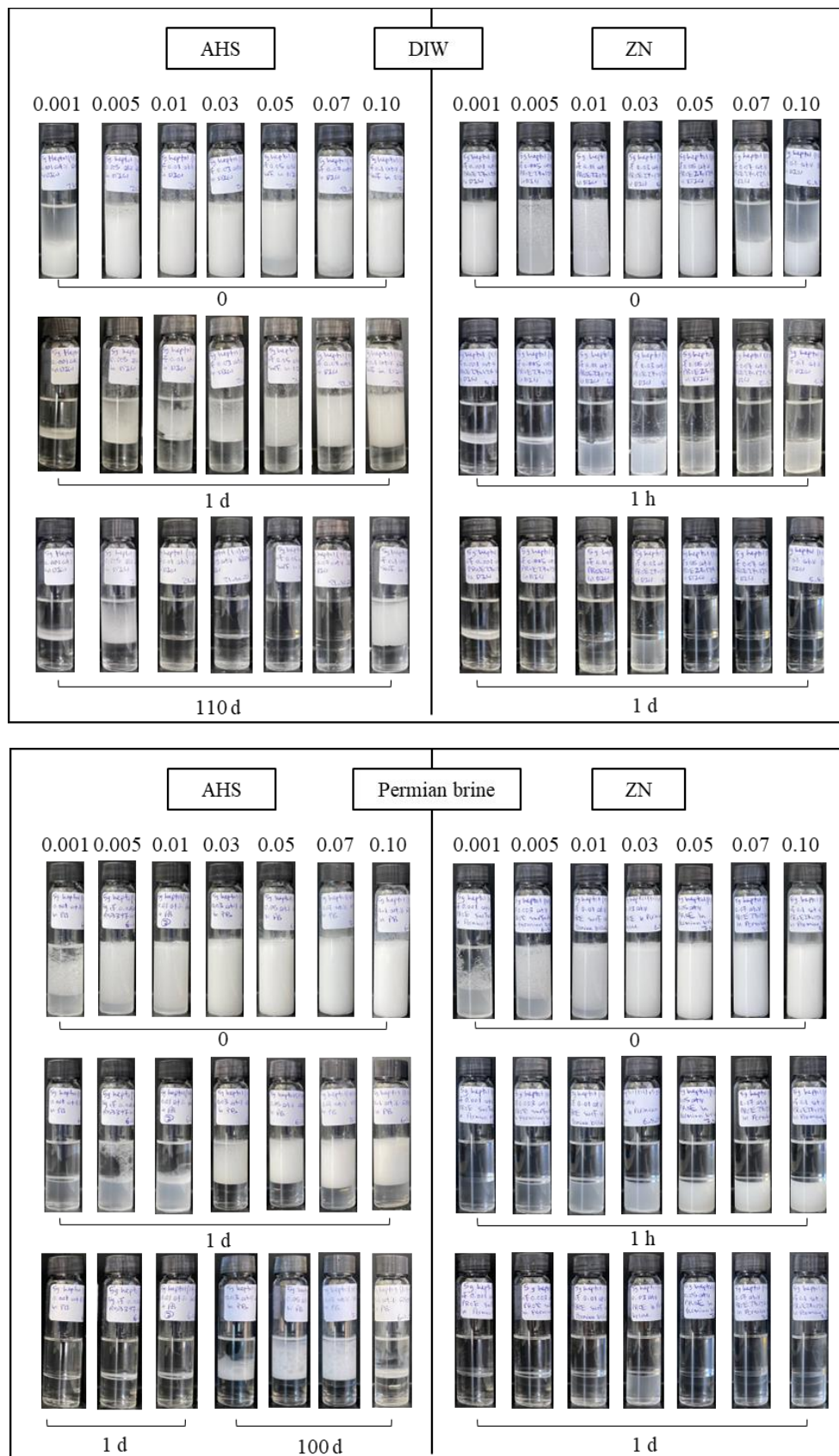
Figure 5.27. Effect of surfactant type and concentration on the fractions of oil (upper) and water (lower) resolved from oil-in-water emulsions from 5 g heptol (1:1 g g^{-1}) and 5 g solutions of AHS in DIW and Permian brine after 100 days.
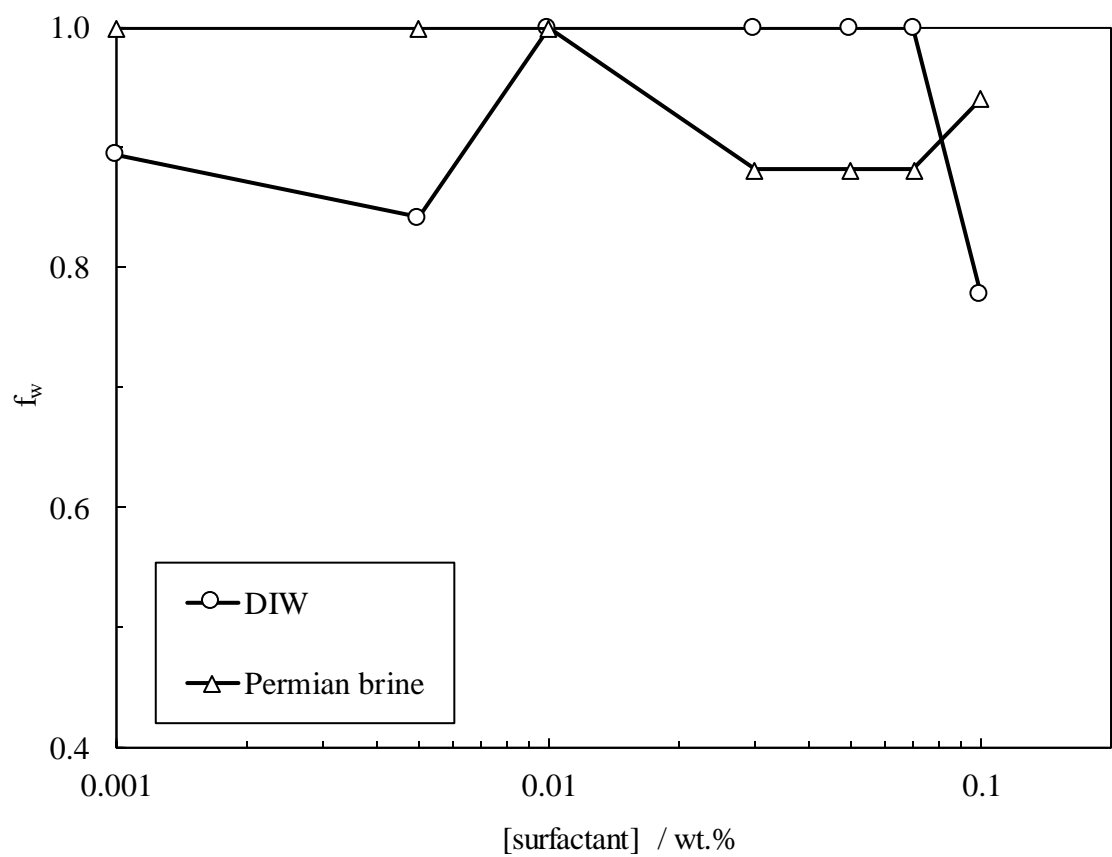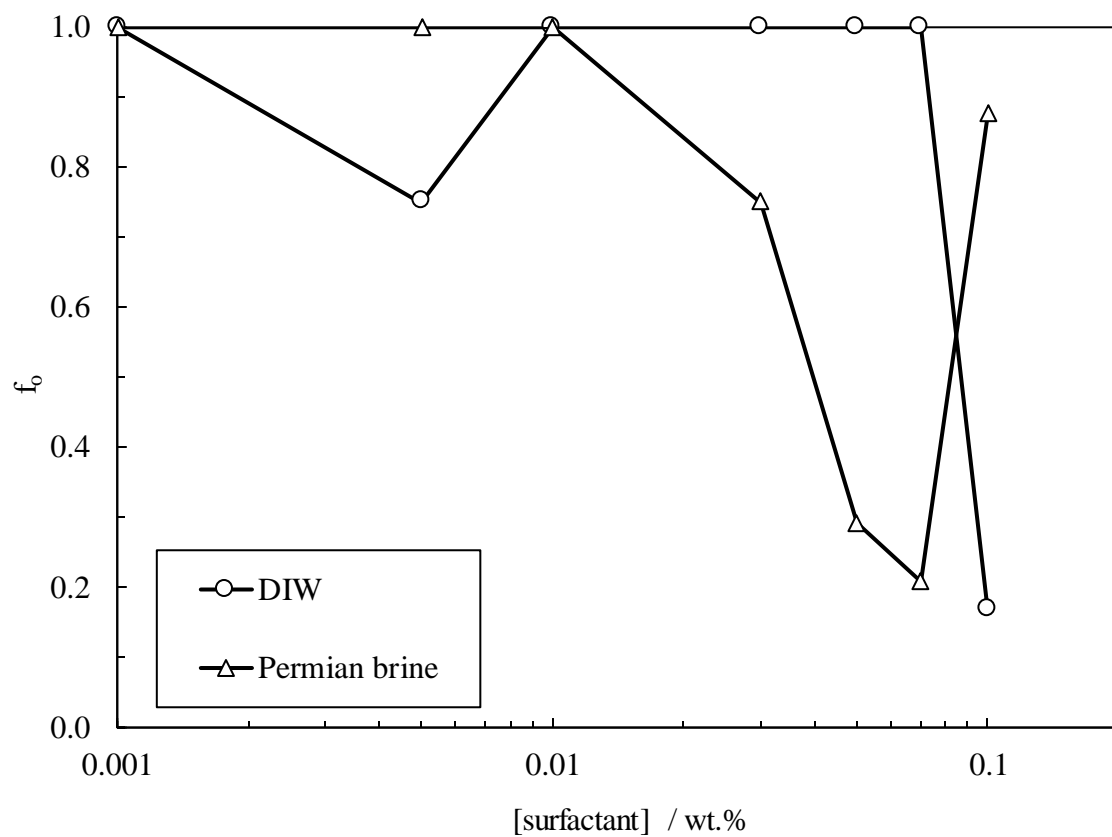
Figure 5.28. Initial emulsion drop diameter vs surfactant concentration for oil-in-water emulsions from 5 g heptol (1:1 g g^{-1}) and 5 g solutions of AHS in DIW and Permian brine.
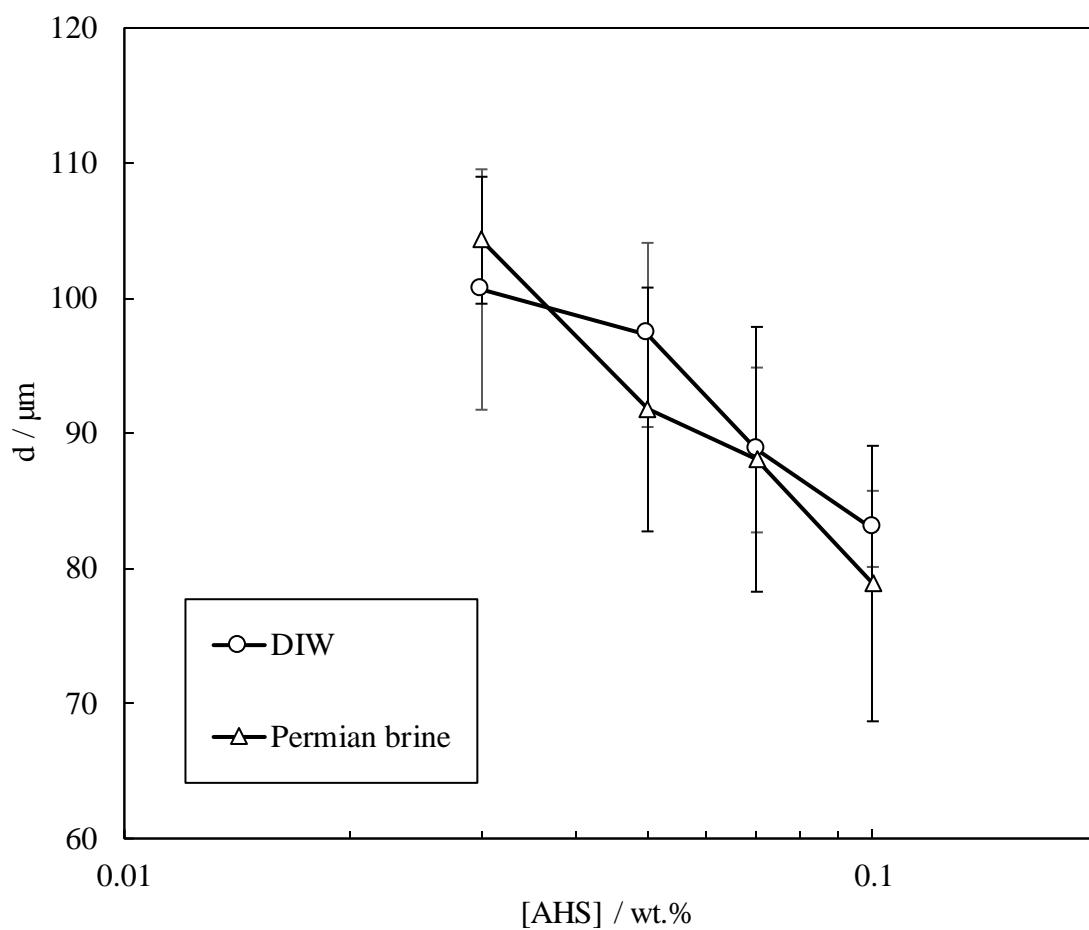
Figure 5.29. Optical microscope images taken immediately after preparation of oil-in-water emulsions from 5 g heptol (1:1 g g^{-1}) and 5 g solutions of AHS (given in wt.%) in DIW and Permian brine.
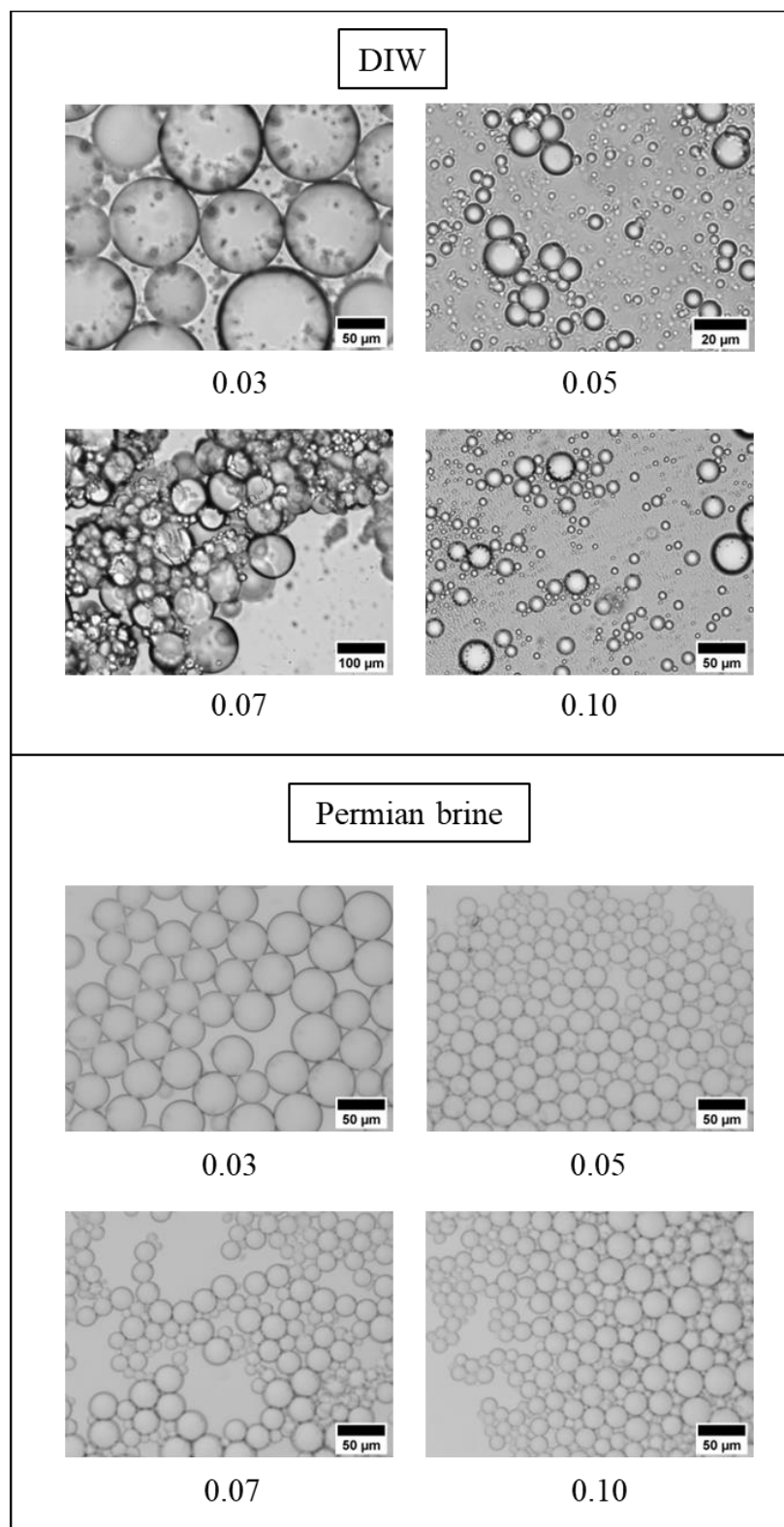
Figure 5.30. Optical microscope images taken immediately after preparation of oil-in-water emulsions from 5 g heptol (1:1 g g^{-1}) and 5 g solutions of ZN (given in wt.%) in DIW or Permian brine.
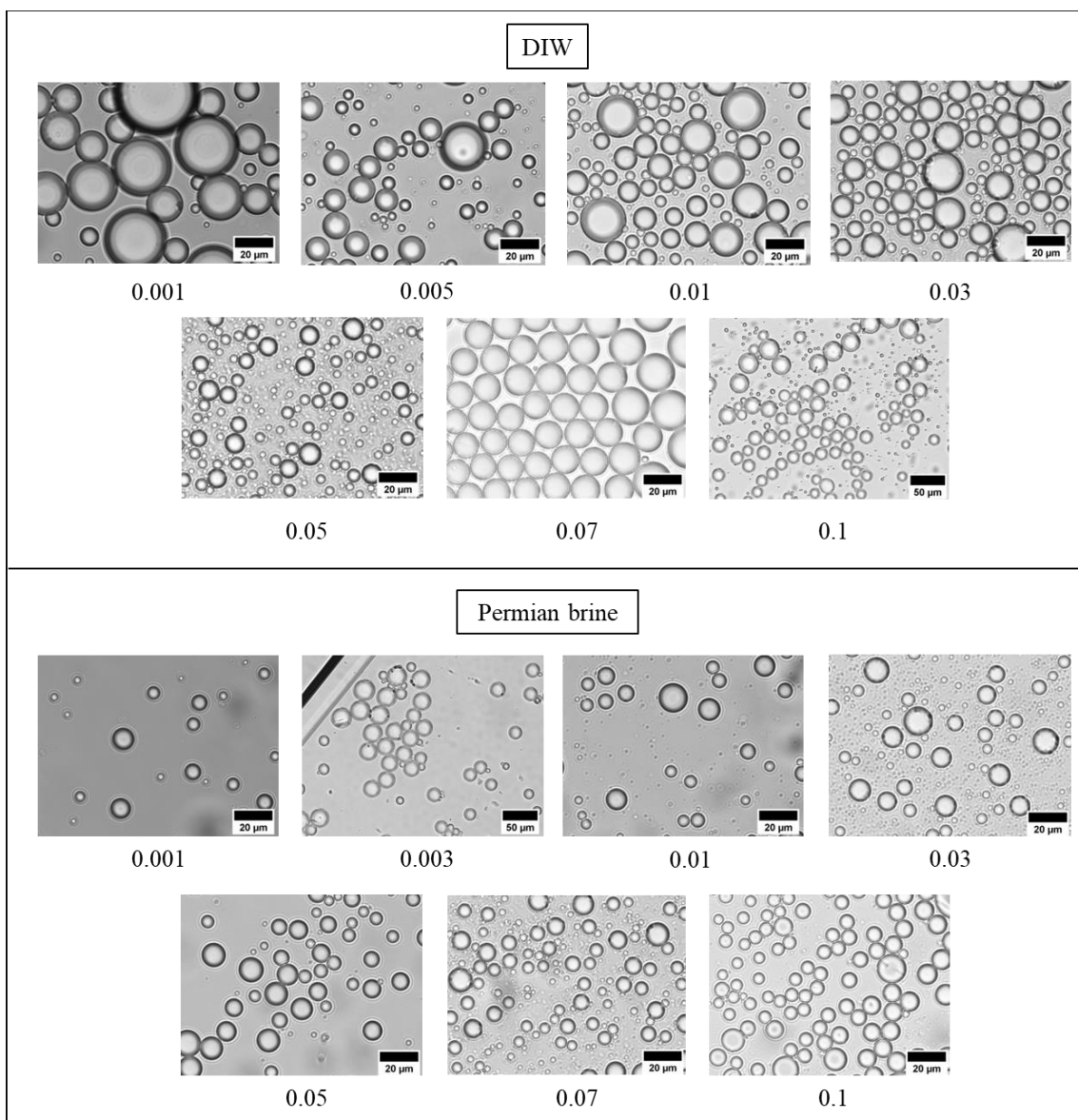
Table 5.3. Summary of results on oil-in-water emulsions from different oils and different concentrations (given in wt.%) of AHS or ZN in DIW and Permian brine (12.6 wt.%). Creaming was high in all emulsions ($f_w > 0.8$).

Surfactant	Oil	f_o after 100 days	Comments

		0.001	0.005	0.01	0.03	0.05	0.07	0.1	
AHS in DIW	Toluene	1							Interfacial charge and interfacial oil molecules at the oil-water interface decreases as follows: toluene > heptol > heptane.
	Heptane	> 0.7							
	Heptol								
AHS in Permian brine	Toluene	1			< 0.2				Ions reduce the surfactant-interface and surfactant-surfactant electrostatic repulsion and result in higher surfactant adsorption at the oil-water interface.
	Heptane								
	Heptol	> 0.7				0.2		0.9	Polar toluene is responsible for emulsification of heptol and water.
ZN in DIW	Toluene								The demulsification design of ZN prevents the long-term stability of emulsions.
	Heptane								
	Heptol								Of different oils, ZN appeared to produce more emulsions with polar toluene.
ZN in Permian brine	Toluene	1			> 0.8				
	Heptane								
	Heptol								

5.3.2 Effect of particles

This part looks into the potential of ES-coated silica particles to emulsify various oils and water. The impact of Permian brine addition on particle emulsification behaviour has also been researched. Also, a series of emulsion experiments were carried out to examine the emulsification power of silica covered with AS (see Appendix C.1).

5.3.2.1 Toluene

Figure 5.31 shows the appearance of oil-in-water emulsions formed by toluene and ES-coated silica dispersions at different times. When the particles were in DIW, raising the particle concentration significantly reduced the coalescence and creaming initially but some oil and water were resolved over time. In the long term, the stability to coalescence in these emulsions became independent of particle concentration above 0.03 wt.% (Figure 5.32). Creaming is less at intermediate particle concentrations (0.03 – 0.1 wt.%) and increases at > 0.1 wt.% which is more significant in the long term. When the particles are in Permian brine, raising the particle concentration has a small effect on reducing coalescence and creaming in the long term (Figure 5.33). High particle concentrations (1 wt.%) in Permian brine were found to destabilise the emulsions very quickly.

Epoxide ring-opening is a chemical process that ES goes through when it is acid- or base-catalysed during which the epoxy group opens to produce two linear hydroxyl groups (–OH). The resultant polar molecule, 3-hydroxyalkyl trimethoxysilane, is covalently grafted on silica particles with the hydroxyl groups on the surface of the particles. Thus, the silane-coated particles used here are polar which allows them to interact with water and other polar solvents through hydrogen bonding and dipole-dipole interactions. This also gives the particles hydrophilicity which leads to longer dispersion stability in polar fluids.[273] Without taking into account the inherent particle hydrophobicity by silane, oil type can have two main effects on the adsorption of particles at an oil-water interface: interfacial oil molecules and interfacial charge. When particles are in DIW, for a sufficient interaction of particles with oil molecules, the particles must approach the interface which is greatly prevented by the electrostatic repulsion between anionic particles and the anionic interface. This is more serious at low particle concentrations and has produced unstable emulsions here. Yet, at high particle concentrations (1 wt.%) where the particles are electrostatically repelled in bulk to approach the oil-water interface, solvophobic interactions between polar particles and low interfacial non-polar heptane molecules can render particles hydrophobic and capable of adsorbing at the oil-water interface and creating Pickering emulsions.[240, 241, 272] Binks and Whitby stated that increasing the polarity of the oil phase makes the polar solvent molecules adsorb to the silica surface, which further alters the particle wettability and improves emulsion stability.[28] This explains the higher emulsification of toluene and particles in DIW (< 1 wt.%) compared to heptane.

The ability to adsorb ions at the oil-water interface is greater for toluene due to its thicker electrical double layer and larger interfacial charge density. The ion adsorption at the

heptane-water interface is lowest while that of heptol lies between toluene and heptane. Ion accumulations at the oil-water interface prevent the adsorption of like-charged particles.[274]

Previous studies show that brine can create an aggregated network of particles in the emulsion's continuous phase to physically stabilize the emulsions by trapping the droplets.[275] Griffith and Daigle investigated the effect of the same particles with two silane coverages (23% and 32%) on the stability and rheology of bromohexadecane-in-water emulsions. They observed that 1 wt.% of weakly aggregated ES-coated silica (23% silane coverage) in 1 wt.% $CaCl_2$ at high pH (9 – 10) can stabilize the emulsions by forming a bridged network of particles while more stable ES-coated silica particles (32%) stabilize the emulsions only at low pH (~ 3) where particles are weakly charged and can be aggregated.[145] The particles used in this study had higher silane coverage (55%) and they were shown to be sterically (by silane) and electrostatically (by particle charge) stable for a long time (refer to stability inspections in Chapter 3). Since original pH dispersions were used here (pH 7 – 10), the particles were moderately to highly charged so both mechanisms are absent (no improvement in emulsification on adding Permian brine to dispersions). Salts can shrink the electrical double layer of the particles and the oil-water interface and lower their charges.[267] While this improves the hydrophobicity of particles to form a dense monolayer at the oil-water interface and stabilize emulsions,[275, 276] it decreases the polarity of toluene and thereby the adsorption of toluene molecules at the oil-water interface which subsequently reduces the interactions between particles and oil molecules at the interface.[241] The salt ions also compete with the solid particles for adsorption at the oil-water interface. High accumulations of ions at the oil-water interface can lessen the adsorption of particles, causing oil droplets to coalesce and eventually phase separate.[275]

Figure 5.34 shows the initial and long-term emulsion drop diameters with particle concentration in DIW and Permian brine. Consistent with visual observations, the plot shows that emulsions with particles in Permian brine have a bigger diameter compared to that of DIW. The emulsion drop diameter is almost unchanged on raising the particle concentration in DIW both in the short and long term but slightly increases with an increase in particle loading in Permian brine. Furthermore, there is a rise in emulsion drop diameter for the emulsions of particles in DIW after 100 days implying oil drop growth and coalescence in the emulsion which is consistent with visual observations. No significant change is observed in the drop diameters of the emulsions made with particles in Permian brine. Figure 5.35 shows the initial microscopy of these emulsions. The drop

shapes are all spherical with more compact, hexagonally arranged smaller droplets in the emulsions formed by 1 wt.% particles in DIW. As observed, the emulsion droplets become significantly bigger when the particles are in Permian brine.

Figure 5.31. Appearance of oil-in-water emulsions from 5 g toluene and 5 g dispersions of ES-coated silica (given in wt.%) in DIW and Permian brine.

258

Figure 5.32. Effect of particle concentration on the fractions of oil (upper) and water (lower) resolved from oil-in-water emulsions from 5 g toluene and 5 g dispersions of ES-coated silica in DIW.

259

Figure 5.33. Effect of particle concentration on the fractions of oil and water resolved from oil-in-water emulsions from 5 g toluene and 5 g dispersions of ES-coated silica in Permian brine.

Figure 5.34. Initial and long-term emulsion drop diameter with particle concentration for oil-in-water emulsions from 5 g toluene and 5 g dispersions of ES-coated silica in DIW or Permian brine.

Figure 5.35. Optical microscope images taken immediately after preparation of oil-in-water emulsions from 5 g toluene and 5 g dispersions of ES-coated silica (given in wt.%) in DIW or Permian brine.

DIW

0.01   0.03   0.05

0.07   0.10   1.00

Permian brine

0.07   0.10
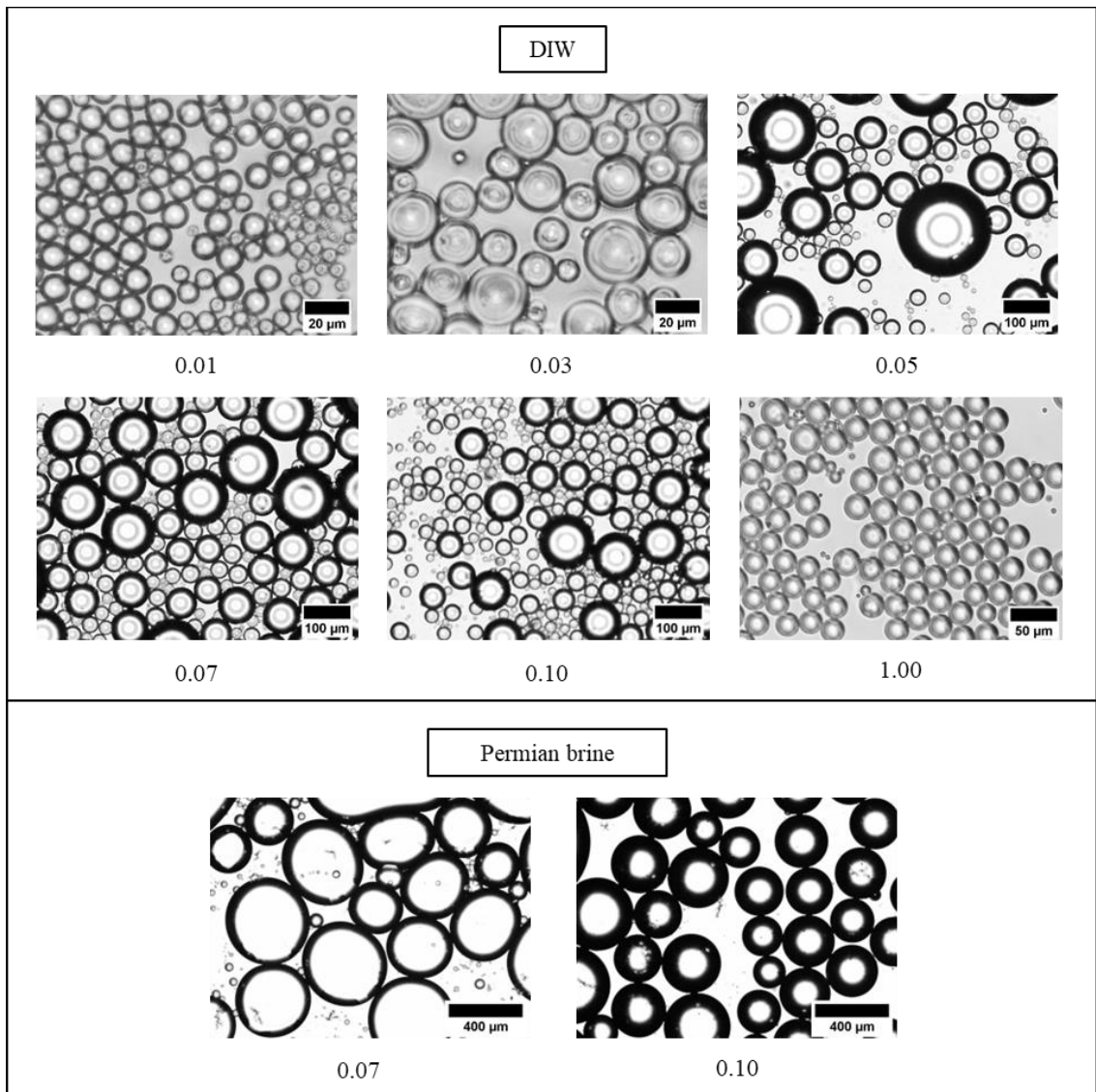
5.3.2.2   Heptane

Figure 5.36 shows the appearance of the oil-in-water emulsions produced by heptane and ES-coated silica dispersions. The ES-coated silica particles used here have low surface activity at the oil-water interface due to the high silane coverage. There is also electrostatic repulsion between the anionic particles and the anionic oil-water interface which prevents high adsorption of particles at the interface. Heptane also has a weak interfacial molecular activity for interactions with particles.[241] Therefore, low particle loading (< 0.1 wt.%) is not expected to create stable Pickering emulsions. However, increasing the particle concentration to 1 wt.% is thought to increase the bulk particle-particle electrostatic repulsion and encourage more particle adsorption at the oil-water interface.[78] This is consistent with the stable emulsion with no initial coalescence and creaming which is observed at the highest particle loading (1 wt.%). The fractions of oil and water resolved from this emulsion after 400 days were 0.65 and 0.8, respectively (Figure 5.37).

In emulsions made with particles in Permian brine, increasing particle concentration was found to increase the emulsification of heptane and DIW after preparation but the emulsions were destabilized after a day. Permian brine screens the particle and oil-water interface charges. The emulsion with 0.1 wt.% particles in Permian brine showed coalescence and creaming after a day and more in the long term ($f_o = 0.6$ and $f_w = 0.8$ after 400 days). Higher particle loadings (1 wt.%) formed unstable emulsions (Figure 5.38). Figures 5.39 and 5.40 show the initial drop diameter measurements and microscopy of these emulsions. A lower drop diameter with the addition of Permian brine to dispersions is observed.

Figure 5.36. Appearance of oil-in-water emulsions from 5 g heptane and 5 g dispersions of ES-coated silica (given in wt.%) in DIW and Permian brine.

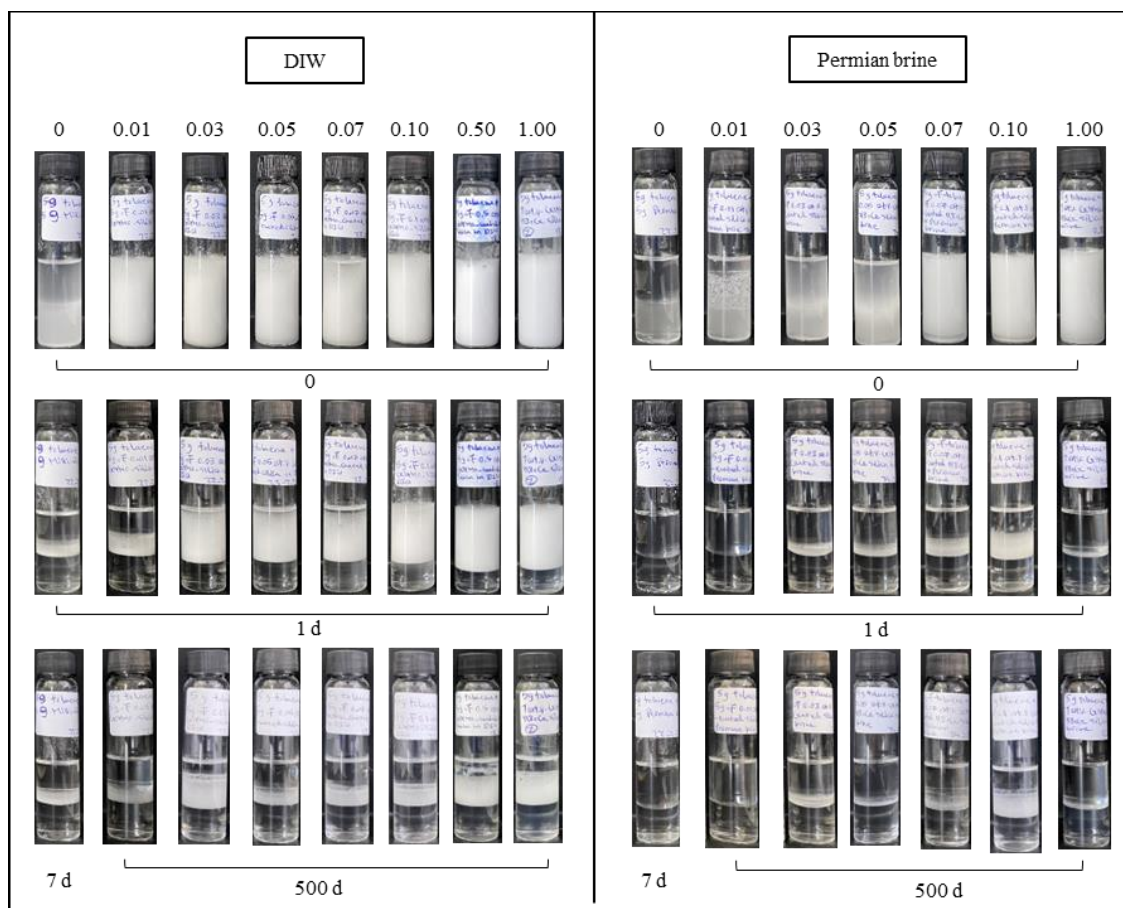**Figure 5.37.** Effect of particle concentration on the fractions of oil (upper) and water (lower) resolved from oil-in-water emulsions from 5 g heptane and 5 g dispersions of ES-coated silica in DIW.
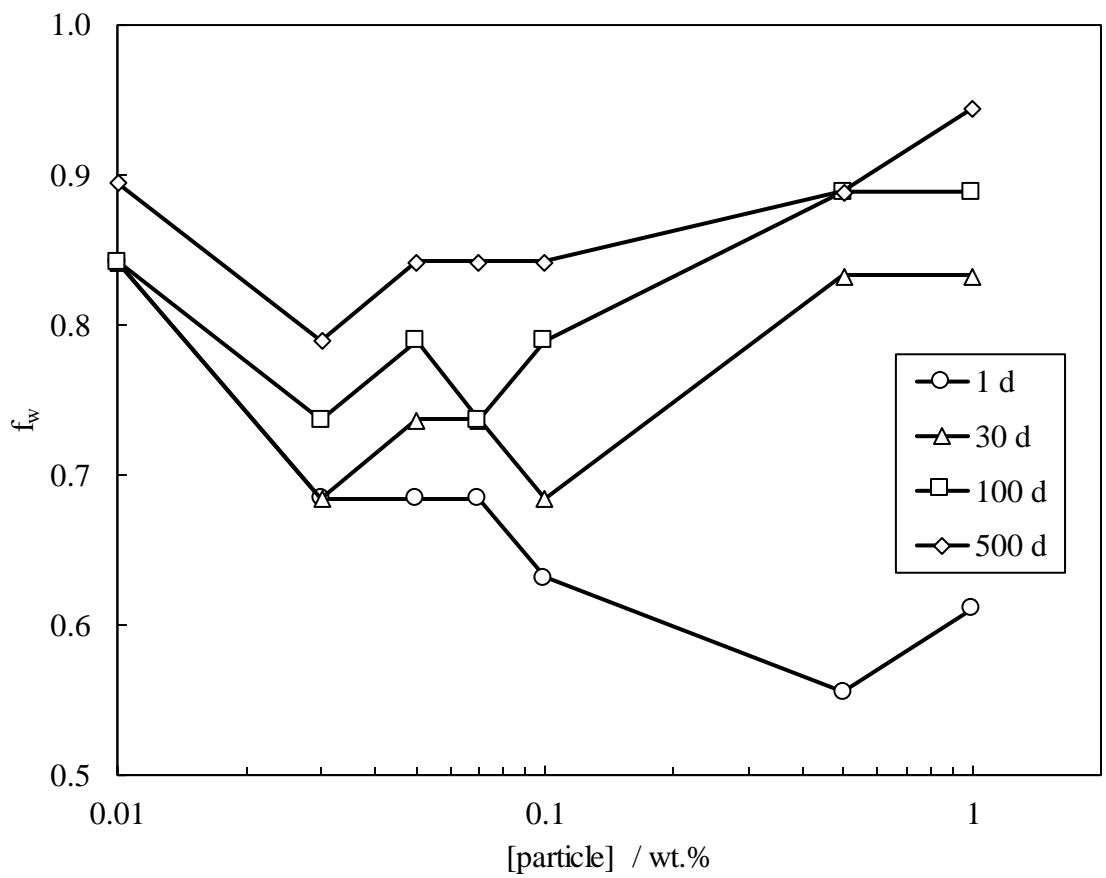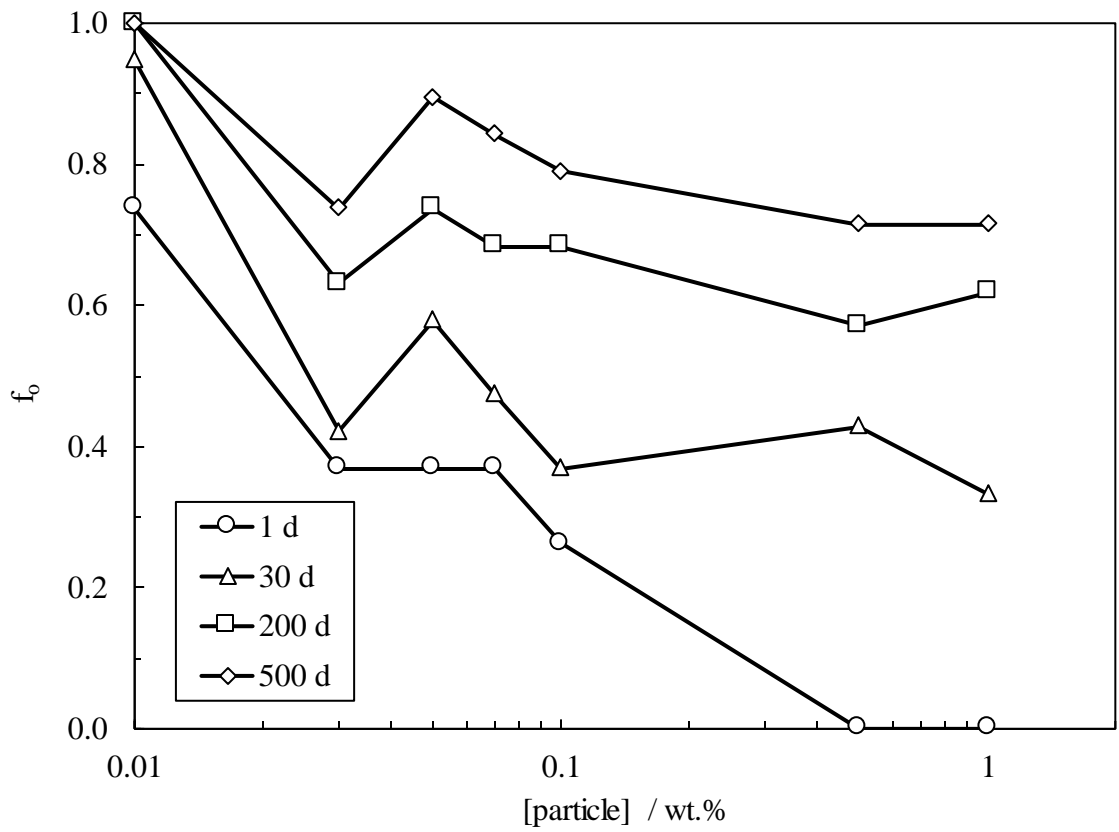
Figure 5.38. Effect of particle concentration on the fractions of oil (upper) and water (lower) resolved from oil-in-water emulsions from 5 g heptane and 5 g dispersions of ES-coated silica in Permian brine.
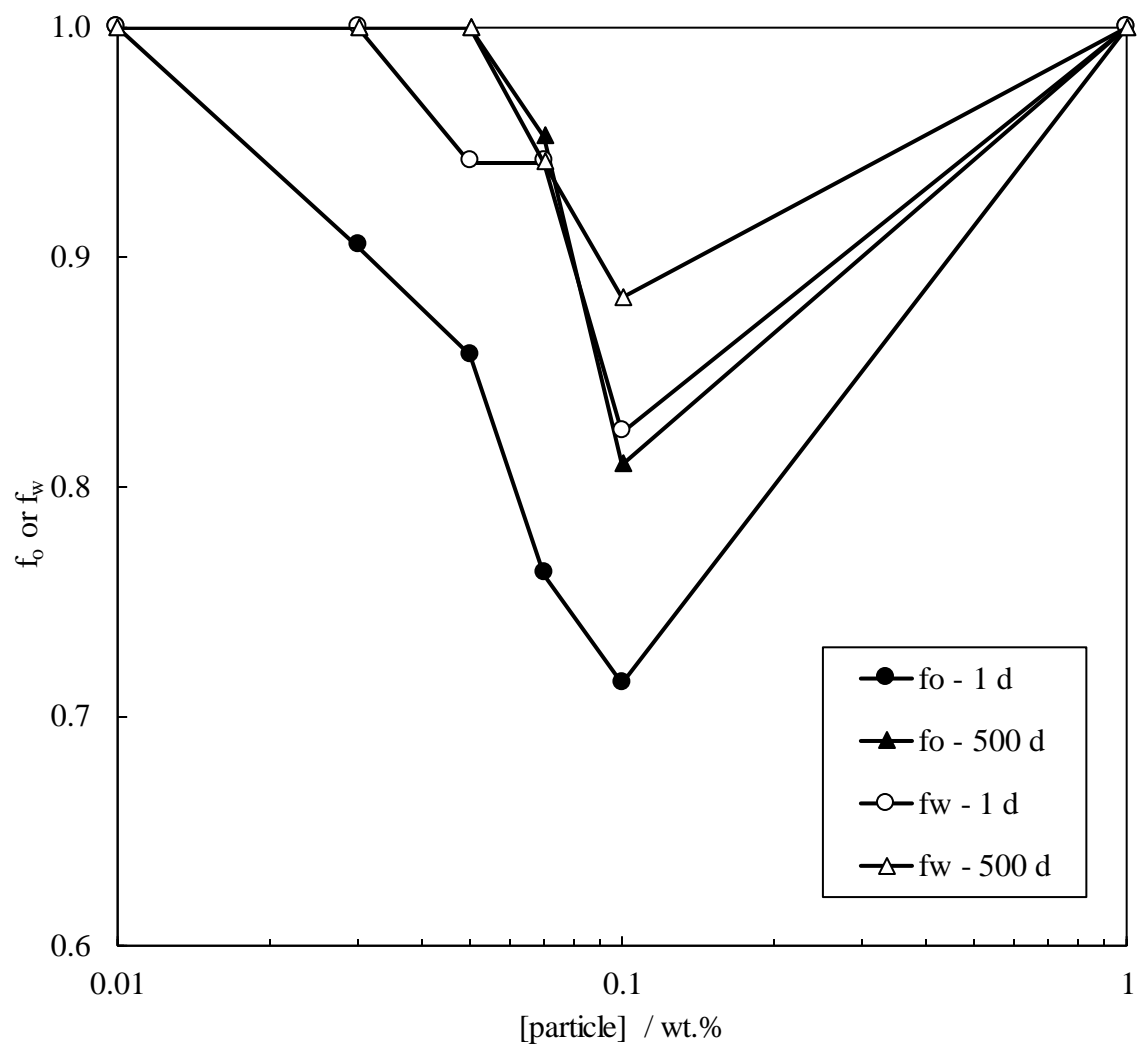
266
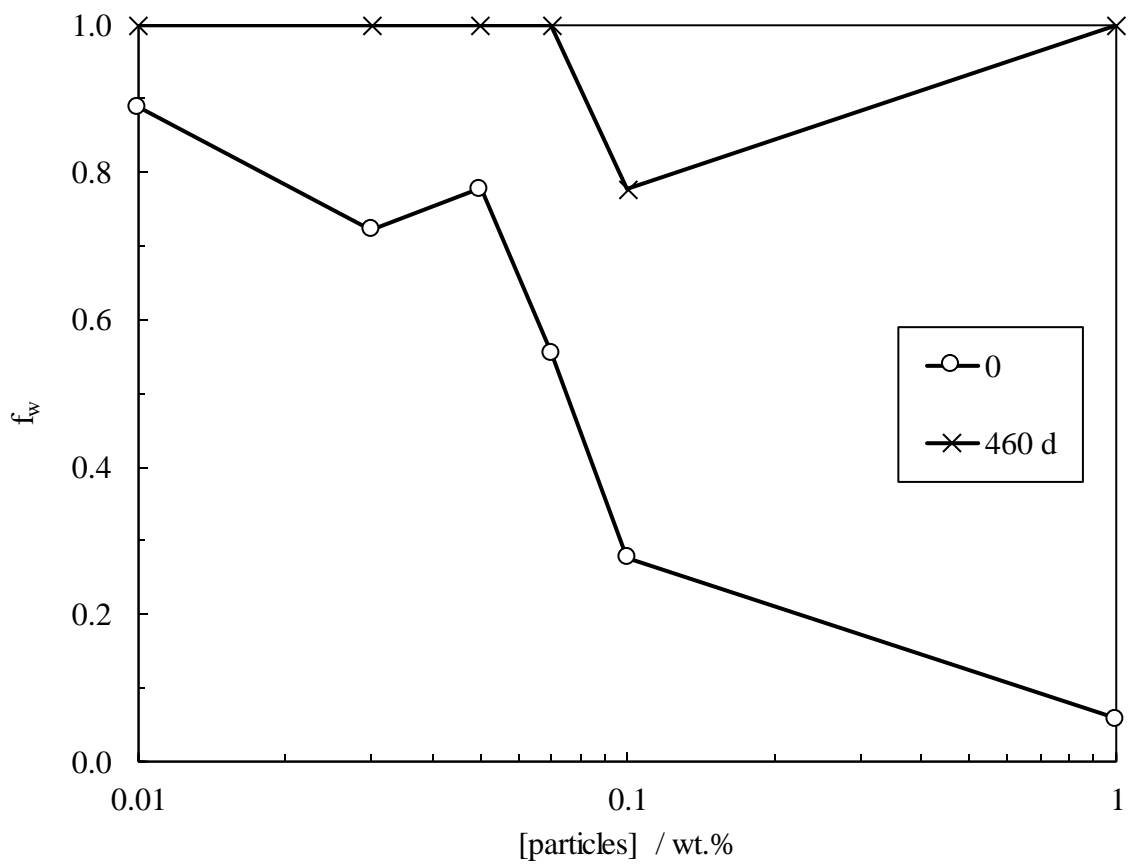
Figure 5.39. Initial emulsion drop diameter vs particle concentration for oil-in-water emulsions from 5 g heptane and 5 g dispersions of ES-coated silica in DIW or Permian brine.
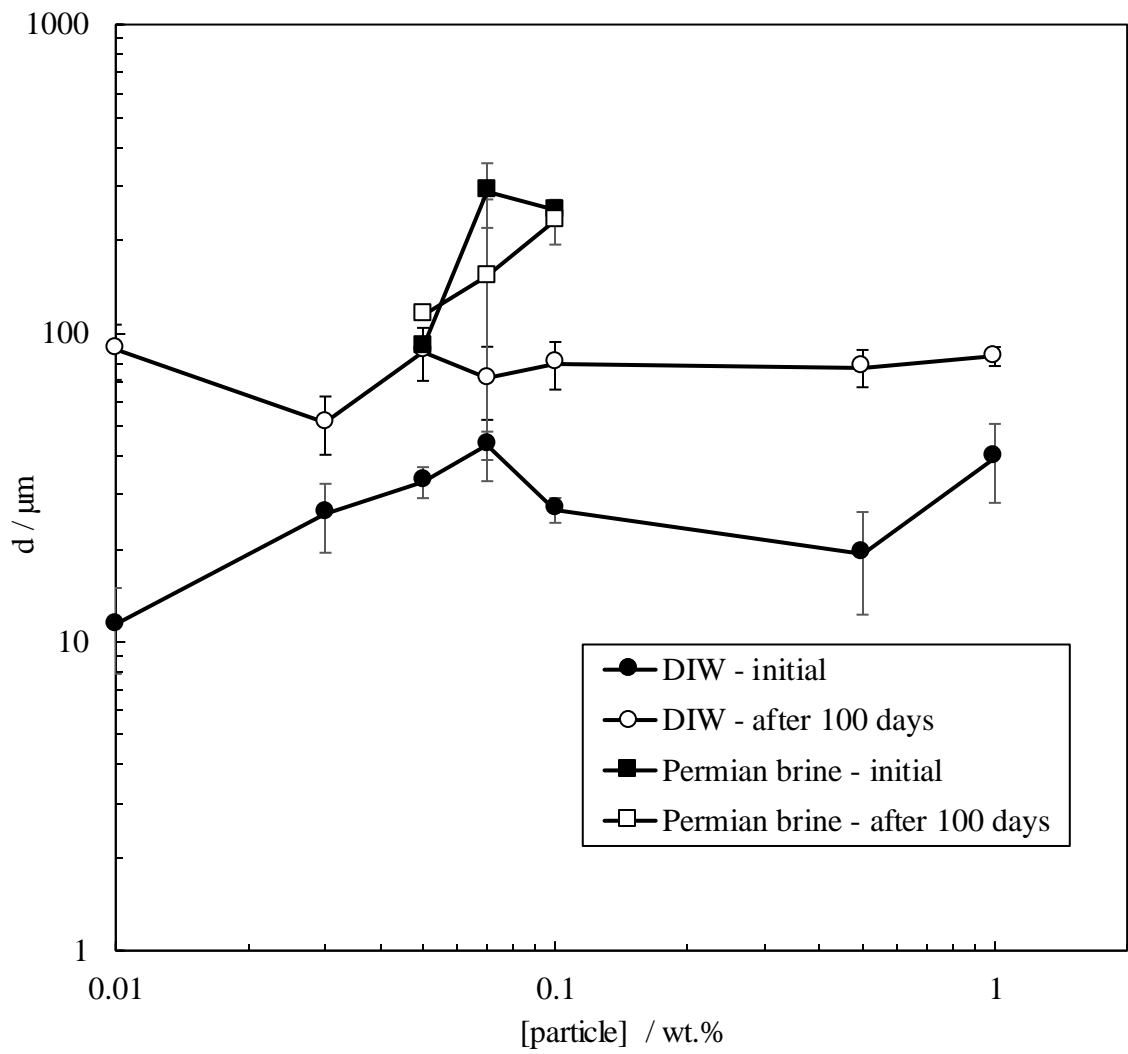
Figure 5.40. Optical microscope images taken immediately after preparation of oil-in-water emulsions from 5 g heptane and 5 g dispersions of ES-coated silica (given in wt.%) in DIW or Permian brine.

DIW

0.01   0.03   0.05

0.07   0.10   1.00

Permian brine

0.03   0.05

0.07   0.10

5.3.2.3 Heptol

269
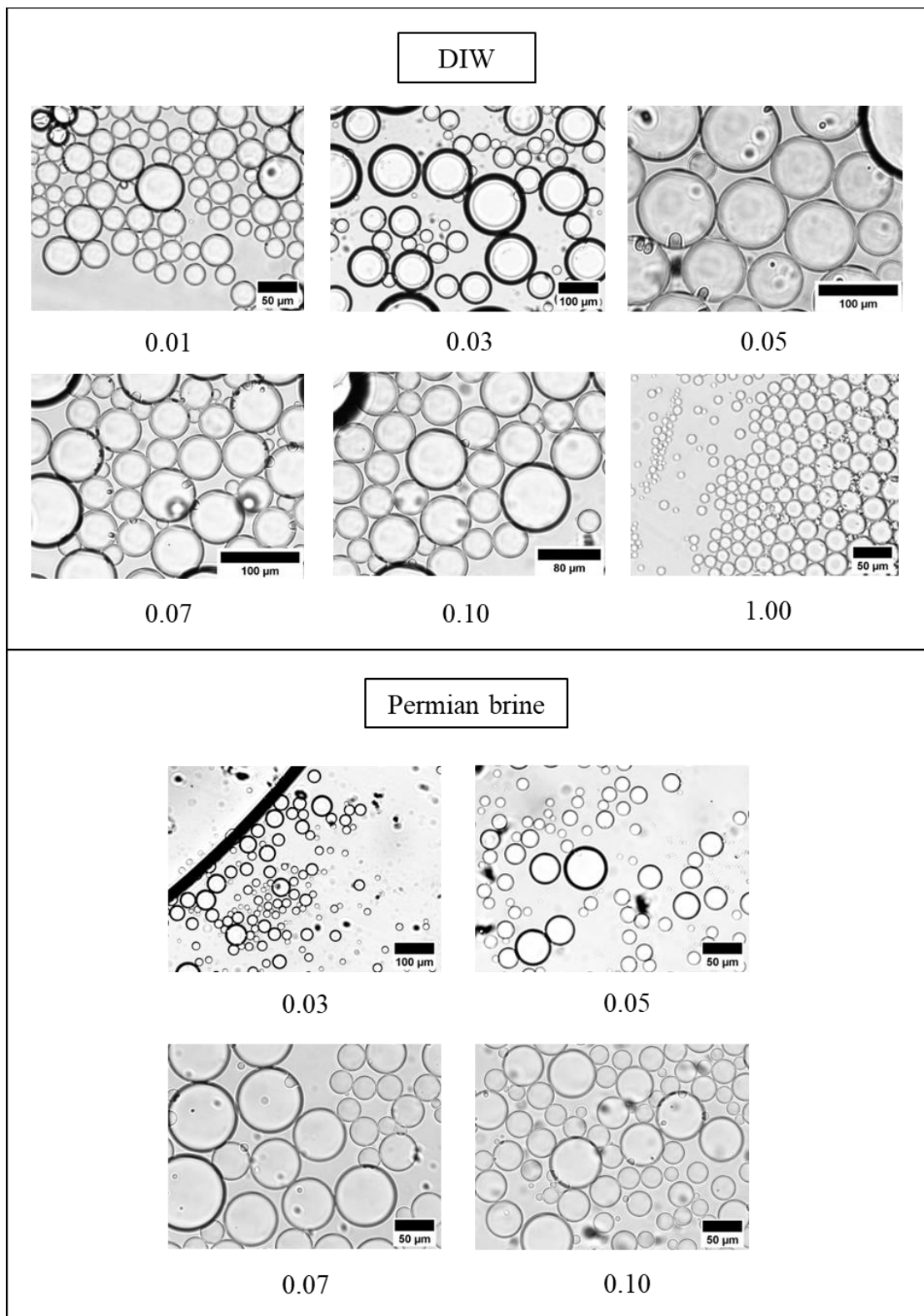
Figure 5.41 shows the appearance of emulsions formed by heptol (1:1 g g^{-1}) and ES-coated silica dispersions. Particles are more hydrophobic in a polar oil (toluene)-water system than in a non-polar oil (heptane)-water system, offering a higher rate of particle adsorption at the oil-water interface in the former. In addition, heptol provides local high interfacial oil molecules at its toluene-water interface and low interfacial charge at its heptane-water interface which leads to synergy in emulsification.[241] At 1 wt.% particles in DIW where heptane begins to hold solvophobic interactions with particles, heptol takes advantage of both hydrophobization mechanisms, *i.e.* polar-polar and polar-nonpolar interactions between particles and oils including toluene and heptane respectively, to create more emulsions. The emulsion made with 1 wt.% particles in DIW had slight coalescence in the long term, lower than that of heptane. The fractions of oil and water resolved from this emulsion after 400 days were 0.2 and 0.5, respectively (Figure 5.42). Like heptane, all emulsions formed by particle loadings below 1 wt.% in DIW experienced significant coalescence and creaming within a day.

When particles were in Permian brine, the emulsions experienced a quick phase separation within a day except for 0.1 wt.% particles in Permian brine which had slight coalescence in the long term. The coalescence in this emulsion was lower than that of heptane. The fractions of oil and water resolved for this stable emulsion after 440 days were 0.2 and 0.7, respectively (Figure 5.43). The effect of Permian brine on the emulsification of heptol and dispersions is thought to be the sum of its effects on individual oil-water systems. The same mechanisms already explained apply here.

Figures 5.44 and 5.45 show the initial drop diameters and microscopy of these emulsions. A decrease and an increase in the initial drop diameter with increasing particle loading in DIW and Permian brine, respectively are observed. The emulsion formed by 1 wt.% particles in DIW had a drop diameter of 42 ± 2 µm after 100 days (nearly twice the initial drop diameter of 21 ± 6 µm) while that of 0.1 wt.% particles in Permian brine was 72 ± 2 µm (20 µm higher than the initial drop diameter).

Table 5.4 summarizes all results on emulsions made from different oils and ES-coated silica.

Figure 5.41. Appearance of oil-in-water emulsions from 5 g heptol (1:1 g g^{-1}) and 5 g dispersions of ES-coated silica (given in wt.%) in DIW and Permian brine.
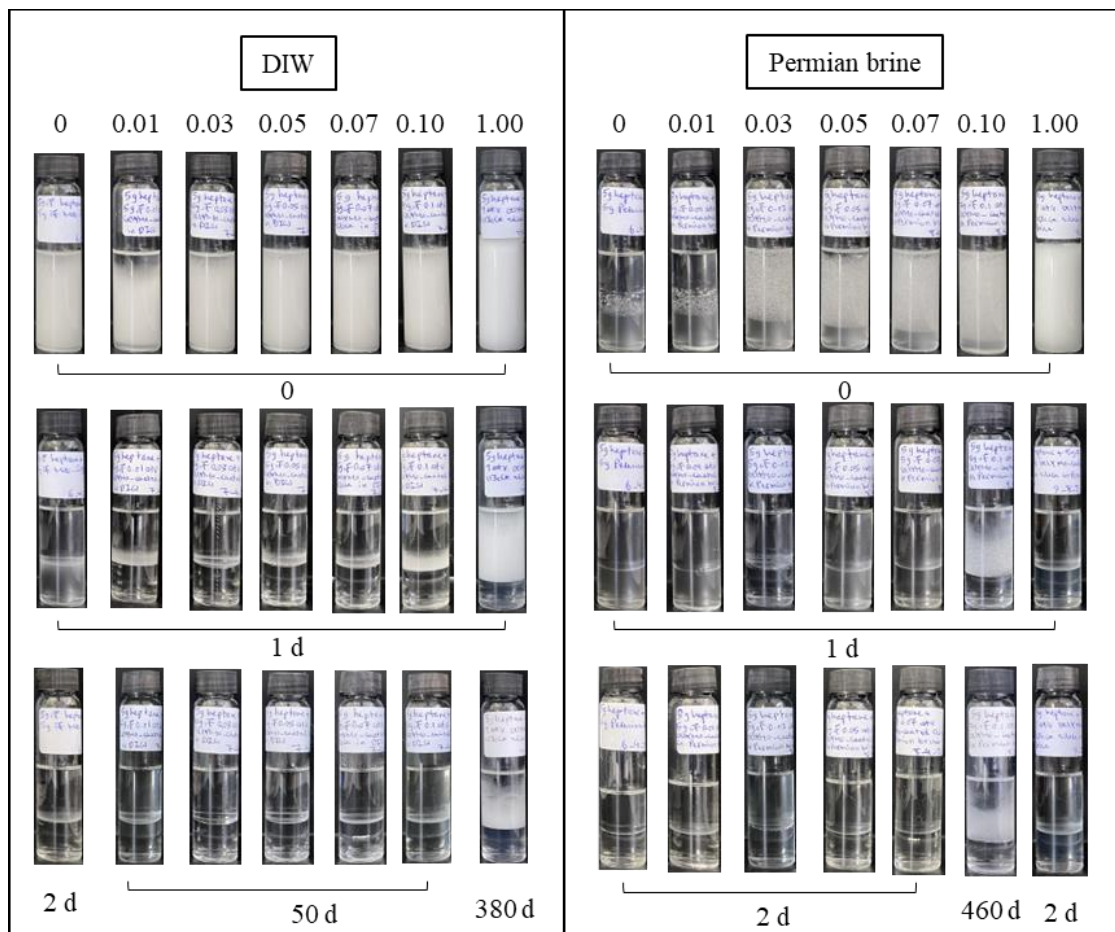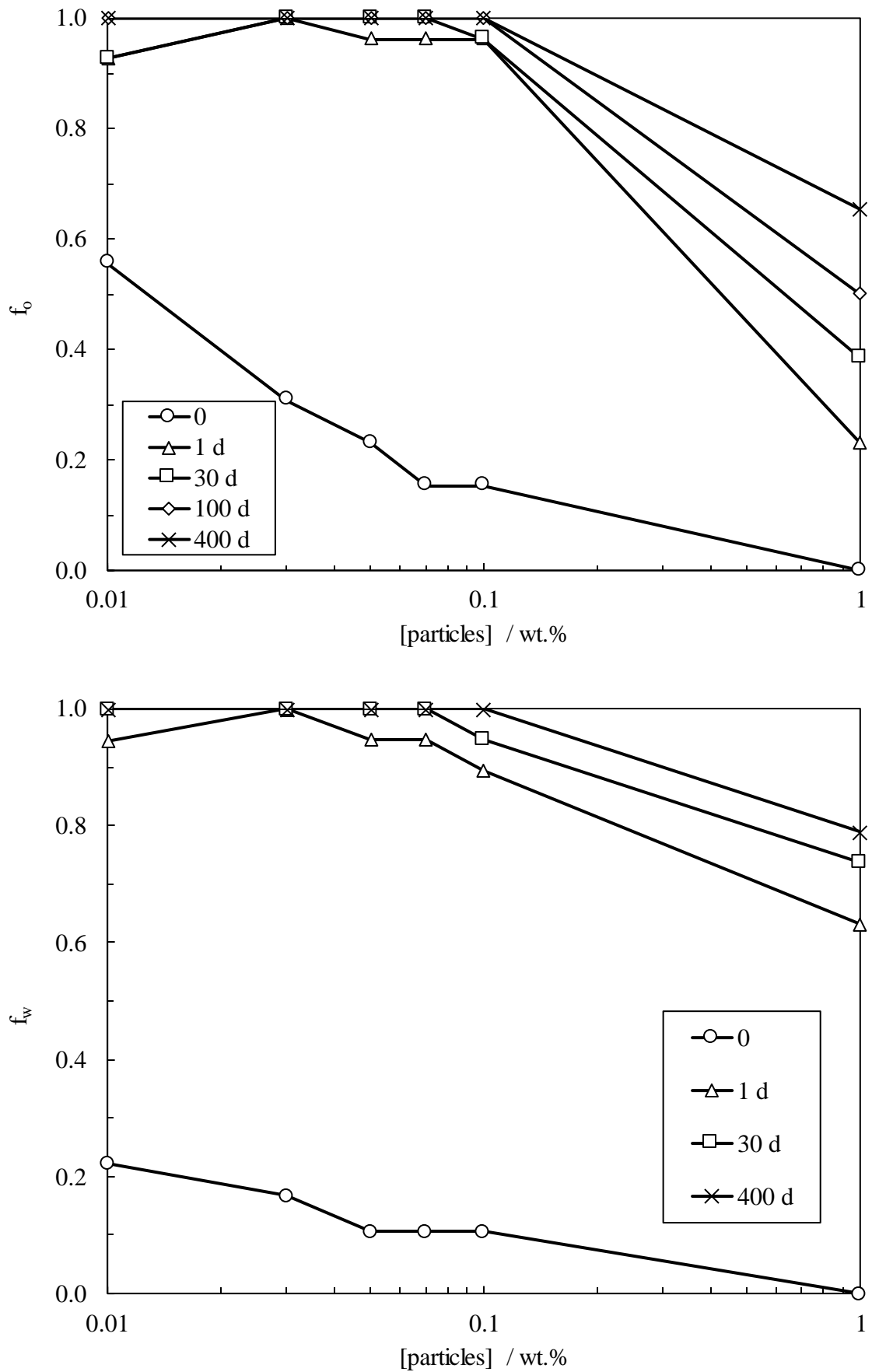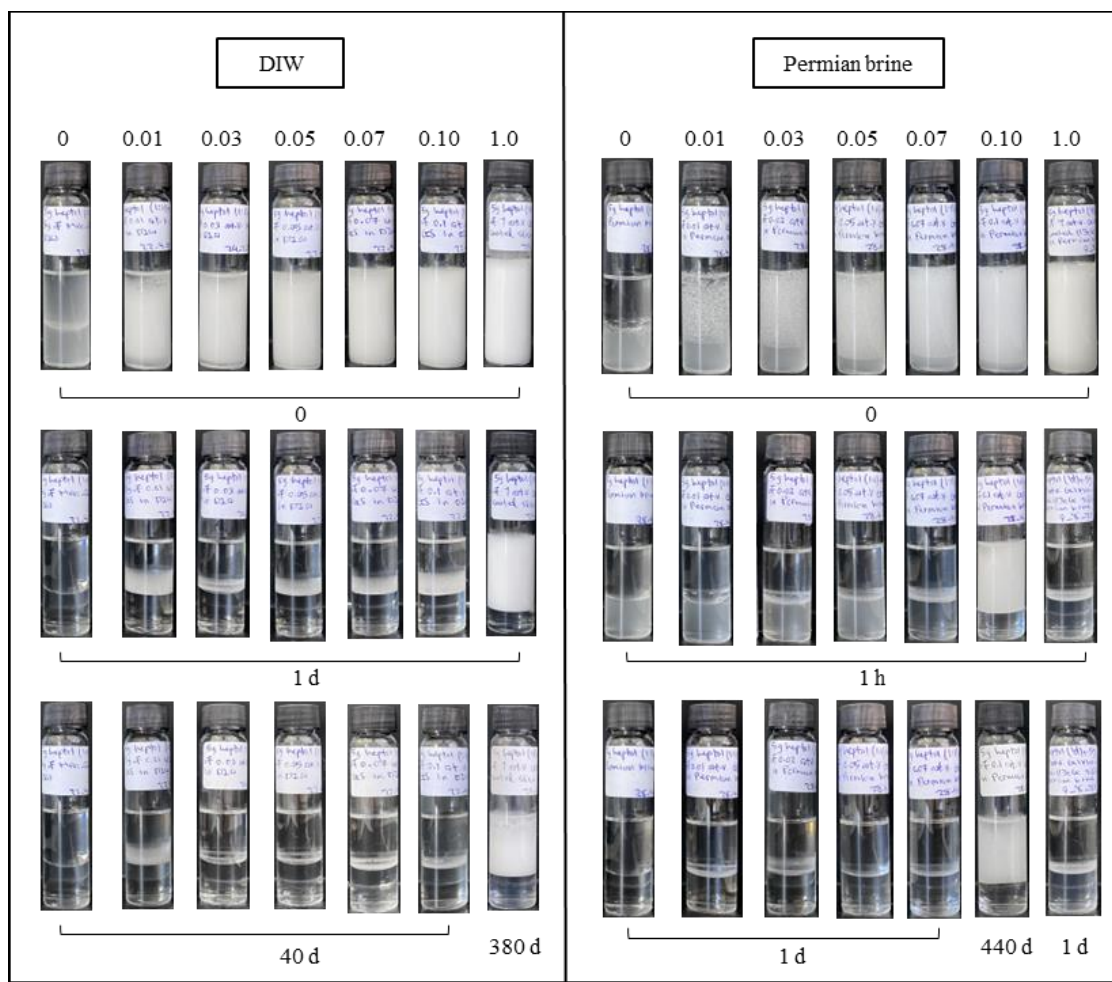
Figure 5.42. Effect of particle concentration on the fractions of oil (upper) and water (lower) resolved from oil-in-water emulsions from 5 g heptol (1:1 g g^{-1}) and 5 g dispersions of ES-coated silica in DIW.

271
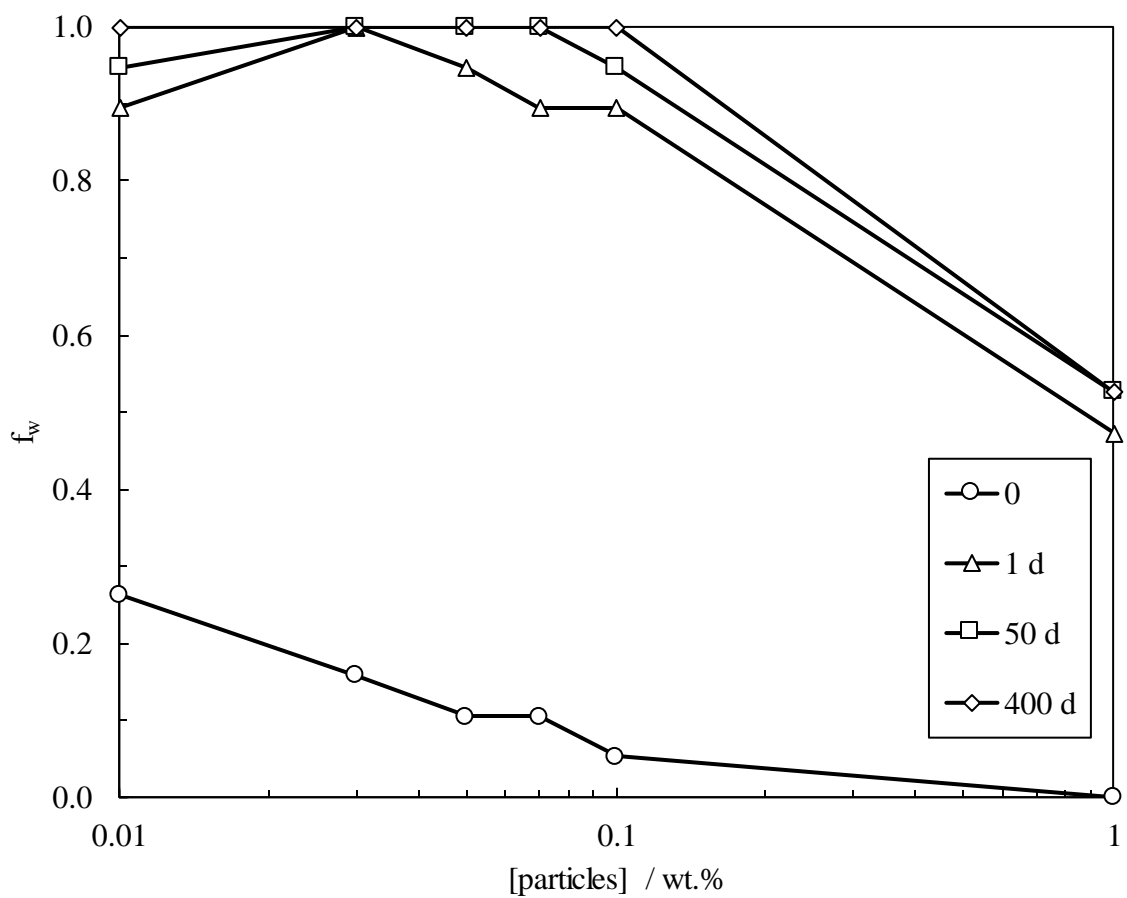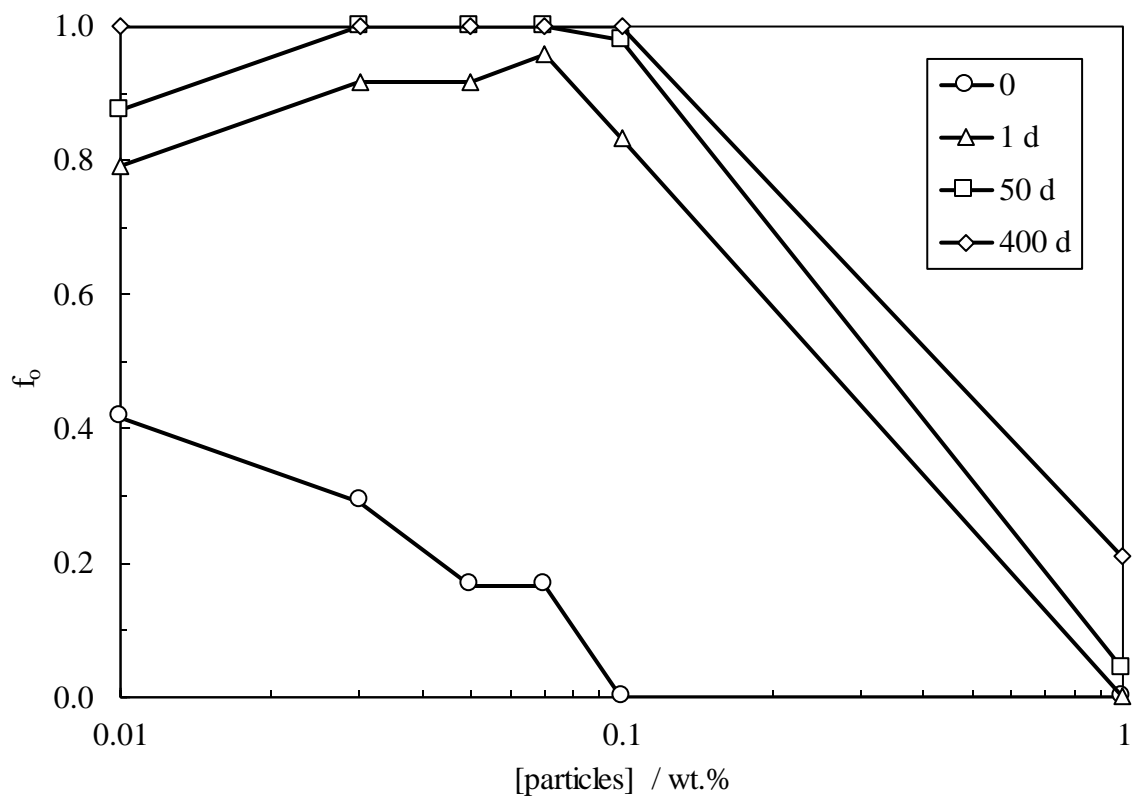
Figure 5.43. Effect of particle concentration on the fractions of oil (upper) and water (lower) resolved from oil-in-water emulsions from 5 g heptol (1:1 g g^{-1}) and 5 g dispersions of ES-coated silica in Permian brine.
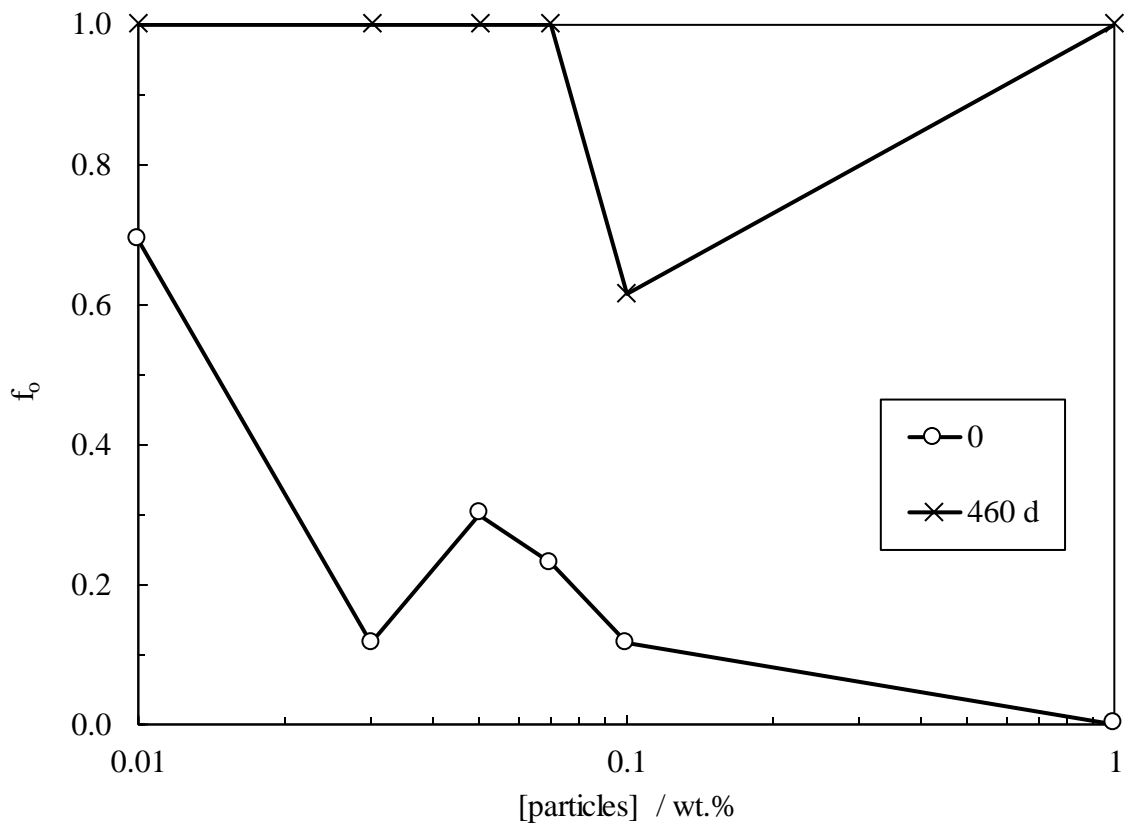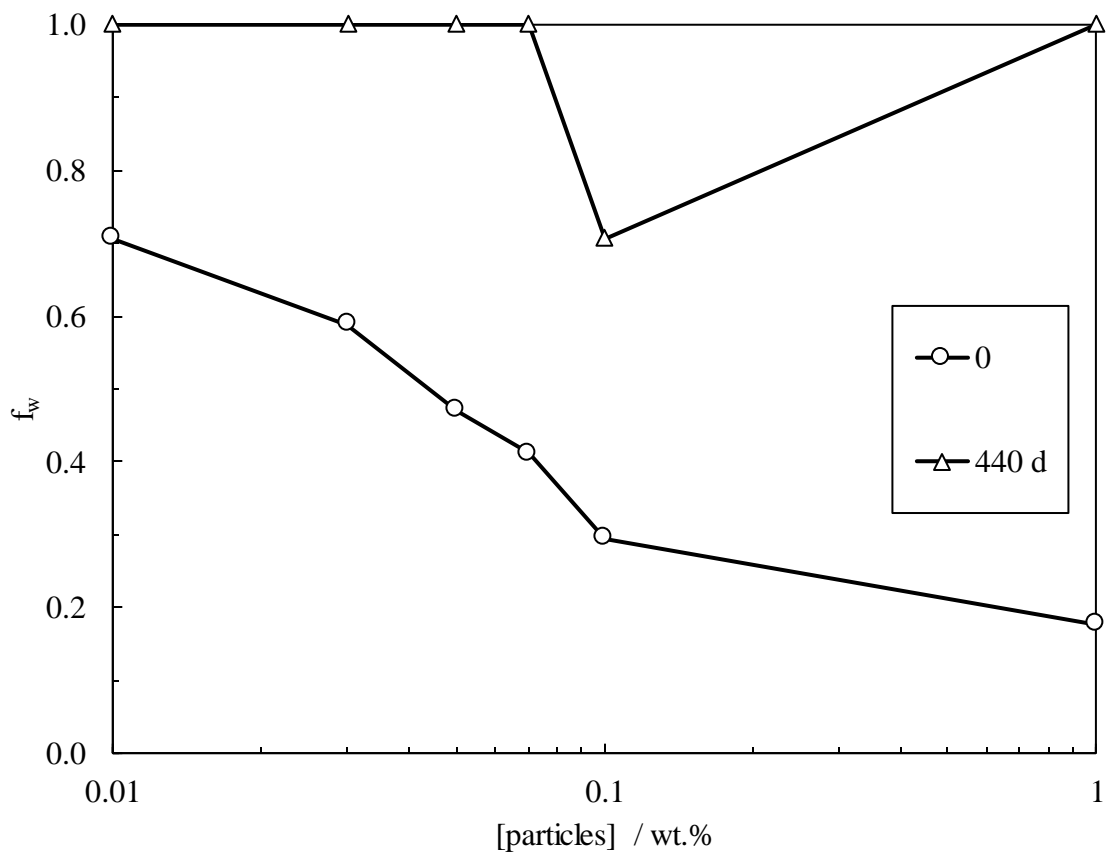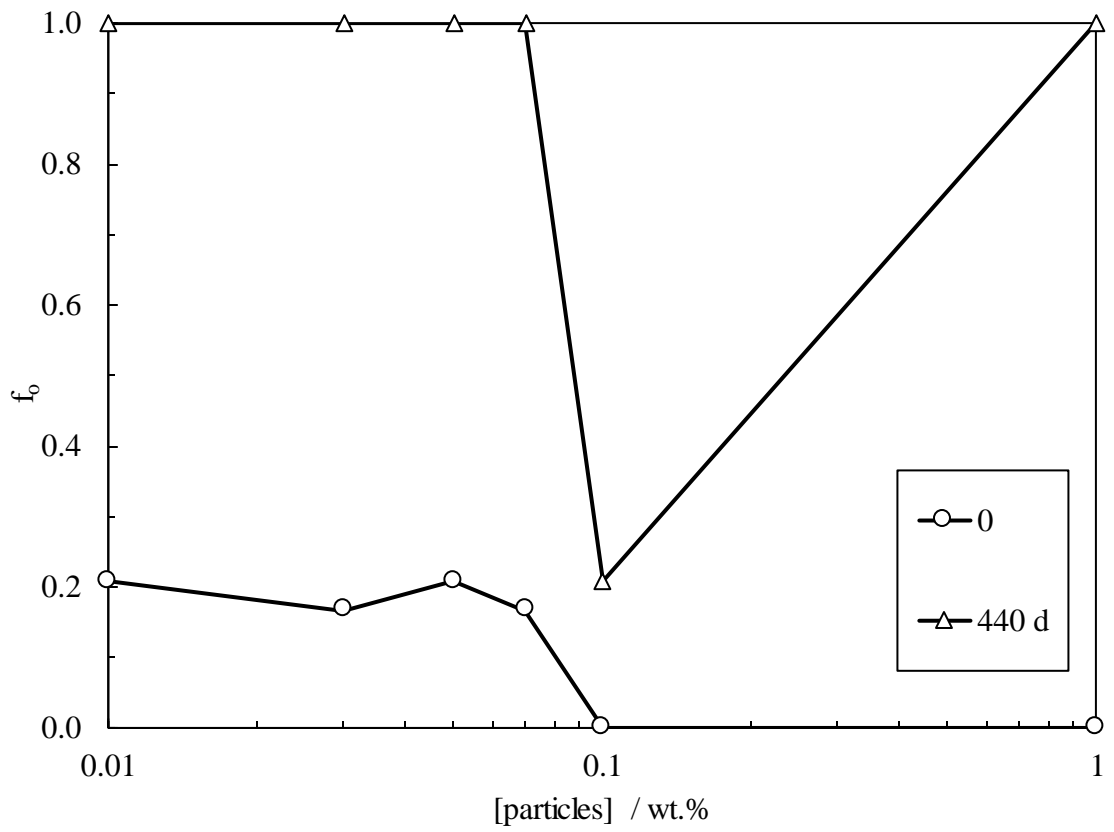
Figure 5.44. Initial emulsion drop diameter vs particle concentration for oil-in-water emulsions from 5 g heptol (1:1 g g^{-1}) and 5 g dispersions of ES-coated silica in DIW or Permian brine.
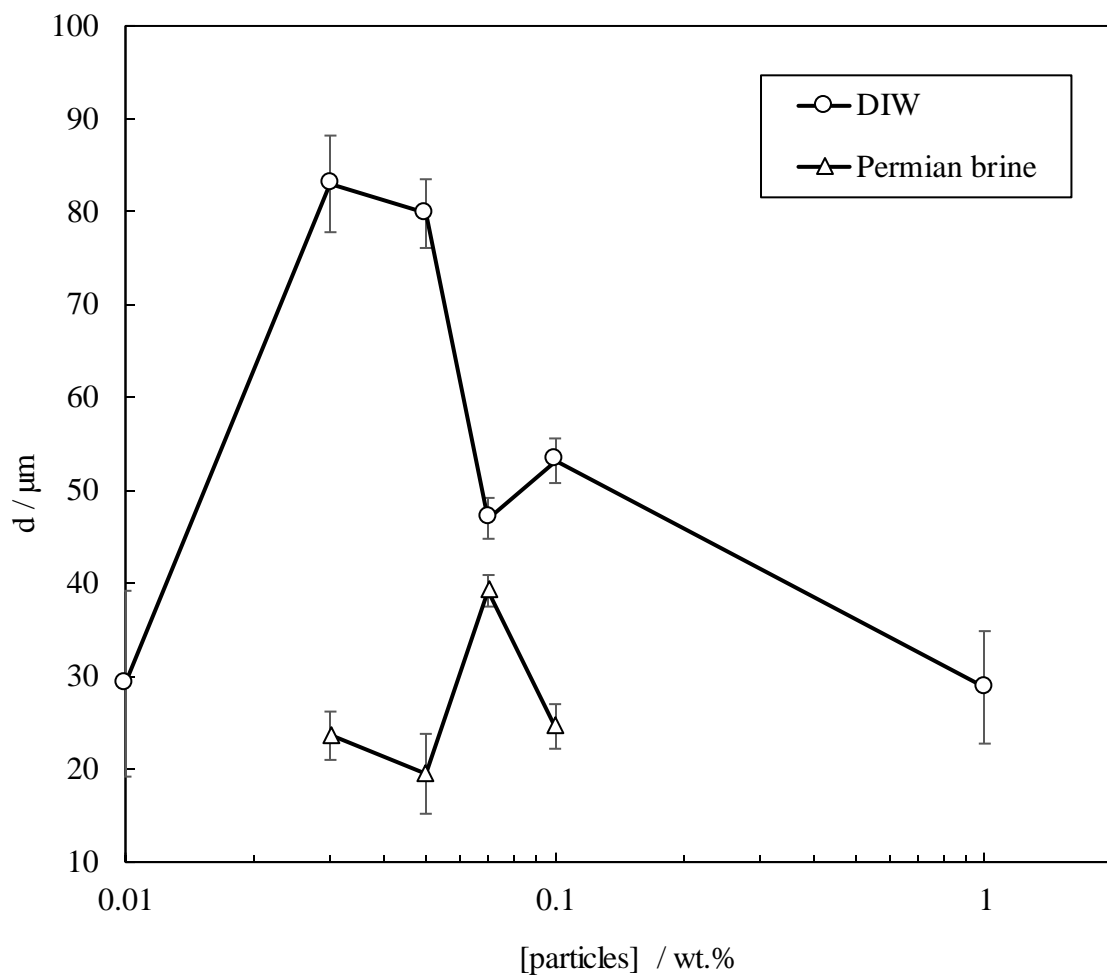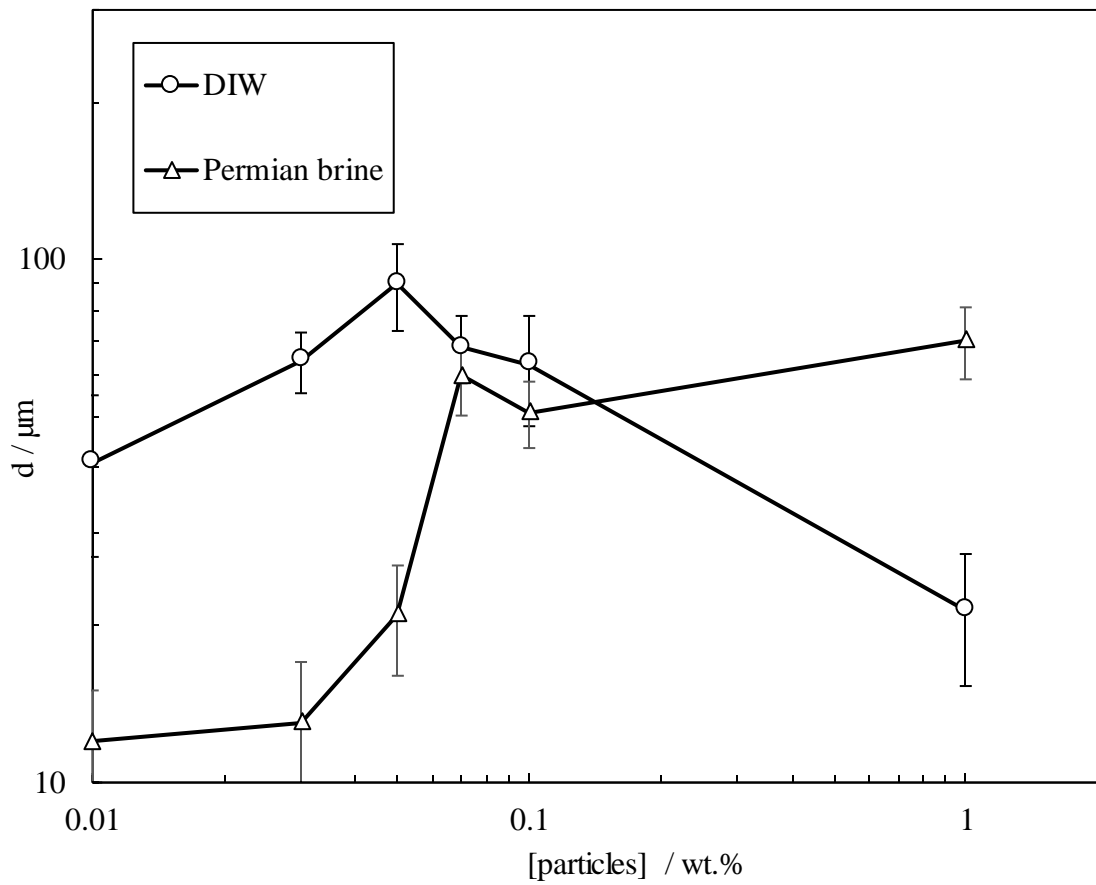
Figure 5.45. Optical microscope images taken immediately after preparation of oil-in-water emulsions from 5 g heptol(1:1 g g⁻¹) and 5 g dispersions of ES-coated silica (given in wt.%) in DIW or Permian brine.
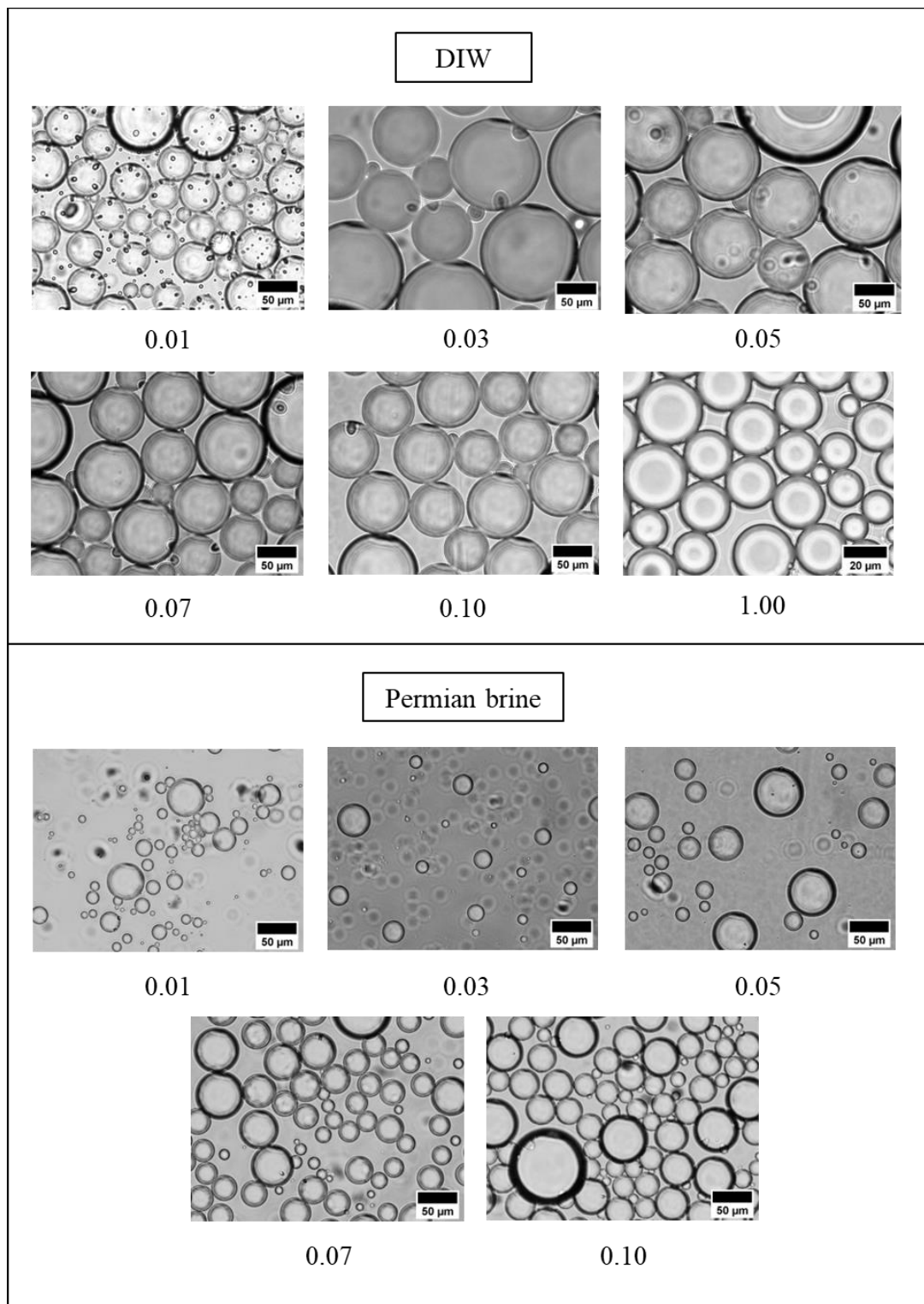
Table 5.4. Summary of results on oil-in-water emulsions from different oils and different concentrations (given in wt.%) of ES-coated silica in DIW and Permian brine (12.6 wt.%).

Particle	Oil	f_o or f_w after 100 days						Comment
		0.01	**0.03**	**0.05**	**0.07**	**0.1**	**1**	
DIW	Toluene		$f_o = 0.4$ to 0.6 with [particle] ↑ $f_w = 0.7$ to 0.9 with [particle] ↑					At low particle concentrations, particle-interface repulsion is large resulting in unstable emulsions.
	Heptane		1				$f_o = 0.5$ $f_w = 0.7$	Interfacial charge and oil molecules: toluene > heptol > heptane Particles can have polar-polar (stronger) and solvophobic interactions with interfacial toluene and heptane, respectively. Heptol takes advantage of both hydrophobization mechanisms.
	Heptol		1				$f_o = 0.04$ $f_w = 0.5$	
Permian brine	Toluene	$f_o > 0.9$ $f_w > 0.9$				$f_o = 0.8$ $f_w = 0.9$		Ions can screen the charges of both particles and the oil-water interface enabling more particle adsorption. However, ion accumulations at the interface prevent the adsorption of like-charged particles. The ability to adsorb counterions at the oil-water interface decreases as follows: toluene > heptol > heptane. Heptol takes advantage of both particle hydrophobization mechanisms.
	Heptane	1				$f_o = 0.6$ $f_w = 0.8$	1	
	Heptol	1				$f_o = 0.2$ $f_w = 0.7$	1	

5.3.3   Blend of surfactant and particles

5.3.3.1   Toluene

The effect of adding ES-coated silica particles to AHS solutions on the emulsification of toluene and water is shown in Figure 5.46. When the blend is in DIW, increasing particle concentration improves the initial emulsion stability to coalescence at low (0.001 wt.%) and high surfactant concentrations (> 0.05 wt.%). The emulsion made with 0.07 wt.% AHS alone in DIW coalesced and creamed significantly in a day but when blending the surfactant solution with 0.01 wt.% and 0.1 wt.% particles, the emulsions did not have any initial coalescence but creamed considerably. The fraction of oil resolved from these emulsions was around 0.6 after 6 months (Figure 5.47). The emulsion with the higher AHS concentration (0.1 wt.%) in the blend in DIW encountered phase separation after a while. All emulsions showed high creaming in the long term (> 0.9). When the blend was in Permian brine, the addition of particles to AHS solutions (> 0.03 wt.%) was found to destabilize the emulsions in the long term. While the emulsions of AHS alone in Permian brine (> 0.03 wt.%) had $f_o < 0.3$ after 190 days, the addition of particles to surfactant solutions significantly increased coalescence in these emulsions ($f_o > 0.8$). All in all, it is concluded that the addition of particles to AHS in DIW slightly improves the stability of emulsions to coalescence but when they are added to AHS in Permian brine, the emulsions become significantly unstable in the long term. On the other hand, the addition of AHS reduces the emulsions made with dispersions of 0.1 wt.% ES-coated silica in DIW at all surfactant concentrations (except for 0.05 wt.% and 0.07 wt.% AHS which show no significant effect) while it increases the coalescence markedly for the particles in Permian brine.

The stability of emulsions made with blends of particles and surfactants is pH dependent. Reducing pH below the isoelectric region of AHS (pH 5.5 – 8.0) renders the surfactant cationic and the ES-coated silica particles weakly anionic. Provided that isopropyl alcohol separating the two headgroups of the surfactant bends for the quaternary ammonium group to interact with the anionic particles while keeping the anionic sulfonate group away from the particle surface (V-shaped adsorption), weak particle hydrophobization can happen which may form Pickering emulsions. At the isoelectric pH, both charges are available in the surfactant headgroup and the particles are moderately charged offering more physical grafting and particle hydrophobicity. In both cases above, since the alkane tail of the zwitterionic surfactant is twice as long as the ES molecules (1.8 nm *vs.* 0.9 nm), the adsorbed surfactant tails first contact other molecules at the oil-water interface. This surface modification is thought to be stronger than the partial hydrophobization caused by the silane itself, as observed by zeta potential measurements in this study. Liu *et al.* studied the stability of emulsions made with silica particles and zwitterionic dodecyldimethylcarboxylbetaine using toluene and n-decane. They found out that the

emulsions can be stable to coalescence at low pH 5 where the surfactant is cationic and can adsorb onto silica particles which renders the particles hydrophobic and flocculated while they are unstable at high pH where the surfactant is zwitterionic. An adjustment of pH can change stable emulsions into unstable ones at different times.[277] This study has some main differences from the one carried out here. First, there is no particle flocculation on the addition of AHS to ES-coated dispersions here due to the steric stabilization of particles by silane. Second, ES-coated silica has a lower negative charge than bare silica at low pH as more than half of the adsorption sites of silica have been occupied by ES here. This reduces the electrostatic interactions between the particles and the surfactant and limits particle hydrophobization. With the grafting of surfactant onto particles, less particle surface charge is achieved which reduces the electrostatic repulsion between anionic particles and the anionic oil-water interface. Thus, the solvophobic interactions between surfactant-modified particles and interfacial oil molecules are strongest for toluene and weakest for heptane. This explains the higher emulsions observed with toluene and water here (compared to heptane).

At pH above the isoelectric region, the particles become highly charged and the surfactant turns anionic, as observed before. Due to their smaller size and larger diffusion, surfactant molecules can adsorb at the oil-water interface faster than particles[272] leading to particles being electrostatically repelled out of thin films between oil droplets and the formation of oil-in-dispersion emulsions. Herein, surfactant adsorption reduces the oil-water interfacial tension and makes droplets charged to prevent flocculation and coalescence *via* electrostatic repulsion while the particles remain dispersed in the continuous phase, unlike Pickering emulsions in which particles adsorb at the oil-water interface.[278, 279]

It is thought that the largest hydrophobization of ES-coated silica particles with the zwitterionic AHS happens at the isoelectric region here. The emulsion type can be switched between an oil-in-dispersion emulsion (high pH (10) – low [AHS]) and a Pickering emulsion (isoelectric pH – high [AHS]). The former does not create stable oil-in-dispersion emulsions here probably due to the low particle/surfactant concentrations used in this study. In the latter, there is a competition for surfactant molecules to adsorb at the particle surface or the oil-water interface [182] which leads to a free-energy minimum in the adsorption energy of particles at the oil-water interface at high surfactant concentrations and prevents particles from adsorbing at the oil-water interface.[280, 281] Recent studies show that the grafted surfactant molecules may leave the particle surface close to the oil-water interface due to their lower adsorption energy at the oil-water interface, suggesting particles as surfactant carriers.[119] If that happens, the surfactant is

available to adsorb at the oil-water interface and lower the interfacial tension. The surfactant molecules can also form a layer around the particles adsorbed on the oil droplets, which further sterically stabilizes them.[245] It is also likely that the hydrophobic-hydrophobic van der Waals interaction between these surfactant tails makes emulsion drops flocculate (see microscopy) and then coalesce.

The addition of brine screens the anionic particles which subsequently lowers the particle-particle and particle-interface electrostatic repulsion. These modifications weaken the electrostatic kinetic barrier while simultaneously increasing the thermodynamic driving force for particle adsorption at the oil-water interface.[282] Here, the individual adsorption of particles or surfactant molecules at the oil-water interface or the particle-surfactant attraction (less particle hydrophobization) is lowered by the addition of ions. A high adsorption of ions at the interface also makes the emulsions unstable, compared to emulsions made with AHS alone. Salinity also reduces the polarity of toluene molecules and makes them less able to adsorb at the oil-water interface for interactions with surfactants and particles.[241]

Figure 5.48 shows the effect of adding particles to surfactant solutions on the drop diameter of the emulsions made with toluene and water. At all particle loadings, a reduction in the drop diameter is seen when Permian brine is added to AHS solutions. However, no significant change is observed in the drop diameter when the particle concentration is raised in the blend in both DIW and Permian brine. The microscopy of these emulsions is shown in Figures 5.49 and 5.50. As observed, the high surfactant concentration and the high salinity cause flocs to appear in the emulsion.

Figure 5.46. Appearance of oil-in-water emulsions from 5 g toluene and 5 g dispersions containing 0, 0.01 and 0.1 wt.% ES-coated silica and different weight percentages of AHS surfactant in DIW and Permian brine.

Figure 5.47. Effect of adding particles on the fraction of oil resolved from oil-in-water emulsions from 5 g toluene and 5 g of dispersions containing 0, 0.01 and 0.1 wt.% ES-coated silica and different weight percentages of AHS surfactant in DIW and Permian brine after 190 days.

Figure 5.48. Initial emulsion drop diameter vs surfactant concentration for oil-in-water emulsions from 5 g toluene and 5 g of dispersions containing 0, 0.01 and 0.1 wt.% ES-coated silica and different weight percentages of AHS surfactant in DIW and Permian brine.

Figure 5.49. Optical microscope images taken immediately after preparation of oil-in-water emulsions from 5 g toluene and 5 g of dispersions containing 0.01 wt.% ES-coated silica and different weight percentages of AHS surfactant in DIW and Permian brine.

Figure 5.50. Optical microscope images taken immediately after preparation of oil-in-water emulsions from 5 g toluene and 5 g of dispersions containing 0.1 wt.% ES-coated silica and different weight percentages of AHS surfactant in DIW and Permian brine.

DIW

0.001   0.05

0.07   0.1

Permian brine

0.03   0.05

0.07   0.10
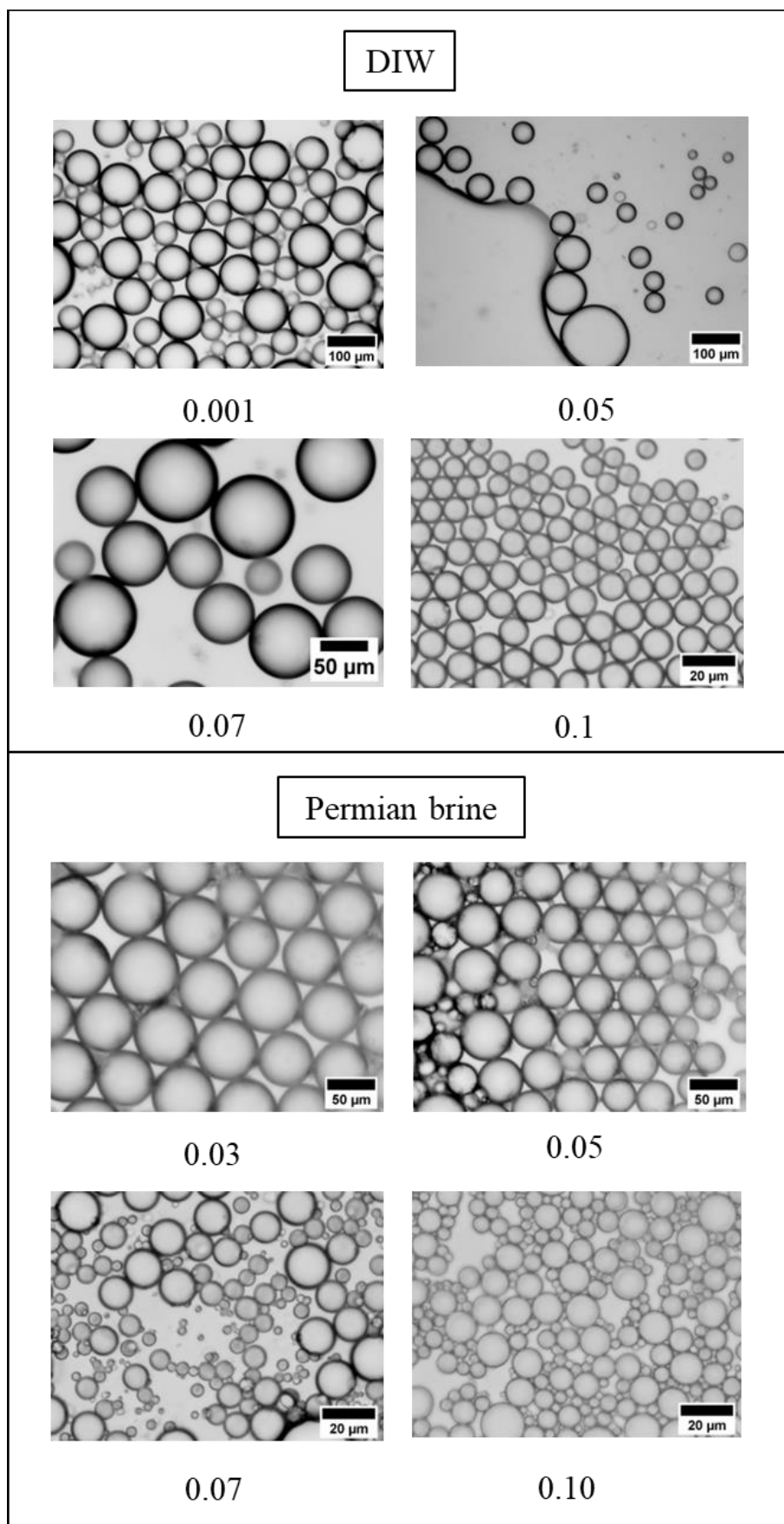
The effect of the addition of ES-coated silica particles to ZN solutions on the emulsification of toluene and water is shown in Figure 5.51. When ZN was in DIW, the addition of particles did not improve the stability of the emulsions against coalescence

284

and creaming at low ZN concentrations in the long term (< 0.03 wt.%). At 0.05 wt.% ZN in DIW, raising particle concentration from 0 to 0.1 wt.% reduced the residual emulsion volume after a month but none of them survived coalescence in 4 months (Figure 5.52). The addition of 0.01 wt.% particles to 0.03 and 0.05 wt.% ZN in Permian brine lowered the emulsification of toluene and water after a day (probably due to the low surfactant concentration) but did not affect the emulsions of higher ZN concentrations in the blend initially. Compared to ZN alone, there is no significant improvement in stability to coalescence in the long term (after 4 months) by adding particles to ZN in Permian brine (Figure 5.52). Serious creaming occurred in all emulsions after 4 months ($f_w > 0.9$). The blueish resolved water in the emulsions made with the blend in Permian brine indicates oil-in-water microemulsions which is more noticeable initially (day 1 photos).

The same interactions explained between AHS and particles are thought to hold here. When the mixture of particles and ZN is in DIW, both zwitterionic and nonionic surfactants can adsorb on the surface of the particles through electrostatic attraction and hydrogen bonding, respectively which render the particles partially hydrophobic and capable of more readily adsorbing to the oil-water interface. More initial emulsions were formed with polar toluene compared to heptane and water when blending ZN and particles.

As shown in Figure 5.53, the initial drop diameter increased upon adding 0.01 wt.% particles to ZN solutions which is more noticeable for the blends in DIW but it decreased again when increasing the particle loading to 0.1 wt.%. The initial microscope images of the emulsions (Figures 5.54 and 5.55) show that increasing the AHS concentration to above 0.07 wt.% in Permian brine widens the drop size distribution in the emulsions at both particle loadings while the drops are uniformly distributed in the emulsions made with the blend in DIW. The presence of Permian brine in the blend of ZN and particles also caused drop flocs.

Figure 5.51. Appearance of oil-in-water emulsions from 5 g toluene and 5 g of dispersions containing 0, 0.01 and 0.1 wt.% ES-coated silica and different weight percentages of ZN in DIW and Permian brine.
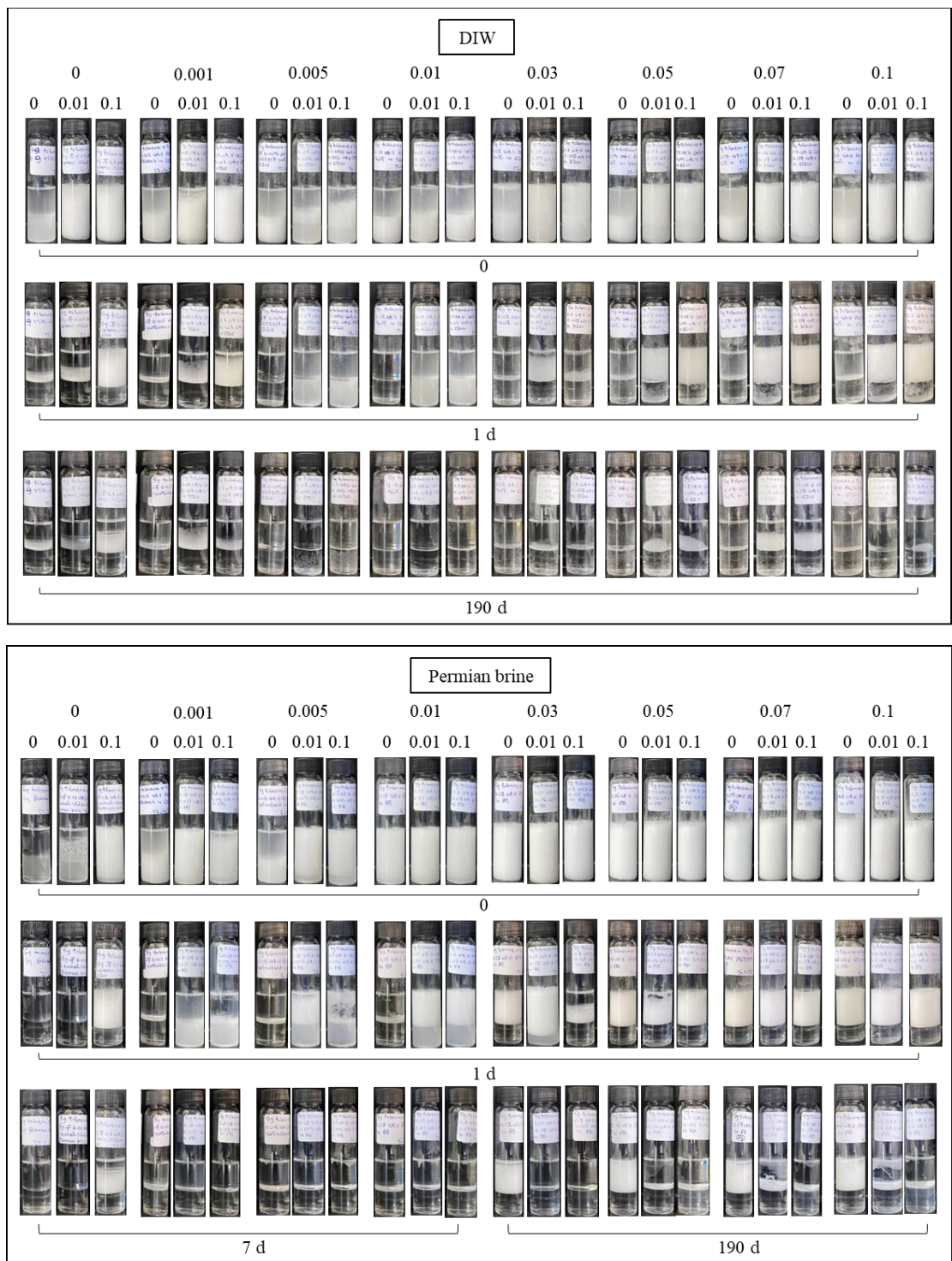
Figure 5.52. Effect of adding particles on the fraction of oil resolved from oil-in-water emulsions formed from 5 g toluene and 5 g of dispersions containing 0, 0.01 and 0.1 wt.% ES-coated silica and different weight percentages of ZN in DIW and Permian brine.
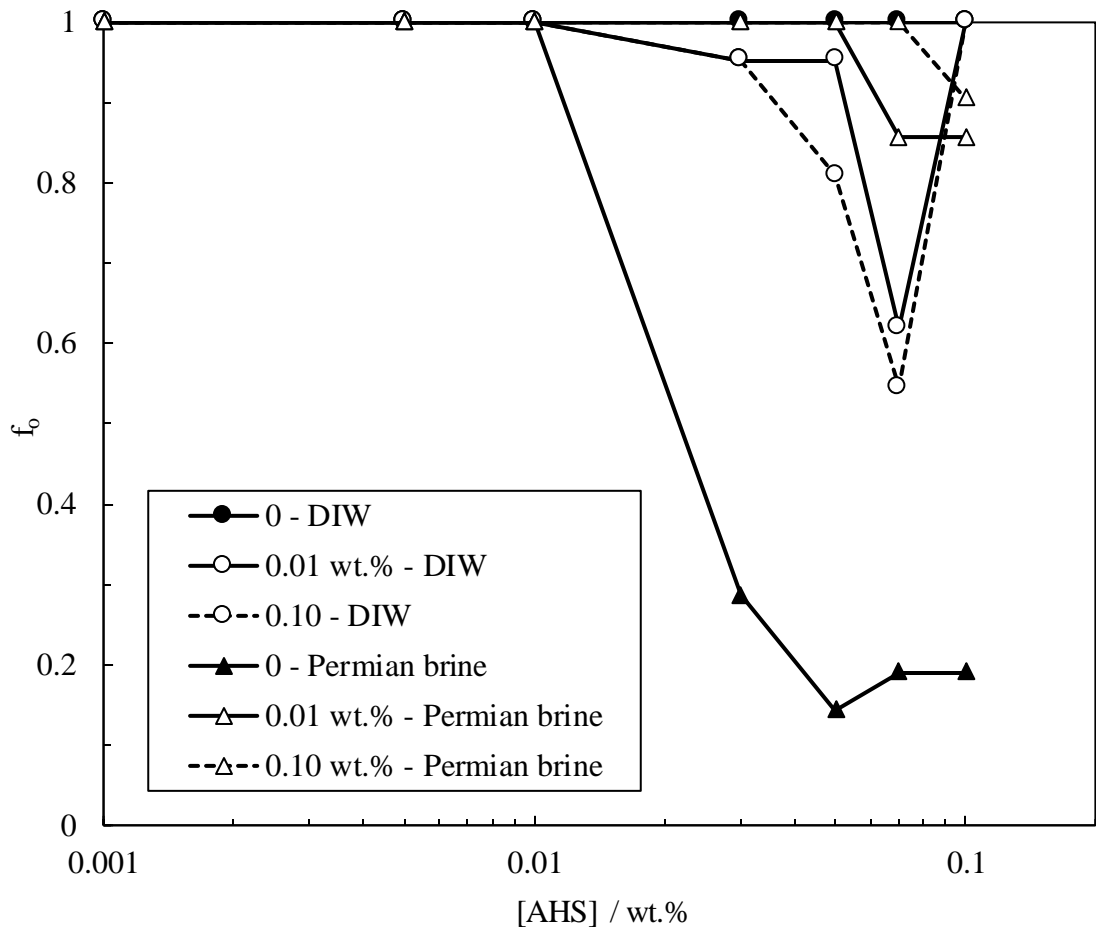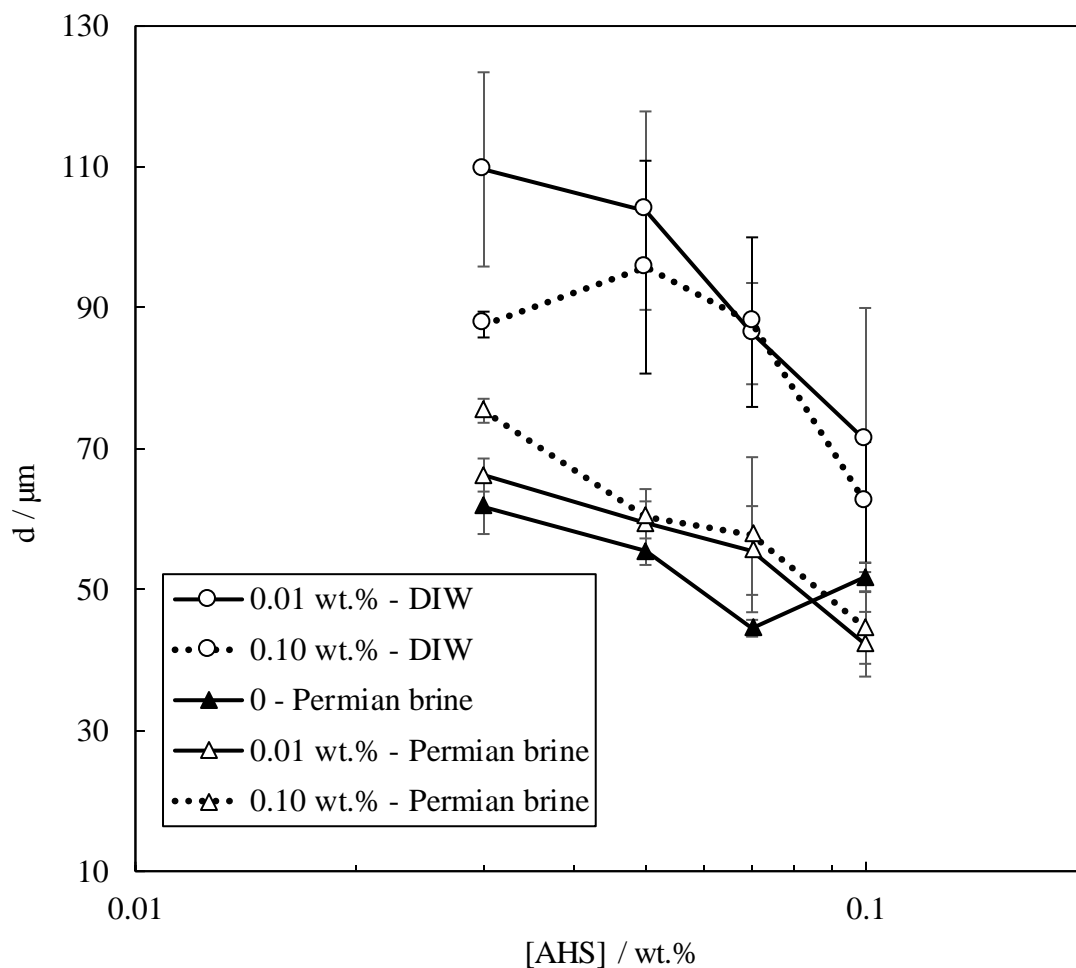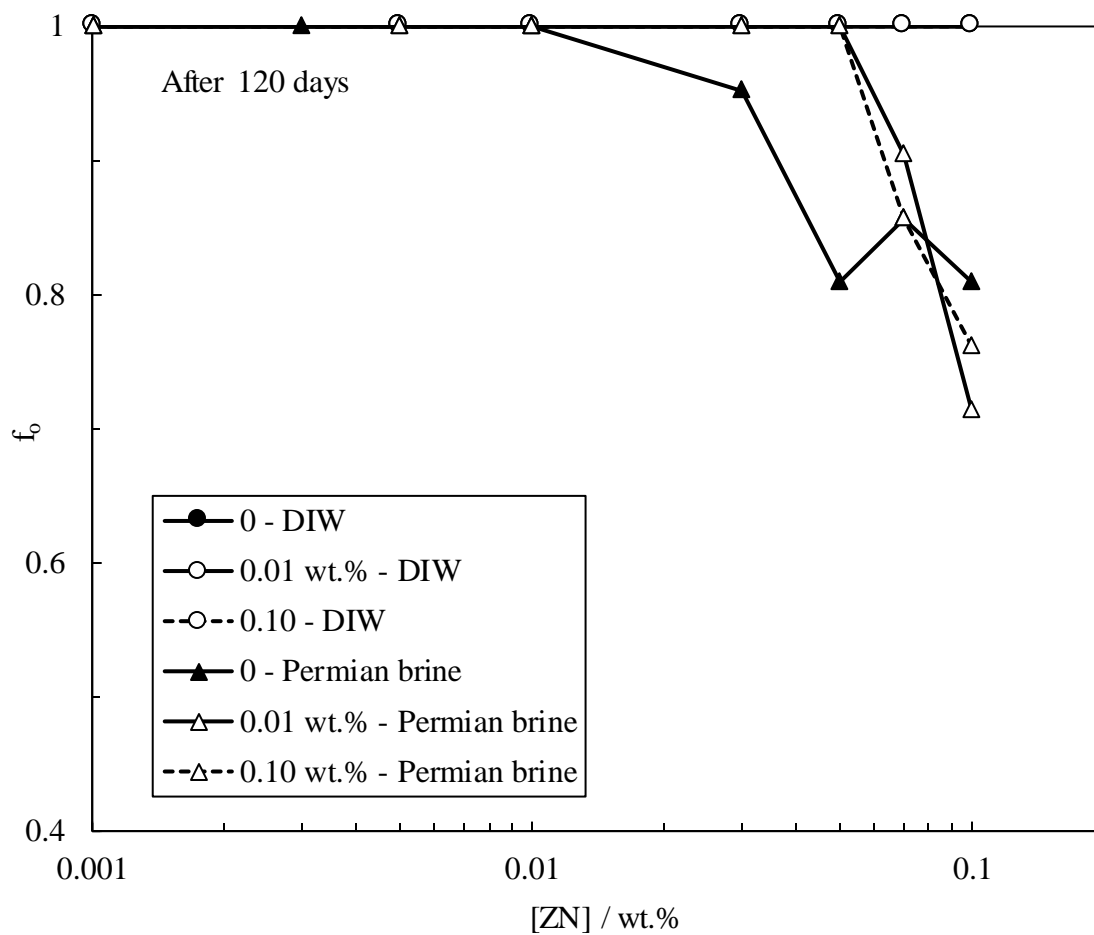
Figure 5.53. Initial emulsion drop diameter vs surfactant concentration for oil-in-water emulsions from 5 g toluene and 5 g of dispersions containing 0, 0.01 and 0.1 wt.% ES-coated silica and different weight percentages of ZN in DIW (upper) and Permian brine (lower).
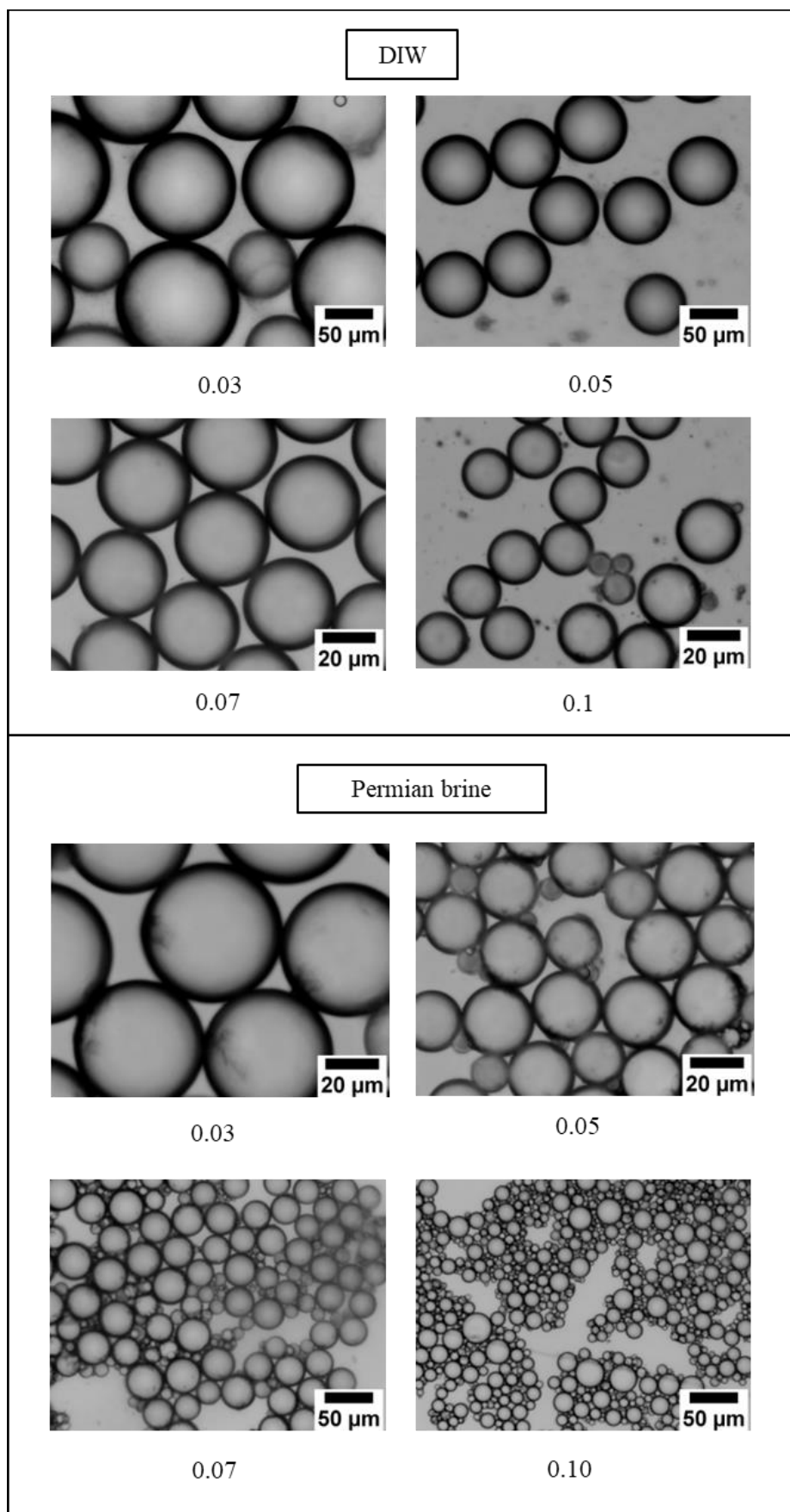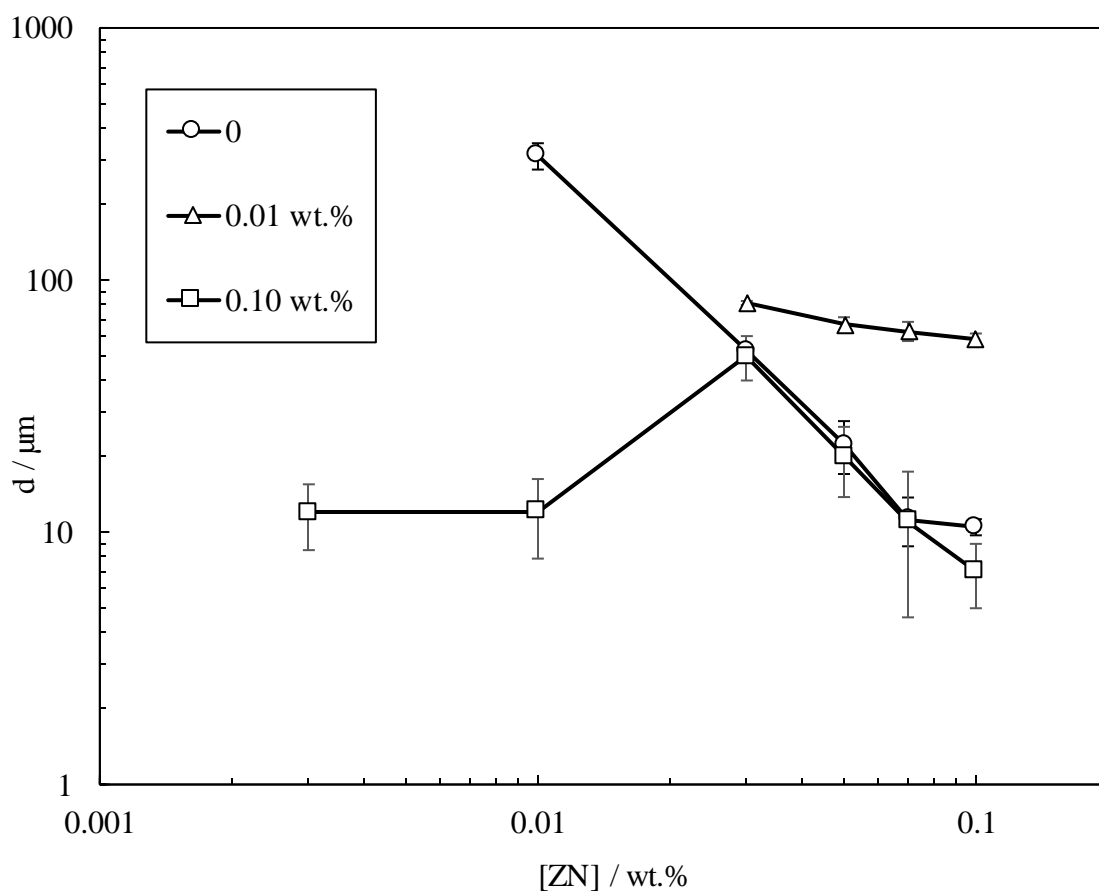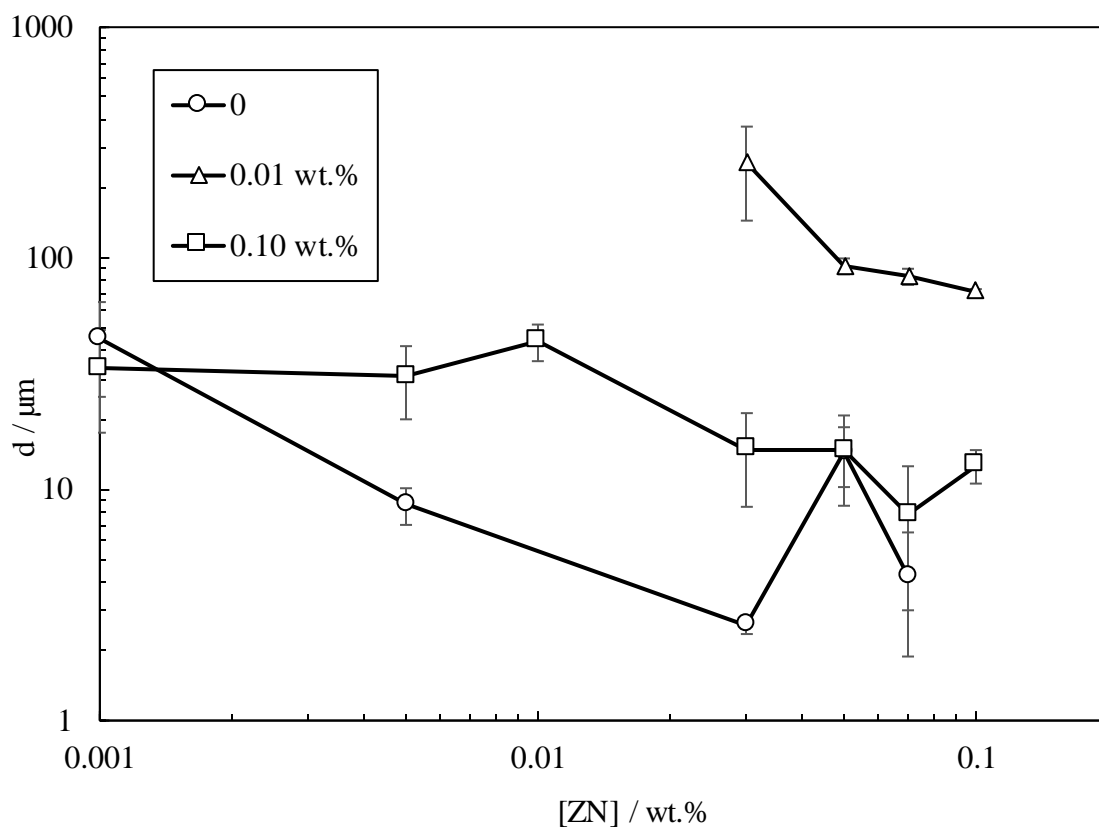
Figure 5.54. Optical microscope images taken immediately after preparation of oil-in-water emulsions from 5 g toluene and 5 g of dispersions containing 0.01 wt.% ES-coated silica and different concentrations of ZN (given in wt.%) in DIW.

288

Figure 5.55. Optical microscope images taken immediately after preparation of oil-in-water emulsions from 5 g toluene and 5 g of dispersions containing 0.1 wt.% ES-coated silica and different weight percentages of ZN in DIW or Permian brine.

DIW

0.001   0.005   0.01   0.03

0.05   0.07   0.1

Permian brine

0.003   0.01   0.03

0.05   0.07   0.1
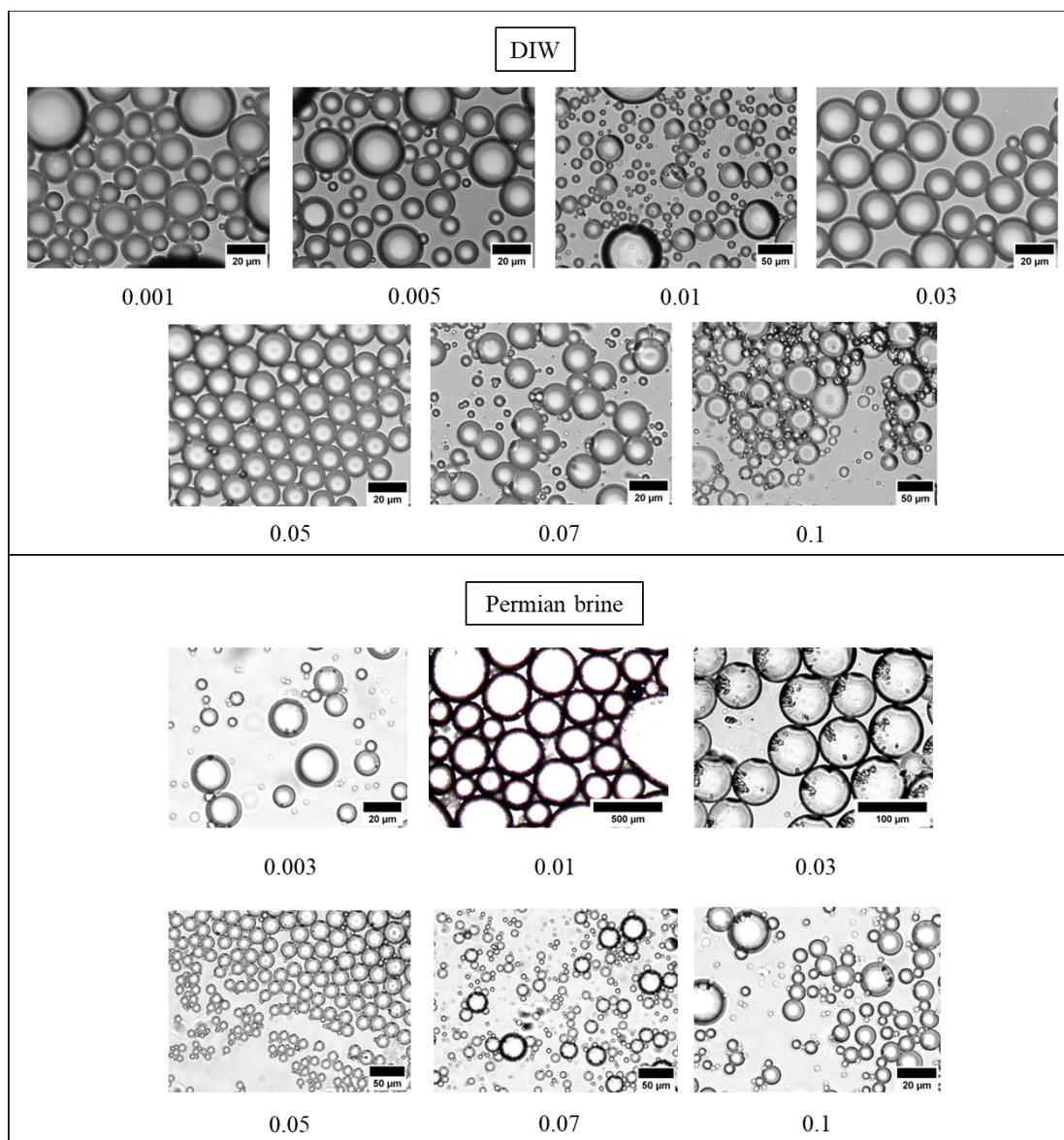
5.3.3.2   Heptane

The impact of increasing particle concentration in AHS solutions on the emulsification of heptane and water is depicted in Figure 5.56. A slight improvement in stability to coalescence is observed in the long term when increasing particle concentrations from 0 to 0.1 wt.% at 0.03 and 0.05 wt.% AHS in DIW, as shown in Figure 5.57 ($f_o = 0.7 \pm 0.05$ after 180 days). No improvement in creaming is observed in the addition of particles to these emulsions. Adding 0.1 wt.% particles to AHS (> 0.05 wt.%) in Permian brine significantly reduces coalescence ($f_o < 0.1$) and creaming ($f_w \sim 0.6$) in the long term while 0.01 wt.% particles were not effective in producing long-term stable emulsions. A decreasing initial drop diameter is observed upon increasing AHS concentrations at all particle loadings in DIW (Figure 5.58). The initial drop diameter decreases with increasing particle concentrations in AHS in DIW but no important effect is observed in Permian brine. The initial microscope images of the emulsions show a monomodal distribution of spherical droplets in DIW and a multimodal distribution in those of Permian brine (Figure 5.59). The high salinity and high surfactant concentration can cause drop flocculation in the emulsion stabilizing it as observed here[270] (Figures 5.59 and 5.60). All in all, it is concluded that the addition of particles to AHS in DIW slightly improves the long-term stability of heptane-in-water emulsions as observed with those of toluene but when the particles are added to AHS in Permian brine, a significant improvement in long-term stability to coalescence is achieved in sharp contrast to those of toluene. On the other hand, the addition of surfactant improves the emulsions made with particles alone which is more pronounced for high particle concentrations in Permian brine.

When the blend is in DIW, the electrostatic repulsion between the anionic oil-water interface and the anionic headgroup of the surfactant or anionic particles prevents the adsorption of particles and surfactants at the interface. However, at high particle and surfactant concentrations, surfactant-grafted particles are formed with surfactant tails having limited interactions with heptane molecules which causes partial emulsification. When salts are added, the ions screen the particles, surfactant headgroups and the oil-water interface. Due to the reduced repulsion between the anionic headgroups of the surfactant and the oil-water interface, the adsorbed surfactants can extend their tails to interact with heptane molecules, causing more emulsification[241] which is more significant at high particle loadings in the long term.

Figure 5.56. Appearance of oil-in-water emulsions formed from 5 g heptane and 5 g of dispersions containing 0, 0.01 and 0.1 wt.% ES-coated silica and different weight percentages of AHS in DIW and Permian brine.

Figure 5.57. Effect of adding particles on the fraction of oil resolved from oil-in-water emulsions formed from 5 g heptane and 5 g of dispersions containing 0, 0.01 and 0.1 wt.% ES-coated silica and different weight percentages of AHS in DIW and Permian brine after 180 days.
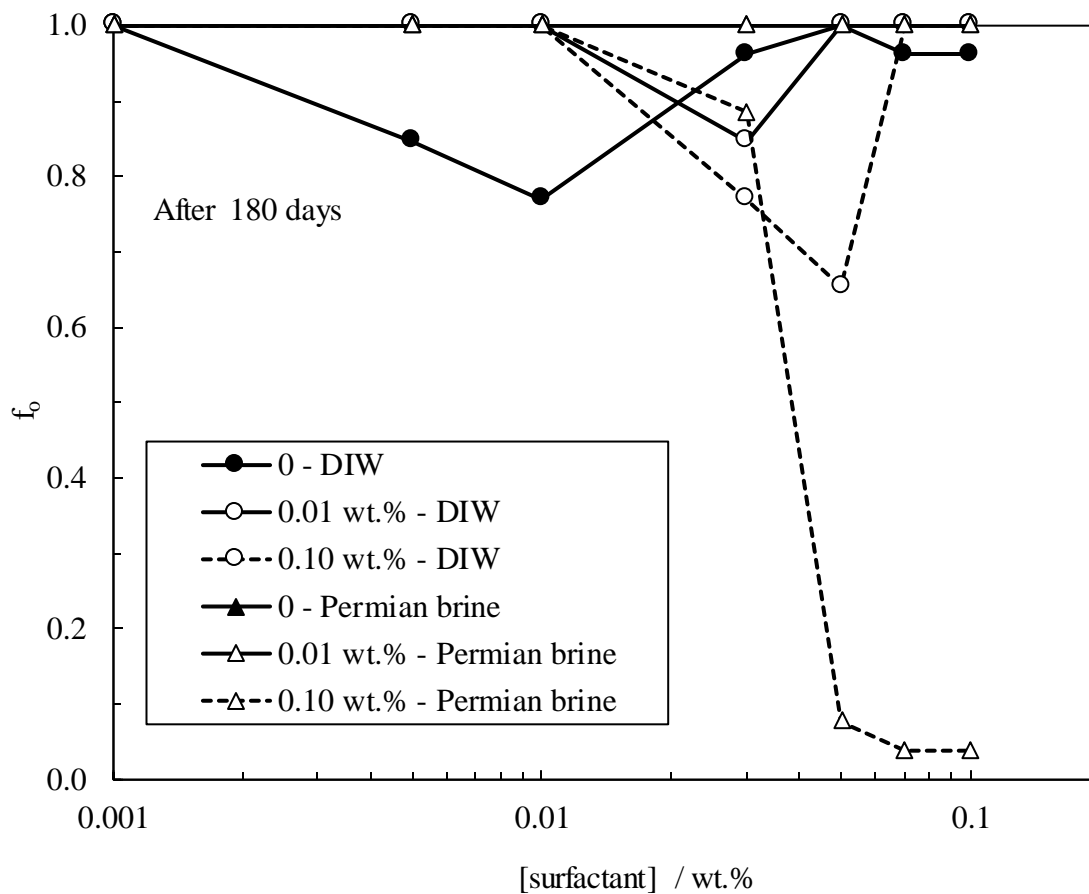
Figure 5.58. Initial emulsion drop diameter vs surfactant concentration for oil-in-water emulsions from 5 g heptane and 5 g of dispersions containing 0, 0.01 and 0.1 wt.% ES-coated silica and different weight percentages of AHS in DIW (upper) and Permian brine (lower).
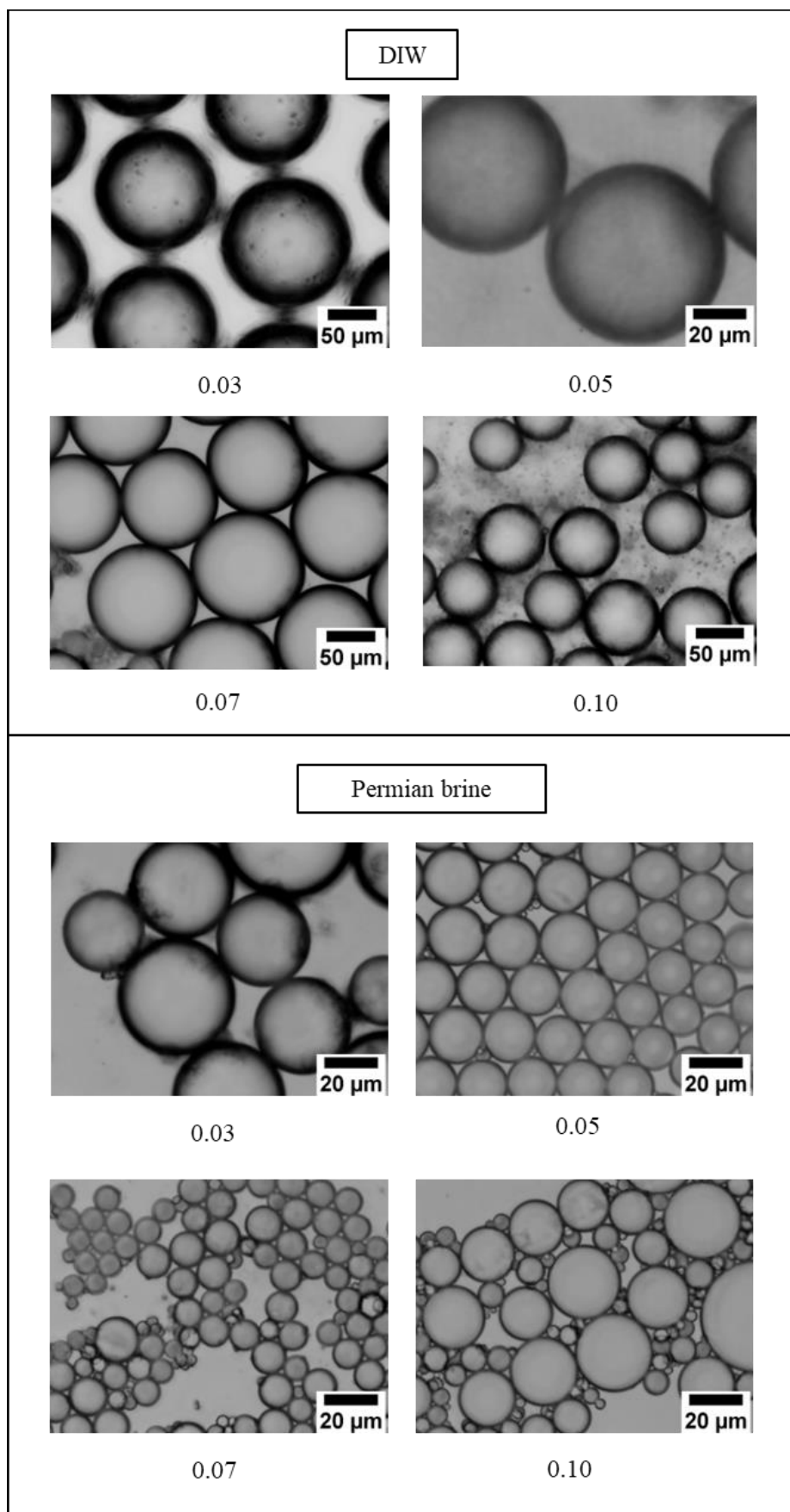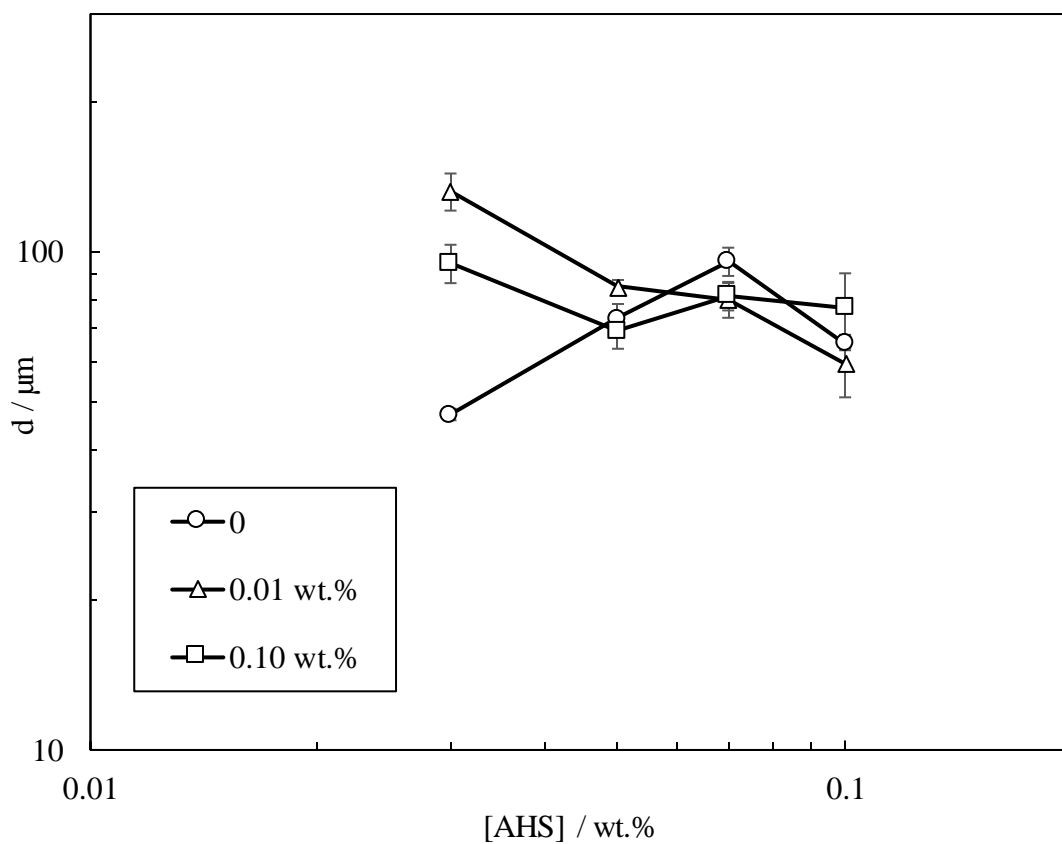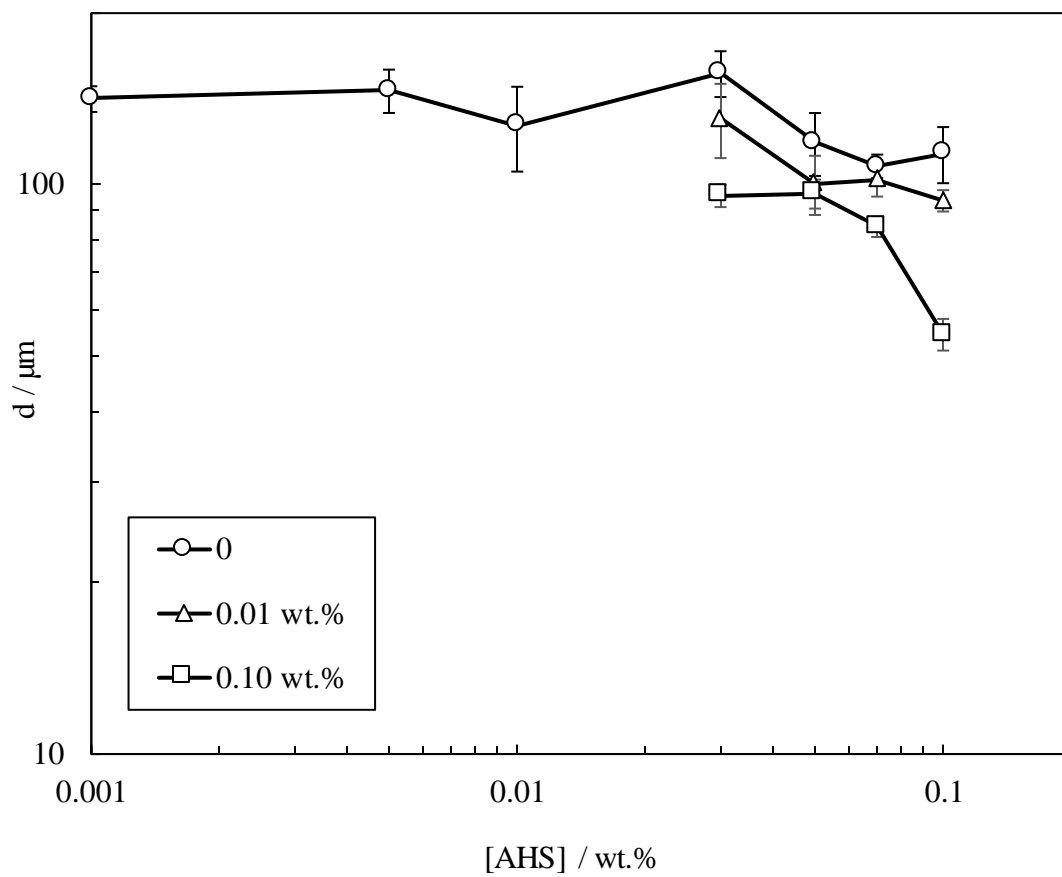
Figure 5.59. Optical microscope images taken immediately after preparation of oil-in-water emulsions from 5 g heptane and 5 g of dispersions containing 0.01 wt.% ES-coated silica and different weight percentages of AHS in DIW and Permian brine.
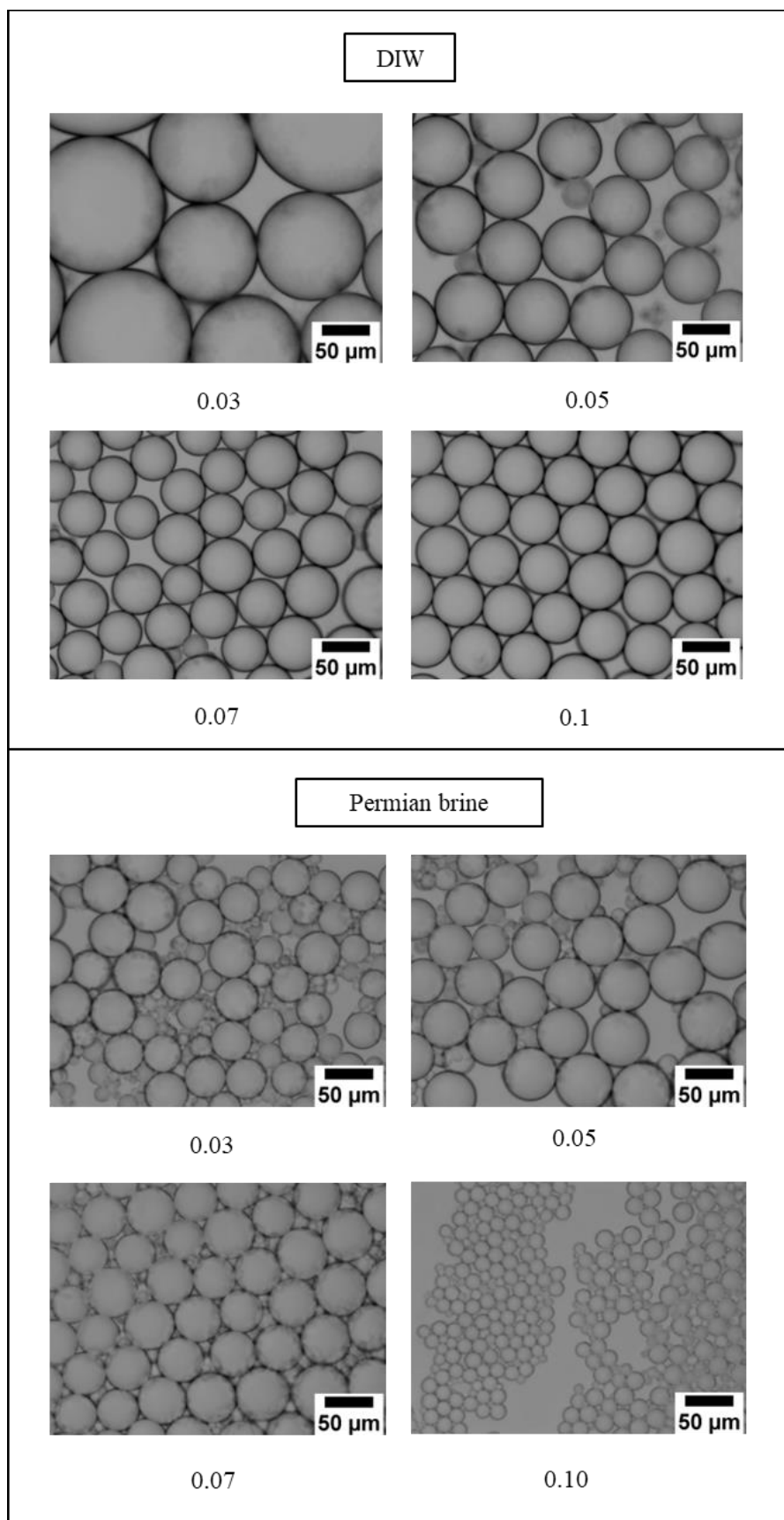
Figure 5.60. Optical microscope images taken immediately after preparation of oil-in-water emulsions from 5 g heptane and 5 g of dispersions containing 0.1 wt.% ES-coated silica and different weight percentages of AHS in DIW and Permian brine.
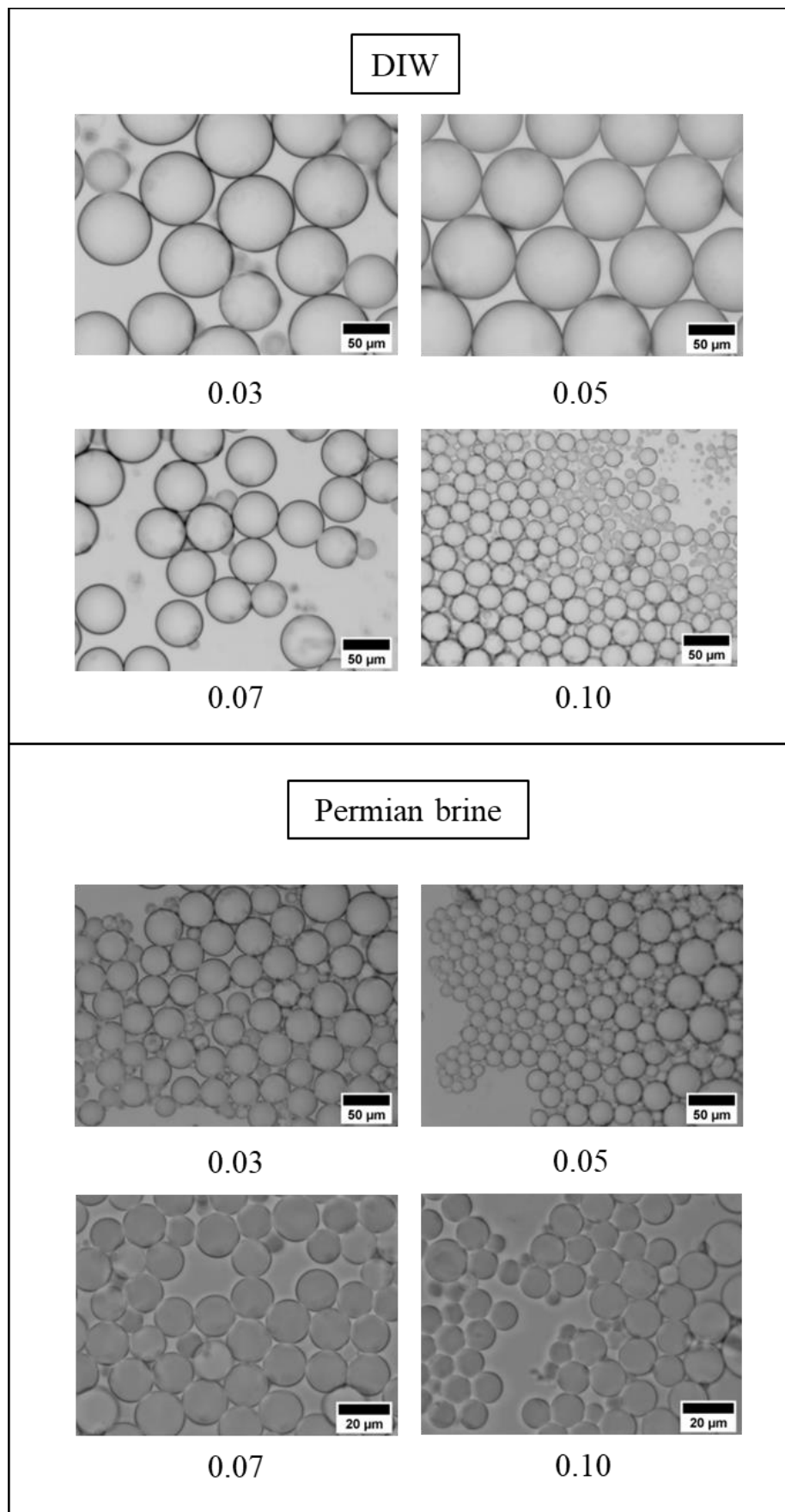
The emulsions made with heptane and blends of particles and ZN in DIW and Permian brine were all phase separated within a day (Figure 5.61). No improvement in emulsion

stability is observed upon increasing particle concentration in ZN solutions but the addition of ZN surfactant to 0.1 wt.% particle dispersions destabilized the emulsions after a day. The initial drop diameter of all emulsions was measured at $20 \pm 10\,\mu m$. Figure 5.62 shows the microscopy of emulsions formed by blends of 0.1 wt.% particles and ZN. The photos of the emulsions made with the blend in Permian brine were taken from the resolved water. Due to emulsion instability, no microscopy was possible for the emulsion formed by the blend of 0.01 wt.% particles and ZN.

Figure 5.61. Appearance of oil-in-water emulsions formed from 5 g heptane and 5 g of dispersions containing 0, 0.01 and 0.1 wt.% ES-coated silica and different weight percentages of ZN in DIW and Permian brine.

Figure 5.62. Optical microscope images taken immediately after preparation of oil-in-water emulsions from 5 g heptane and 5 g of dispersions containing 0.1 wt.% ES-coated silica and different weight percentages of ZN in DIW or Permian brine.

DIW

0.001 0.005 0.01 0.03

0.05 0.07 0.1

Permian brine

0.001 0.003 0.01 0.03

0.05 0.1
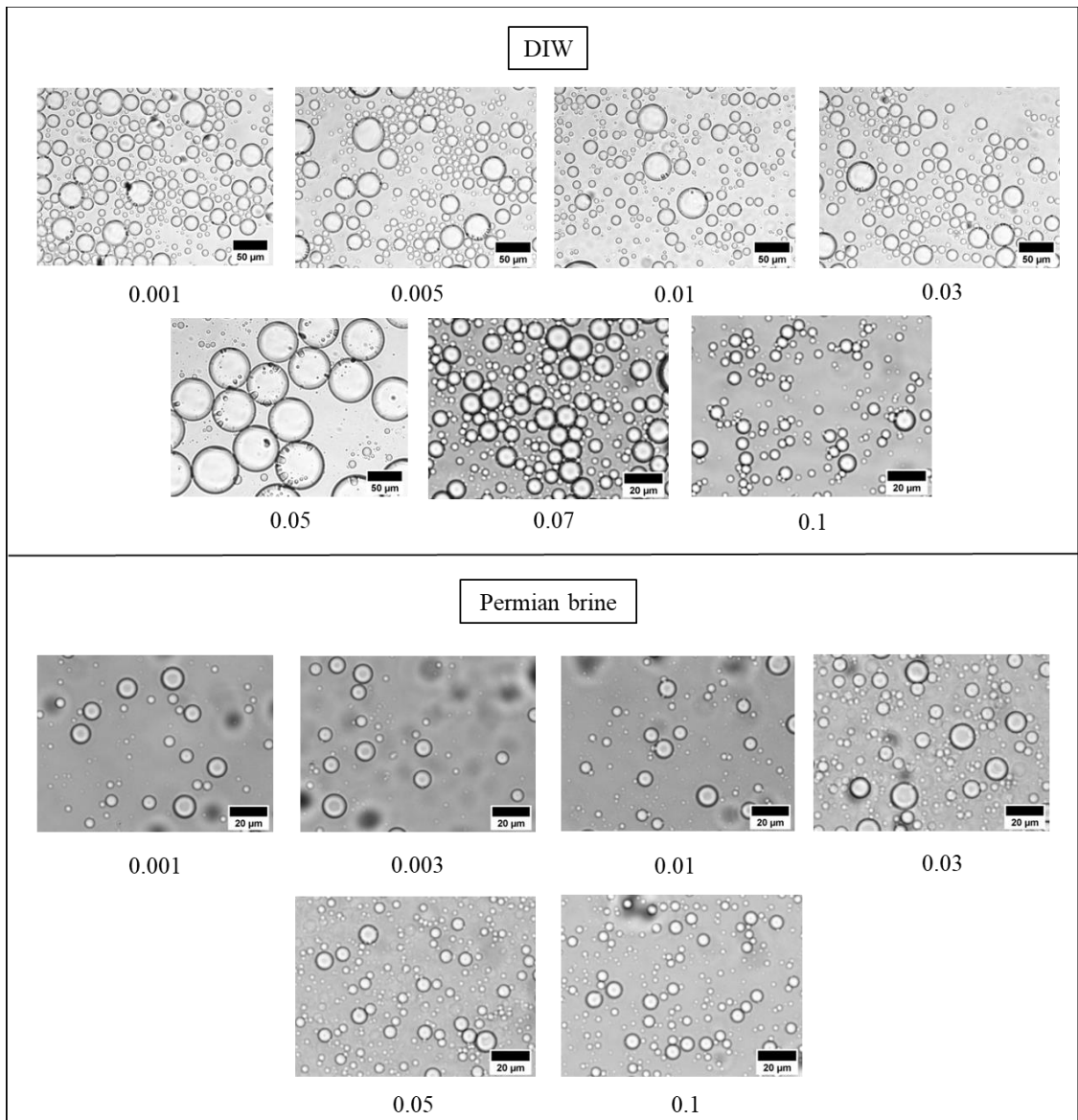
5.3.3.3 Heptol

Figure 5.63 shows the effect of adding ES-coated silica particles to AHS solutions on the emulsification of heptol (1:1 g g^{-1}) and water. The addition of particles to solutions of AHS in DIW at < 0.1 wt.% reduced coalescence slightly in the long term. At 0.1 wt.% AHS in DIW, increasing particle concentration coalesced more oil in 6 months. The emulsion made with 0.1 wt.% AHS alone in DIW had a fraction of oil resolved at ~ 0.3 after 6 months while it increased to > 0.9 with the addition of particles (Figure 5.64). Creaming was high in all emulsions after 6 months with or without particles ($f_w > 0.8$). All emulsions made with AHS in Permian brine at 0.001 – 0.01 wt.% with or without particles were phase separated within a few days. Of the emulsions made with surfactant alone in Permian brine, 0.05 wt.% and 0.07 wt.% AHS solutions formed the most stable emulsions with $f_o = 0.50 \pm 0.05$ after 180 days. The addition of low particle concentrations (0.01 wt.%) to AHS (< 0.1 wt.%) in Permian brine was found to significantly increase coalescence in these two emulsions while raising the particle loading to 0.1 wt.% improved the stability of surfactant-made emulsions to coalescence markedly in the long term ($f_o < 0.1$ after 180 days). Figure 5.65 shows a decreasing drop diameter with an increase in AHS concentration above 0.03 wt.% in both DIW and Permian brine at all particle loadings. There is no major change in drop diameter when raising the particle concentration in the solutions of AHS in DIW while the addition of 0.01 wt.% particles to AHS in Permian brine reduced the initial drop diameter but it remained unchanged upon increasing the particle dosage to 0.1 wt.%. Figures 5.66 and 5.67 show the initial microscopy of these emulsions.

All in all, it is concluded that the addition of particles to AHS in DIW increased the coalescence in the long term while a high particle concentration in the blend in Permian brine reduced the coalescence. This behaviour is thought to be driven by heptane, as explained before. On the other hand, the addition of high AHS concentrations to dispersions of particles in Permian brine can improve the stability of Pickering emulsions while no significant change is seen in those made with particles in DIW.

Figure 5.63. Appearance of oil-in-water emulsions formed from 5 g heptol (1:1 g g^{-1}) and 5 g of dispersions containing 0, 0.01 and 0.1 wt.% ES-coated silica and different weight percentages of AHS in DIW and Permian brine.
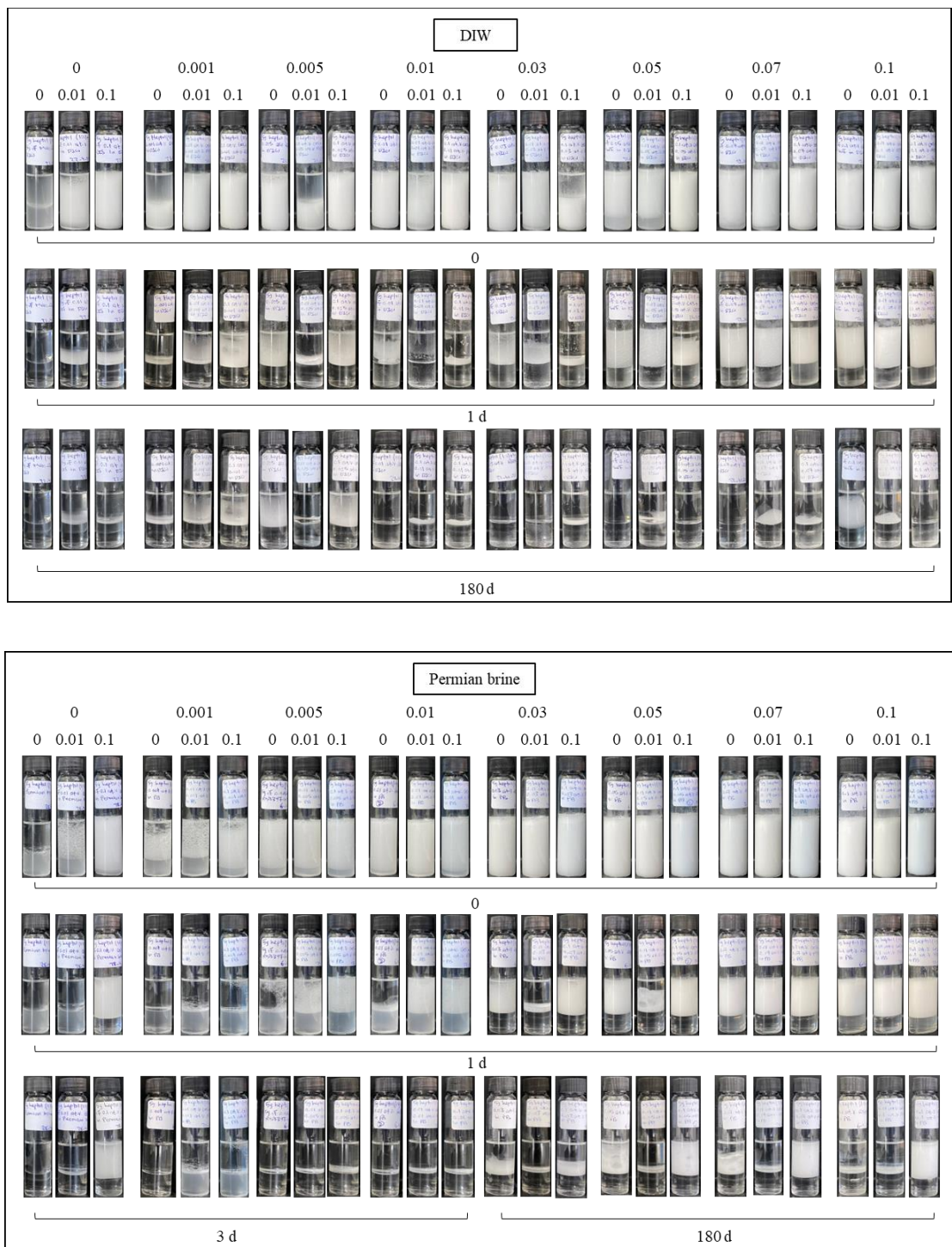
Figure 5.64. Effect of adding particles on the fraction of oil resolved from oil-in-water emulsions from 5 g heptol (1:1 g g^{-1}) and 5 g of dispersions containing 0, 0.01 and 0.1 wt.% ES-coated silica and different weight percentages of AHS in DIW and Permian brine.

301

After 180 days
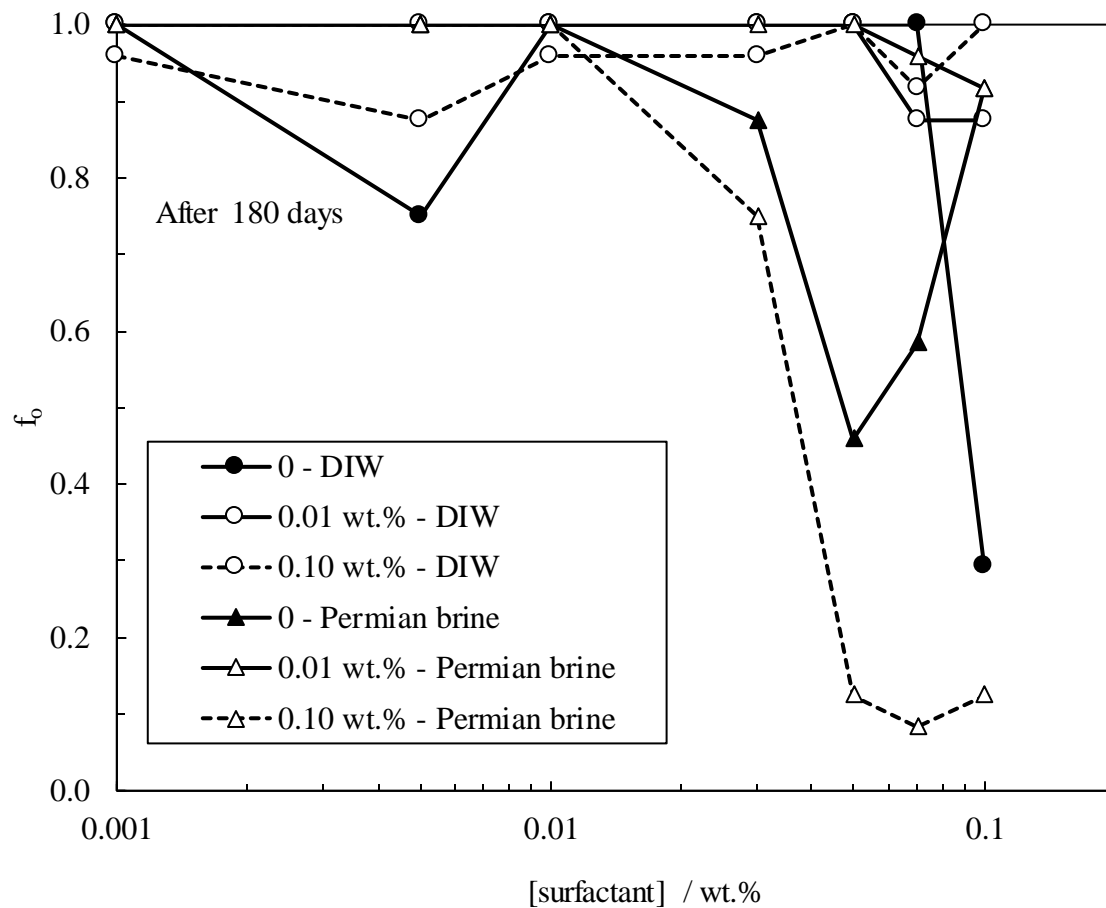
Figure 5.65. Initial emulsion drop diameter vs surfactant concentrations for oil-in-water emulsions from 5 g heptol (1:1 g g^{-1}) and 5 g of dispersions containing 0, 0.01 and 0.1 wt.% ES-coated silica and different weight percentages of AHS surfactant in DIW (upper) and Permian brine (lower).
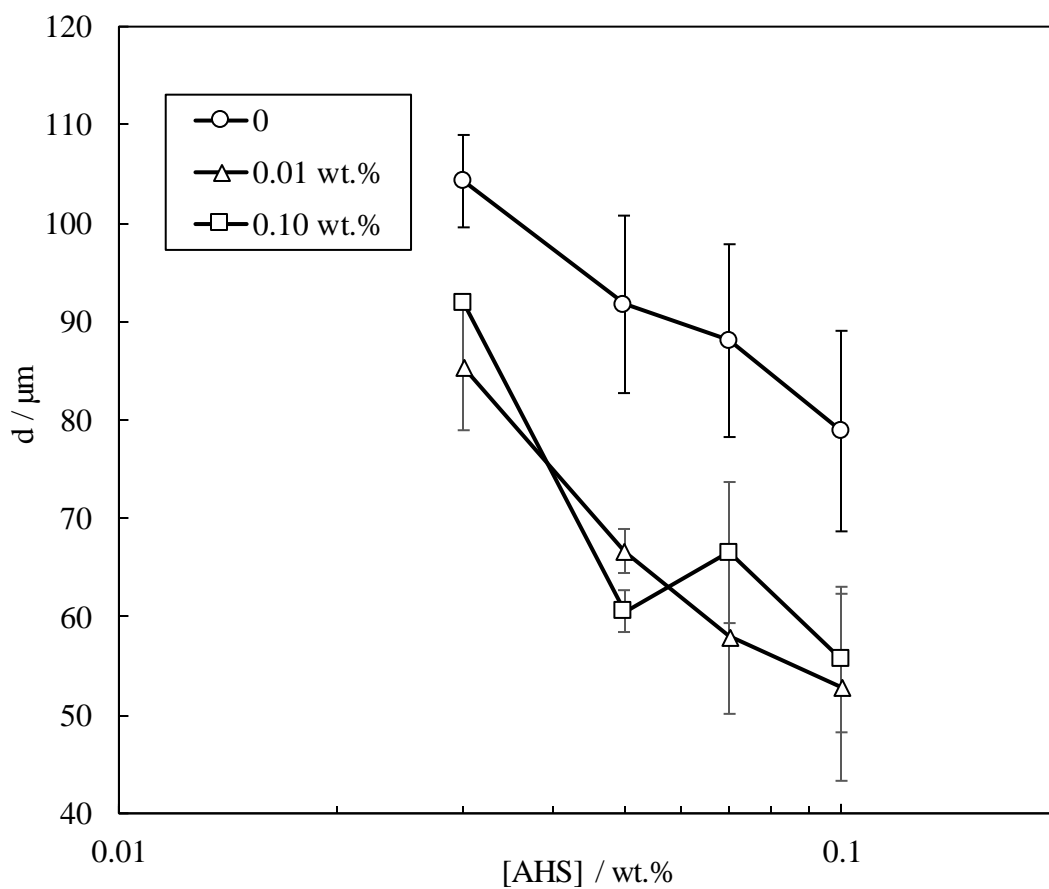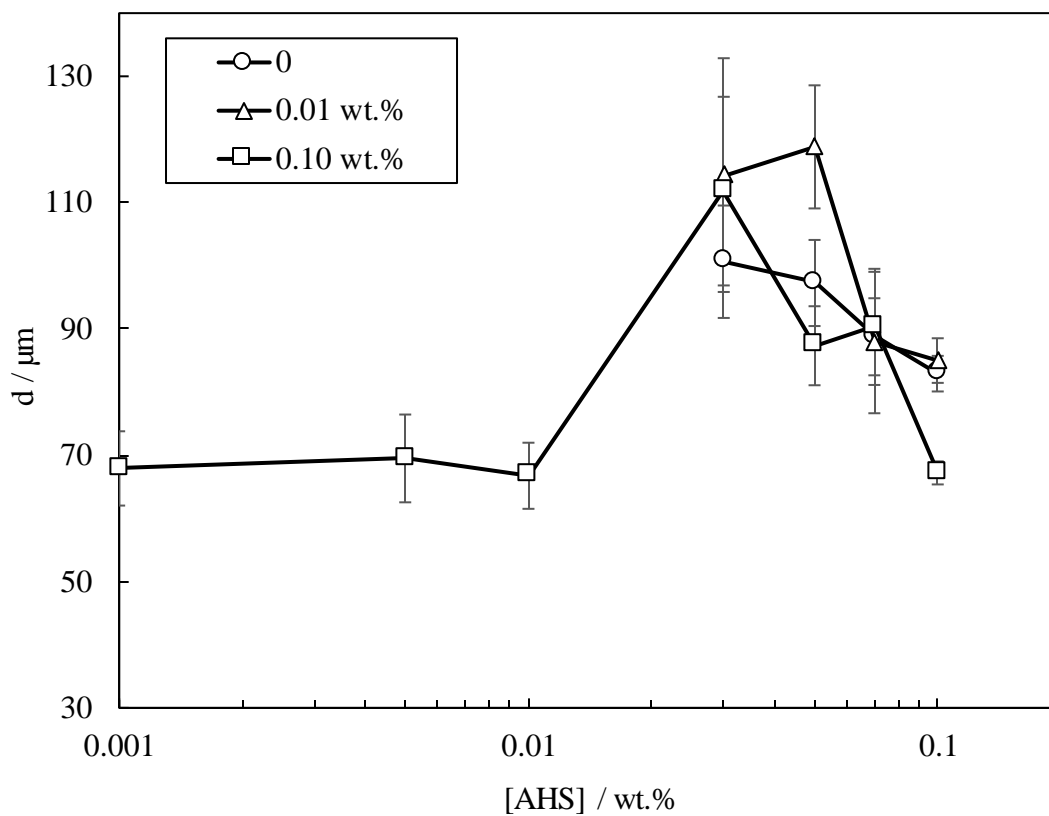
Figure 5.66. Optical microscope images taken immediately after preparation of oil-in-water emulsions from 5 g heptol (1:1 g g^{-1}) and 5 g of dispersions containing 0.01 wt.% ES-coated silica and different weight percentages of AHS surfactant in DIW and Permian brine.
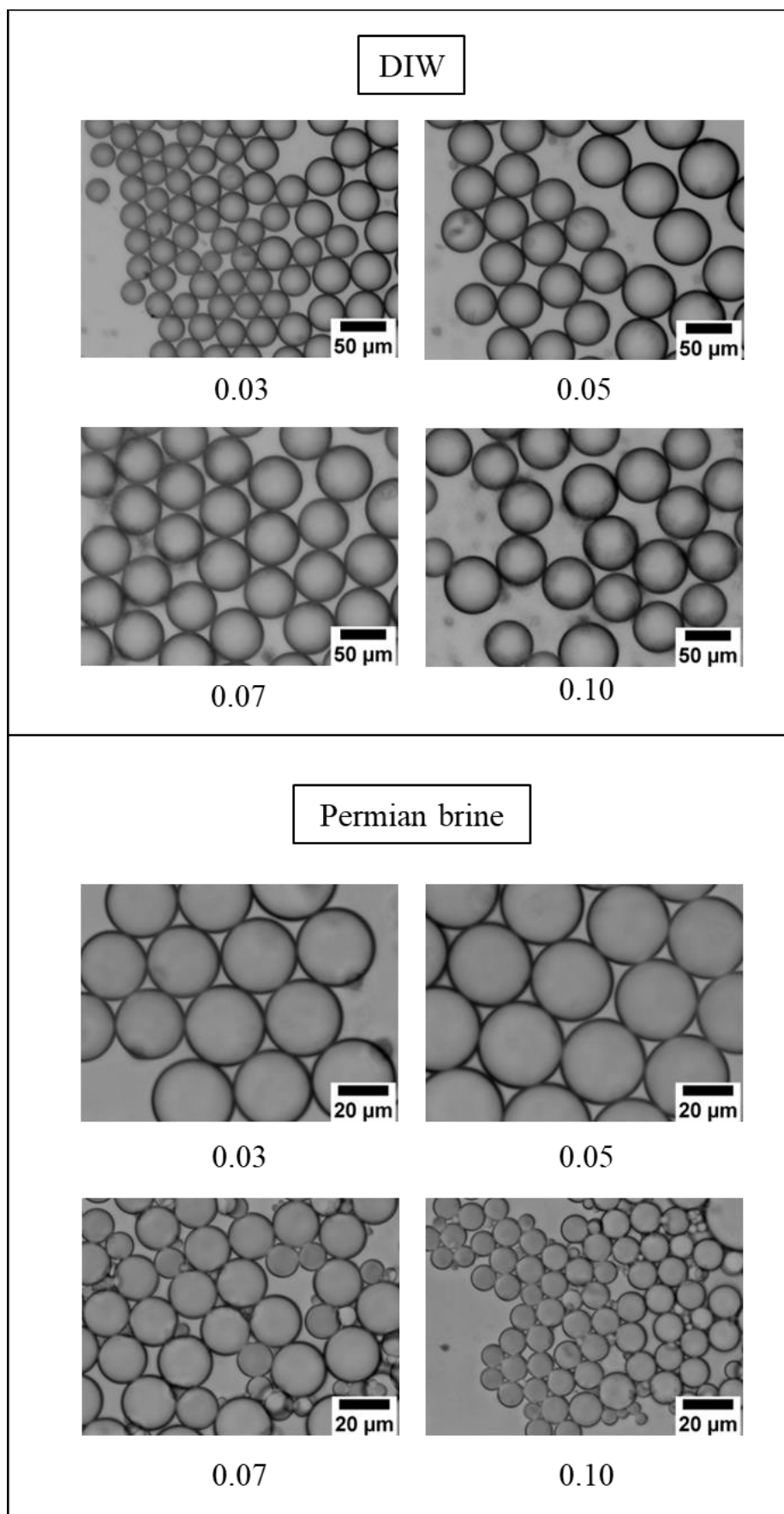
Figure 5.67. Optical microscope images taken immediately after preparation of oil-in-water emulsions from 5 g heptol (1:1 g g^{-1}) and 5 g of dispersions containing 0.1 wt.% ES-coated silica and different weight percentages of AHS surfactant in DIW and Permian brine.

DIW

0.001 0.005 0.010 0.030

0.050 0.070 0.100

Permian brine

0.030 0.050

0.070 0.100
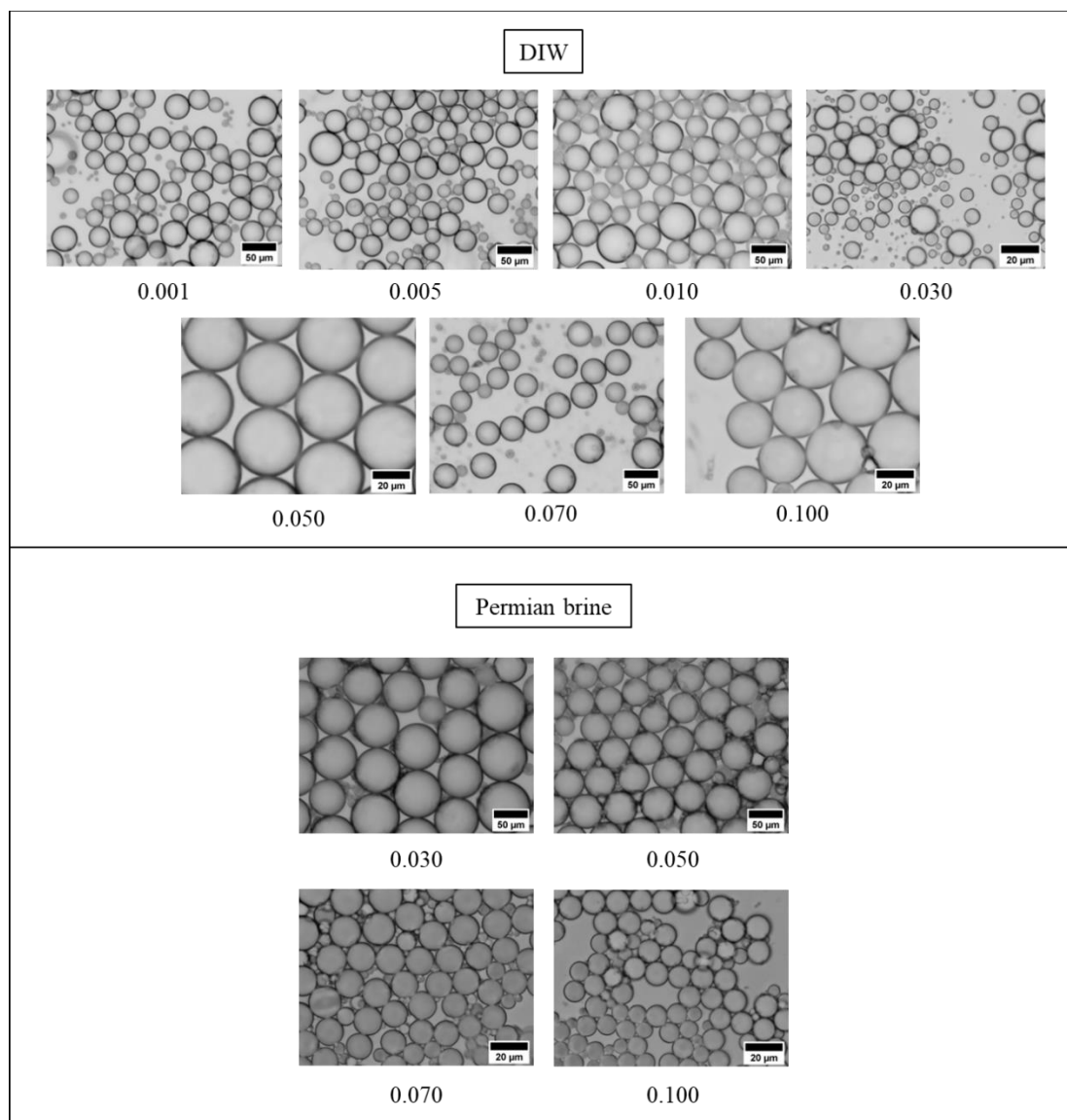
The effect of adding ES-coated silica particles on the emulsification of ZN solutions and heptol is presented in Figure 5.68. All the emulsions made with the blend of ZN and particles in DIW were phase separated within a day except for the one with 0.1 wt.%

particles and 0.03 wt.% AHS in DIW which had residual emulsion after a day ($f_o = 0.6$ and an initial drop diameter of 22 ± 2 µm). This emulsion coalesced more after a few days ($f_o = 0.8$). Creaming occurred seriously in all emulsions within a day ($f_w > 0.9$). All the emulsions made with ZN in Permian brine with or without particles experienced significant coalescence and creaming within an hour. It is also observed that the addition of ZN to the dispersion of 0.1 wt.% particles in Permian brine significantly destabilizes the Pickering emulsions made with particles alone. Figure 5.69 shows the initial microscope images of these emulsions.

A summary of results on emulsions from different oils and blends of ES-coated silica and surfactants is presented in Tables 5.5 – 5.8.

Figure 5.68. Appearance of oil-in-water emulsions formed from 5 g heptol (1:1 g g^{-1}) and 5 g of dispersions containing 0, 0.01 and 0.1 wt.% ES-coated silica and different weight percentages of ZN in DIW and Permian brine.
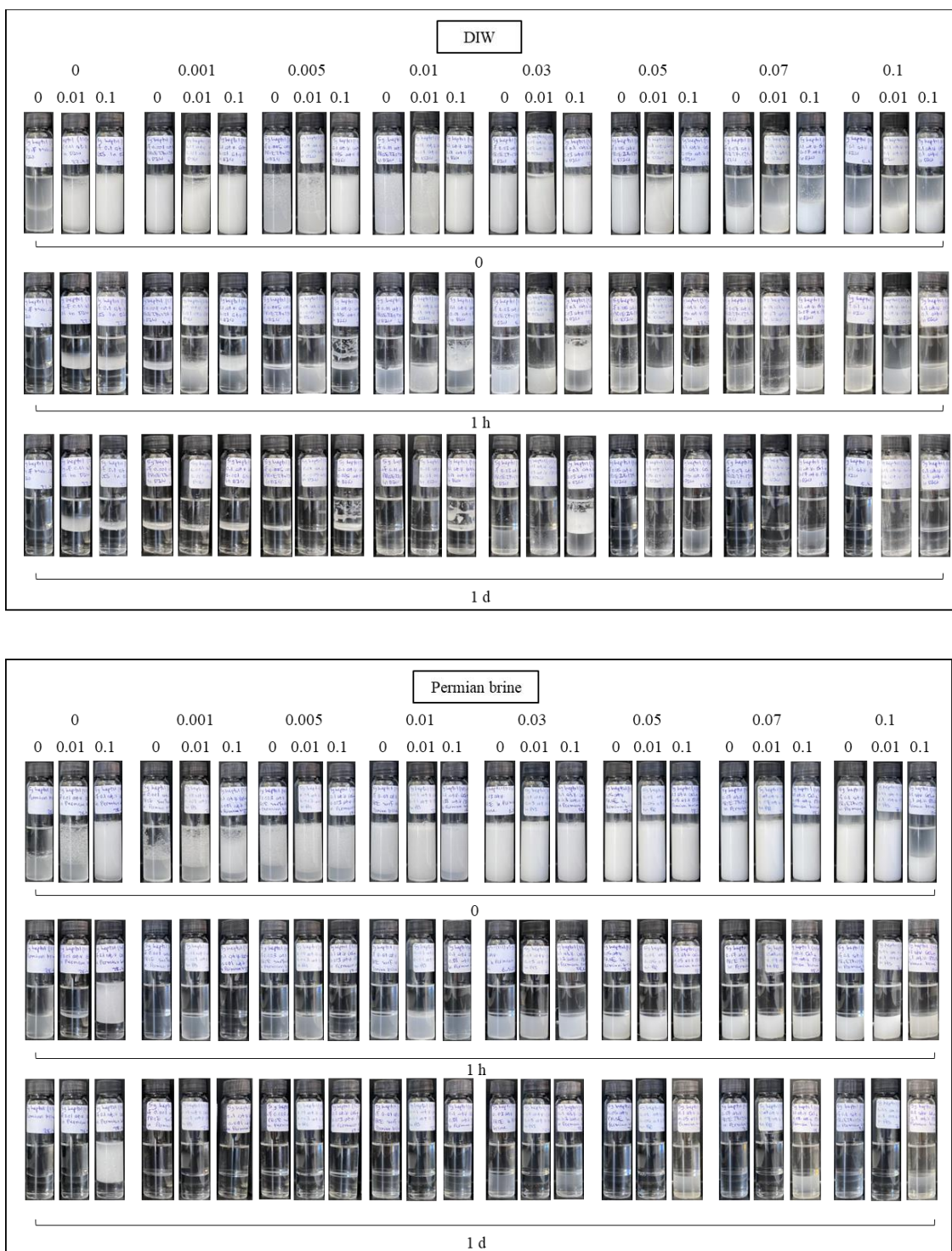
Figure 5.69. Optical microscope images taken immediately after preparation of oil-in-water emulsions from 5 g heptol (1:1 g g⁻¹) and 5 g of dispersions containing (a) 0.01 wt.%, (b) 0.1 wt.% ES-coated silica and different weight percentages of ZN in DIW and Permian brine.

(a)

Permian brine

0.03

0.05

0.07

0.10

(b)

DIW

0.001

0.005

0.01

0.03

0.05

0.07

0.1

Permian brine

0.001

0.003

0.01

0.03

0.05

0.07

0.1
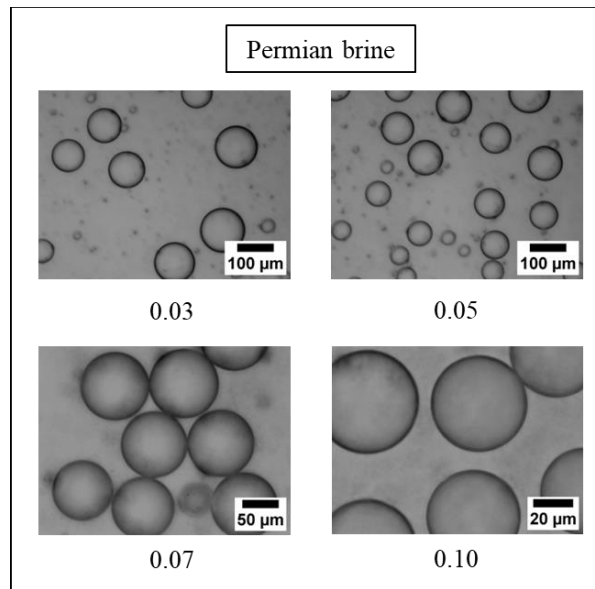
Table 5.5. Summary of results on oil-in-water emulsions from different oils and different blends of 0.01 wt.% ES-coated silica and different AHS concentrations (given in wt.%) in DIW and Permian brine (12.6 wt.%). Creaming was high in all emulsions ($f_w > 0.8$).

308

Particle	Oil	f_o after 100 days								Comment
		0	0.001	0.005	0.01	0.03	0.05	0.07	0.1	
0.01 wt.% in DIW	Toluene						0.7	0.4	0.7	Particle hydrophobization by physical grafting with zwitterionic AHS provids stronger hydrophobization than silane itself. Grafting with surfactant also reduces the particle surface charge and therefore particle-interface repulsion. Solvophobic interactions between surfactant-grafted particles and interfacial oil molecules are highest for toluene and weakest for heptane.
	Heptane					0.8				
	Heptol	1						0.5	0.8	
0.01 wt.% in Permian brine	Toluene							0.7		Ions reduce the particle-surfactant electrostatic attraction resulting in lower particle hydrophobization that is accompanied by the dominance of high concentrations of ions at the oil-water interface.
	Heptane									
	Heptol							0.8	0.6	

Table 5.6. Summary of results on oil-in-water emulsions from different oils and different blends of 0.1 wt.% ES-coated silica and different AHS concentrations (given in wt.%) in DIW and Permian brine (12.6 wt.%).

Particle	Oil	f_o or f_w after 100 days	Comment

Particle	Oil	0	0.001	0.005	0.01	0.03	0.05	0.07	0.1	
0.1 wt.% in DIW	Toluene	$f_o = 0.5$ $f_w = 0.8$	1			$f_o = 0.9$ to 0.4 with [surf.] ↑ $f_w > 0.9$				High particle concentrations in the blend in DIW lead to more residual emulsions of heptane and water due to the higher number of surfactant-modified particles adsorbing at the oil-water interface offering more interactions of surfactant tails with bulk heptane oils.
	Heptane	1				$f_o = 0.8$ to 0.6 $f_w = 0.9$		1		
	Heptol	1	$f_o > 0.8$ $f_w > 0.9$							
0.1 wt.% in Permian brine	Toluene	$f_o = 0.8$ $f_w = 0.9$	1						$f_o = 0.9$ $f_w = 0.9$	Ions prevent interactions between particles and surfactant resulting in less emulsions of water and toluene. Ions also reduce the interfacial heptane-water charge resulting in more emulsions. Heptol benefits from both toluene (high interfacial oil) and heptane (low interfacial charge).
	Heptane	$f_o = 0.6$ $f_w = 0.8$	1			$f_o = 0.3$ to 0 with [surfactant] ↑ $f_w = 0.9$ to 0.6 with [surfactant] ↑				
	Heptol	$f_o = 0.2$ $f_w = 0.7$	1			$f_o = 0.2$ to 0.1 with [surfactant] ↑ $f_w = 0.9$ to 0.7 with [surfactant] ↑				

Table 5.7. Summary of results on oil-in-water emulsions from different oils and different blends of 0.01 wt.% ES-coated silica and different ZN concentrations (given in wt.%) in DIW and Permian brine (12.6 wt.%). Creaming was high in all emulsions.

Particle	Oil	f_o after 100 days								Comment
		0	0.001	0.005	0.01	0.03	0.05	0.07	0.1	

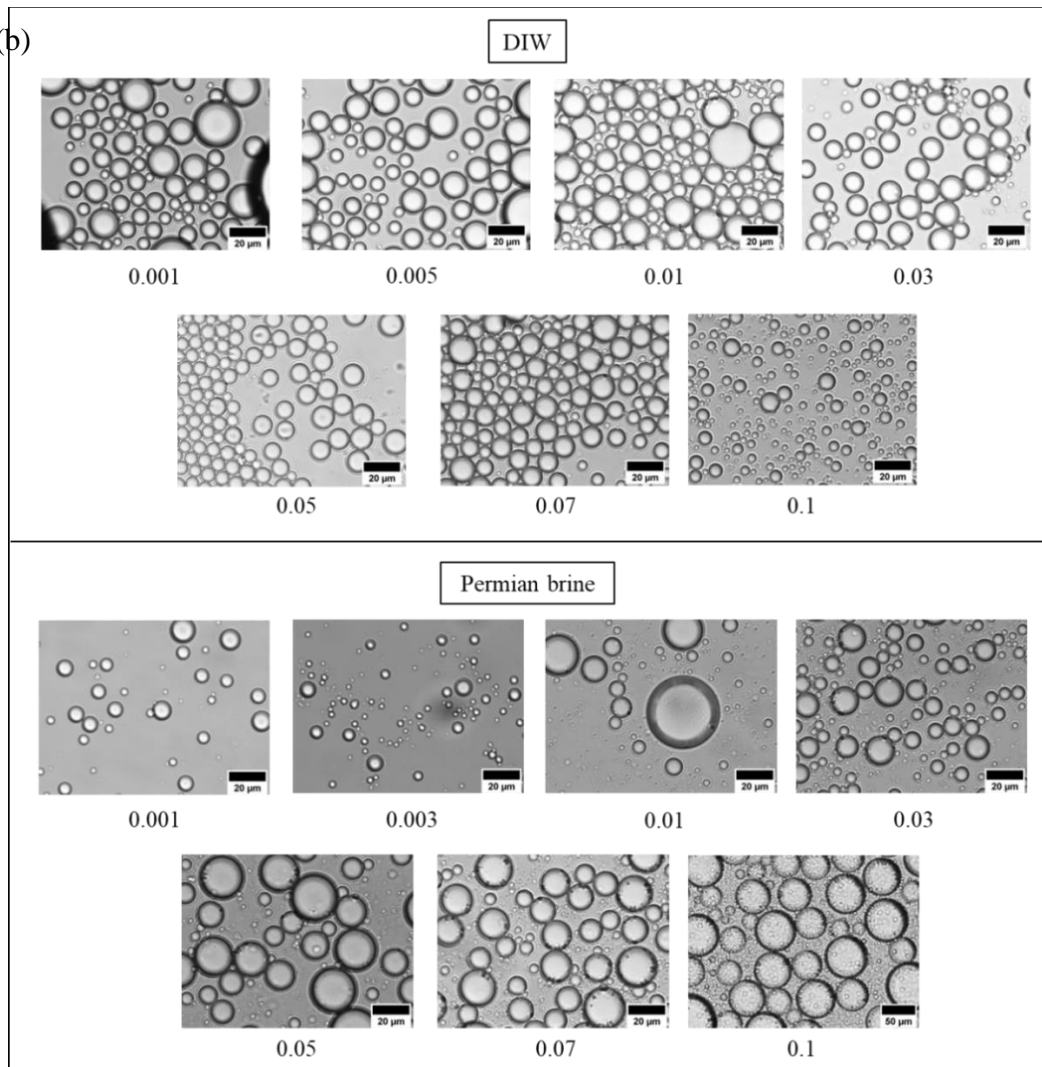| Particle	Oil					0.8	0.6		Comment
0.01 wt.% in DIW	Toluene					0.8	0.6		Zwitterionic and nonionic surfactants can hydrophobize particles through electrostatic attraction and hydrogen bonding, respectively to adsorb at oil-water interface. More initial emulsions were formed with polar toluene (with high interfacial oil) and water when blending ZN and particles. Like emulsions with ZN alone, heptane and heptol produced very unstable emulsions after preparation.
	Heptane								
	Heptol	1							
0.01 wt.% in Permian brine	Toluene						0.8	0.3	When Permian brine was added to the blend, more emulsions of toluene and water were formed probably due to the reduced oil-water interfacial charge. The demulsification ability of ZN prevents long-term emulsion stability.
	Heptane								
	Heptol								

Table 5.8. Summary of results on oil-in-water emulsions from different oils and different blends of 0.1 wt.% ES-coated silica and different ZN concentrations (given in wt.%) in DIW and Permian brine (12.6 wt.%). Creaming was high in all emulsions.

Particle	Oil	f_o after 100 days								Comment
		0	0.001	0.005	0.01	0.03	0.05	0.07	0.1	

Dispersion	Oil	Fractions				Notes
0.1 wt.% in DIW	Toluene	$f_o = 0.5$ $f_w = 0.8$				High particle concentrations in the blend in DIW destabilize the emulsions made with toluene and water probably due to insufficient surfactant concentrations for particle grafting. When surfactant concentration was enough (0.1 wt.%), an emulsion initially stable to coalescence was produced.
	Heptane		1	0.9	1	
	Heptol					
0.1 wt.% in Permian brine	Toluene	$f_o = 0.8$ $f_w = 0.9$			0.75	The addition of Permian brine to the blend produced more Pickering emulsions from water and toluene at high surfactant concentrations.
	Heptane	$f_o = 0.6$ $f_w = 0.8$		1		
	Heptol	$f_o = 0.2$ $f_w = 0.7$				

5.3.4 Effect of pH

The aqueous and adsorption behaviour of both particles and zwitterionic surfactants are affected by pH which in turn affects the emulsification of oil and water. In this part, the effect of pH reduction by hydrochloric acid or aluminium sulphate on the emulsification of different oils and some dispersions or solutions is investigated.

5.3.4.1 HCl

Figure 5.70 shows the effect of pH reduction by HCl on the emulsification of different oils and dispersions of 0.1 wt.% ES-coated silica in DIW. The variations in fractions of oil and water resolved from these emulsions with time are shown in Figure 5.71. At a lower pH, the emulsion of toluene and water is less stable to coalescence and creaming, whereas the emulsions created with other oils show no notable change with pH reduction. Figure 5.72 shows the initial microscopy of these emulsions. On the other hand, reducing the pH of 0.1 wt.% ZN in DIW initially improved the emulsification of water and toluene but the emulsion was phase separated after 40 days (Figures 5.73 and 5.74).

The emulsification of oil and water in the presence of particles was previously observed to be more intense when toluene was used. ES-coated silica particles are highly and weakly anionic when they are at their original pH (9) and reduced pH (4) due to the deprotonation and protonation of silanol groups on the particle surface, respectively. Although a decrease in particle-interface electrostatic repulsion is achieved upon reducing the pH of the dispersions, the residual emulsion is reduced which is probably due to the decreased interfacial toluene molecules on reducing pH which also leads to a rise in the toluene-water interfacial tension.[283]

Upon pH reduction to 4 by HCl, the zwitterionic surfactant in ZN turns cationic due to the protonation of the sulfonate group. As a result of the protonation of the sulfonate group in the surfactant headgroup, lower electrostatic repulsion between headgroups is achieved which is accompanied by higher adsorption of cationic surfactant at the anionic oil-water interface. As previously observed, the emulsification of oil and water in the presence of ZN is more pronounced when using toluene however due to the demulsification power of ZN, the resulting emulsion is not long-term stable.

Figure 5.70. Effect of pH reduction on emulsification of 5 g of different oils including toluene, heptane and 5 g heptol (1:1 g g^{-1}) and 5 g of 0.1 wt.% ES-coated silica in DIW. HCl was used for pH adjustment.

Figure 5.71. Fractions of oil (f_o) and water (f_w) resolved with time from oil-in-water emulsions formed from 5 g of different oils including toluene, heptane and heptol (1:1 g g^{-1}) and 5 g of dispersions containing 0.1 wt.% ES-coated silica in DIW at original and reduced pH. HCl was used for pH adjustment.

Figure 5.72. Optical microscope images taken immediately after preparation of oil-in-water emulsions formed from 5 g of different oils including toluene, heptane and heptol (1:1 g g^{-1}) and 5 g of dispersions containing 0.1 wt.% ES-coated silica in DIW at pH 4. The pH was reduced by HCl.

315
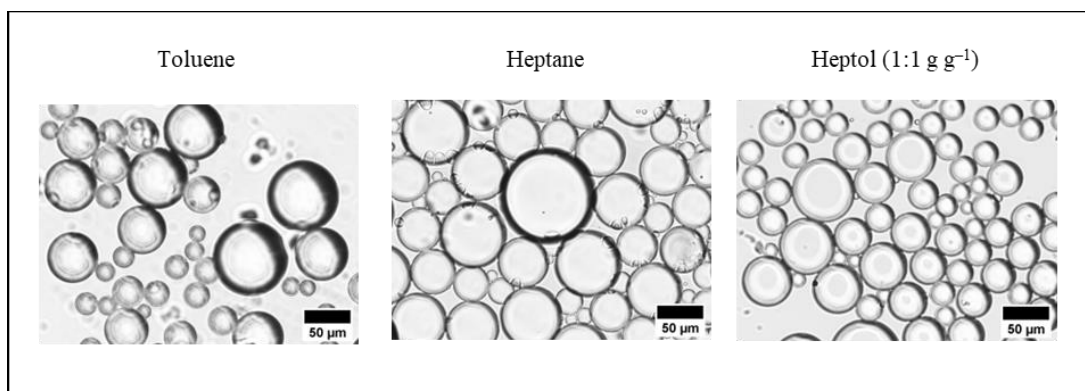
Figure 5.73. Effect of pH reduction on emulsification of 5 g of different oils including toluene, heptane and heptol (1:1 g g^{-1}) and 5 g of 0.1 wt.% ZN in DIW at original and reduced pH. HCl was used for pH adjustment.
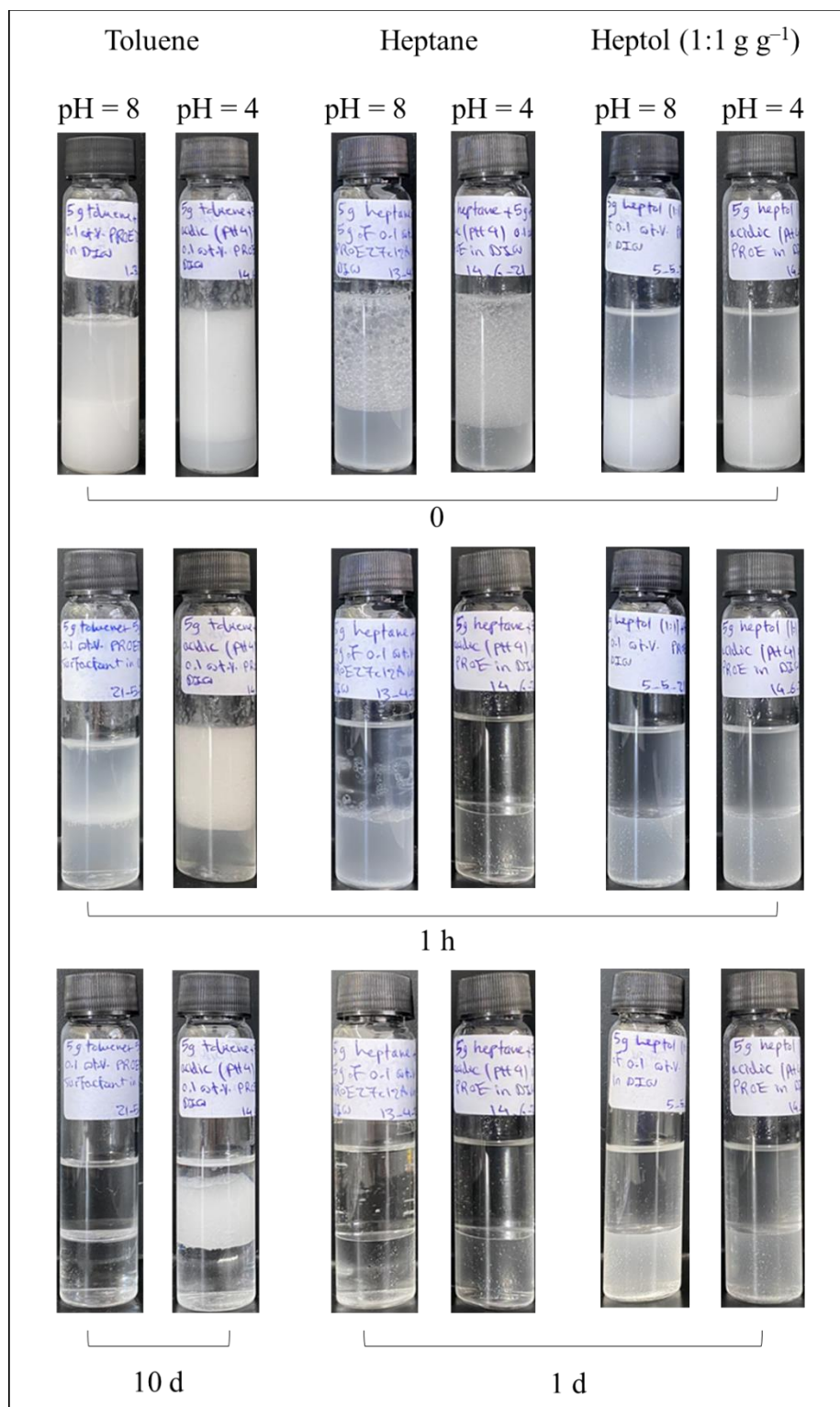
Figure 5.74. Fractions of oil (f$_o$) and water (f$_w$) resolved with time from oil-in-water emulsions from 5 g of toluene and 5 g of 0.1 wt.% ZN in DIW at the original and reduced pH. HCl was used for pH adjustment.
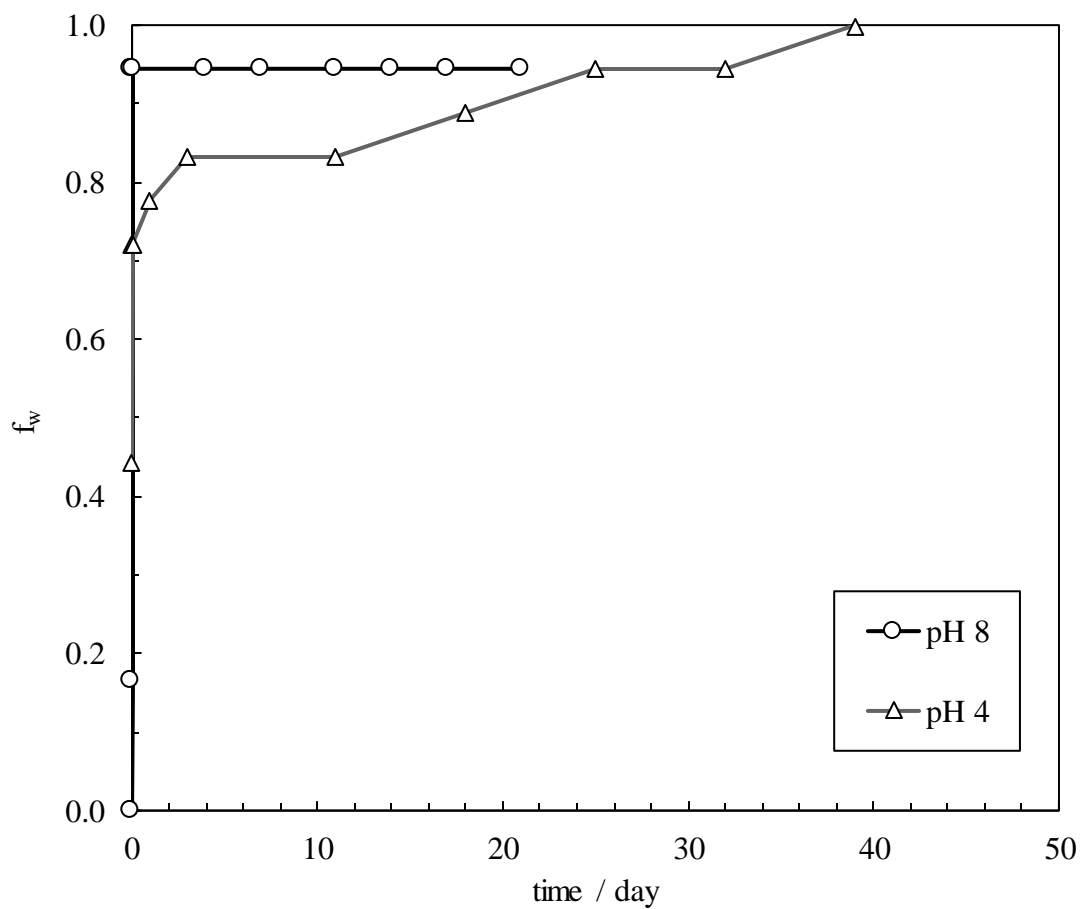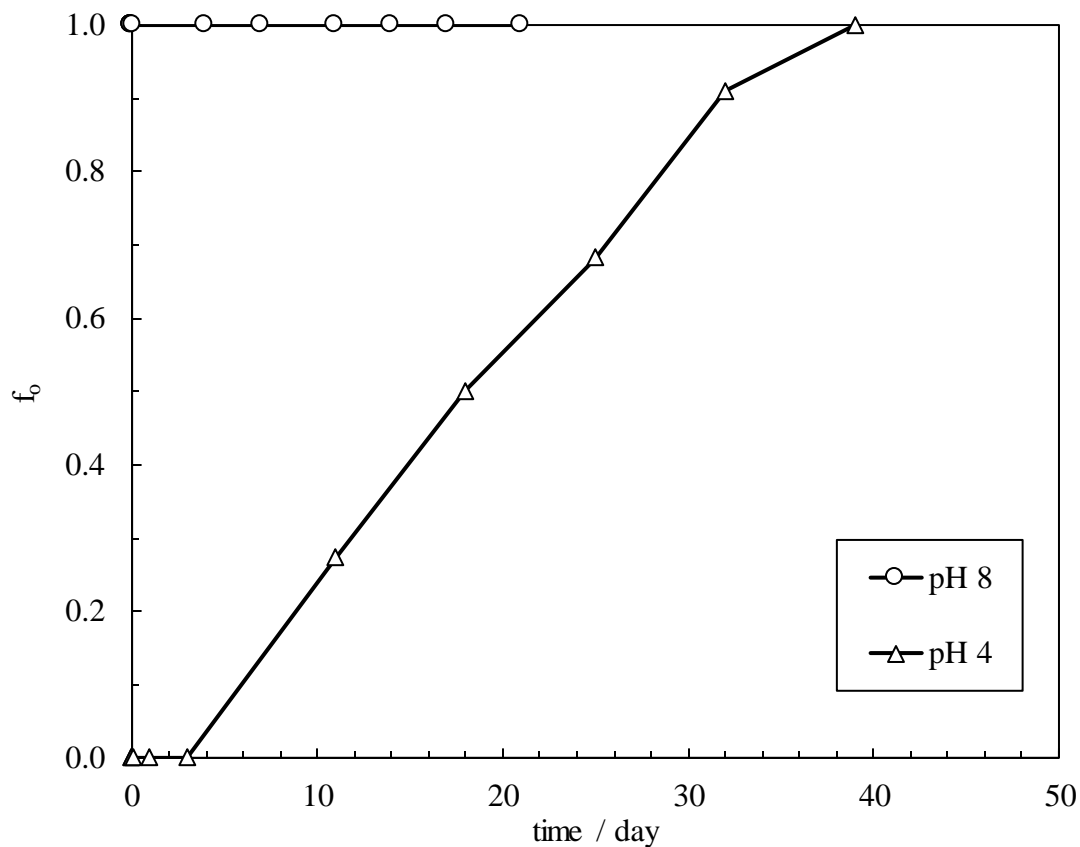
5.3.4.2 $Al_2(SO_4)_3$

The trace addition of aluminium sulphate to dispersions of ES-coated silica lowers the pH to 4 – 5 which was found to enhance the stability of particles in Permian brine for a long time. Figure 5.75 shows the effect of adding 0.01 wt.% aluminium sulphate (10 % of particle concentration) to the dispersion of 0.1 wt.% particles in DIW on the emulsification of different oils with water. In contrast to HCl, initial coalescence did not occur in the emulsions of toluene and dispersions upon the addition of $Al_2(SO_4)_3$ (Figure 5.76). Compared to the emulsion made with the original pH dispersion, the emulsion with toluene and the low pH dispersion had lower coalescence in the first 3 months. The addition of aluminium sulphate to the dispersion did not have a significant effect on the emulsification of water and heptane. When using heptol, an emulsion more initially stable to coalescence was formed with the addition of aluminium sulphate but it was phase separated within a day. The initial microscope images of these emulsions are presented in Figure 5.77. The initial drop diameter of all emulsions made with low pH dispersions was measured as $54 \pm 6 \, \mu m$. The addition of aluminium sulphate to 0.1 wt.% ZN solutions could not improve the emulsification of different oils and water.

The addition of aluminium sulphate electrolyte provides counterions to both reduce particle surface charge (higher hydrophobicity) and form a more compact particle monolayer at the interface which leads to higher emulsification of toluene. The higher emulsification of heptol on adding aluminium sulphate is thought to be due to the presence of toluene.

Figure 5.75. Effect of pH reduction on the emulsification of 5 g of different oils including toluene, heptane and heptol (1:1 g g^{-1}) and 5 g of 0.1 wt.% ES-coated silica in DIW. Aluminium sulphate was used for pH adjustment (10% of particle concentration).
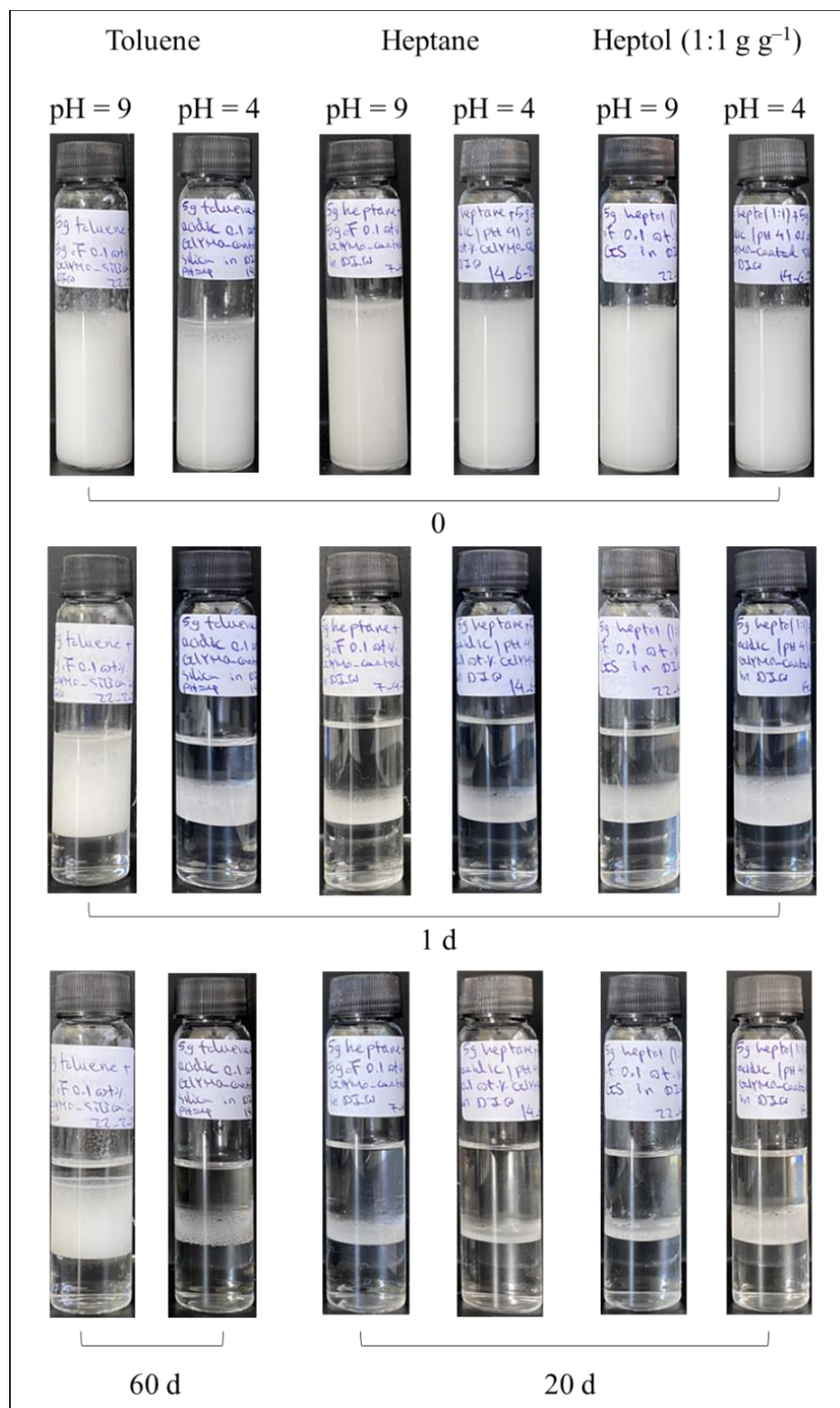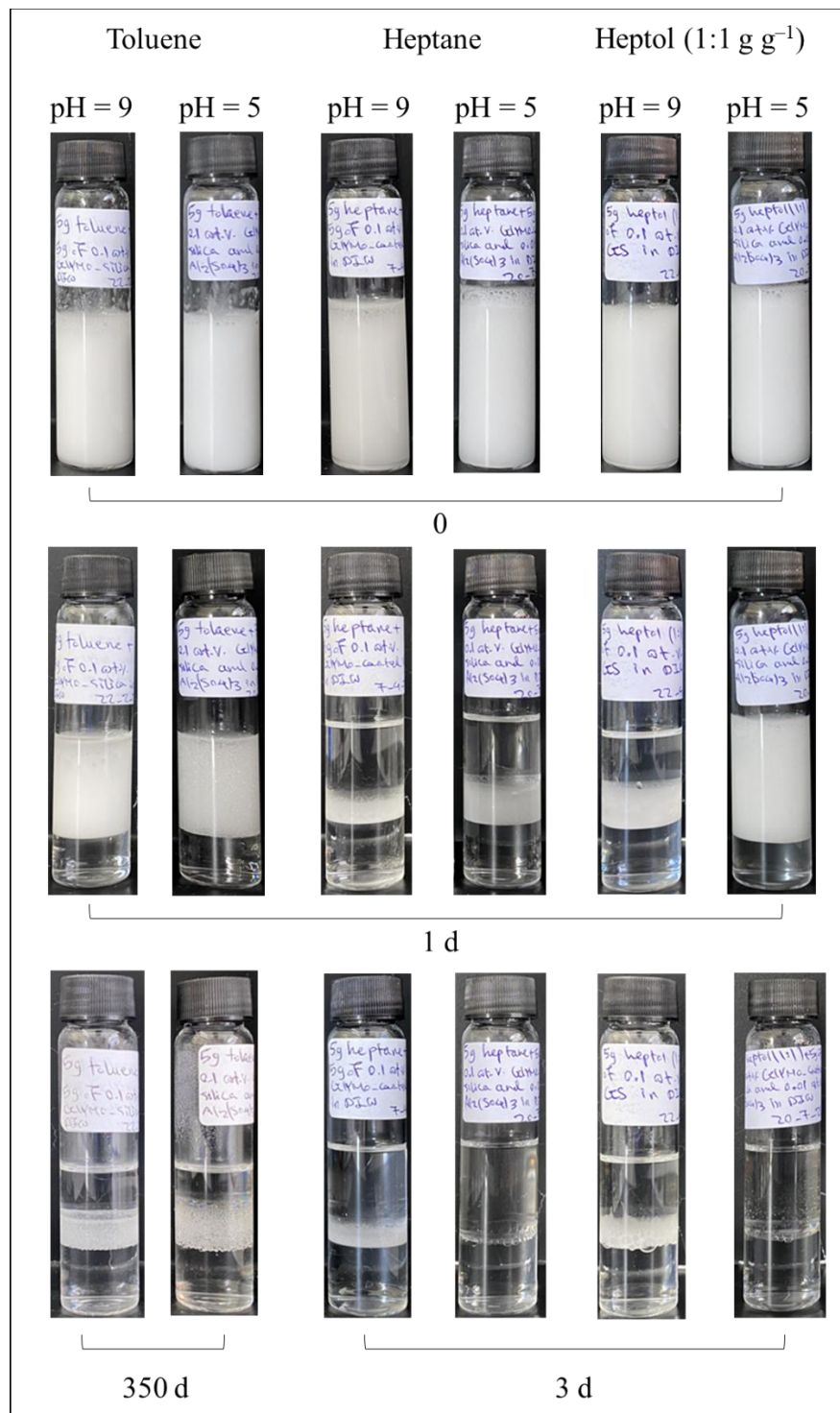
Figure 5.76. Fractions of oil (f$_o$) and water (f$_w$) resolved with time from oil-in-water emulsions from 5 g of different oils including toluene, heptane and heptol (1:1 g g^{-1}) and 5 g of dispersions containing 0.1 wt.% ES-coated silica in DIW at original and reduced pH. Aluminium sulphate was used for pH adjustment (10% of particle concentration).
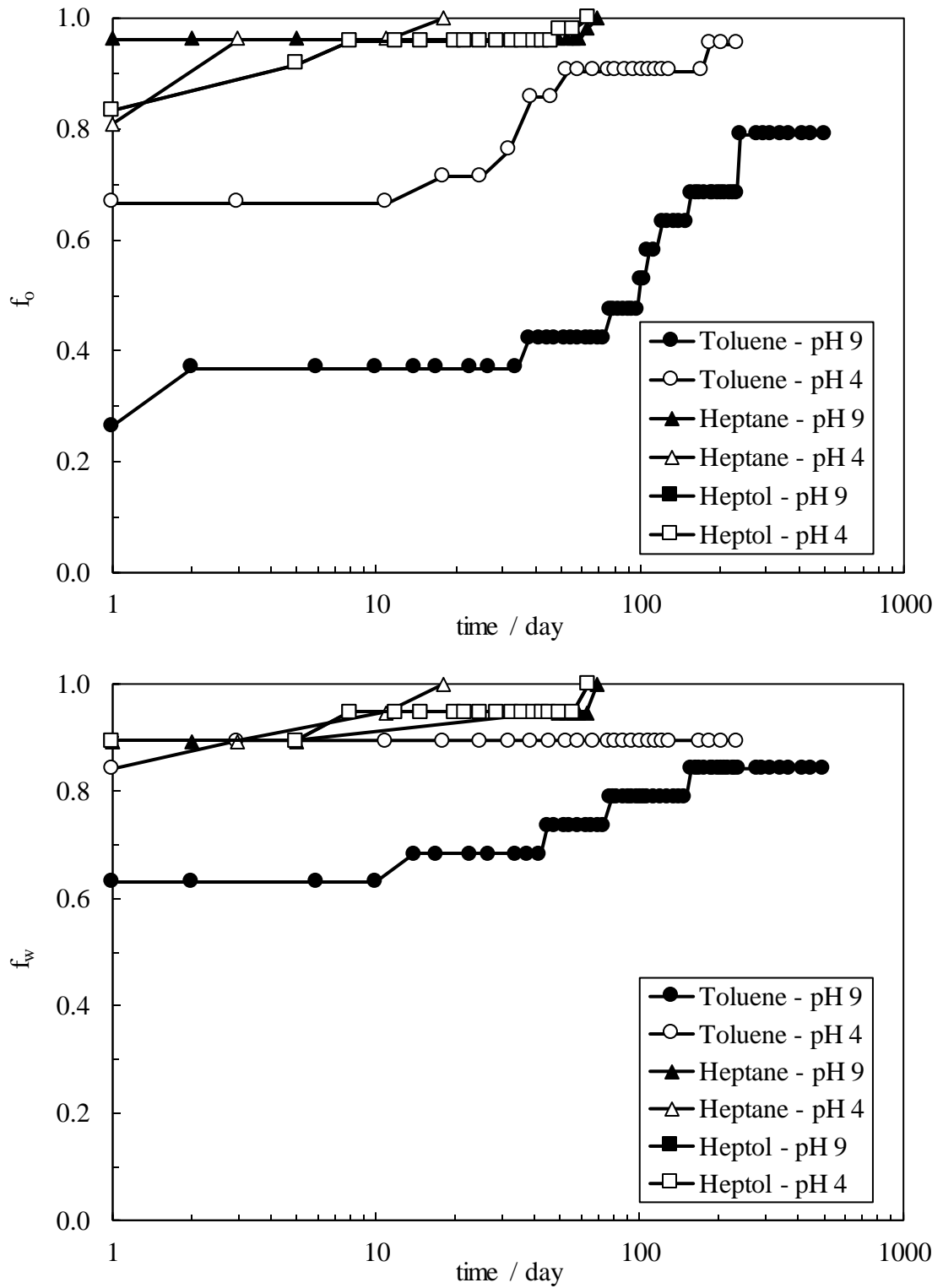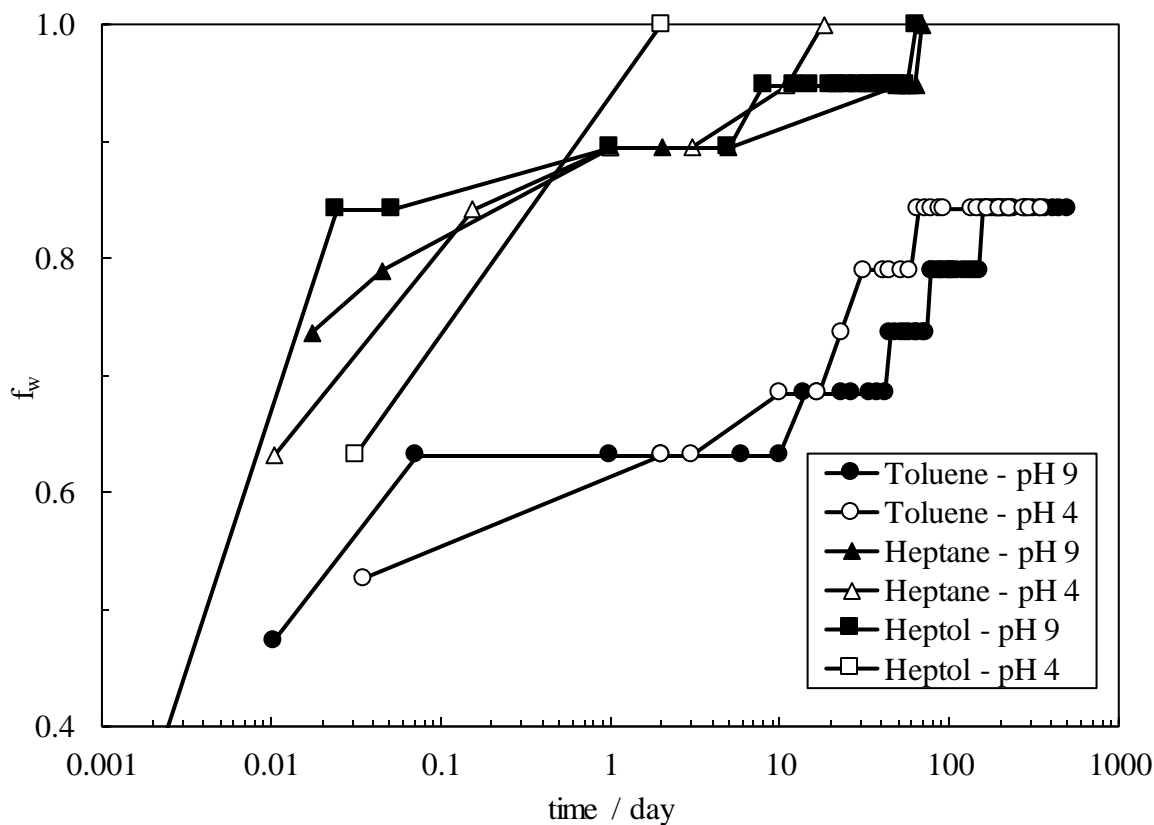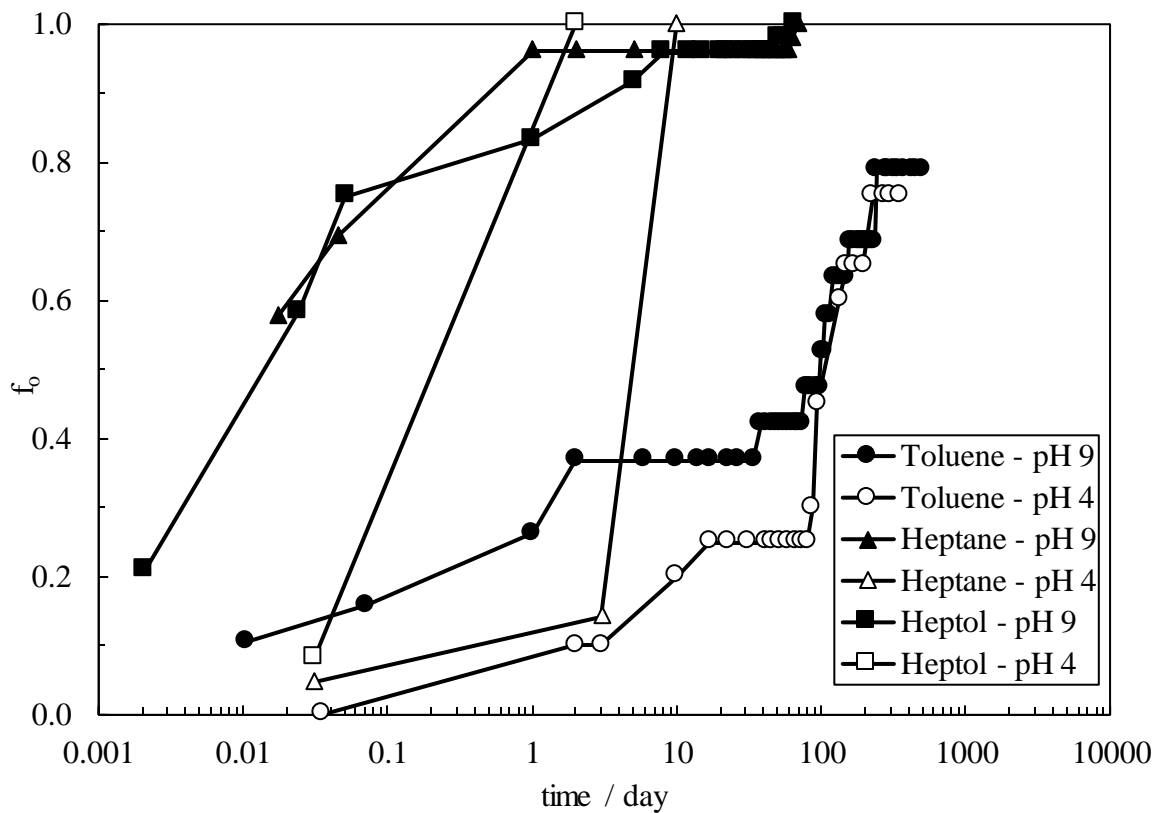
Figure 5.77. Optical microscope images taken immediately after preparation of oil-in-water emulsions from 5 g of different oils including toluene, heptane and heptol (1:1 g g^{-1}) and 5 g of dispersions containing 0.1 wt.% ES-coated silica in DIW at pH 4. Aluminium sulphate was used for pH adjustment (10% of particle concentration).

| Toluene | Heptane | Heptol (1:1 g g^{-1}) |
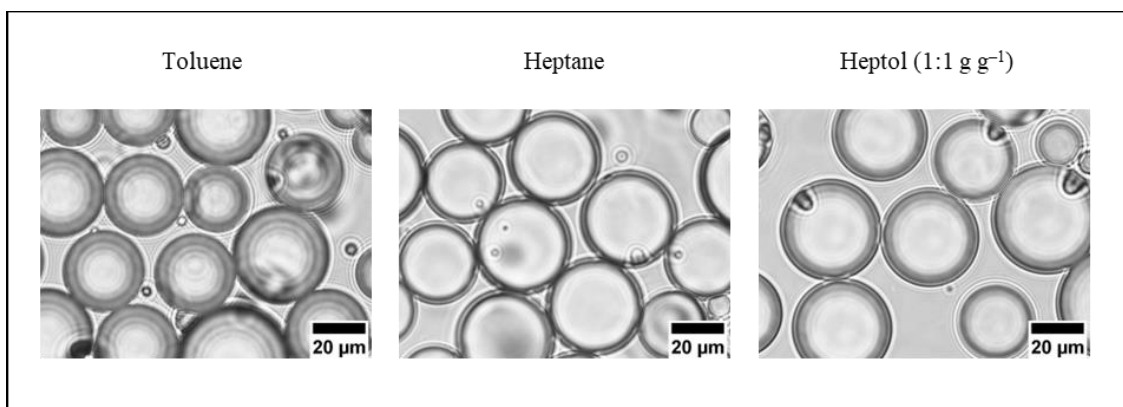
5.4 Summary of findings

This chapter examined the effects of particles and surfactants on the oil-water interfacial tension and emulsification of oil and water. The following findings can be derived from the chapter:

- On the addition of AHS and ZN surfactants to DIW or Permian brine, a considerable reduction in oil-water interfacial tensions was seen for all oils at ~ CMC (more so for ZN surfactant).

- The addition of Permian brine increased the interfacial tension between water and various oils at 25 °C due to large ion adsorption at the interface and increased micellization.

- An increasing interfacial tension was observed with [surfactant] in Permian brine when using crude oil due to the ion-pair formation and increased solubilization. This effect was not observed for other oils.

- Increasing [particle] in AHS in DIW had no clear effect on the crude oil-water interfacial tension but systematically reduced the interfacial tension when blends of ZN surfactant and particles in DIW were used. Increasing interfacial tension between crude oil and water was observed when using ZN surfactant + particles in Permian brine.

- Increasing the temperature from 25 °C to 60 °C increased the crude oil-water interfacial tension both with and without particles probably due to reduced solvation of surfactant molecules at the oil-water interface by counterions like Ca^{2+} or Na^+. The increase was more pronounced for ZN surfactant probably due to the reduced solubility of ethylene oxides of the nonionic surfactant in water at high temperatures.

- Emulsification of toluene, heptane and heptol and AHS in DIW was found to be a function of interfacial charge and oil molecules at the oil-water interface (decreasing as toluene > heptol > heptane. The surfactant-interface electrostatic repulsion prevents large surfactant adsorption at the interface so less emulsion was observed with toluene than heptane.

- A synergy in emulsification was observed when using heptol ($f_o = 0.2$ after 100 days for [AHS] = 0.1 wt.% in DIW) due to the mixed effects of individual oils *i.e.* local high interfacial oil (toluene) and low interfacial charge (heptane).

- Ions reduce the surfactant-interface and surfactant-surfactant electrostatic repulsion and result in a more compact surfactant monolayer at the oil-water interface.

- Stable emulsions of toluene and heptol with small coalescence were observed with the addition of Permian brine to AHS solutions ($f_o < 0.2$ after 100 days for [AHS] = 0.05 – 0.07 wt.%).

- Due to the lack of oil interfacial adsorption and high interfacial tension, emulsions of heptane and AHS in Permian brine were unstable. The nonionic $C_{10-12}E_9$ in ZN surfactant can also adsorb at the oil-water interface to form a more compact

- monolayer with zwitterionic surfactant and more stable emulsions but due to its low concentration (5% in ZN surfactant) and the demulsification ability of ZN surfactant, no long-term stable emulsion was observed.

- Of different oils, ZN surfactant in Permian brine produced more stable emulsions when using polar toluene. Independent of the oil type, surfactant and background electrolyte, all emulsions demonstrated considerable creaming. Large surfactant concentrations (> 0.07 wt.%) in Permian brine were often seen to create a wider drop size distribution with flocs.

- More emulsions of heptane and water were formed by weakly anionic AS-coated silica particles at the original pH, while less emulsification was found at low pH where the particles were protonated and re-dispersed.

- For ES-coated silica in DIW, the particle-interface electrostatic repulsion prevents particle adsorption at the oil-water interface but the particles can interact with interfacial oil through polar-polar (hydrogen bonding and dipole-dipole) interactions and solvophobic interactions in the case of using polar toluene and non-polar heptane, respectively. In both cases, particle hydrophobization results in emulsification (polar-polar interaction is stronger). Therefore, toluene produced more stable emulsions ($f_o = 0.5 \pm 0.1$ for $0.03 – 0.1$ wt.% particles in DIW after 3 months) than heptane. Heptol took advantage of both hydrophobization mechanisms producing an emulsion with almost no coalescence ($f_o \sim 0$ for 1 wt.% particles in DIW after 3 months).

- Ions can screen the charges of both particles and the oil-water interface enabling more adsorption of particles while at the same time reducing the oil polarity leading to fewer interactions between particles and interfacial oil. Ion accumulations at the oil-water interface also prevent the adsorption of like-charged particles.

- Since the surfactant tail is longer than the ES length (1.8 nm *vs* 0.9 nm), the grafted surfactant tails on particles mostly interact with interfacial oil at the oil-water interface. This hydrophobization is thought to be stronger than the partial hydrophobization caused by the silane itself (see zeta potentials). The solvophobic interactions between surfactant-modified particles and interfacial oil molecules were highest for toluene and weakest for heptane leading to higher emulsions of toluene and water with the blend of 0.01 wt.% particles and AHS.

- There was a pH-responsive emulsification behaviour in which the emulsion type was switched between oil-in-dispersion emulsion (high pH, low [AHS]) and Pickering emulsion (isoelectric pH, high [AHS]). The former did not create stable oil-in-dispersion emulsions due to the low particle and surfactant concentrations used.

- Ions were found to reduce emulsification by adsorption at the oil-water interface and lowering particle-surfactant electrostatic attraction (less particle hydrophobization).

- The addition of high AHS surfactant concentrations to dispersions of particles in Permian brine improved the stability of Pickering emulsions while no significant change was seen in those made with particles in DIW.

- Compared to other oils, more initial emulsions of polar toluene and blends of ZN surfactant and particles in DIW were formed which increased with the addition of Permian brine due to the reduced oil-water interfacial charge and increased particle adsorption at the oil-water interface.

- There was no significant improvement in coalescence stability in the long term upon adding particles to ZN surfactant in Permian brine.

- The addition of ZN surfactant to the dispersion of 0.1 wt.% particles in Permian brine significantly destabilized the Pickering emulsions made with particles alone.

- Reducing pH by HCl or $Al_2(SO_4)_3$ had no significant long-term effect on the emulsification of different oils.

- The addition of Permian brine made coalescence and creaming in emulsions of crude oil and water slower probably due to the increased adsorption of crude oil polar groups at the interface by sodium ions. The addition of ions to ZN surfactant solutions was observed to increase coalescence and creaming in the emulsions of water and crude oil probably due to surfactant depletion and the demulsification power of ZN surfactant.

- The extent of particle hydrophobization by cationic polar groups of crude oil is higher for bare silica than ES-coated silica leading to more stable Pickering emulsions with bare silica. The slightly aggregated particles in Permian brine could stabilize the emulsions more than particles in DIW.

Chapter 6 Oil recovery

It is common practice to assess the chemicals used for EOR by flooding experiments since the high efficacy of the chemicals in static studies such as contact angle and interfacial tension measurements does not ensure their effectiveness in porous media. In this study, spontaneous imbibition tests were considered for examining the EOR efficiency of certain dispersions selected from the results obtained earlier. The outcrop shale cores were first tried for these experiments but due to the lack of injectivity, low-permeability Stevn Klint (SK) chalk cores were replaced. The particle stability in porous media (flow mode) was also checked and compared with the static stability investigations performed earlier in sample vials. The effect of adding particles on surfactant adsorption onto rock was tested in dynamic mode and compared with static adsorption results on rock powder. The spontaneous imbibition tests were finally performed and the potential EOR mechanisms of surfactant-particle mixtures are discussed based on the results obtained.

6.1 Candidate injectants

The identification of potential injectants in spontaneous imbibition tests was done using crude oil-water interfacial tensions and contact angles. Due to the necessity of using a brine in field EOR activities, dispersions of ES-coated silica particles and surfactants in only Permian brine were considered. The interfacial tension results demonstrated that the addition of surfactants to Permian brine leads to a considerable reduction in oil-water interfacial tension while the addition of particles to either surfactant solution has little to no impact on the tension at the oil-water interface. The oil-water contact angle measurements showed a maximum reduction at 0.03 wt.% AHS and 0.05 wt.% ZN both in Permian brine in the presence of 0.01 wt.% particles. The dispersions with the lowest contact angles were chosen for spontaneous imbibition experiments because it is thought that rock wettability change is more determining in chemical EOR.

6.2 Cores

Shale reservoirs offer pore throat widths ranging from micro- to nano-metres leading to small injectivity.[284] The injectivity of shale cores was first examined in this work to determine whether they could be used for spontaneous imbibition tests. With a confining

pressure of up to 20 bars, DIW or heptane was injected into two separate shale cores at ambient temperature. Due to the low rock permeability and subsequent pressurization of the core with liquid injection, the pump pressure limit was eventually reached without any liquid being produced. In another experiment, a shale core was vacuumed and saturated with heptane for 24 h at ambient conditions. Alternatively, a five-day high pressure saturation by heptane was also conducted using a shale core at ambient temperature and saturation pressure of 50 bars. Lastly, following the sponsor's protocol, a few shale cores were saturated and pressurized with crude oil to 70 bars, then aged for two weeks at 120 °C. No evidence of a significant weight difference as an indication of liquid saturation was observed in the above experiments. This signifies that the shale cores were too tight to be used for oil saturation and imbibition tests.

Alternatively, SK chalk cores were kindly provided by the Smart Water Group (University of Stavanger) for imbibition tests. The SK chalks are considered highly porous $(45 - 50\%)$ but have low permeabilities $(1 - 5 \text{ md})$ with a pore diameter of 80 nm to a few microns. The similar mineralogy of SK chalks (98% calcite) to Wolfcamp shale and their low pore diameters ensure almost analogous interactions between aqueous/crude oil chemicals and rock minerals.

6.3 Dynamic particle stability and surfactant adsorption onto rock

6.3.1 Particle stability and adsorption in porous media

It was revealed in Chapter 3 that ES-coated silica particles are stable in Permian brine at 75 °C for a long time. Yet compared to static sample vials, the aqueous stability of particles when they flow in porous media may differ. Since the particles must travel through narrow pore channels, any severe aggregation can block the rock and cause formation damage which is more serious in tight reservoir rocks. Therefore, particle stability and rock injectivity should be checked before flooding experiments and field applications. The investigation may also provide useful information on particle adsorption and retention in porous media during fluid flow. Core no. 1 (Table 6.1) and a dispersion of 0.01 wt.% particles in Permian brine were considered for this investigation. The dried core was first injected with Permian brine for 2.5 pore volumes (PV) followed by an 8 PV injection of dispersion, both at 0.1 cm^3 min^{-1} and 75 °C. The initial brine injection was to equilibrate the rock minerals with brine ions prior to the introduction of particles to prevent excess, unbalanced adsorption of particles onto the bare rock. This may make for a more realistic study.

The pressure differences between the inflow and outflow in response to the dimensionless injected pore volume (normalized by the V_p of the core) are depicted in Figure 6.1. It is anticipated that any blockage of the pore throats caused by considerable particle aggregation in the porous media at high temperatures would manifest as a continual growing pressure difference until the eventual termination of the experiment due to the pressurization of the core, which was not seen here. The particles thereby withstood aggregation under high salinity and high temperature conditions while flowing in porous media, just as was observed in static sample vials. Having said that, it is noted that pressure drop fluctuations during dispersion injection are more pronounced than those during Permian brine injection, which will be discussed later.

Following the injection of an adequate volume, sampling was done from the produced dispersion in an effort to evaluate the particle adsorption and retention in the porous medium. Several approaches were explored to determine the particle content of the effluents but all failed. ES-coated silica particles did not exhibit the characteristic absorption peak that is usually seen with bare silica in the UV region (100 – 400 nm), probably as a result of the silane coverage. A concentration-dependent surface tension that may have served as a calibration curve was also not observed by ES-coated silica particles due to their low surface activity, as shown in Chapter 3. As a final attempt, two large samples (2×50 cm^3) were taken for drying; however, due to the high salt concentrations and low particle concentrations used, attempts to determine the particle dosage by weighing the dried samples failed.

SK chalk constitutes a distinctive lithological unit akin to the Ekofisk and Valhall oil reservoir. Its notable attributes encompass a high porosity coupled with a conspicuously reduced permeability, effectively distinguishing it from the broader spectrum of rock formations. This singular geophysical characteristic can be attributed to the presence of a multitude of minute pore spaces dispersed throughout the rock; however, the salient feature is the limited interconnectivity between these pores.

It is pertinent to underscore that SK chalk has been employed as a consistent and enduring subject of investigation within the realm of EOR research, thereby serving as a focal point of scholarly inquiry over an extended temporal horizon. Such high porosity and low permeability measured here have been observed before by other researchers.[137, 138, 285]

Table 6.1. Specifications of the SK chalk cores used for assessing the adsorption of ES-coated silica particles and AHS or ZN surfactants onto rock during flow in porous media. V_p and V_b are the pore and bulk volumes of cores, respectively.

Core No.	Length / cm	Diameter / cm	V_p / cm^3	V_b / cm^3	Porosity / %	Permeability / md	Injectant
1	7.046	3.800	39.2	79.9	49.0	4.2 ± 0.4	0.01 wt.% particles in Permian brine
2	6.740	3.810	38.2	76.8	49.8	4.3 ± 0.1	0.03 wt.% AHS in Permian brine
3	7.056	3.802	39.5	80.1	49.4	3.6 ± 0.5	0.03 wt.% AHS and 0.01 wt.% particles in Permian brine
4	7.024	3.820	40.4	80.5	50.2	3.5 ± 0.3	0.05 wt.% ZN in Permian brine
5	6.700	3.812	37.9	76.5	49.5	3.1 ± 0.2	0.05 wt.% ZN and 0.01 wt.% particles in Permian brine

Figure 6.1. Differential pressure *versus* injected pore volume for a dried SK chalk core injected with Permian brine followed by 0.01 wt.% ES-coated silica particles in Permian brine at 0.1 cm^3 min^{-1} and 75 °C.
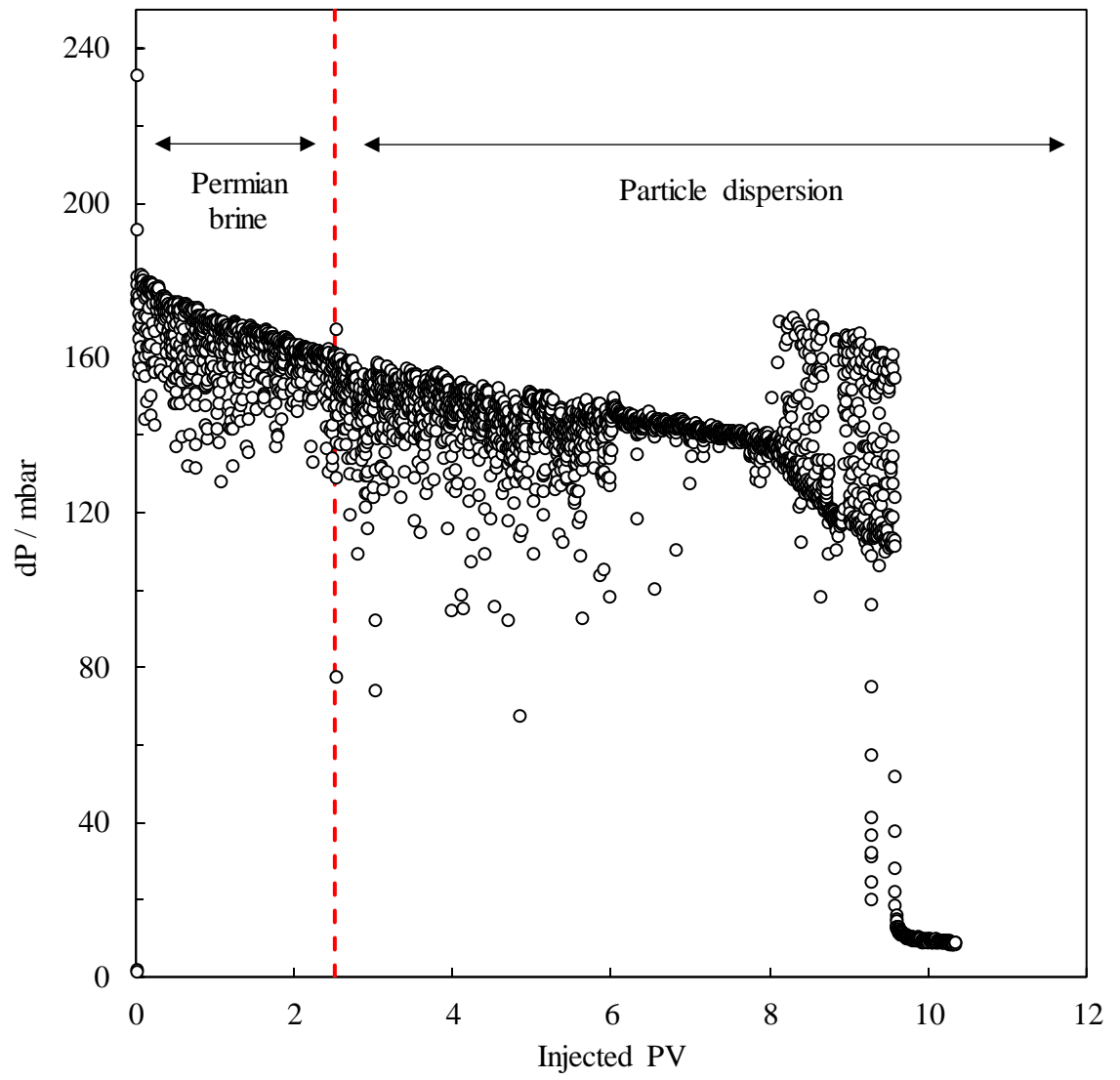
6.3.2 Surfactant adsorption onto rock in porous media

The surfactant adsorption onto rock powder was investigated earlier in this study, however the surfactant adsorption behaviour could be different in porous media. The selected dispersions for spontaneous imbibition tests were considered for this dynamic surfactant adsorption study. Cores 2 – 5 (Table 6.1) were used to study the adsorption of 0.03 wt.% AHS and 0.05 wt.% ZN from Permian brine onto rock at 75 °C in the presence and absence of 0.01 wt.% ES-coated silica particles.

6.3.2.1 Pressure profiles

The pressure profiles created by injecting Permian brine followed by AHS and ZN solutions both with and without 0.01 wt.% ES-coated silica particles at 75 °C are shown in Figures 6.2 to 6.5. Smaller differential pressure oscillations are often seen during Permian brine injection. In addition, dispersions produce greater differential pressure fluctuations compared to surfactant solutions which were also observed during the injection of particles alone in Permian brine (Figure 6.1). These stronger pressure difference fluctuations may represent the local pressure drops brought on by the particles when flowing in pore throats. The particles may temporarily and locally reduce permeability due to the localised log-jamming and pore throat obstruction. These permeability reductions show as more prominent pressure oscillations in the flow pattern (*i.e.* dynamic differential pressure plots). These pore throat obstructions can boost oil recovery in EOR operations by re-routing the injected phase into adjoining oil-filled channels in porous media.[286-288]

Figure 6.4. Differential pressure *versus* injected pore volume for a dried SK chalk core injected with Permian brine followed by 0.05 wt.% ZN in Permian brine at 0.1 cm^3 min^{-1} and 75 °C.

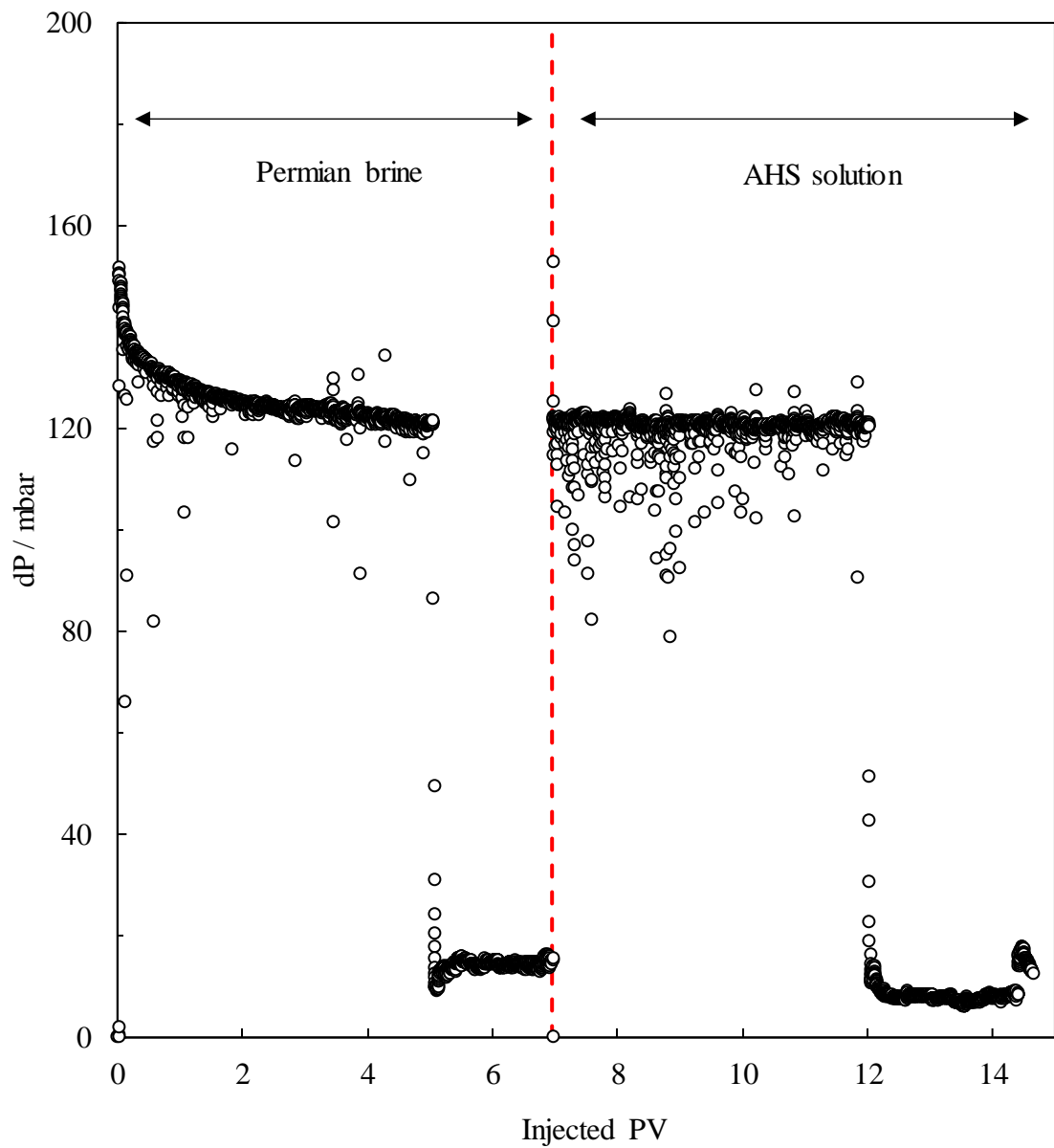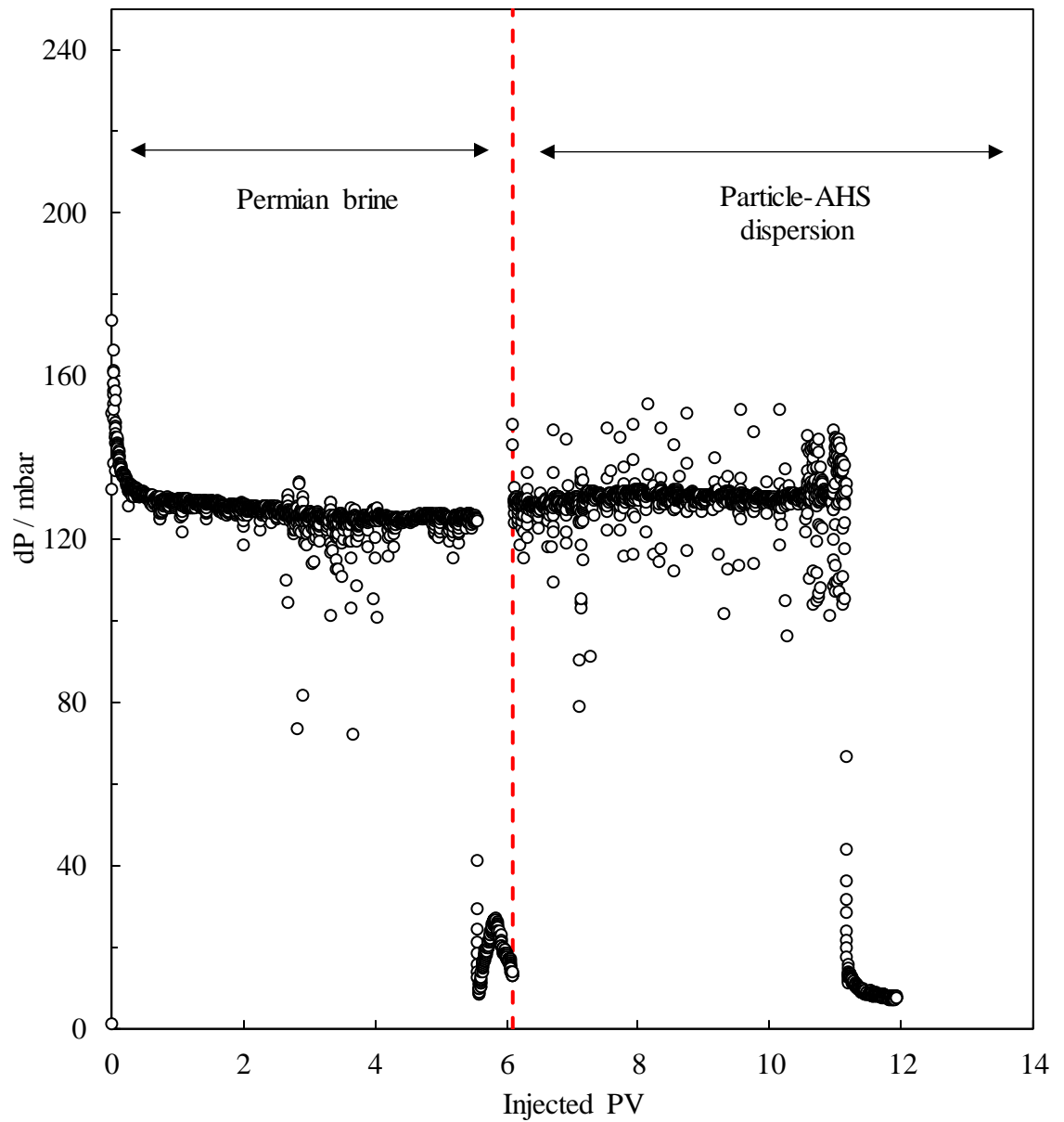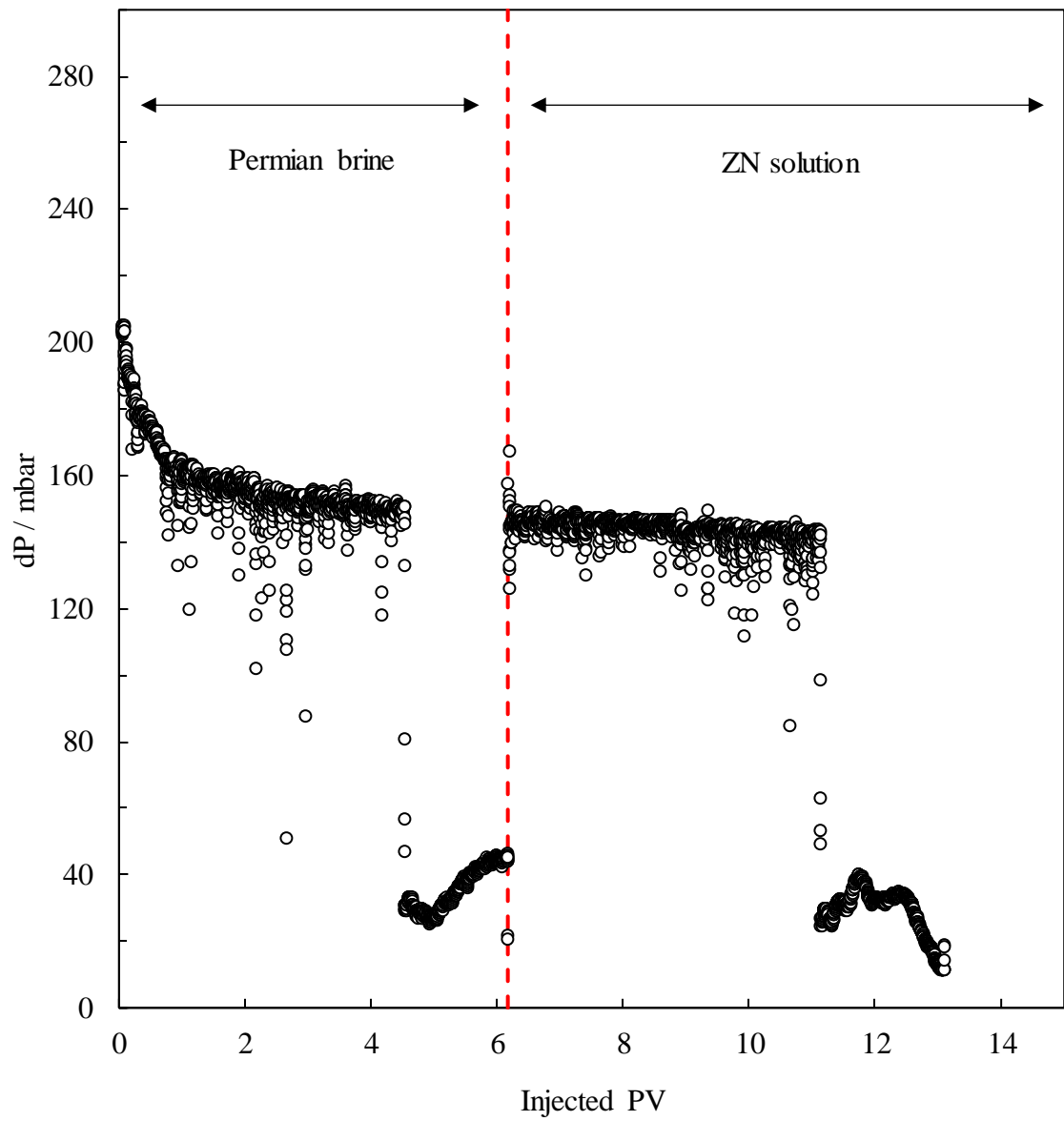**Figure 6.5.** Differential pressure *versus* injected pore volume for a dried SK chalk core injected with Permian brine followed by dispersion of 0.05 wt.% ZN and 0.01 wt.% ES-coated silica particles in Permian brine at 0.1 cm^3 min^{-1} and 75 °C.
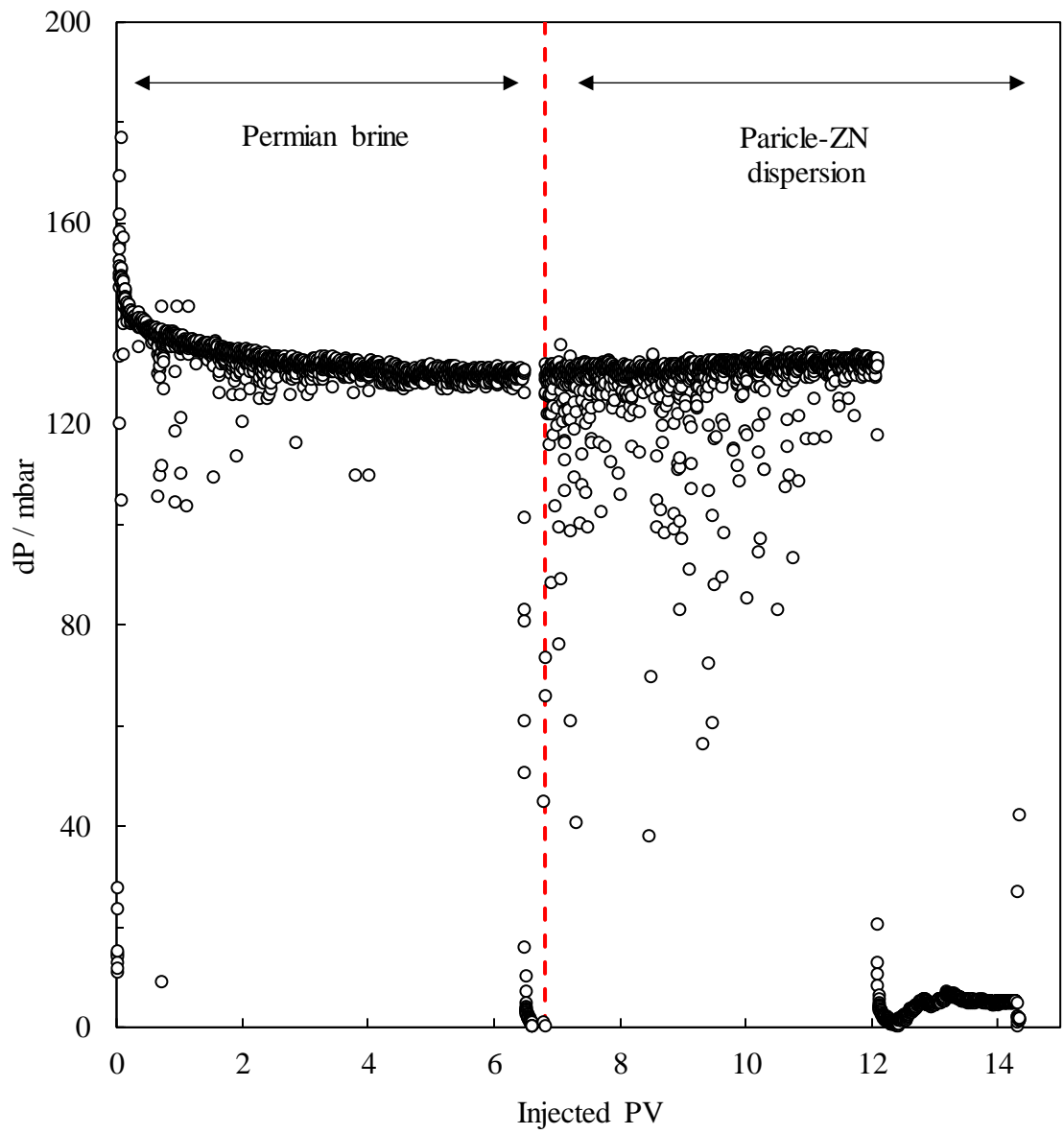
6.3.2.2 Surfactant loss

Figure 6.6 shows the air-water surface tensions of the effluent samples at 25 °C from SK chalk cores injected with Permian brine (7 PV) followed by 0.03 wt.% AHS or 0.05 wt.% ZN in Permian brine (4 – 5 PV) at 0.1 cm^3 min^{-1} and 75 °C. The surface tension of the effluents during Permian brine injection (PV < 7) was almost equal to that of Permian brine (74.3 mN m^{-1}). Therefore, post-brine injection (PV > 7) was considered for comparing the adsorption of two surfactants onto rock. Also, note that the initial surfactant concentrations are almost equal relative to their CMCs (2.5 – 3.0 CMC) enabling comparison. The residual surfactant in the effluent samples can lower the surface tension by which surfactant adsorption onto rock can be assessed. The injected PV (or it could be converted to injection time) can be used as a tool for investigating how early the residual surfactant is observed in the effluent. The figure shows that the surface tension curve for ZN surfactant begins to fall after around 1 PV injection while it is nearly 2 PV for AHS. This cannot be used to judge the final surfactant adsorption onto rock though since they should be compared to their initial concentrations which will be discussed later. The surface tension of AHS solution falls sharply at ~ 2 PV while a gradual decrease followed by a sharp decrease is observed for ZN. In both cases, the surface tension reduction becomes less at large injected pore volumes and tends to reach a plateau. The sharp reduction in surface tension with pore volume is due to the fast diffusion of surfactant molecules in the aqueous phase in porous media.[289, 290]

Figures 6.7 and 6.8 show the effect of adding 0.01 wt.% ES-coated silica particles to surfactant solutions on the surface tension of the effluent samples from core flooding at 75 °C. The surface tension curves for AHS surfactant show no change in breakthrough upon adding particles such that both curves decrease at the same pore volume (Figure 6.7). However, the surface tensions of AHS + particles are higher than those of AHS alone at large pore volumes, implying fewer available surfactant molecules due to the adsorption of surfactant on rock or particles. Figure 6.8 shows that the addition of particles to the ZN solution delays the breakthrough such that the surface tension curve begins to decrease at larger pore volumes. Both solutions and dispersion had the same surface tension at large pore volumes.

Figure 6.6. Air-water surface tension of the effluent samples at 25 °C related to dried SK chalk cores injected with Permian brine followed by 0.03 wt.% AHS or 0.05 wt.% ZN in Permian brine at 0.1 cm^3 min^{-1} and 75 °C. The upper and lower dashed lines show the surface tensions of Permian brine and surfactant solutions at their CMCs, respectively at 25 °C.
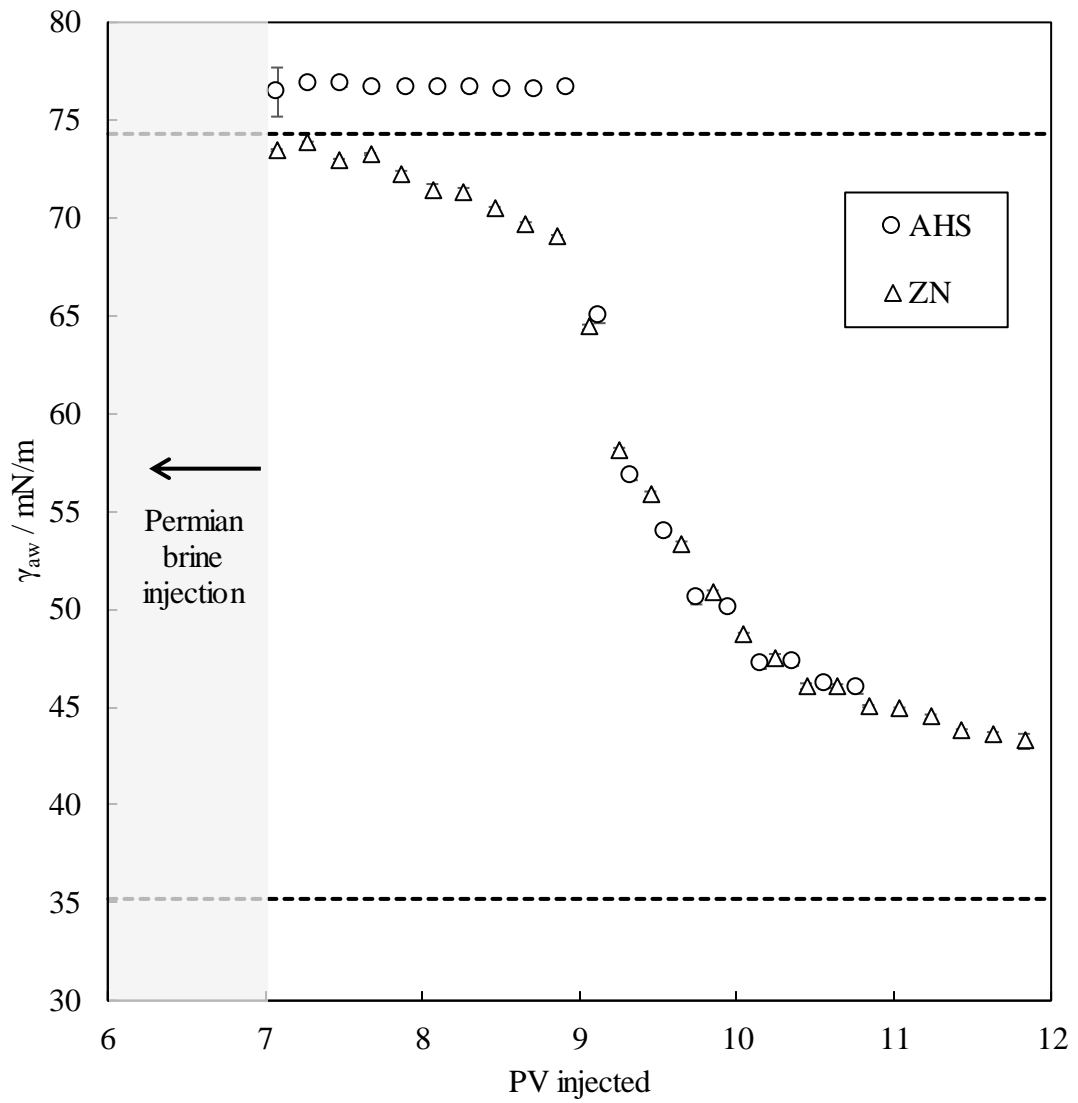
Figure 6.7. Air-water surface tension of the effluent samples related to dried SK chalk cores injected with Permian brine followed by 0.03 wt.% AHS in Permian brine with and without 0.01 wt.% ES-coated silica at 0.1 cm^3 min^{-1} and 75 °C. The upper and lower dashed lines show the surface tensions of Permian brine and surfactant solution at the CMC, respectively at 25 °C.
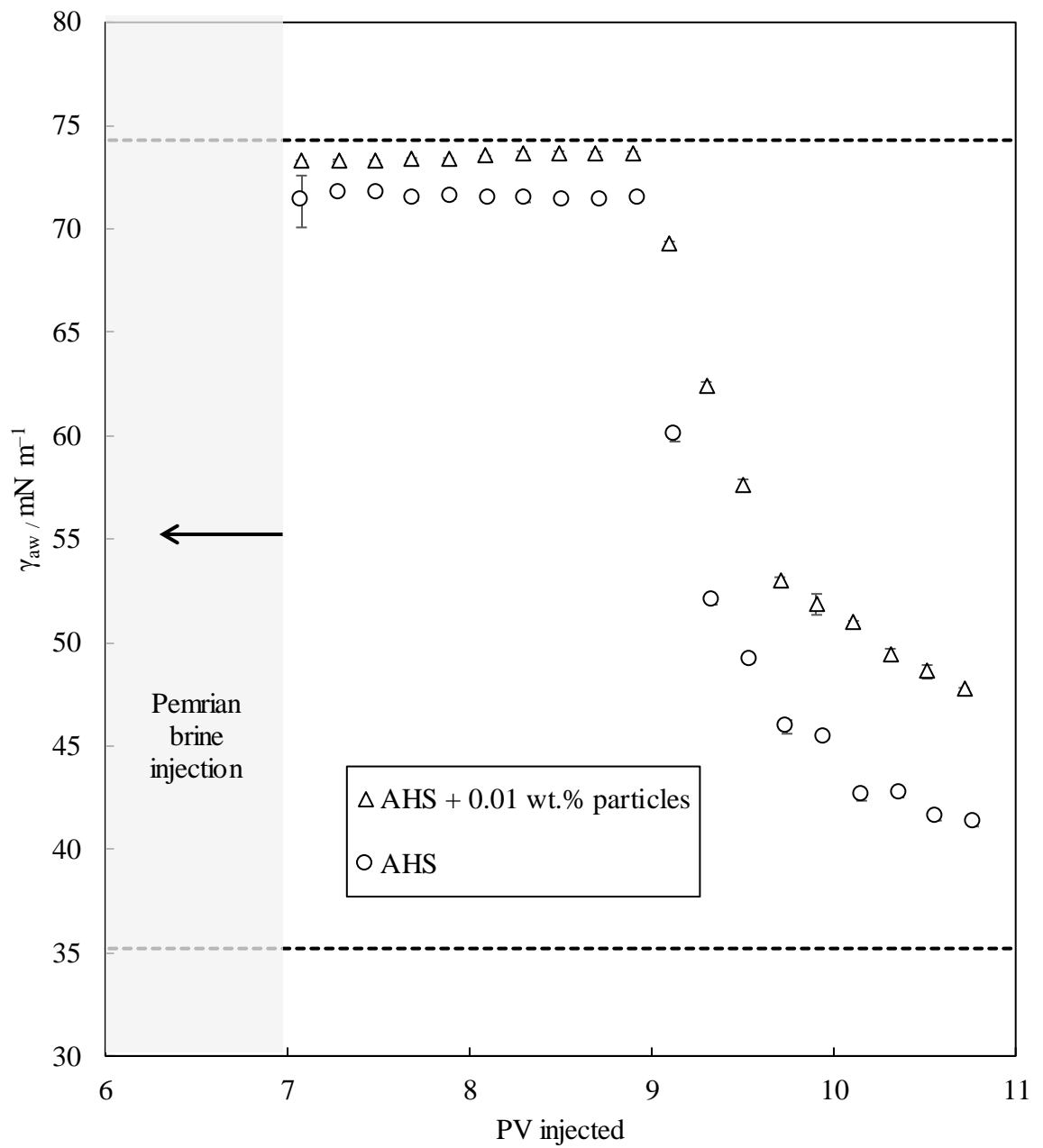
Figure 6.8. Air-water surface tension of the effluent samples related to dried SK chalk cores injected with Permian brine followed by 0.05 wt.% ZN in Permian brine with and without 0.01 wt.% ES-coated silica at 0.1 cm^3 min^{-1} and 75 °C. The upper and lower dashed lines show the surface tensions of Permian brine and surfactant solution at the CMC, respectively at 25 °C.
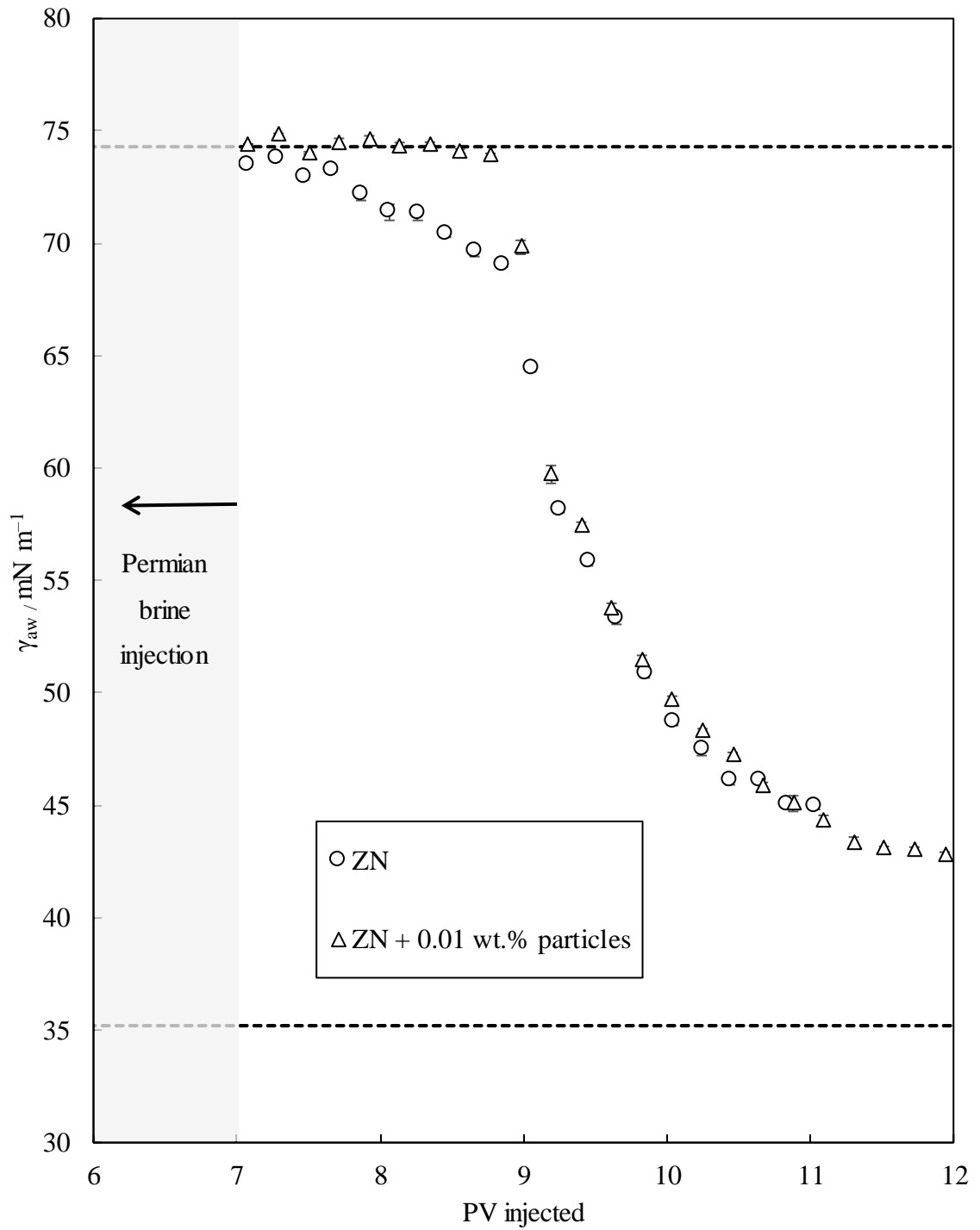
The use of anionic surfactants is common in EOR yet they experience substantial adsorption on cationic carbonate rocks.[291, 292] Zwitterionic surfactants have recently received attention for EOR. Zwitterionic surfactants are thought to have lower adsorption

339

Permian

onto rocks due to their lower pH-dependent charge density but recent results show that they may adsorb largely onto rocks with a large clay content.[134] Previous studies also suggest that sulphate-based zwitterionic surfactants are cheaper than sulfonate-based ones but they may experience sulphur-oxygen bond hydrolysis making them not suitable for EOR.[293, 294] Therefore, sulfonate-based AHS and ZN surfactants are interesting options for EOR but still need to be evaluated for adsorption onto rock. The adsorption limit onto rocks for commercially accepted surfactants for EOR in calcite-based rocks has been reported to be 1 mg m^{-2}.[269] Nanoparticles have received greater attention than polymers and alkali recently due to their EOR effectiveness and low cost but their effects on the adsorption behaviour of zwitterionic surfactants on rocks are less known.

The surfactant concentration in a solution can be determined using a variety of techniques such as titration, UV-vis spectroscopy, conductivity, surface tension, high-performance liquid chromatography (HPLC) and total organic carbon (TOC). In this study, the first three were tried and failed (see Appendix D.1). Therefore, previously measured air-water surface tensions were used as calibration curves.

Figure 6.9 shows the equilibrium surfactant concentration relative to the original surfactant concentration (C_e/C_o) *versus* pore volume injected of Permian brine (7 PV) followed by AHS or ZN solutions with and without 0.01 wt.% ES-coated silica particles in Permian brine ($4 - 5$ PV). In such a plot, a C_e/C_o close to one at sufficient injected pore volumes means low surfactant adsorption onto rock which is ideal for surfactant flooding in EOR. As shown, ZN has a lower C_e/C_o and thus higher adsorption onto rock compared to AHS. The nonionic $C_{10-12}E_9$ in ZN may account for this higher adsorption by further interacting with the rock surface through hydrogen bonding and hydrophobic interactions.[61] The addition of 0.01 wt.% particles increases and lowers the adsorption of AHS and ZN onto rock, respectively (Figure 6.9). However, the changes are not very large here probably due to the low particle concentrations used in the dynamic mode. Greater adsorption changes were obtained in static adsorption results when higher particle and surfactant concentrations were used.

Figure 6.10 compares the static and dynamic adsorption results conducted in this study. The dynamic adsorption behaviours of surfactants, with and without particles, are consistent with the static results on rock powder, however both indicate high adsorption values which might be due to the aerobic lab. conditions. Levitt and Bourrel declared that oil reservoir rocks are in a reduced (or anaerobic) condition while the rocks in labs are mostly in an oxidized condition. Therefore, it is vital to induce a reduced condition in

rocks before implementing surfactant adsorption analysis in labs to have adsorption results analogous to those of reservoirs. They proposed to lower the oxidized potential of the rock using reducing agents like sodium dithionite and buffering or chelating agents like sodium bicarbonate, ethylene diamine tetraacetic acid (EDTA) or sodium citrate[295] which are missing in Permian brine. Previous studies also show that 9 – 10 PV injections of surfactant solutions are required to determine the equilibrium surfactant concentration and saturated adsorption.[289] Therefore, such high surfactant adsorption is thought to be normal. Comparing static and dynamic adsorption, the surfactant adsorption on rock powder is greater than in porous media which is probably due to the larger surface area the rock powder presents and the higher experimental temperature during the dynamic investigation (Figure 6.10), as also observed by previous researchers.[289, 290] Being an exothermic process, the surfactant adsorption onto rock decreases with temperature elevation.[257]

Although there are many studies on the adsorption of ionic surfactants on cationic and anionic rocks mostly in the presence of a single salt,[296-298] the literature lacks systematic studies on the adsorption behaviour of zwitterionic surfactants onto rocks. Having both charges in the headgroup, zwitterionic surfactants can have a more complex adsorption behaviour on rocks than anionics and cationics, especially in the presence of inorganic salts and rock impurities (like clays). For example, it has been reported that due to the lower solvation area of divalent calcium than monovalent sodium (*e.g.* 1.45 nm^2 for Ca^{2+} *versus* 1.96 nm^2 for Na^+), the divalent cation tendency towards anionic rock surfaces is higher leading to a higher cation concentration in the electric double layer of the rock. Therefore, the adsorbed calcium can facilitate interactions between the anionic headgroup of a zwitterionic surfactant and anionic rock minerals by cation bridging and precipitation. These interactions are dependent on the calcium concentration.[218, 290] When no calcium is present in brine, the positive headgroup of the zwitterionic surfactant tends to interact electrostatically with the anionic sites on rock while the sulfonate headgroup is electrostatically repelled largely. At low calcium concentrations, the adsorbed surfactant molecules on rock turn angled with the sulfonate headgroup closer to the rock surface due to the reduced repulsion between the sulfonate headgroup and anionic sites or attractions between the sulfonate headgroup and adsorbed calcium cations on rock. This type of adsorption has the lowest adsorption density on rock. If calcium concentration rises, the anionic sites turn cationic resulting in the vertical adsorption of zwitterionic surfactant on the rock. Even if calcium is absent in the brine, calcite dissolution can supply the dissolved divalent ions in the system. Therefore, if calcite dissolution occurs seriously, an increase in surfactant adsorption onto rock is expected in the presence of Permian brine

ions. Monovalent ions like Na^+ are not potential-determining but they can shrink the electric double layer of the rock or particle.[299]

Permian brine ions lower the electrostatic attraction between anionic particles and zwitterionic AHS. The same effect is expected to happen with ZN since it mainly consists of AHS but the interactions between the headgroup of the nonionic surfactant and the particle surface are independent of the salinity leading to ZN savings by particles. Since the nonionic surfactant and particle concentrations are not large, the ZN savings are also not pronounced. Surfactant adsorption at different surfaces decreases as follows: oil-water > particle-water > gas-water. Therefore, the surfactant molecules tend to stay adsorbed on the particle surface in an air-water system but spontaneously leave the particle surface close to the oil-water. This may prove the role of particles as surfactant carriers.[119] Therefore, it is thought that ES-coated silica particles enhance AHS surface activity but act as surfactant carriers for ZN. This behaviour is probably due to the presence of the nonionic surfactant in ZN.

Figure 6.9. Ratio of equilibrium to original surfactant concentration (C_e/C_o) *versus* injected pore volume for dried SK chalk cores injected with Permian brine followed by 0.03 wt.% AHS and 0.05 wt.% ZN in Permian brine with and without 0.01 wt.% ES-coated silica at 0.1 cm^3 min^{-1} and 75 °C.
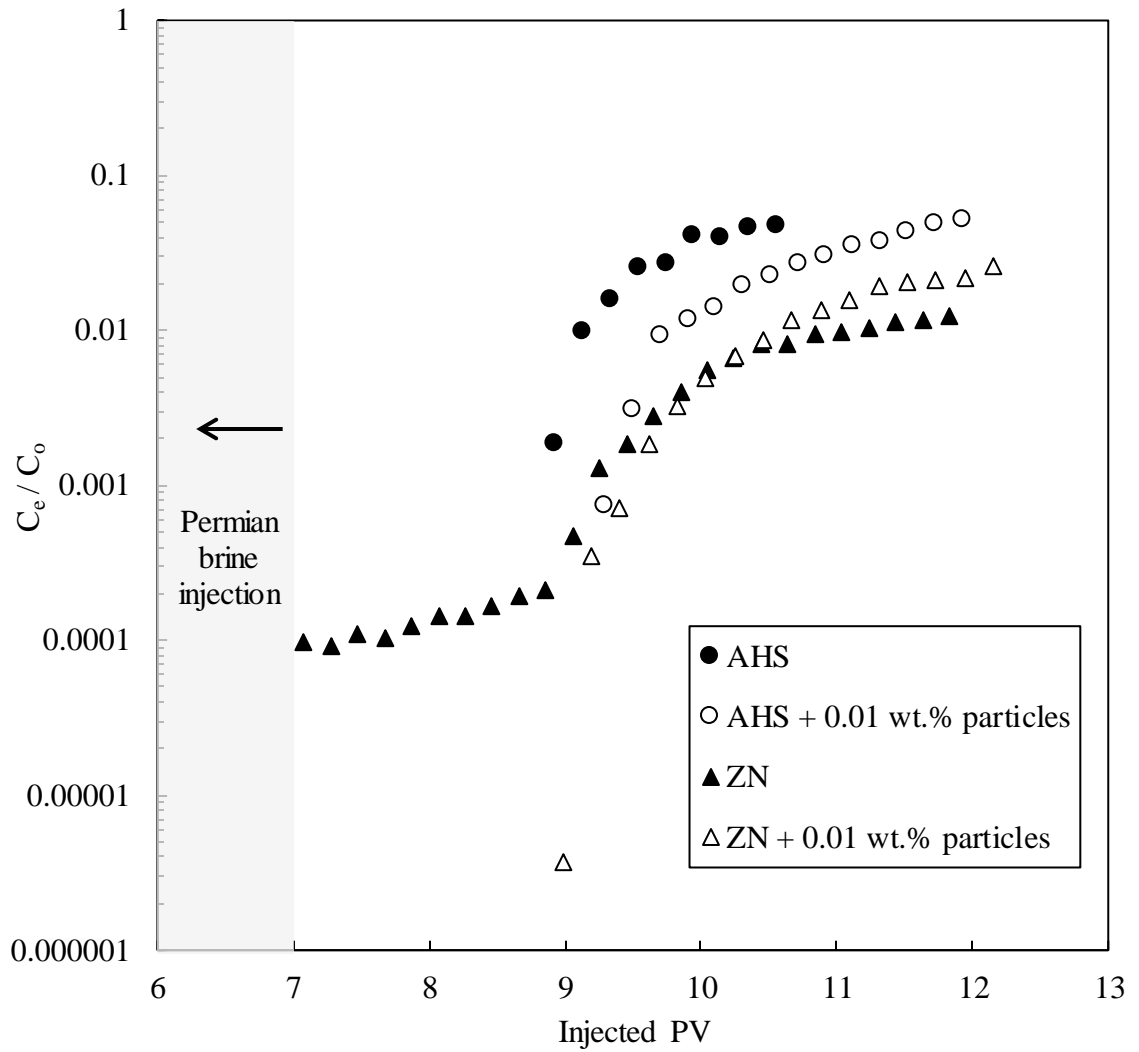
Figure 6.10. Surfactant adsorption values onto rock powder (static adsorption at 25 °C) and porous media (dynamic adsorption at 75 °C) for AHS and ZN solutions with and without 0.01 wt.% ES-coated silica particles.
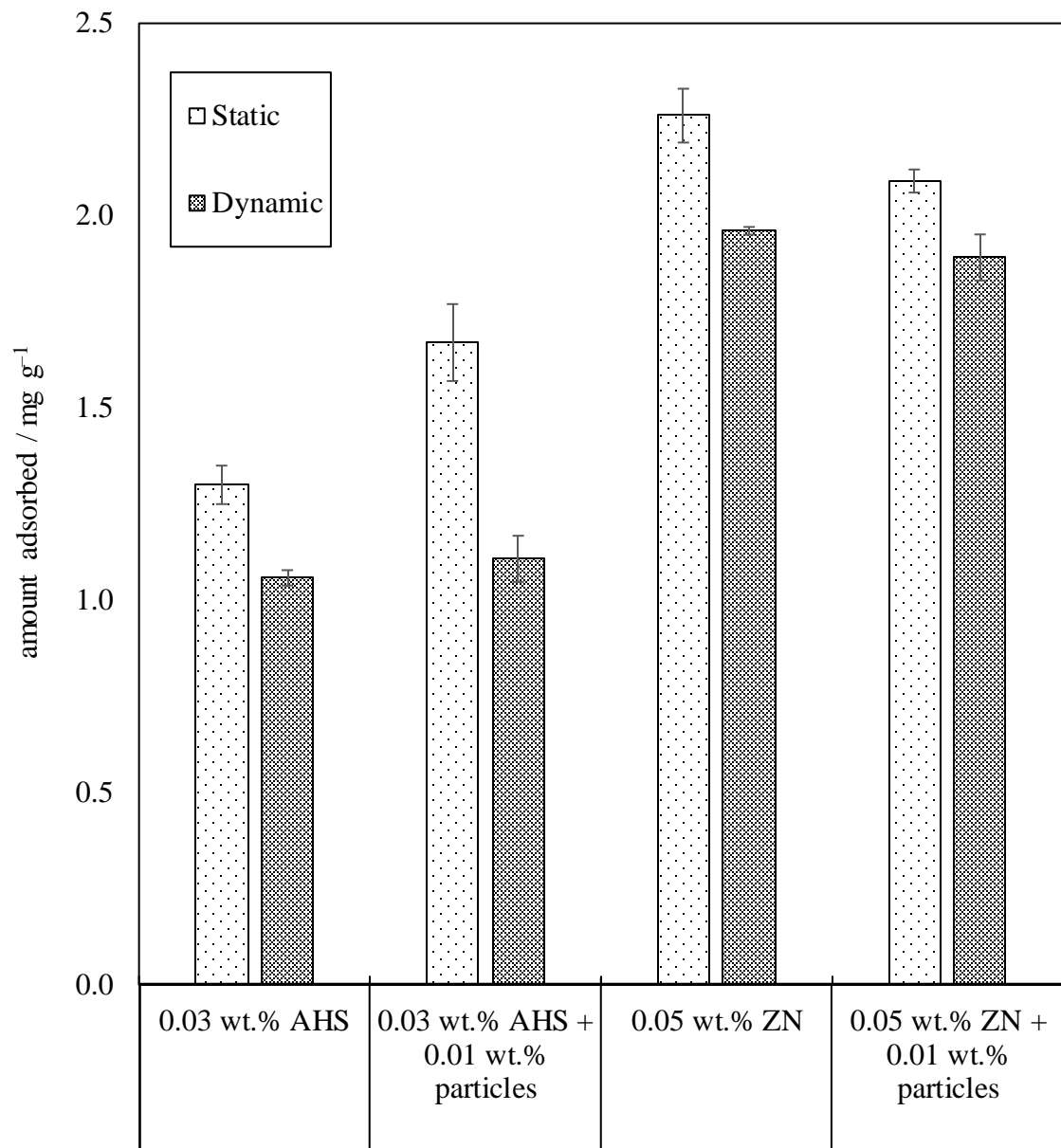
6.4 Oil recovery experiments

Surfactant flooding has been proved effective for EOR in conventional and, more recently, unconventional oil reservoirs. The main idea is that surfactants can reduce oil-water

interfacial tension, lower rock hydrophobicity and prevent asphaltene precipitation.[300] With a decrease in oil-water interfacial tension, the capillary number grows by orders of magnitude, lowering the remaining oil saturation by reducing the resistance that oil droplets encounter as they pass through the pore throats. Recently, nanoparticle-surfactant dispersions have attracted great attention for EOR. It has been suggested that nanoparticles may have a role in decreasing surfactant adsorption onto rocks (like for ZN here) or increasing surfactant activity (like for AHS here). Additional oil recoveries have also been achieved by blending nanoparticles and surfactants.[133, 301]

Spontaneous imbibition tests were used in this study to examine the efficiency of candidate dispersions on oil recovery. They entail immersing an oil-saturated core in the EOR solution and waiting for the solution to spontaneously imbibe into the core to produce oil. Capillary-driven spontaneous imbibition tests provide more precise simulations of fluid flow in porous media compared to core flooding in which the viscous forces that the injection pressure places on the oil within pore throats may lead to larger oil recoveries, especially in rocks with high permeability. In addition, surfactant flooding may not be possible in some cases like in unconventional tight rocks (*e.g.* shale as observed in this study) because of the extremely low permeability and poor injectivity of the rocks.

Aged crude oil-saturated SK chalk cores with brine saturation of $S_w = 10\%$ were used for imbibition tests (Table 6.2). The imbibition test with Permian brine was carried out as a reference, mimicking secondary oil recovery. Candidate dispersions determined earlier in Section 6.1 were used as imbibition fluids. To examine the EOR effectiveness of surfactants alone, two imbibition tests were also carried out with AHS or ZN in Permian brine (without particles). This series of tests allows for the comparison of chemical EOR with secondary brine injection and the impact of adding ES-coated silica particles to surfactant solutions on oil recovery. A single tertiary imbibition was also performed to examine the power of dispersions in producing residual oil after secondary brine imbibition.

Table 6.2. Specifications of crude oil-saturated chalk cores used for spontaneous imbibition tests. The initial brine saturation (S_w) was 10% in all cores. V_p and V_b are the pore and bulk volumes of cores, respectively.

Core No.	Length / cm	Diameter / cm	V_p / cm^3	V_b / cm^3	Porosity / %	Permeability / md	Imbibition fluid

1	7.028	3.822	36.6	80.6	45.4	2.6 ± 0.8	Secondary: Permian brine Tertiary: 0.01 wt.% ES-coated silica + 0.05 wt.% ZN in Permian brine
2	7.080	3.826	38.2	81.4	47.0	3.7 ± 0.2	Secondary: 0.05 wt.% ZN in Permian brine
3	6.972	3.810	37.0	79.5	46.5	3.5 ± 0.4	Secondary: 0.01 wt.% ES-coated silica + 0.05 wt.% ZN in Permian brine
4	7.000	3.812	36.3	79.9	45.5	3.0 ± 0.2	Secondary: 0.03 wt.% AHS in Permian brine
5	6.970	3.814	39.7	79.6	49.9	4.0 ± 0.7	Secondary: 0.01 wt.% ES-coated silica + 0.03 wt.% AHS in Permian brine

6.4.1 Secondary mode

6.4.1.1 Permian brine

The oil recovery factor and oil imbibition rate for the oil-saturated core imbibed with Permian brine in secondary mode are depicted in Figure 6.11. As shown, the oil

production peaked in the first few days and then abruptly stopped after 10 days, producing only 23% of the original oil in place (OOIP) and leaving a significant volume of oil within.

6.4.1.2 Effect of surfactant

Figures 6.12 and 6.13 show the imbibition results for 0.03 wt.% AHS and 0.05 wt.% ZN in Permian brine, respectively. Surfactant solutions retrieved 35 – 37% more oil than Permian brine which is explained by their involvement in lowering the oil-water interfacial tension and rock oil-wetness, as was previously noticed.[302, 303] When comparing surfactants, ZN recovered somewhat more oil than AHS after a month (60.1% OOIP *versus* 58.4% OOIP) but the difference is not substantial. Such high oil recovery factors have been observed with this rock by imbibition of smart water, ionic liquids or surfactants before.[62, 304, 305]

The contact angle of fresh crude oil drops on the halved cores immersed in DIW was measured through the water. Table 6.3 summarizes all the results including contact angles (both on rock chips and halved cores), interfacial tensions and oil recovery for different dispersions and solutions used in imbibition tests. Note that ageing cores with crude oil does not induce uniformly strong hydrophobicity as observed with rock substrates. The cores usually become mixed-wet (locally hydrophobic and hydrophilic) and/or partially hydrophobic after ageing with crude oil.[137, 306] Therefore, oil-water contact angles on cores are lower than on rock substrates probably due to the lower oil-wetness achieved in core ageing. As shown in Table 6.3, both surfactant solutions caused a similar contact angle on halved cores ($\theta_{wo} = 41 \pm 2°$) and rock substrates ($\theta_{wo} \sim 118°$). Both surfactants reduced the oil-water interfacial tension significantly to the same level which plays a role in improving oil mobility. Oil-in-water emulsions are expected to form during imbibition tests by both surfactants. The resulting emulsions have a higher viscosity than water leading to an enhanced mobility ratio.[115] Based on the interfacial tension and emulsion results obtained earlier, neither of the surfactants exhibited Winsor type III (third phase) associated with ultralow interfacial tensions.[307] As the asphaltene content of the crude oil used here is low (< 1 wt.%), prevention of asphaltene precipitation by surfactants is not thought to be strong.

Figure 6.11. Oil recovery factor (RF) and imbibition rate for the crude oil-saturated SK chalk core imbibed with Permian brine in secondary mode at 75 °C. The standard deviations of the oil recovery factor and imbibition rate are below 0.5% and 0.2 cm^3 day^{-1}, respectively.
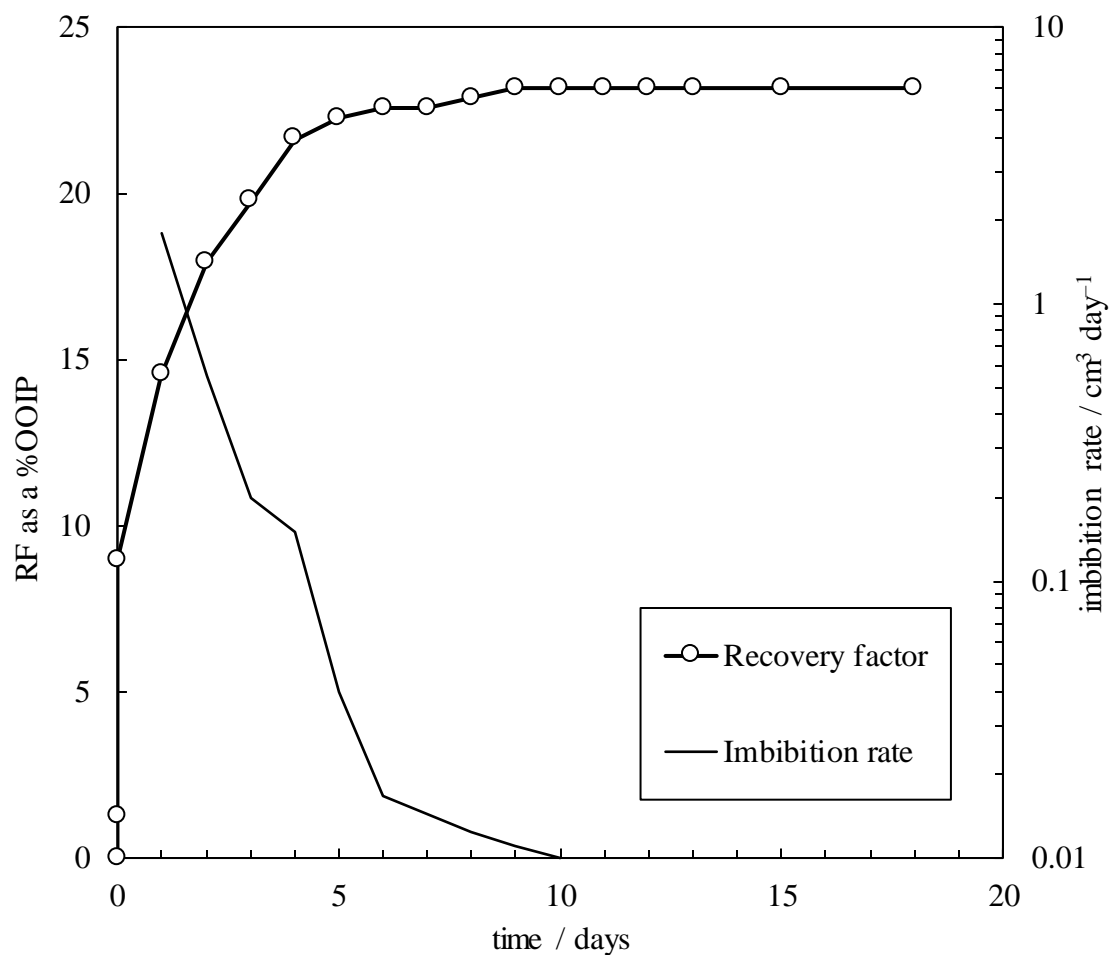
Figure 6.12. Oil recovery factor (RF) and imbibition rate for the crude oil-saturated SK chalk core imbibed with 0.03 wt.% AHS with or without 0.01 wt.% ES-coated silica particles in Permian brine, both in secondary mode at 75 °C. The standard deviations of the oil recovery factor and imbibition rate are below 0.5% and 0.2 cm^3 day^{-1}, respectively.
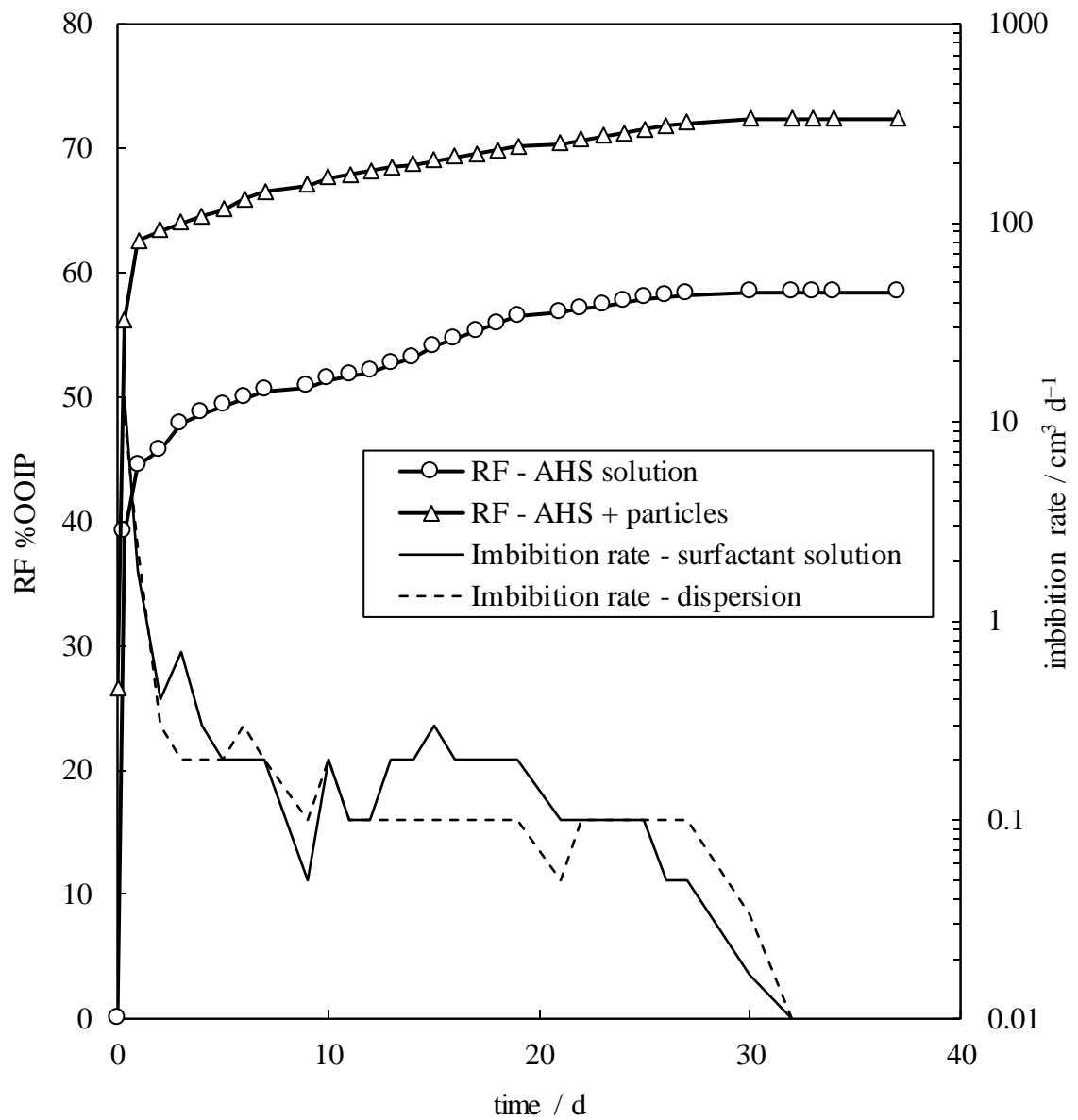
Figure 6.13. Oil recovery factor (RF) and imbibition rate for the crude oil-saturated SK chalk core imbibed with 0.05 wt.% ZN with or without 0.01 wt.% ES-coated silica particles in Permian brine both in secondary mode at 75 °C. The standard deviations of the oil recovery factor and imbibition rate are below 0.5% and 0.2 cm^3 day^{-1}, respectively.
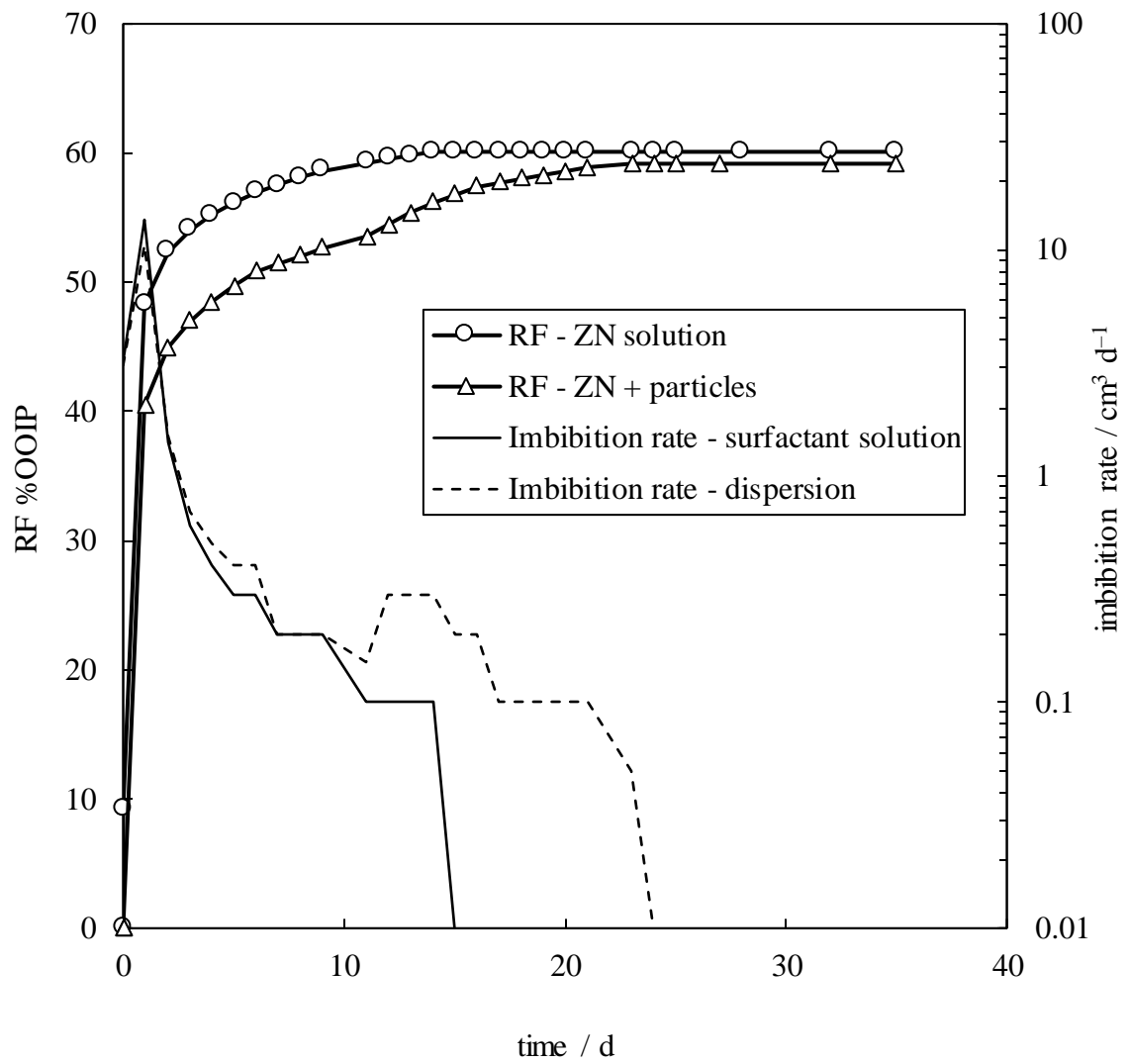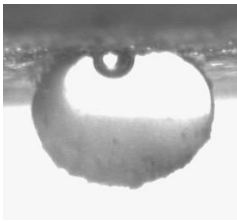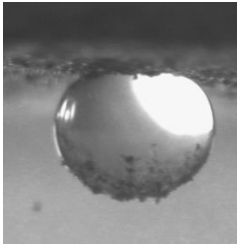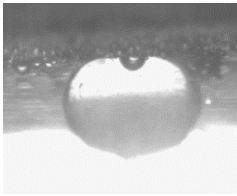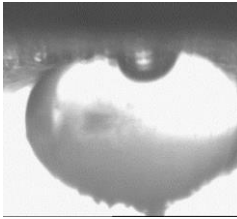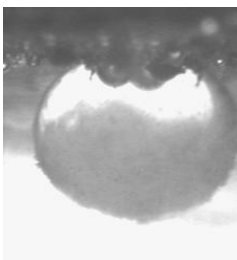
Table 6.3. Summary of EOR results obtained in this study.

	θ_{wo} / °	γ_{ow} / mN m^{-1}

350

Recovery mode	Imbibition fluid	Rock substrates	Cores after imbibition		RF as a %OOIP
	Permian brine	171 ± 8	–	12.6 ± 0.2	23.2
	0.03 wt.% AHS	119 ± 5	43 ± 4	1.07 ± 0.01	58.4
	0.05 wt.% ZN	118 ± 7	39 ± 5	0.87 ± 0.08	60.1
	0.03 wt.% AHS + 0.01 wt.% ES-coated silica	90 ± 12	38 ± 2	1.03 ± 0.03	72.3
Secondary	0.05 wt.% ZN + 0.01 wt.% ES-coated silica	56 ± 9	45 ± 2	0.38 ± 0.01	59.2
Tertiary	0.05 wt.% ZN + 0.01 wt.% ES-coated silica	56 ± 9	40 ± 2	0.38 ± 0.01	6

6.4.1.3 Effect of adding particles

The ultimate oil recovery factor of the AHS solution was 58.4% OOIP which was enhanced by ~ 14% OOIP when 0.01 wt.% particles were added (Figure 6.12). The oil production stopped at the same time for the AHS solution both with and without particles but the dispersion could cumulatively produce more original oil in the rock. Similar synergy in oil recovery by mixing nanoparticles and surfactants has been observed by previous researchers. Zhong *et al.* observed synergy in oil recovery by injecting a mixture of 0.08 wt.% zwitterionic cocamidopropyl hydroxysultaine and 0.2 wt.% ES-coated silica in API brine into sandstone cores. They reported an incremental oil recovery of 3% OOIP and 5% OOIP in the tertiary stage by the blend after the secondary injection of particles alone and surfactant alone, respectively which were linked to the additional oil-water interfacial tension decrease and rock wettability alteration by the blends.[229] Table 6.3 shows nearly similar oil-water contact angles on cores with and without particles but a lower contact angle on substrates when particles were added. Similar oil-water interfacial tensions were also observed when the AHS surfactant solution or surfactant-particle dispersion was used. However, the addition of ES-coated silica to AHS solutions was observed earlier to create more stable oil-in-water emulsions which subsequently produced more residual oil.

On the other hand, ZN and ZN + particles both resulted in a similar oil recovery factor (60.1% OOIP and 59.2% OOIP). The literature contains some studies with no or little additional oil recovery by the addition of nanoparticles.[101, 308] Figure 6.13 shows that the oil production by the ZN solution stops after two weeks but a more continuous oil production is observed in the presence of particles. Thus, although the ZN solution initially produced more oil, the blend could finally reach a similar cumulative oil production after a month. Despite the lower oil-water contact angle on rock substrates upon adding particles to ZN, the contact angles on cores after imbibition are similarly low indicating a water-wet rock (Table 6.3). The oil-water interfacial tensions are also the same with or without particles in ZN solutions. Therefore, it is thought that the inefficiency of emulsification is the reason for the lack of improved oil recovery with the blend of ZN and particles.

The mixture of particles and AHS outperformed that of ZN in terms of ultimate oil recovery (72.3% OOIP *versus* 59.2% OOIP). Considering contact angles on cores, both surfactant solutions and dispersions yielded similar rock wettability. Although both rock wettability alteration and interfacial tension reduction have significant effects on oil recovery, they cannot be used to compare the EOR efficiency of dispersions here. As for surfactants, it is thought that the emulsification of crude oil and water in the presence of

surfactants and particles is mainly the reason for this behaviour. The emulsion results showed that the addition of particles to AHS solutions created oil-in-water emulsions that were more stable to coalescence than ZN. Previous studies argue that Pickering emulsions made with particles and surfactants have a higher viscosity and force on oil droplets trapped in the pore throats which results in improved oil displacement.[115] Using blends of ES- and polyethylene glycol-coated silica and a sulfonate surfactant in API brine, Singh and Mohanty observed a low oil recovery (33% OOIP) by brine injection due to the channelling of the injected brine in the high permeability region leaving the oil in the low permeability region unproduced while the foam made with surfactant and particles was found to create *in situ* emulsions that blocked the high permeability region and diverted the injected phase towards the low permeability zone to produce more oil.[131] Note that other EOR mechanisms *e.g.* water viscosity increment,[309] crude oil viscosity reduction[99, 100] and prevention of asphaltene precipitation[310] by nanoparticles should not be significant here due to the low particle concentrations used, the lack of catalytic behaviour and the low asphaltene content of crude oil, respectively.

6.4.2 Tertiary mode

After the oil production ceased in the imbibition test with Permian brine (Core no. 1 in Table 6.2), the imbibition fluid was replaced with a dispersion of 0.01 wt.% particles + 0.05 wt.% ZN in Permian brine in order to examine the tertiary power of the blend in producing residual oil. Figure 6.14 shows the secondary and tertiary imbibition results with Permian brine and the blend of ZN and particles at 75 °C. Replacement of Permian brine with particle-surfactant dispersion can enhance oil recovery by 6% OOIP in tertiary mode. This additional oil recovered by the blend is the residual oil previously trapped due to the high capillary pressures available in the pore throats of the rock which could not be produced by brine alone. The dispersion took 12 days to produce this amount of oil. It is concluded that EOR by dispersions in the secondary stage is more efficient than in the tertiary stage.

Figure 6.14. Oil recovery factor (RF) and imbibition rate for the crude oil-saturated SK chalk core imbibed with Permian brine in secondary mode and the blend of 0.01 wt.% ES-coated silica particles and 0.05 wt.% ZN in Permian brine in tertiary mode at 75 °C.
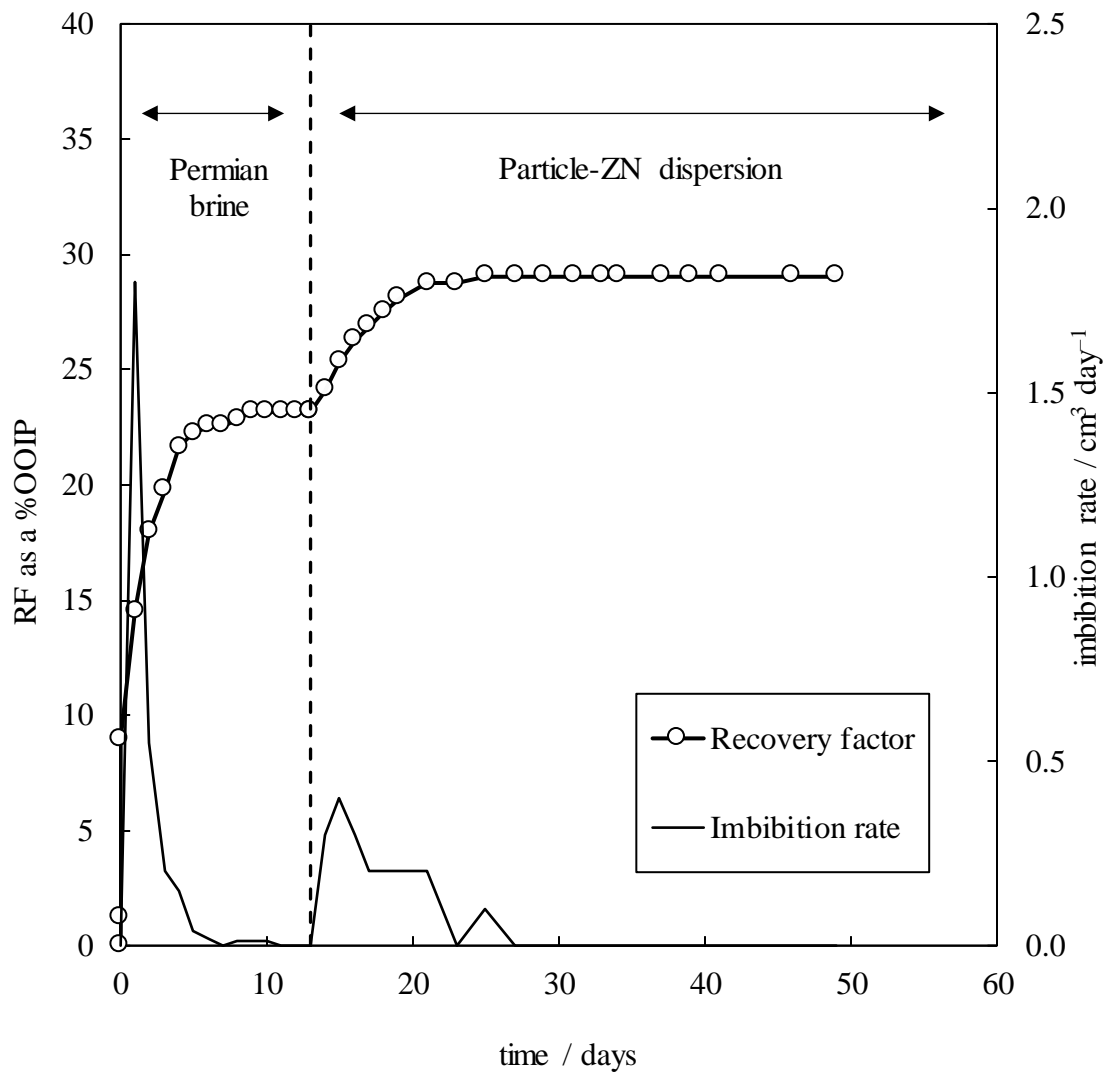
6.5 Summary of findings

This chapter investigated the selective particle-surfactant dispersions to examine their adsorption onto rock during flowing in rock cores. It also studied their efficiency in

producing crude oil from cores in spontaneous imbibition tests. The main findings of this chapter are as follows:

- No fluid saturation or injectivity was found in shale cores due to poor rock permeability and pore connectivity. Therefore, SK chalk cores with high porosity and low permeability but with the same mineralogy were replaced for spontaneous imbibition tests.

- Consistent with stability inspections in sample vials, no particle aggregation was observed during the injection of 0.01 wt.% ES-coated silica in Permian brine implying the suitability of synthesized particles for high temperature and high salinity EOR.

- In dynamic mode, pressure difference fluctuations obtained during the injection of different solutions and dispersions into chalk cores decreased as follows:

  Particles > surfactants + particles > surfactants > Permian brine

  The above results show that the presence of particles increases the pressure fluctuations. Particles can significantly cause local pore blockage and temporary permeability reductions which can re-route the injected phase into adjoining oil-filled channels in porous media and enhance oil displacement.

- The oil recovery by secondary spontaneous imbibition with Permian brine was 23% OOIP which was increased by 35 – 37% OOIP by surfactants (slightly higher by ZN surfactant) in the secondary mode due to their involvement in lowering the oil-water interfacial tension and rock oil-wetness.

- The post-imbibition contact angles of fresh crude oil drops on cores used in the imbibition tests showed rock hydrophilicity (~ 40°) by both surfactant solutions with and without particles. ZN surfactant recovered somewhat more oil than AHS after a month (60.1% OOIP *versus* 58.4% OOIP).

- The ultimate oil recovery factor with AHS surfactant was enhanced by ~ 14% OOIP when 0.01 wt.% ES-coated silica was added while ZN surfactant and ZN surfactant + particles both resulted in a similar oil recovery factor which was consistent with the more stable oil-in-water emulsions formed with the blend of AHS and particles. The resulting emulsions have a higher viscosity than water resulting in more displacement of trapped oil in the pore throats.

- The dispersion of 0.01 wt.% ES-coated silica + 0.05 wt.% ZN surfactant in Permian brine could produce an additional 6% OOIP in tertiary mode after secondary imbibition with Permian brine. This additional oil was the residual oil previously trapped due to the high capillary pressures in the pore throats.

- The secondary and tertiary imbibition results confirm the higher EOR efficiency of the dispersion in the secondary stage.

Chapter 7 Summary of findings and future work

In this thesis, aqueous nanoparticle-surfactant mixtures were investigated in a formation brine, namely Permian brine (12.6 wt.%), for EOR in tight oil reservoirs. Bare silica particles were first covalently grafted using two silanes, namely ES and AS, for long-term stabilization at high temperatures (75 °C) and high salinity. The specifications of silanized particles were determined both alone and in combination with two commercial surfactants, namely zwitterionic alkyl hydroxysultaine (AHS) and binary zwitterionic-nonionic (ZN) (AHS + nonionic C_{10-12} nonaethylene glycol ether). The effect of particles, surfactants or the blend on reservoir properties including rock wettability, oil-water interfacial tension and emulsification of oil and water was studied to choose effective dispersions for spontaneous imbibition in a calcite-rich rock. The surfactant adsorption onto the rock and the way it is affected by particle addition were also investigated both statically (on rock powder) and dynamically (in cores). The key findings of this study along with some potential future works are presented in this chapter.

7.1   Summary of findings

In Chapter 3, the properties of chemicals including particles, surfactants and rocks were determined using different techniques. As steric stabilization using physical grafting of silica with AHS or ZN was determined to be insufficient, covalent grafting with AS and ES was adopted for long-term colloidal stability. A pH-dependent behaviour was observed with AS-coated silica (68% silane coverage) from a positive charge at low pH (+30 mV) to a weak negative charge at its isoelectric point. An optimum ES/silica ratio was determined for ES-coated silica above which excess silane led to particle aggregation. Both particles showed limited colloidal stability in Permian brine at 75 °C at their original pH but were electrostatically stabilized for a long time by pH adjustment. Surfactants were shown to stabilise particle dispersions further sterically in DIW, whereas electrostatic grafting was only moderately successful in brine. Therefore, careful attention must be given to nanoparticles as surfactant carriers since a lack of sufficient steric stabilization may cause particle aggregation and formation damage. Bare silica showed higher electrostatic interactions with surfactants than silane-coated particles. ZN had a narrower zero net charge pH and was more surface-active at air-water and oil-water

interfaces due to its nonionic $C_{10-12}E_9$. The air-water surface tension was observed to consistently decrease with the addition of ES-coated silica to AHS in Permian brine (increasing surface activity) while no discernible effect was detected for ZN. Small pore volumes and a significant BET surface area ($2.21 - 2.95$ m^2 g^{-1}) were revealed by the analysis of shale, signifying a high capacity for chemical adsorption in EOR.

The findings of surfactants (with and without particles) at the rock-fluid interface were described in Chapter 4. Oil-water contact angle variations and surfactant adsorption onto rock were largely consistent. Significant crude oil-water contact angle reductions were observed by both surfactants in DIW (more so for AHS). Permian brine addition increased the minimum contact angle by AHS due to the reduced surfactant-rock electrostatic attraction by ions (consistent with reduced AHS adsorption on rock) but had no effect on that of ZN. Excess surfactant adsorption at high concentrations was revealed to induce hydrophobicity again. A large rock wettability alteration was observed with bare silica alone by interacting with adsorbed cationic crude oil components on the rock. For silane-coated silica particles, this mechanism proved ineffective, resulting in a negligible change in rock wettability. The mixture of ES-coated silica and surfactants showed a pH-responsive behaviour in which particles might serve as carriers (isoelectric pH) or surface activity improvers (high pH) for surfactants. The former provided the largest interactions of zwitterionic surfactant with moderately anionic particles (V-shaped adsorption) and crude oil components (ion pairs) leading to a synergistic contact angle reduction. The latter led to excess surfactant adsorption on rock resulting in a high oil-water contact angle. Although expected to be beneficial, calcite dissolution increased rock hydrophobicity at low pH, probably due to the free rock surface serving as an adsorbent for crude oil components or excess aqueous surfactant. The surface morphology of rock was shown to change in SEM images when treated with blends of ES-coated silica and AHS. The EDX results disclosed the adsorption of anionic particles and AHS onto the cationic rock. Particles and AHS were revealed to serve as an adsorbent for Permian brine ions leading to reduced counterion adsorption onto the rock.

Chapter 5 examined the effects of particles and surfactants on the interfacial tension and emulsification of oil and water. Oil-water interfacial tensions decreased considerably on the addition of AHS and ZN to DIW or Permian brine at ~ CMC with and without particles (more so for ZN). An increasing interfacial tension was observed when using crude oil and surfactants in Permian brine. Increasing particle concentration in AHS in DIW had no clear effect on the crude oil-water interfacial tension but systematically reduced that of ZN. Temperature elevation increased the crude oil-water interfacial

tension in the presence of surfactants (with and without particles) probably due to reduced solvation of surfactant molecules at the interface by counterions (more so for ZN).

Emulsification of toluene, heptane and heptol and AHS in DIW was found to be a function of interfacial charge and oil molecules at the oil-water interface (decreasing as toluene > heptol > heptane). A synergy in emulsification was observed when using heptol (f_o = 0.2 after 100 days for [AHS] = 0.1 wt.% in DIW) due to the mixed effects of individual oils. Ions provided a more compact surfactant monolayer at the oil-water interface and produced more emulsions of toluene and heptol ($f_o < 0.2$ after 100 days for [AHS] = 0.05 – 0.07 wt.%). Emulsions of ZN were unstable due to surfactant demulsification ability. Independent of the oil type, surfactant and background electrolyte, all emulsions demonstrated considerable creaming. Pickering emulsions were formed with weakly anionic AS-coated silica particles and ES-coated silica alone depending on hydrophobization extent with interfacial oil through polar-polar (toluene) or solvophobic interactions (heptane). Heptol took advantage of both and produced an emulsion with no coalescence for up to 3 months ($f_o \sim 0$ for 1 wt.% ES-coated silica in DIW). Physical grafting of ES-coated silica with zwitterionic surfactant was seen to add hydrophobicity to particles (see zeta potential measurements), often resulting in higher emulsification (Figure 7.1). The particle-surfactant mixture exhibited a pH-responsive emulsification behaviour, switching between an oil-in-dispersion emulsion (high pH, low [AHS]) and a Pickering emulsion (isoelectric pH, high [AHS]). Permian brine ions were discovered to slow coalescence and creaming in emulsions of crude oil and water. It was found that bare silica exhibits greater particle hydrophobization by crude oil molecules than ES-coated silica, resulting in more stable Pickering emulsions. However, slightly aggregated bare silica in Permian brine could stabilise the emulsions more than particles in DIW.

Figure 7.1. A silica particle hydrophobized by (a) ES, (b) ES and zwitterionic AHS at an oil-water interface.

(a)
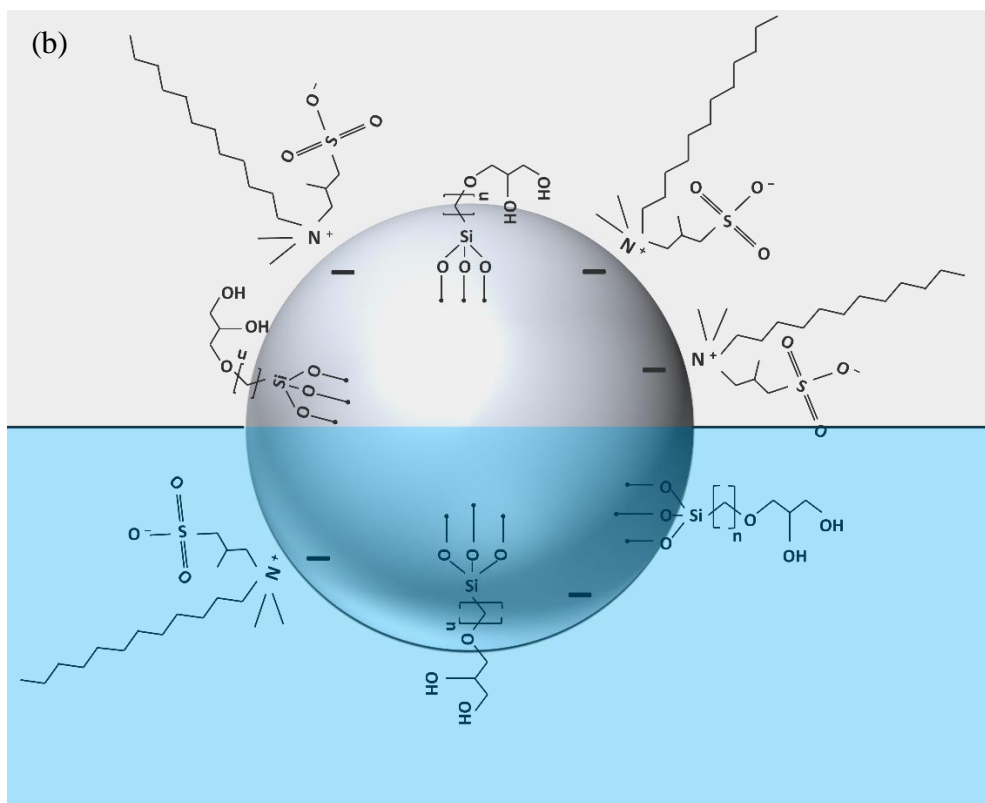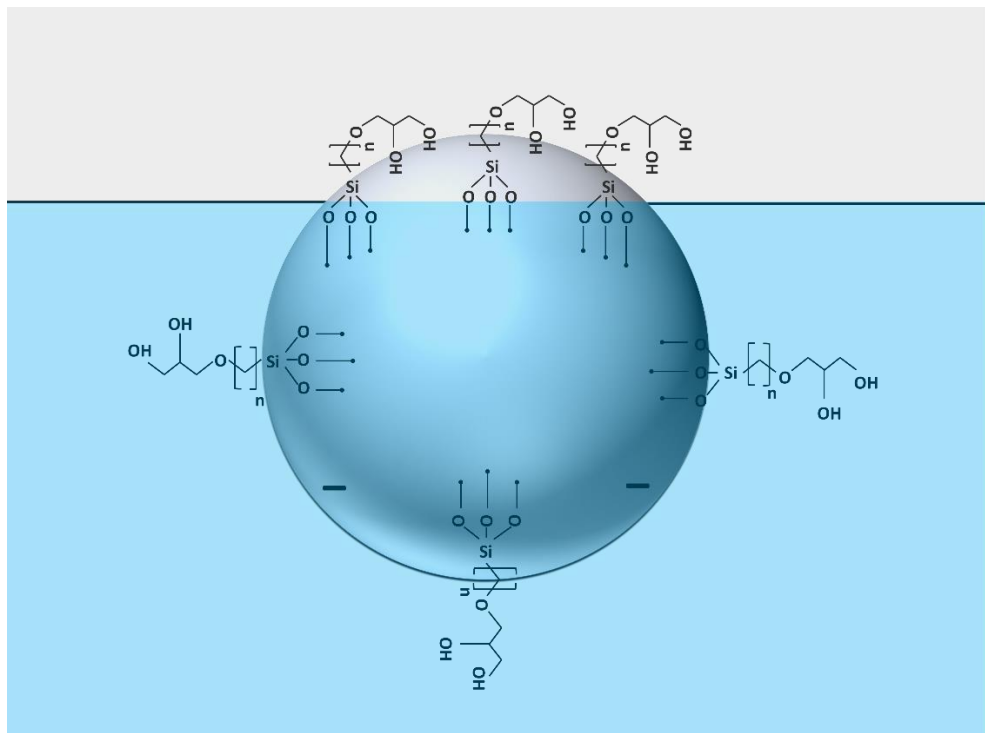
In chapter 6, the effective dispersions selected from previous results were tested in spontaneous imbibition. No particle aggregation was observed in porous media when injecting a dispersion of ES-coated silica in Permian brine implying the suitability of synthesized particles for high temperature and high salinity EOR operations. In dynamic mode, differential pressure fluctuations decreased as follows: particle dispersion > surfactant-particle dispersion > surfactant solution > Permian brine, serving as evidence that particles can drastically cause temporary permeability reductions to re-route the injected phase into adjoining oil-filled channels in porous media and enhance oil displacement. Surfactants increased the oil recovery of brine by 36 ± 1% OOIP in secondary mode due to their involvement in lowering the oil-water interfacial tension and rock oil-wetness. The ultimate oil recovery factor with zwitterionic AHS was enhanced by ~ 14% OOIP on adding only 0.01 wt.% ES-coated silica while no improvement was observed in that of ZN which was linked to the emulsification power of blends. The resulting emulsions have a higher viscosity than water, resulting in more displacement of trapped oil in the pore throats. Hydrophilic wettability (θ_{ow} ~ 40°) was detected in cores after secondary imbibition with both surfactant solutions with and without particles. An additional 6% OOIP oil recovery was also observed in tertiary mode by the blend of particles and ZN implying the efficiency of the formulation in recovering residual oil that could not be produced using brine alone due to the high capillary pressures in the pore throats.

7.2 Future work

- ES-coated silica particles were shown to be colloidally stable in Permian brine at a temperature of 75 °C but it will be fascinating to examine how stability is affected at higher temperatures and salinities with different ionic compositions. The way the particle colloidal stability was assessed in this thesis is more like near wellbore conditions. Further investigations in long cores, for instance, are required to address long-term colloidal stability in deep reservoir injections. Also, more studies are required to address long particle transport in both matrix and fractures. The potential for reservoir blockage and limited application should be addressed in future studies.

- It is noteworthy that shale reservoirs exhibit inherently low levels of porosity and permeability necessitating the utilization of specialized techniques for oil extraction. Hydraulic fracturing is the prevalent method employed for this purpose. Consequently, there is a compelling need to undertake an in-depth investigation of particle transport within these fractures, considering the challenges associated with injecting liquids

into shale rocks and the physical feasibility of nanoparticles penetrating shale rock formations.

- Future research on the impact of specific salts on the effectiveness of surfactants and particles or the mixture in oil-water and rock-water systems is attractive.

- The efficiency of the particle-surfactant formulation should be evaluated using different crude oils (with higher polar groups) and rock types (sandstones, clays, etc.).

- Surfactant partitioning between oil and water was investigated in this study using some conventional techniques but the results were not presented due to irreproducibility. One can employ more precise methods like HPLC.

- Particle adsorption onto rock is crucial from an economic and technological standpoint. Since prior attempts to detect aqueous particle concentration using conventional methods failed, most likely due to the silane coverage, a suitable strategy should be sought out.

- It is important to research how temperature affects the emulsification of different oils and water in the presence of surfactants and particles.

- Future research can greatly benefit from the insightful findings from the emulsification behaviour of surfactants and particles using pure oils here to better understand the emulsification of model oils including polar groups (resin and asphaltene) or crude oil.

- AS-coated silica displayed interesting pH-dependent behaviour in emulsification and rock wettability alteration but further research is required to determine its applicability for EOR. It is important to research its performance (either alone or in blends with surfactants) on interfacial tension and oil recovery.

References

1. D. Myers, *Surfactant science and technology*, John Wiley & Sons, 2005.
2. G. Basu Ray, I. Chakraborty, S. Ghosh, S. P. Moulik, C. Holgate, K. Glenn and R. M. Palepu, *J. Phys. Chem. B.*, 2007, **111**, 9828-9837.
3. L. L. Schramm, *Surfactants: fundamentals and applications in the petroleum industry*, Cambridge University Press, Cambridge, 2000.
4. M. Zaky, A. Badawi, I. Sabbah, R. Abd Elghani, E. Ismaeil and M. Hendawy, *Egypt. J. Chem.*, 2012, **55**, 259-275.
5. M. J. Rosen and J. T. Kunjappu, *Surfactants and interfacial phenomena*, John Wiley & Sons, New York, 4th edn., 2012.
6. B.-Y. Zhu and T. Gu, *Adv. Colloid Interface Sci.*, 1991, **37**, 1-32.
7. R. Zhang and P. Somasundaran, *Adv. Colloid Interface Sci.*, 2006, **123-126**, 213-229.
8. P. C. Hiemenz and R. Rajagopalan, *Principles of Colloid and Surface Chemistry, revised and expanded*, CRC press, New York, 2016.
9. T. W. Healy, A. Homola, R. O. James and R. J. Hunter, *Faraday Discuss.*, 1978, **65**, 156-163.
10. J.-P. Hsu and B.-T. Liu, *J. Phys. Chem. B.*, 1998, **102**, 334-337.
11. L. Liu, L. Moreno and I. Neretnieks, *Langmuir*, 2009, **25**, 688-697.
12. A. J. Worthen, V. Tran, K. A. Cornell, T. M. Truskett and K. P. Johnston, *Soft Matter*, 2016, **12**, 2025-2039.
13. S.-J. Park and M.-K. Seo, *Interface science and composites*, Academic Press, Oxford, 1st edn., 2011.
14. L. Qi, C. Song, T. Wang, Q. Li, G. J. Hirasaki and R. Verduzco, *Langmuir*, 2018, **34**, 6522-6528.
15. A. Ahmed, I. M. Saaid, A. A. Ahmed, R. M. Pilus and M. K. Baig, *Pet. Sci.*, 2020, **17**, 722-733.
16. B. P. Binks, *Curr. Opin. Colloid Interface Sci.*, 2002, **7**, 21-41.
17. F. Reincke, S. G. Hickey, W. K. Kegel and D. Vanmaekelbergh, *Angew. Chem.*, 2004, **116**, 464-468.
18. V. Garbin, J. C. Crocker and K. J. Stebe, *J. Colloid Interface Sci.*, 2012, **387**, 1-11.
19. A. Nelson, D. Wang, K. Koynov and L. Isa, *Soft matter*, 2015, **11**, 118-129.
20. S. J. D. Sofla, L. A. James and Y. Zhang, *J. Mol. Liq.*, 2019, **274**, 98-114.
21. B. P. Binks, *Langmuir*, 2017, **33**, 6947-6963.
22. T. Staszewski, M. Borówko and P. Boguta, *J. Phys. Chem. B.*, 2022, **126**, 1341-1351.
23. A. Gupta, H. B. Eral, T. A. Hatton and P. S. Doyle, *Soft Matter*, 2016, **12**, 2826-2841.
24. J. Mata, V. Aswal, P. Hassan and P. Bahadur, *J. Colloid Interface Sci.*, 2006, **299**, 910-915.
25. P. Winsor, *Chem. Rev.*, 1968, **68**, 1-40.
26. X. Du, L. A. Lucia and R. A. Ghiladi, *ACS Sustain. Chem. Eng.*, 2016, **4**, 1665-1672.
27. N. Anton and T. F. Vandamme, *Pharm. Res.*, 2011, **28**, 978-985.
28. B. P. Binks and C. P. Whitby, *Colloids Surf. A*, 2005, **253**, 105-115.
29. B. P. Binks and D. Yin, *Soft Matter*, 2016, **12**, 6858-6867.
30. J. Zhou, X. Qiao, B. P. Binks, K. Sun, M. Bai, Y. Li and Y. Liu, *Langmuir*, 2011, **27**, 3308-3316.
31. S. Dale, *BP Energy Outlook 2022 Edition*, London, UK, 2022.
32. V. Núñez-López and E. Moskal, *Front. Clim.*, 2019, **1**, 5.
33. T. Ahmed, *Reservoir Engineering Handbook*, Gulf Professional Publishing, Cambridge, 5th edn., 2018.

34. R. Singh and J. Miller, *SPE Western Regional Meeting*, Virtual, 2021.
35. N. Alharthy, T. Teklu, H. Kazemi, R. Graves, S. Hawthorne, J. Braunberger and B. Kurtoglu, *SPE Reserv. Eval. Eng.*, 2017, **21**, 137-159.
36. S. Q. Tunio, A. H. Tunio, N. A. Ghirano and Z. M. El Adawy, *Int. J. Appl. Sci.*, 2011, **1**, 143-153.
37. G. J. Hirasaki, C. A. Miller and M. Puerto, *Soc. Pet. Eng. J.*, 2011, **16**, 889-907.
38. X. Yang, V. J. Verruto and P. K. Kilpatrick, *Energy Fuels*, 2007, **21**, 1343-1349.
39. T. Fan, J. Wang and J. S. Buckley, *SPE/DOE Improved Oil Recovery Symposium*, Tulsa, Oklahoma, 2002.
40. W. K. Seifert and W. G. Howells, *Anal. Chem.*, 1969, **41**, 554-562.
41. L. Cuiec, *SPE annual technical conference and exhibition*, Houston, 1984.
42. Y. Chen, Q. Xie, A. Sari, P. V. Brady and A. Saeedi, *Fuel*, 2018, **215**, 171-177.
43. A. Hiorth, L. Cathles and M. Madland, *Transp. Porous Media*, 2010, **85**, 1-21.
44. A. Dehghan Monfared, M. H. Ghazanfari, M. Jamialahmadi and A. Helalizadeh, *Energy Fuels*, 2016, **30**, 3947-3961.
45. R. Eriksson, J. Merta and J. B. Rosenholm, *J. Colloid Interface Sci.*, 2007, **313**, 184-193.
46. J. S. Buckley, Y. Liu and S. Monsterleet, *Soc. Pet. Eng. J.*, 1998, **3**, 54-61.
47. M. F. Mehraban, S. A. Farzaneh and M. Sohrabi, *Energy Fuels*, 2021, **35**, 3766-3779.
48. Z. Ahsaei, M. Nabipour, A. Azdarpour, R. M. Santos, E. Mohammadian, P. Babakhani, H. Hamidi, M. A. Karaei and A. Esfandiarian, *Energ. Source Part A.*, 2022, **44**, 2811-2822.
49. N. Akhlaghi, S. Riahi and R. Parvaneh, *J. Pet. Sci. Eng.*, 2021, **198**, 108177.
50. R. Anto and U. K. Bhui, *J. Pet. Sci. Eng.*, 2022, **208**, 109803.
51. Z.-H. Zhou, Q. Zhang, Y. Liu, H.-Z. Wang, H.-Y. Cai, F. Zhang, M.-Z. Tian, L. Zhang and L. Zhang, *J. Disp. Sci. Technol.*, 2016, **37**, 1178-1185.
52. F. Moeini, A. Hemmati-Sarapardeh, M.-H. Ghazanfari, M. Masihi and S. Ayatollahi, *Fluid Phase Equilib.*, 2014, **375**, 191-200.
53. R. Aveyard and S. M. Saleem, *J. Chem. Soc., Faraday Trans. 1*, 1976, **72**, 1609-1617.
54. V. C. Santanna, A. C. M. Silva, H. M. Lopes and F. A. Sampaio Neto, *J. Pet. Sci. Eng.*, 2013, **105**, 116-120.
55. M. J. Rosen, H. Wang, P. Shen and Y. Zhu, *Langmuir*, 2005, **21**, 3749-3756.
56. X. Li, X. Yue, J. Zou and R. Yan, *Colloids Surf. A*, 2022, **634**, 127991.
57. B. P. Binks, P. D. I. Fletcher and L. Tian, *Colloids Surf. A*, 2010, **363**, 8-15.
58. R. Gupta and K. K. Mohanty, *SPE Symposium on Improved Oil Recovery*, Tulsa, 2008.
59. F. D. S. Curbelo, V. C. Santanna, E. L. B. Neto, T. V. Dutra, T. N. C. Dantas, A. A. D. Neto and A. I. C. Garnica, *Colloids Surf. A*, 2007, **293**, 1-4.
60. P. Esmaeilzadeh, A. Bahramian and Z. Fakhroueian, *Phys. Procedia*, 2011, **22**, 63-67.
61. S. Paria and K. C. Khilar, *Adv. Colloid Interface Sci.*, 2004, **110**, 75-95.
62. D. C. Standnes and T. Austad, *J. Pet. Sci. Eng.*, 2000, **28**, 123-143.
63. M. Sharma, D. Shah and W. Brigham, *AIChE J.*, 1985, **31**, 222-228.
64. D. C. Standnes and T. Austad, *Colloids Surf. A*, 2003, **216**, 243-259.
65. M. Kahlweit, G. Busse and B. Faulhaber, *Langmuir*, 1996, **12**, 861-862.
66. M. Salehi, S. J. Johnson and J.-T. Liang, *Langmuir*, 2008, **24**, 14099-14107.
67. B. Hou, Y. Wang, X. Cao, J. Zhang, X. Song, M. Ding and W. Chen, *J. Surfactants Deterg.*, 2016, **19**, 315-324.
68. T. Ahmadali, M. V. Gonzalez, J. H. Harwell and J. F. Scamehorn, *SPE Res. Eng.*, 1993, **8**, 117-122.
69. H. Ehtesabi, M. M. Ahadian, V. Taghikhani and M. H. Ghazanfari, *Energy Fuels*, 2014, **28**, 423-430.

70. A. Kumar and A. Mandal, *J. Mol. Liq.*, 2017, **243**, 61-71.
71. S. Liu, D. Zhang, W. Yan, M. Puerto, G. J. Hirasaki and C. A. Miller, *Soc. Pet. Eng. J.*, 2008, **13**, 5-16.
72. J. J. Sheng, *J. Pet. Sci. Eng.*, 2017, **159**, 635-643.
73. C. S. Gregersen, M. Kazempour and V. Alvarado, *Fuel*, 2013, **105**, 368-382.
74. J. Wang, M. Han, A. B. Fuseni and D. Cao, SPE Middle East Oil & Gas Show and Conference, Manama, 2015.
75. M. Van der Lee and E. van den Pol, IOR 2015-18th European Symposium on Improved Oil Recovery, Dresden, 2015.
76. R. Gupta and K. K. K. Mohanty, *Soc. Pet. Eng. J.*, 2010, **15**, 588-597.
77. S. B. Gogoi, *Curr. Sci.*, 2009, **97**, 1059-1063.
78. J. Saien and M. Bahrami, *J. Mol. Liq.*, 2016, **224**, 158-164.
79. L. Wang, Z. Wang, H. Yang and G. Yang, *Mater. Chem. Phys.*, 1999, **57**, 260-263.
80. H. Zhou, R. Cheng, C. Dai, Y. Li, M. Zhao and W. Lv, *IOP Conf. Ser.: Earth Environ. Sci.* , 2019, **218**, 012153.
81. R. R. Jalil and H. Hussein, *IOP Conf. Ser.: Mater. Sci. Eng.*, 2019, **518**, 062004.
82. F. Ravera, E. Santini, G. Loglio, M. Ferrari and L. Liggieri, *J. Phys. Chem. B.*, 2006, **110**, 19543-19551.
83. L. Hendraningrat and O. Torsæter, *Energy Fuels*, 2014, **28**, 6228-6241.
84. A. Roustaei and H. Bagherzadeh, *J. Pet. Explor. Prod. Technol.*, 2015, **5**, 27-33.
85. S. Al-Anssari, Z.-U.-A. Arain, A. Barifcani, A. Keshavarz, M. Ali and S. Iglauer, Abu Dhabi International Petroleum Exhibition & Conference, Abu Dhabi, 2018.
86. B. Wei, Q. Li, F. Jin, H. Li and C. Wang, *Energy Fuels*, 2016, **30**, 2882-2891.
87. S. a. Betancur, F. Carrasco-Marín, A. n. F. Pérez-Cadenas, C. A. Franco, J. Jiménez, E. J. Manrique, H. Quintero and F. B. Cortés, *Energy Fuels*, 2019, **33**, 4158-4168.
88. M. R. Gray, A. Yeung, J. M. Foght and H. W. Yarranton, SPE Annual Technical Conference and Exhibition, Colorado, 2008.
89. C. O. Metin, J. R. Baran and Q. P. Nguyen, *J. Nanopart. Res.*, 2012, **14**, 1-16.
90. H. Zhang, A. Nikolov and D. Wasan, *Energy Fuels*, 2014, **28**, 3002-3009.
91. R. Nazari Moghaddam, A. Bahramian, Z. Fakhroueian, A. Karimi and S. Arya, *Energy Fuels*, 2015, **29**, 2111-2119.
92. A. Chengara, A. D. Nikolov, D. T. Wasan, A. Trokhymchuk and D. Henderson, *J. Colloid Interface Sci.*, 2004, **280**, 192-201.
93. A. D. Monfared, M. Ghazanfari, M. Jamialahmadi and A. Helalizadeh, *Chem. Eng. J.*, 2015, **281**, 334-344.
94. A. Nikolov, K. Kondiparty and D. Wasan, *Langmuir*, 2010, **26**, 7665-7670.
95. S. Al-Anssari, A. Barifcani, S. Wang, L. Maxim and S. Iglauer, *J. Colloid Interface Sci.*, 2016, **461**, 435-442.
96. S. Zendehboudi, A. Shafiei, A. Bahadori, L. A. James, A. Elkamel and A. Lohi, *Chem. Eng. Res. Des.*, 2014, **92**, 857-875.
97. R. B. de Boer, K. Leerlooyer, M. R. P. Eigner and A. R. D. van Bergen, *SPE Prod. Oper.*, 1995, **10**, 55-61.
98. C. A. Franco, R. Zabala and F. B. Cortés, *J. Pet. Sci. Eng.*, 2017, **157**, 39-55.
99. K. Guo, Y. Zhang, Q. Shi and Z. Yu, *Energy Fuels*, 2017, **31**, 6045-6055.
100. S. M. Elahi, C. E. Scott, Z. Chen and P. Pereira-Almao, *Fuel*, 2019, **252**, 262-271.
101. N. A. Ogolo, O. A. Olafuyi and M. O. Onyekonwu, presented in part at the SPE Saudi Arabia Section Technical Symposium and Exhibition, Al-Khobar, 2012.
102. J. Taheri-Shakib, A. Shekarifard and H. Naderi, *Fuel*, 2018, **232**, 704-711.
103. F. M. Caldelas, M. Murphy, C. Huh and S. L. Bryant, SPE production and operations symposium, Oklahoma, 2011.
104. T. Skauge, K. Spildo and A. Skauge, SPE improved oil recovery symposium, Oklahoma, 2010.

105. P. H. Nelson, *AAPG Bull.*, 2009, **93**, 329-340.
106. M. N. Alaskar, M. F. Ames, S. T. Connor, C. Liu, Y. Cui, K. Li and R. N. Horne, *Soc. Pet. Eng. J.*, 2012, **17**, 1160-1171.
107. M. Basavaraj, G. Fuller, J. Fransaer and J. Vermant, *Langmuir*, 2006, **22**, 6605-6612.
108. D. Espinosa, F. Caldelas, K. Johnston, S. L. Bryant and C. Huh, SPE Improved Oil Recovery Symposium, Oklahoma, 2010.
109. T. Austad, S. F. Shariatpanahi, S. Strand, H. Aksulu and T. Puntervold, *Energy Fuels*, 2015, **29**, 6903-6911.
110. A. M. Maia, R. Borsali and R. C. Balaban, *Mater. Sci. Eng. C.* , 2009, **29**, 505-509.
111. Z. Aghaeifar, S. Strand, T. Puntervold, T. Austad and F. M. Sajjad, *Journal of Petroleum Science and Engineering*, 2018, **165**, 743-751.
112. T. Zhang, M. J. Murphy, H. Yu, H. G. Bagaria, K. Y. Yoon, B. M. Nielson, C. W. Bielawski, K. P. Johnston, C. Huh and S. L. Bryant, *Soc. Pet. Eng. J.*, 2015, **20**, 667-677.
113. A. Maghzi, S. Mohammadi, M. H. Ghazanfari, R. Kharrat and M. Masihi, *Exp. Therm. Fluid Sci.*, 2012, **40**, 168-176.
114. L. Yang and K. Du, *Adv. Mater. Res.*, 2012, **347**, 786-790.
115. H. M. Zaid, N. Yahya and N. R. A. Latiff, *J. Nano Res.*, 2013, **21**, 103-108.
116. A. J. Worthen, S. L. Bryant, C. Huh and K. P. Johnston, *AIChE J.*, 2013, **59**, 3490-3501.
117. S. Limage, J. Krägel, M. Schmitt, C. Dominici, R. Miller and M. Antoni, *Langmuir*, 2010, **26**, 16754-16761.
118. T. Sharma, G. S. Kumar, B. H. Chon and J. S. Sangwai, *J. Ind. Eng. Chem.*, 2015, **22**, 324-334.
119. C. Chen, S. Wang, M. J. Kadhum, J. H. Harwell and B.-J. Shiau, *Fuel*, 2018, **222**, 561-568.
120. N. Yekeen, M. A. Manan, A. K. Idris, A. M. Samin and A. R. Risal, *J. Pet. Sci. Eng.*, 2017, **159**, 115-134.
121. N. Saxena, A. Kumar and A. Mandal, *J. Pet. Sci. Eng.*, 2019, **173**, 1264-1283.
122. R. Songolzadeh and J. Moghadasi, *Colloid. Polym. Sci.*, 2017, **295**, 145-155.
123. N. Yekeen, A. M. Ali Elakkari, J. A. Khan, M. Ali, A. Al-Yaseri and H. Hoteit, *Energy Fuels*, 2023, **37**, 5114-5129.
124. G. Xu, J. Chang, H. Wu, W. Shao, G. Li, J. Hou, N. Kang and J. Yang, *Colloids Surf. A*, 2023, **657**, 130545.
125. D. N. P, G. R. Seetharaman, G. Kumar and J. S. Sangwai, *Energy Fuels*, 2023, **37**, 7094-7110.
126. X. Wang, J. Zhou, J. Pang and K. K. Mohanty, *SPE J.*, 2023, 1-11.
127. W. Al-Shatty, M. Campana, S. Alexander and A. R. Barron, *ACS Appl. Mater. Interfaces*, 2022, **14**, 19505-19514.
128. M. Zhao, Y. Li, C. Dai, Y. Chen, Z. Ma, T. Li, Z. Yang and K. Liu, *Fuel*, 2023, **347**, 128481.
129. M. L. d. O. Pereira, K. C. B. Maia, W. C. Silva, A. C. Leite, A. D. d. S. Francisco, T. L. Vasconcelos, R. S. V. Nascimento and D. Grasseschi, *ACS Appl. Nano Mater.*, 2020, **3**, 5762-5772.
130. Y. Zhou, X. Wu, X. Zhong, S. Zhang, H. Pu and J. X. Zhao, *Fuel*, 2020, **277**, 118203.
131. R. Singh and K. K. Mohanty, SPE Annual Technical Conference and Exhibition, San Antonio, 2017.
132. N. Kumar, T. Gaur and A. Mandal, *J. Ind. Eng. Chem.*, 2017, **54**, 304-315.
133. G. Cheraghian, S. Kiani, N. N. Nassar, S. Alexander and A. R. Barron, *Ind. Eng. Chem. Res.*, 2017, **56**, 8528-8534.
134. X. Zhong, H. Pu, Y. Zhou and J. X. Zhao, *Energy Fuels*, 2019, **33**, 1007-1015.

135. H. Green, B. Šegvić, G. Zanoni, S. Omodeo-Salé and T. Adatte, *Geosci.*, 2020, **10**, 381-413.
136. M. A. I. Khan, S. H. Kleiberg, I. D. P. Torrijos, T. Puntervold and S. Strand, 2023.
137. I. Piñerez, T. Puntervold, S. Strand, P. Hopkins, P. Aslanidis, H. S. Yang and M. S. Kinn, *J. Pet. Sci. Eng.*, 2020, **195**, 107654.
138. J. Milter and I. Oxnevad, *Pet. Geosci.*, 1996, **2**, 231-240.
139. T. Fan and J. S. Buckley, *Soc. Pet. Eng. J.*, 2007, **12**, 496-500.
140. E. E. Ureña-Benavides, E. Moaseri, B. Changalvaie, Y. Fei, M. Iqbal, B. A. Lyon, A. A. Kmetz, K. D. Pennell, C. J. Ellison and K. P. Johnston, *Colloids Surf. A*, 2020, **586**, 124276.
141. H. G. Bagaria, Z. Xue, B. M. Neilson, A. J. Worthen, K. Y. Yoon, S. Nayak, V. Cheng, J. H. Lee, C. W. Bielawski and K. P. Johnston, *ACS Appl. Mater. Interfaces*, 2013, **5**, 3329-3339.
142. Z. Xue, E. Foster, Y. Wang, S. Nayak, V. Cheng, V. W. Ngo, K. D. Pennell, C. W. Bielawski and K. P. Johnston, *Energy Fuels*, 2014, **28**, 3655-3665.
143. V. Miloslavsky, E. Makovetsky, L. Ageev and K. Beloshenko, *Opt. Spectrosc.*, 2009, **107**, 811-815.
144. A. Peyman, C. Gabriel and E. H. Grant, *Bioelectromagnetics*, 2007, **28**, 264-274.
145. C. Griffith and H. Daigle, *J. Colloid Interface Sci.*, 2018, **509**, 132-139.
146. H. Jang, W. Lee and J. Lee, *Colloids Surf. A*, 2018, **554**, 261-271.
147. E. Cristiano, Y.-J. Hu, M. Sigfried, D. Kaplan and H. Nitsche, *Clays Clay Miner.*, 2011, **59**, 107-115.
148. S. Brunauer, P. H. Emmett and E. Teller, *J. Am. Chem. Soc.*, 1938, **60**, 309-319.
149. L. Gurvich, *J. Phys. Chem. Soc. Russ*, 1915, **47**, 49-56.
150. ASTM Standard D3049-89R03, Standard Test Method for Synthetic Anionic Ingredient by Cationic Titration, 2003.
151. S. K. Nandwani, M. Chakraborty and S. Gupta, *Sci. Rep.*, 2019, **9**, 14760.
152. J. Wang and X. Guo, *Chemosphere*, 2020, **258**, 127279.
153. T. Puntervold, S. Strand and T. Austad, *Energy Fuels*, 2007, **21**, 3425-3430.
154. M. A. Al-Balushi, M. Karimi and R. S. Al-Maamari, *Energy Fuels*, 2019, **34**, 245-257.
155. B. Liu, L. Bai, Y. Chi, R. Jia, X. Fu and L. Yang, *Mar. Pet. Geol.*, 2019, **109**, 561-573.
156. K. Danov, S. Kralchevska, P. Kralchevsky, K. Ananthapadmanabhan and A. Lips, *Langmuir*, 2004, **20**, 5445-5453.
157. A. P. Gerola, P. F. Costa, F. Nome and F. Quina, *Curr. Opin. Colloid Interface Sci.*, 2017, **32**, 48-56.
158. A. Isah, M. Arif, A. Hassan, M. Mahmoud and S. Iglauer, *Energy Rep.*, 2022, **8**, 6355-6395.
159. H. Demissie and R. Duraisamy, *J. Sci. Innov. Res*, 2016, **5**, 208-214.
160. B. Kang, H. Tang, Z. Zhao and S. Song, *ACS Omega*, 2020, **5**, 6229-6239.
161. A. P. dos Santos, A. Diehl and Y. Levin, *Langmuir*, 2010, **26**, 10778-10783.
162. N. R. Pallas and Y. Harrison, *Colloids Surf.*, 1990, **43**, 169-194.
163. F. M. Menger, A. L. Galloway and M. E. Chlebowski, *Langmuir*, 2005, **21**, 9010-9012.
164. I. Langmuir, *J. Am. Chem. Soc.*, 1917, **39**, 1848-1906.
165. C. Wagner, *Phys. Z.*, 1924, **25**, 474-477.
166. Y. Levin and J. Flores-Mena, *Europhys. Lett.*, 2001, **56**, 187.
167. S. R. Varade and P. Ghosh, *J. Disp. Sci. Technol.*, 2020, **41**, 1174-1191.
168. S. M. S. Hussain, A. Mahboob and M. S. Kamal, *Materials*, 2020, **13**, 1858.
169. T. R. Carale, Q. T. Pham and D. Blankschtein, *Langmuir*, 1994, **10**, 109-121.
170. P. Palladino and R. Ragone, *Langmuir*, 2011, **27**, 14065-14070.
171. L. Zhang, P. Somasundaran and C. Maltesh, *Langmuir*, 1996, **12**, 2371-2373.
172. A. Kroflič, B. Šarac and M. Bešter-Rogač, *Langmuir*, 2012, **28**, 10363-10371.

173. K. Tori and T. Nakagawa, *Colloid Polym. Sci.*, 1963, **189**, 50-55.
174. Z. H. Ren, *Ind. Eng. Chem. Res.*, 2015, **54**, 9683-9688.
175. M. J. Qazi, S. J. Schlegel, E. H. G. Backus, M. Bonn, D. Bonn and N. Shahidzadeh, *Langmuir*, 2020, **36**, 7956-7964.
176. M. Mulqueen and D. Blankschtein, *Langmuir*, 2000, **16**, 7640-7654.
177. J. D. Hines, R. K. Thomas, P. R. Garrett, G. K. Rennie and J. Penfold, *J. Phys. Chem. B.*, 1997, **101**, 9215-9223.
178. P. Somasundaran and L. Huang, *Adv. Colloid Interface Sci.*, 2000, **88**, 179-208.
179. B. P. Binks and T. S. Horozov, *Angew. Chem. Int. Ed.*, 2005, **44**, 3722-3725.
180. H. Vatanparast, F. Shahabi, A. Bahramian, A. Javadi and R. Miller, *Sci. Rep.*, 2018, **8**, 7251.
181. Y.-L. Lee, Z.-C. Du, W.-X. Lin and Y.-M. Yang, *J. Colloid Interface Sci.*, 2006, **296**, 233-241.
182. A. J. Worthen, L. M. Foster, J. Dong, J. A. Bollinger, A. H. Peterman, L. E. Pastora, S. L. Bryant, T. M. Truskett, C. W. Bielawski and K. P. Johnston, *Langmuir*, 2014, **30**, 984-994.
183. S. Partyka, M. Lindheimer and B. Faucompre, *Colloids Surf. A*, 1993, **76**, 267-281.
184. X. Hu, Y. Li, H. Sun, X. Song, Q. Li, X. Cao and Z. Li, *J. Phys. Chem. B.*, 2010, **114**, 8910-8916.
185. J. Zajac, C. Chorro, M. Lindheimer and S. Partyka, *Langmuir*, 1997, **13**, 1486-1495.
186. A. J. Worthen, S. Alzobaidi, V. Tran, M. Iqbal, J. S. Liu, K. A. Cornell, I. Kim, D. A. DiCarlo, S. L. Bryant and C. Huh, Preprint arXiv: 1811.11217, 2018.
187. M. Y. Rezk and N. K. Allam, *Ind. Eng. Chem. Res.*, 2019, **58**, 16287-16295.
188. P. J. Lu, E. Zaccarelli, F. Ciulla, A. B. Schofield, F. Sciortino and D. A. Weitz, *Nature*, 2008, **453**, 499-503.
189. J. T. G. Overbeek, *Pure Appl. Chem.*, 1980, **52**, 1151-1161.
190. J. Lyklema, *J. Colloid Interface Sci.*, 2013, **392**, 102-104.
191. S. Kvech and M. Edwards, *Water Res.*, 2002, **36**, 4356-4368.
192. Z. Briceño-Ahumada, J. F. A. Soltero-Martínez and R. Castillo, *Chem. Eng. J. Adv.*, 2021, **7**, 100116.
193. C. F. Holder and R. E. Schaak, *ACS Nano*, 2019, **13**, 7359-7365.
194. I. Fuchs, Y. Aluma, M. Ilan and Y. Mastai, *J. Phys. Chem. B.*, 2014, **118**, 2104-2111.
195. Y. Bu, B. Cui, W. Zhao and Z. Yang, *RSC Adv.*, 2017, **7**, 55489-55495.
196. A. A. Dongargaonkar and J. D. Clogston, in *Characterization of nanoparticles intended for drug delivery*, ed. S. E. McNeil, Springer, New York, 2018, pp. 57-63.
197. M. Tartagni, M. Crescentini, M. Rossi, H. Morgan and E. Sangiorgi, 2014 IEEE International Electron Devices Meeting, San Francisco, 2014.
198. M. Kosmulski, *Colloids Surf. A*, 2003, **222**, 113-118.
199. Z. G. Estephan, J. A. Jaber and J. B. Schlenoff, *Langmuir*, 2010, **26**, 16884-16889.
200. M. Lashkarbolooki, S. Ayatollahi and M. Riazi, *J. Chem. Eng. Data*, 2014, **59**, 3624-3634.
201. K. Du, E. Glogowski, T. Emrick, T. P. Russell and A. D. Dinsmore, *Langmuir*, 2010, **26**, 12518-12522.
202. P. Somasundaran and G. Agar, *J. Colloid Interface Sci.*, 1967, **24**, 433-440.
203. W. Wang, Y. Zhu, C. Yu, L. Zhao and D. Chen, *J. Nat. Gas Sci. Eng.*, 2020, **5**, 45-55.
204. K. S. W. Sing, in *Stud. Surf. Sci. Catal.*, eds. F. Rodriguez-Reinoso, J. Rouquerol, K. S. W. Sing and K. K. Unger, Elsevier, Amsterdam, 1991, vol. 62, pp. 1-9.
205. S. J. Gregg, K. S. W. Sing and H. Salzberg, *J. Electrochem. Soc.*, 1967, **114**, 279.
206. F. Liu, G.-C. Jiang, K. Wang and J. Wang, *J. Mater. Sci.*, 2017, **52**, 12266-12278.

207. K. S. Sing, *Pure Appl. Chem.*, 1985, **57**, 603-619.
208. J. W. Grate, K. J. Dehoff, M. G. Warner, J. W. Pittman, T. W. Wietsma, C. Zhang and M. Oostrom, *Langmuir*, 2012, **28**, 7182-7188.
209. D. Wang, R. Butler, H. Liu and S. Ahmed, SPE Annual Technical Conference and Exhibition, Colorado, 2011.
210. D. Wang, R. Butler, J. Zhang and R. Seright, *SPE Reserv. Eval. Eng.*, 2012, **15**, 695-705.
211. A. Neog and D. S. Schechter, SPE Improved Oil Recovery Conference, Tulsa, 2016.
212. T. Zeng, C. S Miller and K. Mohanty, SPE Improved Oil Recovery Conference, Tulsa, 2018.
213. Y. Yue, S. Chen, Z. Wang, X. Yang, Y. Peng, J. Cai and H. A. Nasr-El-Din, *J. Pet. Sci. Eng.*, 2018, **161**, 692-702.
214. N. Li, G. Zhang, J. Ge, J. Luchao, Z. Jianqiang, D. Baodong and H. Pei, *Energy Fuels*, 2011, **25**, 4430-4437.
215. G. Jian, M. Puerto, A. Wehowsky, C. Miller, G. J. Hirasaki and S. L. Biswal, *J. Colloid Interface Sci.*, 2018, **513**, 684-692.
216. S. Paria, C. Manohar and K. C. Khilar, *J. Inst. Eng.*, 2003, **43**, 34-44.
217. V. Mirchi, S. Saraji, L. Goual and M. Piri, *Fuel*, 2015, **148**, 127-138.
218. C. T. Gerold and C. S. Henry, *Langmuir*, 2018, **34**, 1550-1556.
219. L. K. Koopal, E. M. Lee and M. R. Böhmer, *J. Colloid Interface Sci.*, 1995, **170**, 85-97.
220. R. G. Chaudhuri and S. Paria, *J. Colloid Interface Sci.*, 2009, **337**, 555-562.
221. D. M. Nevskaia, A. Guerrero-Ruíz and J. de D. López-González, *J. Colloid Interface Sci.*, 1998, **205**, 97-105.
222. A. Bera and H. Belhaj, *J. Nat. Gas Eng.*, 2016, **34**, 1284-1309.
223. E. Sadatshojaei, M. Jamialahmadi, F. Esmaeilzadeh, D. A. Wood and M. H. Ghazanfari, *J. Disp. Sci. Technol.*, 2019, 1-15.
224. S. Rezaei Gomari, Y. Gorra Diallo Omar, F. Amrouche, M. Islam and D. Xu, *Colloids Surf. A*, 2019, **568**, 164-172.
225. N. J. Hadia, Y. H. Ng, L. P. Stubbs and O. Torsæter, *J. Nanomater.*, 2021, **11**, 707.
226. S. Alzobaidi, P. Wu, C. Da, X. Zhang, J. Hackbarth, T. Angeles, N. J. Rabat-Torki, S. MacAuliffe, S. Panja and K. P. Johnston, *J. Colloid Interface Sci.*, 2021, **581**, 656-668.
227. W. G. Anderson, *J. Pet. Technol.*, 1986, **38**, 1125-1144.
228. W. Tang, P. Wu, C. Da, S. Alzobaidi, J. Harris, B. Hallaman, D. Hu and K. P. Johnston, *Fuel*, 2023, **331**, 125752.
229. X. Zhong, C. Li, Y. Li, H. Pu, Y. Zhou and J. X. Zhao, *Energy Fuels*, 2020, **34**, 2893-2902.
230. O. A. Okunade, N. Yekeen, E. Padmanabhan, A. Al-Yaseri, A. K. Idris and J. A. Khan, *J. Pet. Sci. Eng.*, 2021, **207**, 109139.
231. E. L. Sjöberg and D. T. Rickard, *Chem. Geol.*, 1984, **42**, 119-136.
232. M. Arabloo, M. H. Ghazanfari and D. Rashtchian, *Fuel*, 2016, **185**, 199-210.
233. O. Massarweh and A. S. Abushaikha, *Energy Rep.*, 2020, **6**, 3150-3178.
234. A. Durán-Álvarez, M. Maldonado-Domínguez, O. González-Antonio, C. Durán-Valencia, M. Romero-Ávila, F. Barragán-Aroche and S. López-Ramírez, *Langmuir*, 2016, **32**, 2608-2616.
235. A. Martínez-Luévanos, A. Uribe-Salas and A. Lopez-Valdivieso, *Miner. Eng.*, 1999, **12**, 919-936.
236. C. A. Young and J. D. Miller, *Int. J. Miner. Process.*, 2000, **58**, 331-350.
237. T. Zeng, K. T. Kim, C. J. Werth, L. E. Katz and K. K. Mohanty, *Energy Fuels*, 2020, **34**, 5436-5443.
238. A. Bąk and W. Podgórska, *Colloids Surf. A*, 2016, **504**, 414-425.

239.   R. Aveyard, B. P. Binks, S. Clark and J. Mead, *J. Chem. Soc., Faraday Trans. 1*, 1986, **82**, 125-142.

240.   S. Li, Y. Liu, L. Xue and D. Zhu, *J. Pet. Sci. Eng.*, 2022, **212**, 110259.

241.   M. H. Badizad, M. M. Koleini, R. Hartkamp, S. Ayatollahi and M. H. Ghazanfari, *J. Colloid Interface Sci.*, 2020, **575**, 337-346.

242.   M. Lashkarbolooki and S. Ayatollahi, *Fuel*, 2018, **223**, 261-267.

243.   T. R. Underwood and H. C. Greenwell, *Sci. Rep.*, 2018, **8**, 352.

244.   E. A. Guggenheim and N. K. Adam, *Proc. R. Soc. Lond. A Math. Phys. Sci.*, 1933, **139**, 218-236.

245.   A. A. Ivanova, C. Phan, A. Barifcani, S. Iglauer and A. N. Cheremisin, *J. Surfactants Deterg.*, 2020, **23**, 327-338.

246.   J. Zhao, C. Dai, Q. Ding, M. Du, H. Feng, Z. Wei, A. Chen and M. Zhao, *RSC Adv.*, 2015, **5**, 13993-14001.

247.   N. Nadir, S. Shahruddin and J. Othman, *Open Chem.*, 2022, **20**, 1110-1120.

248.   C. J. Lim, C. K. Lim and G. C. L. Ee, *J. Disp. Sci. Technol.*, 2021, **42**, 1660-1672.

249.   L.-m. Yan, Y.-l. Li, Z.-g. Cui, B.-l. Song, X.-m. Pei and J.-z. Jiang, *Energy Fuels*, 2017, **31**, 9319-9327.

250.   Z.-H. Zhou, Q. Zhang, Y. Liu, H.-Z. Wang, H.-Y. Cai, F. Zhang, M.-Z. Tian, Z.-Y. Liu, L. Zhang and L. Zhang, *Energy Fuels*, 2014, **28**, 1020-1027.

251.   H. Alasiri, PhD thesis, Rice University, 2016.

252.   J. R. Premkumar and G. N. Sastry, *J. Phys. Chem. A*, 2014, **118**, 11388-11398.

253.   Y. Li, P. Zhang, F.-L. Dong, X.-L. Cao, X.-W. Song and X.-H. Cui, *J. Colloid Interface Sci.*, 2005, **290**, 275-280.

254.   B. P. Binks and S. Lumsdon, *Langmuir*, 2000, **16**, 8622-8631.

255.   Y. Lin, H. Skaff, T. Emrick, A. Dinsmore and T. P. Russell, *Science*, 2003, **299**, 226-229.

256.   T. Al-Sahhaf, A. Elkamel, A. Suttar Ahmed and A. Khan, *Chem. Eng. Commun.*, 2005, **192**, 667-684.

257.   M. Chorro, N. Kamenka, B. Faucompre, S. Partyka, M. Lindheimer and R. Zana, *Colloids Surf. A*, 1996, **110**, 249-261.

258.   R. Jia, W. Kang, Z. Li, H. Yang, Z. Gao, Z. Zheng, H. Yang, B. Zhou, H. Jiang and S. Turtabayev, *J. Mol. Liq.*, 2022, **368**, 120734.

259.   B. Gao and M. M. Sharma, *J. Colloid Interface Sci.*, 2013, **407**, 375-381.

260.   Z.-Z. Chen, H.-Z. Gang, J.-F. Liu, B.-Z. Mu and S.-Z. Yang, *J. Pet. Sci. Eng.*, 2019, **181**, 106181.

261.   S. S. Adkins, X. Chen, I. Chan, E. Torino, Q. P. Nguyen, A. W. Sanders and K. P. Johnston, *Langmuir*, 2010, **26**, 5335-5348.

262.   A. Miquilena, V. Coll, A. Borges, J. Melendez and S. Zeppieri, *Int. J. Thermophys.*, 2010, **31**, 2416-2424.

263.   W. Karnanda, M. S. Benzagouta, A. AlQuraishi and M. M. Amro, *Arab. J. Geosci.*, 2013, **6**, 3535-3544.

264.   R. A. Nasralla and H. A. Nasr-El-Din, *SPE Reserv. Eval. Eng.*, 2014, **17**, 49-59.

265.   K. H. Chakravarty, P. L. Fosbøl and K. Thomsen, 2015.

266.   A. Zahid, E. H. Stenby and A. A. Shapiro, SPE EUROPEC/EAGE Annual Conference and Exhibition, Barcelona, 2010.

267.   R. Aveyard, B. P. Binks, P. D. I. Fletcher, X. Ye and J. R. Lu, in *Emulsions — A Fundamental and Practical Approach*, ed. J. Sjöblom, Springer Netherlands, Dordrecht, 1992, pp. 97-110.

268.   F. Goodarzi and S. Zendehboudi, *Ind. Eng. Chem. Res.*, 2019, **58**, 8817-8834.

269.   C. Da, S. Alzobaidi, G. Jian, L. Zhang, S. L. Biswal, G. J. Hirasaki and K. P. Johnston, *J. Pet. Sci. Eng.*, 2018, **166**, 880-890.

270.   L. Lobo and D. T. Wasan, *Langmuir*, 1993, **9**, 1668-1677.

271.   L. Xu, M. D. Rad, A. Telmadarreie, C. Qian, C. Liu, S. L. Bryant and M. Dong, *Colloids Surf. A*, 2018, **550**, 176-185.

272. B. P. Binks and S. O. Lumsdon, *Phys. Chem. Chem. Phys.*, 2000, **2**, 2959-2967.
273. H. Sayilkan, Ş. Şsener, E. Şener and E. Arpaç, *J. Mater. Sci.*, 1999, **34**, 5325-5330.
274. P. Jungwirth and D. J. Tobias, *J. Phys. Chem. B.*, 2002, **106**, 6361-6373.
275. T. S. Horozov, B. P. Binks and T. Gottschalk-Gaudig, *Phys. Chem. Chem. Phys.*, 2007, **9**, 6398-6404.
276. S. Arditty, V. Schmitt, F. Lequeux and F. Leal-Calderon, *Eur. Phys. J. B.*, 2005, **44**, 381-393.
277. K. Liu, J. Jiang, Z. Cui and B. P. Binks, *Langmuir*, 2017, **33**, 2296-2305.
278. M. Xu, J. Jiang, X. Pei, B. Song, Z. Cui and B. P. Binks, *Angew. Chem.*, 2018, **130**, 7864-7868.
279. M. Xu, L. Xu, Q. Lin, X. Pei, J. Jiang, H. Zhu, Z. Cui and B. P. Binks, *Langmuir*, 2019, **35**, 4058-4067.
280. B. P. Binks, J. A. Rodrigues and W. J. Frith, *Langmuir*, 2007, **23**, 3626-3636.
281. B. P. Binks, A. Desforges and D. G. Duff, *Langmuir*, 2007, **23**, 1098-1106.
282. V. N. Paunov, B. P. Binks and N. P. Ashby, *Langmuir*, 2002, **18**, 6946-6955.
283. J. Saien and S. Akbari, *J. Chem. Eng. Data*, 2006, **51**, 1832-1835.
284. S. Lu, J. Li, P. Zhang, H. Xue, G. Wang, J. Zhang, H. Liu and Z. Li, *Pet. Explor. Dev.*, 2018, **45**, 452-460.
285. T. Puntervold, A. Mamonov, I. D. Piñerez Torrijos and S. Strand, *Energy Fuels*, 2021, **35**, 5738-5747.
286. H. A. Son, Y. Jang and T. Lee, *Korean J. Chem. Eng.*, 2022, **39**, 3286-3294.
287. A. Bila and O. Torsæter, *Nanomater.*, 2021, **11**, 765.
288. M. A. Endo Kokubun, F. A. Radu, E. Keilegavlen, K. Kumar and K. Spildo, *Transp. Porous Media*, 2019, **126**, 501-519.
289. D. A. Nieto-Alvarez, A. Marín-León, E. E. Luna-Rojero, J. M. Martínez-Magadan, R. Oviedo-Roa, M. Pérez-Alvarez, G. Dominguez-Zacarías and L. S. Zamudio-Rivera, *Ind. Eng. Chem. Res.*, 2018, **57**, 2075-2082.
290. D. A. Nieto-Alvarez, L. S. Zamudio-Rivera, E. E. Luna-Rojero, D. I. Rodríguez-Otamendi, A. Marín-León, R. l. Hernández-Altamirano, V. Y. Mena-Cervantes and T. E. Chávez-Miyauchi, *Langmuir*, 2014, **30**, 12243-12249.
291. J. Lawson, SPE symposium on improved methods of oil recovery, Tulsa, 1978.
292. K. Ma, L. Cui, Y. Dong, T. Wang, C. Da, G. J. Hirasaki and S. L. Biswal, *J. Colloid Interface Sci.*, 2013, **408**, 164-172.
293. M. Puerto, G. J. Hirasaki, C. A. Miller and J. R. Barnes, *SPE J.*, 2012, **17**, 11-19.
294. J. Wolanin, L. Barré, C. Dalmazzone and D. Bauer, *Colloids Surf. A*, 2021, **613**, 126098.
295. D. Levitt and M. Bourrel, SPE Improved Oil Recovery Conference, Tulsa, 2016.
296. T. Amirianshoja, R. Junin, A. K. Idris and O. Rahmani, *J. Pet. Sci. Eng.*, 2013, **101**, 21-27.
297. M. A. Ahmadi and S. R. Shadizadeh, *Fuel*, 2015, **159**, 15-26.
298. Z. Xu, X. Yang and Z. Yang, *J. Phys. Chem. B.*, 2008, **112**, 13802-13811.
299. Y. Wang, J. Ge, G. Zhang, P. Jiang, W. Zhang and Y. Lin, *RSC Adv.*, 2015, **5**, 59738-59744.
300. I. Gupta, C. S. Rai and C. H. Sondergeld, *SPE Reserv. Eval. Eng.*, 2020, **23**, 1105-1117.
301. M. Zhao, W. Lv, Y. Li, C. Dai, X. Wang, H. Zhou, C. Zou, M. Gao, Y. Zhang and Y. Wu, *J. Mol. Liq.*, 2018, **261**, 373-378.
302. E. Alagic and A. Skauge, *Energy Fuels*, 2010, **24**, 3551-3559.
303. N. Saxena, A. Goswami, P. K. Dhodapkar, M. C. Nihalani and A. Mandal, *J. Pet. Sci. Eng.*, 2019, **176**, 299-311.
304. N. Tafur, A. Mamonov, M. A. Islam Khan, A. Soto, T. Puntervold and S. Strand, *Energy Fuels*, 2023, **37**, 11730-11742.
305. S. J. Fathi, T. Austad and S. Strand, *Energy Fuels*, 2010, **24**, 2514-2519.

306. P. Aslanidis, S. Strand, I. D. Pinerez Torrijos and T. Puntervold, *J. Pet. Sci. Eng.*, 2022, **208**, 109531.
307. M. Bourrel, J. L. Salager, R. S. Schechter and W. H. Wade, *J. Colloid Interface Sci.*, 1980, **75**, 451-461.
308. Y. Ding, S. Zheng, X. Meng and D. Yang, *J. Energy Resour. Technol.*, 2019, **141**.
309. L. J. Giraldo, J. Gallego, J. P. Villegas, C. A. Franco and F. B. Cortés, *J. Pet. Sci. Eng.*, 2019, **174**, 40-48.
310. I. Mohammed, M. Mahmoud, D. Al Shehri, A. El-Husseiny and O. Alade, *J. Pet. Sci. Eng.*, 2021, **197**, 107956.

I

Appendix A

A.1   Charge of surfactant micelles

Zeta potential measurements were used to determine the charge behaviour of surfactants with pH. The zeta potential measurements of different concentrations of ZN in DIW at the original pH were first performed to select a suitable surfactant concentration, as seen in Table A.1. It is noted that high surfactant concentrations act as a highly conductive electrolyte which can affect the dip cell electrodes of the instrument and result in wrong measurements. Therefore, 0.1 wt.% was chosen as the candidate concentration.

Table A.1. Zeta potential measurements of different concentrations of ZN in DIW at original pH at 25 ± 0.1 °C. The CMC of ZN in DIW at 25 °C is ~ 0.02 wt.%.

[ZN] / wt.%	pH at 25 ± 1 °C	Zeta potential / mV
0.1 (5 × CMC)	7.6	2.6 ± 0.2
1.0 (50 × CMC)	7.3	− 0.3 ± 0.3
2.0 (100 × CMC)	7.4	− 0.5 ± 0.1

A.2   Stability of ES-coated silica synthesized by route from literature

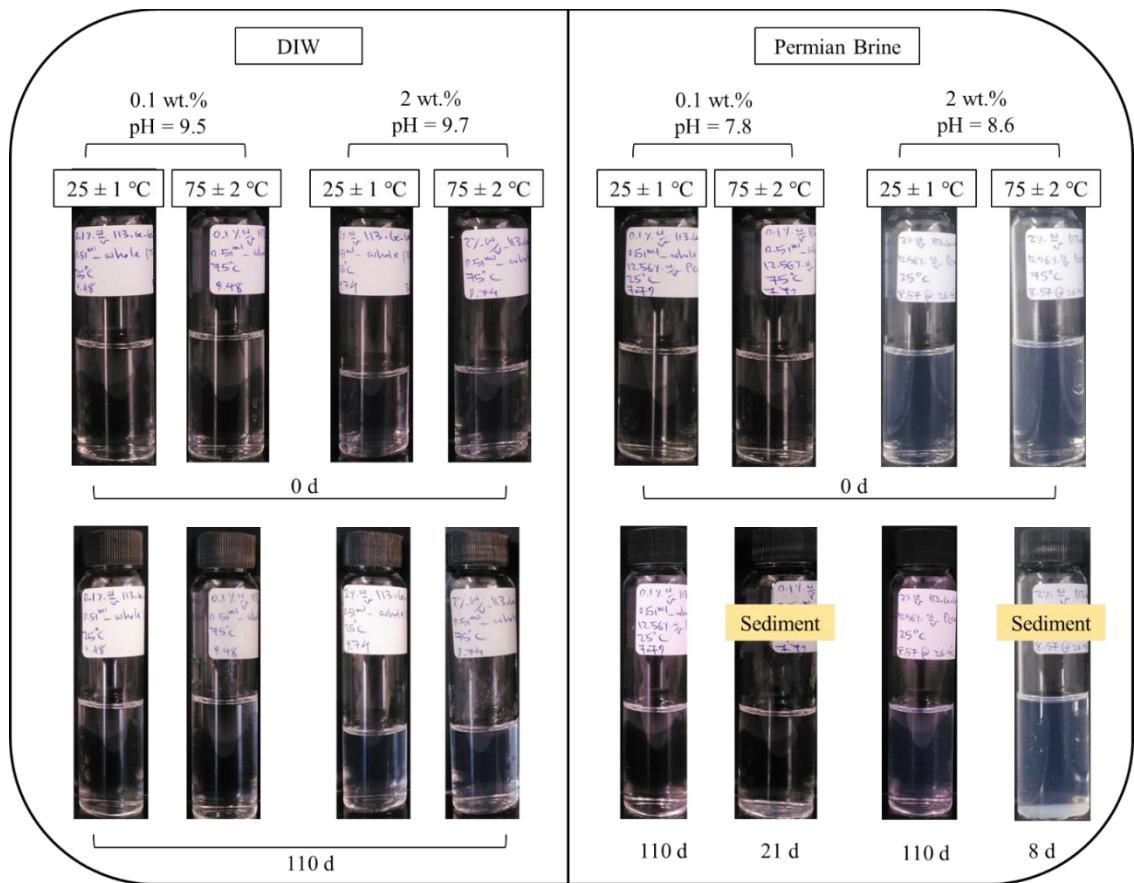### A.2.1   ES/silica dispersion ratio of 0.11 cm^3 g^{-1} – one step synthesis

Figure A.1 shows the stability of 0.1 wt.% and 2 wt.% ES-coated silica particles synthesized with a ES/silica dispersion ratio of 0.11 cm^3 g^{-1} (one-step addition of silane) in DIW and Permian brine. The dispersions containing particles in DIW were stable at both temperatures for a long time while sedimentation was observed in the dispersions with particles in Permian brine at 75 °C after 7 days. However, the comparison of the stability of ES-coated silica and bare silica in Permian brine shows improved stability due to silane coverage on the surface of the silica. It is concluded that this amount of ES (0.11 cm^3 per g of silica dispersion) on the surface of silica particles is not enough to induce sufficient steric hindrance, especially at higher temperatures. The initial particle diameter of dispersions in DIW and Permian brine was measured at 19 ± 2 nm. The zeta potential of 0.1 wt.% ES-coated silica in DIW was measured at − 26 ± 2 mV. The dispersion of 2 wt.% particles in Permian brine kept at low temperature had a particle diameter of 22 nm after 60 days while the one kept at 75 °C faced sedimentation; however, the particle diameter of the supernatant was 21 nm after 60 days.

Figure A.1. Appearance of 0.1 wt.% and 2 wt.% ES-coated silica in DIW and Permian brine at original pH at two temperatures. The particles were synthesized with a ES/silica dispersion ratio of 0.11 cm^3 g^{-1} (top) and 0.25 cm^3 g^{-1} (bottom) in a one-step synthesis based on the synthesis route from the literature.
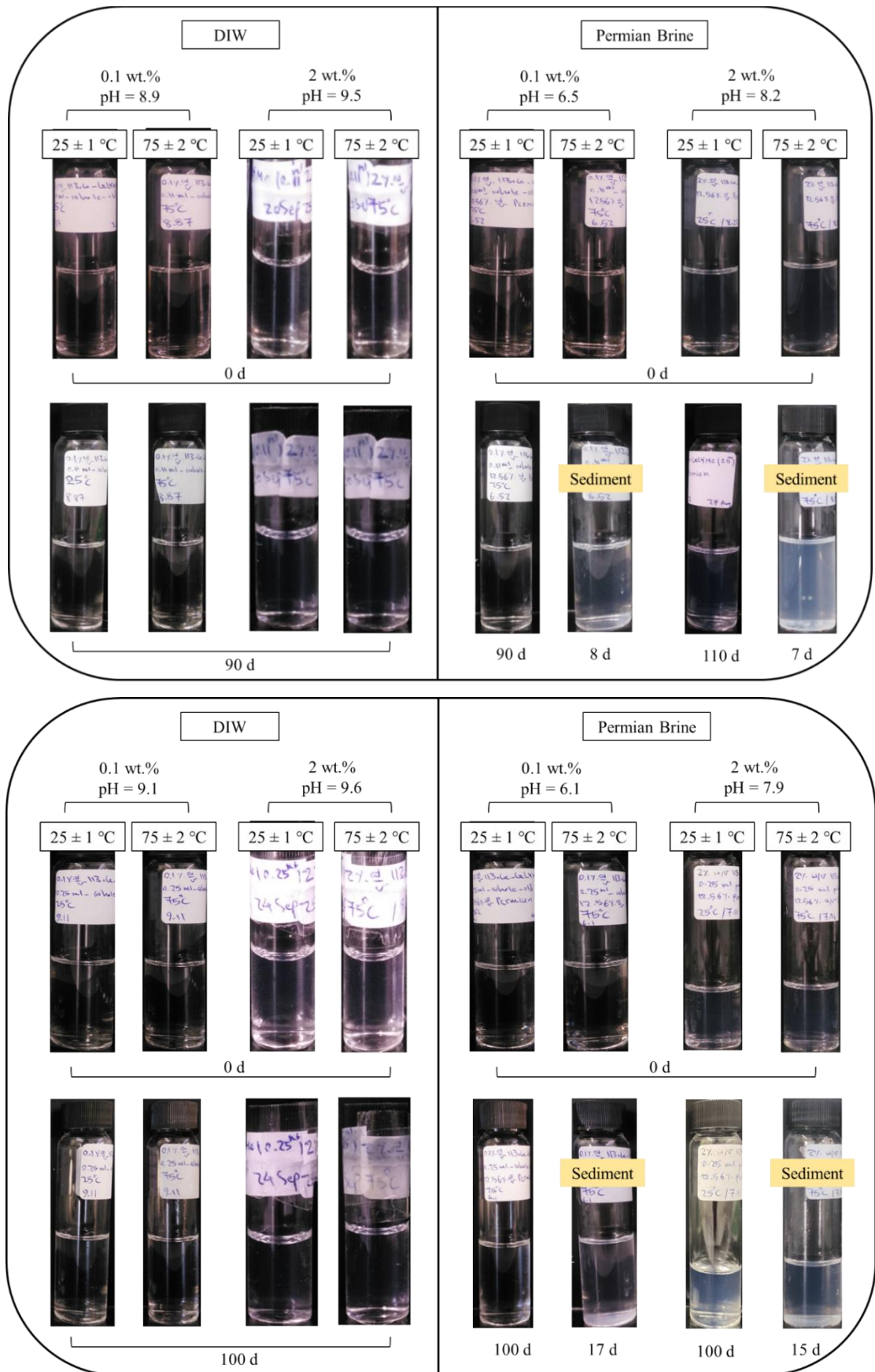
A.2.2   ES/silica dispersion ratio of 0.25 cm³ g⁻¹ – one step synthesis

Figure A.1 shows the stability of 0.1 wt.% and 2 wt.% ES-coated silica particles synthesized with a ES/silica dispersion ratio of 0.25 cm³ g⁻¹ (one step addition of silane) in DIW and Permian brine. The dispersions containing particles dispersed in DIW were stable at both temperatures for ~ 3 months while sedimentation was observed in dispersions containing particles in Permian brine at 75 °C after two weeks. The initial particle diameter of dispersions was 22 ± 4 nm. The zeta potential of 0.1 wt.% ES-coated silica in DIW was measured at -27.4 ± 1.4 mV. The dispersion containing 2 wt.% ES-coated silica in Permian brine at low temperature had a particle diameter of 22 nm after 67 days while the one kept at 75 °C faced sedimentation (the particle diameter of the supernatant was 21 nm after 65 days).

A.2.3   ES/silica dispersion ratio of 0.50 cm³ g⁻¹

A.2.3.1 One step synthesis

Figure A.2 shows the stability of 0.1 wt.% and 2 wt.% ES-coated silica synthesized with a ES/silica dispersion ratio of 0.5 cm³ g⁻¹ (one step addition of silane) in DIW and Permian brine. The dispersions with particles dispersed in DIW were stable at both temperatures for 110 days while sedimentation was observed in the dispersions with 0.1 wt.% and 2 wt.% particles dispersed in Permian brine at 75 °C after 1 – 3 weeks. All of these dispersions had an initial particle diameter of 20 ± 2 nm. The zeta potential of 0.1 wt.% ES-coated silica in DIW was measured at -31.3 ± 1 mV. The dispersion with 2 wt.% particles in Permian brine kept at low temperature had a particle diameter of 22 nm after 60 days while the one kept at 75 °C faced sedimentation; however, the particle diameter of the supernatant of this dispersion was measured at 21 nm after 60 days.

Figure A.2. Appearance of 0.1 wt.% and 2 wt.% ES-coated silica in DIW and Permian brine at original pH at two temperatures. The particles were synthesized with a ES/silica dispersion ratio of 0.5 cm³ g⁻¹ in a one-step synthesis based on the synthesis route from the literature.

DIW				Permian Brine			
0.1 wt.% pH = 9.5		2 wt.% pH = 9.7		0.1 wt.% pH = 7.8		2 wt.% pH = 8.6	
25 ± 1 °C	75 ± 2 °C	25 ± 1 °C	75 ± 2 °C	25 ± 1 °C	75 ± 2 °C	25 ± 1 °C	75 ± 2 °C

0 d (DIW)   0 d (Permian Brine)

110 d (DIW)   110 d | 21 d | 110 d | 8 d (Permian Brine)

A.2.3.2 Two step synthesis

Figure A.3 shows the stability of 1.5 wt.% ES-coated silica synthesized with a ES/silica dispersion ratio of 0.50 cm^3 g^{-1} in a two-step synthesis in DIW and Permian brine. Both

dispersions were stable for a long time at both temperatures. The two-step addition of aqueous ES to the bare silica during the synthesis seems to have improved the stability of particles in Permian brine at high temperatures. The initial particle diameter and zeta potential of 1.5 wt.% ES-coated silica in DIW were 18 ± 4 nm and -33 ± 2 mV, respectively. The particle diameter of the dispersion in Permian brine was initially measured at 26 ± 1 nm. The dispersion in Permian brine kept at the low temperature had a particle diameter of 25 ± 1 nm after 50 days while the one kept at 75 °C showed a particle diameter of 42 ± 2 nm after 50 days.

A.2.3.3 Four step synthesis

To investigate the effect of the addition of ES to the bare silica dispersion during the synthesis on the stability of ES-coated silica particles in Permian brine, a four-step addition of silane to the bare silica dispersion was tried in the synthesis. Figure A.4 shows the stability of 0.1 wt.% and 2 wt.% ES-coated silica synthesized with a ES/silica dispersion ratio of 0.5 cm^3 g^{-1} (four-step synthesis) in DIW and Permian brine. All dispersions were stable in DIW and Permian brine for 110 days. All dispersions had an initial particle diameter of 22 ± 2 nm. The zeta potentials of 0.1 wt.% and 2 wt.% ES-coated silica in DIW were -33.7 ± 1.1 and -17.1 ± 1 mV, respectively.

Figure A.3. Appearance of 1.5 wt.% ES-coated silica in DIW and Permian brine at original pH at two temperatures. The particles were synthesized with a ES/silica dispersion ratio of 0.50 cm^3 g^{-1} in a two-step synthesis based on the synthesis route from the literature.
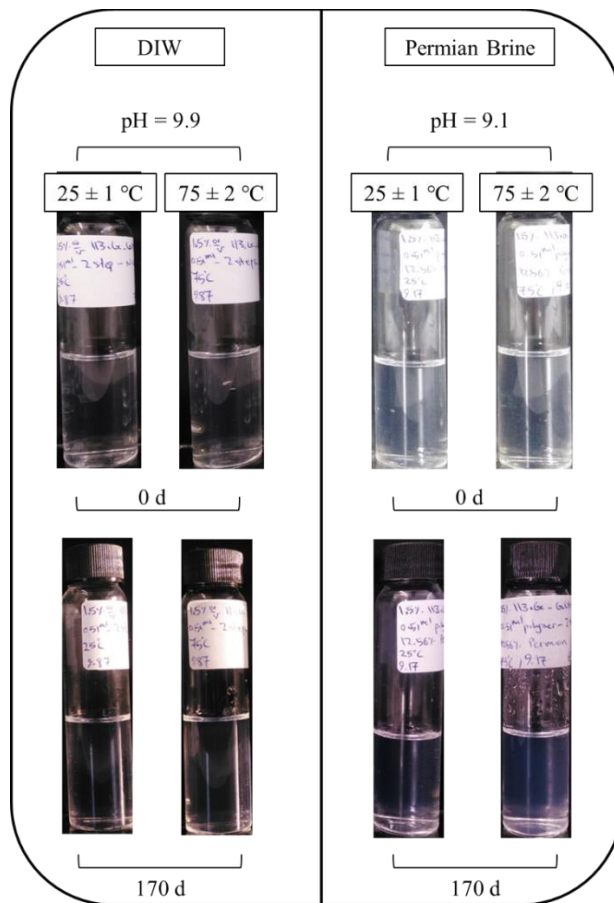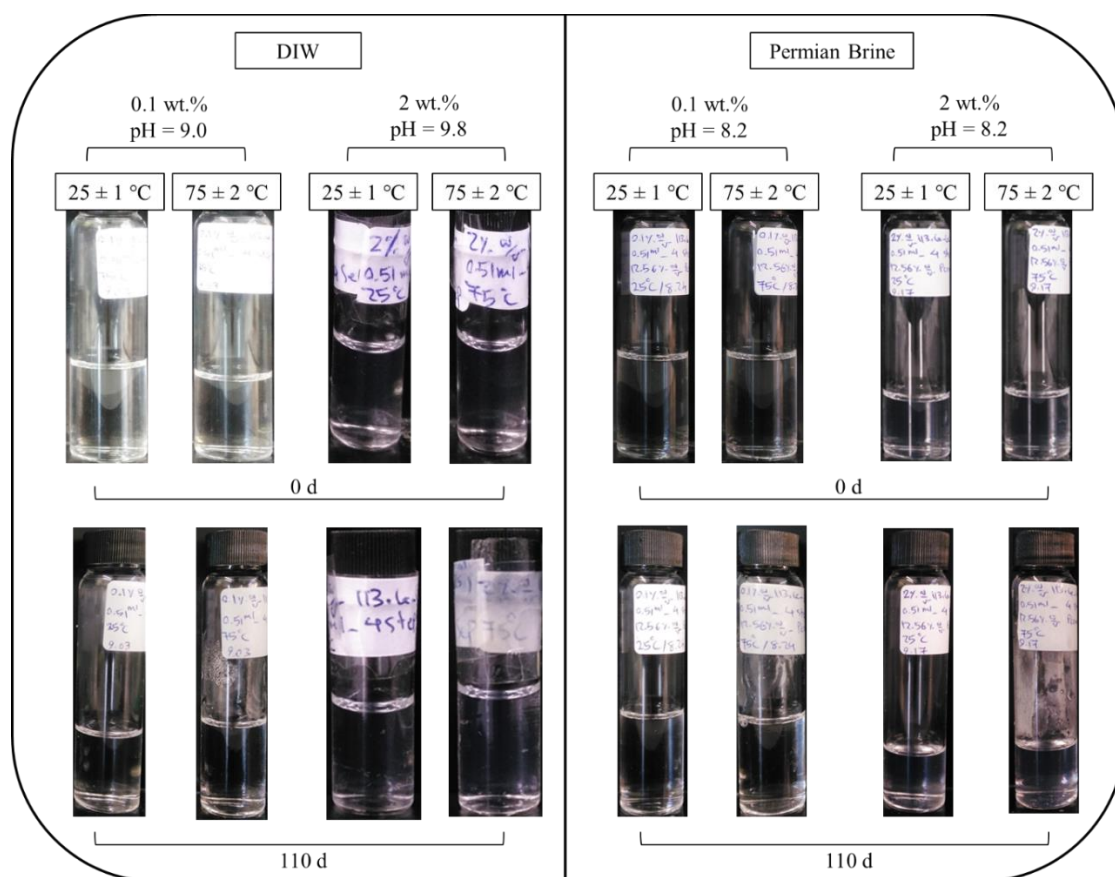
Figure A.4. Appearance of 0.1 wt.% and 2 wt.% ES-coated silica in DIW and Permian brine at original pH at two temperatures. The particles were synthesized with a ES/silica dispersion ratio of 0.5 cm^3 g^{-1} in a four-step synthesis based on the synthesis route from the literature.

A.2.4 ES/silica dispersion ratio of 1.00 cm³ g⁻¹ – one step synthesis

Figure A.5 shows the stability of 0.1 wt.% and 2 wt.% ES-coated silica synthesized with a ES/silica dispersion ratio of 1 cm³ g⁻¹ in a one-step synthesis in DIW and Permian brine at two temperatures. The dispersions with particles in DIW were stable for more than three months at both temperatures while the ones in Permian brine at 75 °C faced

sedimentation after a week. The initial particle diameter of dispersions was 25 – 34 nm. The zeta potential of 0.1 wt.% particles in DIW was measured at -26 ± 2 mV. The particle diameter of the dispersion with 2 wt.% ES-coated silica in Permian brine kept at the low temperature was measured at 23 ± 2 nm after 50 days while no successful measurement was obtained for the one at 75 °C.

A.2.5   Effect of silane volume on initial particle diameter

The effect of silane volume used during the synthesis of ES-coated silica on initial particle diameter in DIW and Permian brine was investigated (Figure A.6). As can be seen, regardless of the ES volume used during synthesis, all particles are between 20 and 25 nm in size. The reason is that the final dispersions made with this synthesis method were filtered, so the aggregates and large particles were all separated.

Figure A.5. Appearance of 0.1 wt.% and 2 wt.% ES-coated silica in DIW and Permian brine at original pH at two temperatures. The particles were synthesized with a ES/silica dispersion ratio of 1 cm^3 g^{-1} in a four-step synthesis based on the synthesis route from the literature.
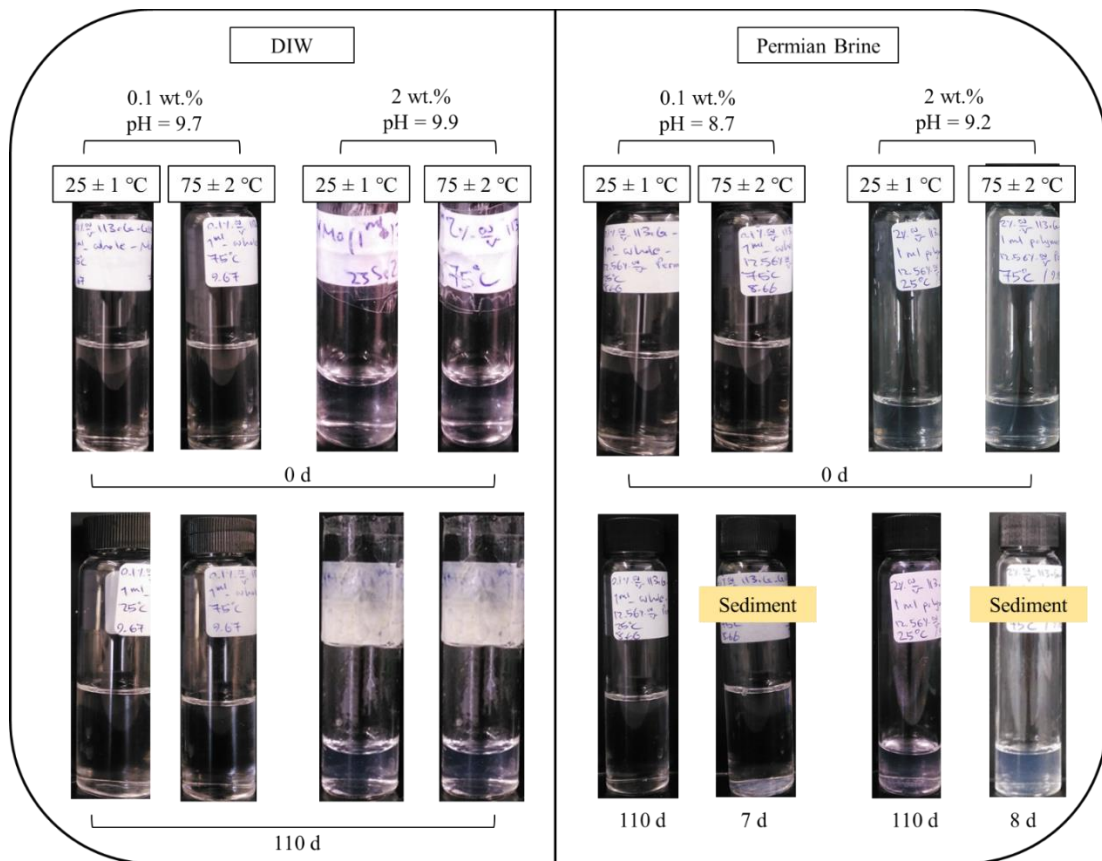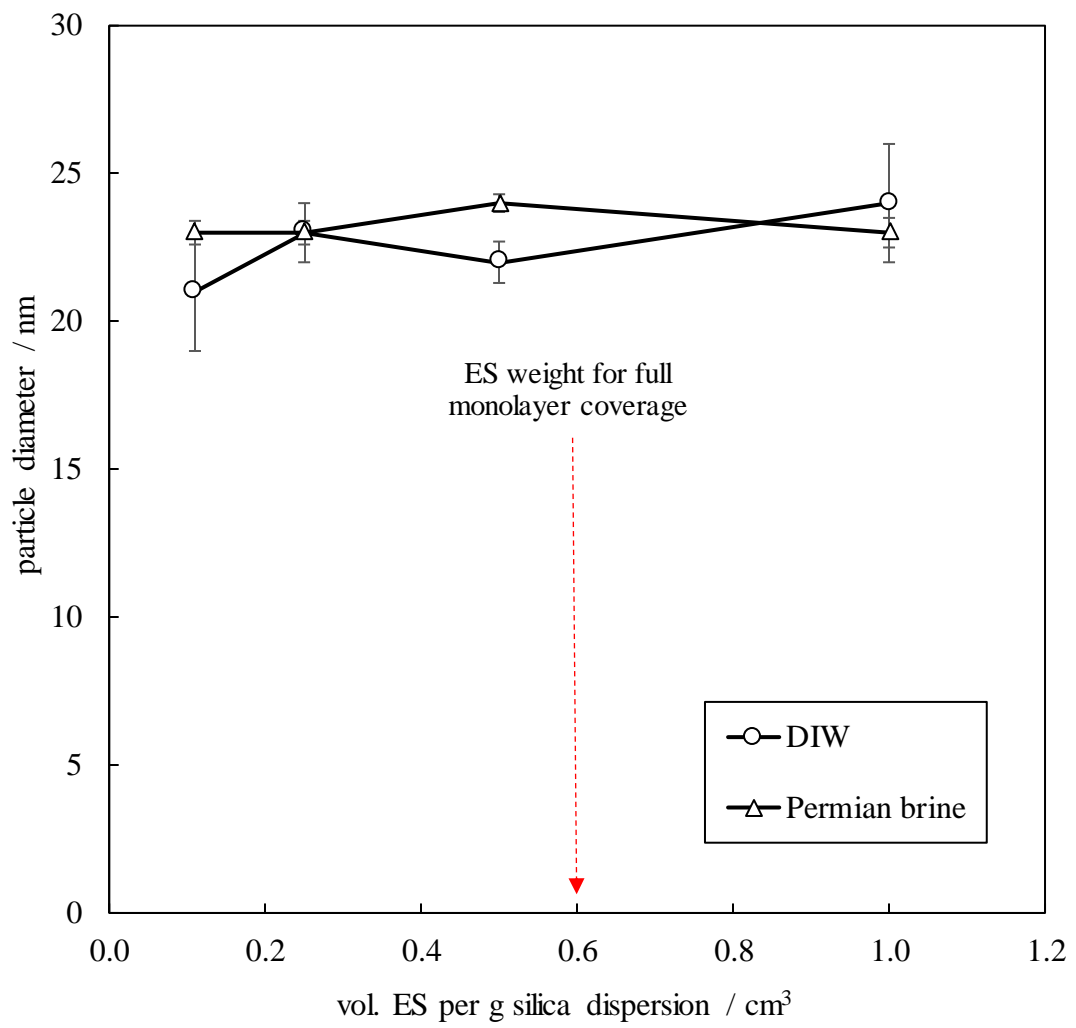
Figure A.6. Effect of silane volume used during the synthesis of ES-coated silica on the initial particle diameter in DIW and Permian brine. The particles were synthesized with different ES/silica ratios in a one-step synthesis based on the synthesis method from the literature. The concentration of particles was 0.1 wt.% in all dispersions.

XI

A.3 Stability of ES-coated silica made by modified synthesis route

### A.3.1 ES/silica particle ratio of 0.25 g g^{-1}

Figure A.7 shows the stability of 0.1 wt.% ES-coated silica synthesized with a ES/silica particle weight ratio of 0.25 g g^{-1} in a two-step synthesis in DIW and Permian brine (unchanged pH). The dispersion with particles in DIW was stable for up to 175 days at both temperatures while the one with Permian brine kept at 75 °C encountered sedimentation after a day. Lowering the pH could reduce the negative charges of particles which weaken the electrostatic attractions between cations and particles resulting in improved stability of particles in Permian brine at high temperatures. All dispersions had an initial particle diameter of 22 ± 1 nm but no successful zeta potential measurements were achieved. The pH decrease had no effect on initial particle diameter, but it did provide long-term particle stability at high salinity and temperature.

A.3.2 ES/silica particle ratio of 0.50 g g^{-1}

Figure A.7 shows the stability of 0.1 wt.% ES-coated silica synthesized with a ES/silica particle ratio of 0.51 g g^{-1} in a two-step synthesis in DIW and Permian brine (unchanged pH). The dispersions containing particles in DIW were stable for up to 8 months at both temperatures while the one in Permian brine at 75 °C encountered aggregation after 2 days and sedimentation after 4 days. Improved stability of particles in Permian brine at 75 °C is observed with pH reduction since the particles become less negative at an acidic pH which was confirmed by the zeta potential measurements. The zeta potential of 0.1 wt.% particles in DIW was measured at − 29 ± 2 mV while it increased to − 4.8 ± 1 mV with pH reduction. Therefore, fewer cations are electrostatically attracted to the particle surface and the dispersion has been stable for a long time. The initial particle diameter of dispersions was 22 ± 2 nm and pH reduction had no effect on the initial particle diameter.

Comparing particle diameters of ES-coated silica synthesized by ES/silica particle ratios of 0.25 and 0.50 g g^{-1}, there is no effect of silane volume on initial particle diameter at 25 °C when dispersed in DIW or Permian brine.

Figure A.7. Appearance of 0.1 wt.% ES-coated silica in DIW and Permian brine at original pH at two temperatures. The particles were synthesized with a ES/silica dispersion ratio of 0.25 g g^{-1} (top) and 0.5 g g^{-1} (bottom) in a two-step synthesis based on the modified synthesis route.

XIII
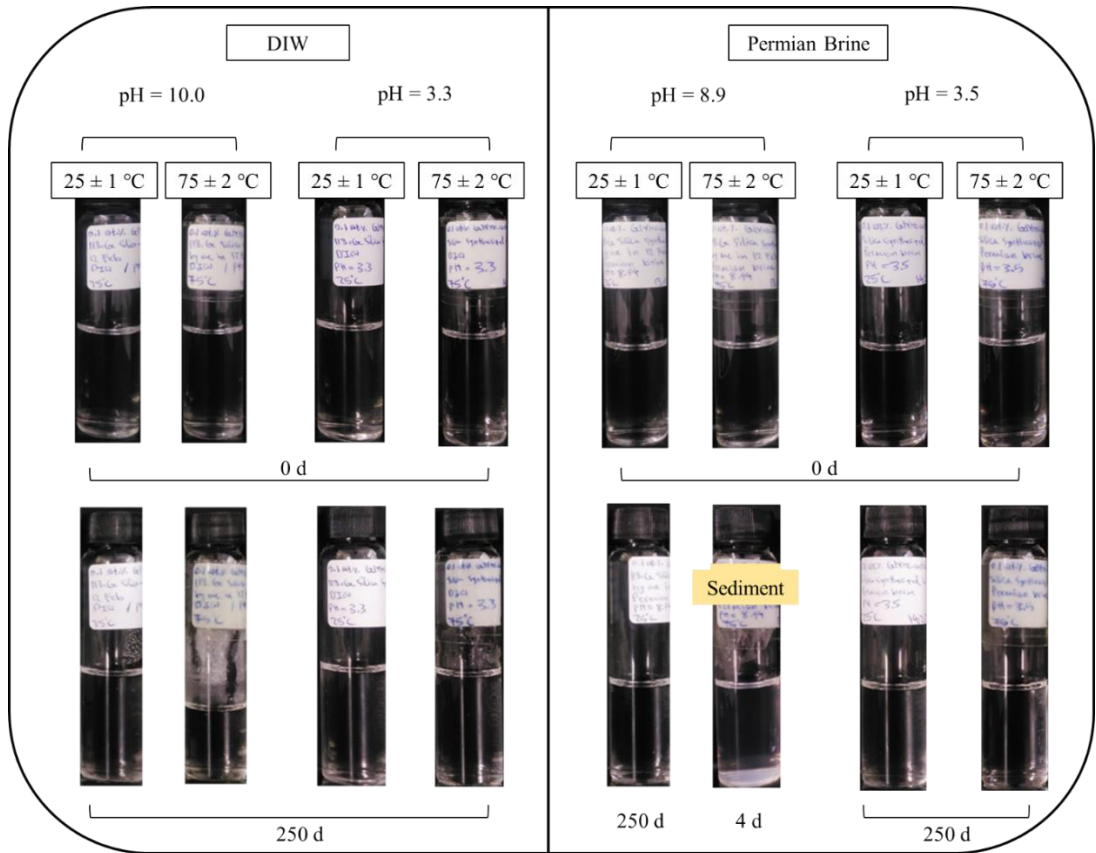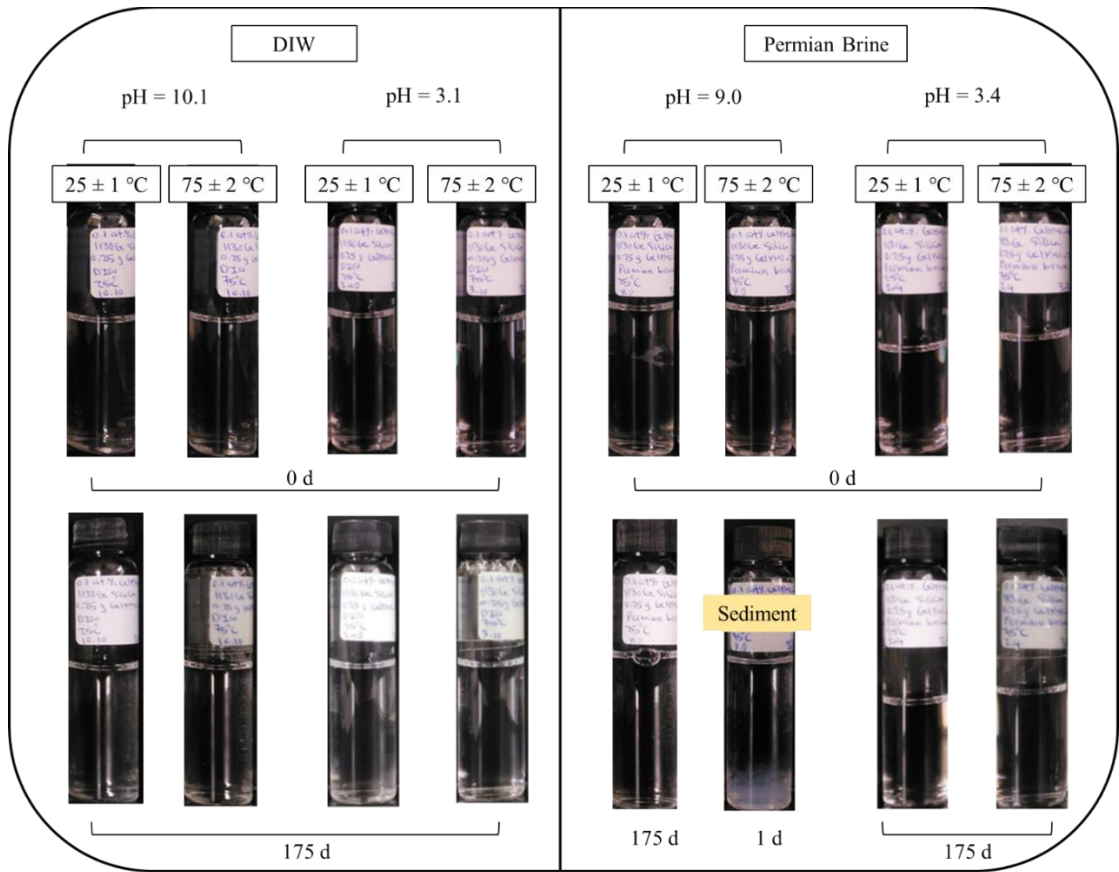
Appendix B

B.1 Effect of immersion liquid on contact angle measurement

This experiment was performed to investigate the effect of the type of liquid in which the rock substrates are immersed on the oil-water contact angle. An oil-conditioned shale substrate was vertically immersed and secured in a solution of 0.05 wt.% ZN in DIW. The solution was gently stirred (100 rpm) for 3 h at 18 ± 1 °C. After treatment, the contact angles of fresh crude oil droplets on the substrate immersed in the equilibrated surfactant solution or DIW were measured and compared (Figure B.1). The contact angles measured by both surrounding liquids are almost the same. However, the low oil-water interfacial tension caused by the surfactant makes it difficult to control the injecting oil droplets when doing the measurement in the equilibrated surfactant solution. Also, unlike the more flattened oil droplet in the presence of surfactant, the droplet profile is clearer for angle measurement when using DIW. For these reasons, it was decided to immerse the substrates in DIW or Permian brine in subsequent contact angle measurements.

Figure B.1. (a) Three-hour equilibration of an oil-conditioned shale substrate in 0.05 wt.% ZN in DIW at 18 ± 1 °C. (b) A small crude oil droplet spontaneously leaving the needle because of low oil-water interfacial tension during contact angle measurement in the equilibrated surfactant solution. (c) The

equilibrated contact angle of oil droplets on an oil-conditioned shale substrate after 3 h treatment with 0.05 wt.% ZN in DIW at 18 ± 1 °C. The contact angle measurement was performed with both fresh DIW or the equilibrated surfactant solution as the fluid surrounding the rock substrate.

(a)

(b)

(c)

$\theta_{w,o}$ / °

□ Equilibrated surfactant solution   ▨ DIW

XV
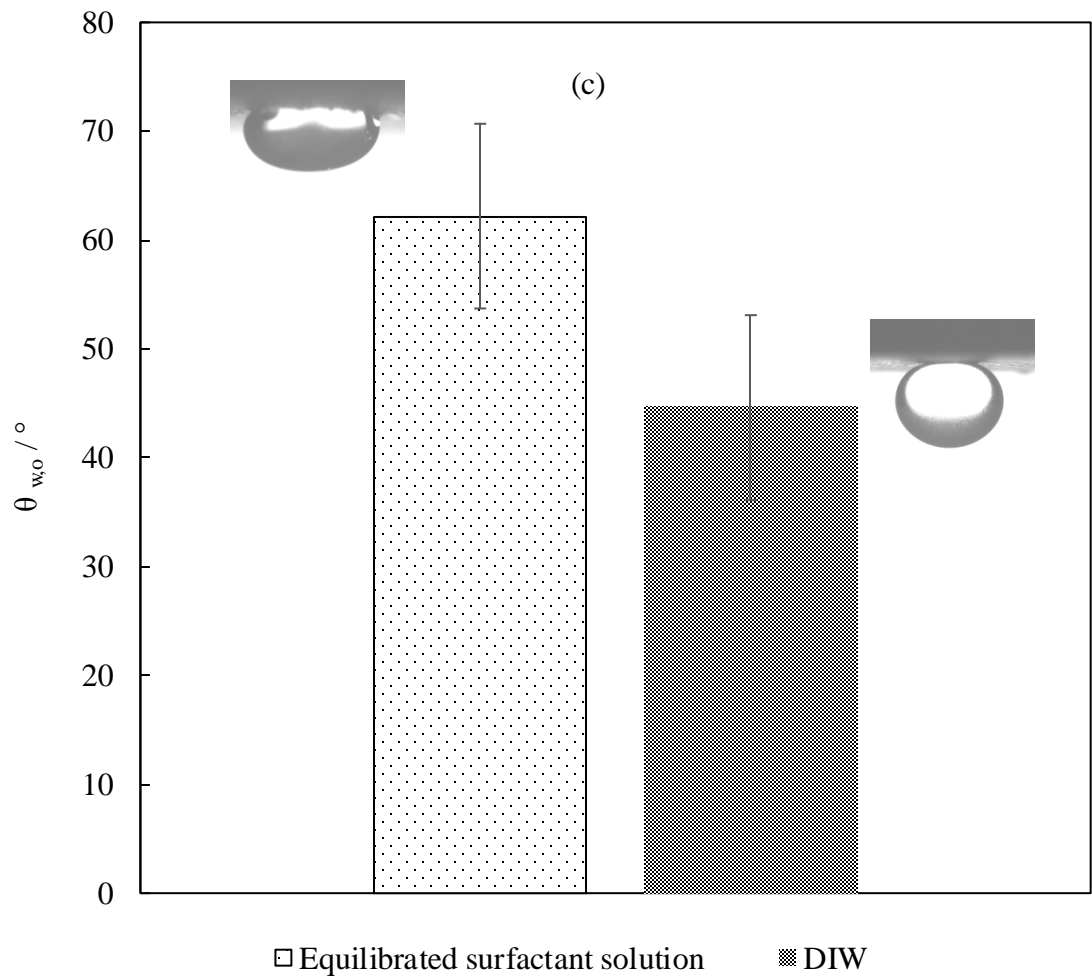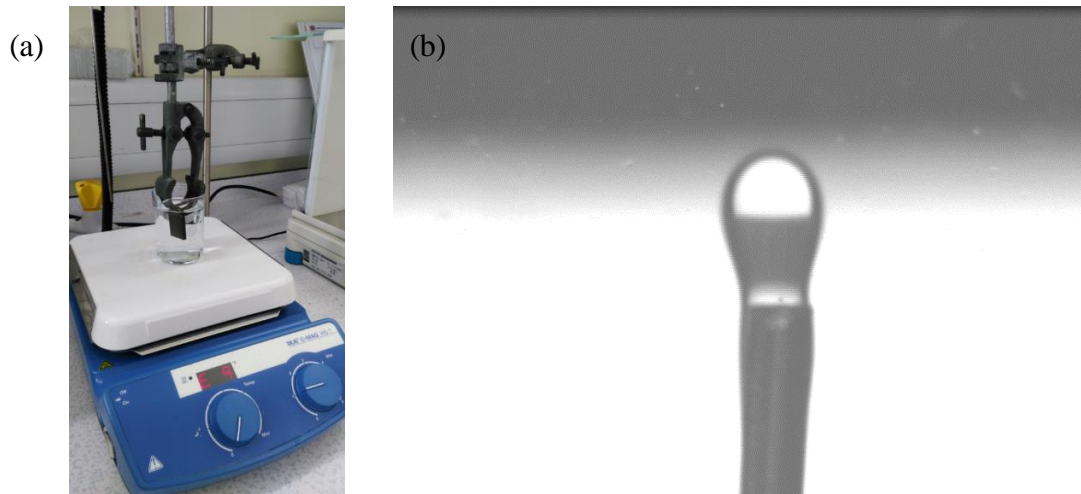
B.2   Contact angle measurements by AS-coated silica particles

Figure B.2 compares the contact angles of crude oil droplets on oil-conditioned shale treated for 24 h with different concentrations of AS- and ES-coated silica particles in DIW at the original pH. As shown, increasing the AS-coated silica concentration in DIW reduces the oil-water contact angle. At low particle loading (low pH) where AS-coated silica is cationic, fewer particles adsorb onto cationic shale due to the similar charge of the adsorbate and adsorbent. On increasing particle concentration, the pH increases from 6.5 towards the isoelectric point at $8 - 9$ [140] where the silane becomes deprotonated and uncharged. In this case, the negative charge on the uncoated sites of AS-coated silica makes the particles overall anionic with a proclivity to adsorb more onto cationic shale. The particles can also interact electrostatically with cationic components of crude oil adsorbed on the shale to promote wettability alteration. As ES is nonionic, this charge reversal with pH is absent for ES-coated silica particles and they are anionic at all pH values above the isoelectric point of bare silica $(2 - 3)$. However, a pH increase due to an increase in particle concentration increases the negative charge on ES-coated silica which subsequently promotes hydrophobicity on the shale again, as explained before. Overall, like with ES-coated silica, there is no significant reduction in the oil-water contact angle for EOR with the addition of AS-coated silica to DIW. The potential reason could be a lack of surface activity of the particles (55% and 77% hydrophilic silane coverage on ES- and AS-coated silica).

Figure B.2. Equilibrium contact angles of crude oil droplets on oil-conditioned shale treated for 24 h with different concentrations of AS-coated silica in DIW at the original pH. The black dashed line shows the contact angle of oil droplets on oil-conditioned shale treated with DIW.
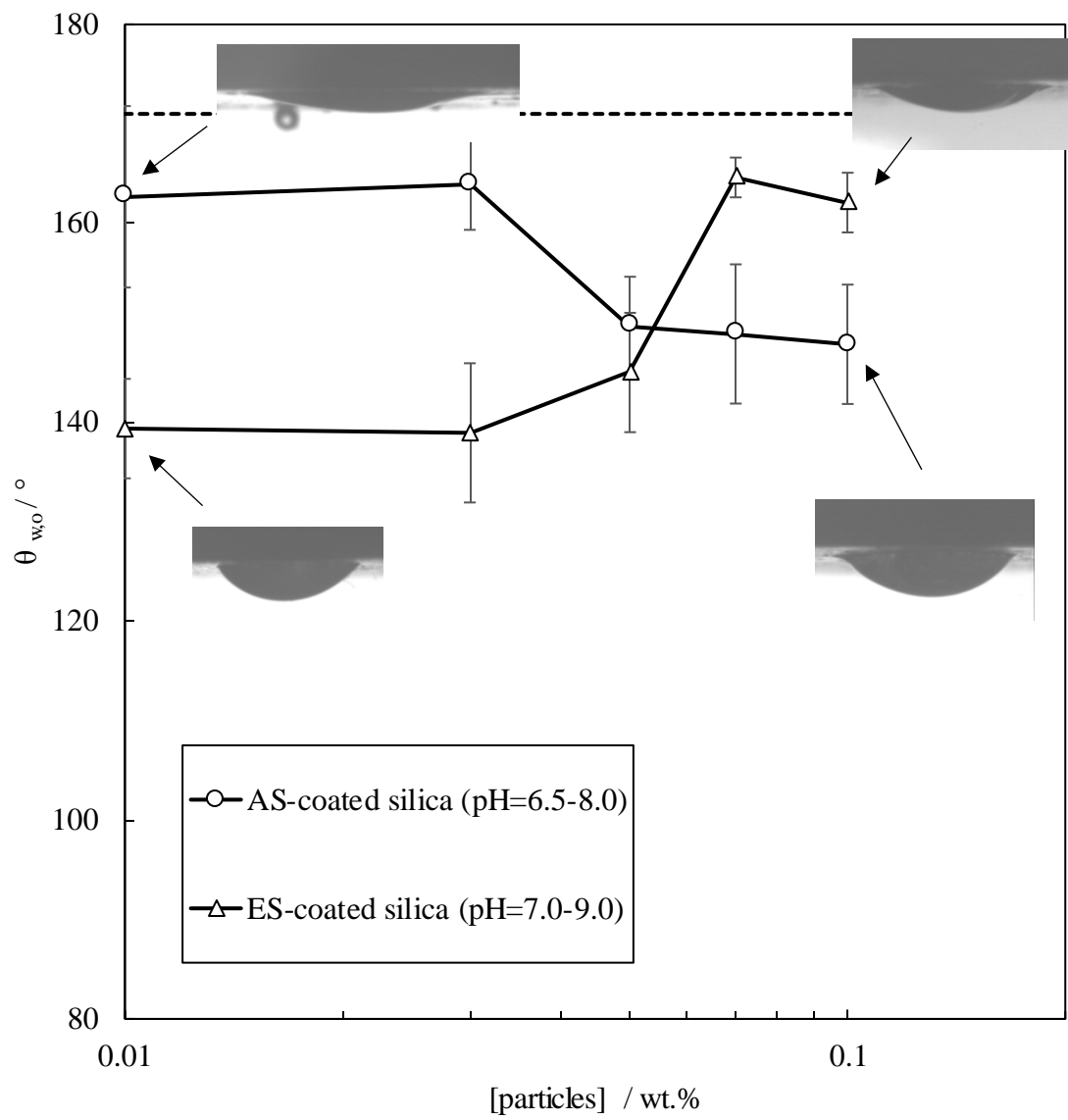
B.3 Surfactant adsorption isotherms

The equilibrium amount of AHS and ZN adsorbed onto bare shale was determined at 25 °C. Different non-linear adsorption models including Sips, Langmuir, Freundlich, Redlich-Peterson and Temkin models were fitted to the experimental data. The model parameters (except for the Redlich-Peterson model which was shown in the main text) are shown in Tables B.1 and B.2. The models were compared based on the correlation coefficients (Figures B.3 and B.4). The plots show that the Redlich-Peterson and Sips isotherms best fit the experimental data (highest R^2). The Redlich-Peterson adsorption isotherm was used in the discussions.

Table B.1. Adsorption parameters related to different models fitted to experimental data for the adsorption of AHS from DIW and Permian brine to the bare shale with or without different concentrations of ES-coated silica at 25 °C.

Solvent	[particle] / wt.%	Sips	Langmuir	Freundlich	Temkin
DIW	0	$Q_m = 12.05$ $n = 0.55$ $K_S = 0.003$	$Q_m = 5.83$ $K_L = 0.037$	$n = 2.42$ $K_F = 0.622$	$K_T = 0.67$ $b = 2448$
	0.01	$Q_m = 2.85$ $n = 3.32$ $K_S = 0.013$	$Q_m = 3.50$ $K_L = 0.010$	$n = 2.53$ $K_F = 0.253$	$K_T = 0.01$ $b = 3195$
	0.05	$Q_m = 4.03$ $n = 4.31$ $K_S = 0.008$	$Q_m = 9.04$ $K_L = 0.002$	$n = 1.33$ $K_F = 0.050$	$K_T = 0.10$ $b = 2848$
	0.10	$Q_m = 5.49$ $n = 2.03$ $K_S = 0.009$	$Q_m = 28.17$ $K_L = 0.0008$	$n = 1.07$ $K_F = 0.027$	$K_T = 0.05$ $b = 1537$
Permian brine	0	$Q_m = 1.14$ $n = 2.43$ $K_S = 0.05$	$Q_m = 1.20$ $K_L = 0.05$	$n = 4.77$ $K_F = 0.30$	$K_T = 1.14$ $b = 13712$
	0.01	$Q_m = 1.26$ $n = 22.50$ $K_S = 0.06$	$Q_m = 1.25$ $K_L = 0.11$	$n = 6.20$ $K_F = 0.44$	$K_T = 5.66$ $b = 15845$
	0.05	$Q_m = 1.26$ $n = 15.36$ $K_S = 0.01$	$Q_m = 1.33$ $K_L = 0.02$	$n = 3.86$ $K_F = 0.22$	$K_T = 0.63$ $b = 12147$
	0.10	$Q_m = 1.69$ $n = 1.77$ $K_S = 0.12$	$Q_m = 1.73$ $K_L = 0.14$	$n = 6.68$ $K_F = 0.65$	$K_T = 9.38$ $b = 12133$

Q_m is maximum adsorption ($mg\,g^{-1}$). K is isotherm constant ($L\,mg^{-1}$). b is Temkin isotherm constant and n is an exponent.

Table B.2. Adsorption parameters related to different models fitted to experimental data for the adsorption of ZN from DIW and Permian brine to the bare shale with or without different concentrations of ES-coated silica at 25 °C.

Solvent	[particle] / wt.%	Sips	Langmuir	Freundlich	Temkin
DIW	0	$Q_m = 3.24$ $n = 26.82$ $K_S = 0.041$	$Q_m = 3.45$ $K_L = 0.04$	$n = 3.94$ $K_F = 0.69$	$K_T = 0.68$ $b = 4223$
	0.01	$Q_m = 3.29$ $n = 19.79$ $K_S = 0.040$	$Q_m = 3.70$ $K_L = 0.03$	$n = 3.29$ $K_F = 0.53$	$K_T = 0.32$ $b = 3463$
	0.05	$Q_m = 2.10$ $n = 40.46$ $K_S = 0.006$	$Q_m = 3.44$ $K_L = 0.003$	$n = 1.70$ $K_F = 0.05$	$K_T = 0.08$ $b = 4681$
	0.10	$Q_m = 2.38$ $n = 3.07$ $K_S = 0.034$	$Q_m = 2.66$ $K_L = 0.03$	$n = 3.25$ $K_F = 0.37$	$K_T = 0.30$ $b = 4803$
Permian brine	0	$Q_m = 70.04$ $n = 0.46$ $K_S = 4 \times 10^{-6}$	$Q_m = 4.08$ $K_L = 0.011$	$n = 2.18$ $K_F = 0.22$	$K_T = 0.58$ $b = 4277$
	0.01	$Q_m = 2.10$ $n = 1.06$ $K_S = 0.06$	$Q_m = 2.12$ $K_L = 0.056$	$n = 4.36$ $K_F = 0.49$	$K_T = 2.49$ $b = 8551$
	0.05	$Q_m = 1.56$ $n = 32.95$ $K_S = 0.18$	$Q_m = 1.54$ $K_L = 0.315$	$n = 8.59$ $K_F = 0.71$	$K_T = 256$ $b = 19485$
	0.10	$Q_m = 1.90$ $n = 7.05$ $K_S = 0.08$	$Q_m = 2.04$ $K_L = 0.074$	$n = 4.39$ $K_F = 0.51$	$K_T = 1000$ $b = 20233$

Q_m is maximum adsorption ($mg\,g^{-1}$). K is isotherm constant ($L\,mg^{-1}$). b is Temkin isotherm constant and n is an exponent.

Figure B.3. Correlation coefficients (R^2) of different adsorption models fitted to the experimental data related to the adsorption of AHS from DIW (top) and Permian brine (bottom) onto shale with or without different concentrations of ES-coated silica at 25 °C.
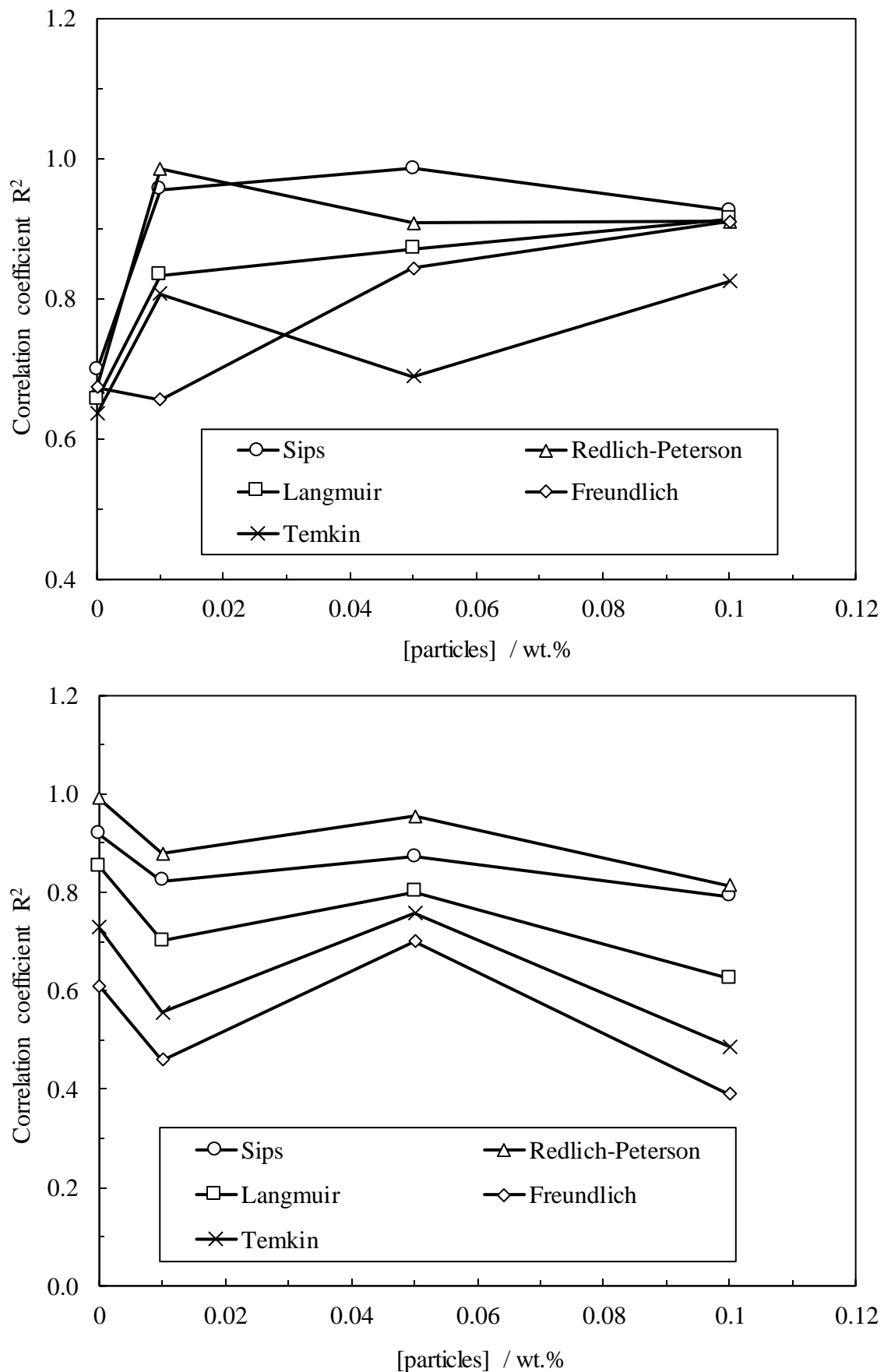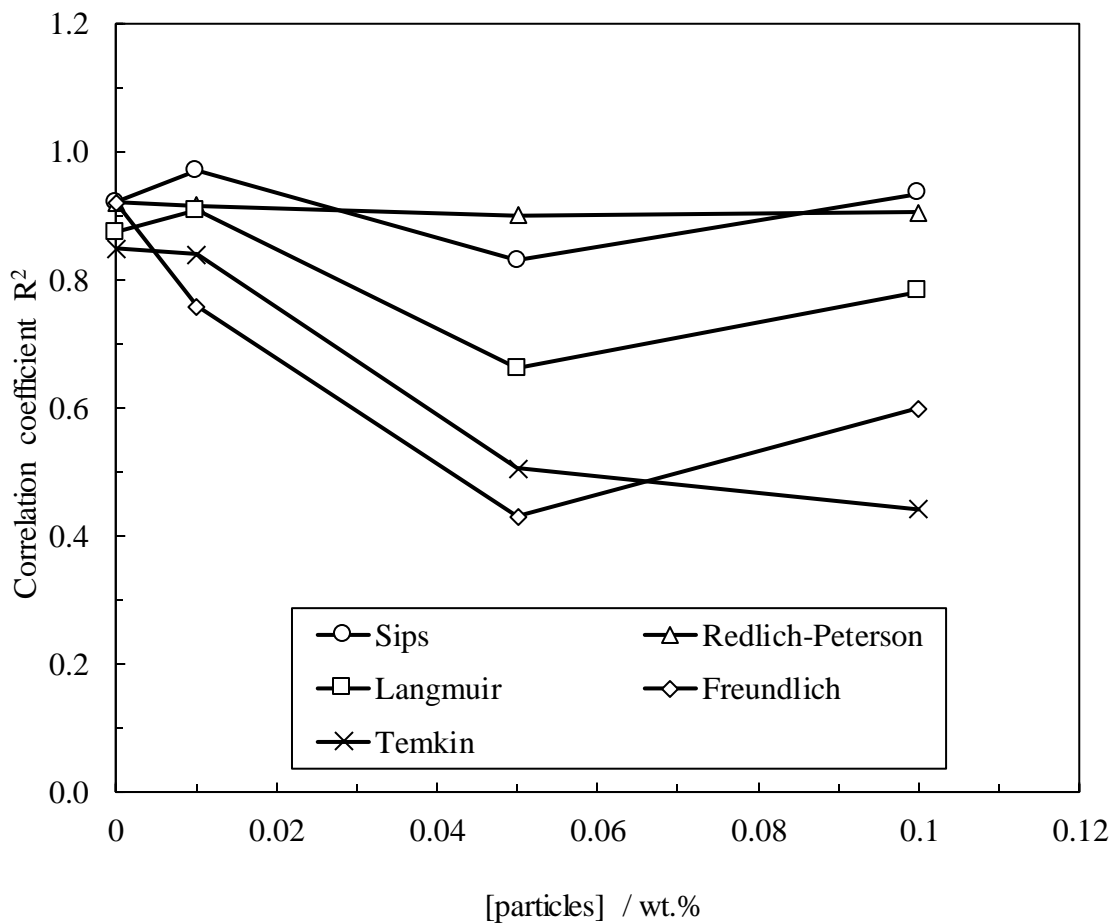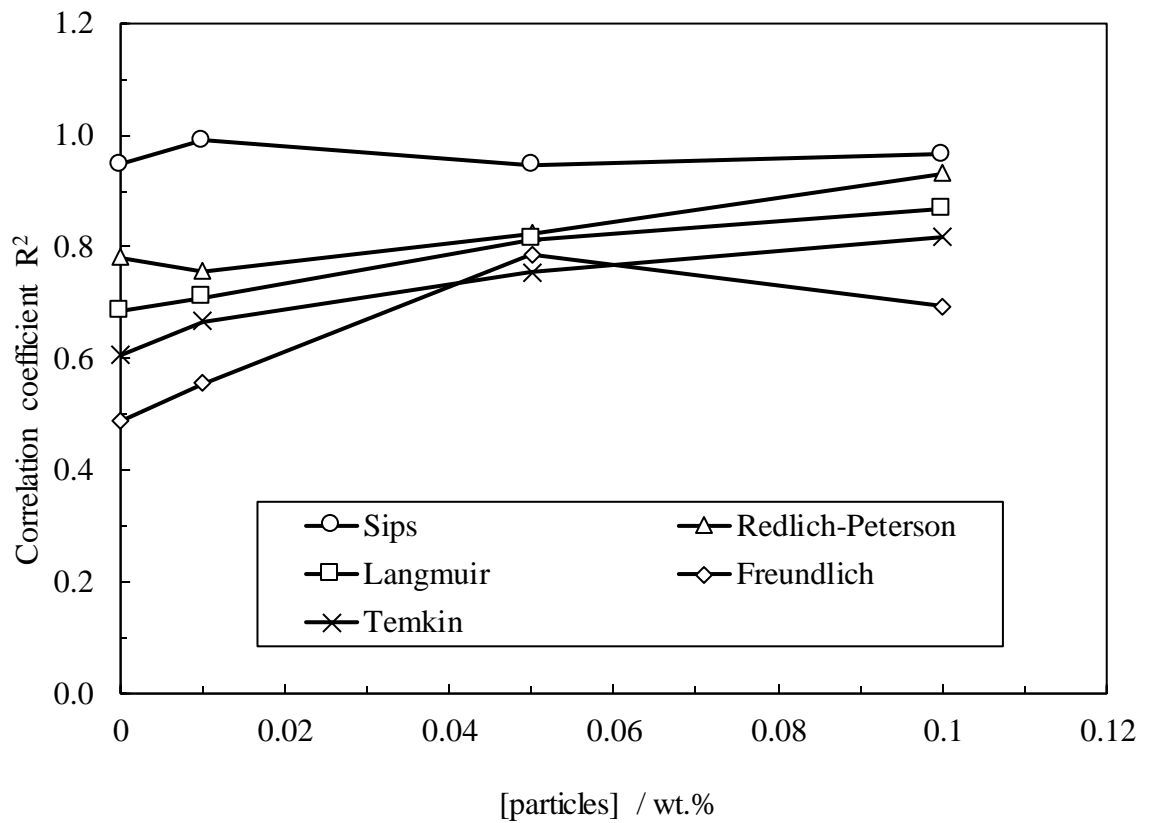
Figure B.4. Correlation coefficients (R^2) of different adsorption models fitted to the experimental data related to the adsorption of ZN from DIW (top) and Permian brine (bottom) onto shale with or without different concentrations of ES-coated silica at 25 °C.

Appendix C

C.1 Emulsions with AS-coated silica particles

The effect of adding AS-coated silica particles on the emulsification of heptane and water at original and reduced pH is shown in Figure C.1. When using original pH dispersions, the initial and long-term coalescence and creaming in the emulsions are reduced noticeably by increasing particle loading from 0.01 wt.% to 0.1 wt.% beyond which they increase slightly (Figure C.2). The emulsions experienced considerable coalescence and creaming within an hour on pH reduction. The initial particle diameter and microscopy of the emulsions are shown in Figures C.3 and C.4, respectively. Spherical heptane droplets are formed in DIW and decrease in size with an increase in particle concentration from 0.03 wt.% to 1 wt.% at the original pH. No drop diameter measurements were possible for the emulsions made with reduced pH dispersions due to quick phase separation.

AS-coated silica particles show pH-responsive behaviour. At the original pH, the amino group of the silane is deprotonated which makes the silane uncharged however the overall charge of particles is slightly negative (due to the charge of uncoated sites on silica). Therefore, higher emulsification of heptane and water is observed at the original pH than at the reduced pH. The amino group is protonated upon pH reduction which makes the particles cationic, redispersed and less efficient for adsorption at the oil-water interface.[28, 179]

Figure C.1. Appearance of oil-in-water emulsions made from 5 g heptane and 5 g of dispersions containing different weight percentages of AS-coated silica in DIW at original pH (6.3 – 7.7) and reduced pH (4.0). HCl was used for pH adjustment.
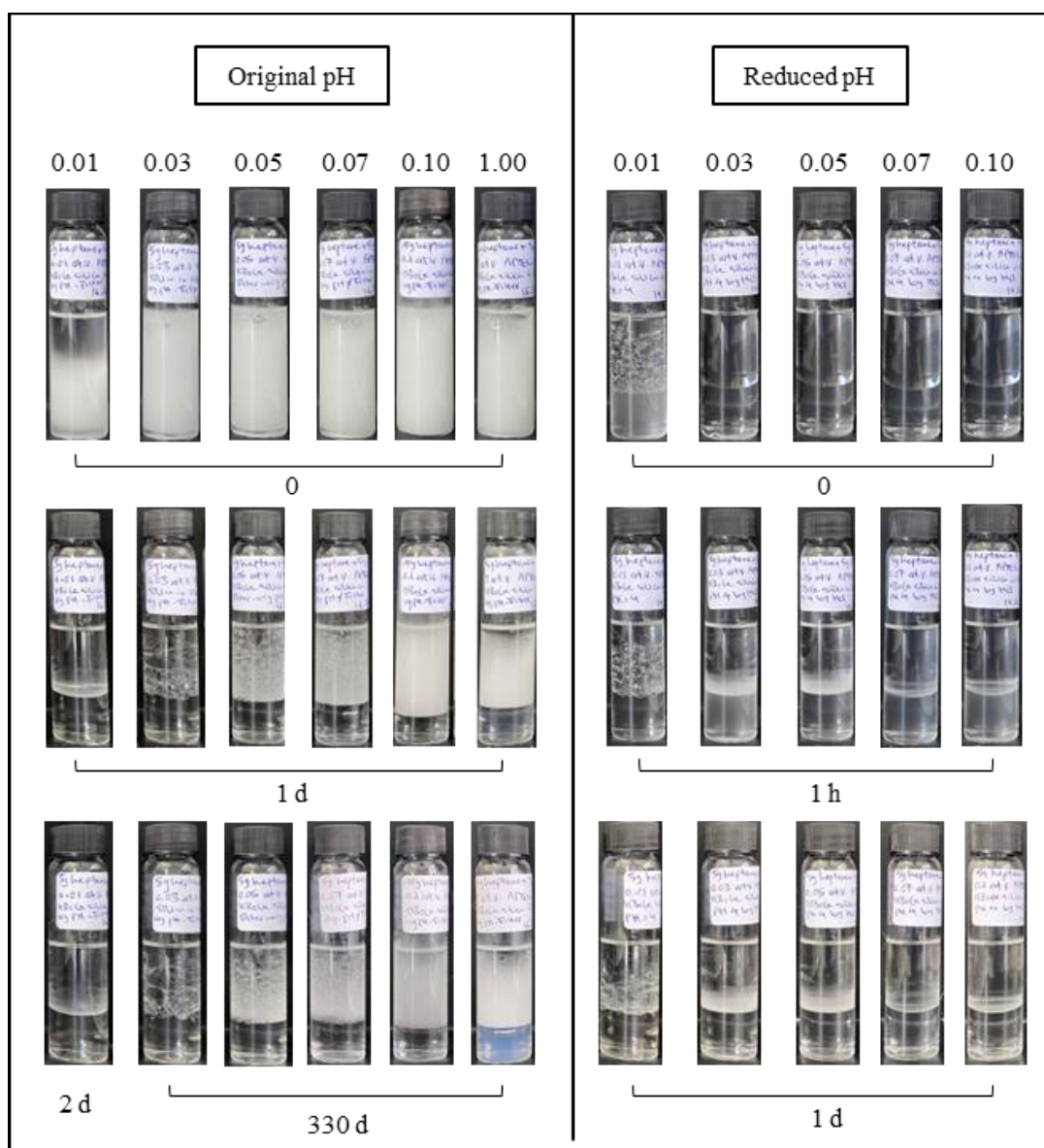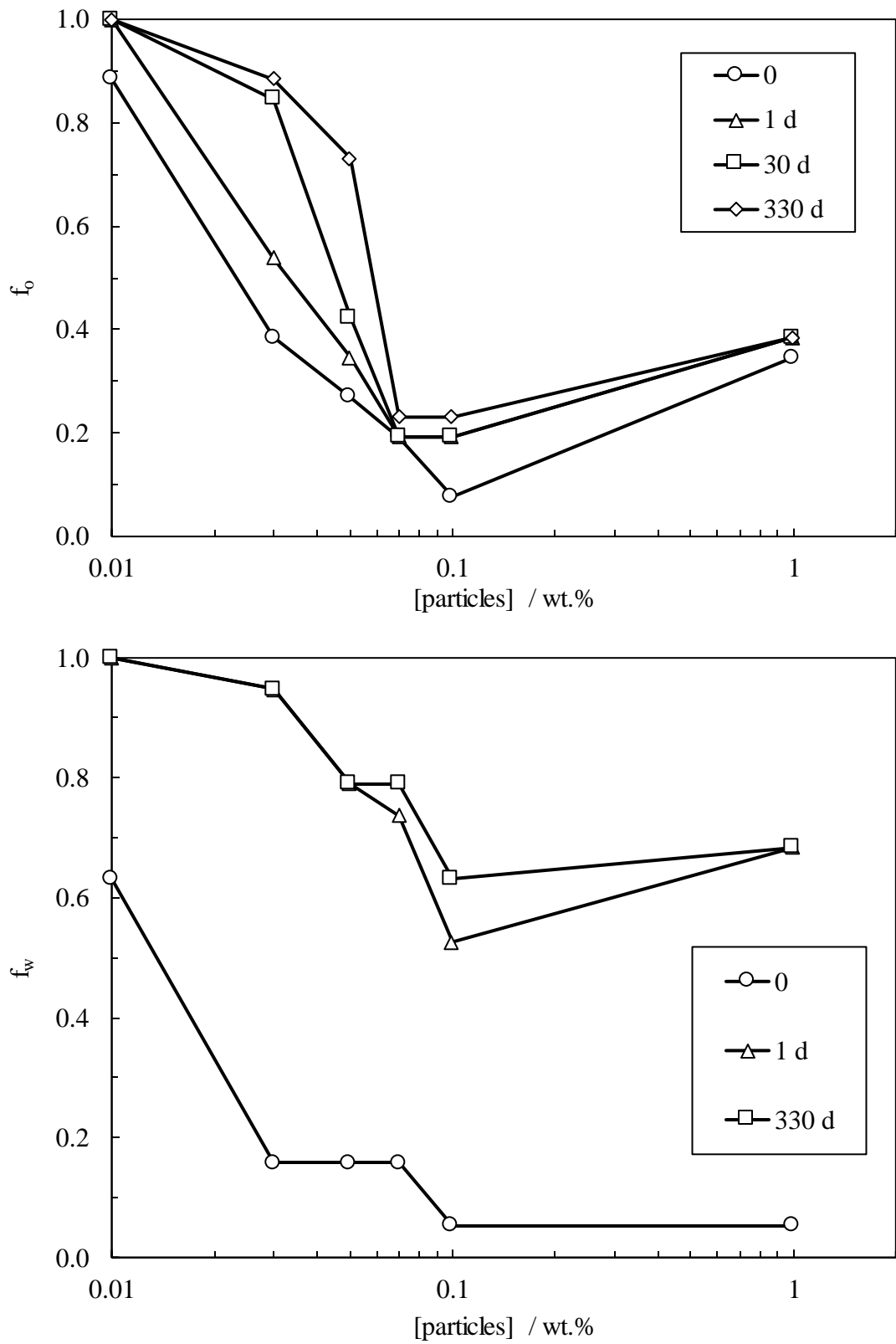
Figure C.2. Effect of particle concentration on the stability against coalescence (upper) and creaming (lower) for oil-in-water emulsions formed from 5 g heptane and 5 g of dispersions containing different concentrations of AS-coated silica particles in DIW at the original pH (6.3 – 7.7).

Figure C.3. Initial emulsion drop diameter vs particle concentration for oil-in-water emulsions formed from 5 g heptane and 5 g of dispersions containing different weight percentages of AS-coated silica in DIW at the original pH (6.3 – 7.7).
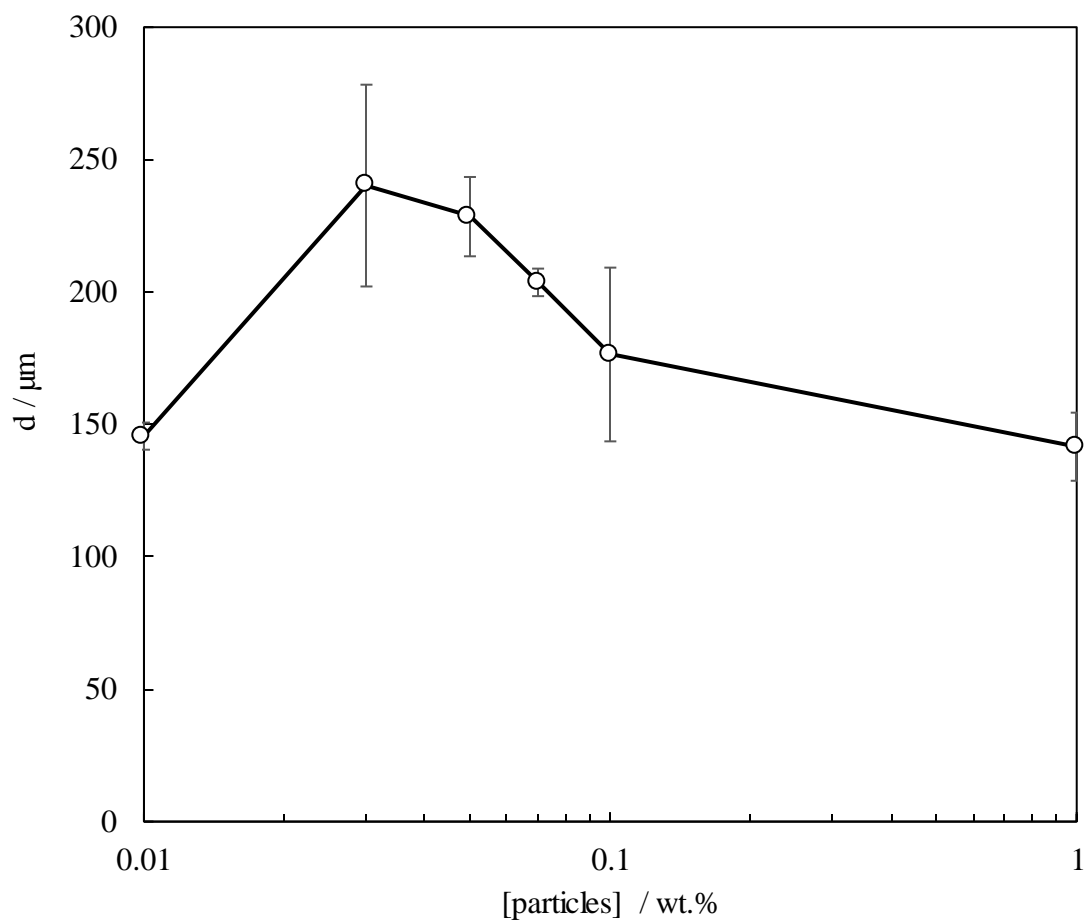
Figure C.4. Optical microscope images taken immediately after preparation of oil-in-water emulsions formed from 5 g heptane and 5 g of dispersions containing different weight percentages of AS-coated silica in DIW at the original pH (6.3 – 7.7) and reduced pH (4). The pH was reduced by HCl.
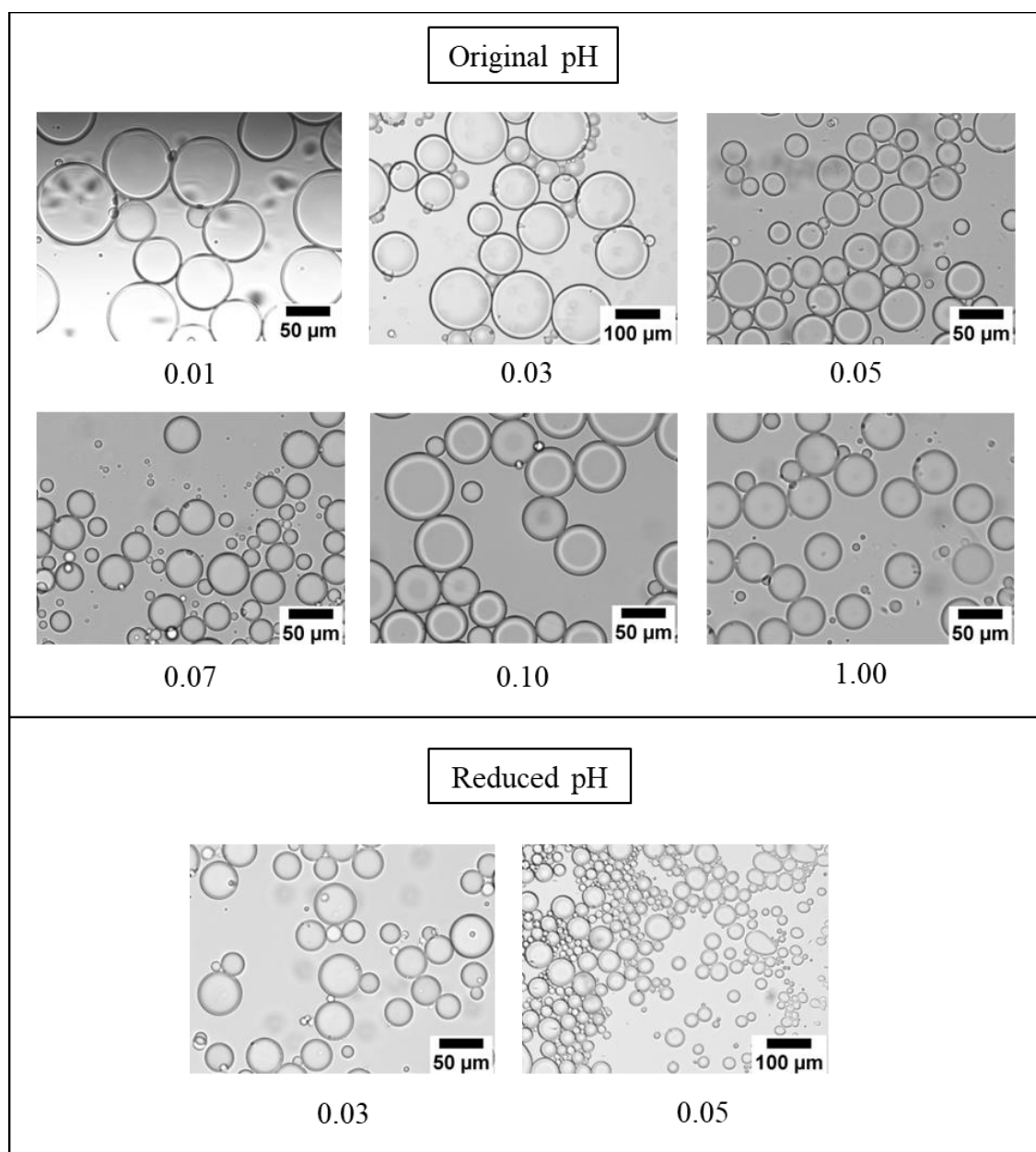
Appendix D

D.1   Determination of surfactant concentration

D.1.1   Epton titration

The Epton titration was used for the determination of aqueous surfactant concentration. As part of the calibration, titration of a basic SDS solution of known concentration (0.1 wt.%) was performed by 0.004 M Hyamine multiple times (Figure D.1). The titration gave an acceptable concentration of 0.10 ± 0.05 wt.%. Then, titrations of known concentrations of AHS and ZN in DIW at low pH (by H_2SO_4) and high pH (by NaOH) using acid indicator solution (0.07 mM disulphine blue, 0.21 mM dimidium bromide and 0.1 M sulfuric acid) or alkali indicator solution (0.07 mM disulphine blue, 0.21 mM dimidium bromide and 0.2 M sodium hydroxide) were performed. In all cases, the endpoint occurred earlier than expected resulting in incorrect concentration estimates (Figures D.2 to D.4). Therefore, this method could not be used for the determination of surfactant concentration.
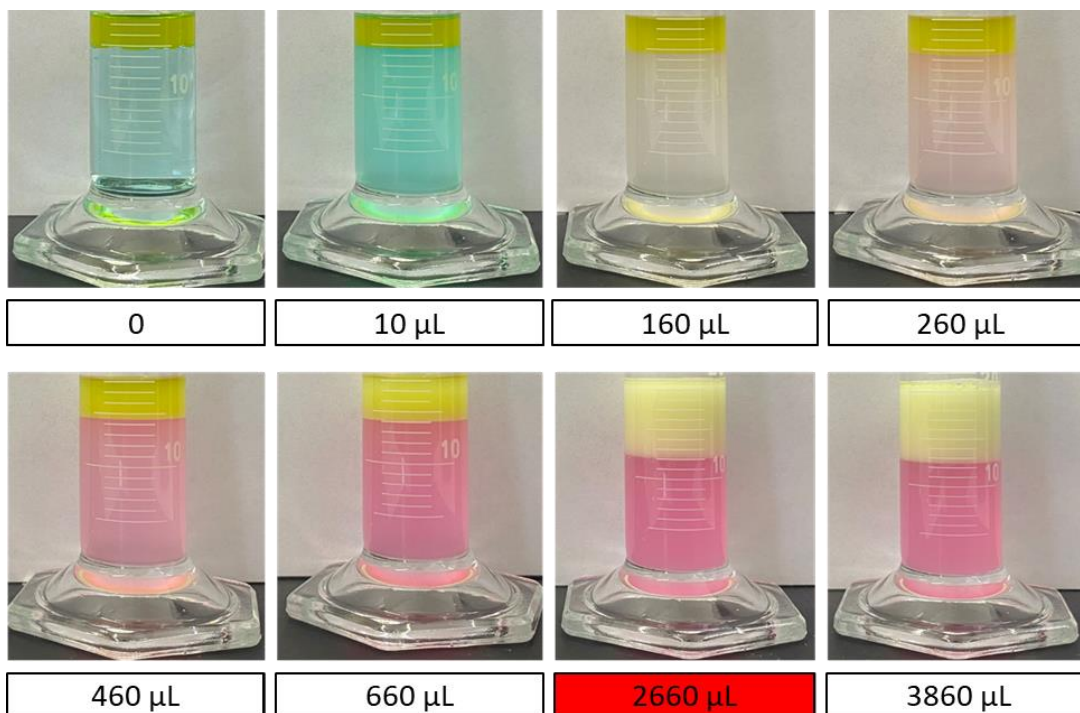
Figure D.1. Titration of 0.1 wt.% SDS in DIW (pH = 7.7 at 20 °C) with a 0.004 M Hyamine solution. The titration was performed with 1 cm^3 of the basic sample (pH was increased to 9.5 at 20 °C by 1 N NaOH) mixed with a few drops of 1 wt.% phenolphthalein (in 95% ethanol), 2 cm^3 of the acid indicator solution (containing 0.07 mM disulphine blue, 0.21 mM dimidium bromide and 0.1 M sulfuric acid) and 15 cm^3 of chloroform. The yellow titrant volume shows the endpoint which gives a concentration of 0.095 wt.%.
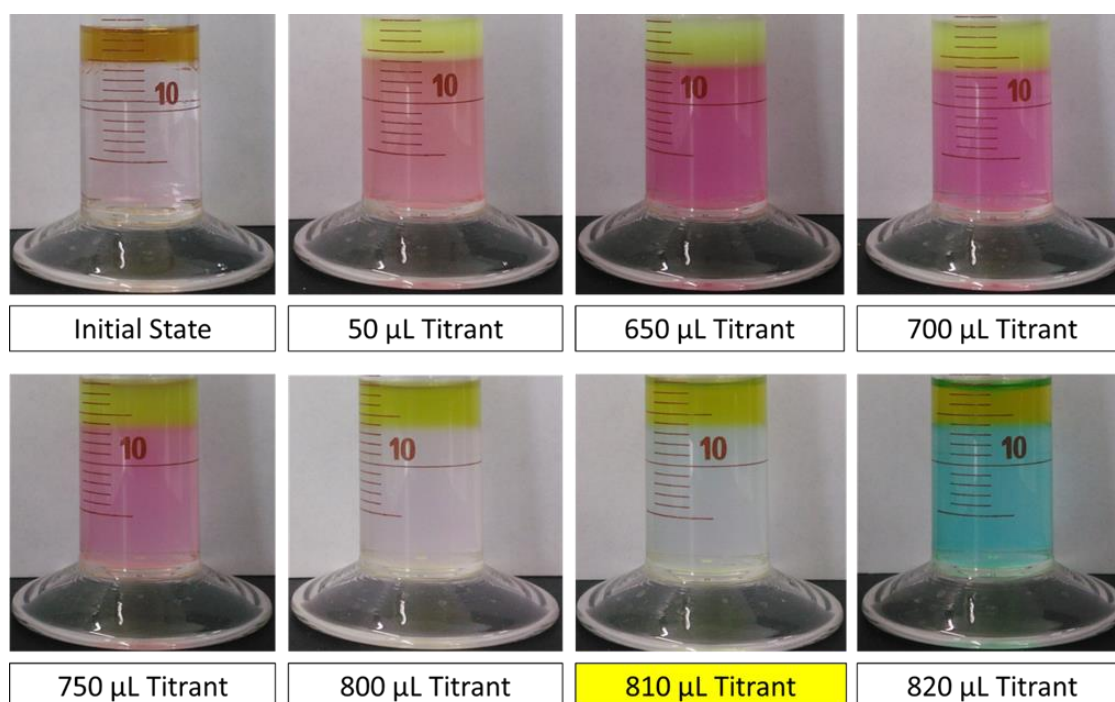
D.1.1.1 Acid indicator solution

Figure D.2. Titration of 0.1 wt.% AHS surfactant in DIW (pH = 7.8 at 20 °C) with 0.001 M SDS in DIW. The titration was performed with 1 cm^3 of the acidic sample (pH was reduced to 3.2 at 20 °C by 1 N H$_2$SO$_4$) mixed with a few drops of 1 wt.% phenolphthalein (in 95% ethanol), 2 cm^3 of the acid indicator solution (containing 0.07 mM disulphine blue, 0.21 mM dimidium bromide and 0.1 M sulfuric acid) and 15 cm^3 of chloroform. The red titrant volume shows the expected endpoint which was not observed.

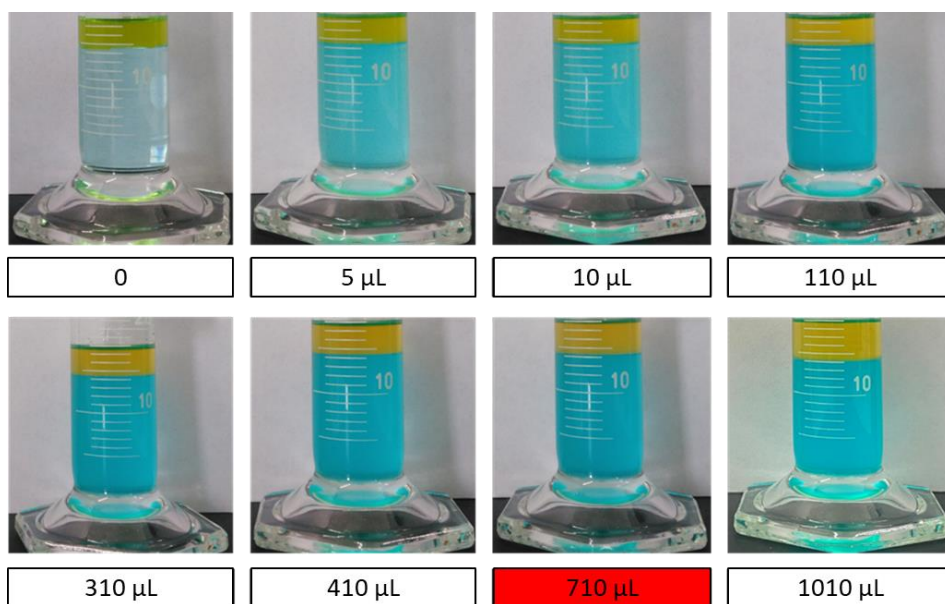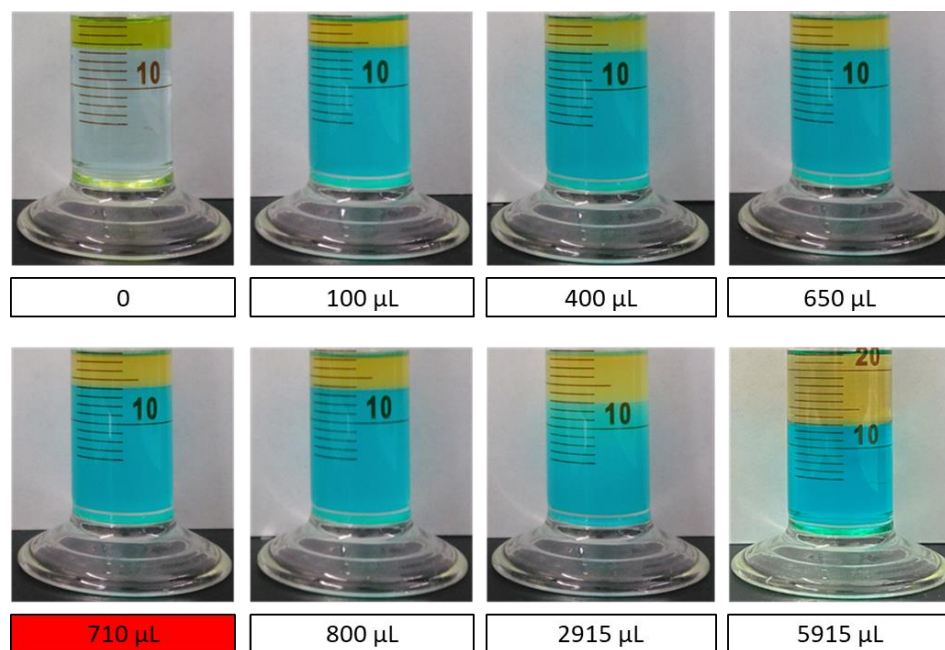| 0 | 10 µL | 160 µL | 260 µL |
| 460 µL | 660 µL | 2660 µL | 3860 µL |

Figure D.3. Titration of 0.1 wt.% (a) AHS and (b) ZN in DIW (pH = 7.5 ± 3 at 20 °C) with a 0.004 M Hyamine solution. The titration was performed with 1 cm^3 of the basic sample (pH was increased to 9.5 at 20 °C by 1 N NaOH) mixed with a few drops of 1 wt.% phenolphthalein (in 95% ethanol), 2 cm^3 of the acid indicator solution (containing 0.07 mM disulphine blue, 0.21 mM dimidium bromide and 0.1 M

sulphuric acid) and 15 cm^3 of chloroform. The red titrant volume shows the expected endpoint which was not observed.

(a)

0	5 µL	10 µL	110 µL

310 µL	410 µL	710 µL	1010 µL

(b)

0	100 µL	400 µL	650 µL

710 µL	800 µL	2915 µL	5915 µL

D.1.1.2 Alkali indicator solution

Figure D.4. Titration of 0.1 wt.% AHS surfactant in DIW (pH = 7.8 at 20 °C) with 0.001 M SDS in DIW. The titration was performed with 2 cm^3 of the acidic sample (pH was reduced to 3.2 at 20 °C by 1 N H$_2$SO$_4$) mixed with a few drops of 1 wt.% phenolphthalein (in 95% ethanol), 2 cm^3 of the alkali indicator solution (containing 0.07 mM disulphine blue, 0.21 mM dimidium bromide and 0.2 M sodium hydroxide) and 15 cm^3 of chloroform. The red titrant volume shows the expected endpoint which was not observed.
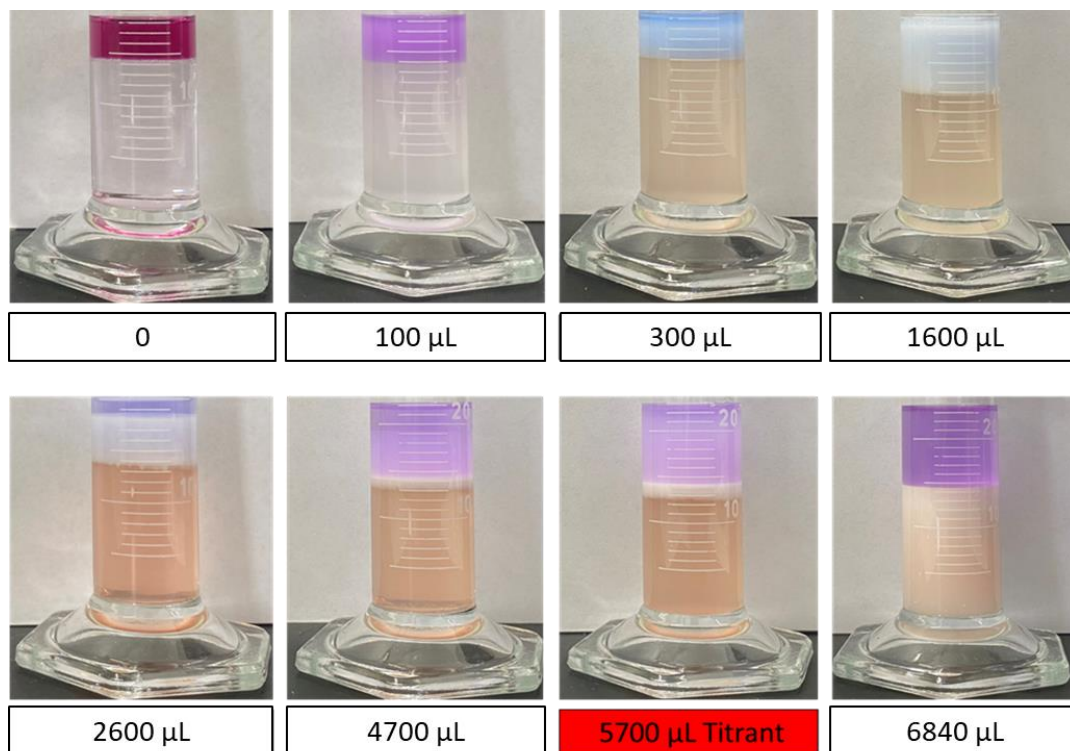
D.1.2 Conductivity measurement

The conductivity of different concentrations of AHS or ZN in DIW and Permian brine were measured at 25 °C to make calibration curves (Figures D.5 and D.6). As shown, a straight line with high accuracy can be fitted to conductivity values when surfactants are in DIW while no obvious trend is observed for surfactants in Permian brine. Therefore, this method cannot be used for the determination of surfactant concentration.

Figure D.5. Conductivity measurements of different concentrations of AHS in DIW (pH = 6.4 – 7.2) (upper) and Permian brine (pH = 5.6 – 6.1) (lower) at 25 °C.
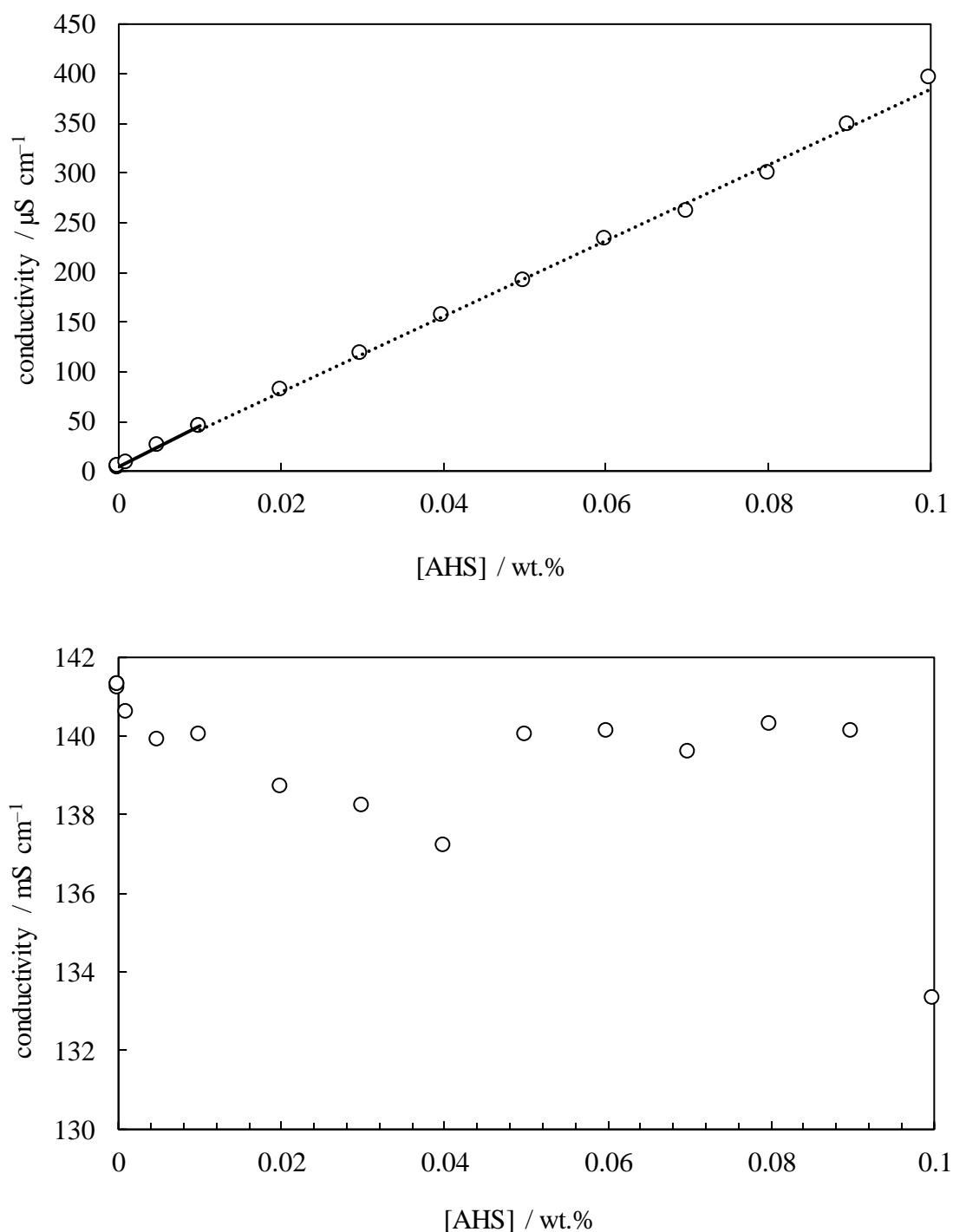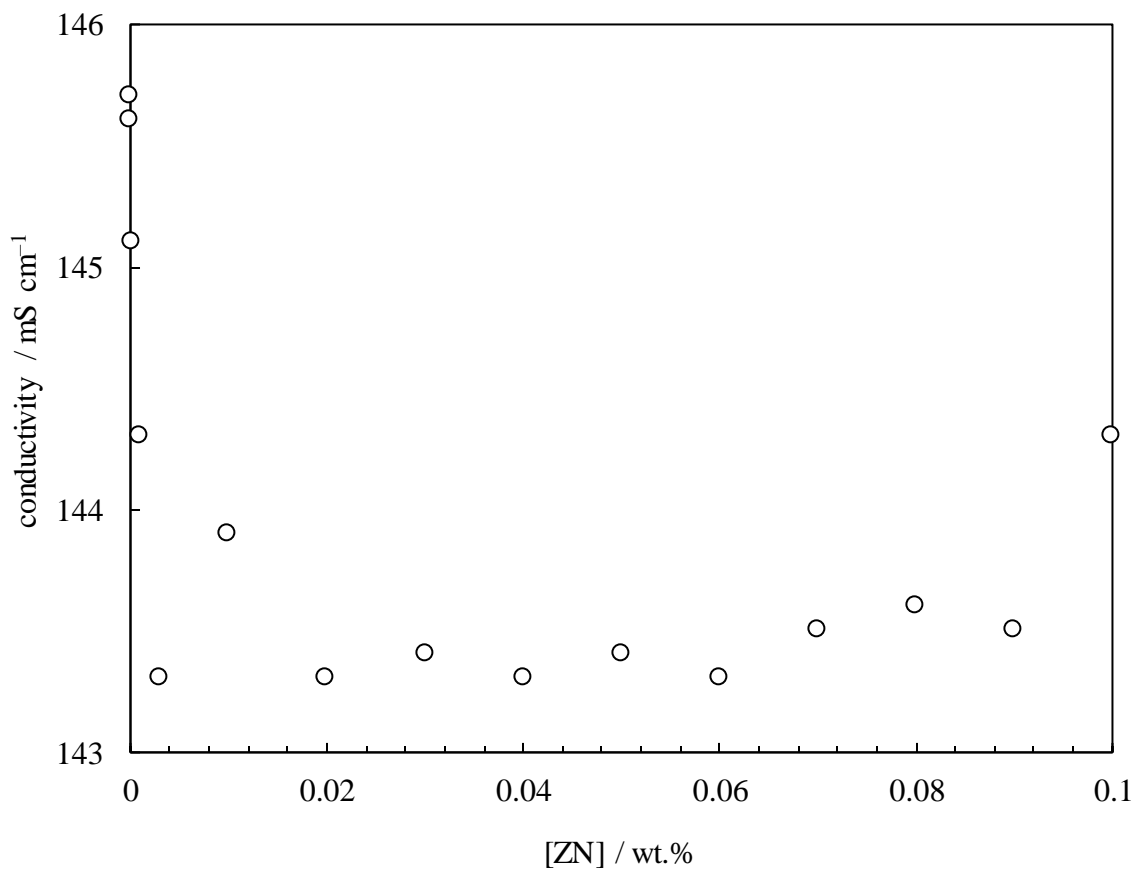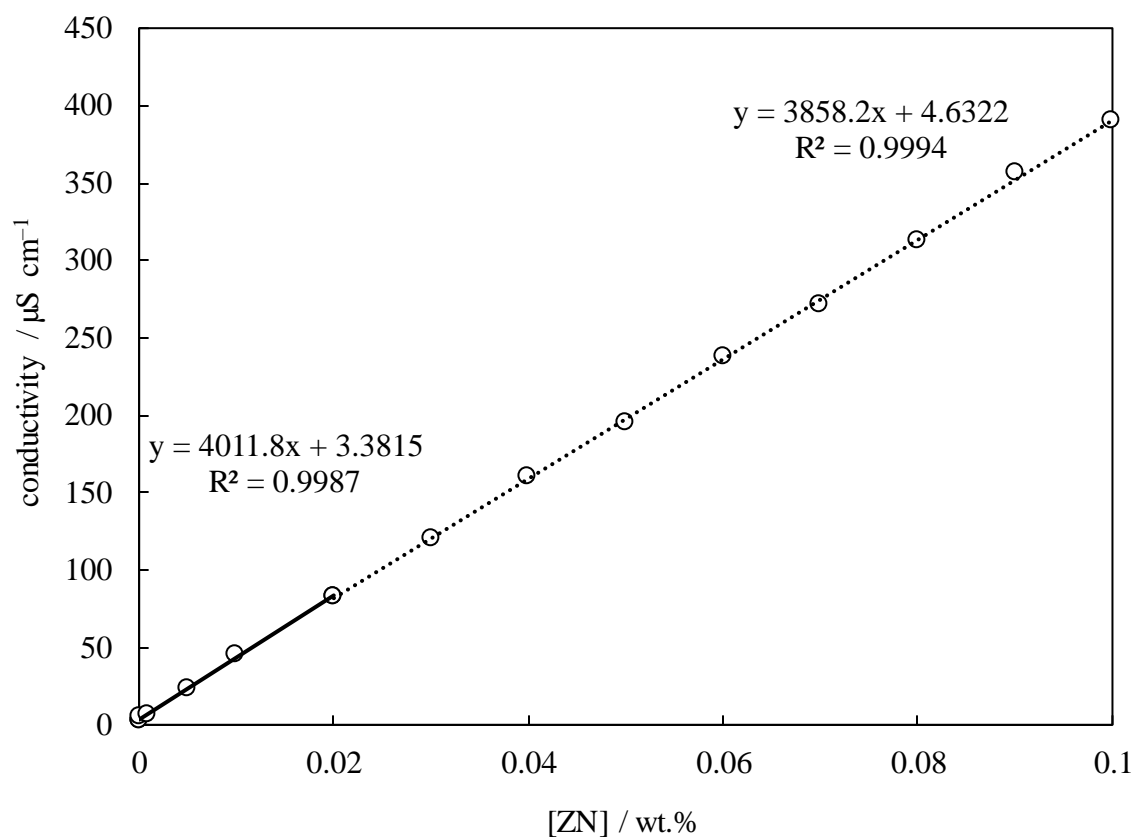
Figure D.6. Conductivity measurements of different concentrations of ZN in DIW (pH = 6.3 – 7.6) (upper) and Permian brine (pH = 5.2 – 6.0) (lower) at 25 °C.

D.1.3   UV-vis spectroscopy

The absorbance of AHS in DIW was measured at 25 °C. However, the surfactant did not show any characteristic behaviour to be used for calibration (Figure D.7). This behaviour is expected due to the lack of an absorbing group in the surfactant structure.

Figure D.7. Absorbance of 0.1 wt.% AHS in DIW (upper) and Permian brine (lower) at 25 °C.